ProQuest LLC.
789 East Eisenhower Parkway
P.O. Box 1346
Ann Arbor, MI 48106 – 1346

THE EFFECT OF OXIDE IMPURITIES ON THE MICROSTRUCTURE AND PROPERTIES OF Y-T.Z.P.

SIMON NICHOLAS HODGSON

A thesis submitted in partial fulfilment of the requirements of Sheffield Hallam University, for the degree of Doctor of Philosophy

March 1994

Collaborating Organisation: Magnesium Elektron

The Effect of Oxide Impurities on the Microstructure and Properties of Y-T.Z.P.

A thesis submitted in partial fulfilment of the requirements for the degree of Doctor of Philosophy.

Simon Nicholas Hodgson

Abstract.

An investigation has been carried out into the effects of three common oxide impurities, TiO_2, Al_2O_3, and SiO_2, on the properties and behaviour of Y-T.Z.P. These impurities are present in varying amounts in almost all commercially available Y-T.Z.P. materials, and substantial costs are incurred in removing them in the purest systems.

However, the effects of these impurities, both individually and in combination have received relatively little study in the published literature, and it has not been made clear to what degree these impurities influence the properties and behaviour of the material.

To carry out the investigation it has been necessary to develop a novel technique for introducing the impurities as dopants into a high purity, commercially available Y-T.Z.P., whilst retaining a high degree of chemical homogeneity in the material. The technique developed uses a variant on the alkoxide sol-gel process to coat the individual powder particles with a thin layer of dopant atoms and offers a number of advantadges over other doping techniques. The process could be exploited to solve a variety of ceramic processing problems.

The results obtained from impurity doped materials showed that alumina and silica reduced the sintering temperature and promoted enhanced densification at lower sintering temperatures, whilst titania impaired the sintering at lower temperatures. Alumina additions resulted in pronounced grain growth and associated destabilisation of the tetragonal phase of zirconia, particularly for higher sintering temperatures. A factorial experiment was carried out to obtain additional, and previously unreported information. This showed that there were significant interactions occurring between all of the additives investigated some of which appeared to be beneficial.

An investigation into the effect of the additives on the mechanical properties (hardness and fracture toughness) was carried out for a range of sintering temperatures. The results of these experiments suggested that the impurities had very limited direct effects on the transformation toughening mechanism, although there were differences in properties associated with the effects of the impurity additions on the microstructures of the sintered materials.

The Effect of Impurities on the Microstructure and Properties of Y-T.Z.P.

This thesis is based upon an investigation sponsored by Magnesium Elektron ltd. and carried out at Sheffield Hallam University during the period September 1988 to February 1994.

To the best of my knowledge, the methodologies, theories and results presented in this work are original, except where reference is made to other authors.

With the exception of the particle size determinations, which were carried out by Magnesium Elektron, and the X-ray Fluorescence analysis of the powder compositions all work in this thesis was carried out by myself.

No part of this thesis has been submitted for any other award.

Acknowledgements.

I would like to thank Mr. M. Clubley and Magnesium Elektron for their support of this work, and my supervisors Dr. J. Cawley, and Dr. E. Wilson for their help and encouragement.

I would also like to thank Dr. S. Jones, and Dr. C. Norman of Alcan Chemicals, and Dr. H.V. Atkinson of the University of Sheffield for their contributions.

The support of the School of Engineering at Sheffield Hallam University, in allowing me the opportunity to complete the work, is gratefully acknowledged.

Contents.

Page

3. Experimental Methods.

Page

4. Experimental Results.

1. Introduction.

Yttria stabilised, polycrystalline tetragonal zirconia (Y-T.Z.P.) is amongst the most promising of the transformation toughened zirconia ceramics. These materials generally exhibit superior strength, toughness, defect tolerance, hardness and wear resistance compared to other ceramic materials.

The best Y-T.Z.P. powders are produced by a complex chemical process which produces fine, easily sintered powders with extremely low levels of impurity.

This work is concerned with an investigation into the effect of commonly occurring oxide impurities in Y-T.Z.P. on the behaviour of the material.

1.1 Background to work.

Despite the outstanding potential of Y-T.Z.P. ceramics, in a range of applications, the widespread commercial exploitation of the material has been relatively slow to develop, although it is now beginning to find limited application[1].

One major factor behind the slow pace of commercialisation of the material has been its prohibitively high cost, and there is considerable commercial interest in the development of lower cost zirconia powders, via alternative, less costly production processes to those currently employed.

The industrial sponsors of this work wished to identify the key parameters which determine the performance of a Y-T.Z.P. material, particularly the effect of residual impurities, with a view to producing a lower cost material with acceptable performance[2].

The material used as the comparative basis for this study is a Japanese manufactured yttria stabilised T.Z.P. material (TOSOH TZ3Y). This material is generally accepted to be amongst the best Y-T.Z.P. ceramics, and has excellent properties[3]. However, the cost of this

material is of the order of £100 per Kg. The Tosoh T.Z.P. powder is produced by a complex chemical route[3], involving the hydrolysis of zirconium and yttrium chlorides followed by distillation of the product. The product consists of ultra-fine (nm) size particles, which are then heat treated, milled, and spray dried to produce homogenously sized, weakly bonded, porous spherical agglomerates, approximately 50 microns in diameter.

The chemical purity of this material is extremely high, with levels of the major impurities being typically <0.005 mass %[3].

The effect of oxide impurities was identified as a particular area of interest bearing in mind the exceptional purity of the Tosoh material and that one of the major costs and difficulties encountered in the manufacture of T.Z.P. has been the reduction of impurities to perceived acceptable levels.

Whilst it is highly probable that impurities will produce significant effects on the properties and behaviour of the material, there have been few (published) systematic studies of these, and accepted models to explain the effects of impurities in this material have not been developed to date.

Furthermore, it is probable that impurity elements will interact and that their combined effect will be different from the sum of their individual effects due, for example to compound formation, mutual solid solubilty, or solute partitioning effects. However, there appears to be no published work investigating the effects of such interactions on the zirconia system, and it was decided that these would also be investigated in this work through the use of factorially designed experiments. This is a key technique used to identify the effects of interactions in systems containing a number of different factors.

One major difficulty encountered in carrying out

investigations which involve making additions to ceramic systems arises from the inherently poor homogeneity which occurs when two or more powders are mixed. Consequently, it is often not possible to attain chemical equilibrium in the system during the normal sintering process, nor to produce a reliable model for the effect of homogenously dispersed species in a system, as required in this work.

Although various techniques have been developed to attempt to find a solution to this problem, none of these was thought to be appropriate to this investigation. Thus in order to carry out the study, it has been necessary to develop a novel technique for producing a range of materials with systematically varied composition, whilst maintaining a representative degree of chemical homogeneity

1.2. Aims and objectives of research programme.

The primary aims of the research programme were twofold.

(1) To develop an appropriate experimental technique to introduce dopants into commercially produced powders.

(2) To carry out a systematic study into the effects of common oxide impurities on the properties and behaviour of Y-T.Z.P., and identify whether high degrees of chemical purity are prerequisite for the manufacture of Y-T.Z.P. ceramics with good properties.

The objectives of the development of the doping technique were as follows:

(i). To ensure that controlled and reproducible additions of dopant could be made.

(ii). To maximise the degree to which the dopant additives were homogenously dispersed in the doped powders.

(iii). To minimise the effects of the doping process on the physical characteristics and morphology of the powders.

It was decided to carry out the study by making dopant additions to a high purity commercially produced T.Z.P. powder as opposed to attempting to produce a completely new material since it was not considered feasible to synthesise T.Z.P. powders in the laboratory with comparable sintering properties to commercially produced material.

It was also thought that the results of such a study might be easier to interpret since the number of additional variables introduced into the system, particularly regarding the sintering behaviour, was minimised.

The objectives of the study into the effect of the impurities on Y-T.Z.P. were as follows:

(i) To identify the effects of single impurities in the 0-1 mass % range on the sintering behaviour of T.Z.P.

(ii) To identify the effects of multiple impurities on the sintering behaviour of T.Z.P. and to identify any interactions occurring.

(iii) To attempt to quantify these effects.

(iv) To identify the effects of single and multiple impurities on the phase composition and microstructure developed under various sintering conditions.

(v) To identify the effects of impurity additions on the mechanical properties of T.Z.P.

(vi) To explain the effects identified in (i)-(v) by the development of a suitable model.

The impurities to be investigated were chosen as alumina, silica, and titania.

Silica and titania are the major contaminants in the precursor minerals for zirconia production. Alumina is also a contaminant in certain minerals used for zirconia production, particularly Australian zircon. However,

alumina is also frequently introduced into ceramic materials as a contaminant during powder processing. In particular milling and grinding operations tend to introduce this impurity.

The level of impurity addition chosen for the investigation was influenced by the levels of impurity in commercially available T.Z.P. and its precursor minerals, and by the need to be able to accurately identify the impurity contents of the doped powders to ensure the effectiveness of the doping technique. This effectively limited the minimum level of impurity addition investigated to 0.25 mass % which is substantially higher than in the Tosoh powder, but in the same range as the impurity level in some of the less costly commercially produced materials.

The upper level of impurity level added was 1 mass percent, which represents the approximate (total) impurity level in the lowest purity commercially available T.Z.P. powders.

2. Literature review.

2.1 Development of zirconia ceramics.

Zirconia has long been regarded as a potential engineering ceramic of some importance. This is particularly due to the extremely high melting point of the material, approximately 2850°C.

However, zirconia is a polymorphic material, and (in its pure form) undergoes a reversible monoclinic to tetragonal phase transformation on heating at approximately 1170°C, and a reversible tetragonal to cubic transformation on heating at approximately 2370°C. The structures of the polymorphs can be considered as increasingly distorted forms (M>T>C) of the cubic (Fluorite type) structure[4].

The tetragonal to monoclinic transformation is accompanied by a 3 to 5% volume expansion on cooling which results in extensive microstructural damage, and for many years, the exploitation of the otherwise excellent properties of zirconia was precluded by the effects of this disruptive phase transformation[5].

In 1929, Ruff and Ebert[6] discovered that the material could be completely stabilised in the high temperature, cubic form, by the addition of certain oxides, thus avoiding the deleterious effects of the tetragonal-monoclinic phase transformation. This material is normally referred to as cubic stabilised zirconia (C.S.Z.) or fully stabilised zirconia (F.S.Z.).

The discovery of the stabilising effect was followed by the observation by Curtiss in 1947[7], that enhanced mechanical properties, particularly thermal shock resistance, were obtained when smaller quantities of the stabilising additive were present, resulting in the formation of a microstructure consisting of a dispersion of monoclinic phase present in the cubic phase. The nomenclature, partially stabilised zirconia (P.S.Z.) was adopted for this system.

Various mechanisms[8][9][10][11] were suggested, to account for the improved properties of the cubic/monoclinic P.S.Z. materials, these being reviewed and confirmed by Garvie and Nicholson[12].

In 1985, Garvie et al published a paper entitled "Ceramic Steel?"[13], which led to a new generation of ceramic materials based upon zirconia.

In this paper, it was demonstrated that it was possible to produce a P.S.Z. material with a microstructure consisting of retained metastable tetragonal grains in a cubic matrix which had greatly improved properties compared with the conventional (cubic/monoclinic) P.S.Z.

Garvie et al[13] identified the primary toughening mechanism in these materials as arising from an increase in the work of fracture. This was due to the absorption of energy associated with the martensitic tetragonal-monoclinic phase transformation.

Significantly, this was the same transformation which had earlier been responsible for the limitations in the use of zirconia in the unstabilised form due to its disruptive nature. The phenomena was given the title "transformation toughening". It was also concluded that the transformation was initiated by the interaction of the complex tensile stress fields associated with a crack tip, and the dispersed metastable tetragonal phase in the material.

The elucidation of the transformation toughening mechanism by Garvie[13] and others[14], led to a great deal of interest in these materials, and facilitated the rapid development of a range of transformation toughening zirconia ceramics with properties of strength and toughness greatly superior to the majority of other engineering ceramics[3][15].

A variety of stabilising additives are used in the zirconia system, including yttria, magnesia, calcia, ceria etc, each of which results in different

microstructure and properties. The stabilising cation is usually added to the description of the ceramic e.g. Mg-P.S.Z..

The zirconia system with which this work is concerned consists of zirconia stabilised with approximately 3 mole % of yttria. This causes a microstructure consisting of almost 100% tetragonal phase to be retained on cooling to room temperature[16]. The nomenclature Y-T.Z.P. (yttria stabilised tetragonal zirconia polycrystal) is adopted for this system[5].

The properties and applications of zirconia ceramics and T.Z.P. have been reviewed by Subbarao[17], Stevens[18], and Nettleship and Stevens[19].

There are a wide range of current and potential applications for zirconia ceramics, exploiting the improved strength, toughness and wear resistance arising from the transformation toughening effect. The fine grain size of Y-T.Z.P. materials makes them particularly suited for the fabrication of finely machined artefacts requiring accurate dimensional tolerances.

Examples of current applications of Y-T.Z.P.[1][18] include ceramic knives and cutting tools, grinding and milling media, dies for extrusion and drawing of metals, guide rollers, bushings and bearing shells, spray nozzles, biomedical applications and connectors for optical fibres. Within the U.K. and Europe, these applications are little more than experimental curiosities in many cases at present, however Japanese industry has been keen to develop these applications and in many cases these are now a commercial success.

It is also envisaged that the material will find commercial applications as engine components such as valves, guides and pistons, rotors and turbine blades.

2.2 Polymorphism and crystallography of zirconia.

Early models of the crystal structures of zirconia[20]

Table 2.1

Comparative properties of transformation toughened zirconia and other engineering ceramics.

Material.	Strength. M.O.R. (MPa)	Toughness. K_{1c} ($MNm^{-1.5}$)
Yttria stabilised Tosoh TZ3Y T.Z.P.	1300	10
MgO stabilised Nilcra TS P.S.Z.	720	15
MgO stabilised Feldmuhle ZN40 P.S.Z.	520	8
SiC.	600	4
Alumina.	500	3

* All figures quoted are from manufacturers data, measured at room temperature. Due to non-standardised test procedures, the results are not directly comparable and should be considered as a guide to the relative performance only.

concluded that as many as six crystalline modifications existed, whilst others claimed the existence of various alternative high temperature polymorphs, later thought to be due to the effects of impurity elements. There has also been some dispute over the existence of the cubic modification in pure zirconia[21] although this is now generally recognised as correct[4][22][23][24].

Zirconia is now recognised as existing in three polymorphs at atmospheric pressure, the stable form being dependent on the temperature and composition. These exhibit monoclinic[25][26][27][28], tetragonal[26][27][29], and cubic[38] structures.

The cubic to tetragonal phase transformation is thought to occur by a diffusion controlled eutectoid reaction[30], whilst the tetragonal to monoclinic phase transformation is thought to occur by a diffusionless, martensitic type mechanism[31][32][33].

It has also been demonstrated that an alternative, non transformable tetragonal or cubic related phase (normally referred to as t') with different cell parameters to the normal phases can be formed, by a martensitic type phase transformation from the cubic phase during rapid cooling from high temperature[30][34][35][36][37]. This phase will undergo gradual decomposition into the equilibrium cubic and transformable tetragonal phase if heat treated at a temperature in the two phase field of the equilibrium diagram[36].

The lattice parameters of the polymorphs have been shown to vary with the amount of stabilising oxide present. The effect of yttria content on the cell dimensions is shown in figure 2.2.

The nucleation of the tetragonal to monoclinic phase transformation is of particular importance in the stabilisation of the tetragonal phase in T.Z.P.

Studies of the transformation[38] have discovered the occurrence of "burst phenomena", characteristic of

Figure 2.2

Effect of Y_2O_3 stabiliser content on the unit cell dimensions of zirconia polymorphs.

(Reproduced from reference[30]).

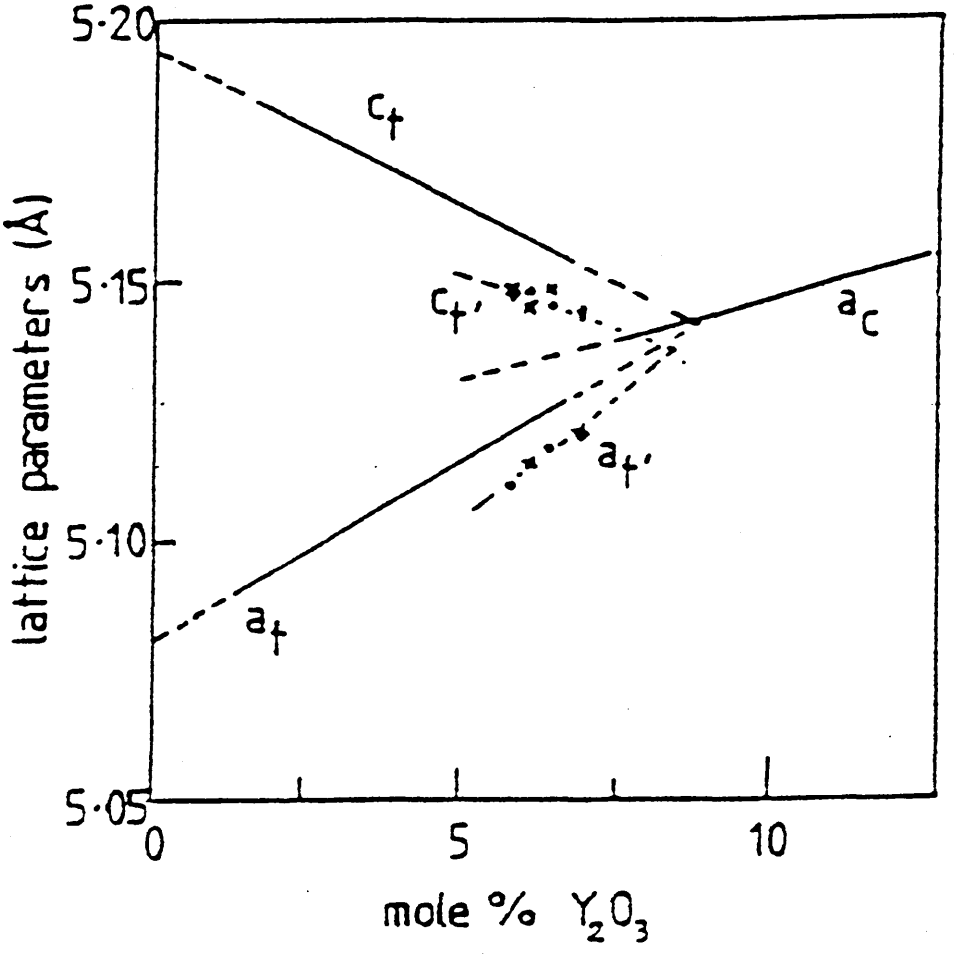

martensitic transformations in many metallic systems and provides evidence for heterogeneously nucleated transformation mechanism.

Heterogeneous nucleation of the martensitic transformation at grain edges and small angle grain boundaries in T.Z.P. has been demonstrated by Ma and Ruhle[33][40].

Autocatalytic nucleation, in which transformation of one grain induces transformation in neighbouring grains, is also important in T.Z.P. and results in the formation of a characteristic transformed zone or "wake" around a propagating crack in the material[41][42].

2.2.1 Lattice defect structure

One consequence of making stabilising additions to zirconia, in which the valencies of the zirconium ions (4^+) and the substituting solute ions (variously 3^+ and 2^+) differ, is that in order for the structure to maintain overall charge neutrality, it is necessary to produce charge compensating vacancies in the co-ion sublattice (the oxygen or anion sublattice in this case)[43]. The positions of the vacancies in the structure are described as the defect structure of the material.

Ordinarily, it is expected that thermal and statistical factors will produce a random arrangement of ionic vacancies within the material. However, the distribution of defects within stabilised zirconia is not always random, particularly for higher levels of stabiliser addition, and ordering of the defects within the crystal structure can occur[44][45]. This implies that there is some interaction between the defects in the crystal structure.

The oxygen vacancies, or lattice defects, in zirconia give rise to a number of useful electronic properties with commercial applications.

At high temperatures, typically around 1000°C, the vacancies in the zirconia lattice become mobile. Since the vacancies possess a net charge, behaving as "holes" in the lattice, they can act as charge carriers enabling the material to become electrically conducting at high temperatures[18]. This vacancy conduction is exploited in applications such as furnace elements for high temperature furnaces.

There is some contradiction in the literature regarding the structural relationships between the defects (vacancies), the zirconium ions and the stabiliser ions. In particular, whether the charged defects will be situated adjacent to the Zr^{4+} or the stabiliser (Y^{3+}) ions in the structure[44]. These structural relationships may be of significance in determining the sintering characteristics of the material via changes in the free vacancy concentration (see section 2.5.4), and similar effects might be significant for impurity ions in solid solution in zirconia.

Yashima et al[45] have investigated a number of possible structural models, based upon ion packing around the (charged) defects, and suggest that for the yttria stabilised zirconia system, the Y^{3+} ions and the charge compensating vacancies occur adjacently.

2.3 Stabilisation of zirconia.

With respect to the behaviour of zirconia, stabilisation can be defined as preventing or impeding the phase transformations between the high temperature and low temperature polymorphs, allowing one of the high temperature polymorphic forms (i.e. cubic or tetragonal crystal structures) to be retained at ambient temperature.

It has long been known that the tetragonal zirconia polymorph can occur at room temperature in material with a very fine particle size (around 30 nm), even where no stabiliser is present[46].

This phenomena has been attributed to the effect of surface energy on the thermodynamics of the phase transformation[13]. The surface energy of the tetragonal zirconia polymorph is lower than that of the monoclinic form and compensates for the (higher) internal energy as the particle size is reduced [47].

A variety of additives have been found to result in the stabilisation of zirconia. The most commonly used of these are CaO[48], MgO[49], Y_2O_3[34], and CeO_2[19].

A complete explanation of the mechanism by which these additives produce stabilisation has not been developed to date, although various explanations, described below, have been given. These have not been reviewed in the published literature.

There are four main theories proposed for the stabilisation mechanism, which may be jointly involved. These are based upon (i) ionic size effects, (ii) ion - vacancy interactions, (iii) nucleation effects and (iv) lattice vibration effects.

(i) Ionic size effects.
The ionic sizes in zirconia are such that the cation:anion size ratio lies outside the normal range of stability of the fluorite crystal structure as predicted by Pauling's rules[50].

McColm[51], suggested that additions of stabilising oxide, in solid solution in substitutional sites in zirconia, result in an increase in the average cation:anion size ratio, to a value closer to that at which Pauling's rules would predict a stable cubic structure, thus reducing the (thermodynamic) instability of the high temperature polymorph.

Evidence cited for this mechanism was that the sizes of Ca^{2+} and Y^{3+} ions are larger than the Zr^{4+} ion, this being consistent with the theory of increased stabilisation by increasing the cation:anion size ratio.

McColm[51] also suggested that further evidence for this type of mechanism is offered by the stabilising effect produced by substitution of N^{3-} ions for the O^{2-} ions in zirconia. Since N^{3-} ions are larger than O^{2-} ions, this would increase the average anion size, and produce a similar decrease in the cation:anion size ratio to that described for cation substitution. This theory cannot account for the stabilising effect observed with additions of MgO to ZrO_2. Mg^{2+} ions are **smaller** than Zr^{4+} ions, and should therefore not have any stabilising effect by this mechanism. McColm attributed the stabilisation in this system to the effect of the very slow transformation kinetics in this system, and the subsequent retention of the metastable high temperature form on quenching.

(ii) Ion-vacancy interactions.
Heuer et al[4] proposed an alternative theory for the stabilisation mechanism based upon the effect of the charged crystal defects produced by the substitution of stabiliser ions (of valency/ionic charge other than 4^+) in the Zr^{4+} lattice.

This theory suggested that the interaction of the lattice defects with the surrounding ions results in a reduction in the electron energy levels of the (displaced) ions of the high temperature polymorphs, and a consequent increase in the thermodynamic stability of these structures (i.e. a decreased driving force for transformation).

Further evidence for the defect-ion interaction theory is given by recent work by Lu and Chen[52], who showed that a decrease in stabilisation (high temperature phase stability) occurred when Y^{3+} (acceptor ion) doped zirconia was co-doped with Ta^{5+} (donor) ions, which reduce the number of ion vacancies in the structure.

The formation of nitride stabilised zirconia (as discussed in (i)) can also be explained by this mechanism, since substitution of N^{3-} ions for O^{2-} may

also result in the formation of charge compensating vacancies in the anion lattice.

The defect interaction mechanism may also explain the observed stabilisation effects of zirconia sintered in a reducing atmosphere[53], since this would produce an oxygen deficient structure.

There are a number of areas which this theory does not explain. In particular, defect - ion interactions cannot account for the observed stabilisation of zirconia when ions of the same valency as Zr (eg 4^+) are added. i.e. CeO_2 or TiO_2 stabiliser additions, since substitution of these ions in the zirconia lattice should not produce charge compensating defects.

(iii) Nucleation effects.

Nucleation effects are thought[33] to be of particular importance in the martensitic tetragonal to monoclinic phase transformation.

The transformation is thought to occur by nucleation controlled kinetics, with both kinetic and thermodynamic factors determining whether the t-m transformation takes place, and thus whether the crystal structure remains in the (stabilised) tetragonal form[33].

The free energy for the transformation is affected by the stabiliser content of the parent and product phases. Thus, above a certain stabiliser content the tetragonal phase has the lowest free energy, precluding the transformation, whilst below this critical stabiliser level the monoclinic form is the low energy polymorph and the transformation may take place according to nucleation controlled kinetics provided that no activation energy barrier exists, or that sufficient energy is supplied to surmount this.

In unstabilised material the nucleation takes place spontaneously. However, the addition of a stabilising additive reduces the driving force for the transformation and as a result, the nucleation sites

become operative only in the presence of an additional applied stress (i.e. a crack tip stress field). The material is therefore stabilised in the tetragonal form (as in T.Z.P.) in the absence of an applied (tensile) stress field[33].

(iv) Lattice vibration effects.
An attempt has been made (by Cormack and Parker)[54] to produce an atomistic simulation to model the effects of stabiliser atoms on the structure, bonding and thermodynamic stability of the zirconia polymorphs.
The model used comprised a static element, to account for the effects of structural parameters such as atomic positions and lattice vectors, and a dynamic element to account for the effect of thermal vibrations, based upon an assumption of quasi harmonic motion.

This work suggested that the stabilisation mechanism involved a change in the modes of thermal vibration (due to changes in the inter-atomic force constants when stabilising additives were present) to delay or eliminate the onset of unstable modes of oscillation on cooling, thereby reducing the free energy of the high energy polymorphs.

This model was partially successful in predicting the stabilising effects of various types and amounts of dopant additives, but was not able to correctly predict the absolute temperatures at which the phase transformations took place in real systems.

Depending upon the relative ionic sizes, valency, and solid solubility, impurity ions might affect the stabilisation, and resultant phase composition and mechanical properties of T.Z.P. by all of the above mechanisms, and a study into the effects of impurities on these parameters therefore formed a significant part of this work.

2.3.1 The Zirconia-Yttria System.

The phase diagrams for the various zirconia-stabilising additiv

systems have received extensive study, due to their importance in the production of transformation toughened ceramics, and according to Heuer et al[4], it is possible to have a high degree of confidence in the latest studies.

In the case of the Y_2O_3 - ZrO_2 system, there have been numerous modifications[55] [56] [57] [58] [59] [60] to the phase diagrams by different workers. The phase diagram of Scott[34] is normally considered to be the most accurate. This is illustrated in figure 2.3.1 (a), with the zirconia rich portion of the system illustrated in figure 2.3.1 (b).

A set of thermodynamic functions have been produced for the ZrO_2-Y_2O_3 system by Du et al, enabling a calculated phase diagram to be obtained[60]. This was in general agreement with the experimentally determined diagram of Scott[34]. The attainment of equilibrium in zirconia ceramics is relatively slow, due to the low cation diffusivities in these systems[61], this being of considerable significance for the addition of dopant oxides to the system in this work.

2.4 Mechanical properties of transformation toughened ceramics.

2.4.1 The transformation toughening mechanism.

The transformation toughening mechanism is responsible for the enhanced mechanical properties of partially stabilised zirconia ceramics such as Y-T.Z.P. The nature of this mechanism and its effects are reported here in so far as is necessary to support the mechanisms proposed to account for the effects of impurities on the mechanical properties identified in this study.

Although there is no doubt that the transformation toughening phenomena is associated with the (martensitic) tetragonal to monoclinic phase transformation, there is still no single accepted model for the mechanism by which the transformation produces the increased fracture toughness. Indeed it is possible that a combination of

Figure 2.3.1 (a) The ZrO_2 - Y_2O_3 phase diagram.
Reproduced from Reference[34].
Note 2 mol% $YO_{1.5}$ = 1 mol% Y_2O_3

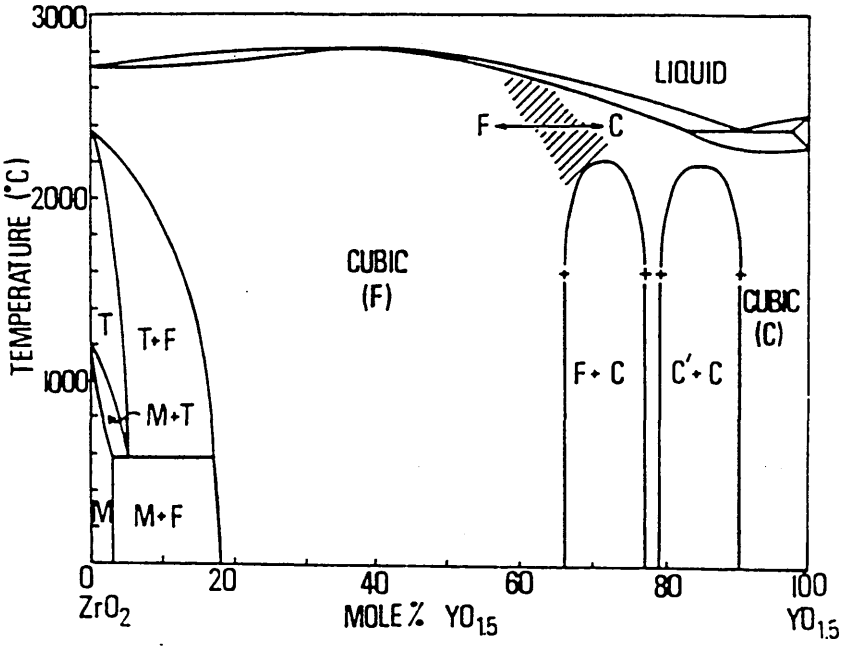

Figure 2.3.1 (b) ZrO_2 rich portion of The ZrO_2-Y_2O_3 phase diagram.
Reproduced from Reference[34].

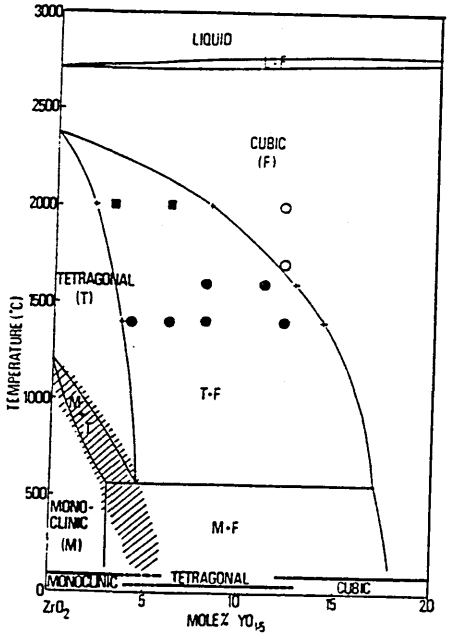

several processes are operating.

Generally, there are two schools of thought regarding the toughening mechanism, these can be thought of as those based upon energetic considerations, ie (i) an increase in the work of fracture, or (ii) those based upon elastic considerations, ie the reduction of crack tip tensile strain fields. There is some doubt whether the two mechanisms would give rise to equivalent behaviour[62].

The mechanism of transformation toughening originally proposed by Garvie[13] for partially stabilised zirconia, was that the tetragonal to monoclinic transformation could be initiated in metastable tetragonal precipitates, by an interaction with an advancing crack. The same principle applies to T.Z.P.

The tetragonal phase is retained in a metastable form in P.S.Z. and T.Z.P. ceramics by constraining effects in the matrix allied with the effect of the stabilising additives. The removal of this constraint, by the interaction with a crack or defect results in spontaneous transformation to the monoclinic form.

(i) Energetic models.
Garvie et al[13] proposed that the toughening effect arose from the energy absorbed by the martensitic phase transformation. This was thought to increase the work of fracture. This model is the basis for a variety of mechanisms proposed for transformation toughening.

The martensitic transformation is accompanied by a change in shape and volume in the material. The resultant strains are accommodated by the development of a very fine twin structure, commonly referred to as martensitic laths.

The shear and deformation accompanying the transformation are very similar in effect to conventional plastic deformation[63], and allow the structure to relieve internal stresses. The process is often referred to as transformation plasticity or pseudoplastic deformation[64].

It has been suggested that the increased work of fracture is

associated with the pseudo-plasticity accompanying the tetragonal to monoclinic phase transformation[65].

This mechanism can be considered as analogous to that thought to operate in TRIP steels[66].

The pseudoplastic deformation is thought to play a particularly important part in the toughening mechanism for smaller crack lengths. In these cases it has been suggested that plastic flow at the crack tip may result in the relief of stress concentrations, thus increasing the toughness[67]. It is also possible that this phenomena might affect the hardness of the material, and transformation plasticity is considered as a possible explanation of some of the effects observed on the hardness of doped Y-T.Z.P. in this work.

A theoretical model for the effect of various energy dissipative mechanisms was developed by Pomphe and Kreher[68]. The model was based upon the Griffith type model where the energy dissipated by the martensitic phase transformation was included in the energy balance criteria. This model did not consider plastic deformation as a dissipative mechanism however.

(ii) Elastic models.

The idea that the toughening mechanism was due to elastic stress fields rather than energy absorption was first proposed by Porter and Heuer[14] and forms the basis of a variety of similar models. The tetragonal -> monoclinic transformation has a 3-5% volume expansion associated with it. Thus the phase transformation and this volume change introduce compressive stress into the material at the crack tip where the transformation is initiated. The compressive forces arising from the volume expansion oppose the tensile stress fields at the crack-tip, and inhibit further crack growth.

Quantitative theories for toughening by elastic type mechanisms were developed by Evans et al[69] and McMeeking and Evans[70].

It has been shown that in order for the transformation to exert sufficient toughening effect to account for the observed behaviour, the transformation must occur not only at the crack tip, but also in the "wake" of the advancing crack. This transformed zone around the crack is often described as having a "crack shielding effect"[69][70].

2.4.2 R Curve behaviour.

The most significant departure between the behaviour of transformation toughened and conventional ceramics is the non linear strength-toughness relationship in transformation toughened materials.

In particular, it has been found in a number of studies[71][72] that the resistance to crack growth (R) in transformation toughened ceramics, is not a constant determined solely by the increase in surface energy associated with crack growth (as in a conventional Griffith model). In these materials the resistance to crack growth (R) and the related crack resistance stress intensity (K_R) increase with increasing crack length. This type of behaviour is termed "R-curve" behaviour, and is characteristic of systems exhibiting some plastic deformation[73].

The occurrence of R curve behaviour in these materials has been suggested to arise because it is necessary for a substantial wake of transformed material to build up behind the crack tip before complete crack shielding occurs. At this point steady state values of R are attained[71].

In these materials, failure is controlled not by a constant fracture toughness K_{1c} for the material, but by the slope of the R Curve[5]. The fracture behaviour is determined by the point where the stress intensity factor K_1 curves and the crack resistance stress intensity curve K_R are tangential (see figure 2.4.2)[74].

Cracks of length greater than C^* will grow by

Figure 2.4.2 - R-curve behaviour.
Reproduced from reference[106].

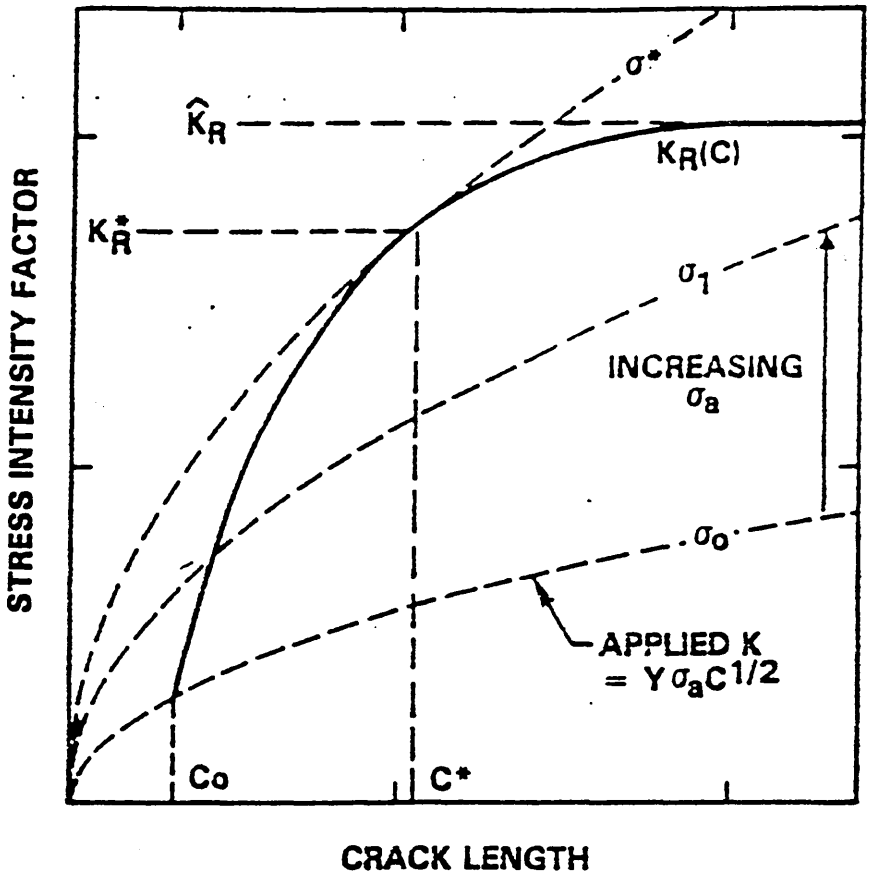

catastrophic fracture as in a conventional brittle material, but for crack lengths below C^*, the strength is determined by the shape of the R (or K_R) curve, with the cracks undergoing slow stable crack growth to an equilibrium length corresponding to point of intersection between the K_1 and K_R curves.

A consequence of this behaviour is that the strength

toughness are not directly related in transformation toughened ceramics, and the best values of strength and toughness are not exhibited by the same materials[15]. Also, the strength and fracture toughness values exhibited by the material are dependent upon the applied load, specimen and loading geometry, all of which influence the shape of the K_1 curves. This is of some significance as a possible source of error and confusion in mechanical property determinations on zirconia ceramics as carried out in this work.

2.4.3 Effect of surface stress.

Spontaneous tetragonal to monoclinic phase transformation of unconstrained grains on the surface of T.Z.P. and P.S.Z. ceramics has been shown to occur, giving rise to a resultant surface compressive stress in the material[75][76]. This results in an increase in strength in the component by a similar mechanism to that commonly used to strengthen glasses by tempering[77][78].

The amount of surface transformation, and consequently the magnitude of the (strengthening) surface compressive stress can be increased by grinding or abrading the surface of the ceramic, whilst polishing of the material results in a gradual reduction of the effect as the transformed material is removed.

The effects of these surface stresses are believed[79] to be of significance as a possible source of error in the determination of fracture toughness by indentation as used in this work, and it is important that standardised specimen preparation procedures are used to

avoid this.

2.4.4 Strength degradation in Y-T.Z.P.

Y-T.Z.P. has been shown to undergo a degradation in it's mechanical properties by a chemical reaction in air at temperatures ranging from room temperature to around 300°C[80][81]. This so called "ageing" phenomena has been a major cause of concern in the commercial application of T.Z.P. ceramics.

Reviews of the effects and the possible causes of the degradation effect have been carried out by Nettleship and Stevens[19], and Swab[82], whilst Hirano[83] has reviewed the methods to inhibit the degradation effect.

Studies by Masaki[84], found that the effect was maximised at around 200°C and that increasing the stabiliser content to 5 mole % appeared to prevent it, whilst work by Sato et al[85], has shown that the ageing is accelerated by the presence of water.

Two mechanisms have been proposed to account for the observed phenomena.

Sato and Shimada propose a crack tip corrosion process occurs with water molecules, causing crack growth. The phase transformation accompanying crack growth was suggested to induce further cracking, thus accelerating the surface transformation[86].

Lange et al[87] propose a mechanism involving chemical destabilisation of the surface grains by reaction of solid solution yttria with water. The presence of $Y(OH)_3$ crystallites on the grain boundaries of aged foils was cited as evidence for this phenomena.

The work of Lange et al[87] also showed that the process was independent of the amount of grain boundary phase. This finding suggests that increased levels of impurity and associated grain boundary phases is not likely to impair the resistance to this phenomena. Some additives\impurities have been found to improve the resistance to this effect.

Attempts have been made to control the phenomena by reducing the transformability of the surface grains. This has been achieved by sintering in an yttria bed[88] or, more significantly in terms of this work, by controlling the grain size (and thus the driving force for transformation) by alumina addition[89].

Additions of titania in solid solution in T.Z.P. have also been shown to reduce the transformation phenomena, and multicomponent Ti-Y-T.Z.P. materials resistant to the ageing phenomena have been developed[90].

These findings suggests that the presence of Al_2O_3 and TiO_2 impurities might be expected to improve the resistance to the ageing phenomena, and although this was not examined directly in this study, suggests that the effects of these impurities on other properties (which might be adversely affected) such as sintering behaviour, and fracture toughness are therefore of particular interest.

2.5 Sintering and microstructural development.

2.5.1 Sintering processes.

Sintering can be defined as "the process whereby a heat treatment is used to convert a powder compact into a dense polycrystalline solid"[91]. The process is driven by the reduction in free energy associated with the decreasing surface area (& energy) which results from consolidation of the individual particles into a solid[77].

There are essentially three types of sintering process of importance for sintering of these ceramics, these being solid state sintering, reactive liquid phase sintering (where the primary grains exhibit solubility in the liquid phase), and non reactive liquid phase sintering (where the primary grains are not soluble in the liquid phase).

The theory and effects of these sintering processes have received extensive study and review in both standard

texts (See McColm and Clark[91], Kingery et al[77]) and journal publications (e.g. references[92] to [102], for solid state sintering, and [103] to [110] for liquid phase assisted sintering).

2.5.2 Sintering additives.

Both liquid phase forming, and solid solution impurity elements may enhance sintering rates by promoting densification during the sintering process, whilst retarding the grain growth process. Impurities acting in this way are frequently used as "sintering aids"[111], and it was thought that the impurities added during this work might produce similar effects. Sintering additives for Y-T.Z.P. have received little study, although some work has been carried out for P.S.Z. with other stabiliser additions[111].

Impurity elements can affect the sintering process either by forming a second (liquid) phase at the grain boundaries/particle interfaces, or by various interactions with grain boundaries and vacancies whilst remaining in solid solution.

(i) Solid state additives.
There is some disagreement in the literature about the mechanism by which solid solution impurities affect the grain growth behaviour. For example it has been suggested by Cahn[112] and Jorgensen and Westbrook[113] that segregated impurities exert a drag force on the moving grain boundary, reducing the grain growth rate.

Alternatively, it has been suggested by Kroger and Vink[114] that segregated impurities may reduce that rate of grain growth by forming a continuous barrier (or impediment) to diffusion at the grain boundary, thus reducing the rate of mass/vacancy flow across it and consequently the grain growth rate.

A perhaps more complete explanation of the effect of sinter enhancing impurities was suggested by Brook[97],

who considered the effect of the solute impurities was due to changes in the respective rates of lattice and surface diffusion, thus promoting densification (increased D_L)*, whilst reducing the rate of grain growth (reduced D_s)**

Impurity elements may also form an independent (and non melting) second phase within the microstructure of the material (ie a microstructure with grains of the impurity material present).

These second phase precipitates may affect the sintering and grain growth behaviour by preventing grain boundary advance[77]. This mechanism has been used to good effect in T.Z.P. where alumina is used to control, grain size and prevent the low temperature strength degradation in Y-T.Z.P..

(ii) Liquid phase forming additives.
Impurities which form a liquid phase at the sintering temperature may enhance the sintering behaviour, by the normal liquid phase assisted (reactive or non reactive) sintering mechanisms, particularly in the early stages of sintering.

There are two types of liquid phase forming additives, used as sintering aids[91][115]. These are:-

(a) Permanent liquid phase sintering additives.
ie the liquid phase remains at the grain boundaries throughout the sintering process, forming a glassy grain boundary phase on cooling.

(b) Transitory liquid phase sintering additives.
Liquid phase is formed during the sintering process to give enhanced densification, but is redissolved into the grains on further heat treatment or cooling.

* Lattice Diffusivity ** (Particle) Surface Diffusivity.

2.5.3 Effect of precursor powder structure.

The effect of the powder structure on the sintering behaviour and microstructural development of advanced ceramic materials has been reviewed by Kendall[116].

The main factors determining the sintering behaviour of a ceramic powder are conventionally thought to be particle size and chemical purity. Kendall[116] also discussed the effect of agglomeration and agglomerate strength, and identified these as the limiting factor in the production process.

Agglomeration occurs in all fine powders due to Van der Waals attractive forces between particles[116]. These agglomerates have been shown to be sufficiently strong (strength typically >100MPa)[117] to remain unbroken during the shaping and pressing operations carried out in the manufacture of the green compact.

Unbroken agglomerates act as sources of density inhomogeneity in the green compact, and undergo differential shrinkage compared to the bulk material, shrinking away from the matrix and forming defects in the microstructure[118].

The agglomeration behaviour of Tosoh TZ3Y, and other Y-T.Z.P. materials produced by different fabrication routes have been studied by Groot Zevart et al[119]. This work included measurements of agglomerate strength and pore structures for green compacts pressed at 4, 100, and 400 MPa.

The Tosoh powder was shown to consist of regular spray dried 30-50 um granules which themselves comprised dense aggregates of around 60nm diameter. The strength of these agglomerates was shown to be approximately 40 Mpa, indicating that the agglomerates should have been broken down during the green pressing operation.

However, recent work by Kim et al[120], using optical techniques and porosimetry to characterise the internal structure of commercial Y-T.Z.P. appears to show that some

agglomerates may survive at pressures as high as 600 MPa.

The source of the T.Z.P. powder tested is not given in this work, and it is therefore difficult to make objective comparisons between these two apparently contradictory studies.

Shi et al[121] have produced a study of the effect of agglomerates on the microstructural development of zirconia, and suggest that the source of strong agglomeration in zirconia powders may be hydrogen bonding from chemically co-ordinated water molecules on the particle surfaces, or oxygen linkages between powder particles formed by loss of hydroxyl groups from chemically bound water molecules.

Agglomeration was thought to be a potentially significant factor in this work, due to the possible effects of the powder doping technique on the agglomerate strength.

2.5.4 Sintering of T.Z.P.

The sintering of high purity T.Z.P. is often considered to take place by a liquid phase sintering mechanism, and the presence of a grain boundary phase has been identified in T.E.M. studies of a range of commercially produced T.Z.P. ceramics[122]. However, some uncertainty arises with regard to the nature of the sintering process.

The amount of liquid phase produced is extremely small in commercial high purity materials, with the grain boundary phase in the final microstructure being between 2 and 10 nm thick[19]. The microstructures of these materials tend to comprise straight sided grains (characteristic of solid state sintering), rather than the curved grain boundaries expected for a liquid sintered material[19].

It is not clear whether the liquid phase is formed in the early stages of sintering, in which case liquid phase sintering mechanisms should operate provided sufficient liquid is present, or whether the liquid phase forms in

the later stages of sintering (by which time a solid network may have formed thus rendering the liquid phase sintering mechanisms inoperative).

Theunissen et al[123] have studied the microstructural development during the sintering of T.Z.P. and this work suggests that segregation of yttria to the grain boundaries takes place only at higher temperatures. This was thought to explain the rapid grain growth in the initial stages of sintering of the material.

A number of studies have been carried out into the densification of stabilised zirconia, to attempt to identify the sintering mechanisms. However, the results of the work have been contradictory.

Young and Cutler[124] carried out an investigation into the sintering of yttria stabilised zirconia, using the constant rate of heating method to determine the sintering mechanism. This work suggested that the sintering process was controlled by grain boundary diffusion.

A more comprehensive study was undertaken by Wu and Brook[125], using isothermal sintering, fast firing and hot pressing techniques to characterise the sintering behaviour of CaO and Y_2O_3 stabilised zirconias of various composition.

This work, identified problems with the constant heating rate method used by Young et al[124], and suggested that the kinetics of the diffusion process were controlled by lattice diffusion of cation species in both cases.

This work also showed that the densification rate underwent a maxima with increasing stabiliser content at around 10 mole % Y_2O_3, which also coincides with a maxima in the ionic conductivity.

Since conduction is controlled by anion (O^{2-}) mobility, and diffusion by cation mobility, such a relationship is not immediately expected. The relationship was explained by the fact that the concentrations of oxygen vacancies and cation (Zr^{4+} or stabiliser ion) interstitials are

related through the Schottky and Frenkel disorder reactions as follows:

Schottky:

$$0 = 2V_o^{\cdot\cdot} + V_{Zr}^{''''}$$

where $K_{Schottky} = [V_O^{\cdot\cdot}]^2[V_{Zr}^{''''}]$ (2.5.4 - 1)

or $[V_{Zr}^{''''}] = K_{Schottky}/[V_O^{\cdot\cdot}]^2$ (2.5.4 - 2)

Frenkel:

$$Zr_{Zr} = V_{Zr}^{''''} + Zr_i^{\cdot\cdot\cdot\cdot}$$

where $K_{Frenkel} = [Zr_i^{\cdot\cdot\cdot\cdot}]\ [V_{Zr}^{''''}]$ (2.5.4 - 3)

Substituting for $[V_{Zr}^{''''}]$ in (2.5.4 - 3) gives:

$$[Zr_i^{\cdot\cdot\cdot\cdot}] = (K_{Frenkel}/K_{Schottky})\,[V_O^{\cdot\cdot}]^2 \quad (2.5.4 - 4)$$

Note: V_X = A vacancy on X sublattice.

X_i = An ion of substance X on an interstitial site.

'''' = An effective charge of -4

$^{\cdot\cdot}$ = An effective charge of +2

e.g. $V_{Zr}^{''''}$ = Zr ion vacancy with effective charge 4-

Thus any increase in oxygen vacancy concentration, for example from charge balancing requirements of increasing the amount of Y^{3+} stabiliser content should give rise to an increase in zirconium interstitial ion concentration according to equation (2.5.4 - 4).

By extension, it can be seen that the substitution of any cation of valency less than 4 for zirconium ions should produce an increase in rate controlling cation vacancies, and thus sintering rate. This might be of some significance as a possible effect of impurity ions in solid solution.

Wu and Brook[125] also attributed the maxima, and subsequent decrease in both densification rate and ionic conductivity with increasing stabiliser concentration to the formation of defect associates or clusters which reduce the number of free vacancies and thereby number of interstitial cations according to equation (2.5.4 - 4).

This relationship also suggests that it is the interstitial cations formed at the sintering temperature

which are the rate controlling species for densification.

A detailed study of the microstructural development and densification processes in yttria stabilised zirconia has been carried out by Slamovich et al[126]. This study concluded that the densification of these materials was controlled by kinetic factors, which included the effect of microstructure (grain size and porosity).

2.5.5 Microstructure of T.Z.P..

Tetragonal zirconia polycrystal is the name given to zirconia ceramics with a microstructure ostensibly consisting of 100% tetragonal phase.

In order to produce this microstructure, it is necessary to have an appropriate level of stabiliser addition (Y_2O_3 in this case) in solid solution in the zirconia, and to have a small grain size.

In order to retain the tetragonal phase in zirconia with 3 mole% Y_2O_3 stabiliser, the grain size must not exceed 0.8um[127], although smaller grain sizes (<0.3um) are required where protection against destabilisation from low temperature ageing is required[128].

The effect of a range of sintering conditions on the density and microstructure of T.Z.P. was studied by Gupta[129]. This work showed that over-firing of the samples resulted in a decrease in density, associated with spontaneous transformation of the tetragonal phase. This occurred when grain growth increased the grain size to the point when the tetragonal phase became unstable.

Ruhle et al[122] have investigated the microstructure of a range of Y-T.Z.P. ceramics using S.E.M., T.E.M., and E.D.X.

The main conclusions of this work being as follows.

- All T.Z.P. materials investigated exhibited an amorphous grain boundary phase consisting of Y_2O_3, SiO_2, possibly together with ZrO_2 and Al_2O_3

- Some microcracking was present in the as fired samples, even where the martensitic phase transformation had not occurred.

- Many of the samples contained a proportion of large cubic phase grains in the microstructure.

- Some chemical inhomogeneity was identified with regards to the distribution of the Y_2O_3 stabiliser, although this varied between different materials.

The amorphous grain boundary phase identified by Ruhle[122], was found at all grain boundaries, indicating highly wetting behaviour, and the surface tension of the liquid phase produces rounded grains. However, this effect does not occur for all wetted grain boundaries, despite the presence of the liquid phase, and as such is not fully understood[122].

The formation of cubic phase grains in the microstructure is due to the sintering conditions used. T.Z.P. ceramics are normally fired in the two phase (cubic plus tetragonal) region. The amount of cubic phase is therefore determined by the stabiliser content and sintering temperature used.

Lange[127], has proposed that the formation of increasing amounts of cubic phase, may have been responsible for the decrease in fracture toughness with increasing stabiliser addition of the range 2-6 mole % Y_2O_3.

In Y-T.Z.P. which has been subjected to rapid cooling from the sintering or heat treatment temperatures in the two phase region, the cubic phase transforms by a shear transformation to the t' (cubic related) form, with a high stabiliser content, which is retained to room temperature[34] [35] [36].

In samples subjected to slow furnace cooling, the equilibrium microstructure expected at room temperature is completely tetragonal[34]. However, the microstructure frequently contains appreciable amounts of cubic phase grains[122].

This suggests that chemical equilibrium does not occur in the samples, and that yttria rich grains exist or are formed in the microstructure (possibly from stabiliser inhomogeneity in the starting powder) resulting in the retained cubic phase[122].

Under slow cooling conditions, Nettleship and Stevens[19] have shown that the cubic grains may undergo a diffusion controlled transformation in which tetragonal precipitates are formed within the cubic grains by homogenous nucleation.

The composition of the cubic and tetragonal grains has been studied by Tsukama et al[130]. This work showed that the cubic grains contained higher than normal levels of yttria, whilst other grains were depleted in stabiliser.

2.6 Impurities in zirconia ceramics.

Impurities play an important role in determining the behaviour and properties of zirconia (and other) ceramic materials. In particular, impurities may result in changes to the microstructure and sintering behaviour, and to the mechanical properties.

As previously explained, the basic aim of the project was to attempt to model the behaviour of homogenously dispersed impurities in order to determine the requirement for extensive chemical purification during the powder manufacturing process.

For the purpose of this work, the term impurity is used to mean any component present in the material apart from zirconia, and the stabilising additive (Y_2O_3).

Typical levels of impurity contamination in commercial Y-T.Z.P. ceramics vary from about 0.1 mass % (e.g. TZ3Y as studied in this work)[3], to around 1 mass % (eg. Magnesium Elektron SC15 ZrO_2[131], Zirconia Sales HSY-3 ZrO_2[132]). However the effects of these impurities have received little attention in the published literature.

2.6.1 Sources of zirconia and levels of impurities.

Zirconia is derived primarily from two major mineral sources. These are zircon ($ZrO_2.SiO_2$), and baddelyite (ZrO_2).

Zircon is the more abundant mineral source, and commercial production of the mineral usually takes place as a by-product of the mining of titanium ores from beach sands.

The major sources of Zircon are Australia, South Africa, the U.S.A., India and China[133].

Baddelyite is found in South Africa (suffers from uranium contamination), and in smaller quantities in Brazil. The South African mineral is extracted as a by-product of copper and phosphate production.

The major impurities present in the minerals are silica, titania, alumina, ferric oxide, and lime[18]. In addition, virtually all commercial zirconia contains around 2 mass % HfO_2 which is extremely difficult and costly to remove[18][54].

Stevens[18] has given compositional details of the main mineral sources, and this information is reproduced in table 2.6.1.

2.6.2 Phase equilibria of zirconia/impurity systems.

The behaviour of various oxide impurities in zirconia under conditions approaching equilibrium can be illustrated by reference to the relative phase diagrams.

However, there is some cause for scepticism in the application of equilibrium phase diagrams to sintered zirconia ceramics due to the extremely low cation diffusion rates within the zirconia lattice[61].

The slow cation diffusivities in this system[61] makes the attainment of true chemical equilibrium extremely slow. Consequently, it is unlikely that this is attained within the relatively short heat treatment schedules used

Table 2.6.1: Chemical compositions of raw materials used for the production of zircon and zirconia.
(reproduced from reference[18])

Chemical Analysis	Australian Zircon	S. African Foskor	Baddeleyite Foskor (purified)	PMC *
Zirconia %	66·90	96·00	> 99·00	98
Silica %	32·60	1·5	< 0·5	0·2
Titanium oxide %	0·12	1·0	< 0·3	0·4
Ferric oxide %	0·04	1·0	< 0·05	0·5
Alumina %	0·43			
Lime %	trace			
Magnesia %	0·03			
Phosphoric anhydride %	0·007	0·20	< 0·03	0·05

* PMC = Palabora Mining Co., South Africa.

during the fabrication of these materials (see experimental methods section).

Although the phase equilibria for (pure) zirconia-stabilising additive systems have been extensively studied[4] [34] [59] [122] [134], impure systems, such as those studied in this work, have received far less investigation, and in many cases, the equilibrium diagrams have not been produced to date. Where these do exist, these are often poorly characterised, particularly for three or more component systems, systems with very low levels of impurity as in T.Z.P., and/or the low temperature phase equilibria.

Phase diagrams of the binary systems ZrO_2-Al_2O_3[135], ZrO_2-SiO_2[136], and ZrO_2-TiO_2[137] have been investigated. Phase diagrams are also available for the ternary systems ZrO_2-Y_2O_3-Al_2O_3[138], as investigated in this work, and the system ZrO_2-Al_2O_3-SiO_2[139]. The quaternary system, ZrO_2-Al_2O_3-SiO_2-TiO_2 has also been characterised by Pena et al[140] [141] [142]. The equilibrium diagrams for these systems are illustrated in figures 2.6.2(i)-(vi) respectively.

However, phase diagrams are not available for the ternary systems ZrO_2-Y_2O_3-SiO_2 and ZrO_2-Y_2O_3-TiO_2 , nor the complex quaternary and quinternary systems, ZrO_2-Y_2O_3-SiO_2-Al_2O_3, ZrO_2-Y_2O_3-SiO_2-TiO_2, ZrO_2-Y_2O_3-Al_2O_3-TiO_2, and ZrO_2-Y_2O_3-SiO_2-TiO_2-Al_2O_3 as studied in this work.

The system Al_2O_3-SiO_2-Y_2O_3 is thought[122] to be relevant to the behaviour of grain boundary phases in impure T.Z.P.. This system has been studied (for amorphous materials) by Hyatt and Day, with the properties of the glasses of various composition investigated[143]. The phase diagram for this system is illustrated in figure 2.6.2 (vii).

2.6.3 Effect of impurities on microstructure.

The largest single effect of impurities on the material is likely to be changes in the microstructural

Phase diagrams of zirconia-impurity systems.

Figure 2.6.2(i) The ZrO_2-Al_2O_3 system.
(Reproduced from reference[135])

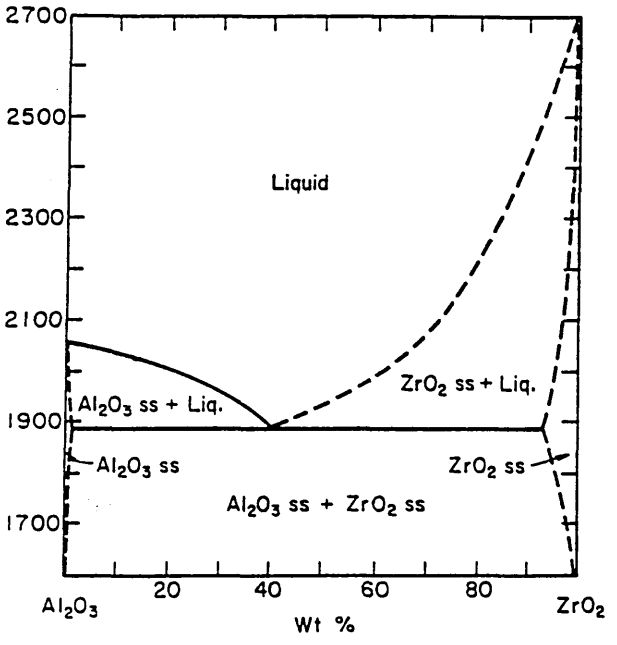

Figure 2.6.2(ii) The ZrO_2-SiO_2 system.
(Reproduced from reference[136])

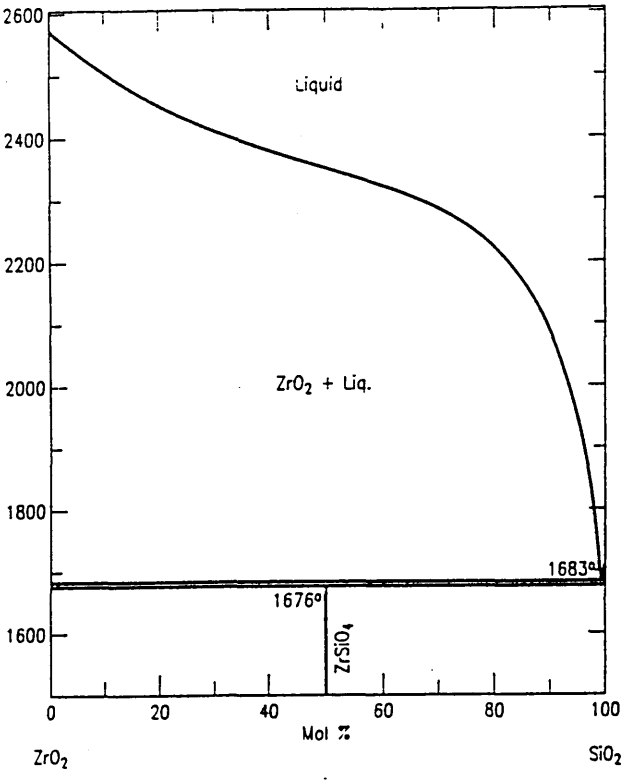

Figure 2.6.2(iii) The ZrO_2-TiO_2 system.

(Reproduced from reference[137])

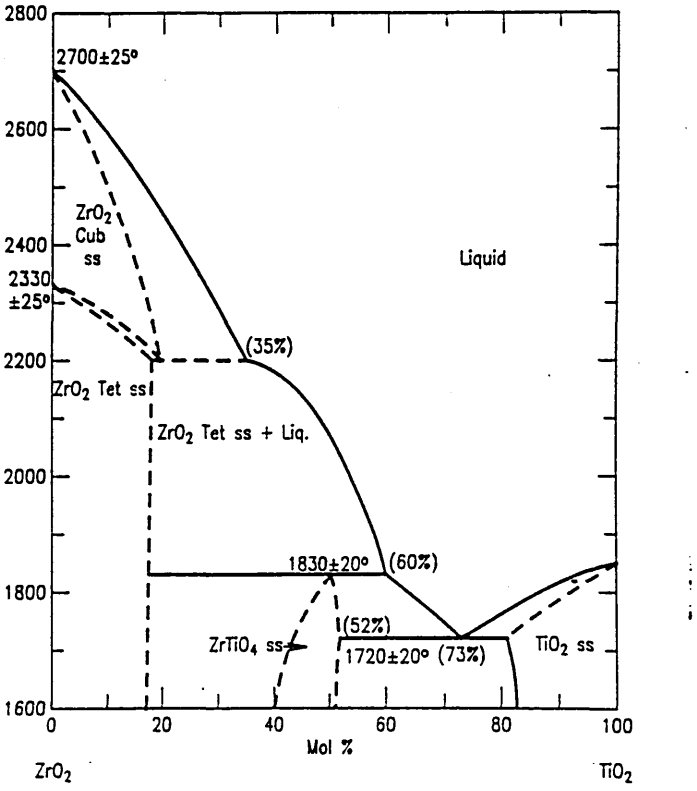

Figure 2.6.2(iv) The ZrO_2-Y_2O_3-Al_2O_3 System.

(Reproduced from reference[138])

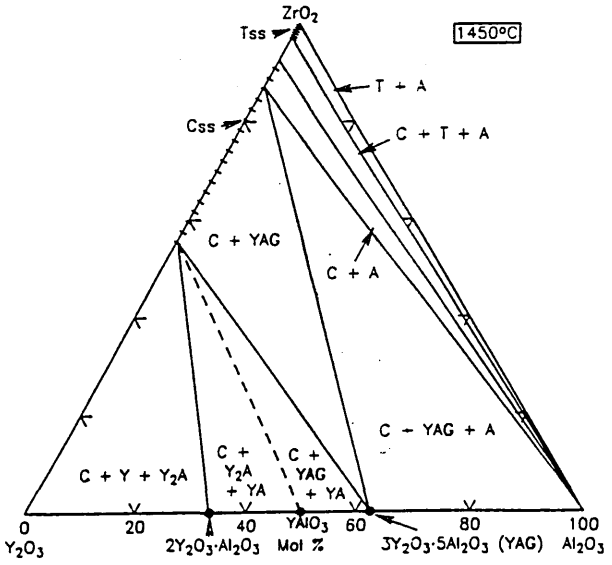

Figure 2.6.2(v) The ZrO_2-Al_2O_3-SiO_2 System.
(Reproduced from reference[139])

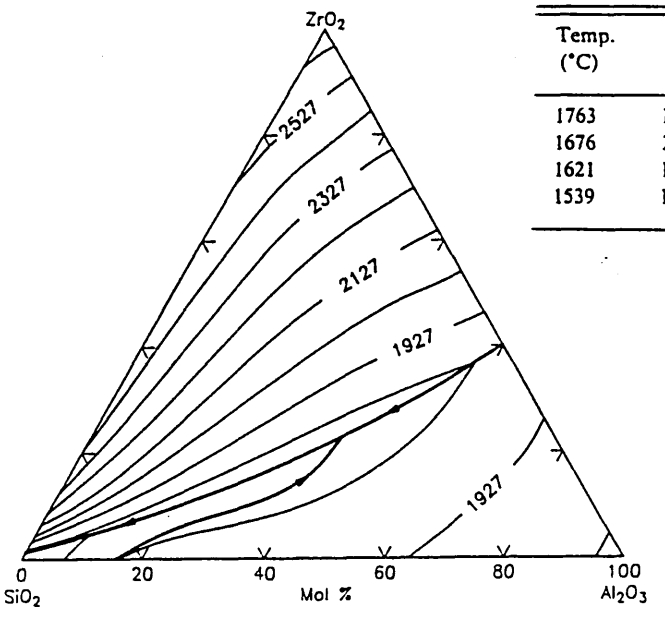

Temp. (°C)	Phases
1763	Liquid + Al_2O_3(s) = $ZrSiO_4$(s) + Mullite
1676	ZrO_2(s) + SiO_2(s) = $ZrSiO_4$(s) + Liquid
1621	Liquid + ZrO_2(s) = Mullite + $ZrSiO_4$(s)
1539	Liquid = Mullite + $ZrSiO_4$(s) + SiO_2(s)

Figure 2.6.2(vi) The ZrO_2-Al_2O_3-SiO_2-TiO_2 System.
(Reproduced from reference[142])

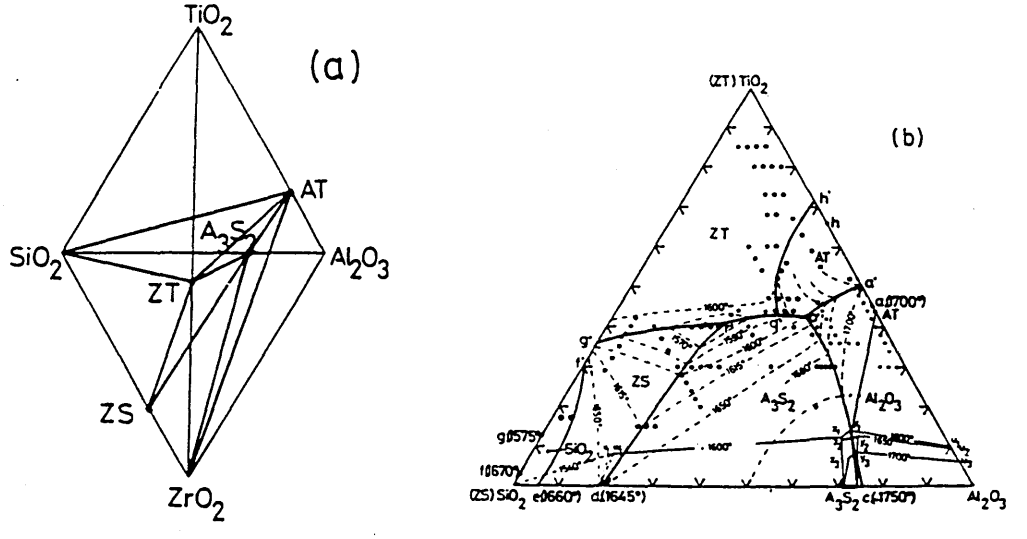

(a) Solid-state compatibility relationships in the ZrO_2–Al_2O_3–SiO_2–TiO_2 system; (b) Projection through the ZrO_2 corner showing secondary phases crystallizing during freezing from ZrO_2–Al_2O_3–SiO_2–TiO_2 mixtures containing 60 wt % ZrO_2. The various symbols represent experimental compositions.

Figure 2.6.2(vii) The Al_2O_3-SiO_2-Y_2O_3 System.
(Reproduced from reference[143])

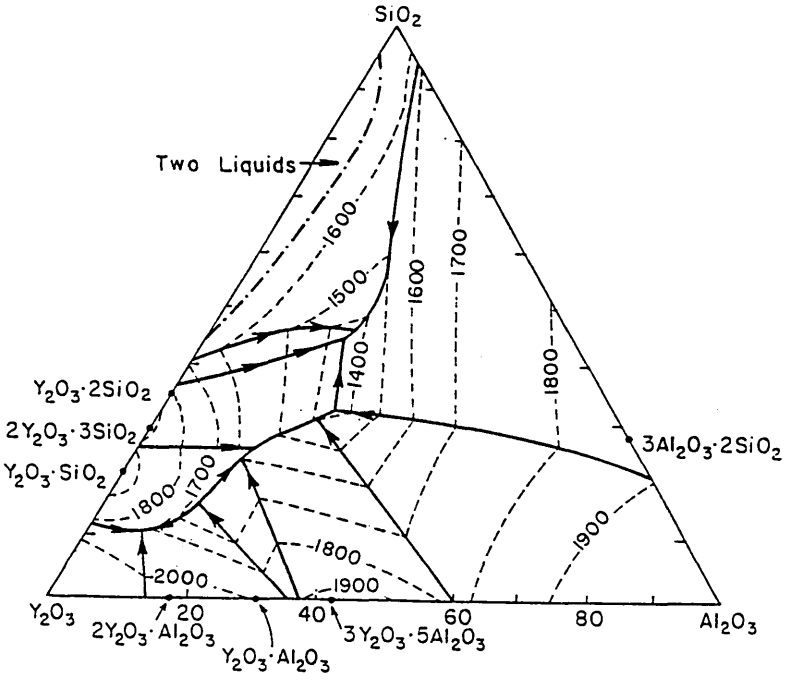

development due to changes in the sintering process i.e. enhanced or impaired sintering rates, grain growth or grain growth inhibition.

Where impurities are homogenously dispersed in the material these effects would also be expected to occur consistently throughout the microstructure, whilst uneven dispersions of impurities might be expected to produce differential sintering behaviour. This has been demonstrated by Lange and Hirlinger for zirconia toughened alumina, where the zirconia additions produced discontinuous grain growth in the material when poorly (i.e. inhomogenously) dispersed[144].

Even if subsequent homogenisation of the impurities did occur during heat treatment, the effects of inhomogeneity on the sintering and microstructure would precede this and be irreversible.

For the Y-T.Z.P. system with which this project is concerned, impurity elements appear to interact to form low melting temperature grain boundary glassy phases in the microstructure[145].

The presence of an amorphous grain boundary film along all the grain boundaries in sintered Y-T.Z.P. has been confirmed in a number of studies[122] [146].

Ruhle et al[146] have studied the structure and composition of the grain boundaries in T.Z.P., and suggested that the composition of the grain boundary phase is that of a low melting eutectic in the yttria-alumina-silica system. However, later work[122] suggests that the amount, and composition of this phase is dependent upon the starting material used, and may contain yttria,silica, alumina, and perhaps zirconia.

Impurity elements, including Al,Si,Fe have been shown to have significant effects on the electrical properties of the grain boundaries in zirconia[147], indicating substantial segregation effects do occur.

Most of the studies of the effect of impurities on the properties and behaviour of zirconia have concentrated on their effects on the sintering behaviour, and on the electrical properties.

2.6.3.1 Effect of silica impurities.

The effect of silica on the sintering behaviour and microstructural development has been extensively studied for calcia and magnesia stabilised P.S.Z.[148][149]. but less information has been published for the yttria stabilised systems.

Shackelford et al[148] investigated the use of silica as a sintering aid in CaO and MgO stabilised P.S.Z., and Mallincrodt et al[149] carried out similar investigations into P.S.Z. with a range of additives including silica and alumina over the range 0-1% addition.

Both of the above studies concluded that silica produced enhanced densification through a liquid phase sintering mechanism, with Mallincrodt[149] et al also demonstrating that the enhanced densification effect was only operative at low sintering temperature.

Shackelford concluded that the liquid phase formed consisted of a stabiliser-silicate phase, since liquid phase sintering was not identified when no stabiliser was present in the system[148].

Similar studies carried out on yttria stabilised zirconia by Mecartney[150], showed that the presence of silica resulted in enhanced densification of the material by a liquid assisted sintering mechanism.

Microstructural studies on Y-T.Z.P. by Ruhle et al[122], show a similar effect, with an amorphous grain boundary phase (liquid at sintering temperature) being identified, consisting of yttria and (impurity) silica.

Lin et al[151] studied the effect of silica and silicate impurities on the microstructure of Y-T.Z.P. and concluded that the grain morphology, chemical composition

of the primary grains, and crystallisation behaviour of second phases were all influenced by the presence of these impurities as grain boundary phases.

Silica is known to exhibit extensive solid solubility in zirconia (see figure 2.6.2(ii)). However, microstructural studies carried out by Radford and Bratton on yttria stabilised zirconia showed that only very low silica levels were present within the grains, with increased silica levels at the grain boundaries[152].

This work also identified silica containing inclusions within some of the grains, although other work[122] failed to reproduce these.

Further evidence for segregation of silica to grain boundaries is provided by conductivity measurements. Yttria stabilised (cubic) zirconia has been shown to exhibit a 100 fold decrease in conductivity when 2% silica was present in the material[153].

The liquid phase produced when silica is present in partially stabilised zirconia has been shown to have a de-stabilising effect[149], this is due to the partitioning of yttria into the liquid phase during sintering[154]. Silica grain boundary phases have also been shown to produce an increase in yttria mobility during heat treatment[155].

2.6.3.2 Effect of alumina impurities.

Alumina is frequently used as a sintering additive in P.S.Z. and T.Z.P. However, there is some confusion in the literature regarding the mechanism by which alumina promotes densification in these materials.

Radford and Bratton[152] proposed that impurities/additions of alumina produced a liquid phase sintering in Y-F.S.Z., and noted characteristic rounded grains in their material.

Later work by Bernard[156], discussed by Butler and

Drennan[153] appeared to contradict this, and no amorphous grain boundary phase was identified in this work, with alumina being present mainly as particles or inclusions within the microstructure.

Alumina has been identified in the grain boundary phase of T.Z.P. in a number of materials investigated by Ruhle et al[146], but it appears from these and the earlier results[122], that this only occurs in the presence of silica.

Work by Stoto et al[155], suggests that alumina grain boundary phases facilitate enhanced rates of yttria migration and homogenisation in the microstructure, which they suggested accounted for increased rates of grain growth.

Ruhle et al[122] identified alumina as second phase grains within the microstructure, and for higher levels of alumina content (20 wt.%) Rossi et al[157], showed the alumina to be present as dispersed grains in the microstructure, approximately equivalent in size to the tetragonal zirconia grains. Butler and Drennan[153] found the alumina to be present primarily as intra-granular particles containing inclusions of silica and zirconia. The differences between this and the previous study may be due to the larger grain size (11-18um) or to Yb_2O_3 (n.b. not Y_2O_3) which was present in the material studied by Butler and Drennan[153].

Silica-zirconia inclusions, identified by Butler and Drennan in the alumina particles, were presented as evidence that alumina could act as a scavenger for silica impurities in the material[153].

A number of alternative mechanisms have been advanced to account for the effect of alumina on the sintering of yttria stabilised zirconia when no liquid phase sintering mechanism could be identified.

Bernard[156] identified that alumina exhibited slight solubility (0.1% at 1300°C) in zirconia. It was suggested

that this may account for an enhanced rate of sintering and solid state diffusion in the material by substitution of Al^{3+} ions in the Zr^{4+} lattice.

This was suggested to be a similar mechanism to that identified by Wilhelm et al for Fe^{3+} impurities in yttria stabilised zirconia[158].

Radford and Bratton[152] identified a decrease in grain growth rates with alumina additive in Y-F.S.Z. material (12um cf. 35um in pure F.S.Z.). This grain growth inhibition, has been explained by Butler and Drennan as arising from grain boundary pinning by the second phase alumina particles[153].

This may also explain the increased densification observed in these materials, since a reduction in grain size would lead to an enhanced rate of removal of porosity during sintering.

A study of the effect of a range of alumina additions on the sintering behaviour of Y-T.Z.P. has been carried out by Lu and Chen[159]. This work showed a complex relationship between the amount of alumina present, the sintering temperature and the sintered density of the material.

For sintering temperatures from 1250-1400°C, the density was found to increase with increased alumina content, going through a maxima at around 0.5-0.75 mole %, and decreasing for addition levels greater than this.

For sintering temperatures above 1450°C, the density was found to decrease with increasing alumina content, with a minima at around 1 mole %, and with the density increasing for addition levels greater than this. These results are shown in figures 2.6.3.2(i) & (ii).

Lu and Chen also calculated the activation energies for sintering of T.Z.P., and alumina doped T.Z.P.[159]. The alumina doped material exhibited a substantial lower activation energy than the undoped material in the early

Figure 2.6.3.2 - Effect of alumina additions on properties of sintered T.Z.P™.
Reproduced from reference [159]

(i) Sintering temperatures up to 1450°C

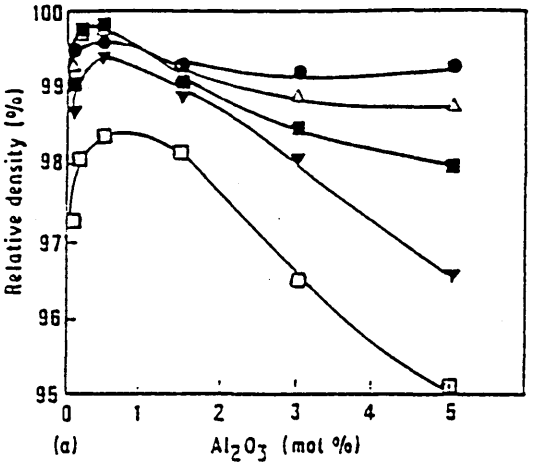

(●) 1450°C. (△) 1400°C. (■) 1350°C. (▼) 1300°C. (□) 1250°C.

(ii) Sintering Temperatures above 1450°C.

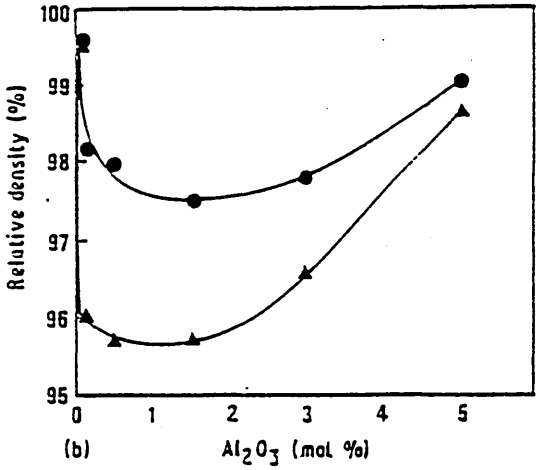

(●) 1500°C. (▲) 1600°C.

stages of sintering indicating that a liquid assisted sintering process took place in the doped specimens. At higher densities, a smaller difference between alumina doped and undoped T.Z.P. was noted, indicating that both mechanisms were predominantly solid state sintering.

A study carried out by Lange et al[160] on the sintering characteristics of chloride derived Y-T.Z.P. material indicated a de-densification (or bloating) effect, which became increasingly pronounced at higher heat treatment temperatures. This pore formation was attributed to the effect of alumina contamination from milling media, and was thought to be due to the release of high pressure oxygen in the structure during the formation of cubic phase.

2.6.3.3 Effect of titania impurities.

The effect of TiO_2 on the sintering behaviour and other properties of partially and fully stabilised

zirconia has been less extensively studied than the effect of alumina and silica impurities, although there have been a number of recent detailed structural and microstructural studies of the effect of titania.

The main studies carried out have been an investigation into the effects of titania on the sintering and electrical properties of yttria stabilised zirconia by Radford and Bratton[152][161], a microstructural analysis analysis by A.E.S. and X.P.S. by Theunissen et al[162], and a structural study by Zschech et al[163].

The phase diagram for the ZrO_2-TiO_2 system indicates that TiO_2 shows substantial solid solubility in zirconia (figure 2.6.2(iii)).

Radford and Bratton[161] carried out electron microprobe studies of the microstructure of doped Y-F.S.Z., which showed that the TiO_2 was distributed evenly throughout the grains with a slightly enhanced level detected at grain boundaries

Further evidence for a slight segregation was provided

from electrical measurements which showed a decrease in conductivity when TiO_2 additions were made to F.S.Z., which was smaller than the decrease obtained when SiO_2 additives were present.

This work also showed that titania acted as a grain growth inhibitor for Y-F.S.Z., with an average grain size 19um for TiO_2 doped material as opposed to 35um in the undoped material. However other studies have shown that additions of TiO_2 result in an increase in the grain growth rate in T.Z.P.[164].

A.E.S. and X.P.S. studies on Y and Ti doped zirconia by Theunissen et al[162] also found evidence for a significant amount of segregation of Ti^{4+} and Y^{3+} ions at the grain boundaries.

Microstructural studies carried out on the material by Radford et al[152] indicated that the TiO_2 doped material underwent a liquid phase sintering process, although the grains were less rounded than those observed with alumina doped samples.

Since no liquid phase is predicted at temperatures below 1700°C in the ZrO_2-TiO_2 phase diagram (see figure 2.6.2(iii)), this was attributed to a reaction with the stabilising additives or other impurities, particularly SiO_2 and MgO.

Radford and Bratton also studied the effect of combinations of alumina and titania additives. A multiple addition of 1 mole % Al_2O_3 and TiO_2 was found to further improve the sintering[152].

Crystallographic studies of TiO_2-Y_2O_3 stabilised T.Z.P. carried out by Zschech et al[163], using X-ray absorption near edge spectroscopy (XANES), showed that titanium occurs as Ti^{4+} charged ions, which substitute for the Zr^{4+} ions in the lattice. This work also found that the Ti^{4+} ions were not randomly distributed, and tended to form clusters in the structure due to inter-ion interaction effects, where the Ti^{4+} ions occupy off-

centre positions in the lattice.

2.6.4 Effect of impurities on mechanical properties.

The effects of impurities on the mechanical properties of Y-T.Z.P. has received little attention in the published literature and this was therefore one of the principal areas of investigation for this work.

The presence of impurity elements may affect the mechanical properties of the material by a number of mechanisms, however, the most important effects on mechanical properties are likely to result directly from changes to the microstructure of the material, from the presence of stress raising flaws and defects, or from modifications to the stabilisation and transformation toughening mechanisms.

Wang et al[165] have carried out a study into the effects of grain size on the mechanical properties of Y-T.Z.P. with various levels of stabiliser addition, and found a complex relationship between these.

Both strength and toughness were found to initially increase with increasing grain size, going through a maximum at a grain size value which depended upon the level of stabiliser present. This was attributed to increasing transformability of the grains with grain growth.

Above a certain grain size, both properties were found to decrease with increasing grain size, this phenomena being attributed to spontaneous transformation of the tetragonal grains.

Grain growth normally occurs over a relatively well defined temperature range in these materials[129]. However, although the effects of certain impurities on the grain size have received some study, as discussed in the previous section, their effect on the the grain growth behaviour over a range of sintering temperatures has not been systematically studied, and this was considered to

be one area of interest for this study.

Inclusions of impurity, possibly arising from inhomogenous distribution of the elements in the starting materials, or from phase separation effects may act as stress raising flaws in the structure[118]. These flaws may grow by brittle fracture mechanisms, resulting in lower strengths.

Discontinuous grain growth arising from chemical inhomogeneity, as discussed in the section 2.6.2 may have a similar effect. The characteristic failure mode of T.Z.P. has been shown to be intergranular for the tetragonal phase, and transgranular for the cubic grains[18].

Glassy grain boundary phases caused by the segregation of impurity to grain boundary sites are frequently observed in Y-T.Z.P. as described previously[122]. This glassy phase may act as low fracture toughness cleavage paths in the material, which might be expected to decrease the overall strength and toughness.

However, according to Ruhle et al[146], virtually all high strength and toughness ceramic materials contain some grain boundary phase, which it was suggested may lower the grain boundary energy and thus increase the toughness (and thereby) strength of the material, provided that that it is of an appropriate thickness.

However, segregation of the yttria stabilising additive into grain boundary glassy phase is likely to be an important and potentially deleterious effect of impurities in the structure. This effect has been demonstrated for T.Z.P.[122], and may produce an impairment of the mechanical properties due to spontaneous transformation of the retained metastable phase as the stabilising additive is removed.

A study into the effects of alumina addition on the mechanical properties of T.Z.P. carried out by Tsubakino et al[166] offers some evidence for both a change in

grain boundary energy, and stabiliser segregation to a grain boundary phase, and suggested that increased grain boundary integrity associated with the impurity addition might be a possible mechanism to explain the lack of an apparent destabilising effect in their specimens.

Impurity elements in solid solution in zirconia are liable to have some direct effect on the stabilisation mechanism, particularly in the case of TiO_2 which has been shown to have a stabilising effect[90] [137]

Al^{3+} ions in alumina, have the same valency as the Y^{3+} stabilising additive, and substitution of Al^{3+} for the Zr^{4+} ions in the lattice would produce charge compensating defects in the same way as Y^{3+} ions. Lu et al [159] describe Al^{3+} and Y^{3+} as acceptor ions in zirconia.

Since these defects are thought to play a part in the stabilising mechanism, it is possible that a similar stabilising effect could occur. However, this effect would be limited by the low (approximately 0.1 mass %) solubility of alumina in zirconia.

Both alumina and titania have been shown to improve the resistance of the material to the low temperature ageing phenomena[90] [167]. This is usually attributed to a decrease in grain size and subsequent decrease in transformability for alumina[167]. However, an increase in stability arising from the stabilising effect of TiO_2 or Al_2O_3 in solid solution may also contribute to this behaviour.

Alumina additions (at 5 mass percent) have also been shown to increase the toughness of Y-P.S.Z. by Tu et al[168]. This was attributed to an increase in the amount of retained metastable tetragonal phase present after heat treatment.

2.7 Mixing and homogeneity in materials processing.

The mixing of two or more species is a statistical

phenomenon. The statistical nature of the process limits the degree to which even mixing can occur[169] [170] [171]. The degree of chemical homogeneity is a function of the sample size (ie the number of particles involved in the mixing process), and will improve with increasingly large sample space (or number of particles).

The relatively poor mixing encountered by solid state powder mixing compared with liquid or gaseous phase mixing, is primarily due to the small numbers of solid particles involved compared with the numbers of molecular species involved when mixing occurs at a molecular level in miscible fluids.

It is not possible to produce a homogenous microstructure, nor good mechanical properties in a ceramic manufactured from a starting material containing significant levels of chemical or physical heterogeneity[172].

The degree of mixedness must be described in terms of the scale with which we are concerned. This is measured in terms of the "characteristic volume" for the mixture. The characteristic volume, is a measure of the number of particles (sample size) required to produce a mixture whose composition matches the bulk composition to within a certain predefined level of deviation[173] [174].

The homogeneity of particulate mixtures has received extensive study, due to its importance in terms of chemical (and ceramic) processing[175] [176], and a number of different measures of the extent of mixing, or degree of mixedness have been devised. A review of the measures of mixing for similar sized particles is given by Drew and Hoopes[177]. For systems involving particles of different sizes[178] or systems with three or more components[179], modified statistical approaches are adopted.

The characteristic volume also defines the diffusion distances required for the system to attain true chemical homogeneity within the defined limit, or the diffusion

distances required by reactive species in a mixture, to enable the reaction to proceed to completion[173]. This was therefore of particular significance when attempting to add dopants to a commercial T.Z.P. powder in this work to model the effect of homogenously dispersed impurities.

The primary aim of the development of the doping process carried out in this work was to improve the homogeneity and thereby reduce the characteristic volume for the mixture to a volume within which homogenisation could occur during heat treatment.

2.8 The alkoxide/sol-gel process.

The alkoxide/sol-gel process is a chemical technique for the production of high purity oxide ceramics or glasses by the reaction of organo-metallic (metal alkoxide) precursors in alcoholic solution.

The technique was initially developed, for bulk glasses, by Levene and Thomas[180] in the period 1967-1971 (patent published 1972), and also by Dislich[181] and Schroeder[182].

The use of alkoxides to produce particulate oxide products had been demonstrated much earlier[183], as had the use of alkoxides to produce thin films. A review of this was published by Schroeder in 1969[184]. A review of the history and principles of sol-gel processing has been produced by Dislich and Hinz[185], and also by Thomas[186].

The alkoxide sol-gel process has been the subject of much interest, particularly regarding the low temperatures required to produce dense oxide materials[187], and the excellent compositional control and homogeneity afforded by the process in multi component systems[188] [189] [190] [191] [192].

The low processing temperatures arise from the extremely high sintering activities of the gel products. Densification occurs by a number of mechanisms including capillary contraction, condensation, structural

relaxation and primarily viscous flow[193] [194].

The chemical homogeneity of multi-component gel systems arises from the fact that the constituents are mixed at the molecular level prior to gel formation[188].

The homogeneity, low heat treatment temperature and ability to produce thin films associated with sol-gel processing were exploited during this work in the development of the alkoxide doping process.

The sol-gel process essentially involves the production of a solution of the alkoxide species in a compatible medium (normally alcohol), the addition of water to the system, either directly, or via the absorption of atmospheric moisture, reaction between the alkoxide and water leading to gel formation, drying of the gel, and sintering to a fully dense product[195] [196].

There are two types of gel produced in the process. The polymer gel formed initially in ethanol is called an alcogel, the dried product is called an aerogel or xerogel[195].

2.8.1 Precursor alkoxides.

One of the major advantages of the alkoxide/sol-gel process over other chemical methods of oxide production is the wide range of oxides which can be produced by this method. Alkoxides can be prepared from virtually all the metal elements[197] [198], and a wide range of single and multicomponent oxide ceramics and glasses have been produced. Suitable alkoxide precursors were commercially available for all of the oxide impurities investigated in this work.

Metal alkoxide molecules comprise a central metal atom covalently bonded to a number of organic groups via oxide linkages. The number of side groups is determined by the valency of the metal ion.

The side group is generally a saturated linear alkane, with the length of this organic group determining the nature and reactivity of the alkoxide species.

2.8.2 The mechanism of reaction.

The formation of an oxide ceramic or glass from an alkoxide precursor essentially occurs by a two step chemical reaction.

The reactions which occur are basically similar for all alkoxide systems, although the rates of reaction in particular may vary significantly[199] [200] [201] [202]. The reaction mechanism has been reviewed by Klein for the sol-gel processing of silicates[195].

The stages in the reaction are (a) hydrolysis, which occurs by the reaction of one or more of the ethoxide groups of the alkoxide precursor with dissolved water in the alcoholic solution, followed by a second stage consisting of (b) polymerisation or condensation-polymerisation (polycondensation) reaction.

The process can be represented in terms of the the following reactions[203].

(a) $M(OR)_n + xH_2O \rightarrow M(OH)_x(OR)_{n-x} + xROH$

(b) $M(OH)_x(OR)_{n-x} \rightarrow MO_{n/2} + (x/2)H_2O + ((n-x)/2)R_2O$

For complete reaction, this can be simplified as follows

(a) $M(OR)_n + nH_2O \rightarrow M(OH)n + nROH$

(b) $M(OH)n \rightarrow MO_{n/2} + n/2H_2O$

(NET) $M(OR)_n + n/2H_2O \rightarrow M(OH)_n$

2.8.2 Effect of catalyst.

The rate and yield of the sol-gel production of silicates in particular can be significantly enhanced by the addition of acid or basic catalysts to the system. In addition, and more dramatically, the nature of the product can be completely changed by using different catalysts.

The means by which catalysts affect the process is thought to be primarily due to electrophilic or nucleophilic attack by OH^-, or H_3O^+ species[204]

In addition, the respective rates of the hydrolysis and

polycondensation reactions are affected by the presence of acid and base catalysts, although there is some disagreement in the literature regarding the details of this[204] [205] [206].

The mechanism of the polycondensation reaction depends primarily on the type of catalyst present, and this determines the properties of the reaction product.

For acid catalysis, the polycondensation reaction occurs preferentially at the chain ends of linear molecules, resulting in the formation of increasingly large chains. Some reaction does occur at the side groups, and this ultimately results in the formation of 3 dimensional cross links between the molecules, and the production of a rigid gel.[203] [204] [205]

For base catalysis, reaction occurs at equal rates at all sites on the hydrolysed alkoxide species, and the resultant product thus consists of growing, approximately spherical, particles[203] [204]. Optimisation of the catalyst system to give a high yield of reaction and suitable physical characteristics in the reaction product was a major part of the development of the alkoxide doping process in this work.

2.8.3 Effect of water addition.

The mole ratio of the water:alkoxide reactant species has also been found to have a significant effect on the reaction mechanism and the nature of the product[196] [203]. For sub stoichiometric levels of water addition (ie < 2 moles of water : 1 mole alkoxide), the hydrolysis will occur at the chain end sites resulting in linear molecules (with the size and structure controlled by the catalysis conditions). In these cases gelation occurs by the entanglement of the polymer chains and bond formation[203].

With higher levels of water addition, the molecular species formed from the reaction tend to be more highly branched due to the greater number of reactions occurring

at side groups. In the case of basic hydrolysis, these molecular clusters remain discrete, resulting in the formation of colloidal particles rather than gelation[203]. The effect of the water:alkoxide ratio on the nature of the reaction product was expected to be an important factor determining the agglomerate strength of the doped powders produced in this work.

2.8.4 Effect of reaction modifiers.

For alkoxide systems other than tetra ethyl silicate (TEOS), the reaction rates for both hydrolysis and polycondensation reactions are generally very much more rapid.

The effect of rapid hydrolysis and polycondensation (which tends to occur at similar rates at all positions on the hydrolysed alkoxide species) is that these alkoxides undergo rapid hydrolysis in the presence of water to form precipitates rather than network polymer gels. These reactions are usually extremely difficult to control[201][202].

Various reaction modifying additives have been used in order to attempt to slow the hydrolysis reaction and produce the polymer gel structure in the reaction product as opposed to a particulate product. These have included (beta) diketones and ketoamines, carboxylic acids and alkanolamine all of which act by replacing alkoxy groups with the protecting ligand species[197][207].

Acetic acid has been used to slow the hydrolysis of aluminium[207] and titanium alkoxides[208] by this mechanism, with acetylacetone also used in the case of titanium alkoxides[208].

Another method of preventing the formation of particulate reaction products from titanium alkoxide was demonstrated by Yoldas[202], who showed that the addition of 0.014 to 0.3 mole % of HNO_3 or HCl per mole alkoxide to the alcoholic solution, and controlling the water level

resulted in the formation of clear sols/gels. Identification and use of suitable reaction modifying additions was an essential element in the development of the alkoxide doping process for TiO_2 and Al_2O_3 additions and for multicomponent additions in this work.

2.9 Factorial experimental design.

A factorial experimental design is a technique for planning and analysing experimental investigations involving a number of variables which may undergo interaction. It involves the use of statistical techniques to determine which if any of the factors under investigation are significant, and to identify any significant interaction between combinations of factors[209] [210] [211] [212] [213]

Factorial experimental designs have been shown to be the most effective method for carrying out this type of experiment[210]. This is explained by Daniel[213], as being due to the fact that in a factorial experiment each piece of information can "be made to work twice".

The factorial method for experimental design was first developed by Fisher in 1926, for agricultural trials at Rothampsted research station[214] [215], and these formed the basis of much of the early work using the method. A number of developments were made to the technique to improve its efficiency and accuracy, these being discussed by Yates, also working at Rothampsted, in 1937[216].

Since this time, the technique has been extensively developed, particularly for industrial experiments[212], where the results of each series of experiments can be used to produce improvements in the industrial process being investigated. This process is known as "evolutionary operation"[217].

A factorial experiment varies from a conventional experimental technique in which one factor is varied at

a time. In the factorial experiment the effect of each factor (the main effect) is calculated as the difference in the (average) effect on the system (the response) at the levels of that factor investigated.

In a factorial experiment, the response is also calculated for each factor when other factors are varied simultaneously. If the effect of the individual factors at the levels investigated changes when the levels of other factors are altered, the factors are said to have an interaction.

Factorial experiments are said to offer the maximum efficiency in identifying effects and interactions, reduce the possibility of drawing misleading conclusions from investigations in which interactions exist, and enable conclusions to be drawn which are applicable for a wide range of conditions[210].

In systems in which there is significant interaction between the factors, the main effects of the individual factors may be obscured by the interaction effects, and it is possible to draw misleading conclusions from the results. This is the principal disadvantage of one factor at a time experiments (which cannot identify the presence of interactions), and the reason for carrying out factorial experiments[210].

However, where this does occur, it may be necessary to carry out additional experiments on the effects of each individual factor, with the levels of the other factors held constant[210].

The analysis of the results of factorial experiments can be a complex task. However, various methods have been developed to simplify the process. The most commonly used of these was devised by Yates.

Yates[216] has developed a process whereby the effects of each factor may be calculated using a simple algorithm (or numerical procedure) which involves adding and subtracting the response values of the treatments in a

standard order. The use of Yates' method is described in more detail in the experimental methods section of this thesis.

There are a number of variants on the factorial experimental designs including 2^k (ie investigation of the effects of k different factors at 2 different levels) and 3^k (k factors at 3 levels) experiments, partial factorial designs (to reduce number of tests carried out) and confounded experiments (where the experiment is broken down into a series of smaller experiments).

2^k factorial designs are the most efficient and simplest type of factorial experiments. However in this type of experiment, where only two levels of the factors are investigated, it is necessary to assume an approximately linear response over the range of the levels of factors investigated. This type of design was adopted for this work.

Where the behaviour is expected to be non linear over the range of factors investigated, it is necessary to use 3^k type of factorial design[210].

Although factorial experiments are commonly used in industrial experimentation and process development[213], their application in more fundamental research has been somewhat limited. In the field of materials science and engineering, of 72,000 publications abstracted on the "Metadex" system for the years 1991 to 1994, only 39 refer to the use of factorial experimental methods, with the large majority of these being related to process development in the polymers and composites industries. Only 6 publications concerned with the application of the technique to ceramics research are listed[218] [219] [220] [221] [222] [223].

The limited exploitation of this useful technique in scientific research can perhaps be explained as being due to the fact that whilst factorial experiments provide useful empirical information regarding the effects of factors and their interactions, the technique offers little assistance in identifying the causes of, and

mechanisms responsible for these effects.

For this reason, it was decided to combine both factorial experimental design and more traditional and detailed single factor (i.e. one factor varied at a time) experiments for both the mechanical property and the microstructure and phase development of variously doped and heat treated T.Z.P. in this work, to attempt to identify correlations between these.

3. Experimental methods.

This section of the report is intended to outline the experimental techniques used and developed to carry out the investigation.

The methods described fall into two categories:

- Those concerned with the development of the doping technique and the production of the doped powders. (sections 3.1 - 3.3)

- Those concerned with the investigation of the effects of the impurities on the sintered ceramic. (sections 3.4 - 3.12)

3.1 The alkoxide powder doping process.

3.1.1 Background to the development of the doping process.

The development of a suitable method for introducing the impurity oxides into the system was considered to be prerequisite for carrying out this investigation.

In particular, it was considered necessary to produce the highest possible level of homogeneity within the doped powders, whilst producing the minimum possible change to the other physical properties (particle size, size distribution, morphology, agglomeration) of the doped powders.

A number of alternative methods were considered at the outset of the project to produce the doped T.Z.P. compositions. These included:-

(a) Mechanical mixing and milling of commercial T.Z.P. powder with particulate dopant additives.

This method was discounted on two grounds. Firstly, the degree of mixedness, defined in terms of the "characteristic volume" of the mixture would remain relatively poor, with the maximum homogeneity attainable being further limited by the relative sizes of the two

types of particles, and the size of the agglomerates in the spray dried TZ3Y powder. Milling of the material would also be expected to produce significant contamination of the powder due to wear of the milling media.

(b) Manufacture of doped powder particles by co-precipitation of zirconia, stabiliser and dopant oxides from metal alkoxide precursors in solution.

Although this would have produced the greatest possible degree of homogeneity, the powder particles produced would be unlikely to exhibit the same size, and agglomeration characteristics as the doped powder, and therefore, a comparison with the properties of commercial T.Z.P. would not be possible. Furthermore, it was thought that the development of a suitable process route to synthesise T.Z.P. powder particles with the necessary characteristics and sintering activity would have been an extremely complex task, which could not have been accomplished within the original remit of the research programme.

(c) Pyrolysis of suitable precursor materials (e.g. metal chlorides, nitrates)

It was thought that the pyrolysis of a mixture of T.Z.P. powder with a suitable precursor material might be one possible means of producing the doped powders with the stabiliser distributed uniformly around (although not within) the T.Z.P. particles. A similar technique is used to add yttria stabiliser to certain commercial T.Z.P. products[18].

Although this method was attractive in terms of its simplicity, drawbacks included identifying suitable precursor materials, and particularly, the effect of the (normally) high temperatures required for pyrolysis on the particle (and grain) size and the sintering characteristics of the doped powders.

(d) The alkoxide doping process.
This was the new technique developed during this work, using alkoxide precursors to produce an oxide coating on each of the powder particles of a commercially available T.Z.P. material of high purity, using a variant on sol-gel coating technology.

3.1.1.1 Advantages of the alkoxide doping route

There were a number of advantages associated with the alkoxide doping process developed in this work over the other doping processes considered (apart from the increase in homogeneity compared to conventional powder mixing). These included:-
(a). The dopant coating produced by this process would be expected (due to the presence of surface oxide and/or OH^- groups at the particle surface) to be chemically bonded to the surface of the particles, thus preventing segregation or demixing processes from occurring during subsequent processing operations.

(b). The heat treatment temperatures necessary to produce an oxide from the precursor material were significantly lower than for other pyrolysis type process routes (see 3.1.1(c)). A temperature of approximately 500°C was found (by mass loss experiments) to be required to remove any residual water and organic material from the reacted alkoxide. This was sufficiently low as to effectively preclude any significant grain growth or sintering processes from occurring during the doping process and associated heat treatments.

(c) A wide range of suitable alkoxide precursor materials existed, allowing the technique to be developed for a range of oxide additives and/or applications.

(d) The homogeneity of the doped powders produced by this process should be substantially greater than obtainable by particulate mixing processes, with the characteristic volume for the alkoxide doped powders expected to be of the order of the volume of a few powder particles.

This can be compared with the characteristic volumes predicted for ideal random homogenous mixtures (i.e. of particle mixtures), which are of the order of the volume of many hundreds or thousands of particles to get reasonable homogeneity of the minor component in a given sample batch.

If characteristic volumes of this scale had been achieved, subsequent homogenisation by solid state diffusion would be expected to occur during heat treatment. The characteristic volume gives a measure of the diffusion distances required for homogenisation.

3.1.2 Development of the doping process.

The objective of the doping process was to attempt to produce a homogenous dispersion of impurity in the T.Z.P. powder to model the effects of impurities in the system, whilst minimising the changes to the other physical properties of the powder. The experiments carried out were thus concerned with:

(i) Developing the doping process to ensure that controlled and reproducible dopant additions could be made at the desired level.

(ii) Attempting to determine the degree of homogeneity in the doped powders.

(iii) Determining the effect of the doping process on the properties of the powder.

The essential stages in the process developed during this work are illustrated in Figure 3.1.2(a).

The Tosoh TZ3Y T.Z.P. powder used as the base material for the doping process was supplied in the form of spherical spray dried powder agglomerates approximately 50 microns in diameter. The agglomerates, which were relatively easily disrupted, consisted of primary particles approximately 100 nm in diameter (section 3.3).

The doping process began with the production of a dynamic suspension of the principal component powder (TZ3Y) in

Figure 3.1.2 (a).

FLOW CHART INDICATING THE MAJOR STAGES IN THE ALKOXIDE DOPING PROCESS

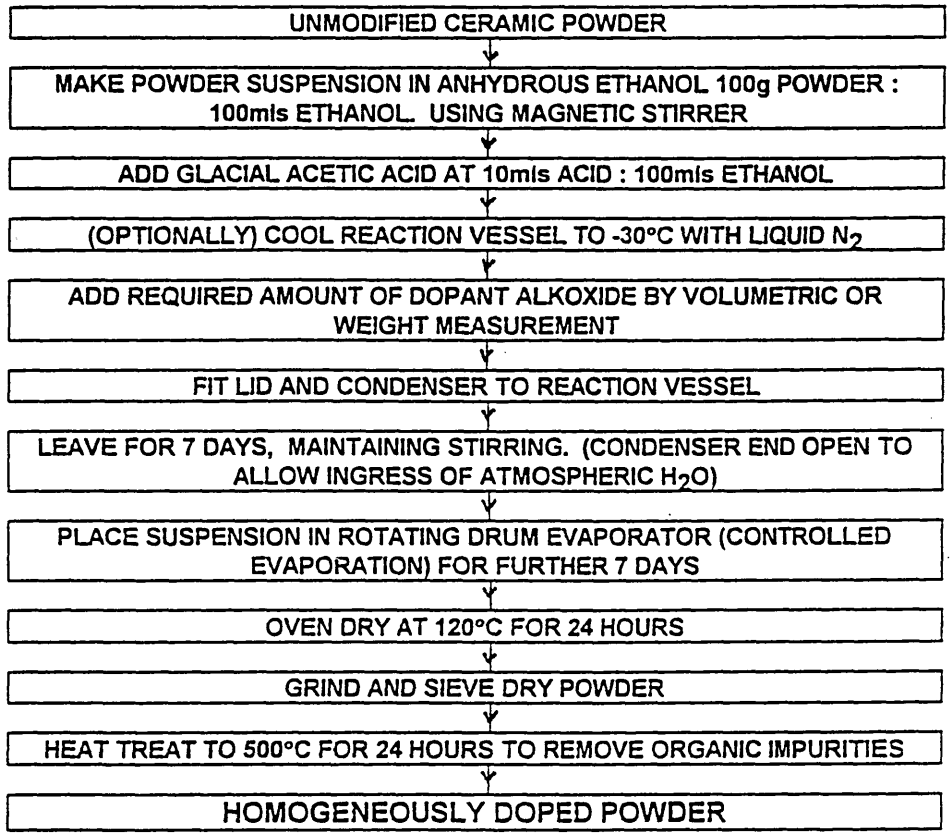

absolute ethanol, the suspension being maintained by the action of a magnetic stirrer. Prior to the addition of the alkoxide, various reaction modifying/catalysing additions were made to the ethanol. These are described below.

The function of the modifying/catalysing additions was to ensure that the reaction of the alkoxide precursors produced a gel coating, on the surface of the primary powder particles surface rather than forming precipitates. This was essential to obtain the highest possible degree of homogeneity in the doped powders (see section 2.8.4).

The system was developed to allow the same process route to be employed for all of the dopant additions used. This was achieved by the use of acetic acid additions which functioned differently according to the system. The addition acted as a catalyst for the less reactive systems, and as a reaction inhibitor for the more rapid reacting systems. However, a number of other potential additives were also investigated with varying degrees of success.

It was important that the additives used would not otherwise interact with the system and introduce further variables into the investigation. This effectively constrained the choice of potential additives to those, notably organic compounds, which could be subsequently removed by oxidation or volatilisation.

The suitability of potential modifying additives was assessed by allowing a small portion of alkoxide-ethanol solution (at concentrations equivalent to those used for the doping process) to dry on a petri dish or glass slide. Visual examination of the reaction product was then carried out, with systems which formed precipitates being rejected.

Acetylacetone was investigated as a potential additive to reduce the reactivity of aluminium butoxide and titanium isopropoxide precursors, and avoid precipitate formation.

This was carried out according to the method of Livage[208]. Equal volumes (7cm^3) of the alkoxide and acetylacetone were mixed, prior to the addition of 100 mls of ethanol.

In the case of titanium isopropoxide, the addition of acetylacetone did produce a clear, but yellow coloured, sol which formed a yellow coloured, gel reaction product after 3 days. However addition of acetylacetone to the aluminium alkoxide was less successful, with the two chemicals undergoing a violent exothermic reaction on mixing, with some precipitation occurring.

The use of acetic acid addition was investigated, as this had been shown by Livage[208] to produce a clear, stable colloidal sol with titanium isopropoxide for pH values <3. This technique was found to be successful, and was subsequently adopted for this study, giving rise to clear stable sols, and gel type reaction products with both titanium isopropoxide, and also aluminium alkoxide precursors.

The alkoxide species were added to ethanol solution, to which glacial acetic acid (at the rate 10 mls acid to 100 mls ethanol) had previously been added . This was found to give a pH (prior to alkoxide addition) of approximately 2. The alkoxide addition resulted in a small increase in pH, but for the addition levels used in this work (less than 0.5 moles alkoxide per mole acetic acid) the sols remained stable.

In the case of the tetraethyl silicate alkoxide precursor, it was necessary to employ conditions of acid catalysis to avoid precipitate formation as described in section 2.8.2. Although HCl or H_2SO_4 are the normal catalysts used in the sol-gel production of silica[195], it was decided to attempt to use acetic acid in this work, for the reasons explained above regarding its choice as a reaction modifier, and to develop a single consistent process route for all of the alkoxide additives. It was found that additions of glacial acetic

acid at the same 10mls acid to 100mls ethanol level chosen for the reaction modifying addition described above were successful in producing a clear stable sol, and gel type reaction product for this precursor.

Additional control over the nature of the reaction product was attained through choice of appropriate alkoxide precursors. The alkoxide precursors used were tetra-ethyl ortho silicate (TEOS) for silica, titanium isopropoxide for titania, and for alumina, a chemically modified form of aluminium isopropoxide, obtained from Alcan chemicals which had been pre-treated with a protective ligand species to reduce its reactivity (Alcan AOC 1010X). Other aluminium alkoxides investigated were aluminium butoxide and isopropoxide, but unlike the Alcan material these resulted in some precipitation during trials.

The process was developed to allow both single and multiple additions to be made. However, the reaction in systems containing multiple alkoxide additions tended to be more difficult to control. In these systems, the addition of acetic acid reaction modifier used in the single alkoxide doped systems was not adequate to fully prevent precipitation from taking place.

To overcome this problem, a method was developed involving the use of temperature control. This entailed the careful addition of liquid nitrogen to the mixture prior to the alkoxide addition, until a temperature of -30°C was achieved. Rapid formation of mixed alkoxide compounds appeared to take place on alkoxide addition in the multi-component systems, evidenced by substantial exotherms and colour changes in the solution, however no precipitation was observed. The formation of mixed alkoxides was considered to be advantageous as it avoided problems associated with incompatible reaction rates of the different alkoxide precursors.

The reactant mixture was then contained within a flat bottomed glass culture vessel, agitated with a magnetic

stirrer to prevent sedimentation, and equipped with a Leibig condenser for a period of seven days (figure 3.1.2(b)). This apparatus was used since initial experiments carried out in open beakers, with direct additions of water to the system were found to give low reaction yields and poor repeatability, particularly for silica dopant addition. It was found that the yield could be increased by reducing the water:alkoxide ratio and/or the overall evaporation rate, by use of acid catalysis or by partially pre-reacting the alkoxide (in a suitable condenser equipped reaction vessel) prior to evaporation of the ethanol (see table (i)). Trials were carried out to determine the optimum timescale for this pre-reaction, with no further improvement in yield identified after 7 days. An explanation for this phenomena is given in the discussion section of the thesis.

By adopting the above process conditions, it was possible to obtain yields of reaction in excess of 90%. At these levels, provided that conditions were kept constant, the reproducibility of the process was excellent. Adjustments were made to account for the sub-theoretical yields at the dopant addition stage to achieve the desired bulk powder compositions. Although it did not appear necessary to take such precautions with some of the more rapid reacting alkoxide systems, a similar process route was used in all cases for consistency.

The suspension, which increased in viscosity slightly during the pre-reaction stage, was then decanted into a polythene drum, which was mechanically rotated to continue mixing of the system. The drum lid contained a limited number of small holes in its centre, which enabled slow evaporation of the ethanol from the system (See figure 3.1.2(c)). This was found to take around 5 days at ambient temperature, during which time the system gradually increased in viscosity, eventually forming a dry "cake" of agglomerated particles. This was then transferred to a pyrex container and heat treated to

Figure 3.1.2(b)
Reaction vessels used for doping process.

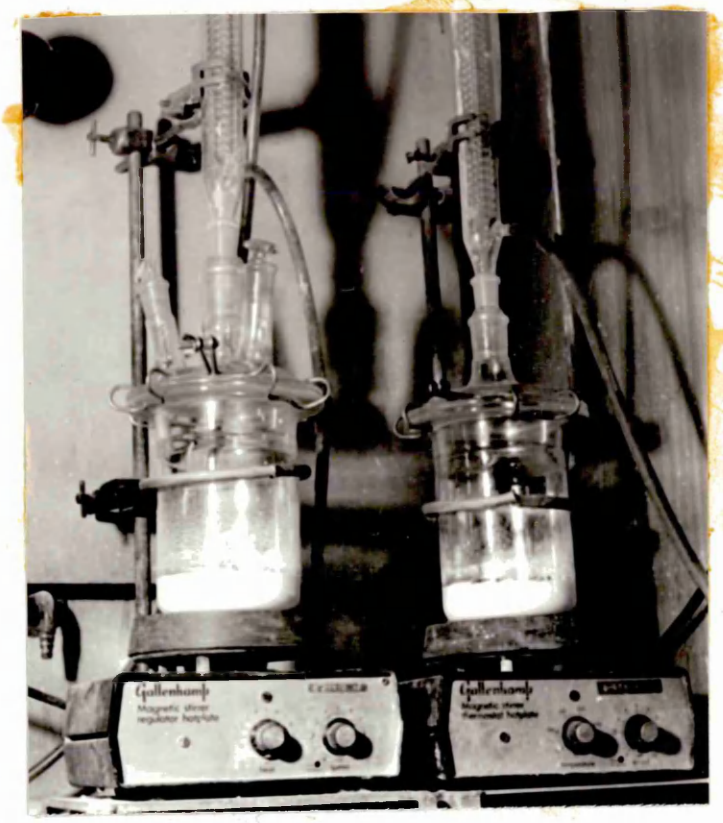

Figure 3.1.2(c) Drum drier/mixers used during doping process.

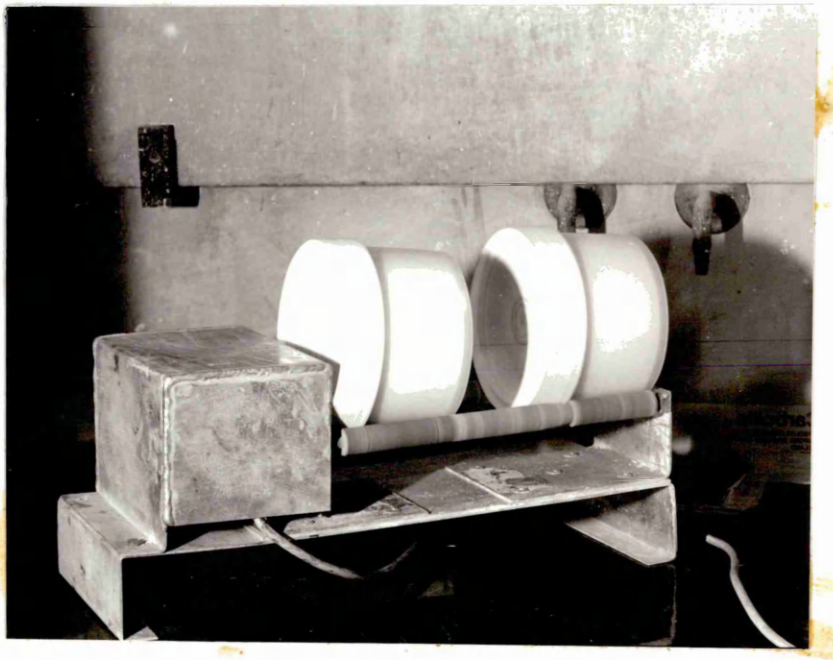

120°C to ensure complete solvent evaporation.

The resultant "cake" of agglomerated particles in the dried material was then broken down, initially using a glass rod to break up the large agglomerates. However breaking down the smaller agglomerates could not be accomplished in this manner, and it was necessary to grind the material, (by hand) using an agate mortar and pestle to disrupt these. The material was ground until it would all pass through a mesh size of first 150 um, and then 75 um. Typically this process took around an hour to complete for a 150g sample. The agglomerates were relatively easy to break down, although there were a small proportion of these which were more strongly bonded.

The final stage in the process was a heat treatment for 24 hours at 500°C, to eliminate any residual organic material arising from the gel or ethanol. This heat treatment temperature was the lowest at which complete removal of the organic material could be achieved, as evidenced by infra-red absorption spectroscopy, and mass loss measurements. This temperature was considered to be sufficiently low as to preclude any significant changes from taking place in the original bulk powder. This was confirmed by X-ray diffraction studies and particle size analysis as discussed in the following sections.

3.1.3 Confirmation of dopant additions and doped powder compositions.

To ensure that the doping technique was producing the desired levels of dopant additions in the powders, it was necessary to develop a sufficiently sensitive analytical technique to determine the dopant concentrations at the low levels used.

Two techniques were used to determine the powder compositions, these being an Inductively Coupled Plasma (I.C.P.) technique to analyse solutions derived from the

doped powder, and X-Ray Fluorescence (X.R.F.) analysis of fused beads containing the doped zirconia powders.

The following method was used to obtain solutions of the zirconia and dopant additives for analysis by the I.C.P. technique:

0.5g of doped/undoped T.Z.P. sample was weighed into a Nickel crucible, together with 4.0g of Na_2CO_3 and 2.0g of Na_2O_2. These weights were accurately recorded to 0.0001g. A nickel foil lid was placed on the crucible which was then heated over 2 Meka burners for 5 minutes, with the mixture stirred by agitation of the crucible at 1 minute intervals to ensure complete mixing and dissolution. The crucible and lid were then cooled and placed in a clean 400 ml beaker to which 20ml distilled and deionised H_2O and 3.5 ml conc. HCl were slowly added. An additional 10 ml of this solution was used to wash out the crucible and lid as they were removed from the mixture. a watch glass cover was placed on the beaker, and the contents were then boiled for 15 minutes, or until a clear solution was obtained. Finally, any condensate on the lid was washed into the solution, and the solution volume made up to 500 ml with distilled and deionised H_2O. A 10 ml aliquot of the solution was then taken for analysis.

Analysis of the solutions was performed using a Jarrel-Ash ICAP 9000 inductively coupled plasma (I.C.P.) atomic emission spectrometer. An R.F. frequency of 27 MHz was used at a 1.1 KW power output. Samples were supplied to the plasma as spray droplets in argon gas via a nebuliser. The equipment was calibrated using matrix matched (i.e. ZrO_2) reference sample solutions to which known quantities of SiO_2, TiO_2 and Al_2O_3 were added.

The reliability and reproducibility of the results was tested by supplying unidentified duplicate specimens for analysis, and comparing the results obtained. It was found that variations of 0.05% were obtained for TiO_2,

0.15% for Al_2O_3, and 0.35% for SiO_2. Furthermore, samples of known composition were submitted for analysis, with the results obtained for SiO_2 found to be substantially underestimating the true value. These errors were highly significant in relation to the levels of additions being made in this work, and for much of the project, the compositions of most of the specimens had to be assumed from the known addition levels (the nominal dopant additions).

In the final stages of the work, the facility to analyse the specimens by X-ray fluorescence spectroscopy became available. This was found to give much more reliable and reproducible results (again being confirmed by duplicate samples and samples of known composition), with the reproducibility found to be within plus or minus 0.05 mass percent for all dopant additions. The analysis was carried out using a Philips PW2400, wavelength dispersive spectrometer, using the fused bead technique to eliminate errors from particle size effects, and calibrated using samples of known composition.

Fused lithium tetraborate (glass) beads containing the samples for analysis were prepared as follows:
1g of the sample was weighed (to 0.0001g), into a platinum crucible, together with 10g (also to 0.0001g) of lithium tetraborate powder. The powders were then mixed using a small spatula, and transferred to a furnace at 1250°C and heat treated for 12 minutes to melt and homogenise the material, the crucible being removed and agitated to mix the contents after 3 and 6 minutes heat treatment. The melt was then removed from the furnace and poured into a platinum casting dish (40mm diameter x 5mm deep), with forced air cooling.

To obtain accurate results, it was essential that the fused bead produced for analysis had a planar, smooth surface. To ensure this, the casting dish was prepared by forming in a die using a 40 tonne hydraulic press to give a perfectly flat surface, with the bottom surface polished.

The analysis parameters for the X.R.F. spectrometer for each of the elements analysed were as follows:

Element	Line emission	X-ray parameters KV	mA	Detection parameters Crystal	d space (2d (nm))	Angle
Zr	L alpha	50	60	PE	0.8742	87.7917
O	K alpha	24	125	PX1	5.0000	55.2501
Si	K alpha	50	60	PE	0.8742	108.9954
Ti	K alpha	50	60	LIF200	0.4027	86.1355
Al	K alpha	50	60	PE	0.8742	144.793

Note: PE, PX1, and LIF200 are the trade names used to identify the crystals used in the X-ray detection system for the Philips PW2400 spectrometer. The d spacings quoted refer to these crystals. The detection angle quoted is a function of the wavelength of the excited X-rays from the analysed elements, and the d spacings of the detector crystal used according to the Bragg equation.

Analysis for other material, such as residual carbon from the sol-gel reaction was carried out qualitatively by infra-red spectroscopy, using a Perkin Elmer PE780 spectrometer. The samples were prepared for analysis by dispersing in KBr, at the rate of 2mg sample in 200mg KBr, and pressed in a die under vacuum for 5 minutes to produce a 1 cm diameter disc of material.

Samples of undoped and variously doped samples were analysed by this technique prior to and after various heat treatments. Comparison of the absorption spectra confirmed the presence of Carbon by the presence of a broad range of overlapping absorption peaks over the range 4000-1500 cm^{-1}.

3.1.4 Determination of powder and dopant homogeneity.

If the doping technique behaved according to our predictions, the dopant species should have been present as an approximately mono-molecular layer, evenly dispersed over the surfaces of the powder particles.

The positive determination of chemical homogeneity on this scale was extremely difficult to achieve, since the

scanning electron microscopy and energy dispersive x-ray analysis analytical techniques available were not sufficiently sensitive to determine the locations of individually dispersed dopant ions within a homogenous mixture, nor the presence of a monolayer of dopant ions on the surface of the (100nm sized) zirconia particles.

Confirmation of the effectiveness of the doping technique, and the degree of homogeneity was thus based upon a negative result. That is if the analytical techniques confirmed the presence of the desired level of dopant within the bulk of the sample, but were unable to identify the presence of inclusions or concentrations of dopant within the sample, it was considered reasonable to assume that the dopant ions must have been dispersed throughout the sample, and that chemical homogeneity had been achieved.

Analysis of the unsintered powders was carried out on sections of unsintered, green pressed pellets, which had been carbon coated to reduce charging effects. The analysis was performed using A Link Systems, energy dispersive x-ray analysis apparatus and software coupled to a Philips XL40 scanning electron microscope. Bulk compositional analysis was performed using X-ray signals obtained from a comparatively large volume of the specimen at low (200x) magnification, to confirm the presence of the dopants by the energy dispersive X-ray analysis technique. X-ray mapping was also carried out using this equipment and software, over 16384 points (128 x 128), with a 0.5 second analysis (dwell time) at each point. After accounting for the "dead time" during which the detector is not available for analysis (around 25% of total elapsed time), the information required for each map took around three hours to acquire. An accelerating voltage of 20KV was used for all these experiments.

For comparative purposes, samples mixed by conventional mechanical powder mixing, with alumina, silica and titania additions were compared to samples containing

similar quantities of these additives but prepared using the alkoxide doping technique.

X-ray mapping was carried out on samples of both types, initially at low (200 X) magnification, to identify the presence of large scale inhomogeneity (i.e. inclusions/precipitates up to around 200 microns in size), and then at progressively increased magnification, to identify inhomogeneity on a finer scale. The highest magnification used was 10,000 X (photomagnification), to identify the presence of particles or precipitates of the order of a micron or less in diameter.

3.2 Particulate dopant additions.

In order to assess the effects and effectiveness of the alkoxide doping technique (as opposed to the effects of the dopant additions), it was necessary to produce a number of reference specimens of similar compositions to the alkoxide doped materials, but with the dopant additives added by conventional mechanical powder mixing techniques.

One mass percent of the dopant additions were made to the Tosoh T.Z.P. material using ANALAR grade alumina, (fumed) silica, and titania powders. These were mixed for 12 hours using a "turbula" mixer in a polythene container.

The samples were not subjected to ball milling (which would have improved the distribution and homogeneity of the dopant addition) as there was a high probability that this would have introduced additional contamination into the samples.

3.3 Determination of powder characteristics.

In order to produce a material with high sintering activity (i.e. sintering occurs at reduced temperature), the manufacturers, of the T.Z.P. used in this study, have developed powders with extremely fine and homogenous particle size and low agglomerate strength. This is thought to be fundamental to the properties of sintered

ceramic bodies produced from these materials.

It was therefore necessary to determine the powder characteristics both prior to and after the doping process in order to estimate the likely effect on the sintering behaviour arising from changes in the powder characteristics. Four parameters were investigated: Particle size, morphology, agglomerate strength and phase composition.

3.3.1 Determination of particle size.

Two techniques were used to determine the particle size of the unsintered powder.

A direct measurement of particle size was made by observation of the powder particles using a Jeol 840A scanning electron microscope. Specimens for analysis were prepared as follows:

The powders were dispersed in ethanol at the rate of 1g powder : 100 mls ethanol and ultrasonic treated for 15 minutes (by placing the beaker containing the suspension in an ultrasonic cleaning bath) to break up and disperse the powder agglomerates. A single drop of the suspension was then applied to a polished aluminium microscope stub. After evaporation of the ethanol, the powder particles were then platinum coated to reduce charging effects prior to examination. It was found that ultrasonic treatment of the dispersion for 15 minutes resulted in the (virtually complete) break up of the original powder agglomerates, and enabled the primary powder particles to be observed.

Some problems were encountered with specimen charging even after platinum coating of the specimens and degraded the quality of the images which were obtained using secondary electron mode to achieve the maximum topographical information. To attempt to reduce this phenomena, low accelerating voltages were used (5 KV).

A second technique used to measure particle size, and

size distribution was a sedimentation method using a Sedigraph 5100 particle size analyser. This instrument measures the rate of sedimentation of a suspension of known concentration by the absorption of an X-ray beam passing through the suspension at different points. The X-ray intensity is inversely proportional to the concentration of the powder particles in suspension at any point, and the change in concentration between two points at different heights in the suspension is related to the particle size via Stoke's law. The instrument gives a direct readout of particle size and size distribution.

Samples were prepared for analysis as aqueous suspensions (1g powder to 100 mls deionised water). These were subjected to ultrasonic agitation using an ultrasonic probe for two minutes on full power, to break down the agglomerates into the primary particles, followed by stirring to maintain the particles in suspension prior to the measurement.

Although this method obtains data from a large number of powder particles, and is therefore of greater statistical reliability than direct measurement techniques on a few particles, it is not easy to differentiate between the behaviour of individual particles and unbroken powder agglomerates by this technique. The results of the two techniques used can therefore be seen as complimentary.

3.3.2 Determination of powder morphology.

The powder morphology was determined directly by scanning electron microscopy using the specimen preparation technique described in section 3.3.1. However, in order to determine the morphology of both the primary powder particles, and the particle agglomerates, two variants on the technique were used as follows:

(i) To observe the size and morphology of the primary particles, the suspension was subjected to 15 minutes ultrasonic treatment (a beaker containing the suspension was placed in an ultrasonic cleaning bath)

to break down the agglomerates.

(ii) To observe the size and morphology of the particle agglomerates, no ultrasonic treatment was given to the suspension.

Specimen coating and electron microscope imaging conditions were as described in the previous section.

3.3.3 Determination of agglomerate strength.

The agglomerate strength, which was expected to be an important factor determining the sintering characteristics in both doped and undoped powders was estimated by a number of methods.

A preliminary estimation of agglomerate strength was made from the effectiveness of ultrasonic treatment in dispersing the agglomerates in powders prepared for study by electron microscopy as described in sections 3.3.1.& 3.3.2. If a dramatic increase in agglomerate strength had occurred as a consequence of the doping process, it was expected that the stronger agglomerates would prove more difficult to break down.

A second determination of agglomerate strength was carried by carrying out particle (or agglomerate) size determinations on suspensions of the powder particles in water, using the Sedigraph 5100 particle size measuring instrument. Sample preparation was identical to that described in section 3.3.1, with 2 minutes ultrasonic treatment of the suspensions prior to testing. As with the previous method, it was expected that an increase in agglomerate strength would increase the relative volume fraction of particles remaining unbroken after ultrasonic treatment (measured as large rapidly sedimenting particles).

The particle size distributions obtained by this technique were thus used to give a crude, semi quantitative measure of relative agglomerate strength.

Although this method is similar in principle to that described above for direct observation of agglomeration by microscopy, since the results obtained in this method represent the average behaviour of a large number of particles, these may be of greater statistical reliability.

An attempt was also made to obtain a more accurate quantitative estimate of agglomerate strength using the "break-point" method described by Groot Zevart et al[119]. Two gramme quantities of the variously doped powders were subjected to uniaxial compression in a steel die at loads corresponding to pressures of up to 500 MPa. An Instron testing machine was used to apply and measure the applied loads and the die plunger displacements. This enabled the relative density of the powder to be determined from the original mass, the die diameter, and the plunger length.

A graph was plotted of relative density versus the logarithm of the applied pressure. According to the method of Groot Zevart et al, this was expected to produce a graph with two distinct linear regions of different slope, with point of discontinuity corresponding to the break-point, or strength of the agglomerates in the material.

These experiments were discontinued at an early stage, after preliminary tests failed to identify any discrete point of discontinuity, making it impossible to accurately determine the agglomerate strength by this method. It is now thought that these findings may have been significant, possibly indicating that the powders contained a range of agglomerates of varying strength.

3.3.4 Determination of powder phase composition.

The phase composition of the doped and undoped powders was determined by X-ray powder diffractometry to determine whether the doping process and associated heat treatments had changed the phase composition of the

unsintered powder.

A number of alternative methods and formulas have been proposed for phase analysis in zirconia systems, based upon X-ray diffraction. There are two types of theoretically based methods, which are described as the "matrix" method and the "polymorph" method[226].

The Matrix method uses a comparison of the intensity of a particular peak in a pure single phase material against its intensity in a multi phase material. After appropriate correction has been made for the mass absorption coefficients of the phases present, the amount of the phase present can be calculated from the intensity ratio[227].

This method does not incorporate any correction for intensity differences between samples arising from other factors, and consequently "significant errors can arise if sample preparation procedures are not rigorously controlled"[228].

The method used in this work is described as the "polymorph" method.

The polymorph method uses the relative peak intensities (areas) of the different polymorphs (the stabilised tetragonal or cubic forms are treated as high temperature polymorphs) in the same sample. The relative proportions of the polymorphs present can be calculated, from the relative intensities of the equivalent peaks, using correction factors (R values) to account for the contributions of the Lorentz polarisation factor, absorption factor, structure factor, multiplicity factor, and temperature factor for each of the phases.

The relative proportions of the two phases eg the cubic and monoclinic polymorphs of zirconia) are thus given by the expression[228] [229]

$$\frac{V_c}{V_m} = \frac{R_m I_c}{R_c I_m} \text{ or } \frac{[R(11\bar{1})_m + R(111)_m].I(111)_c}{R(111)_c.[I(11\bar{1})_m + I(111)_m]}$$

Porter and Heuer have calculated values for the R values for the various polymorphs and diffraction peaks, based upon the crystal structure of McCullough and Trueblood[25].

However, Evans et al[229], suggest that calculations based upon calculated R values are unreliable, due to the large effect on the structure factor and R values associated with small displacements of the Zr^{4+} ions from their normal positions and suggest that accurate quantitative analysis requires the production of calibration curves to account for the effect of the errors in R value correction for each specific system to be studied.

In these studies, the main purpose of the x-ray diffraction studies was to compare the phase development between systems with different impurities, thus the development of calibration curves was not considered essential, and was not carried out.

One of the most significant problems encountered when attempting to determine the phase composition of polymorphic mixtures of zirconia is the substantial overlap, and superposition of diffraction peaks which occurs particularly for the (111) reflections of the cubic and tetragonal phases. These two diffraction peaks occur at approximately 30.5 degrees two theta, and are impossible to resolve by normal methods. Consequently, to ascertain whether a peak identified at this position is due to the presence of tetragonal phase and/or cubic phase, it is necessary to investigate the high angle (400) diffraction peaks from these phases, found at diffraction angles between 72 and 75 degrees two theta, which are discrete and resolvable.

The analysis was carried out using a Philips PW1710 x-ray diffractometer, using a monochromated (K alpha) copper radiation source operating at a voltage of 35KV, and current of 45mA. Philips APD 3 X-ray diffraction analysis software was used to calculate the peak areas

and correct for the effect of background intensity and contributions of the K alpha 2 component of the peaks.

Samples of the ground and sieved powders used for analysis in this work were pressed into the (recessed) diffractometer specimen holder, using a glass plate to ensure a flat surface.

The samples were then scanned over the ranges 20 to 76 degrees 2 theta, at a rate of 1 degree per minute from 20 to 70 degrees, and 1/4 degree per minute over the range 70 to 76 degrees where the intensities were substantially lower, and greater sensitivity and resolution was required.

The X-ray diffraction peaks of interest and their approximate positions were as follows:

Peak	Diffraction Angle. (approximate peak position) °'s two theta.
$(11\bar{1})_m$	28.2°
$(111)_m$	31.5°
$(111)_{c,t}$	30.6°
$(400)_c$	88.5°
$(400)_t$	89.2°
$(004)_t$	87.8°

Studies of the high angle diffraction peaks failed to find any evidence for the existence of the cubic (400) peak, suggesting that the amount of any cubic phase present in these samples was below the limits of detection for the technique used. The phase composition of the samples was therefore determined as a two phase, tetragonal and monoclinic system, according to the low angle expression derived by Miller et al[36].

$$\frac{M_m}{M_t} = (0.82) \cdot \frac{I_m(11\bar{1}) + I_m(111)}{I_t(111)}$$

where:

$M_{m,t}$ = mole fraction of monoclinic or tetragonal polymorph.

$I_{m,t}(XYZ)$ = integrated intensity (peak area) of (XYZ) peak for monoclinic or tetragonal polymorph

3.4 Powder dopant additions and sample identification.

A total of 23 powder compositions were investigated during the project. These comprised the TZ3Y powder as supplied from the manufacturer (unmodified powder), a blank treated reference consisting of the TZ3Y powder, which had undergone all stages of the alkoxide doping route, but with no alkoxide additions actually made, alkoxide doped TZ3Y with additions of silica, alumina, or titania over the 0 to 1 mass % range, alkoxide doped samples with combinations of the three oxide dopants (multiple doped samples), and mechanically mixed samples with 1 mass % addition of particulate (single) oxide dopants.

In order to produce statistically reliable results, the doped samples which comprised the factorial experiments, were produced in a random sequence. The duplicate compositions and the mechanically mixed samples were produced on a separate occasion. Each sample was allocated a batch number according to the sequence in which they were produced.

The range of compositions investigated, and the batch numbers corresponding to the chronological order of their production are shown in table 3.4

3.5 Test sample fabrication and sintering schedules.

Test specimens were prepared by uniaxial, double ended compaction of preweighed (1.5g) quantities of the powder in a steel die of internal diameter 16 mm. A hydraulic test machine was used to apply the load in a reproducible manner, with a load of 37.5 KN being applied to the die plunger. This corresponds to a pressure of approximately 187.5 MPa or around 1900 Kg/cm^2 applied to the powder.

Table 3.4 Powder dopant additions.

Powder Batch No.	Dopant Addition. (nominal)	Doping Method.
1	0.25% Al_2O_3	Alkoxide Doped.
2	0.75% Al_2O_3	Alkoxide Doped.
3	1% SiO_2	Alkoxide Doped.
4	0.25% TiO_2	Alkoxide Doped.
5	0.25% SiO_2	Alkoxide Doped.
6	1% SiO_2,1% Al_2O_3	Alkoxide Doped.
7	0.75% SiO_2	Alkoxide Doped.
8	0.75% TiO_2	Alkoxide Doped.
9	1% SiO_2, 1 % TiO_2	Alkoxide Doped.
10	1% SiO_2, 1% Al_2O_3, 1% TiO_2	Alkoxide Doped.
11	Blank treatment.	Alkoxide Doped.
12	1% TiO_2	Alkoxide Doped.
13	1% Al_2O_3	Alkoxide Doped.
14	1% Al_2O_3, 1% TiO_2	Alkoxide Doped.
15	TZ3Y as supplied (unmodified).	Alkoxide Doped.
16	0.75% Al_2O_3 (Duplicate batch).	Alkoxide Doped.
17	0.5% SiO_2	Alkoxide Doped.
18	0.5% Al_2O_3	Alkoxide Doped.
19	0.5% TiO_2	Alkoxide Doped.
20	0.25% Al_2O_3 (Duplicate batch).	Alkoxide Doped.
MA	1% Al_2O_3	Mechanically Mixed.
MS	1% SiO_2	Mechanically Mixed.
MT	1% TiO_2	Mechanically Mixed.

The plunger faces were coated with VYCOAT acrylic plastic coating spray to prevent surface adhesion and delamination effects within the pressed pellets which caused great difficulties in preliminary work, with an additional coating coating of ROCOL anti stick, non silicon release agent also being applied to the coated plunger faces and die internal surfaces.

The load was applied gradually, increasing from 0 - 37.5 KN over approximately 10 seconds, with the pressure being maintained for 15 seconds. The pressure was then gradually released at approximately the same rate by slowly operating the manual pressure release valve on the press.

The green pressed pellets were carefully placed on a bed of TZ3Y powder to avoid contamination, and sintered in an alumina crucible tray, in air.

Due to limitations on the operating range of the furnaces available, one of two furnaces were used depending upon the sintering temperature used. Both furnaces were controlled by a Eurotherm programmer controller which enabled the furnace temperature to be cycled through a controlled ramp up, dwell and cooling rate.

Samples sintered at temperatures of 1350°C or greater were heat treated in a Carbolite HTF 18/8 furnace with Super Kanthal elements, whilst samples sintered at temperatures below 1350°C were heat treated in a Carbolite MFHT/T/1 furnace (SiC elements).

The heat treatment schedule used for all of the specimens consisted of a preheat stage to 500°C followed by a two hour dwell to remove residual organic material (from the TZP manufacturing or the powder doping process) and other volatile contaminants. The main heat treatment stage then followed consisting of a controlled heating rate of 2°C per minute to the sintering temperature, a two hour dwell at this temperature, followed by controlled cooling at 2°C per minute to room temperature.

Figure 3.5 Heat treatment schedule used for sintering the T.Z.P. specimens.

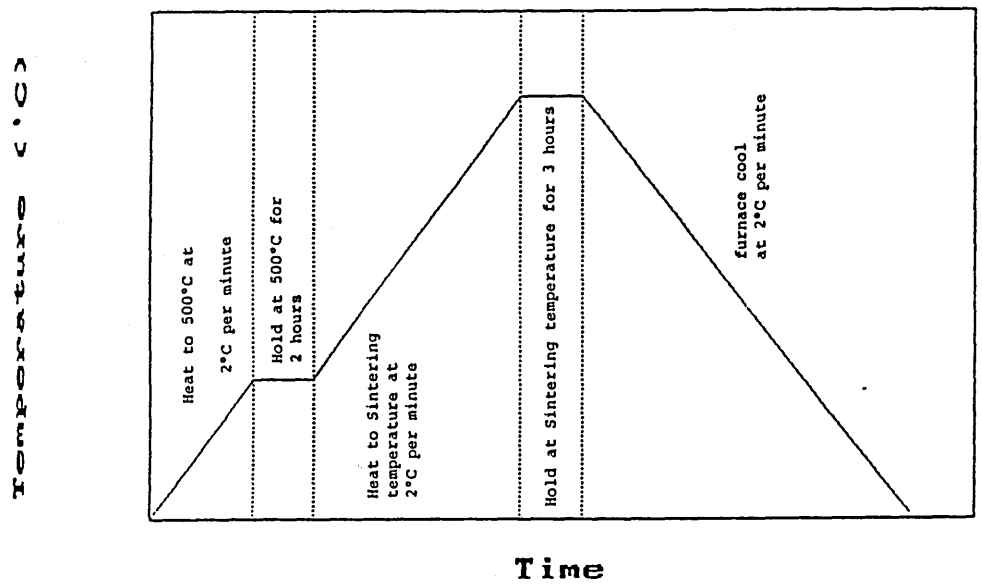

In practise the furnace cooling rate in the latter stages of cooling below approximately 350°C occurred at a somewhat slower rate than this due to the high thermal mass of the furnace.

Sintering treatments were carried out at 950° 1050°, 1150°, 1250°, 1350°, 1450°, 1550°, 1650°, 1700°, and 1750°C, with the typical heat treatment schedules used illustrated in figure 3.5. It should be noted that the overall heat treatment time increased as higher sintering temperatures were used.

3.6 Determination of sintering shrinkage.

The sintering shrinkage obtained from the variously doped samples at different sintering temperatures was determined by direct measurement of the pellets before and after sintering, using a (vernier) micrometer calibrated to 0.01 mm. In practise, the pre-sintering diameters of all the pellets were found to be identical, these being determined by the internal dimensions of the pressing die.

To obtain reliable values, it was found to be necessary to take a number of readings of the pellet diameter, as is was found that there was some slight variation in the diameter values at different points.

An average of 10 readings were taken across the diameter of the pellet using a micrometer.
The linear shrinkage was then calculated as:

(Sintered Diameter/Original Diameter) X 100%

The shrinkage results were subject to relatively large measuring errors, and were therefore considered to be essentially confirmatory evidence for the effect of the impurities on the densification mechanism (also studied by density determinations). However it was possible to obtain values for shrinkage determinations for samples produced over a significantly wider range of sintering temperatures than was possible by wet density

determination (due to breakdown of the partially sintered specimens in water). Consequently these measurements did offer useful additional information, particularly regarding the initial stages of sintering.

3.7 Determination of density and porosity.

The effect of composition and sintering temperature on the density, and porosity of the specimens was determined by an archimedean technique.

The specimens were weighed dry, immersed in water, and after immersion in water to generate the apparent density, bulk density, and apparent porosity of the samples. In addition, an estimate of the true porosity was made by assuming a theoretical density of 6.1 Kgm^{-3} for tetragonal zirconia. The last of these figures is for comparative purposes only since it takes no account of the effect of cubic phase development, nor the effects of the impurity phases on the density of the material.

The samples were immersed in water for 10 minutes prior to the "wet" weighing, and each sample was immersed and weighed 5 times (or until 5 stable readings were obtained) to produce a mean figure, together with an estimate of the measuring error.

Although this method did give reproducible results, there is some doubt whether the experimental technique used would have achieved complete penetration of water into the pore spaces, and it is probable that this resulted in an underestimation of the apparent porosity, and an overestimation of the density.

The following definitions[224] are relevant:

Apparent Porosity = % of material comprising open\reticulated porosity

Total Porosity = % of material comprising both open and closed pores.

Apparent volume = volume of (solid) material and the closed pores.

Bulk volume = volume of (solid) material including both open and closed porosity.

Apparent Density = mass / apparent volume.

Bulk Density = mass / bulk volume.

The apparent density (A.D.), bulk density (B.D.), apparent porosity (A.P.), and total (or true) porosity (T.P.) were calculated as follows[224]:

Weight of dry sample in air = W_a
Weight of sample soaked and suspended in water = W_b
Weight of soaked sample suspended in air = W_c
Density of water = D_L

$$B.D. = \frac{W_a}{W_c - W_b} \times D_L$$

$$A.D. = \frac{W_a}{W_a - W_b} \times D_L$$

A.P. = 100 x (1-(Bulk Density/Apparent Density))

T.P. = 100 x (1-(Bulk Density/Theoretical Density))

3.8 Specimen preparation.

A standardised and reproducible technique was developed for the metallographic preparation of the sample surfaces prior to microstructural examination. This being considered to be extremely important given the long preparation times involved, and the susceptibility of ceramic materials to surface damage during these operations[225].
The use of standardised sample preparation techniques was also essential for the preparation of samples prior to the fracture toughness measurements, since it has been shown that surface finish has a peculiarly large effect on the mechanical properties of transformation toughened materials such as T.Z.P. due to surface phase transformations[75][76].

Table 3.8 Grinding & Polishing Schedule.

Grinding platten.	Grinding/ polishing compound	Polishing time used.	Mean stock removal rate
Kemet iron composite	14 um diamond slurry.	60 mins	0.40 mm/hr
Kemet copper composite	6 um diamond slurry.	30 mins.	0.15mm/hr
Lamplan 9450 polishing cloth	1 um diamond slurry.	30 mins.	0.01 mm/hr
Lamplan 9450 polishing cloth	1/4 um diamond slurry.	30 mins.	<0.01 mm/hr

Applied load : 1Kg handweight.
(each handweight was applied to 6 specimens)

Platten speed : 50 Revolutions per minute.

Diamond sprays : Applied for 2 seconds every 30 seconds.

Lubricant : Applied for 2 seconds every 120 seconds with (Kemet) composite plattens, not used with (lamplan) polishing cloths.

The preparation schedule developed during this work utilised a commercial sample preparation system based upon an Engis 15 lapping/polishing machine with composite grinding plates and soft cloth polishing plattens. An automated pneumatic spray dispenser was used to supply lubricant and polishing compound to the grinding/polishing platten at regular intervals.

Engis type K, 14, 3, 1 and 1/4 um diamond slurries were used as the polishing compound.

Samples were prepared under standardised conditions for applied load, platten speed, and polishing compound and lubricant application, these conditions being identified from a preliminary investigation into the rate of stock removal and surface finish obtained under various conditions. The grinding\polishing schedule and conditions used are shown in table 3.8.

3.9 Quantification of sintering defects and surface damage, by optical microscopy and Seescan image analysis.

Although shrinkage, density and porosity results all enable the sintering behaviour to be determined, all of these techniques are limited in that they are essentially bulk measurements.

In particular, although these measurements give estimates of the effect of relatively large numbers of (usually small) defects on the sintering behaviour, they are insufficiently sensitive to determine the effects of defects which (although often quite large, and highly significant in determining the properties of the material) are present in smaller numbers.

It was therefore considered useful to carry out an additional determination of the sintering characteristics of the various compositions under a range of sintering temperatures by the use of microstructural investigation.

Image analysis techniques combined with optical

microscopy were used in this part of the work, using a SEESCAN image analysis system coupled to a Zeiss microscope.

This measurement also gave additional information regarding the polishing characteristics of the material, particularly the susceptibility of the sintered ceramic to surface damage such as grain pull out induced during the lapping and polishing operations. This was thought to offer some semi quantitative evidence for the comparative mechanical properties of the materials.

The Seescan package was used to generate figures for the number of defects present over ten fields of view, the percentage of the total sample area occupied by defects (mean defect area %) and the average size of the defects measured (in mm^2).

The number of fields of view and total number of defects measured were limited by the information storage capacity of the machine.

The system was programmed to reject any defects at the lower limit of resolution at this magnification to minimise signal noise effects and to give acceptable statistical distributions, and was calibrated using a scale graticule.

3.10 X-ray diffraction study of sintered phase composition.

The phase composition of the samples after heat treatment was determined by X-ray diffraction, carried out on the unpolished surfaces of the sintered specimens prior to any thermal etching process.

A Philips PW 1710 diffractometer, with Cu radiation source and crystal monochromator was used for the X-ray diffraction studies. The equipment was controlled using Philips APD 3 control and analysis software. Standard conditions were adopted for all the measurements as follows:

Generator Voltage 35 KV
Generator current 45 mA

The sintered pellets were located at the centre of the specimen holder using plasticine to hold them in position. A glass side was used to press the specimens into the plasticine ensuring that they were level, and that the sample height was correct. This was aided by the recessed design of the specimen holder, with the samples being mounted flush with, the edges of the recess.

The specimens were scanned, in continuous scan mode, over the range 20 to 76 degrees 2 theta to determine the relative proportions of the expected cubic, tetragonal, and monoclinic phases, and to identify the presence of any other new phases formed. The low angle region of the diffraction scan, was carried out a scan speed of 1 degree (two theta) per minute, whilst the high angle end of the scan in the range 70 to 76 degrees was carried out at 1/4 degree per minute. The slower scan rate over the 70-76 degrees two theta range was found to be necessary to improve the resolution and reduce the problems associated with the low signal to noise ratio of the low intensity, broad diffraction peaks in this range.

The arguments regarding the application of the different quantitative methods for phase determination in zirconia have been discussed previously, with respect to the phase determination in the unsintered specimens in section 3.3, and the polymorph method discussed in that section was adopted for these measurements, with modified formulae to account for the different phase composition (notably the presence of cubic phase) in the sintered specimens. The key diffraction peaks used in the phase determination were as follows:

Peak	Diffraction Angle. (approximate peak position) °'s two theta.
$(11\bar{1})_m$	28.2°
$(111)_m$	31.5°
$(111)_{c,t}$	30.6°
$(400)_c$	88.5°
$(400)_t$	89.2°
$(004)_t$	87.8°

As discussed in section 3.3, the superpositioning of the (100) cubic and tetragonal diffraction peaks, necessitates the need to consider the high angle diffraction peaks to distinguish between the cubic and tetragonal phases. However, quantitative phase analysis in systems containing both cubic and tetragonal phases is hampered by the broad profile, low intensities, and overlap of these high angle diffraction peaks.

To attempt to ameliorate this problem, the areas under the peaks were calculated using Philips APD 3, curve fitting software to separate and identify the contributions to the peak intensities made by peak overlap. Figure 3.10(a) illustrates the peak profile fitting results for the high angle (400) peaks. Resolution of the low angle $(111)_m$ and $(11\bar{1})_m$ peaks was straightforward. However the (virtually) coincident $(111)_c$ and $(111)_t$ peaks could not be separated and were treated as a single peak as per the method of Miller and Garlick. This led to slight errors in the curve fitting process (which is based upon the profile of a normal peak) as evidenced by the form of the residual term after curve fitting (figure 3.10 (b)). However, these errors would be expected to be approximately consistent for all the results.

Some difficulties also arose in identifying and measuring the high angle cubic (400) peak. The peak profile fitting programme used to determine the $(400)_c$ peak areas indicated an extremely broad peak profile.

This presented some problems in the analysis (and significant errors in the phase determination results) due to the low signal to noise ratio associated with this broad, low intensity peak.

The broad peak profile suggested the possibility of the presence of the unpredicted cubic related (t') phase rather than the cubic (f or c) phase, since the characteristic X-ray diffraction pattern of the cubic related material contains two smaller peaks in the approximate range 73-75 degrees two theta corresponding to the $(004)_{t'}$ and $(400)_{t'}$ reflections (figure 3.10(c)).

Several attempts were made to use the curve fitting software to calculate peak areas based upon two t' peaks rather than the single $(400)_c$ peak in this range. However in each case, the software rejected this, moving the fitted peak positions closer with each iteration of the fitting calculation, until a single peak was obtained. It was therefore assumed that the peak was produced from the cubic as opposed to the cubic related phase.

The phase composition of the sintered pellets was calculated using expressions developed by Miller and Garlick[36] for the mole ratios of the phases, based upon the polymorph method of Porter and Heuer[228] discussed in section 3, but with modified R values for the high angle peaks. The expressions used were:

$$\frac{M_m}{M_{c,t}} = (0.82) \cdot \frac{I_m(11\bar{1}) + I_m(111)}{I_{c,t}(111)}$$

$$\frac{M_c}{M_t} = (0.88) \cdot \frac{I_c(400)}{I_t(400) + I_t(004)}$$

$M_{m,c,t}$ = mole fraction of m,c or t polymorph.
$I_{m,c,t}(XYZ)$ = integrated intensity (peak area) of (XYZ) peak for (m,c, or t) polymorph.

Figure 3.10 (a)
Fitted peak profiles for high angle peaks, showing overlap, and effect of alpha 2 component.

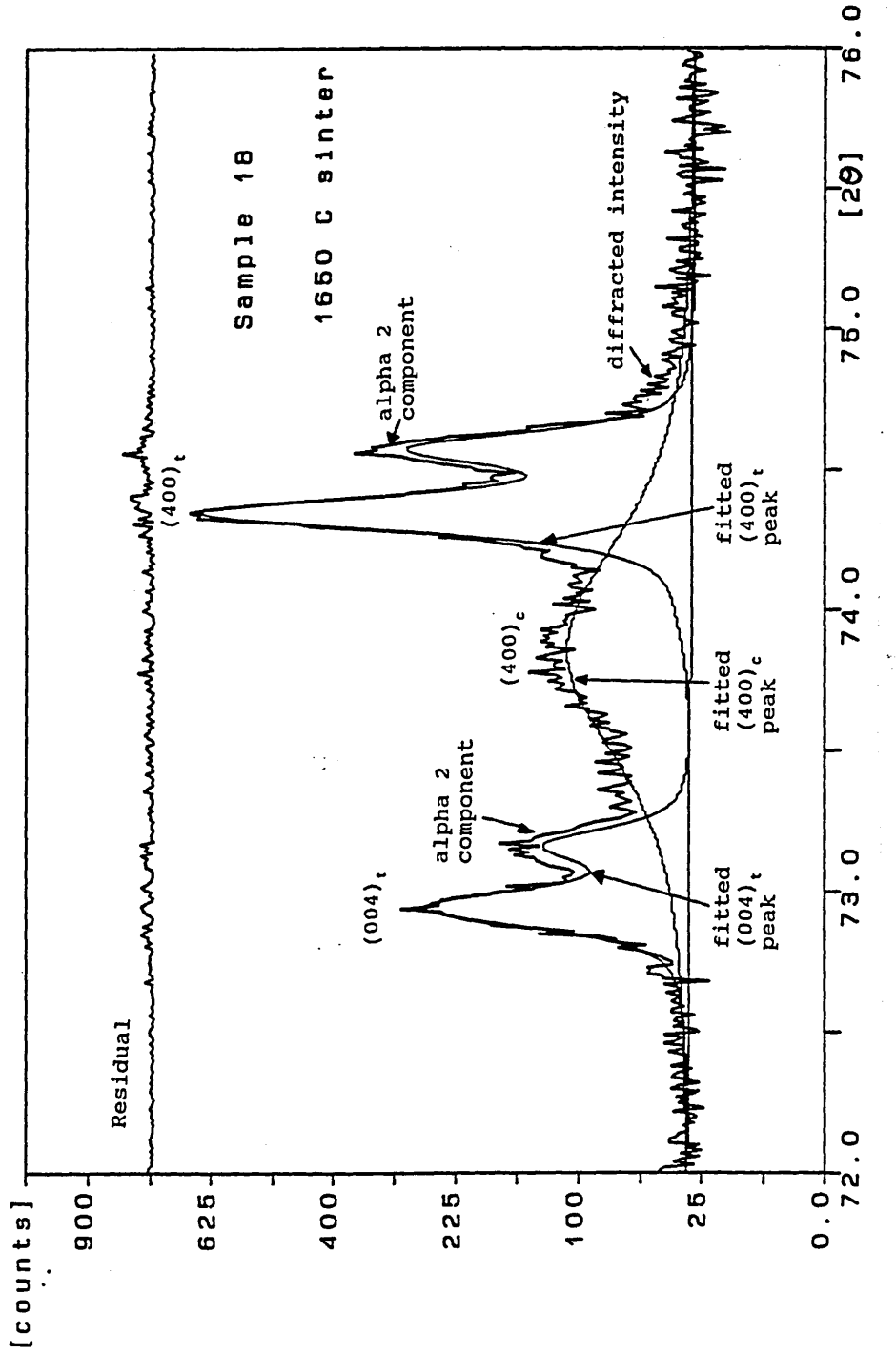

Figure 3.10 (b)
Fitted peak profiles for low angle peaks, showing coincident $(111)_c$ and $(111)_t$ peaks, and effect on residual after curve fitting.

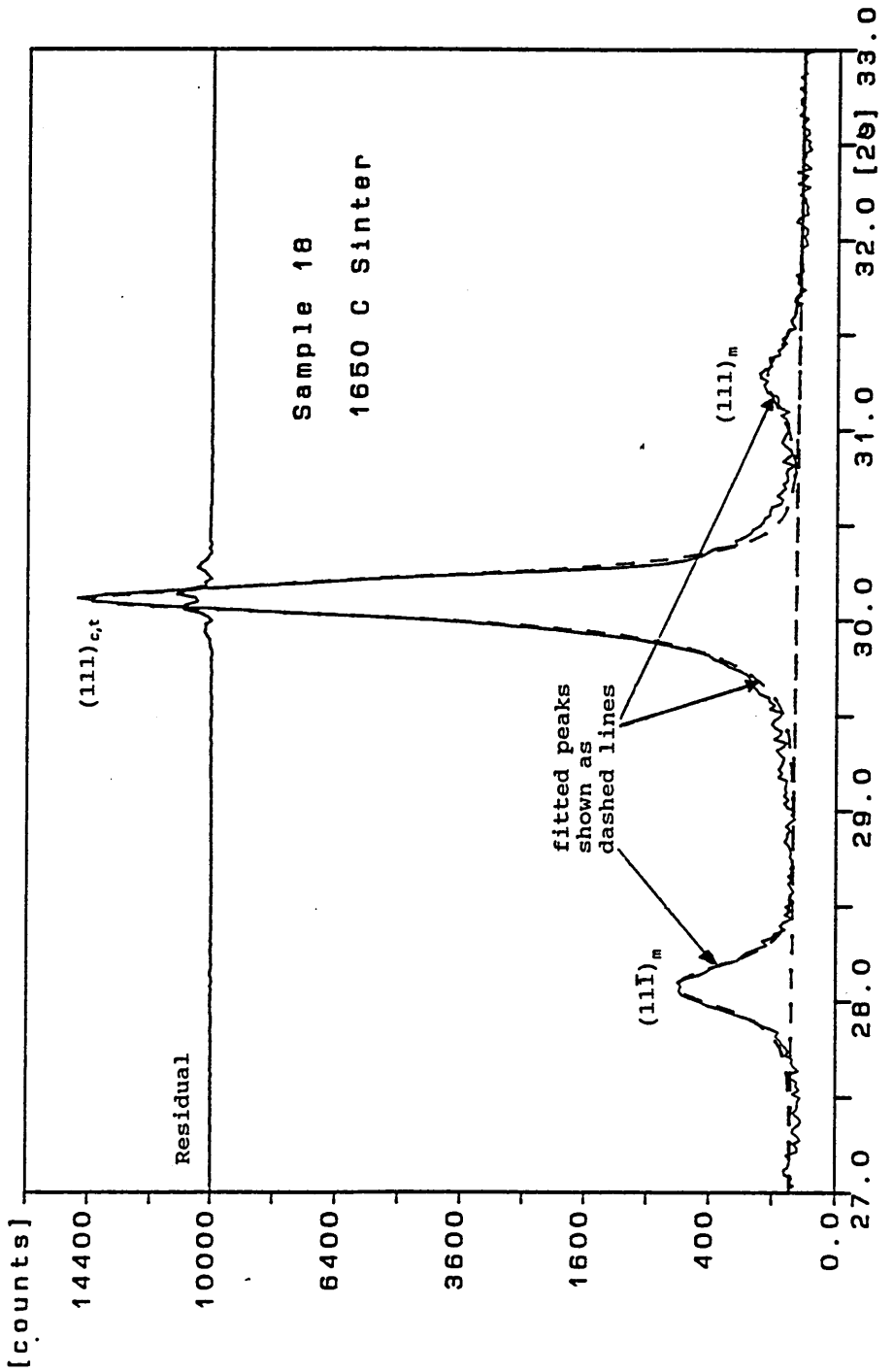

Figure 3.10(c) X-ray diffraction peaks for the t' (cubic related) zirconia polymorph in the range 73-75 degrees two theta. Reproduced from reference[230].

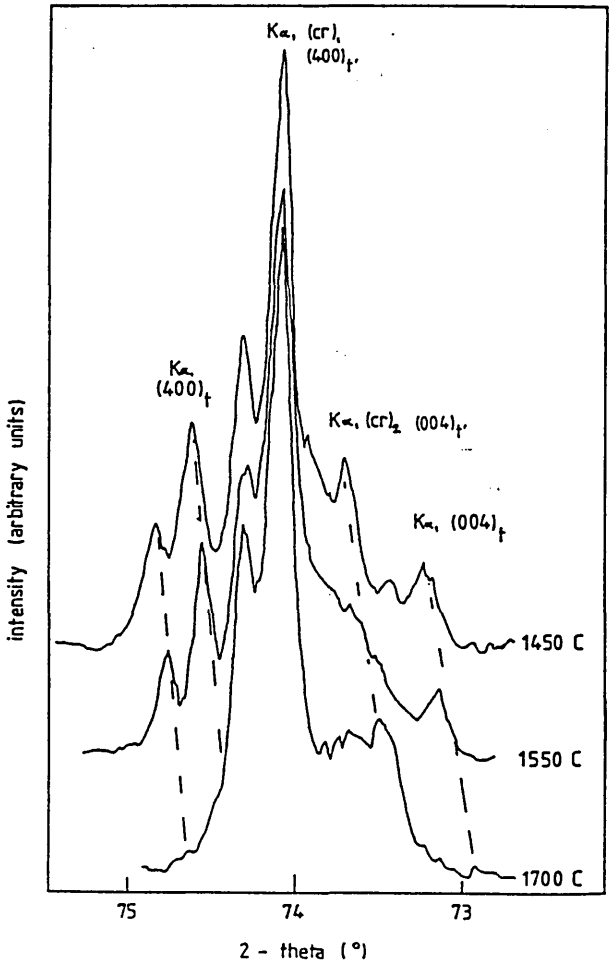

XRD traces between 72.5° and 75.5° 2θ as a function of thermal treatment temperature. Two reflections, $(cr)_1 \equiv (400)_{t'}$ and $(cr)_2 \equiv (004)_{t'}$, are considered to be related to the cubic phase developed at the thermal treatment temperature.

Note:
Miller and Garlick[36] refer to the tetragonal phase identified in their work as T', as it appeared to be non transformable when cooled or stressed. However, the structure and R factors used were calculated as a normal tetragonal structure, using Teuffer's model[29] for the crystal structure. It is therefore reasonable to extend this analysis for tetragonal as opposed to T' (cubic related tetragonal) phase.

If the additional assumption is made that there are no additional phases present (this seemed to be justified from the results), then it can also be assumed that:

$$M_c + M_m + M_t = 1$$

The above three equations can be solved for the three unknown quantities (the mole fractions) as simple simultaneous equations, in terms of the experimentally determined molar ratios.

ie. Let the mole ratios

$$M_c / M_t = x$$

$$M_m / (M_c + M_t) = y$$

then rearranging gives

$$M_t = 1/(1+x+y(x+1))$$

$$M_c = x/(1+x+y(x+1))$$

3.11 Determination of mechanical properties.

Two related experiments were carried out to determine the effects of the impurities and sintering temperature on the mechanical properties of the material. These consisted of a hardness determination using a Vickers indentation, and a determination of fracture toughness using indentation crack length.

The hardness of the material was calculated from the average diameter of 10 Vickers indentations, made where possible under a constant load of 37.5 Kg. In some specimens, notably those with significant residual or induced porosity from the sintering process it was found

necessary to apply a smaller load.

In order to carry out the calculation of fracture toughness, it was necessary that the hardness values were calculated in terms of S.I. units (N/m^2), rather than the more conventional Vickers Hardness Number.

The following formula was used for the hardness calculation[231]:

$$\text{Hardness } (N/m^2) = 0.47 \times \frac{\text{Applied load (N)}}{(1/2 \times \text{indentation diameter (m)})^2}$$

The fracture toughness of the material was determined from the lengths of the indentation induced cracks in the material. This is a standard technique for toughness determination in brittle materials, although there are some problems in its use for materials which undergo transformation toughening. A review of the principles and applications of indentation fracture has been carried out by Lawn and Wilshaw[232]

The toughness values recorded in these materials are found to be a function of the applied load (due to the R curve behaviour), and the specimen history, in particular the surface finishing procedure and annealing/heat treatment[233].

Since this work was more concerned with the comparative effects of the impurity and sintering temperature on the material than obtaining absolute values for toughness it was considered reasonable to use this method for property determination.

To avoid introducing spurious effects arising from the specimen preparation or history, a standardised procedure for polishing and preparing the specimens was used (section 3.8), and wherever possible a standardised load of 40 kg was used to indent the specimens, although for very porous or extensively microcracked specimens reduced loads were applied.

There are two forms of indentation induced crack used in

fracture toughness determinations, depending upon the fracture toughness of the material and the applied load[234]. The interpretation of the results is carried out differently in each case.

For high applied loads, (and/or less tough materials) the indentation cracks extend across the entire indentation, forming characteristic half penny type crack morphology known as median cracks (figure 3.11(a)). For smaller applied loads (and/or more tough materials) the indentation cracks emanate from the basal corners of the Vickers pyramid indentation, and extend across the surface layers of the specimen only. These cracks are known as Palmqvist cracks (figure 3.11 (b)).

The loads and material used in this work produced the Palmqvist type cracking in all cases, this being confirmed by microscopical examination of the bottom of the indentation, at which point no evidence of cracking could be observed.

The formula used in this work to calculate the fracture toughness follows the work of Niihara et al[234], and is the same method used by the T.Z.P. manufacturers in producing their data. The formula for Palmqvist type cracks (defined as those with a l/a ratio <2.5) is given as:

$$((K_{1c}\Phi) \ / \ (H \times (a)^{1/2}) \times (H \ / \ E\Phi)^{0.4} = 0.35 \times (l/a)^{-1/2}$$

This simplifies to:

$$K_{1c} = 0.0117 \times (l/a)^{-1/2} \times H \times a^{1/2} \times (H/(3 \times E))^{-0.4}$$

where:

H = hardness in N/m^2 a = 1/2 x indent diameter (m).

l = measured crack length (m).

E = Modulus of elasticity (N/m^2)

Φ = constraint factor = approximately 3

K_{1c} = mode 1 fracture toughness ($Nm^{3/2}$)

The modulus of elasticity value used in the equations was taken from manufacturers data sheets for TZ3Y[3]. This

Figure 3.11(a) Vickers indentation cracking Median crack morphology.
(reproduced from reference[235]).

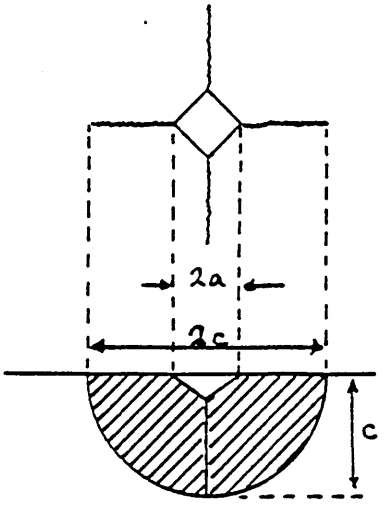

Figure 3.11(b) Vickers indentation cracking Palmqvist crack morphology.
(reproduced from reference[235]).

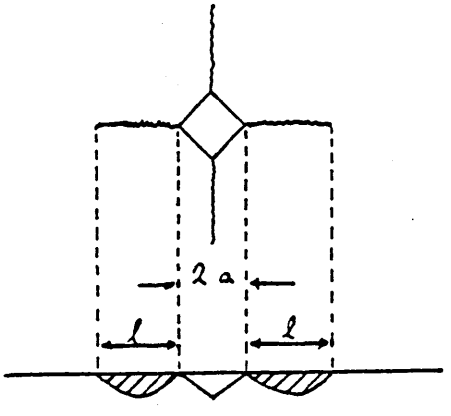

was 200 GPa, or 200 x 10^9 N/m^2.

The values of the indentation diameters and crack lengths were obtained from measurements on photomicrographs (videoprints) produced using optical microscopy. These were calibrated using a scale graticule, photographed at the same magnification.

No investigations were carried out on the thermally etched specimens as it was thought that the possible effects of the heat treatment and surface transformations may give rise to spurious results. In retrospect, it is considered that such a study would have yielded valuable information, most notably on the microstructure : fractography relationship, for example whether the fracture behaviour was consistently intergranular or transgranular for all impurity and heat treatment conditions.

3.12 Microstructural examination by scanning electron microscopy and E.D.X. analysis.

The grain size, and phase distribution in the samples were analysed by scanning electron microscopy and E.D.X. spectroscopy. The examinations were carried out using a Philips XL40 scanning microscope, equipped with a LINK EDX detection system and analytical software.
The microstructural investigations were generally performed using secondary electron generated images, with an accelerating voltage of 20 KV. However under some circumstances, particularly in the examination of porous or extensively microcracked specimens which exhibited charging behaviour, lower accelerating voltages were used, and either backscattered electron images, or mixed secondary and backscattered electron images were used. Backscattered electrons are less affected by specimen charging effects but yield less topographical information than secondary electrons.

3.12.1 Sample preparation and etching procedure.

The samples for examination were polished as described in section 3.8.

Etching of the polished specimens samples was then required in order to allow the grains and phases to be clearly resolved.

A number of techniques were used to etch the specimens. The best results were obtained when the samples were thermally etched for 1 hour at 1450°C, The samples were heated and cooled at 2°c per minute (i.e. as used in the original sintering schedule) to reduce the possibility of introducing changes in phase composition.

It is nevertheless probable that the thermal etching process will have resulted in some changes in phase composition in the samples. However, since the main objective of this part of the work was to obtain comparisons between the behaviour of variously doped samples, rather than absolute values this was considered to be acceptable, for the investigation of the 1550° and 1750°c sintered samples. It should be noted that the thermal etching process was carried out AFTER the determination of the phase composition by X-ray diffraction and the mechanical property determinations.

The etching of the 1350°C sintered samples was also carried out by a thermal etching process, however in this case an etching temperature of 1350°C was used. This gave significantly poorer resolution than the 1450°C etched samples, but it was not thought reasonable to etch the samples at a temperature higher than the original sintering temperature. An etching time of two hours was required to give adequate resolution at this temperature.

The thermal etching procedure could not be used on the lower temperature sintered samples, since the temperatures required to etch the samples would have introduced substantial changes to the microstructure.

Other etching techniques investigated were longer etching

times and reduced temperatures (from 2-12 hours at temperatures between 1050°C and 1300°C), which resulted in less grain boundary definition, or shorter etching times at higher temperatures.

A significant proportion of the total heat treatment time involved heating and cooling the samples to and from the etching temperature, and an attempt was made to reduce the heat treatment time by placing samples (which had been preheated to 800° C) directly in the furnace at the etching temperature, and by removing them on completion of the etching time, initially into a furnace at 800°C and then cooling.

The rapid heating and cooling of the specimens appeared to result in surface damage to the specimens, presumably due to thermal shock, with the intermediate heat treatment and cooling step at 800°C being introduced to attempt to prevent this. Although the intermediate step did reduce the magnitude of this effect relative to samples which were not subjected to this, appreciable damage remained clearly visible in all cases, and this procedure was abandoned in favour of controlled furnace heating and cooling at the 2°C per minute ramp rate.

Chemical etching of the samples using boiling concentrated orthophosphoric acid was also attempted. However, short immersion times (e.g. up to 1 minute) in this medium did not appear to generate topographical contrast, whilst immersion for periods in excess of this appeared to result in the virtual disintegration of the surface, although it was still not possible to clearly identify the grains and boundaries in these specimens.

All of the samples were mounted on aluminium stubs, using conductive paint as an adhesive, and carbon coated prior to examination to reduce charging effects.

3.12.2 Grain size determination.

The grain size of the specimens was determined from

scanning electron photomicrographs (obtained under the conditions described previously) of the etched samples using the mean linear intercept method.

A series of random lines of known length were drawn on the micrographs and the number of grain boundaries intercepted by the lines measured, for a minimum of 100 grains per specimen. The number of grain boundaries intercepted in a given length can then be used to calculate the grain size as follows:

$$\text{2 dimensional grain size} = \frac{\text{no. of grain boundaries intercepted}}{\text{Total length of lines}} \times \text{magnification}$$

The true grain size is larger than the value calculated from 2 dimensional measurements since the two dimensional sections of three dimensional grains are generally smaller than the true grain size. The true three dimensional grain size was estimated by applying a correction factor (x 1.56) to the two dimensional values according the method of Mendelson[236].

3.13 The factorial experiments

The form of factorial experiment used for this work was a 2^4 design. That is, the effects of four factors (the alumina, silica and titania content together with sintering temperature) were investigated at two levels (low and high)[209][210].

This form of experimental design was chosen for two main reasons:

(i) It was expected that the factorial experiment would yield information on the presence and effect of any (hitherto unreported) interactions between impurities (this information could have been obtained from a 2^3 design).

(ii) It was postulated that the temperature-impurity interaction effect might offer evidence on the

effect of impurities on the sintering/densification, phase transformation and toughening mechanisms for specimens sintered at various temperatures.

In order to gain the maximum possible information from the experiments, a series of "back to back" factorial experiments were used (with various temperature intervals) to cover the entire range of sintering conditions investigated.

Separate factorial experiments were carried out to investigate the effects of impurities on the densification mechanisms and behaviour (the density results), the phase transformations and development (the X-ray diffraction results), and the toughening mechanisms (the mechanical property results).

A standard notation is used in factorial experiments[210], and has been adopted in this work.

Thus lower case letters a,b,c,d are used to denote high levels of the treatments (and the associated responses), whilst the absence of a lower-case letter (or the figure (1) in its place) signifies that this factor is present at the lower level.

In this work the letter a indicates that alumina was present at the high level, b indicates silica, and c titania, whilst d denotes that the higher sintering temperature (e.g. of two) was used. The high level of the dopant additions (a,b,c) was the (nominal) 1 mass % addition of each dopant, and the low level no addition. The high and low values of temperature (d) refer to the upper and lower limits of the particular temperature interval being investigated.

The treatment combinations are thus written as (eg):

ab - Alumina and silica present at the high (1%) level, all other factors at low level {no titania addition, lower sintering temperature temperature}.

bcd - Silica and titania present at high level (1 mass %) and higher sintering temperature used.

The upper-case letters A,B,C,D represent the factorial effects of that particular factor or their interaction.
eg AB - The factorial effect corresponding to the interaction between A and B.

Square brackets [A], [BD] represent the total effects of that/those factor(s), whilst curved brackets (A), (BD) represent the average (mean) effects of that/those factor(s).

The main effect (of a factor) is calculated as the average difference between the effect of that factor at the low and high levels, taken over all the levels and combinations of the other factors. The total effect of a factor is the sum of these differences.

For example:
The main effect of temperature (D) in this work was calculated as the average difference between the responses at the low and high temperature values when:

(i) No dopants were present (d-1)
(ii) alumina dopant was present alone (ad-a)
(iii) silica dopant was present alone (bd -b)
(iv) titania dopant was present alone (cd-c)
also
(v) when alumina and silica were present (abd -ab)
(vi) when alumina and titania were present (acd-ac)
(vii) when silica and titania were present (bcd - bc)
(viii) when Al_2O_3, SiO_2 and TiO_2 were present (abcd-abc)

This can be written as

$$(D) = 1/8 \{(d-1)+(ad-a)+(bd-b)+(cd-c)+(abd-ab) +(acd-ac)+(bcd-bc)+(abcd-abc)\}$$

or

$$(D) = 1/8 \{(d+ad+bd+cd+abd+acd+bcd+abcd) - (1+a+b+c+ab+ac+bc+abc)\}$$

The total effect of this factor [D] is calculated as the sum of these differences. [D] =
$\{(d+ad+bd+cd+abd+acd+bcd+abcd) - (1+a+b+c+ab+ac+bc+abc)\}$

Similarly, the main effect of an impurity, eg alumina (A) is calculated as :

$$(A) = 1/8 \{ (a-1)+(ab-b)+(ac-c)+(ad-d)+(abc-bc) +(acd-cd)+(abd-bd)+(abcd-bcd) \}$$

$$(A) = 1/8 \{(a+ab+ac+ad+abc+acd+abd+abcd) - (1+b+c+d+bc+ad+bd+bcd)\}$$

Thus for example, taking the data in table 4.3.8(a), the total effect of temperature [D] is given by:

$$[D] = \{5.61+5.92+5.81+5.92+5.04+5.78+5.91+5.90\} - \{3.95+5.42+3.99+5.75+3.50+4.50+3.82+5.59\}$$
$$= \{45.89\}-\{36.52\} = \mathbf{9.37}.$$

Similarly, the mean effect of alumina addition (A) is given by:

$$(A) = 1/8 \{(5.42+5.75+4.50+5.92+5.59+5.78+5.92+5.90) - (3.95+3.99+3.50+5.61+3.82+5.04+5.81+5.91)\}$$
$$= 1/8 \{(44.78)-(37.63)\} = 1/8\{7.15\} = \mathbf{0.89}$$

The **two factor interaction effects** were calculated as the average difference between the the effects of the first factor at the high and low levels of the second factor, taken over all the levels and combinations of the other factors. Thus the presence of a significant two factor interaction indicates that the effect of the first factor was dependent upon the level of the second (or vice versa).

e.g. The interaction term (AD) in this experiment represents the average <u>difference</u> between the response of a at the high level of d (for the various levels of b and c)

i.e. ((ad-d)+(acd-cd)+(abd-bd)+(abcd-bcd))

and the response of a at the low level of d (sintering temperature).

i.e. ((a-1)+(ac-c)+(ab-b)+(abc-bc))

This gives:

$$1/8 \{(1+c+b+bc+ad+acd+abd+abcd)-(a+ac+ab+abc+d+cd+bd+bcd)\}$$

e.g. in table 4.3.8(a)

(AD) = 1/8{(3.95+3.50+3.99+3.82+5.92+5.78+5.92+5.90
- (5.42+4.50+5.75+5.59+5.61+5.04+5.81+5.91))}

(AD) = 1/8 {(38.78)-(43.63)} = 1/8{-4.85} = -0.61

Similarly the **three factor interaction effects** were calculated as the difference between the two factor interaction effects at the low and high levels of the third factor, and the **four factor interaction effect** was calculated from the difference in the three factor interaction effects at the two levels of the fourth factor.

Thus a significant three factor interaction effect (eg ABD) indicates that the interaction between the factors A (Al_2O_3 addition) and B (SiO_2 addition) was different at the high and low levels of D (temperature), whilst a four factor interaction effect (e.g. ABCD indicates that the interaction between the factors A, B, and C was different at the two levels of D.

The information obtained from the experiments was analysed using Yates' method[216]. This involves using a simple algorithm (or numerical procedure), adding and subtracting the response values of the treatments in a standard order to produce a table from which the effects of each factor and interaction are calculated[209] [210] [211] [212].

The results are quantified in terms of the main effects (the effects of the individual factors), and the two, three and four factor interactions.

Yates' method to calculate the factorial effects for a 2^4 experiment operates as follows:

First write down all the treatment combinations in standard order beginning with the untreated sample and adding in each factor and its possible combinations in turn (in alphabetical order).
e.g. for a 2^4 experiment, the standard order is
1,a,b,ab,c,ac,bc,abc,d,ad,bd,abd,cd,acd,bcd,abcd.

Referring to table 4.3.8(a) as a worked example, the factorial effects are then calculated by Yate's method as follows:

The effects of each treatment are then written beside the corresponding letter, thus in Table 4.3.8(a), the density achieved in an undoped sample (designated 1) was $3.95gcm^{-3}$, and in a sample containing 1% alumina was $5.42gcm^{-3}$. This is continued for all factors and combinations as far as abcd (1% additions of alumina,silica and titania, 1250°C sintering temperature in table 4.3.8(a)), which gave a density of $5.90gcm^{-3}$.

Then a series of columns are generated (four columns for a 2^4 design) as follows. The first 8 numbers in each column are obtained by adding together successive pairs of numbers in the preceding column (e.g. the first number in column (1) is **9.37** which is (3.95+5.42)), with the final 8 numbers being obtained by subtracting successive pairs of numbers in the preceding column (e.g., the last figure in column (1) is **-0.01** which is (5.90-5.91)).

This process is continued for columns (2) to (4) (e.g. the final figure in column (4) = **-1.03**, which is (-0.55)-(0.48)). The figures in column (4) represent the total factorial effects of the factors and interactions [A] to [ABCD]. As a computational check, the first figure in column (4) should equal the sum of the treatment effects (e.g. **82.41**).

Finally, the mean factorial effects eg (A),(B),(C),(D) and the Interaction Effects e.g. (AB),(ABCD) are calculated by dividing the total factorial effect by 2^{n-1}., where n = the number of factors investigated (4 in this case). Thus in table 4.3.8(a), the mean factorial effects e.g. **(A) = 0.89**, are obtained by dividing the total factorial effect (e.g. [A] = 7.15) by eight.

The effects of the treatments, and the calculation of the associated factorial effects by Yates' method for each sintering temperature interval used are shown for all of

the factorial experiments in appendix 1.

The sum of squares of a particular effect was calculated using the formula[213]:

$$\text{Sum of Squares (of effect)} = \frac{[\text{effect of factor}]^2}{2^n \times r}$$

where n = number of factors investigated (4 in these experiments).

r = number of replicates (1 in these experiments)

e.g. in table 4.3.8(a), the sum of squares of the effect of temperature [D]

$$S.S_{[D]} = \frac{[9.37]^2}{2^4 \times 1} = \frac{87.7969}{16} = \mathbf{5.487}$$

This term is used to estimate the statistical significance or otherwise of any apparent effect, using an analysis of variance (ANOVA).

This entails calculating the sums of squares of both the calculated factorial effects as described above and the experimental error.

The magnitude of the factorial effects (sum of squares) is compared with the experimental error (sum of squares). The latter term normally being derived from a series of replicates, or repeat experiments. The value of the ratio of the sum of squares is then used to test the null hypothesis (ie the hypothesis that no significant effects or interactions are present) using the F distribution[213].

However, in the case of this work, it was not possible to replicate the experiments, given that this would have (at a minimum) doubled the amount of experiments to be carried out. A number of alternative strategies are available to deal with this situation, some of which were attempted and are described in the following section.

3.13.1 Estimation of error in factorial experiments.

As explained above, the estimation of statistical

significance of the factorial experiments requires an estimate of experimental error in the results. Two methods were used to estimate this:-

The conventional method of producing an estimate of experimental error in unreplicated four (or more) factor factorial experiments is based upon an empirical observation that high order interactions are rarely significant in practice[210]. Thus the standard technique is to pool the calculated sums of squares corresponding to third order and fourth order interactions, and use these as an (internal) estimate of experimental error.

An example of this is given in table 4.3.8(g)

The error term is derived from the sum of squares of the third and fourth order interaction terms.

The total sum of squares of these terms in table 4.3.8(g) is therefore calculated as follows:

Error sum of squares = (0.0003+0.2525+0.0371+0.0039+0.0663)
= **0.3601**

The mean squares of the factorial effects are derived by dividing the sum of squares of the factorial effects by the number of degrees of freedom associated with each. (n.b. for a 2^k experiment, each effect has only one degree of freedom associated with it).

Similarly, the mean square of the experimental error is given by the sum of the mean squares of the (high order interaction) factorial effects, divided by the total number of degrees of freedom associated with the 5 values.

i.e. (0.0003+0.2525+0.0371+0.0039+0.0663)/5
hence error mean square = (0.3601)/5 = **0.0702**

The significance of the effects is then obtained by dividing the mean square of each of the factorial effects by the pooled error mean square.
e.g. In table 4.3.8 (g):

For effect of Alumina (A) = 3.1952/0.0702 = **44.37**
This number is then compared with the relevant f test values for significance (from statistical tables), for the appropriate numbers of degrees of freedom of both terms being compared.
i.e. degrees of freedom of pooled error term = 5
degrees of freedom of calculated effect (A) = 1

The f test value for f(1%) level, i.e. 1 % probability that null hypothesis is true, for 5 and 1 degrees of freedom is $\mathbf{f_{5,1}(1\%) = 16.3}$. Similarly, $f_{5,1}(5\%) = 6.61$, and $f_{5,1}(10\%) = 4.06$.

Since **44.37** is greater than **16.3**, we can assume from this that this result is **significant at the f(1%) level**, or alternatively, there is more than a 99% probability that this represents a significant effect. Effects significant at the f(1%) level are indicated as *** in the results, with **, and * being used to denote values significant at the f(5%) and f(10%) level respectively.

Although the pooled interaction effects method was used for estimation of experimental error and significance testing in this work, the results suggested that the estimates obtained by this method were somewhat unreliable, as it appeared that significant 3rd order interactions did indeed occur in these experiments. The results of the analysis by this method have been included for comparison in the tabulated results and analysis of variance (ANOVA) tables.

An alternative method of estimating experimental error for the variance analysis is to use an external estimate of error from other (related) experiments[212].
This technique is normally used where the reliability of estimated error is greater (having been derived from a greater number of data points) for the external estimate.

In this experiment, the external error estimate used was that from the one factor at a time experiments. Although this method was not statistically much better than the

internal estimate method (as the estimate was based upon a relatively small sample), the reliability of this estimate was thought to be significantly better since the effects of multi-factor interactions appeared to produce a greatly exaggerated estimate of experimental error with the internal method.

Thus in table 4.3.8 (g), the estimate of experimental used for this technique was that derived from density measurements on duplicate powder batches (table 4.3.1(c)).

The mean difference between the (16) measurements was 0.03 gcm^{-3}, with the mean square of these differences (i.e. the mean of the difference values squared) being 0.0009, and the sum of squares of the differences approximately 0.0144. Taking the mean square difference as the sum of squares of differences divided by the total number of degrees of freedom of the (16) measurements gives the Mean square difference = 0.0144/16 = **0.0009**

The significance of the various effects is then tested similarly to the pooled error method by dividing the mean square of the factorial effects by the error mean square.

e.g. in table 4.3.8 (g), For SiO_2 addition (B), the significance test value = 0.5513/0.0009 = 612.56. This is then compared with the relevant f test values for significance which in this case are as follows:

The f test value for f(1%) level, i.e. 1 % probability that null hypothesis is true, for 16 and 1 degrees of freedom is $f_{16,1}(1\%) = 8.53$. Similarly, $f_{16,1}(5\%) = 4.49$, and $f_{16,1}(10\%) = 3.05$.

Thus for example, the mean square /error mean square value for the BCD (i.e. silica plus titania plus sintering temperature) interaction effect in table 4.3.8(g) gives a value of 4.44 suggesting that this result is significant at the f(10%) level, but not quite at the f(5%) level.

4. Experimental results.

The findings of the experiments carried out during the project are reported in this section.
As for the experimental methods, the results can be considered in two sections:

- Those results describing the effects of the alkoxide doping process and the process parameters on the composition and properties of the doped powders.
  (section 4.1 and subsections)

- Those results describing the effects of the dopant additives on the properties and behaviour of the sintered ceramic.
  (sections 4.2 - 4.7 and subsections)

Note.
Throughout the following sections of the report, the figures quoted for the dopant addition level refer to the nominal dopant addition calculated from the amount of alkoxide precursor added to the powder, rather than the amount of dopant measured in the powders by XRF analysis (see section 4.1.3.4). It was decided to refer to this figure rather than the analysis results for a number of reasons:

(i) There remains some doubt regarding the accuracy of the XRF analysis technique, particularly for low levels of alumina addition.
(ii) This would have added a further uncertainty to the results, whereas the amount of dopant added to the powders could be accurately and precisely determined.
(iii) This simplified the reporting of the results, and the explanation of the mechanisms.
(iv) The magnitude of the discrepancy between the nominal dopant addition and the XRF analysis results was in all cases, small and predictable. Consequently, this made no significant difference to the results, or to the nature of the proposed mechanisms.

4.1 Powder Doping Process.

The development of the powder doping process was considered to be a prerequisite to carrying out the later parts of the study.

The following sections of the report describe the effect of the doping process and the process conditions on the composition and properties of the doped powders.

These results are reported to explain the significance of the various stages in the doping process, and to facilitate future developments of the process to a wider range of oxide systems.

4.1.1 Effect of reaction precursors, modifying additives and conditions (water:alkoxide ratio) on the alkoxide reaction product.

A number of potential reaction modifying additions were investigated, in order to produce systems which did not undergo (often immediate) precipitation when the alkoxide reactants were added. The results of these experiments are reported in this section

The system eventually used in the doping process was that found to be effective for all the alkoxide dopants used. However many of the additives investigated were effective to various degrees, and the results are reported to facilitate future work using these systems.

The water to alkoxide ratio used was also found to have a significant effect. The water additions are reported as 3 levels:

(a) Excess - i.e. more than theoretical requirement for complete reaction.

(b) Limited - i.e. H_2O addition is less than theoretical requirement for complete reaction.

(c) Atmospheric - i.e. no H_2O addition made. Water for reaction supplied by (slow) absorption of atmospheric moisture.

Table 4.1.1

Effect of reaction precursors, modifying additives and process conditions on alkoxide reaction product.

(i) SiO_2 additions.

Alkoxide precursor	Water addition	Reaction modifier or catalyst addition	Reaction product.
Silicon tetraethoxide (T.E.O.S.)	Excess	None	Precipitate (-> particulate on drying)
"	Limited	None	Precipitate (-> particulate on drying)
"	Atmos.	None	clear gel.
"	Excess	NH_4OH	Precipitate (-> particulate on drying)
"	Limited	NH_4OH	Precipitate (-> particulate on drying)
"	Atmos.	NH_4OH	Precipitate (-> particulate on drying)
"	Excess	HCl	Clear gel.
"	Limited	HCl	Clear gel.
"	Atmos.	HCl	Clear gel.
"	Excess	Glacial acetic acid	Clear gel.
"	Limited	Glacial acetic acid	Clear gel.
"	Atmos.	Glacial acetic acid	Clear gel.

Table 4.1.1
Effect of reaction precursors, modifying additives and process conditions on alkoxide reaction product.

(ii) TiO_2 additions.

Alkoxide precursor	Water addition	Reaction modifier or catalyst addition	Reaction product.
Titanium isopropoxide.	Excess	None	Precipitate (-> particulate on drying)
"	Limited	None	Precipitate (-> particulate on drying)
"	Atmos.	None	Precipitate (-> particulate on drying)
"	Atmos.	Acetylacetone (ligand)	Yellow gel (very slight precipitation).
	Atmos.	Conc. HCl	Clear gel.
"	Atmos.	Glacial acetic acid	Clear gel.

(iii) Al_2O_3 additions.

Alkoxide precursor	Water addition	Reaction modifier or catalyst addition	Reaction product.
Aluminium butoxide. (T.E.O.S.)	Excess	None	Precipitate (-> particulate on drying)
"	Limited	None	Precipitate (-> particulate on drying)
"	Atmos.	None	Precipitate (-> particulate on drying)
"	Atmos.	Glacial acetic acid	Cloudy gel (some precipitation).
"	Atmos.	Acetylacetone (ligand)	Vigorous exothermic reaction -> yellow precipitate (-> particulate on drying)
Aluminium isopropoxide.	Atmos.	None	Precipitate (-> particulate on drying)
"	Atmos.	Glacial acetic acid	Cloudy gel (limited precipitation).
Modified Alcan Aluminium Isopropoxide 1010 X	Atmos.	None	slight precipitation (-> cloudy gel)
"	Atmos.	Glacial acetic acid	Clear gel.

4.1.2 Effect of doping process conditions on yield of doping process

The results of the chemical analysis carried out on the doped powders produced under various conditions are shown in table 4.1.2 (a) to (c).

The yield of reaction was calculated by comparing the results of the chemical analysis of the doped powders with the theoretical dopant level calculated from the amount of alkoxide added.

The importance of catalyst, water addition level, and reaction vessel on the yield of the doping process and the final doped composition are clearly indicated in the results.

(a) Silica doped samples.

Table 4.1.2 (a). Chemical analysis results - Effect of process conditions on yield of reaction.

Sample	dopant	Process Conditions: treatment	catalyst	H_2O	Chemical Analysis SiO_2 mass %	SiO_2 yield (%)	Al_2O_3 mass %	Al_2O_3 yield (%)	TiO_2 mass %	TiO_2 yield (%)	Y_2O_3 mass %
(i)	4.75% SiO_2	reacted and dried in beaker.	None	excess	4.20	88	< error	N/A	< error	N/A	5.14
C	9.10% SiO_2	reacted and dried in beaker.	NH_4OH	excess	3.62	39.8	< error	N/A	< error	N/A	5.13
D	9.10% SiO_2	reacted and dried in beaker	NH_4OH	excess	2.39	26.3	< error	N/A	< error	N/A	5.21
G	4.75% SiO_2	reacted and dried in drum drier (slow evaporation)	NH_4OH	limited	3.80	80	< error	N/A	< error	N/A	4.95
H	4.75% SiO_2	reacted and dried in drum drier (slow evaporation)	HCl	limited	4.40	92.6	< error	N/A	< error	N/A	5.07
I	4.75% SiO_2	reacted and dried in drum drier (slow evaporation)	NH_4OH	excess	0.85	17.9	< error	N/A	< error	N/A	5.01
J	4.75% SiO_2	reacted and dried in beaker	HCl then NH_4OH	excess	1.10	23.2	< error	N/A	< error	N/A	5.06
M	4.75% SiO_2	reacted and dried in beaker	NH_4OH then HCl	excess	3.67	77.3	< error	N/A	< error	N/A	4.91
N	4.75% SiO_2	reacted one week in condenser vessel, then drum dried (slowly).	NH_4OH	excess	4.37	92	< error	N/A	< error	N/A	5.06
O	4.75% SiO_2	reacted and dried in beaker	NH_4OH->HCl->NH_4OH	excess	4.56	96	< error	N/A	< error	N/A	5.18
P	4.75% SiO_2	reacted and dried in drum drier (slow evaporation)	HCl then NH_4OH	excess	4.75	100	< error	N/A	< error	N/A	5.40
Q	4.75% SiO_2	reacted one week in condenser vessel, then drum dried (slowly).	NH_4OH	atmos.	4.37	92	< error	N/A	< error	N/A	5.07
R	4.75% SiO_2	reacted and dried in beaker	glac. acetic acid	atmos.	4.51	95.8	< error	N/A	< error	N/A	5.10
R2	4.75% SiO_2	reacted one week in condenser vessel, then drum dried (slowly).	glac. acetic acid	atmos.	4.60	96.8	< error	N/A	< error	N/A	5.14

Table 4.1.2 (b and c). Chemical analysis results - Effect of process conditions on yield of reaction.

(b) Alumina doped samples.

Sample	dopant	Process Conditions: treatment	catalyst	H_2O	Chemical Analysis: SiO_2 mass %	SiO_2 yield (%)	Al_2O_3 mass %	Al_2O_3 yield (%)	TiO_2 mass %	TiO_2 yield (%)	Y_2O_3 mass %
F	9.10% Al_2O_3	reacted and dried in beaker.	None	limited	< error	N/A	9.78	> 100	< error	N/A	4.39
T	1.0 % Al_2O_3	reacted and dried in beaker.	None	atmos.	< error	N/A	0.93	93	< error	N/A	5.21
U	1.0 % Al_2O_3	reacted and dried in beaker.	None	atmos.	< error	N/A	0.85	85	< error	N/A	5.30
V	1.0 % Al_2O_3	reacted and dried in beaker (25 % ethylene glycol addition)	None	atmos.	< error	N/A	0.91	91	< error	N/A	5.28
W	1.0 % Al_2O_3	reacted and dried in beaker (5% ethylene glycol addition)	None	atmos.	< error	N/A	0.93	93	< error	N/A	5.24
X	1.0 % Al_2O_3, 5.0% SiO_2	reacted and dried in beaker (1 % ethylene glycol addition)	glac. acetic acid	atmos.	3.15	70	0.81	81	< error	N/A	5.14

(c) Titania doped samples.

Sample	dopant	Process Conditions: treatment	catalyst	H_2O	Chemical Analysis: SiO_2 mass %	SiO_2 yield (%)	Al_2O_3 mass %	Al_2O_3 yield (%)	TiO_2 mass %	TiO_2 yield (%)	Y_2O_3 mass %
E	9.10% TiO_2	reacted and dried in beaker.	None	excess	< error	N/A	< error	N/A	8.32	91.4	4.87
K	4.75% TiO_2	reacted and dried in beaker.	None	limited	< error	N/A	< error	N/A	4.72	99.3	4.83
L	4.75% TiO_2	reacted and dried in beaker.	NH_4OH	limited	< error	N/A	< error	N/A	4.45	93.7	5.03
S	4.75% TiO_2	reacted one week in condenser vessel, then drum dried (slowly).	glac. acetic acid	atmos.	< error	N/A	< error	N/A	4.82	> 100	5.02

4.1.3 Effect of doping process conditions on physical properties of doped powders.

The effect of the doping process on the physical condition of the powders (prior to the grinding and sieving operations) was determined qualitatively by visual examination of the appearance of the dried powder produced after doping. An attempt was made to break up the dried powder "cake" using a glass rod.

The properties of the powders after doping varied dramatically according to the process conditions. Some of the powder cakes produced were broken down with minimal effort, with these being classified as "friable", whilst other powders required a substantial amount of work to break them down.

The effects of the process conditions on the properties of the doped powders are shown in tables 4.1.3 (a) and (b).

In all cases, the doped powders were ground and sieved as part of the doping process to produce a fine powder. The resultant powders all had impaired powder flow characteristics compared with the original unmodified TZ3Y material, although this could only be assessed qualitatively by examination of the powders.

Table 4.1.3 (a). Effect of doping process conditions on properties of doped powders.

(a) Silica doped samples.

Sample	dopant	Process Conditions..... treatment	catalyst	H_2O	Alkoxide reaction product.....	Physical nature of doped powder .....
(i)	4.75% SiO_2	reacted and dried in beaker.	None	excess	clear gel.	Hard, lumpy powder. Difficult to break down.
C	9.10% SiO_2	reacted and dried in beaker.	NH_4OH	excess	precipitate -> particulate	Friable powder, very weakly agglomerated.
D	9.10% SiO_2	reacted and dried in beaker	NH_4OH	excess	precipitate -> particulate	Friable powder, very weakly agglomerated.
G	4.75% SiO_2	reacted and dried in drum drier (slow evaporation)	NH_4OH	limited	precipitate -> particulate	lumpy, but weakly agglomerated powder.
H	4.75% SiO_2	reacted and dried in drum drier (slow evaporation)	HCl	limited	clear gel.	Hard, lumpy powder, strongly agglomerated.
I	4.75% SiO_2	reacted and dried in drum drier (slow evaporation)	NH_4OH	excess	precipitate -> particulate	Friable powder, very weakly agglomerated.
J	4.75% SiO_2	reacted and dried in beaker	HCl then NH_4OH	excess	precipitate -> particulate	Friable powder, very weakly agglomerated.
M	4.75% SiO_2	reacted and dried in beaker	NH_4OH then HCl	excess	precipitate -> particulate	Lumpy, but weakly agglomerated powder.
N	4.75% SiO_2	reacted one week in condenser vessel, then drum dried (slowly).	NH_4OH	excess	precipitate -> particulate	Friable powder, very weakly agglomerated.
O	4.75% SiO_2	reacted and dried in beaker	NH_4OH->HCl->NH_4OH	excess	precipitate -> particulate	Lumpy, but weakly agglomerated powder.
P	4.75% SiO_2	reacted and dried in drum drier (slow evaporation)	HCl then NH_4OH	excess	precipitate -> particulate	Friable powder, very weakly agglomerated.
Q	4.75% SiO_2	reacted one week in condenser vessel, then drum dried (slowly).	NH_4OH	atmos.	precipitate -> particulate	Friable powder, very weakly agglomerated.
R	4.75% SiO_2	reacted and dried in beaker	glac. acetic acid	atmos.	clear gel.	Lumpy powder, but relatively weak agglom. cf. (H)
R2	4.75% SiO_2	reacted one week in condenser vessel, then drum dried (slowly).	glac. acetic acid	atmos.	clear gel.	Lumpy powder, but relatively weak agglom. cf. (H)
Y	5.00% SiO_2	reacted and dried in beaker. [1% ethylene glycol (anti caking agent) addition.]	glac. acetic acid	atmos.	clear gel.	Hard, lumpy powder. Strongly agglomerated.

Tables 4.1.3 (b) & (c). Effect of doping process conditions on properties of doped powders.

(b) Alumina doped samples.

Sample	dopant	Process Conditions..... treatment	catalyst	H_2O	Alkoxide reaction product.....	Physical nature of doped powder .....
F	9.10% Al_2O_3 (aluminium n butoxide)	reacted and dried in beaker.	None	atmos.	Precipitate -> particulate	Friable powder, very weakly agglomerated.
T	1.0 % Al_2O_3	reacted and dried in beaker.	None	atmos.	Precipitate -> particulate	Friable powder, very weakly agglomerated.
U	1.0 % Al_2O_3	reacted and dried in beaker.	None	atmos.	Precipitate -> particulate	Friable powder, very weakly agglomerated.
U2	1.0 % Al_2O_3	reacted one week in condenser vessel, then drum dried (slowly)	glac. acetic acid	atmos.	clear gel.	lumpy powder, but agglomerates quite weak.
V	1.0 % Al_2O_3	reacted and dried in beaker (25 % ethylene glycol addition)	None	atmos.	Precipitate -> particulate	Hard lumpy powder, strong agglomerates.
W	1.0 % Al_2O_3	reacted and dried in beaker (5% ethylene glycol addition)	None	atmos.	Precipitate -> particulate	Hard lumpy powder, strong agglomerates.
X	1.0 % Al_2O_3, 5.0% SiO_2	reacted and dried in beaker (1 % ethylene glycol addition)	glac. acetic acid	atmos.	clear gel.	lumpy powder, but agglomerates quite weak.

(c) Titania doped samples.

Sample	dopant	Process Conditions..... treatment	catalyst	H_2O	Alkoxide reaction product.....	Physical nature of doped powder .....
E	9.10% TiO_2	reacted and dried in beaker.	None	excess	Precipitate -> particulate	"sticky", weakly agglomerated, friable powder.
K	4.75% TiO_2	reacted and dried in beaker.	None	limited	Precipitate -> particulate	"sticky", weakly agglomerated, friable powder.
L	4.75% TiO_2	reacted and dried in beaker.	NH_4OH	limited	Precipitate -> particulate	"sticky", weakly agglomerated, friable powder.
S	4.75% TiO_2	reacted one week in condenser vessel, then drum dried (slowly).	glac. acetic acid	atmos.	Clear gel.	slightly "sticky", and lumpy powder. (weakly agglomerated).

4.1.4 Characterisation of doped powders prior to sintering experiments.

The results of the characterisation of the doped powder compositions prepared according to the standard doping process conditions discussed in section 3.1 are covered in the following sections.

4.1.4.1 Physical appearance of doped powders.

At the end of the doping process, all of the powders appeared to be very fine, and were less free flowing than the as received material.

No discolouration or other change in visual appearance could be identified at this stage.

Handling of the treated powders was generally more difficult, as a result of the change in flow properties, and also to the presence of large proportion of very fine particles which tended to stick to the surfaces of containers, spatulas, and pressing dies. The presence of these very fine particles was thought to be a potential health hazard, and wherever possible the powder handling operations were carried out in a fume cabinet.

The properties of the doped powders prior to the grinding and sieving stages of the doping process showed more variability. In particular, the strength of the "cake" of powder particles formed on drying (in terms of the difficulty in grinding down the powder) was different for the different dopant types, and was found to increase in the order:
blank treatment < TiO_2 addition < Al_2O_3 addition < SiO_2 addition.
There was also some evidence that a similar increase occurred as the dopant addition level was increased although this could not be quantified.

4.1.4.2 Determination of particle size and morphology by S.E.M. examination.

The micrographs and results of S.E.M. examination of ultrasonic treated and untreated samples of doped and undoped compositions is shown in figures 4.1.4.2 (a) - (d).

The main feature to note in these results is that the doping process, presumably the grinding and sieving operation, has changed the particle morphology from regular approximately spherical particles prior to ultrasonic treatment into asymmetric particles of various shape and size.
The impaired flow properties of the doped powders were thought to be due to this.

Figure 4.1.4.2

S.E.M. photomicrographs of powder morphology.

(a) Undoped TZ3Y powder, from ethanol suspension.
No ultrasonic treatment.
Suspension applied to aluminium stub, Pt coated after evaporation of ethanol.

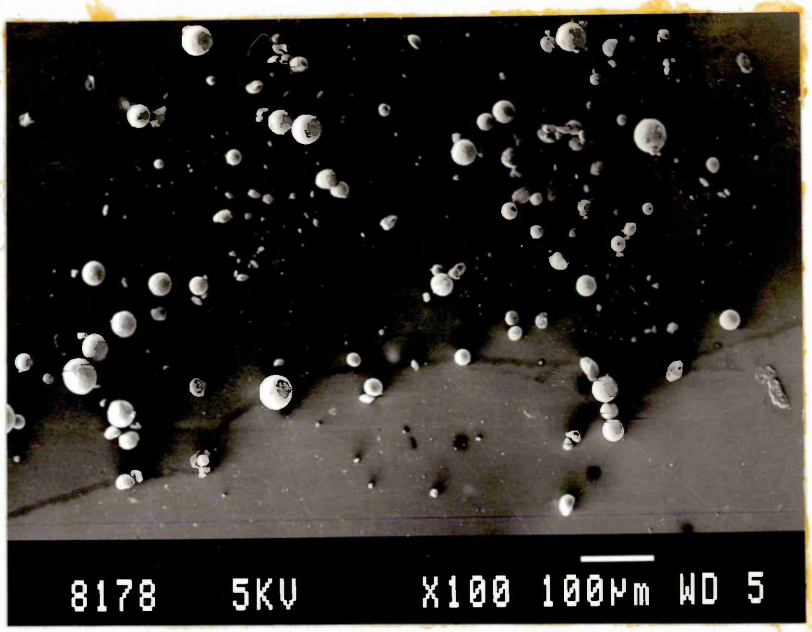

Figure 4.1.4.2

S.E.M. photomicrographs of powder morphology.

(b) Undoped TZ3Y powder, from ethanol suspension. Ultrasonic treated for 15 minutes. Suspension applied to aluminium stub, Pt coated after evaporation of ethanol.

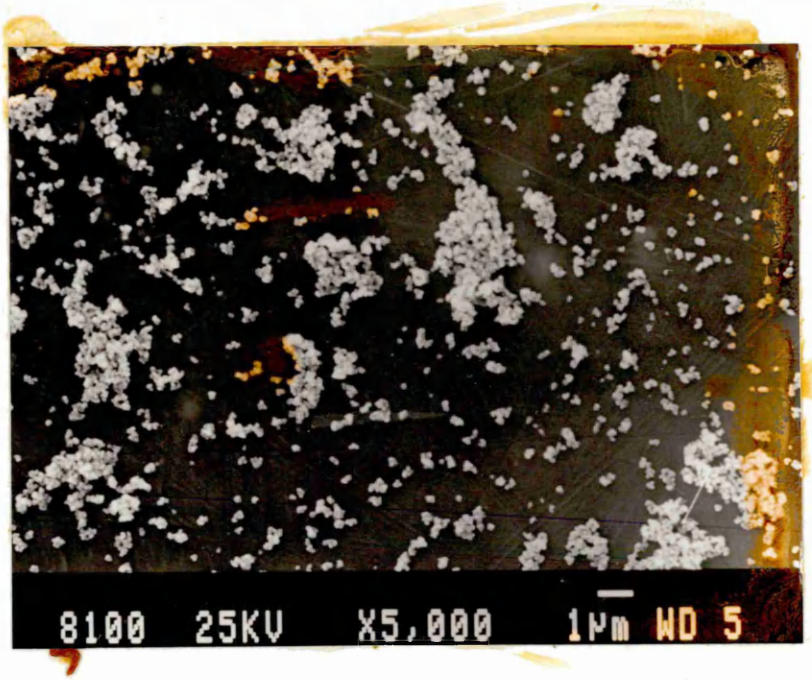

Figure 4.1.4.2

S.E.M. photomicrographs of powder morphology.

(c) Alkoxide doped TZ3Y powder (nominal 1% SiO_2 addition) from ethanol suspension.
No ultrasonic treatment.
Suspension applied to aluminium stub, Pt coated after evaporation of ethanol.

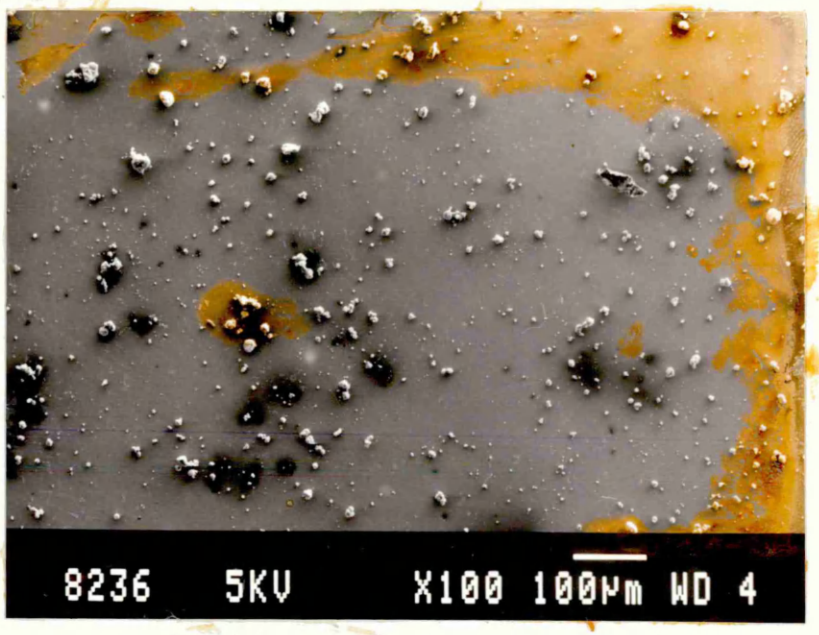

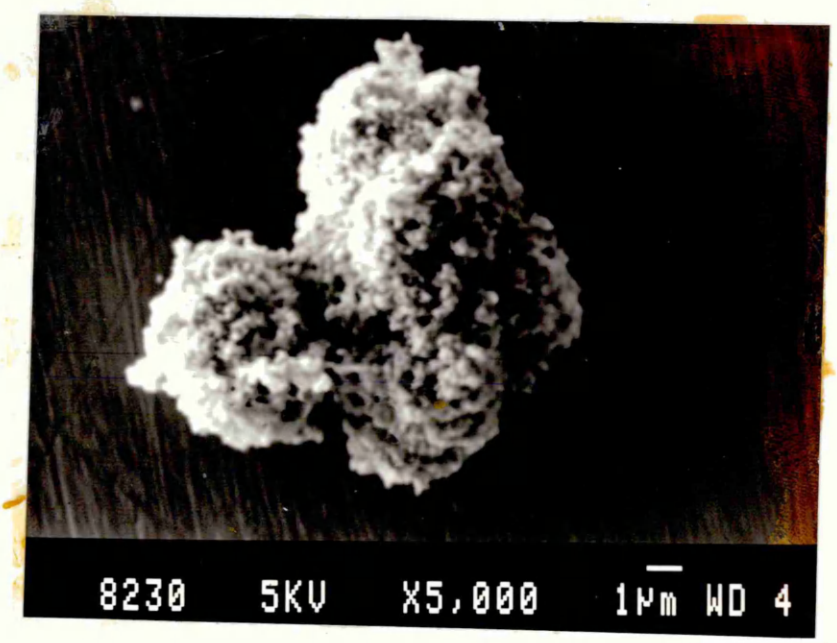

Figure 4.1.4.2
S.E.M. photomicrographs of powder morphology.

(d) Alkoxide doped TZ3Y powder (nominal 1% SiO_2 addition) from ethanol suspension.
Ultrasonic treated 15 minutes.
Suspension applied to aluminium stub, Pt coated after evaporation of ethanol.

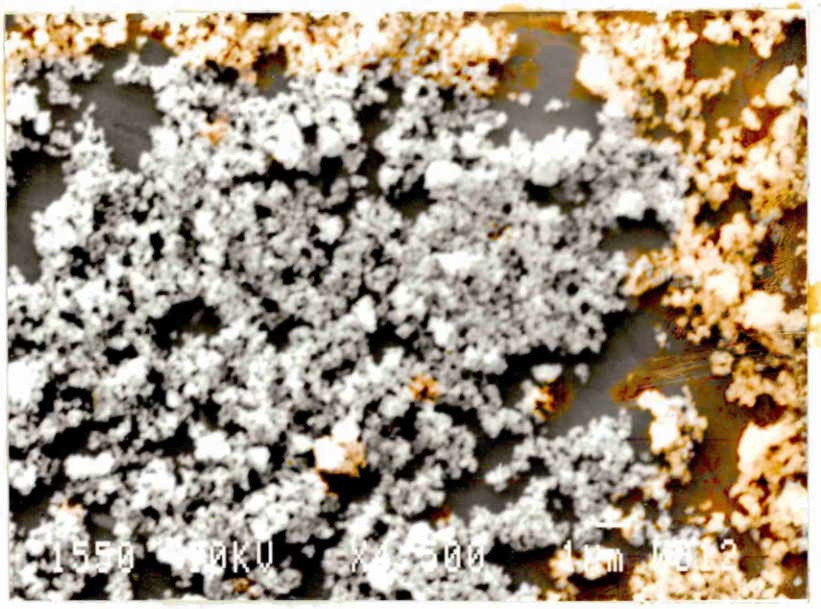

4.1.4.3 Determination of particle size by Sedigraph apparatus.

The results of the Sedigraph particle size, and size distribution measurements carried out on variously doped and undoped particles are shown in figures 4.1.4.3 (a)-(d). The results show little change between the results for untreated samples and samples after the doping process indicating that the overall size distribution was broadly similar between the powders.

The results indicate a slight increase in the large size fraction in the powders subjected to the doping process. There does not appear to be a significant difference between samples treated with different dopant additions or different addition levels.

Figure 4.1.4.3 Sedigraph Particle Size Distribution Results.

(i) As supplied TZ3Y powder.

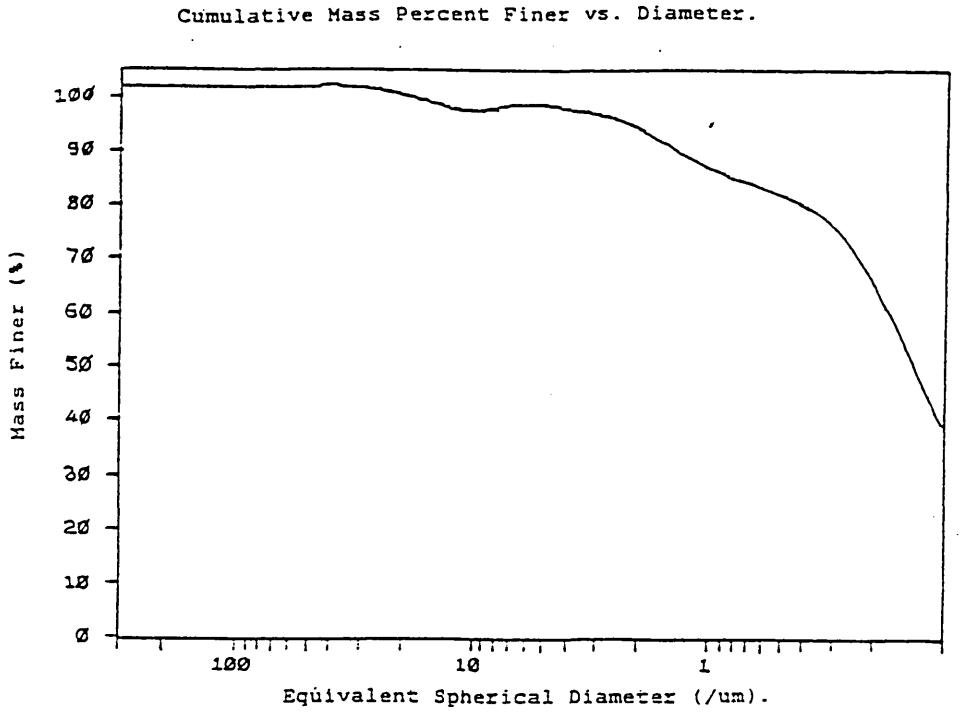

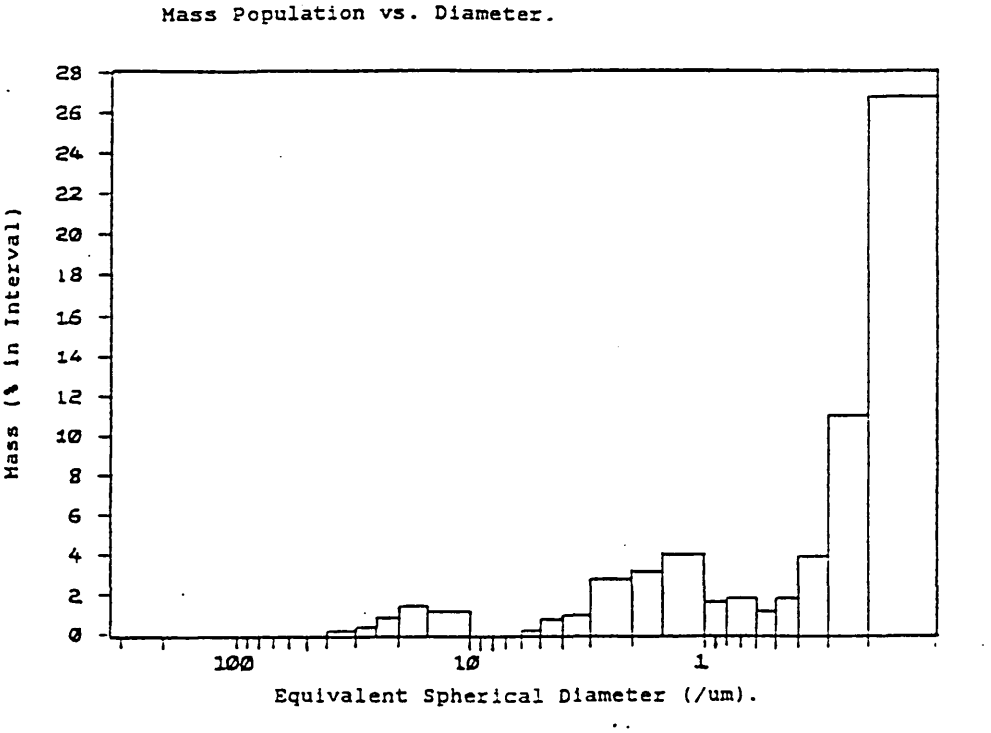

Figure 4.1.4.3 Sedigraph Particle Size Distribution Results.

(ii) Alkoxide doped TZ3Y powder (nominal 0.25% Al_2O_3 addition).

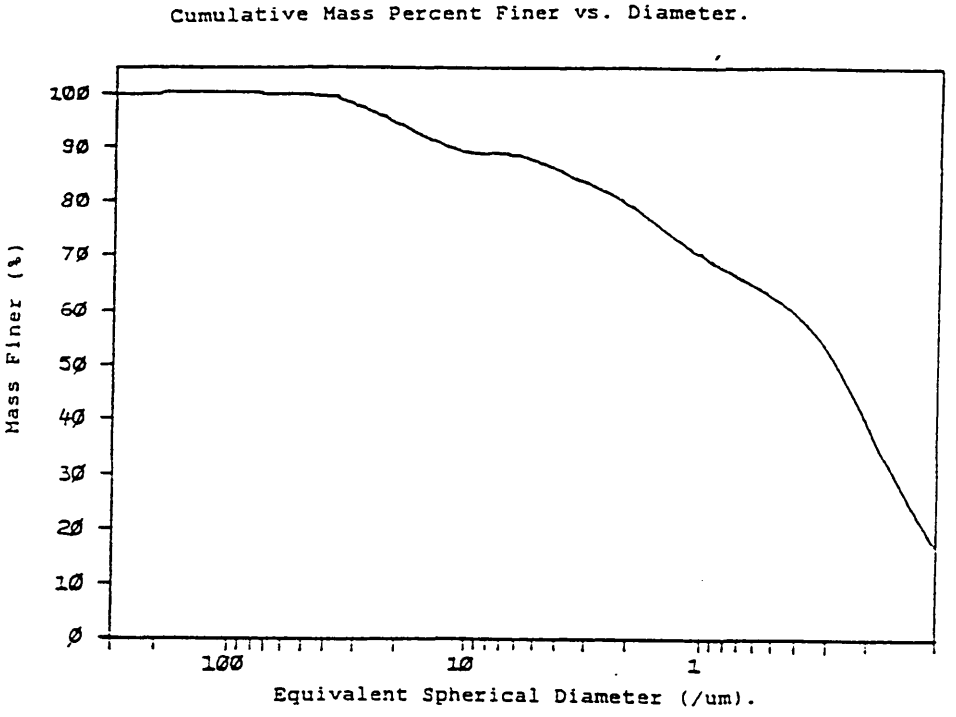

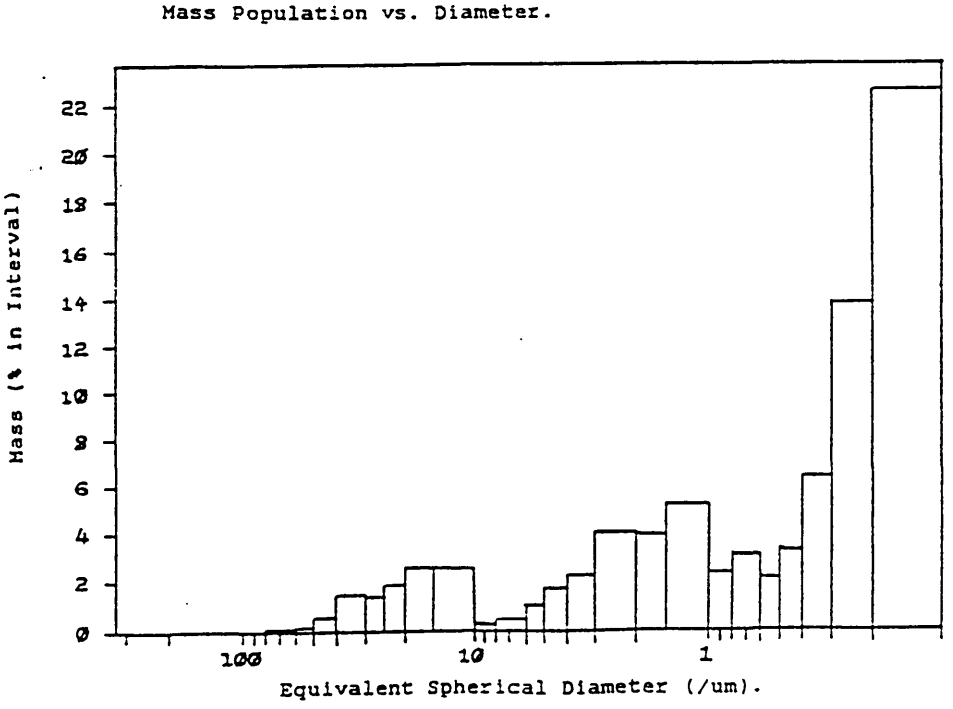

Figure 4.1.4.3 Sedigraph Particle Size Distribution Results.

(iii) Alkoxide doped TZ3Y powder (nominal 0.75% Al_2O_3 addition).

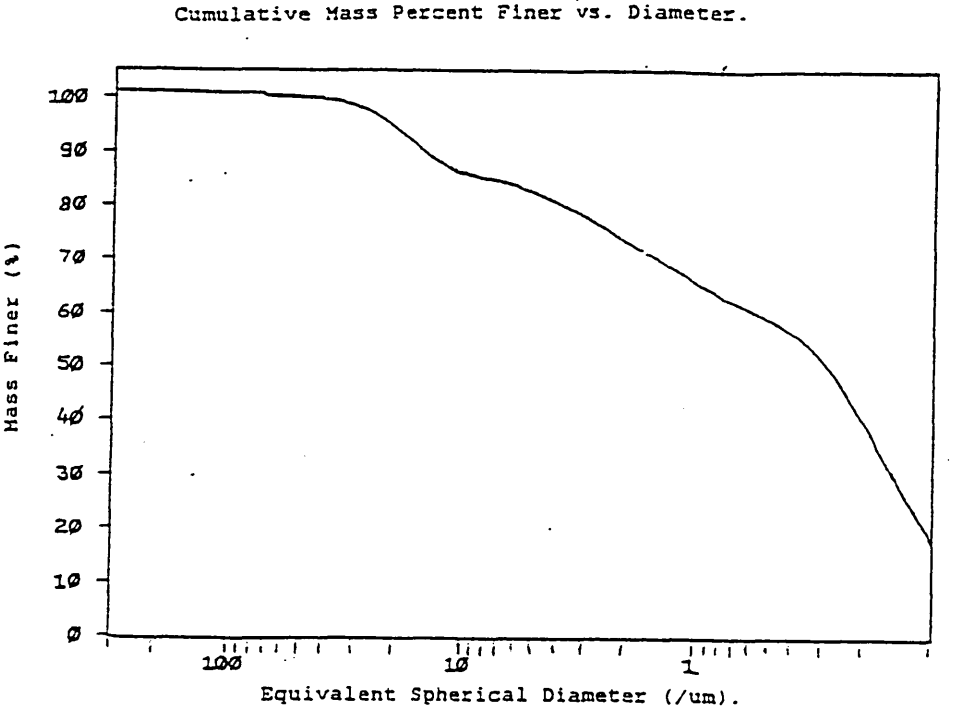

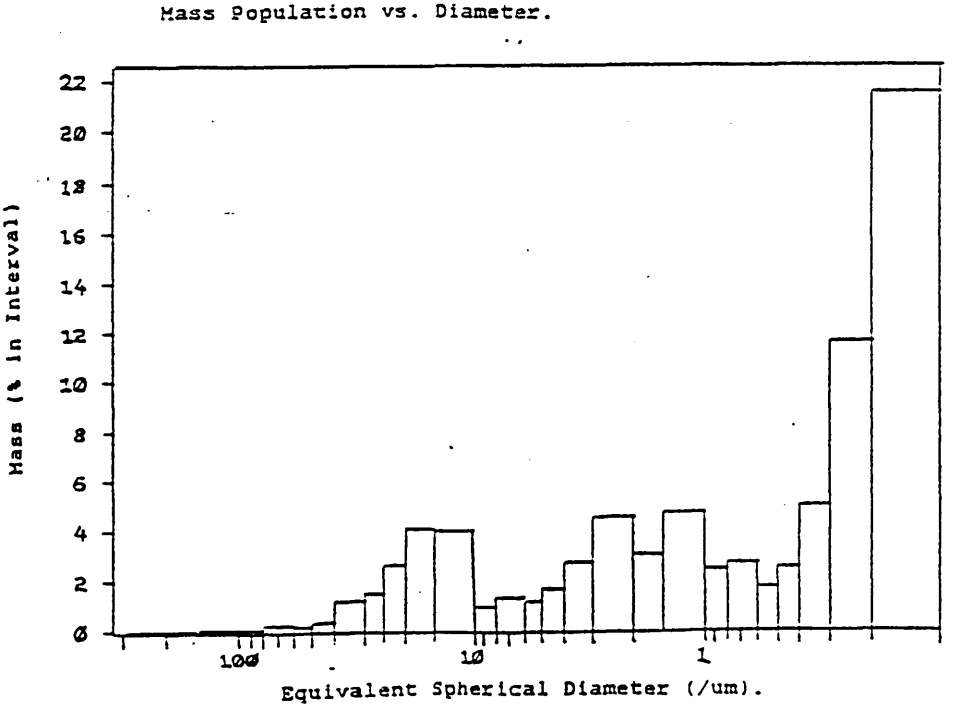

Figure 4.1.4.3 Sedigraph Particle Size Distribution Results.

(iv) Alkoxide doped TZ3Y powder (nominal 1.0% SiO_2 addition).

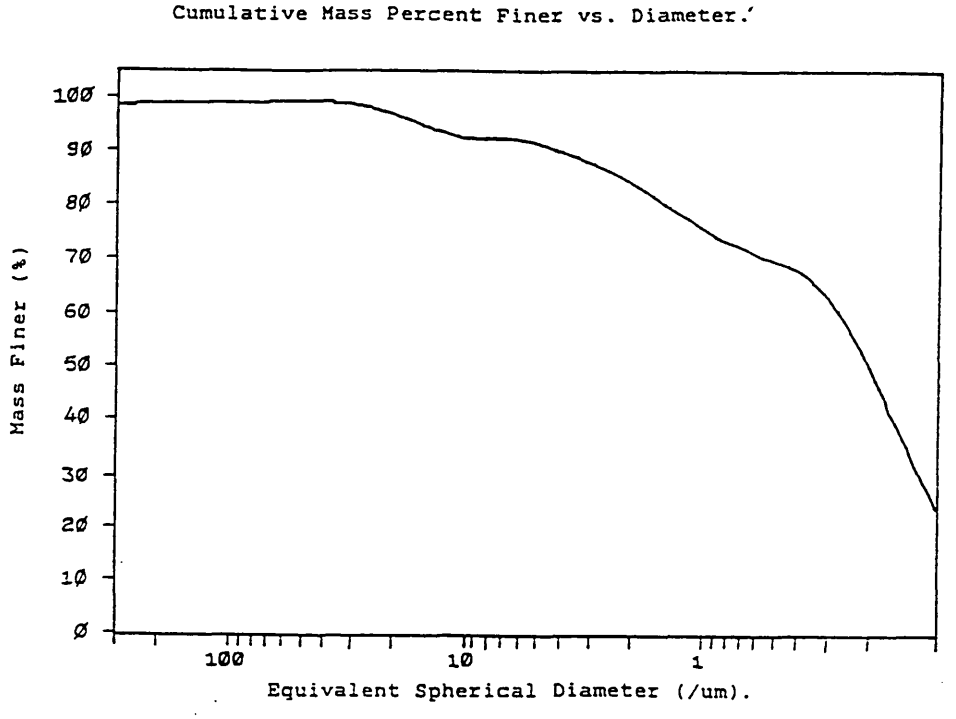

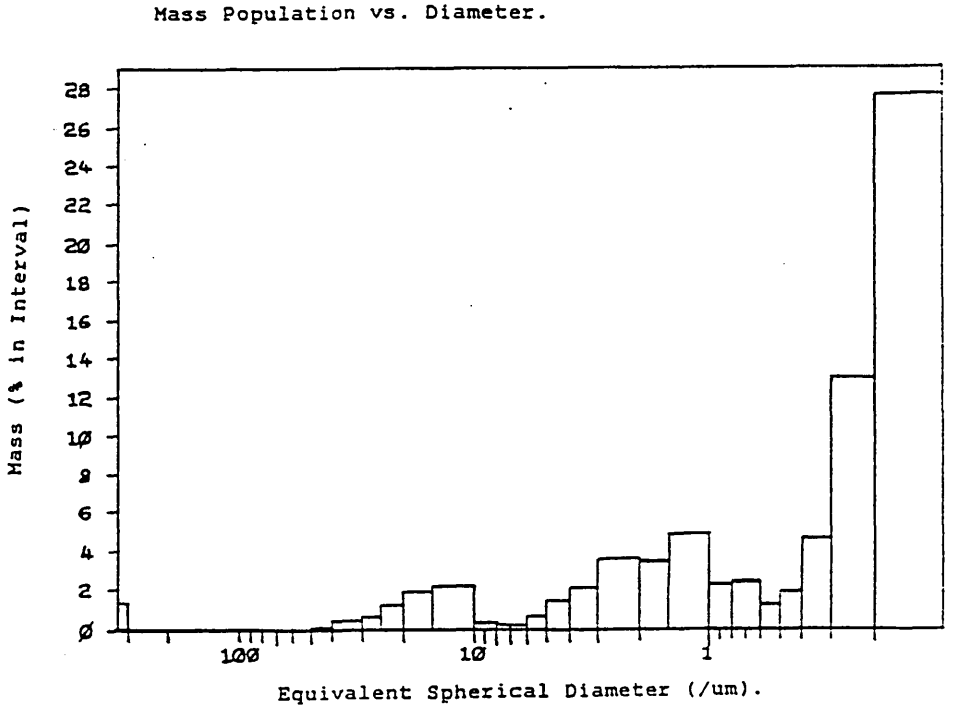

Figure 4.1.4.3 Sedigraph particle size distribution results.

(v) Alkoxide doped TZ3Y powder (nominal 0.25% TiO_2 addition).

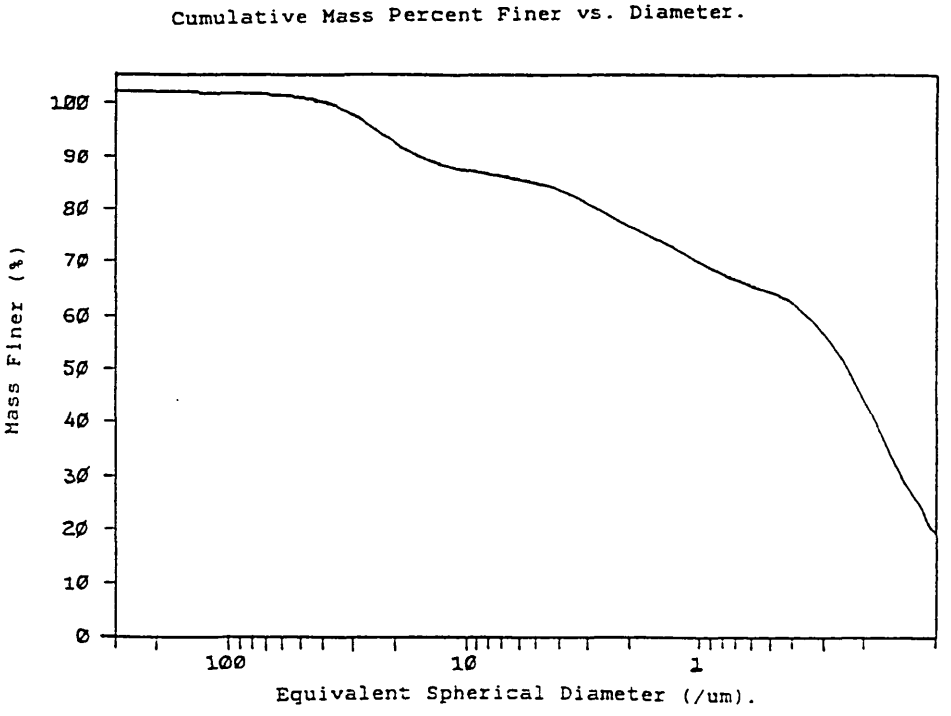

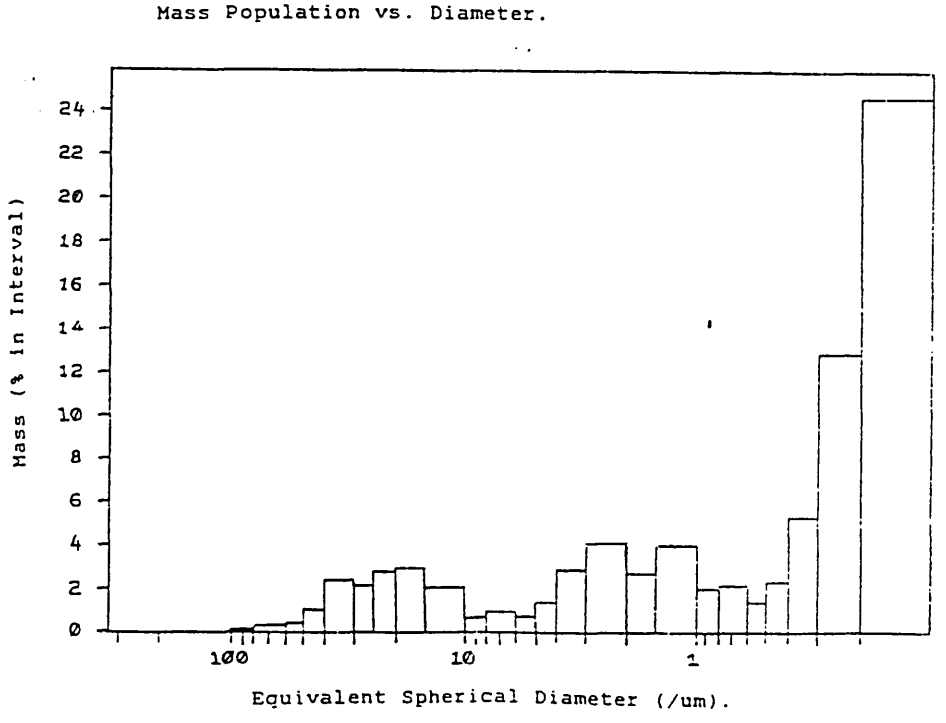

4.1.4.4 Determination of powder phase composition by X-ray diffraction.

The results of the phase composition analysis by x-ray powder diffraction are shown in table 4.1.4.4

No additional crystalline phases were identified arising from the dopant addition. Typical diffraction patterns obtained from the samples are illustrated in figures 4.1.4.4 (a)-(d)

Table 4.1.4.4 X-ray powder diffraction results
Unsintered powders - effect of doping process.

Powder Number.	Integrated Peak Intensity [counts]. 111_t	$\bar{1}11_m$	111_m	004_t	400_c	400_t	M_m/M_{ct}	M_c/M_t	mol fract. Tetragonal (M_t)	mol fract. Cubic (M_c)	mol fract. Monoclinic (M_m)
15	1904.07	310.34	293.38	18.19	0	66.56	0.260	0.000	0.79	0.00	0.21
11	2399.78	276.85	218.51	31.68	0	92.85	0.169	0.000	0.86	0.00	0.14
3	2088.29	315.21	270.53	22.72	0	77.97	0.230	0.000	0.81	0.00	0.19
12	1897.77	291.41	225.94	23.67	0	76.14	0.224	0.000	0.82	0.00	0.18
13	2251.90	380.12	296.58	25.71	0	81.42	0.246	0.000	0.80	0.00	0.20
10	2252.04	371.24	277.25	28.33	0	85.27	0.236	0.000	0.81	0.00	0.19

Figure 4.1.4.4 - X-ray powder diffraction trace.

(a) Undoped (blank treated) TZ3Y Powder*, compared to unmodified (as received) TZ3Y.

(* baseline shifted for clarity)

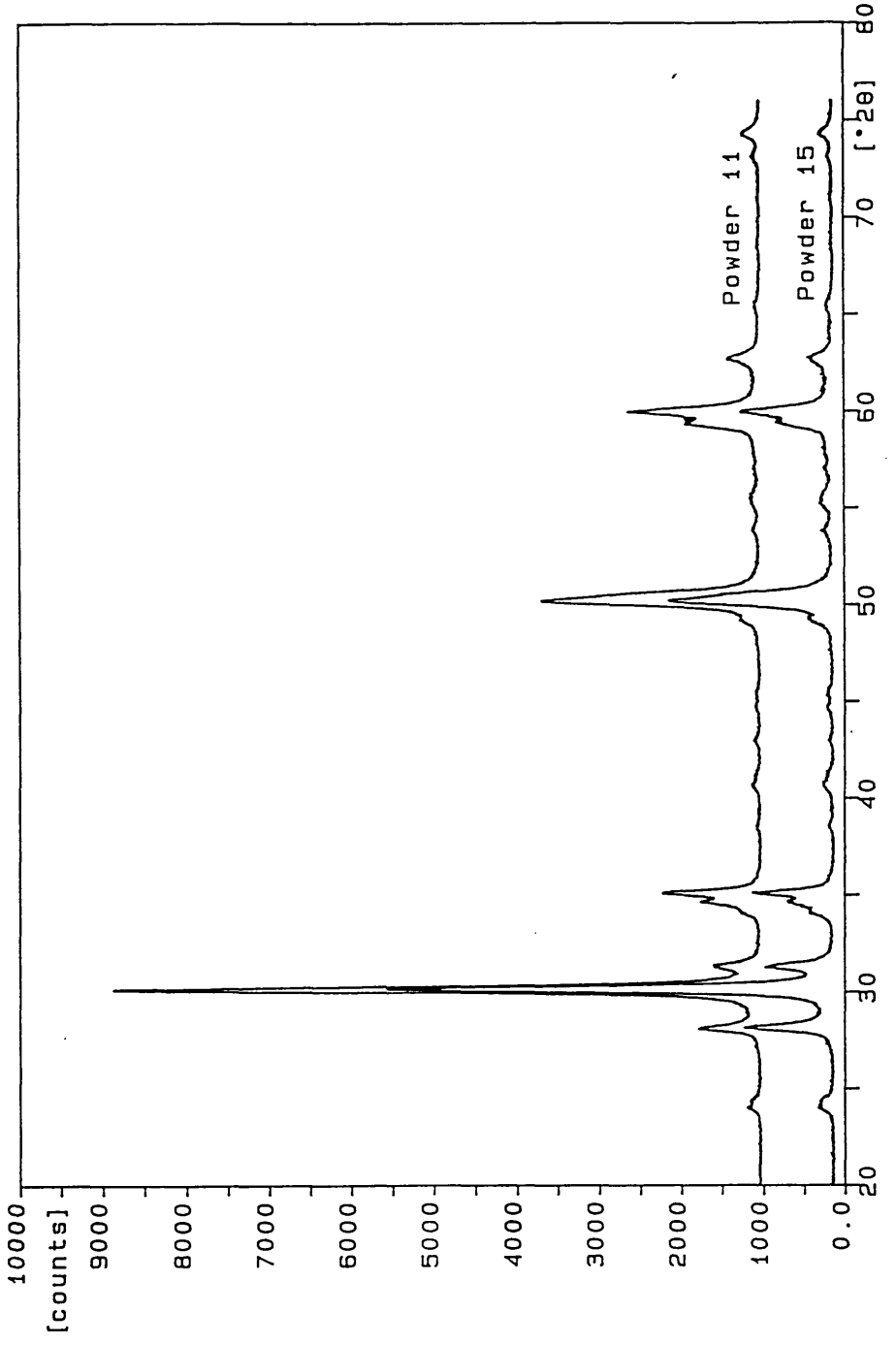

Figure 4.1.4.4 - X-ray powder diffraction trace.
(b) Alkoxide doped TZ3Y powder* (nominal 1% Al_2O_3 addition), compared to unmodified (as received) TZ3Y.
(* baseline shifted for clarity)

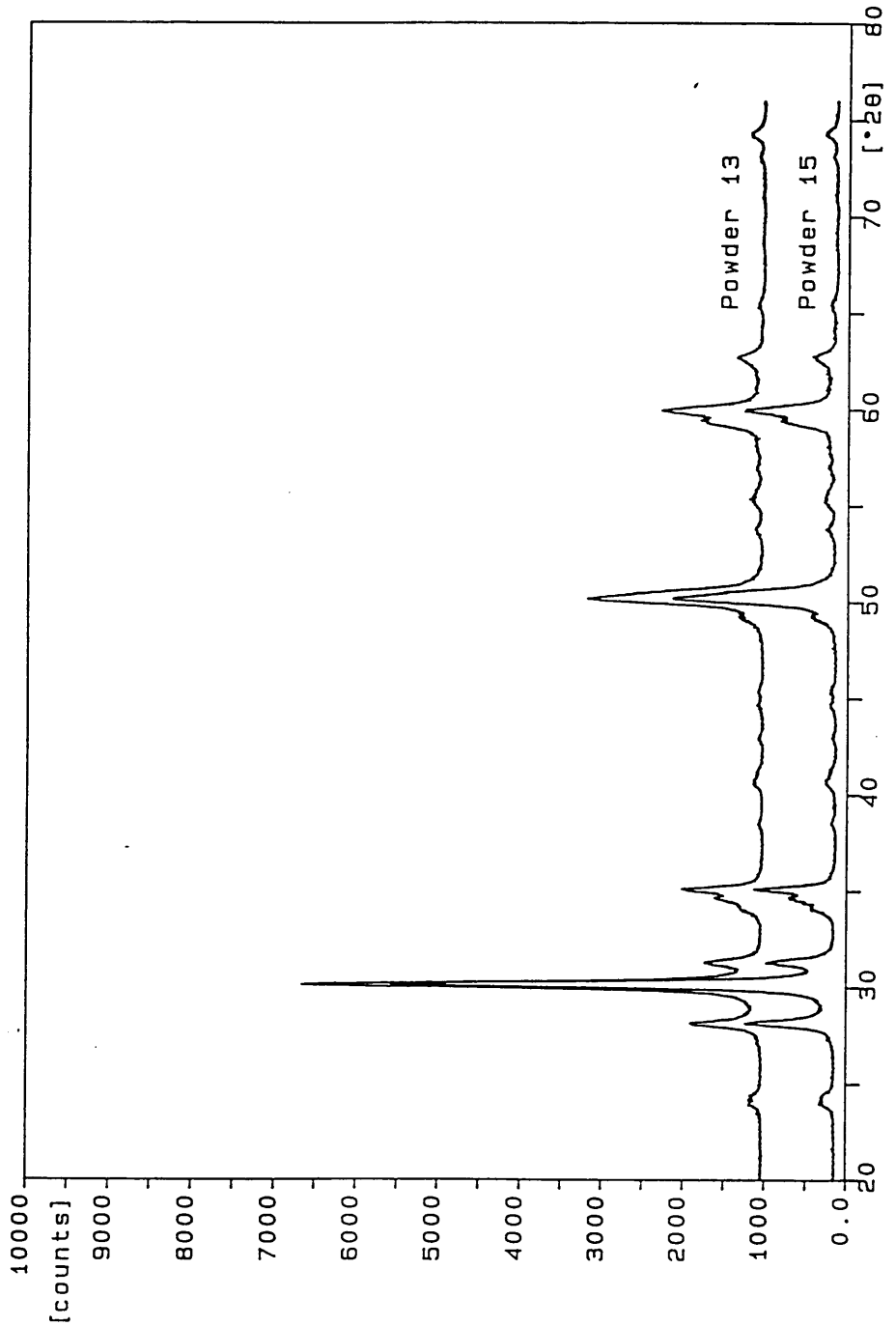

Figure 4.1.4.4 - X-ray powder diffraction trace.
(c) Alkoxide doped TZ3Y powder* (nominal 1% SiO_2 addition), compared to unmodified (as received) TZ3Y.
(* baseline shifted for clarity)

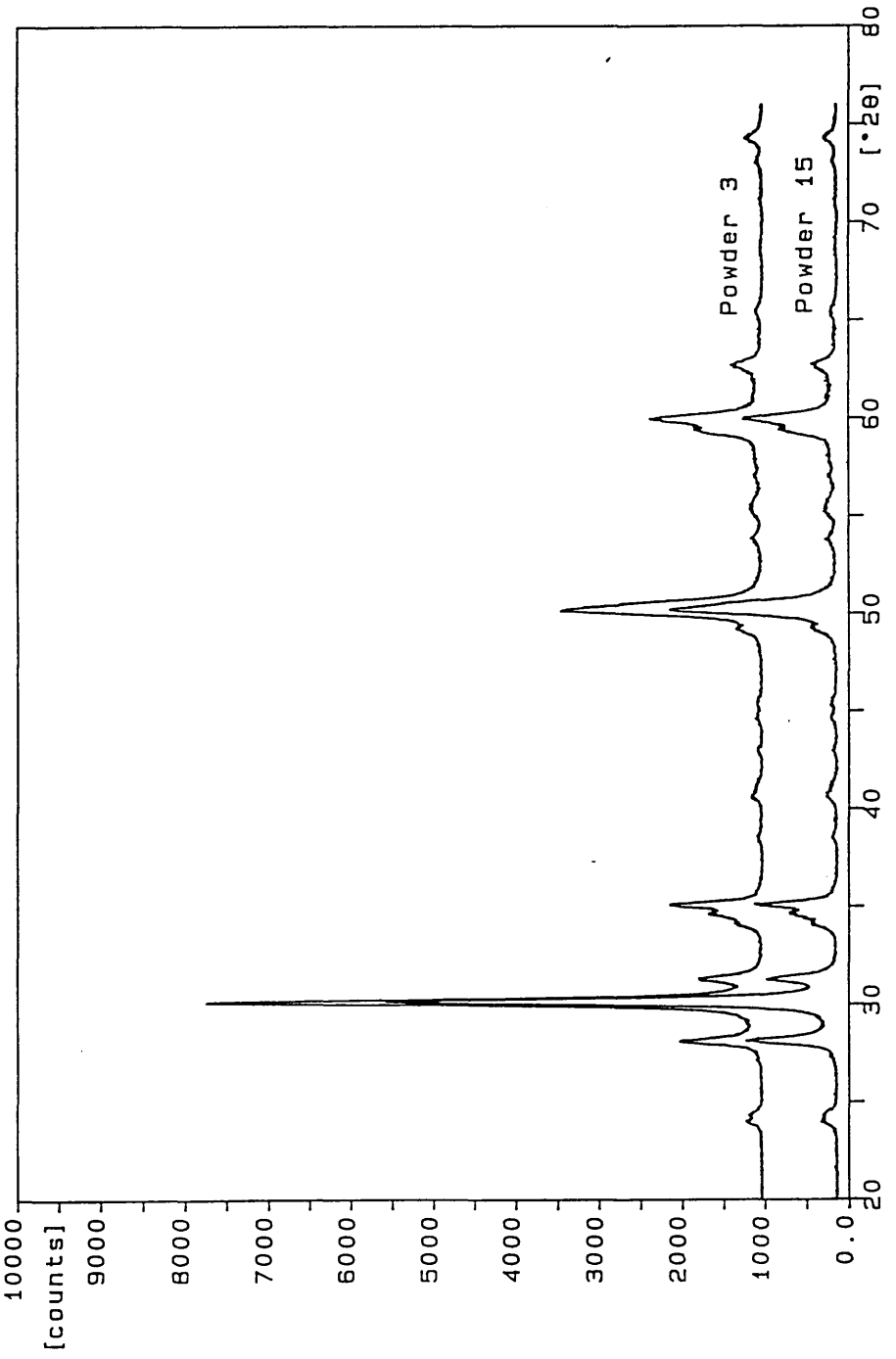

Figure 4.1.4.4 - X-ray powder diffraction trace.
(d) Alkoxide doped TZ3Y powder* (nominal 1% TiO_2 addition), compared to unmodified (as received) TZ3Y.
(* baseline shifted for clarity)

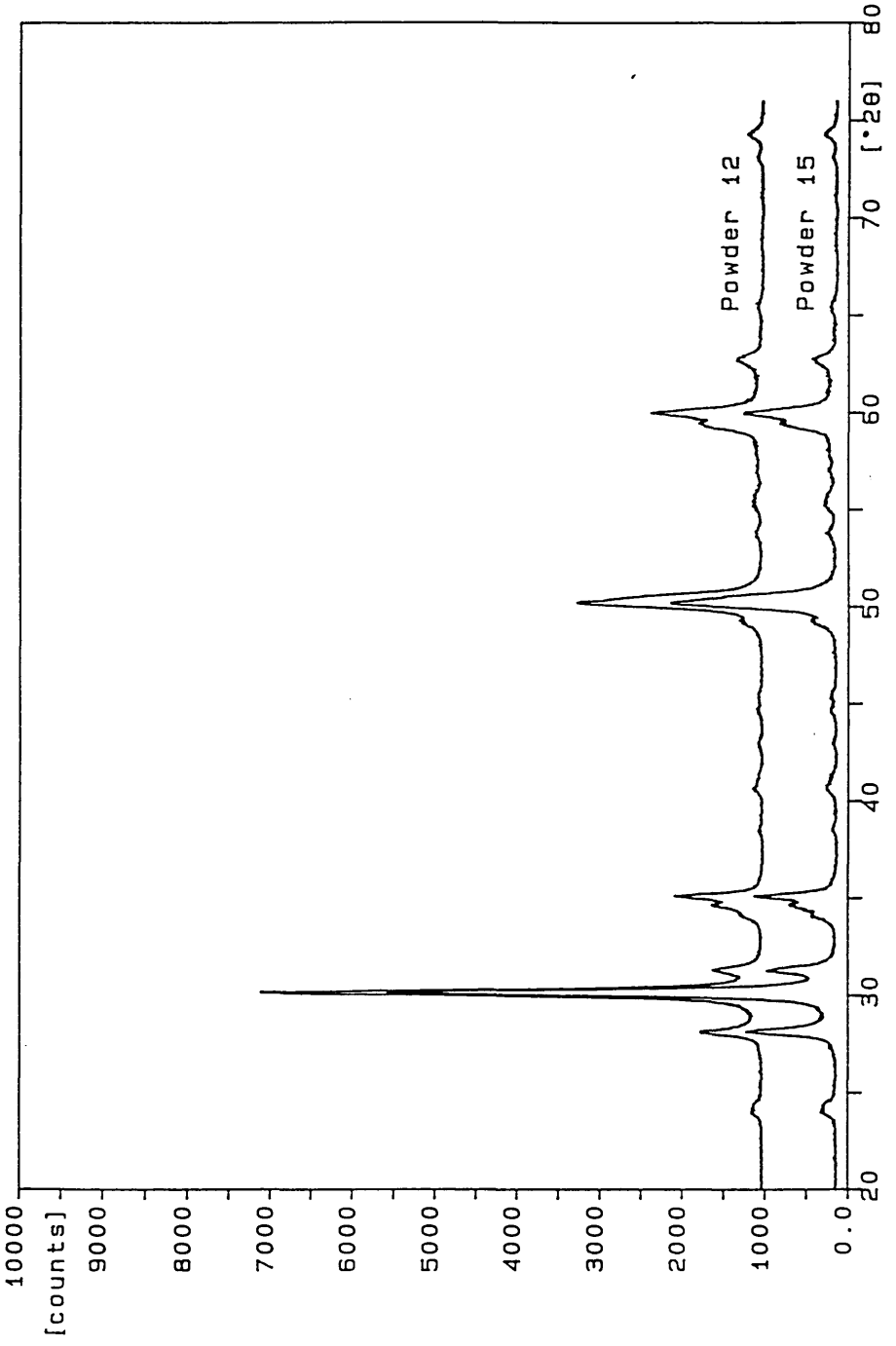

4.1.4.5 Determination of powder homogeneity.

The results of the E.D.X. dot mapping experiments carried out on the (alkoxide) doped powders are shown in figures 4.1.4.5 (a),(c) and (e).

These are compared with the results of similar analysis carried out on mechanically mixed powders in figures 4.1.4.5 (b), (d) and (f).

No concentrations, inclusions or inhomogeneities could be identified in the alkoxide doped powders other than signal noise effects, indicating that homogeneity was achieved in these samples.

Figure 4.1.4.5 (a)

Compositional X-ray dot map of alkoxide doped TZ3Y (with nominal 1% Al_2O_3 addition)

Unsintered, pressed pellet.

(i) Electron image of mapped area.

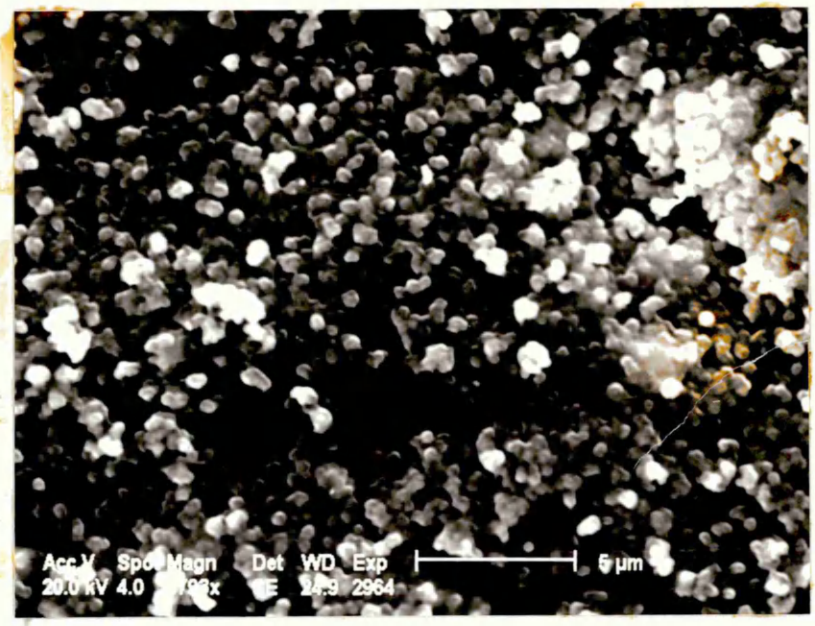

(ii) X-ray dot map

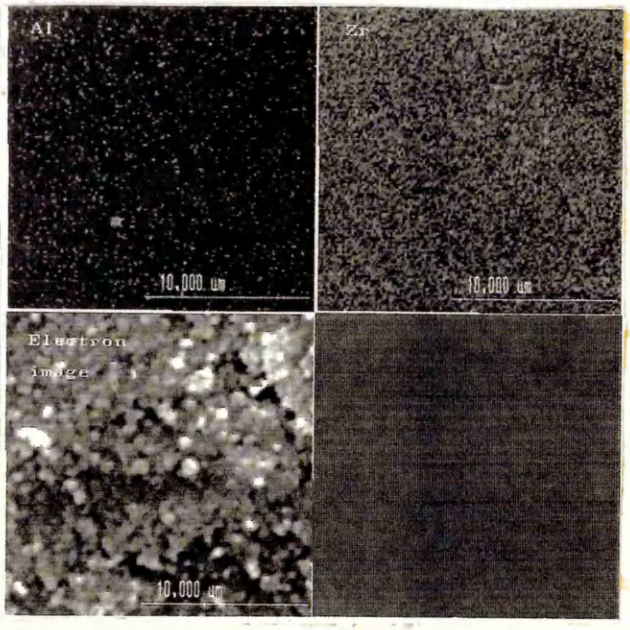

Figure 4.1.4.5 (b)

Compositional X-ray dot map of mechanically mixed TZ3Y with 1% Al_2O_3 (powder) addition.

Unsintered, pressed pellet.

(i) Electron image of mapped area.

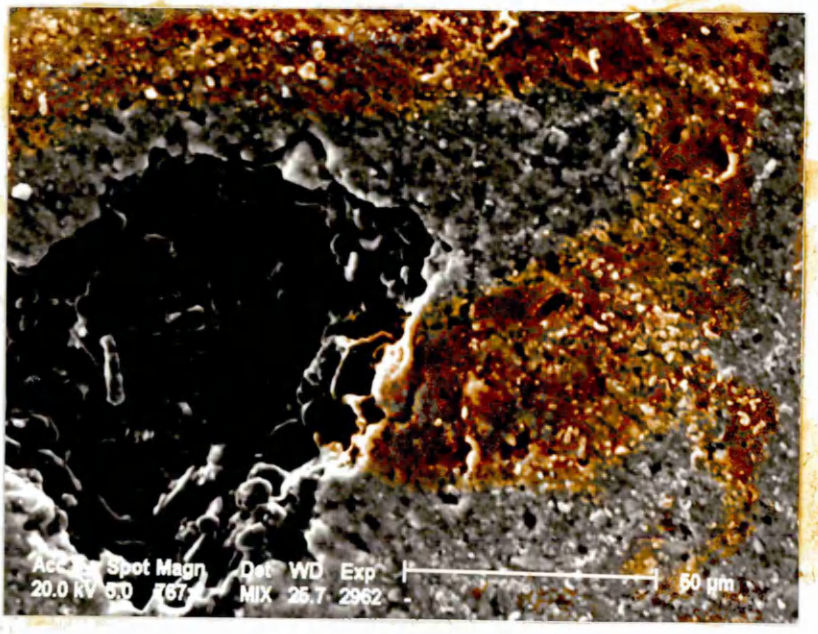

(ii) X-ray dot map

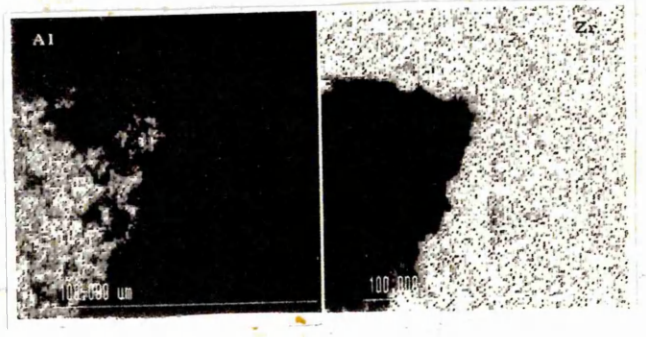

Figure 4.1.4.5 (c)

Compositional X-ray dot map of alkoxide doped TZ3Y (with nominal 1% SiO_2 addition)

Unsintered, pressed pellet.

(i) Electron image of mapped area.

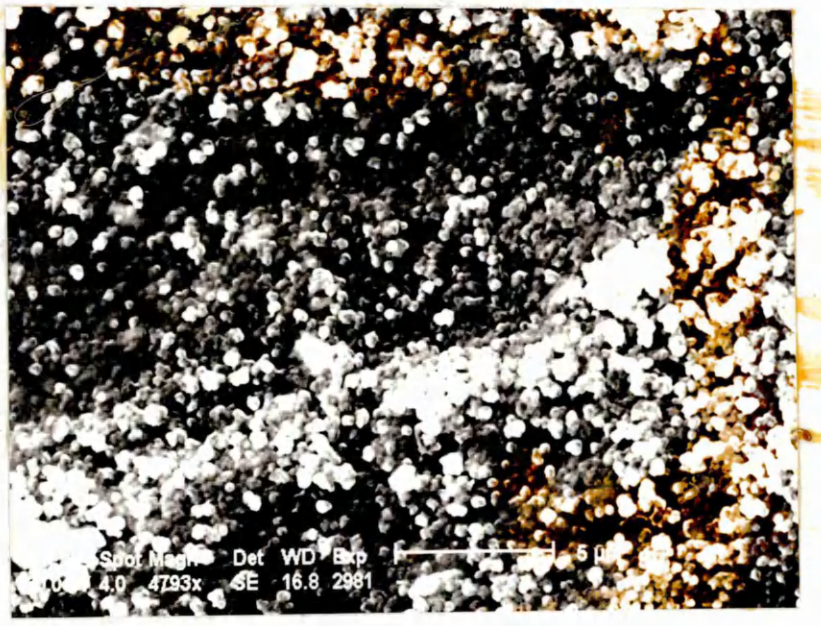

(ii) X-ray dot map

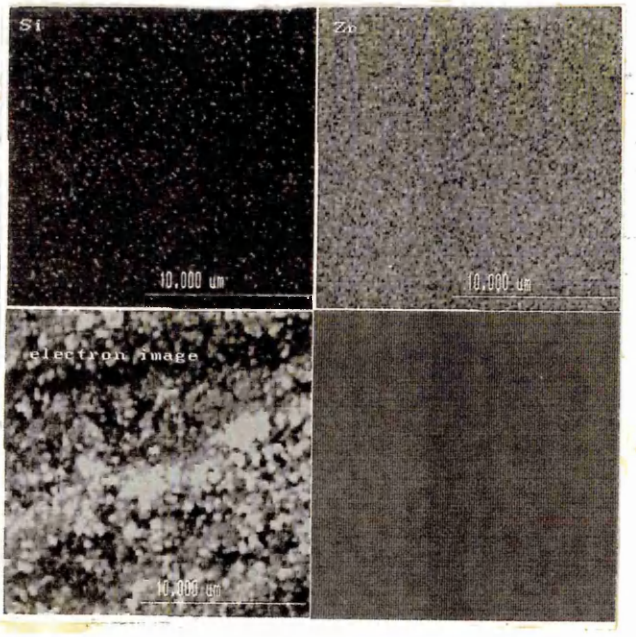

Figure 4.1.4.5 (d)

Compositional X-ray dot map of mechanically mixed TZ3Y with 1% SiO_2 (powder) addition.

Unsintered, pressed pellet.

(i) Electron image of mapped area.

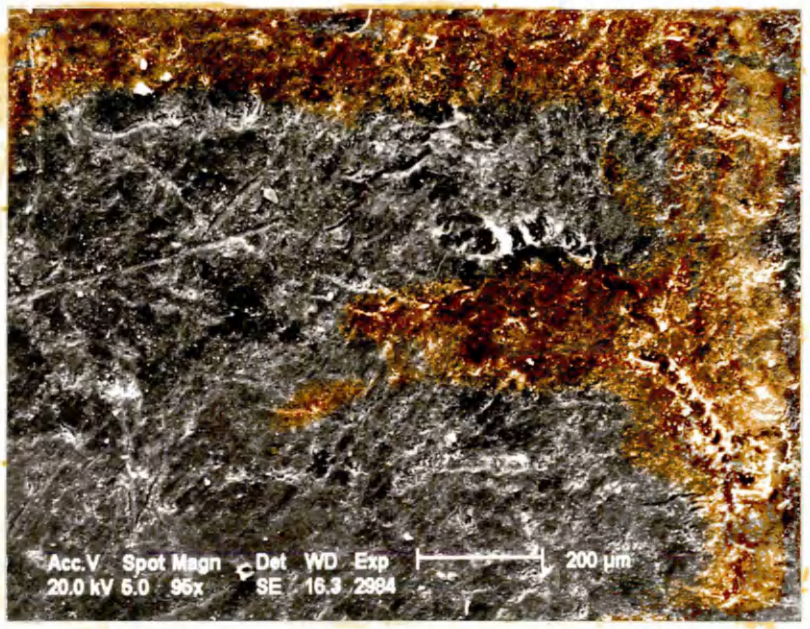

(ii) X-ray dot map

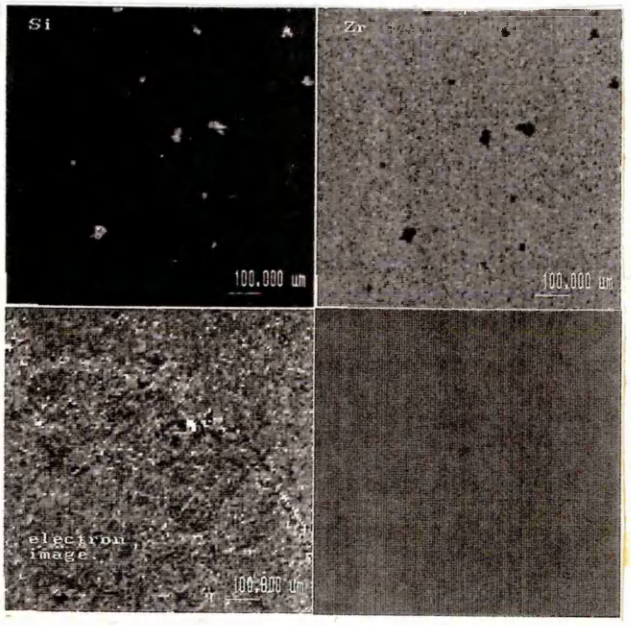

Figure 4.1.4.5 (e).

Compositional X-ray dot map of alkoxide doped TZ3Y (with nominal 1% TiO_2 addition)

Unsintered, pressed pellet.

(i) Electron image of mapped area.

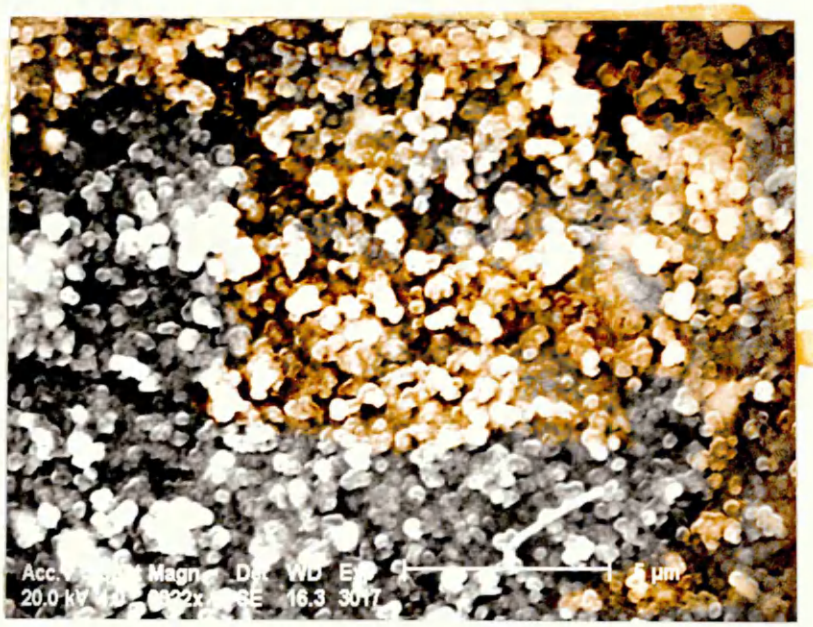

(ii) X-ray dot map

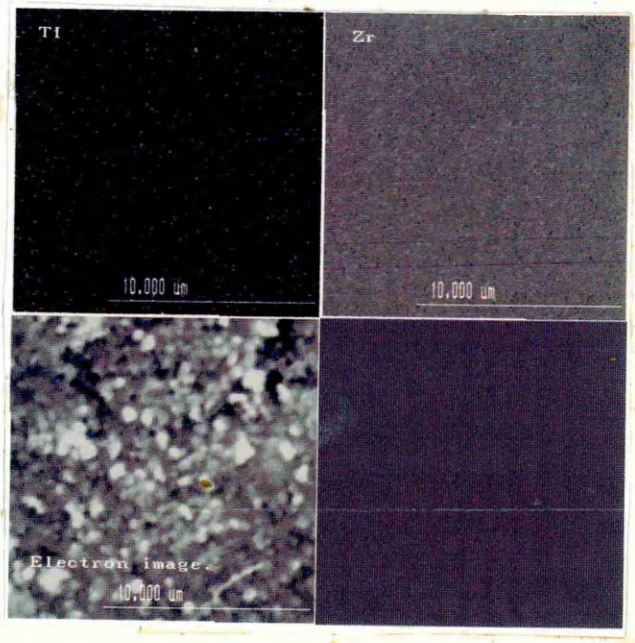

Figure 4.1.4.5 (f).
Compositional X-ray dot map of mechanically mixed TZ3Y with 1% TiO_2 (powder) addition.
Unsintered, pressed pellet.

(i) Electron image of mapped area.

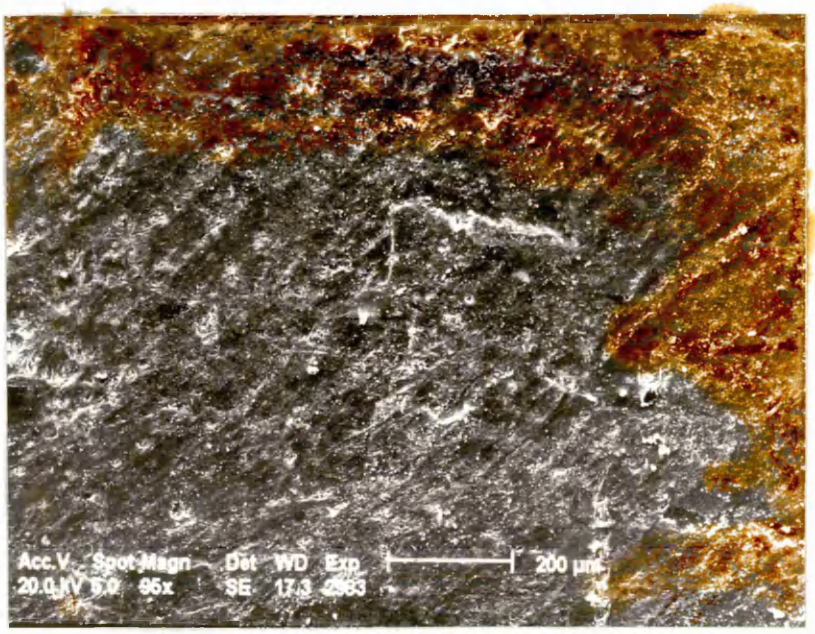

(ii) X-ray dot map

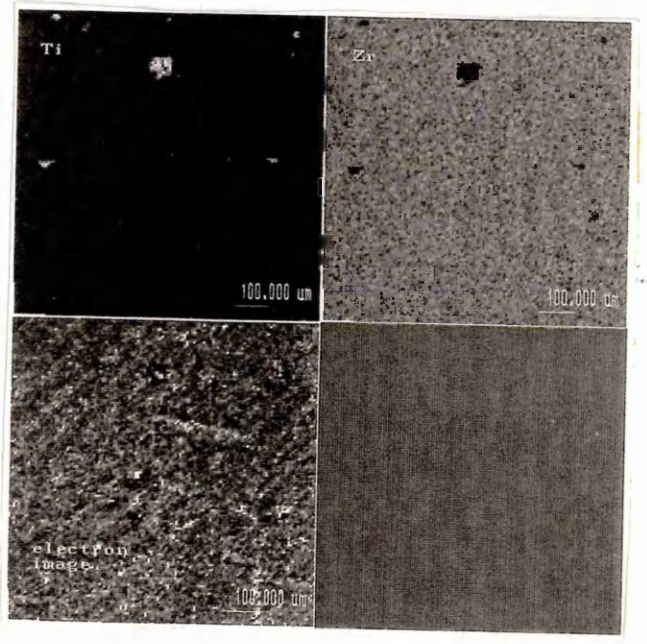

4.1.4.6 Analysis of doped powder compositions.

The results of the chemical analysis carried on the doped and undoped powder compositions are shown in table 4.1.4.6.

The samples were analysed for a wide range of potential oxide impurities. However the main impurities present were found to be Al_2O_3, SiO_2, and TiO_2 (the oxide dopants), Na_2O, and HfO_2, with smaller amounts of Fe_2O_3 and MgO.

The reproducibility of the analysis technique is claimed to be such that 1 standard deviation about the concentration value is approximately
$0.4 \times (\text{concentration in mass percent})^{1/2}$
Thus for any single result, the range of possible values representing the 95% confidence limits is given by the expression:
$1.96 \times 0.4 \times (\text{concentration in mass percent})^{1/2}$

Table 4.1.4.6

X.R.F. Chemical analysis results, doped and undoped powder compositions.

Powder	Nominal Dopant Addn. (mass%)			Analysis Results (Mass %)							
	Al_2O_3	SiO_2	TiO_2	ZrO_2	Y_2O_3	HfO_2	Al_2O_3	SiO_2	TiO_2	Na_2O	MgO
1	0.25	----	----	91.64	5.27	1.85	0.21	0:00	0.03	0.13	0.09
2	0.75	----	----	91.54	5.30	1.84	0.69	0.00	0.02	0.12	0.08
3	----	1.00	----	91.53	5.28	1.85	0.00	1.02	0.04	0.30	0.08
4	----	----	0.25	91.57	5.28	1.86	0.00	0.00	0.30	0.12	0.08
5	----	0.25	----	92.08	5.31	1.84	0.00	0.26	0.03	0.17	0.09
6	1.00	1.00	----	90.61	5.22	1.80	0.90	0.97	0.03	0.13	0.09
7	----	0.75	----	92.53	5.33	1.85	0.00	0.74	0.04	0.13	0.09
8	----	----	0.75	92.42	5.37	1.86	0.00	0.00	0.77	0.13	0.07
9	----	1.00	1.00	90.85	5.24	1.83	0.00	1.03	1.00	0.11	0.09
10	1.00	1.00	1.00	90.76	5.26	1.84	0.89	0.99	1.03	0.12	0.08
11	----	----	----	92.20	5.31	1.86	0.00	0.00	0.04	0.12	0.08
12	----	----	1.00	91.60	5.28	1.85	0.00	0.00	0.97	0.12	0.08
13	1.00	----	----	91.29	5.25	1.83	0.89	0.00	0.03	0.12	0.08
14	1.00	----	1.00	91.06	5.28	1.85	0.90	0.00	0.72	0.11	0.09
15	----	----	----	92.24	5.30	1.83	0.00	0.01	0.03	0.36	0.09
16	0.75	----	----	91.48	5.26	1.82	0.64	0.00	0.04	0.11	0.09
17	----	0.50	----	91.91	5.30	1.82	0.00	0.47	0.03	0.13	0.08
18	0.50	----	----	92.38	5.32	1.84	0.47	0.00	0.03	0.11	0.08
19	----	----	0.50	92.31	5.33	1.84	0.00	0.00	0.62	0.12	0.09
20	0.25	----	----	92.48	5.34	1.85	0.20	0.00	0.04	0.12	0.08

4.2 Sintering shrinkage results.

The results of the sintering shrinkage results on the doped and undoped powder compositions at various sintering temperatures are shown in the following sections.

4.2.1 Sources and estimation of experimental error

The main sources of experimental error and variation in these experiments were expected to be:

- Measuring errors in the micrometer readings.
- Errors arising from the doping process, e.g. variable yield of reaction, changes to other physical parameters.
- Errors arising during the fabrication and sintering stages. e.g. variations in green density, temperature gradients in furnace.

The results given for the shrinkage measurements include three estimates of error, as follows:-

(a) The first error estimate is a measure of the error present in the shrinkage measurement (ie the measuring error), which was thought to arise from the limited accuracy of the measurement technique used.

The measuring error was calculated from the standard error in the mean of the 10 diameters measured for each pellet, with the 95% confidence limits for the mean being used as an estimate of the measuring error.

These were calculated using the formula:

$$\text{95\% confidence limits} = \text{+ or - } 1.96 \times \text{(standard error)}$$
$$\text{(around mean value)}$$

where:

$$\text{standard error} = \frac{\text{standard deviation of results}}{(\text{no. of measurements})^{1/2}}$$

The measuring error was calculated separately for the undoped, alumina, silica, titania and multiple doped specimens, and an overall average value for all specimens taken (see table 4.2.1(a) - appendix 1).

It was thought that this measure of error would produce an underestimate of the true value, since it is an estimate of error in the measurements only, and does not account for errors arising from the doping process, specimen fabrication or heat treatment.

(b) A second figure for the experimental error was generated by fabricating a duplicate series of pellets from two of the doped powders, and recording the discrepancies between the shrinkage values recorded between the original and duplicate pellets.

The difference between the two sets of values was taken as a measure of error present in the experiment.

The mean difference value between the original and duplicate experiments at equivalent temperatures was calculated, together with the standard deviation of the differences.

The error in the experiment (after powder doping stage) was then estimated from the 95% upper confidence limit of the mean experimental error as follows:

e.g.

experimental error	=	mean difference between original and duplicate specimens.	+ 1.96 x	std. error in the difference values.

This gave a value of plus or minus 0.43% shrinkage. The results and calculations used to generate this estimate of error are shown in table 4.2.1(b) (appendix 1).

An assumption was made that the mean error recorded in the samples tested was representative of the error in the experiment as a whole (evidence for the validity of this assumption is offered by the similar errors recorded between the different doped powders).

However, it was thought that this estimate of experimental error might also underestimate the total error present in the experiment as it does not account for errors (or variability) introduced during the doping process.

The above estimate of error also assumes that the experimental error was similar between samples sintered at all sintering temperatures. In reality, this assumption was probably an over-simplification, since the errors in the samples sintered at high and low temperatures (where properties were varying rapidly with dopant level and temperature) were greater than the errors at intermediate sintering temperatures (typically 1350-1650°C)

(c) A third figure for experimental error was estimated, similarly to the above, but using pellets fabricated from separate batches of doped powders (alumina doped powders of composition 0.25 and 0.75%). These powders and pellets were produced separately to the other samples. This estimate should account for the error present in the entire experiment. However, as the duplicate powder batches were produced and sintered separately to the main batch of doped powders, it is probable that the differences measured between these and the original powders will be greater than the actual errors present in the main experiment which was carried out as a single batch.

The estimate of error by this method was approximately plus or minus 0.6%. This magnitude of error is significant when compared to the differences recorded between samples, particularly for samples approaching their maximum density, and makes it difficult to draw clear conclusions from the shrinkage measurements alone.

The calculated and estimated values of experimental error show an increase in estimated error between the three methods.

There is a relatively large increase in error between the measuring error (a), and the estimated error from duplicate pellets by method (b). This suggests that the measuring error makes a relatively small contribution to the overall experimental error, with a larger

contribution arising from variability introduced during pressing and sintering of the pellets.

The estimated error also shows a small increase between methods (b) (ignoring the doping process) and (c) (accounting for variability from the doping process).

This suggests that the doping process is introducing an additional source of error into the experiments but that this is relatively small compared to the errors arising from other sources.

4.2.2 Shrinkage results - undoped specimens.

The shrinkage results of the unmodified TZ3Y powder as supplied from TOSOH, were compared with the same powder which had undergone the doping process, but with no dopant additions actually made (the blank treatment).

The results of the shrinkage measurements on the undoped powders are shown in tables 4.2.2 (a) and (b) (appendix 1) and illustrated in figure 4.2.2. These tables show the range and spread of the data observed from each specimen and have been shown in full.

The majority of the shrinkage recorded for the undoped specimens took place between a sintering temperature of 950 and 1350°C, with the maximum shrinkage being recorded at a sintering temperature of 1450-1550°C.

The overall profile of the curves is virtually identical for the two materials, and the differences recorded between the undoped and blank treated specimens lie within the range of possible experimental error.

Figure 4.2.2
Effect of sintering temperature on shrinkage of undoped specimens.

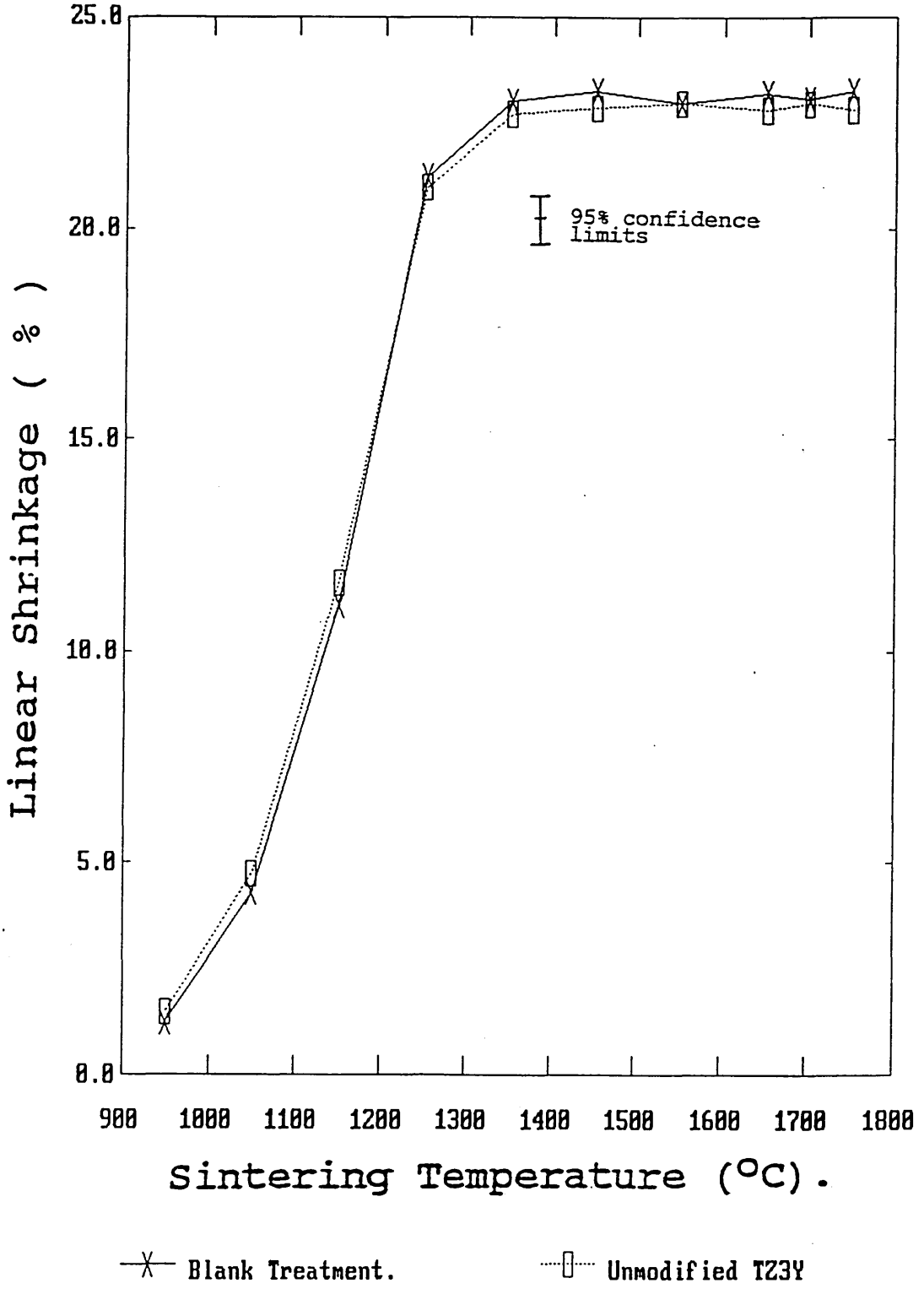

4.2.3 Sintering shrinkage - alumina doped samples.

The shrinkage results for the alumina doped samples are tabulated in table 4.2.3 (appendix 1).

Figure 4.2.3(a) shows the effect of sintering temperature on the shrinkage of the alumina doped samples.

The majority of the shrinkage recorded for the alumina doped samples took place at sintering temperatures between 950 and 1250° C, with the maximum shrinkage occurring at approximately 1350°C.

Figures 4.2.3(b)-(d) show the effect of alumina content on the shrinkage of the doped samples. The behaviour appears to fall into three distinct regions.

For lower sintering temperatures, the alumina content appears to produce a marked increase in shrinkage. This is most pronounced for the 1050 and 1150°C sintered samples between 0 and 0.25% alumina addition. A similar effect also appears to take place for the 1250°C sintered sample, although the magnitude of this effect is within the limit of possible experimental error (figure 4.2.3(b)).

For sintering temperatures between 1350 and 1650°C, additions of alumina appear to have little or no effect over the 0-1 weight % level (figure 4.2.3 (c)).

For sintering temperatures in excess of 1650°C, alumina additions show a large effect on the shrinkage behaviour, with a large decrease in shrinkage being recorded for between 0.25% and 0.5 mass % additions of alumina (figure 4.2.3(d)).

Figure 4.2.3 (a) Effect of sintering temperature on shrinkage of alumina doped specimens.

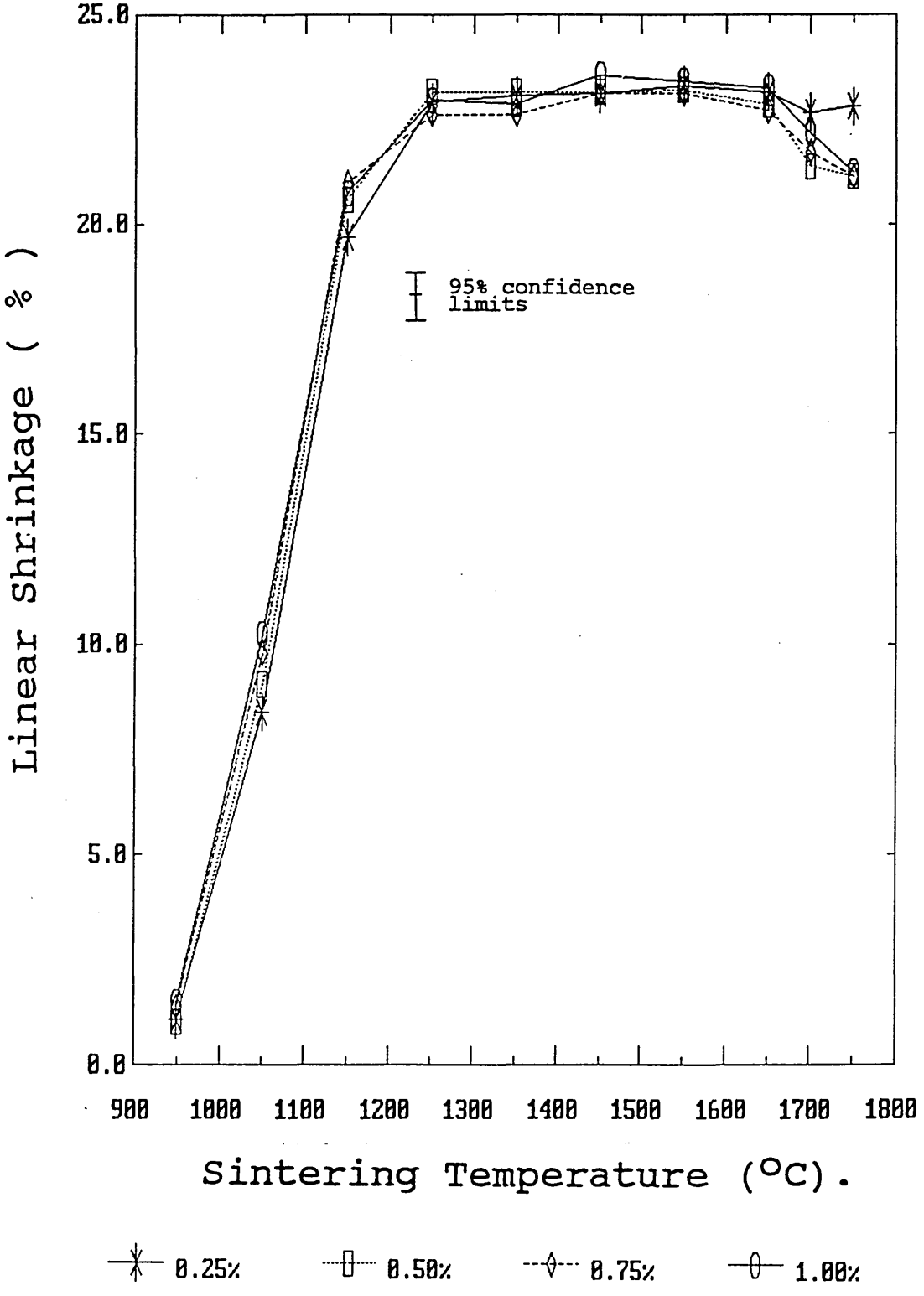

Figure 4.2.3 (b) Effect of alumina dopant addition on shrinkage for 1050 - 1250°C sintering temperature.

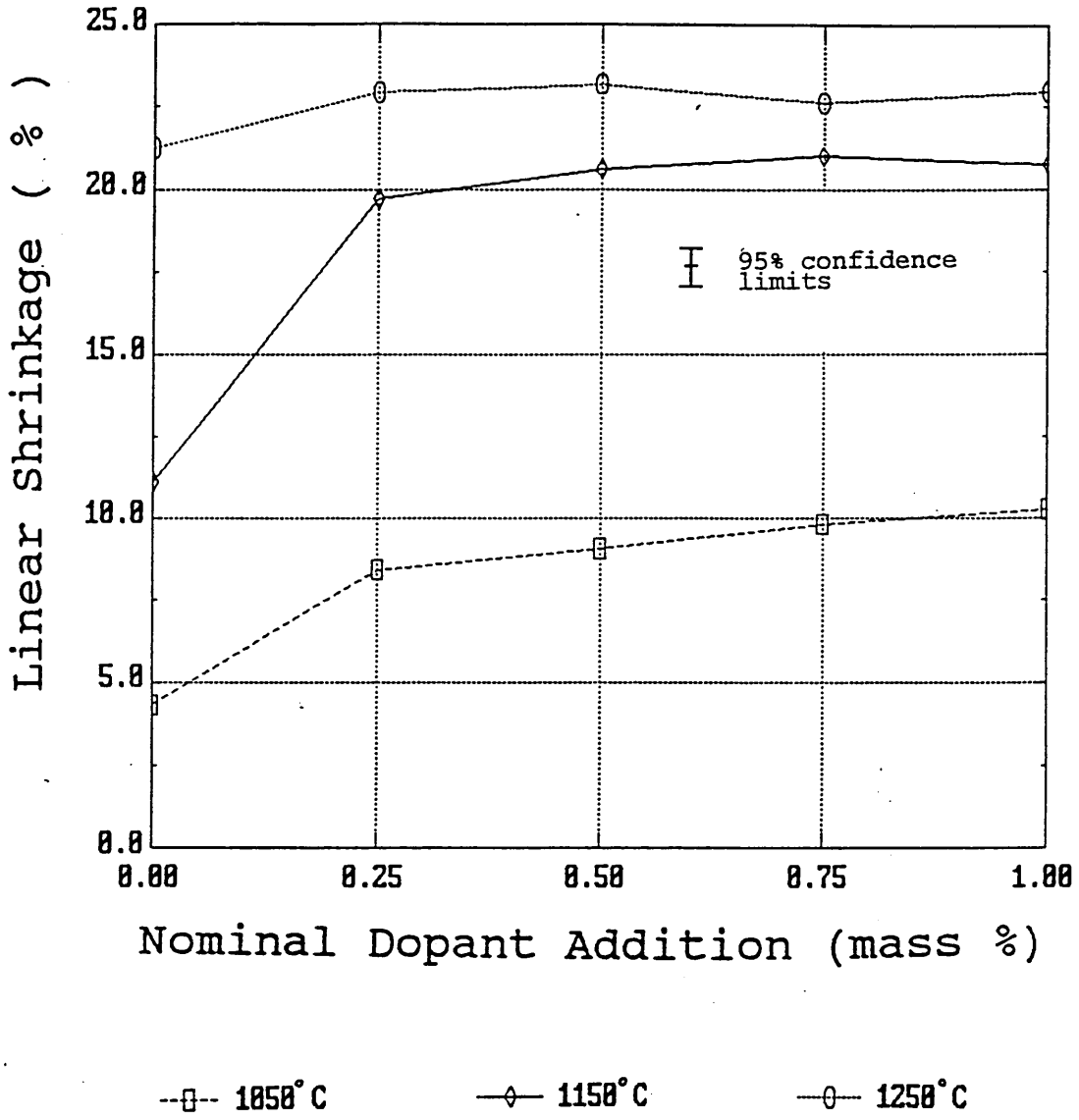

Figure 4.2.3 (c) Effect of alumina dopant addition on shrinkage for 1350-1650°C sintering temperature.

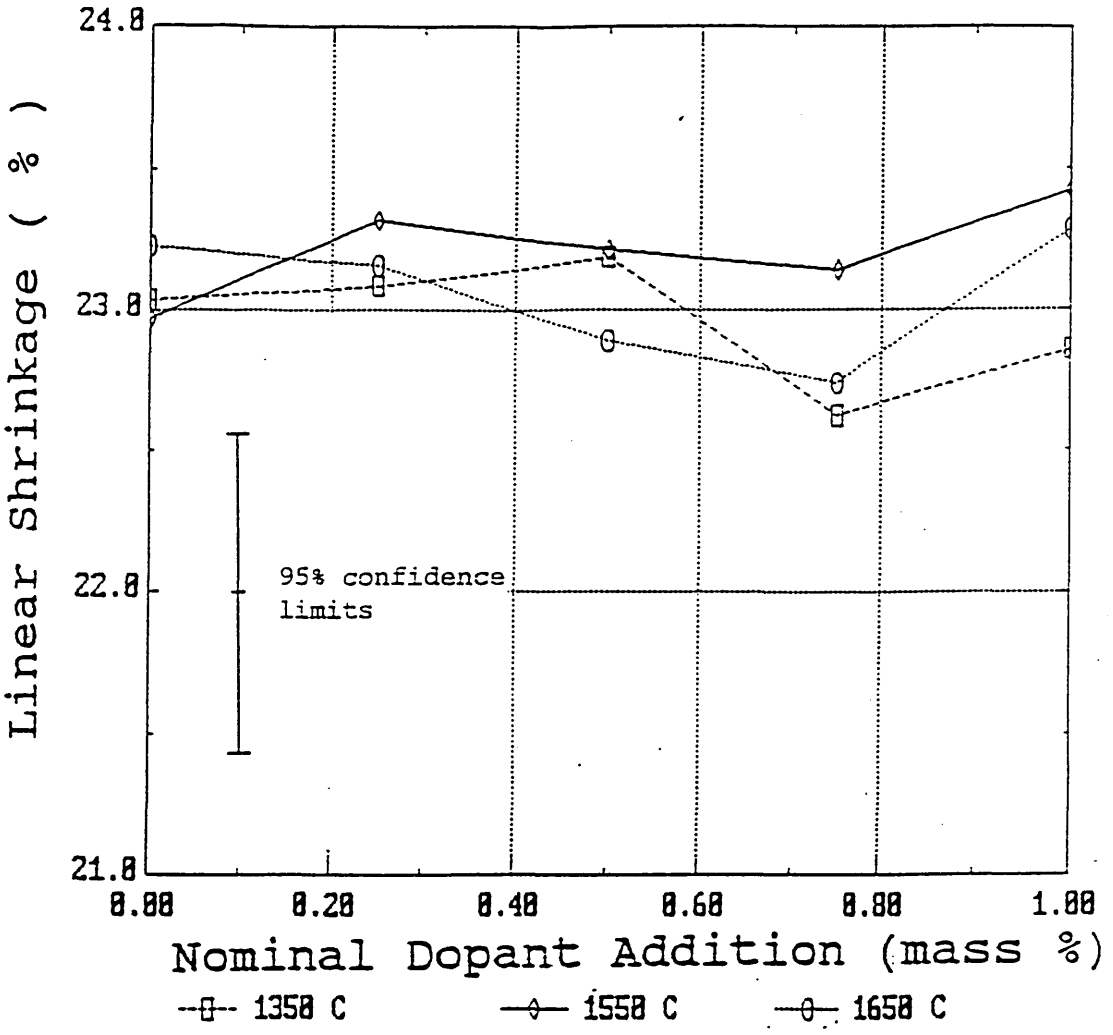

Figure 4.2.3 (d) Effect of alumina dopant addition on shrinkage for sintering temperatures in excess of 1650°C.

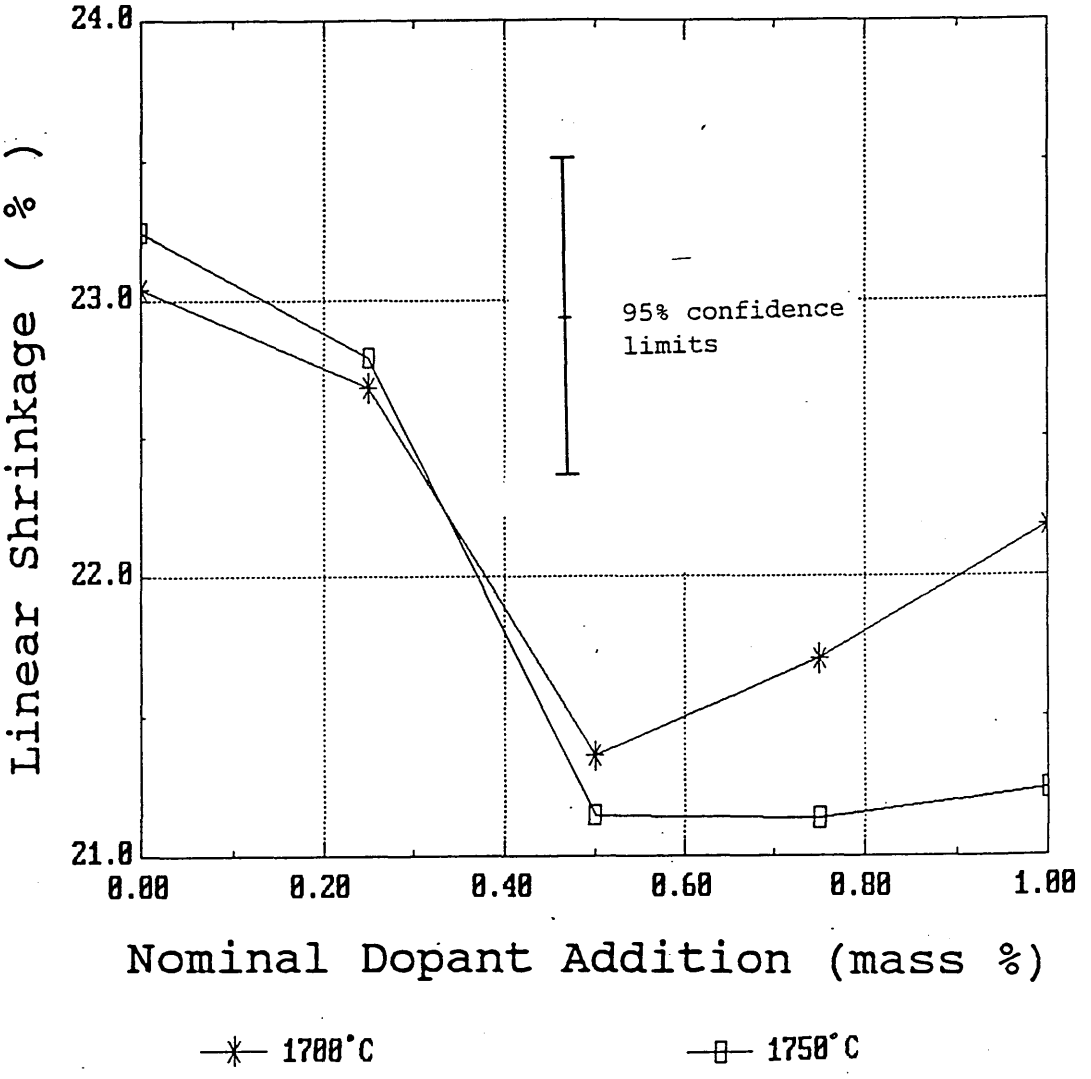

4.2.4 - Shrinkage results - silica doped samples.

The shrinkage results for the silica doped samples are tabulated in table 4.2.4 (appendix 1).

The majority of the shrinkage recorded for the silica doped samples took place at sintering temperatures between 950 and 1250° C, with the maximum shrinkage occurring at approximately 1350°C.

The 0.75% silica addition appears to give consistent, but anomalous results (this is confirmed in other experiments).

The effect of the remaining silica additions on the shrinkage over the range of temperatures investigated is shown in figure 4.2.4(b)-(d).

The shrinkage results (figure 4.2.4 (a)) appear to show that for higher sintering temperatures the sintering shrinkage is reduced with silica additions compared to the blank treated specimen. With little difference between the behaviour of the material at the 0.25,0.5 and 1% addition level.

Closer inspection of the results, plotting the % silica addition against shrinkage does appear to suggest that there are consistent trends in the behaviour of the doped specimens.

At lower sintering temperatures, ie 1350° or less, the 0.25% silica additions appear to promote increased shrinkage. This is particularly pronounced at 1150°C where the shrinkage is shown to be greatest for the 0.25% addition of silica, and to gradually decrease with increasing silica content (see figures 4.2.4 (b) and (c)).

At higher sintering temperatures, the specimens all appear to undergo similar behaviour, showing a slight decrease in shrinkage with increasing silica addition. The magnitude of the decrease in shrinkage recorded between different silica contents is within the range of

estimated experimental error, however the consistency of the effect across all the sintering temperatures and addition levels suggests that the trend may be significant (see figure 4.2.4 (d)).

Figure 4.2.4 (a) Effect of sintering temperature on shrinkage of silica doped specimens.

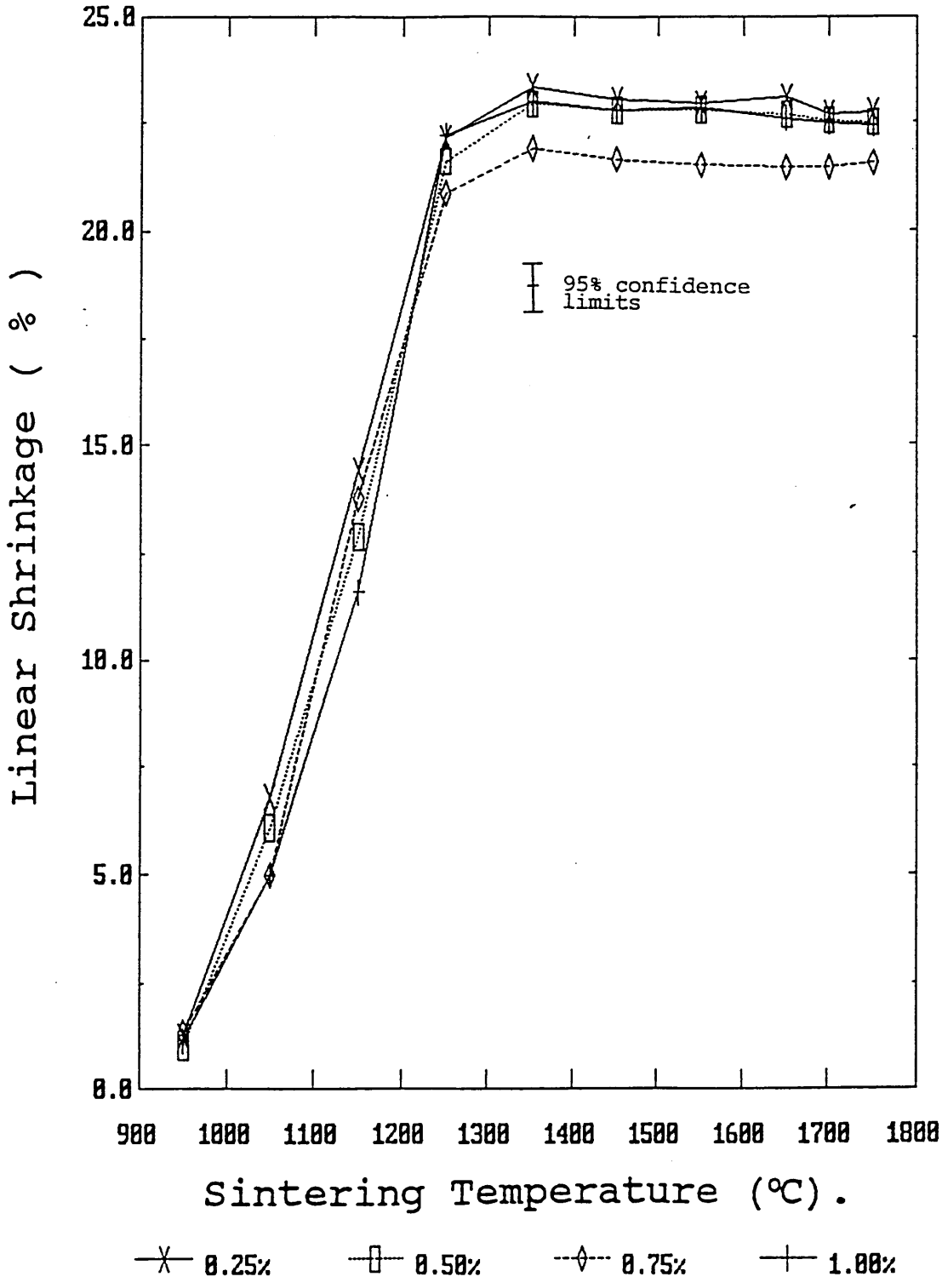

Figure 4.2.4 (b) Effect of silica dopant addition on shrinkage for 1050 - 1150°C sintering temperature.

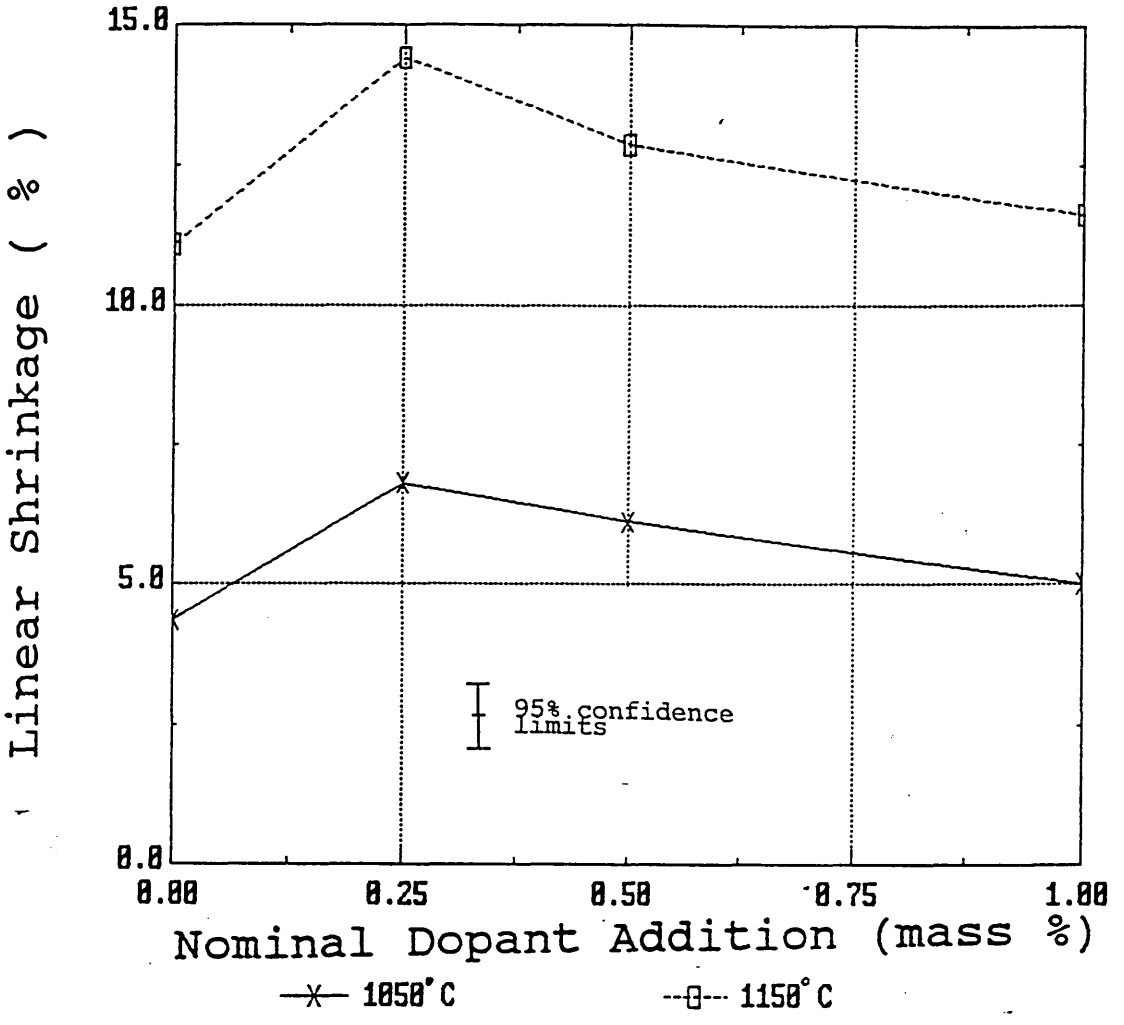

Figure 4.2.4 (c) Effect of silica dopant addition on shrinkage for 1250 - 1350°C sintering temperature.

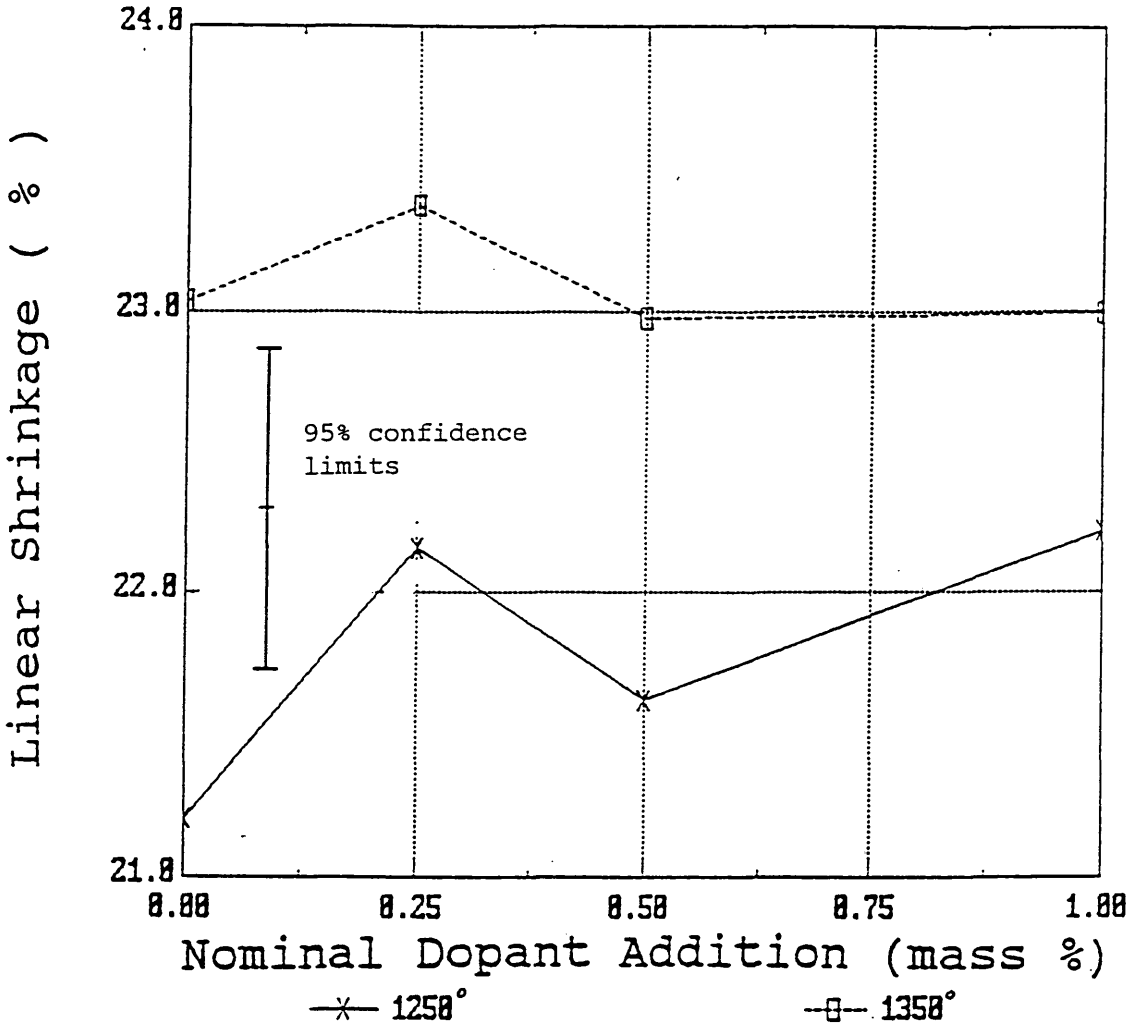

Figure 4.2.4 (d) Effect of silica dopant addition on shrinkage for sintering temperatures in excess of 1450°C.

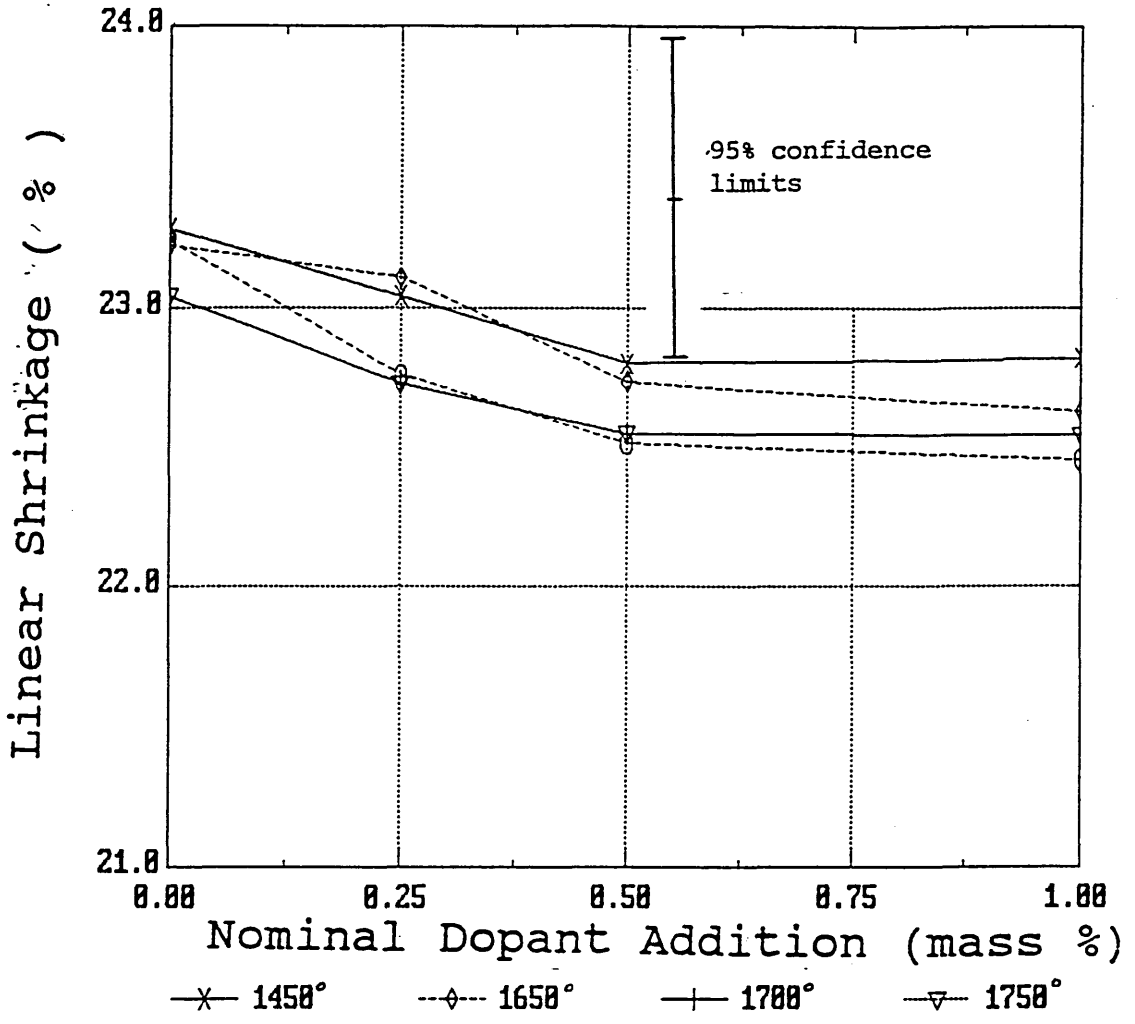

4.2.5 Sintering shrinkage - titania doped samples.

The shrinkage results for the titania doped samples are tabulated in table 4.2.5 (appendix 1).

The majority of the shrinkage recorded for the titania doped samples took place at sintering temperatures between 950 and 1350°C, with the maximum shrinkage occurring at approximately 1550°C (figure 4.2.5 (a)).

Figures 4.2.5 (b)-(c) show the effect of TiO_2 content on the shrinkage for a range of sintering temperatures. The behaviour appears to fall into two types, with the change in behaviour occurring for a sintering temperature of approximately 1350°C.

For sintering temperatures up to 1250°C, the shrinkage decreases with increasing titania addition. This effect appears to continue (to a lesser degree) for the 1350°C sintered material, although the magnitude of the decrease lies within the range of possible experimental error in this case (figure 4.2.5 (b)).

For sintering temperatures in excess of 1350°C, the shrinkage appears to be independent of titania addition (figure 4.2.5 (c)).

Figure 4.2.5 (a) Effect of sintering temperature on Shrinkage of titanium oxide doped specimens.

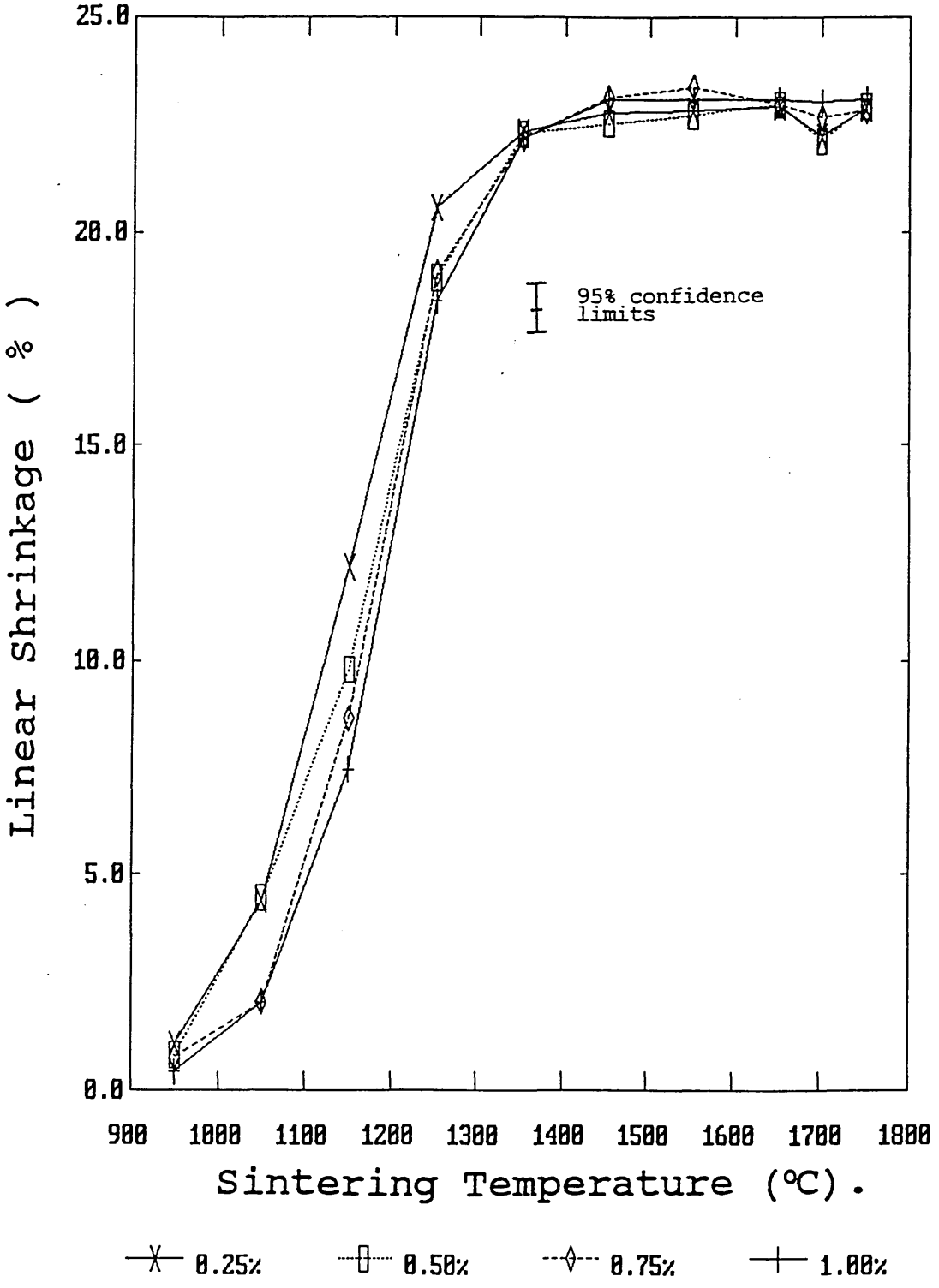

Figure 4.2.5 (b) Effect of titanium oxide dopant addition on shrinkage for sintering temperatures up to 1350°C.

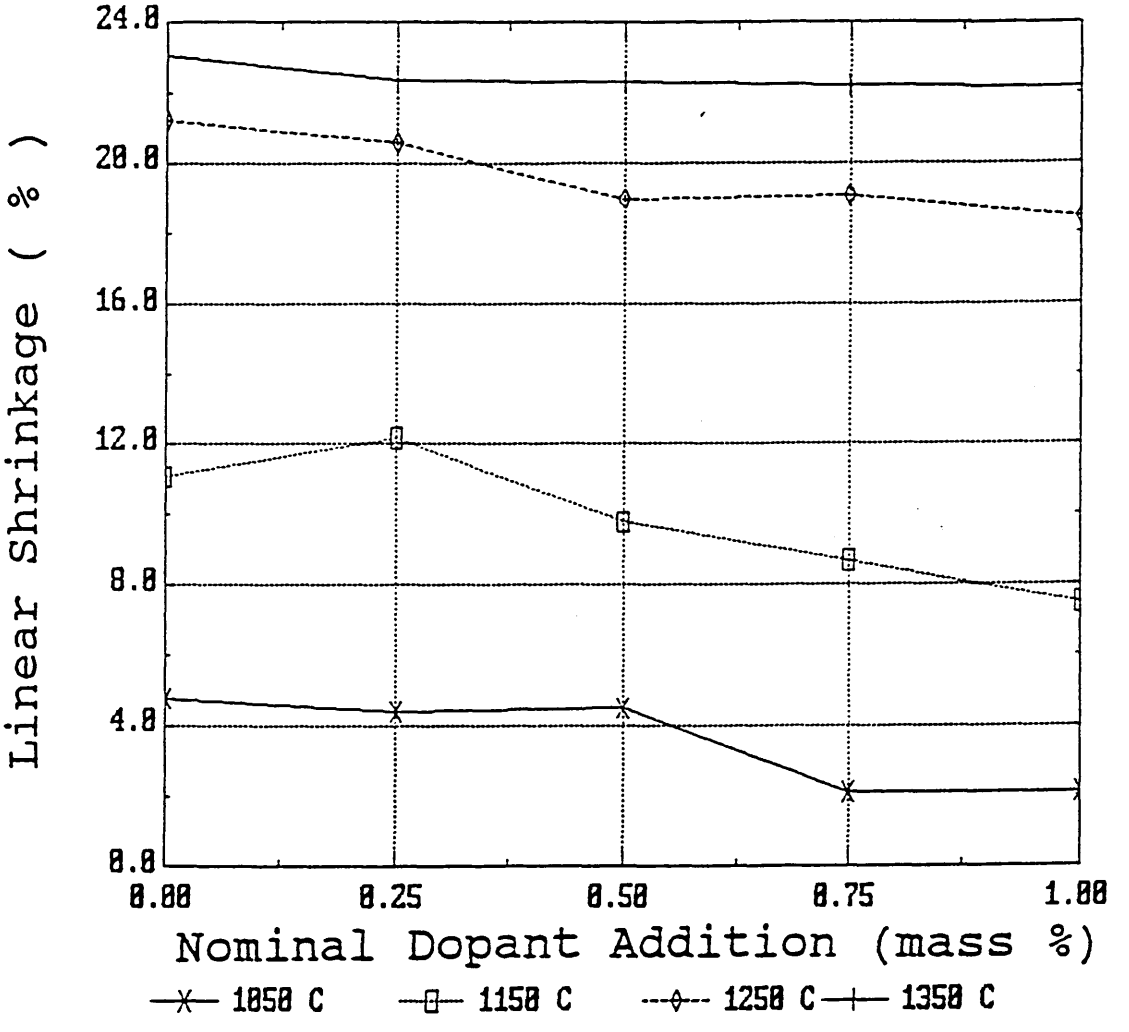

Figure 4.2.5 (c) Effect of titanium oxide dopant addition on shrinkage for sintering temperatures of 1350°C and above.

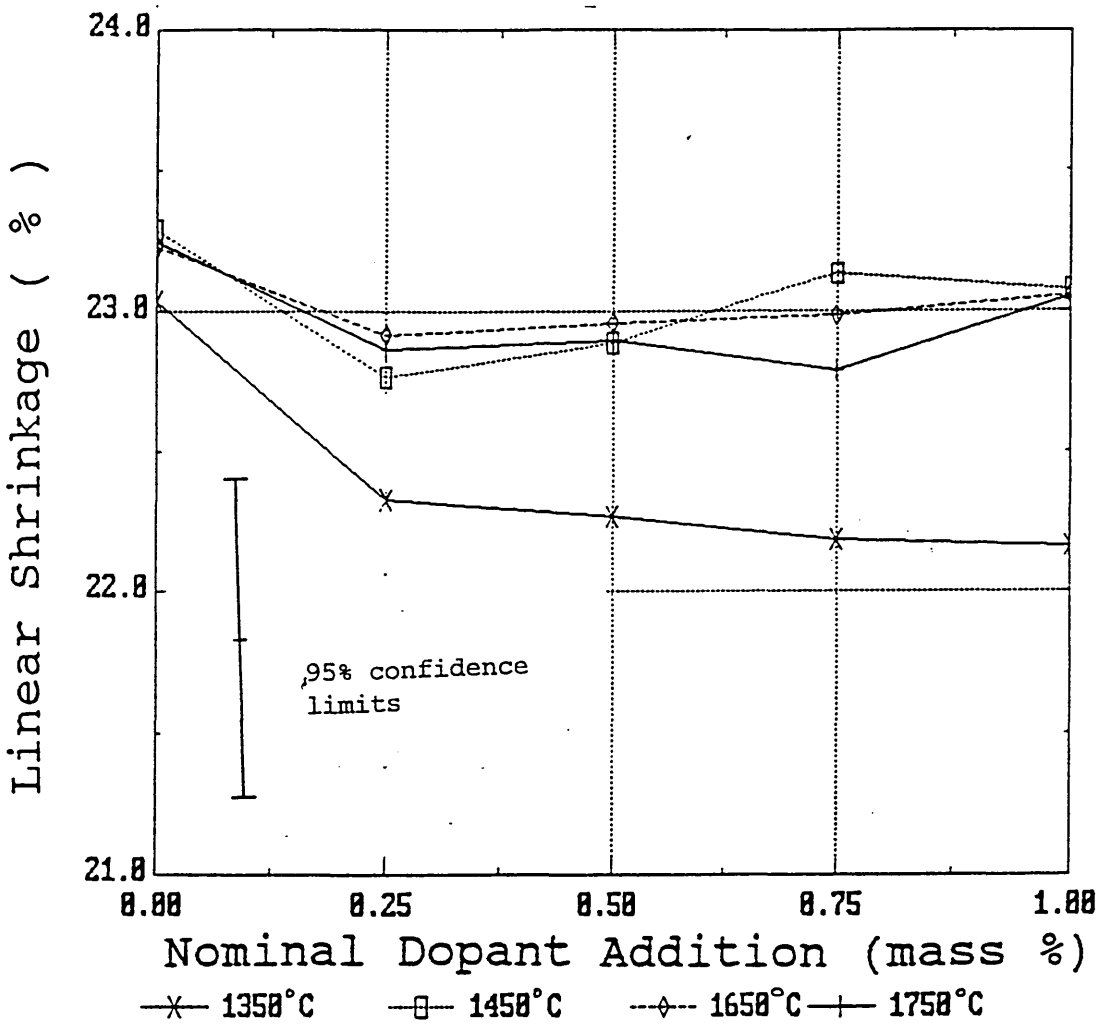

4.2.6 Multiple doped samples.

The shrinkage results for the samples containing multiple oxide dopant additions are shown in table 4.2.6 (appendix 1), with the results illustrated graphically in figure 4.2.6.

These results appear to show that samples containing silica and alumina in combination (ie the SiO_2 with Al_2O_3, and the Al_2O_3 with TiO_2 and SiO_2 undergo the majority of shrinkage at a reduced sintering temperature of between 950 and 1150°C compared to the other doped powders, whilst the SiO_2 with TiO_2 and the Al_2O_3 with TiO_2, containing samples undergo the majority of shrinkage for sintering temperatures between 950 and 1350°C.

The samples containing Al_2O_3 with SiO_2 also appear to show a slight reduction in shrinkage with increasing sintering temperature above 1250°C, although this is within the limits of experimental error for the shrinkage determination.

All of the samples containing alumina show a marked reduction in shrinkage with increasing sintering temperatures above 1650°C, whilst this was not apparent in the SiO_2 with TiO_2 doped specimens.

Figure 4.2.6 Effect of sintering temperature on shrinkage of multiple doped specimens.

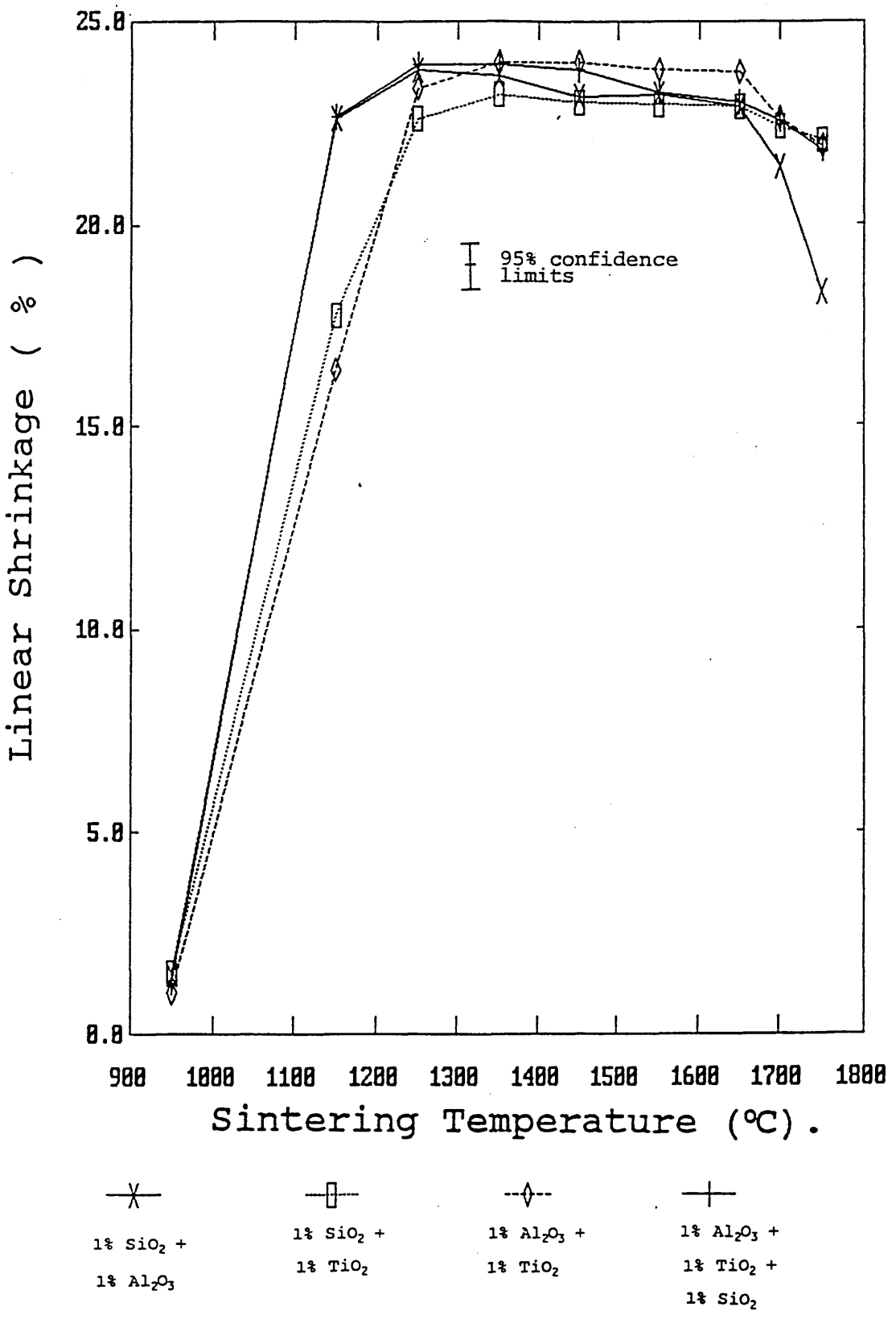

4.2.7 Mechanically mixed specimens.

The shrinkage results for the doped powders produced by mechanically mixing the TZ3Y and dopant powders are shown in table 4.2.7 (appendix 1), with the effect of sintering temperature on the shrinkage of these samples being shown, and compared with the behaviour of the undoped TZ3Y material (as supplied) in figure 4.2.7 (a).
The results show a similar trend to the alkoxide doped specimens with silica addition producing enhanced densification at low temperatures (particularly pronounced at 1150°C), and alumina additions giving decreased shrinkage for high sintering temperatures (1750°C). All dopant additions resulted in a lower value for the maximum shrinkage compared to the undoped material.

The main differences between the mechanically mixed samples and the alkoxide doped materials were the effects of titania additions at low sintering temperatures. The decrease in shrinkage noted with titanium (alkoxide) doped powders were not observed in the mechanically mixed materials.

Figure 4.2.7 (a). Effect of sintering temperature on shrinkage of mechanically mixed doped specimens.

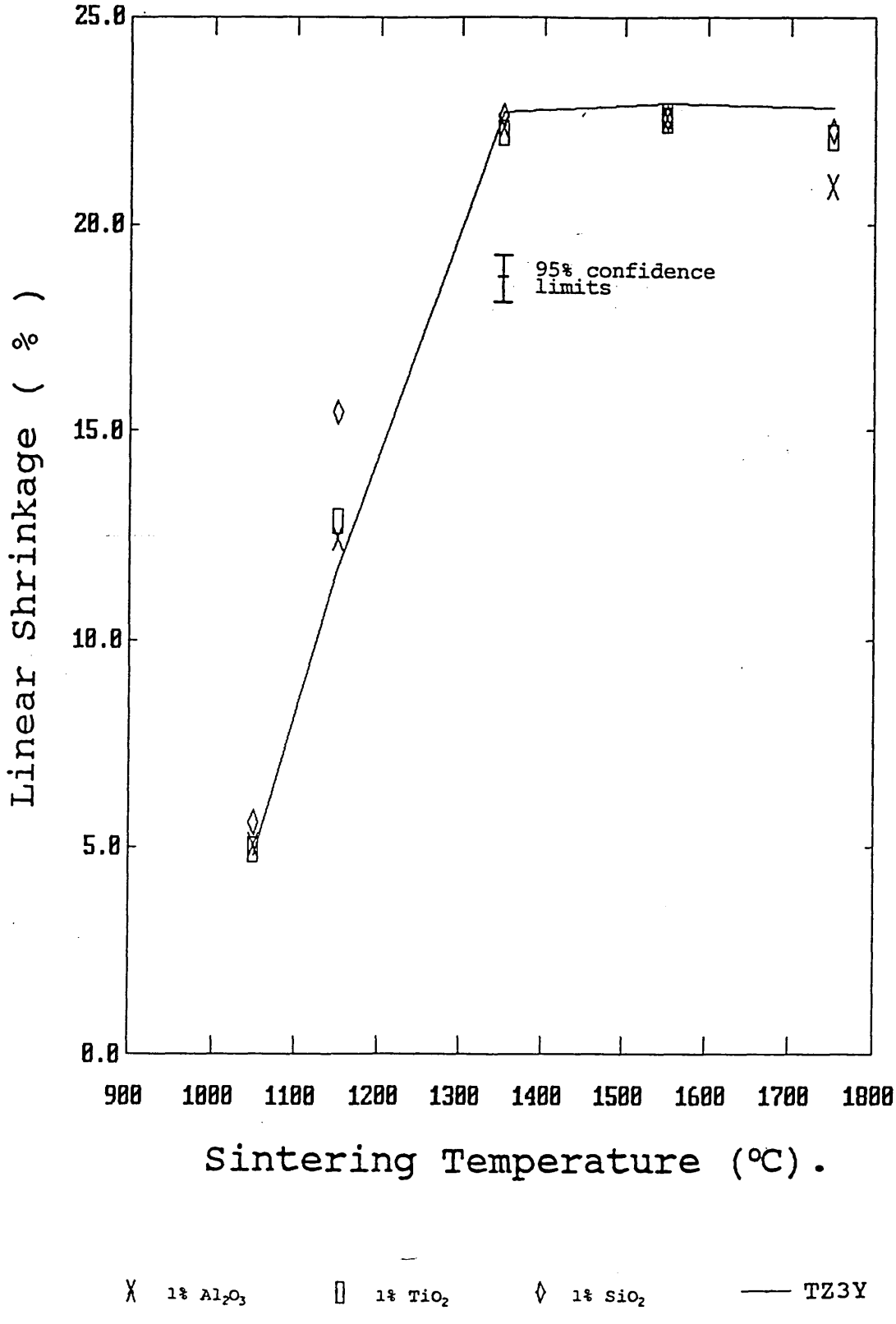

4.3 Density and porosity results.

The results of the density and porosity determinations on the sintered samples are reported in this section.

4.3.1 Sources and estimation of experimental error.

Three estimates of experimental error in the density determinations were made, using similar methods to those described for error estimation in the shrinkage results (section 4.2.1).

i.e. (a) Estimate of measuring error.
(b) Estimate of (post doping) experimental error
(c) Estimate of total experimental error.

(a) The error in the measurement of density and porosity was thought to be due to the limitations in accuracy of the balance (a Mettler AE 100 electronic balance reading to four decimal places [0.0001g]), the presence of trapped air bubbles in or on the specimens, and the (non) penetration of water into the pore structure of the test specimens. The removal of water from internal pores during the specimen surface drying operation was also a possible source of error.

To attempt to estimate the errors present in the measurement (and to give more reliable results) the wet density measurements were repeated four times and the mean and standard deviation calculated. These values are shown in the tabulated results.

The measuring error was estimated from these as the 95% confidence limits for each of the measurements, with an overall average value for all specimen types being calculated as described for the shrinkage results.

Table 4.3.1 (a) (appendix 1) shows the calculations used and results obtained for the estimation of measuring error by this method.

The 95% confidence limits, representing the range of possible error in each of the measurements varied between < 0.001 to $0.003 g$ per cm^3, with the mean value of the

range of possible error (for 95% confidence) being approximately plus or minus 0.02 g per cm^3.

(b) The errors in the fabrication and sintering results were thought to arise from density variations between the green pressed specimens, and from temperature inhomogeneities in the heat treatment furnace. These errors were estimated from measurements on a series of duplicate pellets made from 3 of the doped powders and produced under the same experimental conditions.

As with the equivalent error estimate in the shrinkage calculations, the upper confidence limit of the mean density difference was used as the estimation of the error in this part of the experiment. A value of plus or minus 0.05 g/cm^3 was calculated for the experimental error by this method. The calculations used to generate the estimate of experimental error, and the results obtained by this method are shown in table 4.3.1(b) (appendix 1).

(c) The error present in the whole experiment (including the effects of the doping process) was estimated from density measurements on pellets produced from separate (repeat) batches of powders of two of the compositions (0.25% and 0.75 wt. % doped alumina).

As with the equivalent error estimate in the shrinkage measurements, the 95% upper confidence limit in the mean difference between the density of pellets of the two powder batches (of each composition) under the same experimental conditions was used as the estimate of total experimental error. The estimated experimental error by this method gave a value of plus or minus 0.05g/cm^3.

Table 4.3.1(c) (appendix 1) shows the data and calculations used to generate this estimate of experimental error. The total experimental error is shown in the graphs as error bars representing the 95% confidence limits about the data points.

4.3.2 Undoped powders.

The density and porosity results for the undoped TZP samples are shown in table 4.3.2 (appendix 1), with the effect of sintering temperature on the sintered density of the undoped specimens illustrated in figure 4.3.2(a).

The graph shows the behaviour of the unmodified TZ3Y material, as supplied by the manufacturer, and the blank treated material which had undergone the doping process, but with no dopant additions made.

The results show that no difference could be determined in the densification behaviour of the two materials by this method.

The majority of the densification took place at sintering temperatures below 1350°C, with only a slight increase in density possibly occurring (less than possible experimental error) for sintering temperatures in excess of this.

Figure 4.3.2
Effect of sintering temperature on the density of undoped TZP.

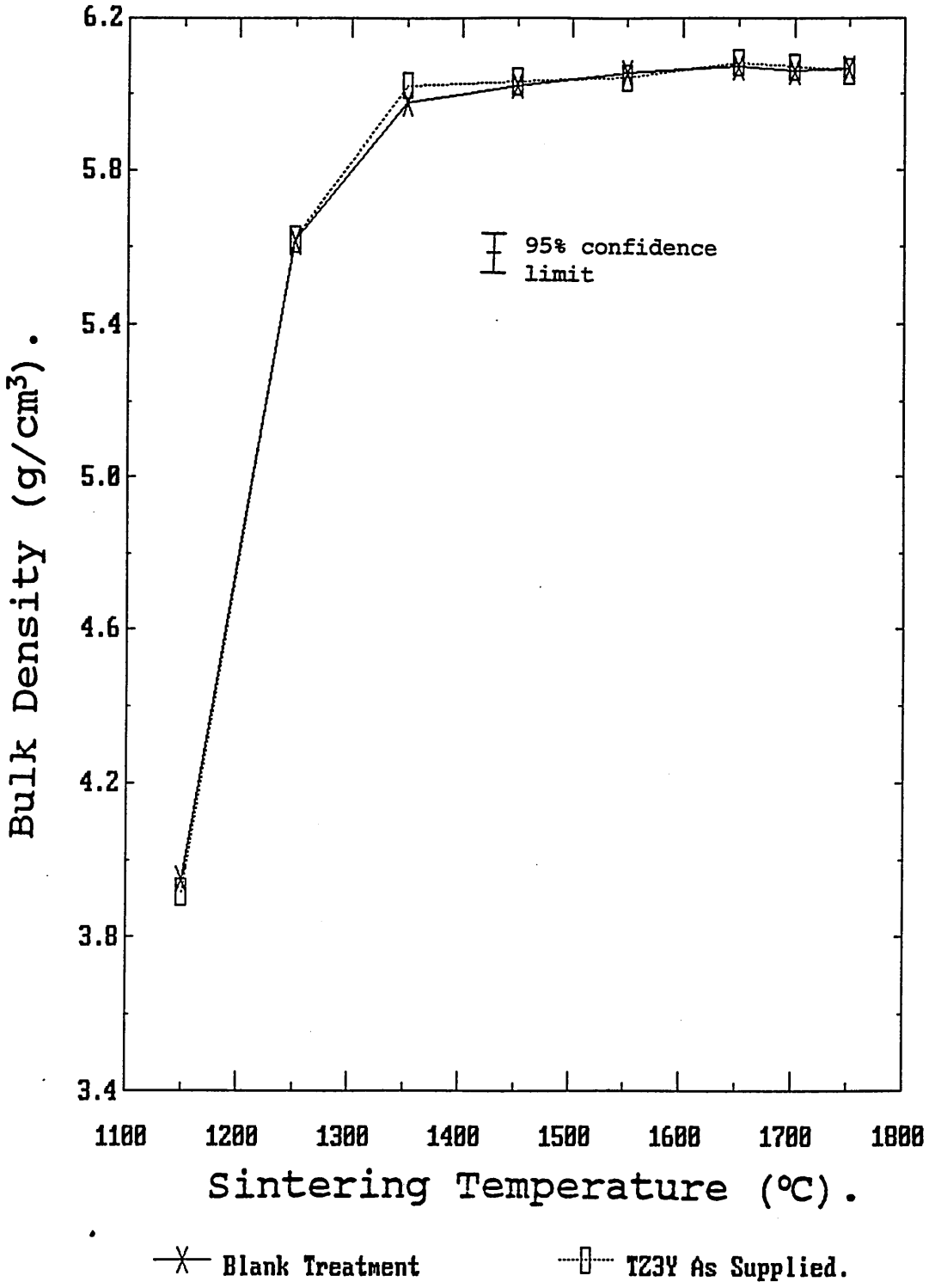

4.3.3 Alumina doped powders.

The density results for the alumina doped samples are shown in table 4.3.3 (appendix 1), with the effect of sintering temperature on the densification behaviour shown in figure 4.3.3(a).

The results show that the majority of the densification in these materials took place at sintering temperatures up to 1250°C, with a significant decrease in density in the majority of the specimens for sintering temperatures in excess of 1650°C.

The effect of alumina addition on the densification for different sintering temperatures is shown in more detail in figures 4.3.3(b)-(d).

The effect of alumina additions appears to give rise to four types of behaviour depending upon the sintering temperature used.

The results show a significant increase in density with alumina addition for sintering temperatures below 1350°C, the majority of this occurring for alumina additions of 0.25% or less.

For sintering temperatures of 1350-1450°C, the effects of alumina addition are less significant, and less clearly defined, being within the range of possible experimental error. However, there appears to be a slight increase in density with alumina addition up to 0.25-0.5 mass %.

For sintering temperatures of 1550-1650°C, there appears to be a small decrease in density for increased alumina addition, this becoming more pronounced at the higher sintering temperature.

For sintering temperatures in excess of 1650°C, the effect of increased alumina additions becomes increasingly significant on the density, with a large decrease in density apparent for alumina additions in excess of 0.5 mass %.

Figure 4.3.3 (a).
Effect of sintering temperature on the densification behaviour of alumina doped TZP.

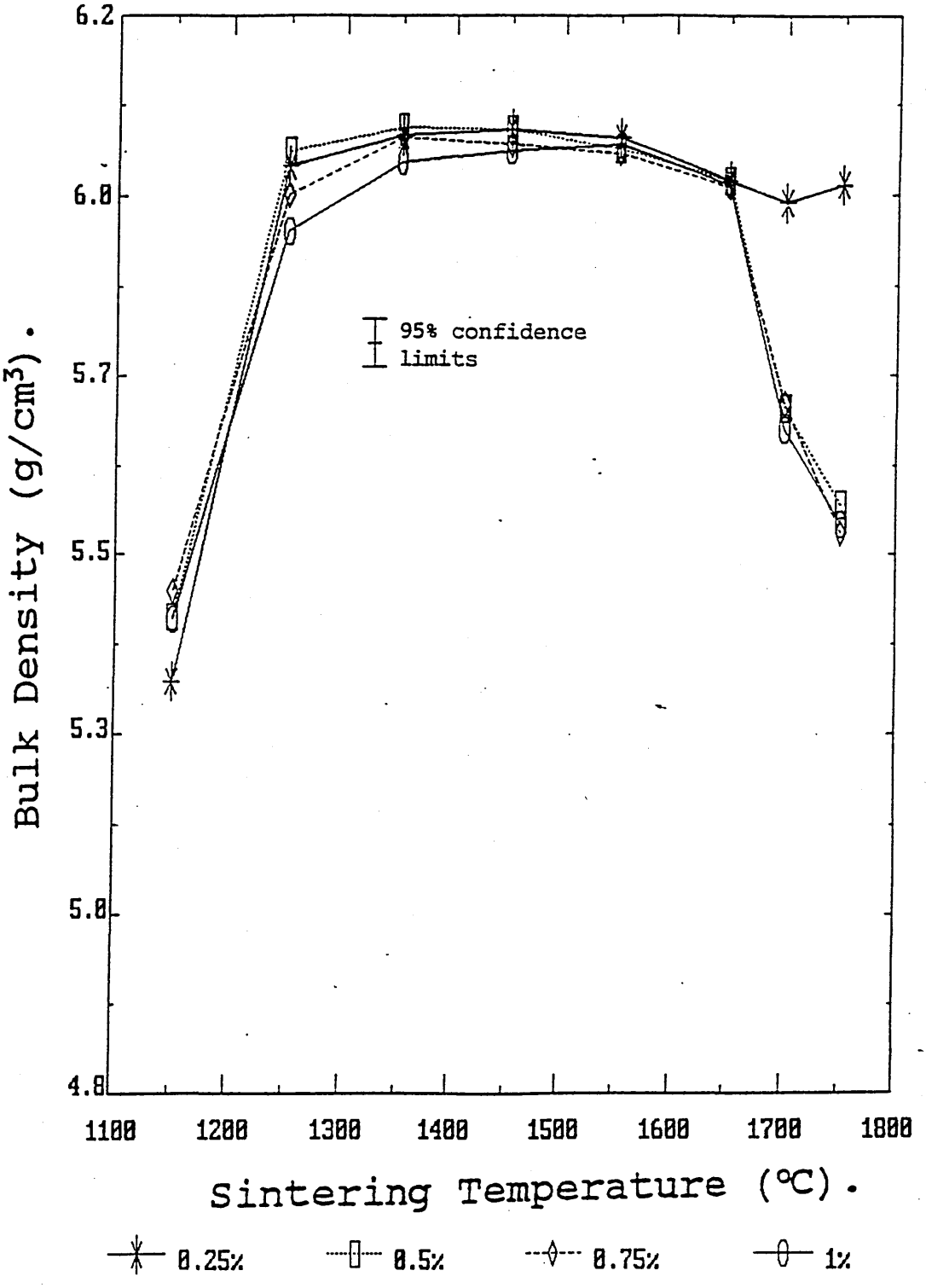

Figure 4.3.3 (b).

Effect of Alumina addition on densification behaviour of doped TZP for sintering temperatures up to 1350°C.

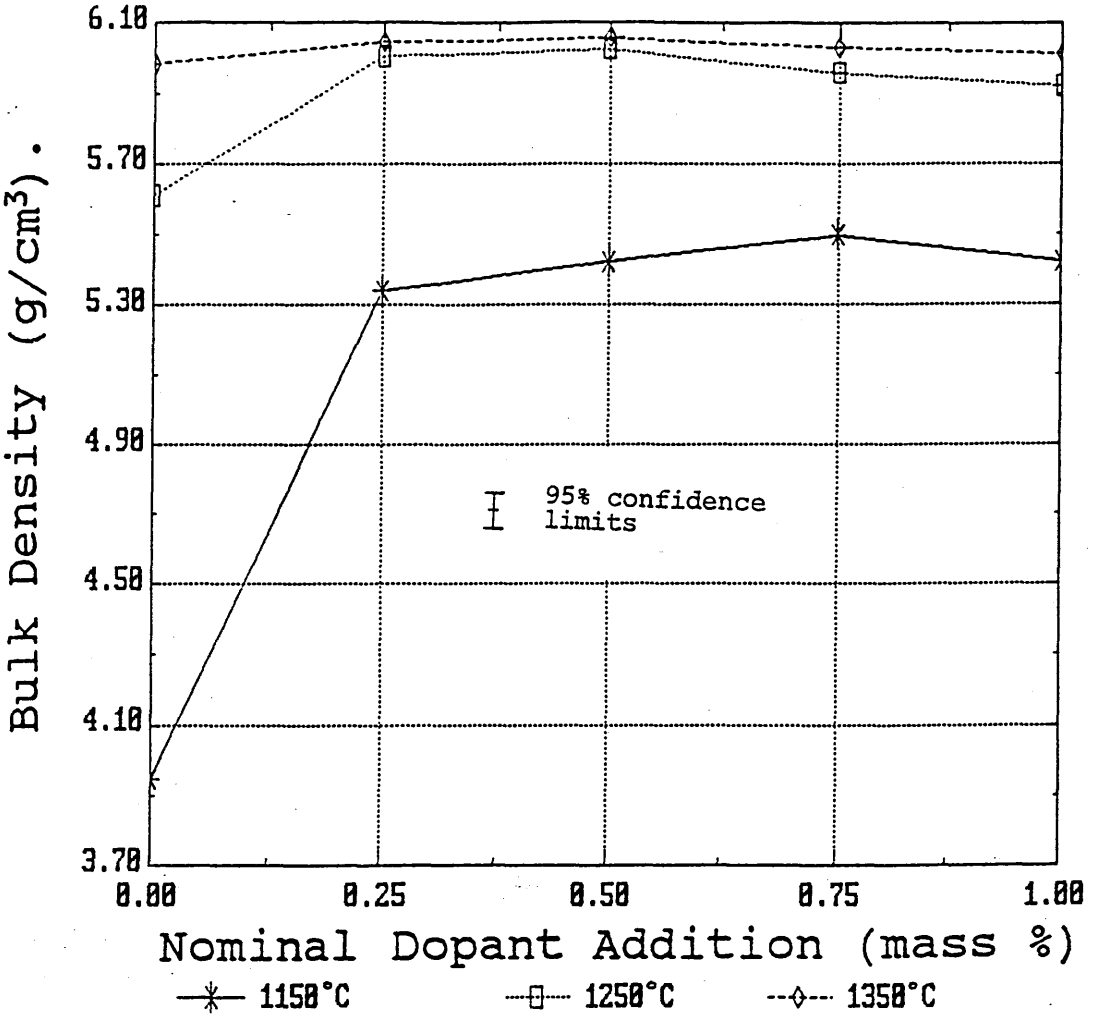

Figure 4.3.3 (c).
Effect of alumina addition on densification behaviour of doped TZP for 1350-1450°C sintering temperature.

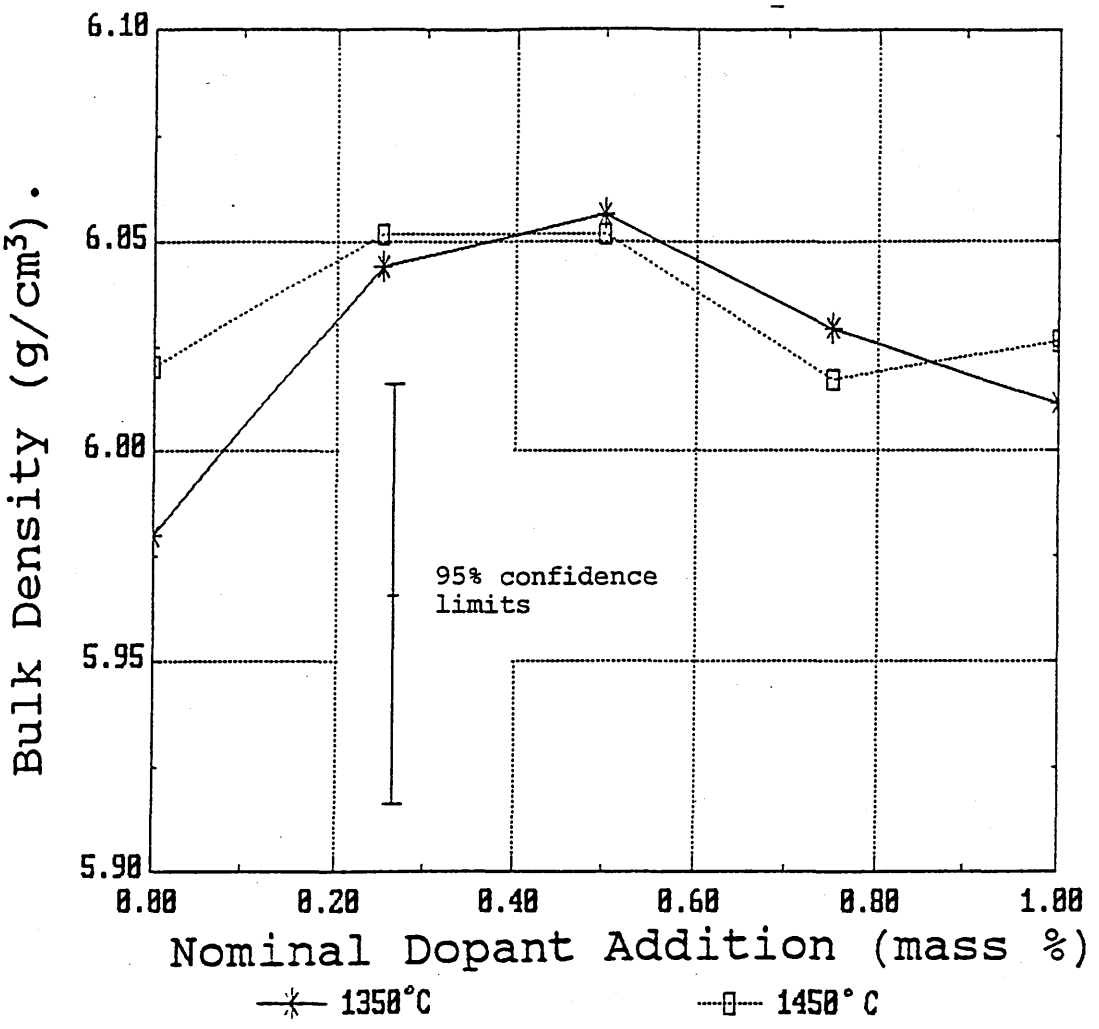

Figure 4.3.3 (d).
Effect of alumina addition on densification behaviour of doped TZP for 1550-1650°C sintering temperature.

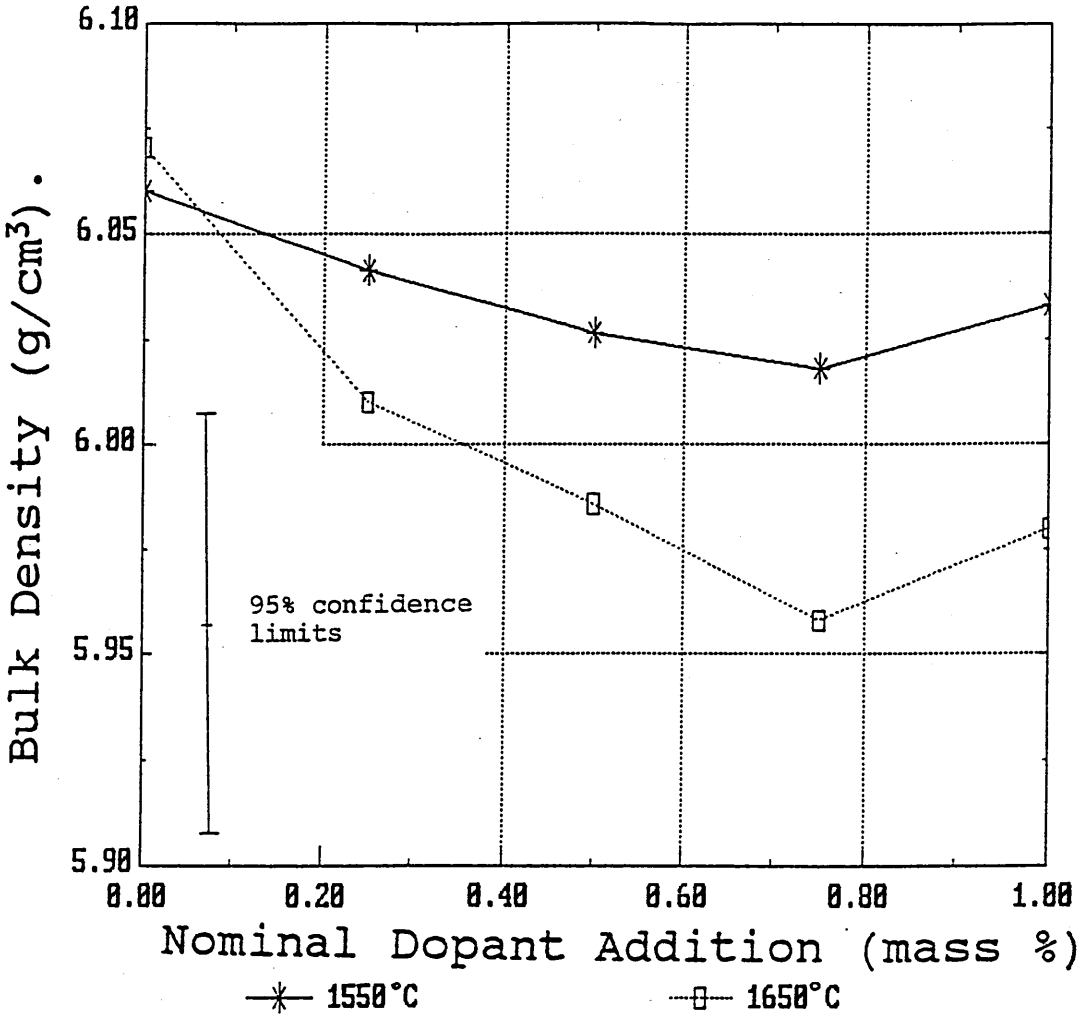

Figure 4.3.3 (e).

Effect of alumina addition on densification behaviour of doped TZP for sintering temperatures in excess of 1650°C.

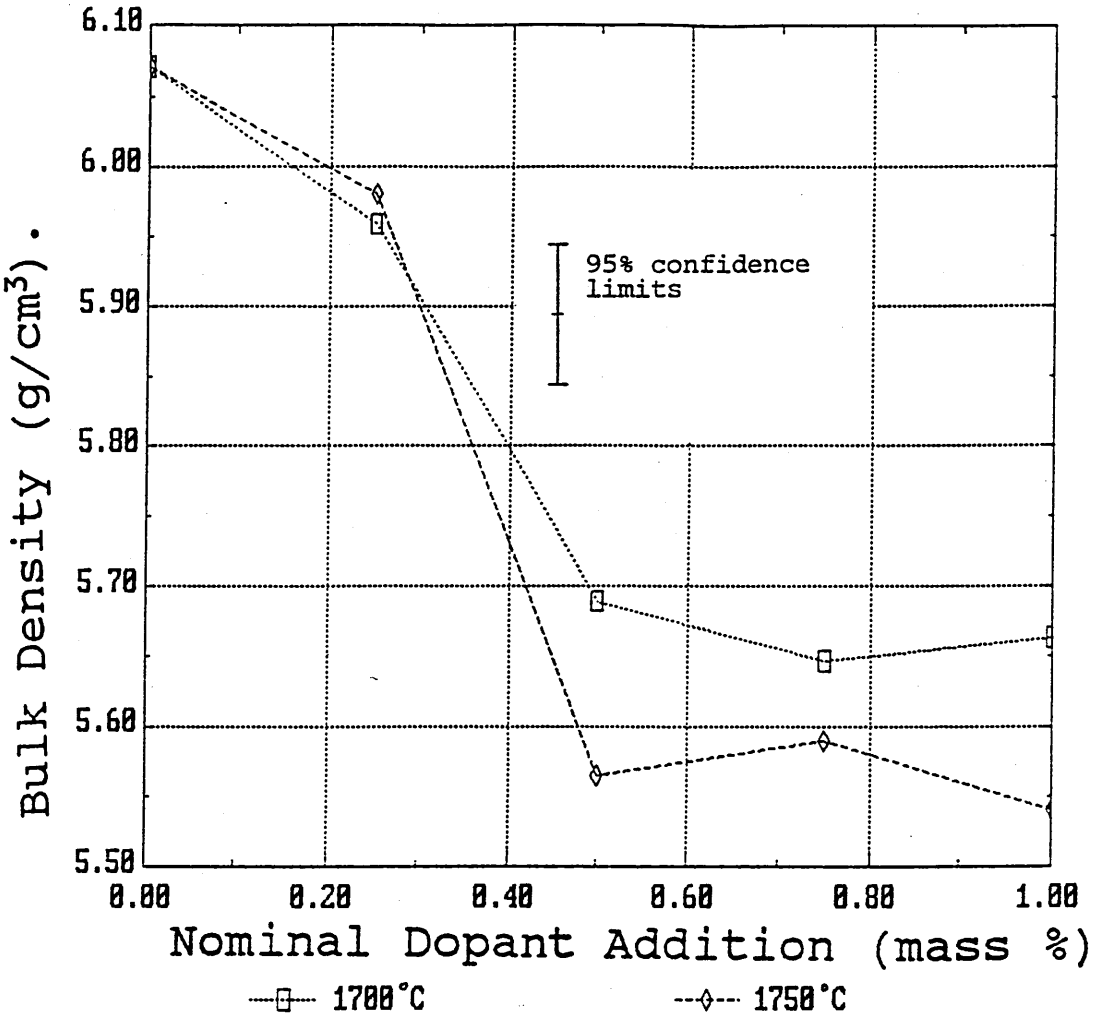

4.3.4 Silica doped powders.

The density results for the silica doped samples are shown in table 4.3.4 (appendix 1), with the effect of sintering temperature on the densification behaviour of silica doped TZP shown in figure 4.3.4 (a).

The results show that the densification in these materials took place at sintering temperatures up to 1350°C. No increase in density appeared to occur for samples sintered at temperatures in excess of this.

The effect of silica addition on the densification for different sintering temperatures is shown in more detail in figures 4.3.4(b)-(d). There appear to be three types of behaviour depending on the sintering temperature used.

Figures 4.3.4(b) and (c) show the effect of silica addition on the density of samples sintered at temperature up to 1350°C. These results appear to show a maxima in density for silica additions of 0.25 mass %, with a small decrease in density for higher silica additions.

For the 1450°C sintered sample, the magnitude of any effect lies within the range of possible experimental error, although these results could possibly be interpreted as similar (although less significant) effect to that seen in the 1150-1350°C sintered samples (see figure 4.3.4 (d)).

For sintering temperatures in excess of 1450°C, all of the samples show a decrease in density with increased silica content.

Figure 4.3.4 (a)
Effect of sintering temperature on the densification behaviour of silica doped TZP.

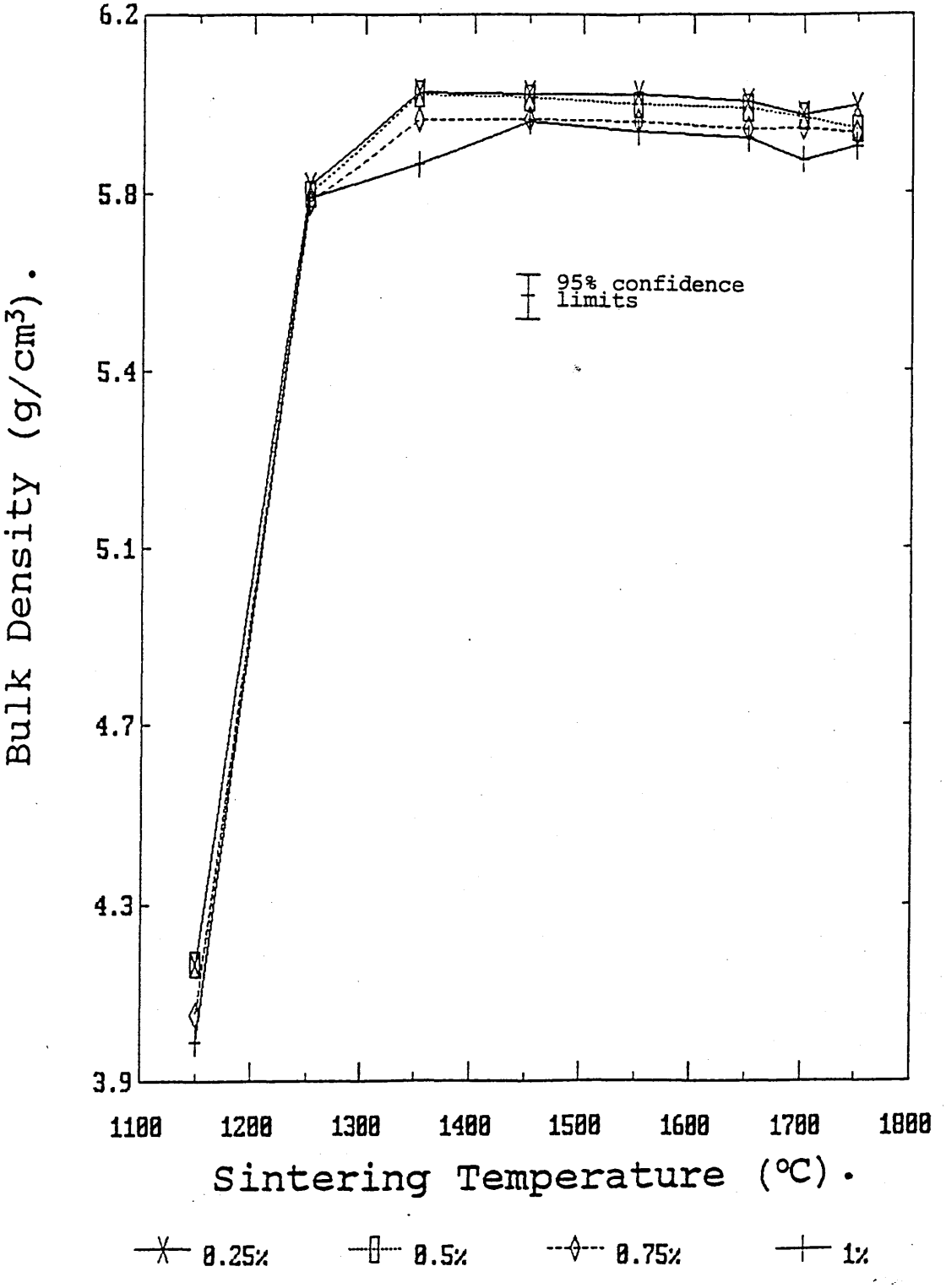

Figure 4.3.4 (b).
Effect of silica addition on densification behaviour of doped TZP for 1150°C sintering temperature.

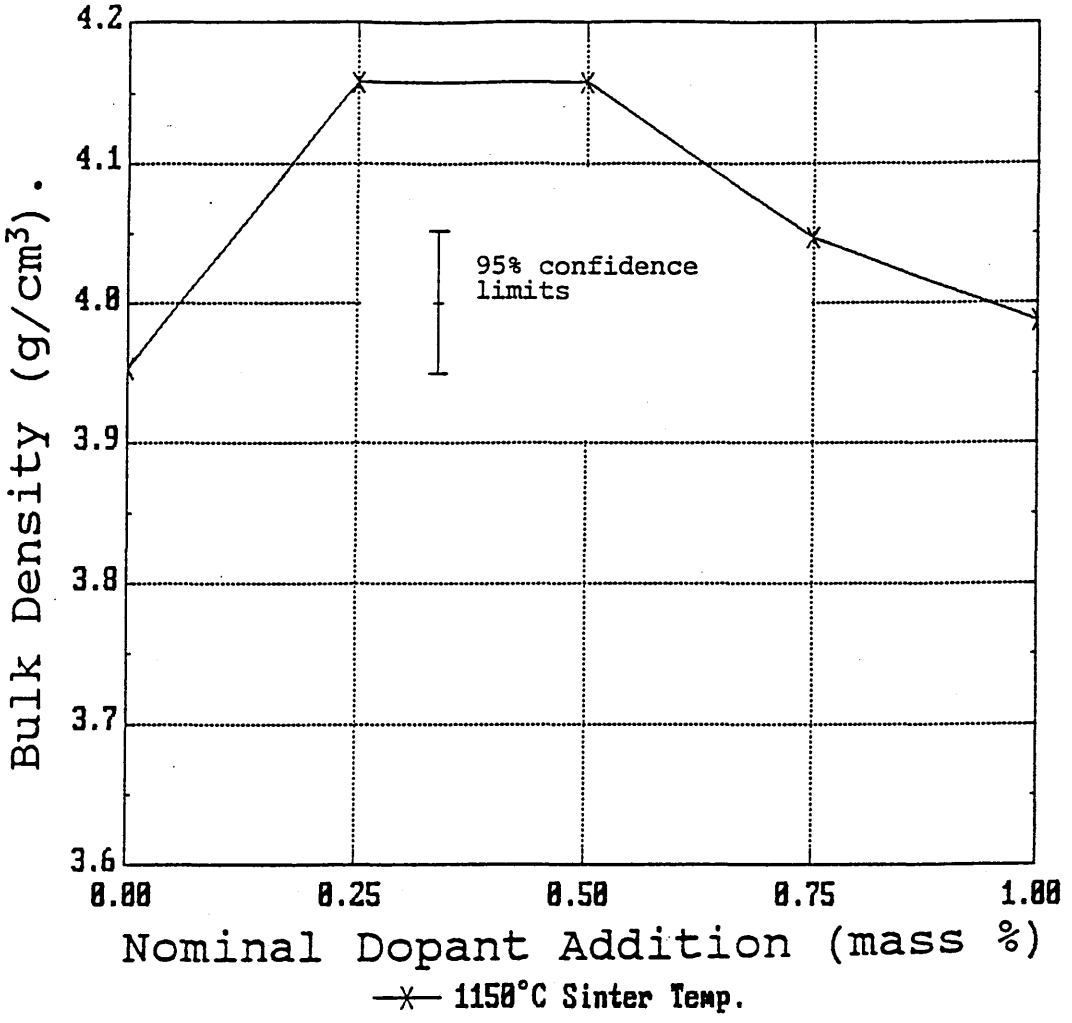

Figure 4.3.4 (c).

Effect of silica addition on densification behaviour of doped TZP for 1250-1350°C sintering temperature.

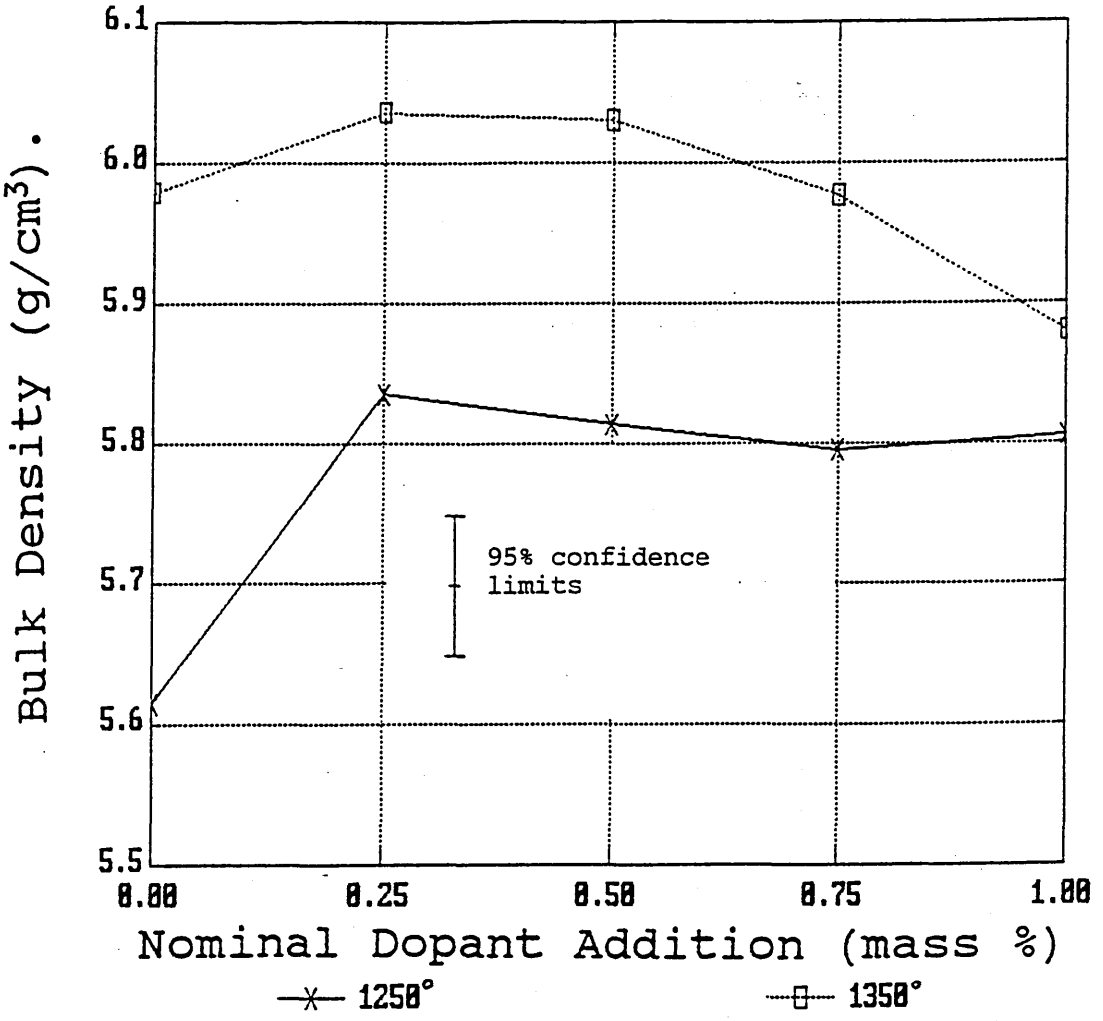

Figure 4.3.4 (d).
Effect of silica addition on densification behaviour of doped TZP for 1450°C sintering temperature.

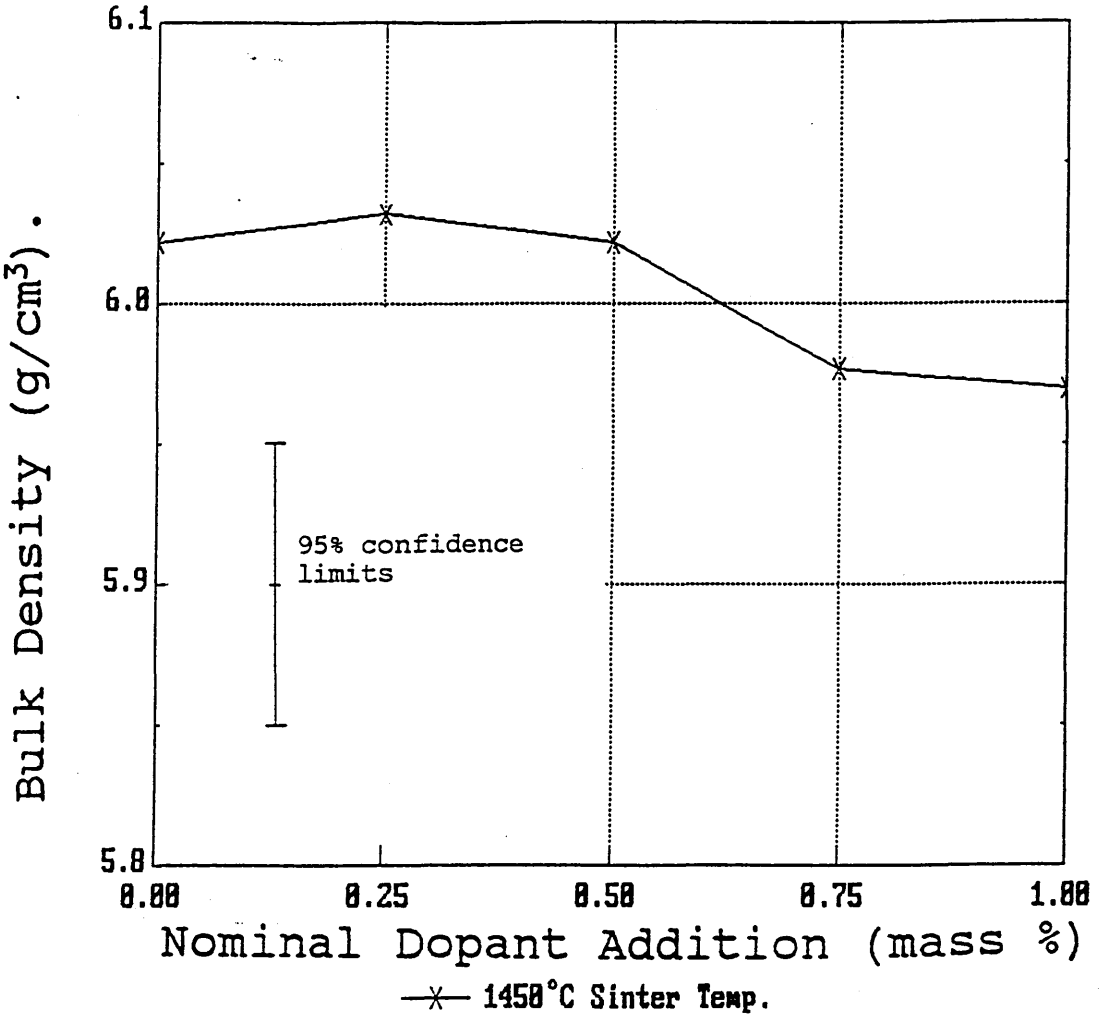

Figure 4.3.4 (e).
Effect of silica addition on densification behaviour of doped TZP for sintering temperatures in excess of 1450°C.

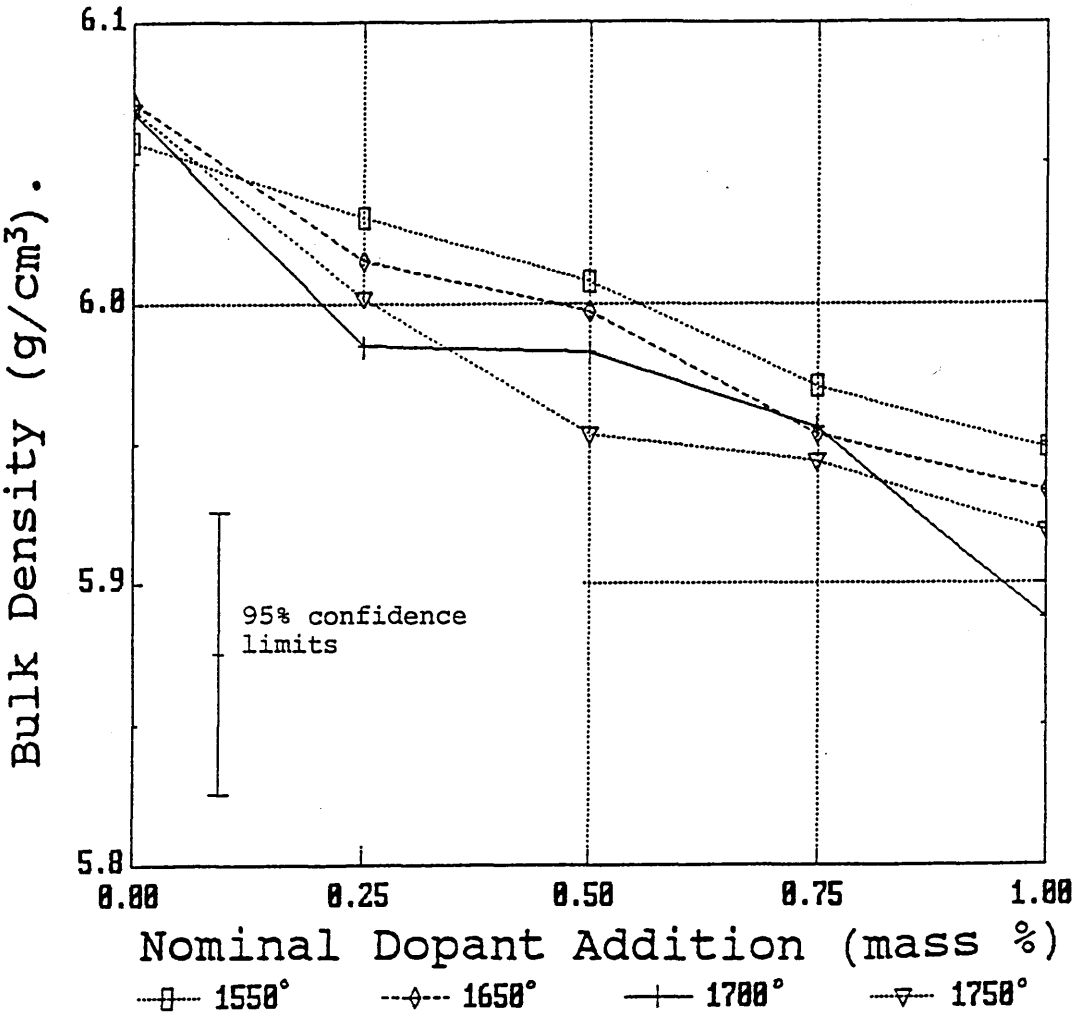

4.3.5 Titania doped samples.

The density results for the titania doped samples are shown in table 4.3.5 (appendix 1), with the effect of sintering temperature on the densification behaviour shown in figure 4.3.5(a).

The results show that the majority of the densification in these materials took place at sintering temperatures up to 1450°C.

The effect of titania addition on the densification for different sintering temperatures is shown in more detail in figures 4.3.5 (b)-(d).

The results show two types of behaviour depending upon the sintering temperature used.

For specimens sintered at temperatures between 1150 and 1350°C, the density appears to show a general decrease with increasing TiO_2 content. The 1150°C sintered material appears to show a slight increase in density for TiO_2 additions in the range 0 - 0.25 mass %, although this may be due to experimental error.

For sintering temperatures in excess of 1350°C, no significant effect can be determined for increases in TiO_2 content in the range 0-1 mass %.

Figure 4.3.5 (a)
Effect of sintering temperature on the densification behaviour of titania doped TZP.

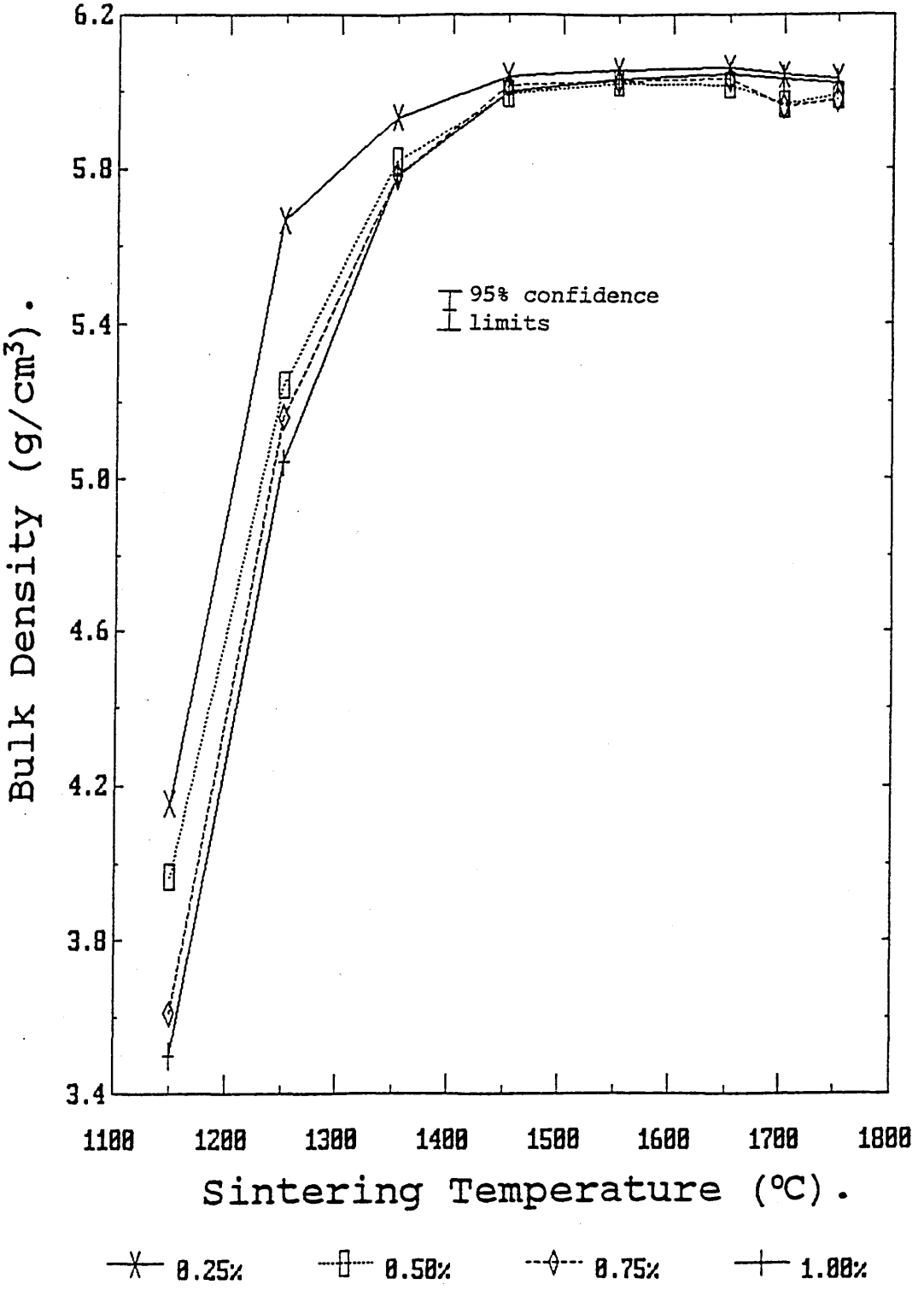

Figure 4.3.5 (b).
Effect of titania addition on densification behaviour of doped TZP for 1150-1250°C sintering temperature.

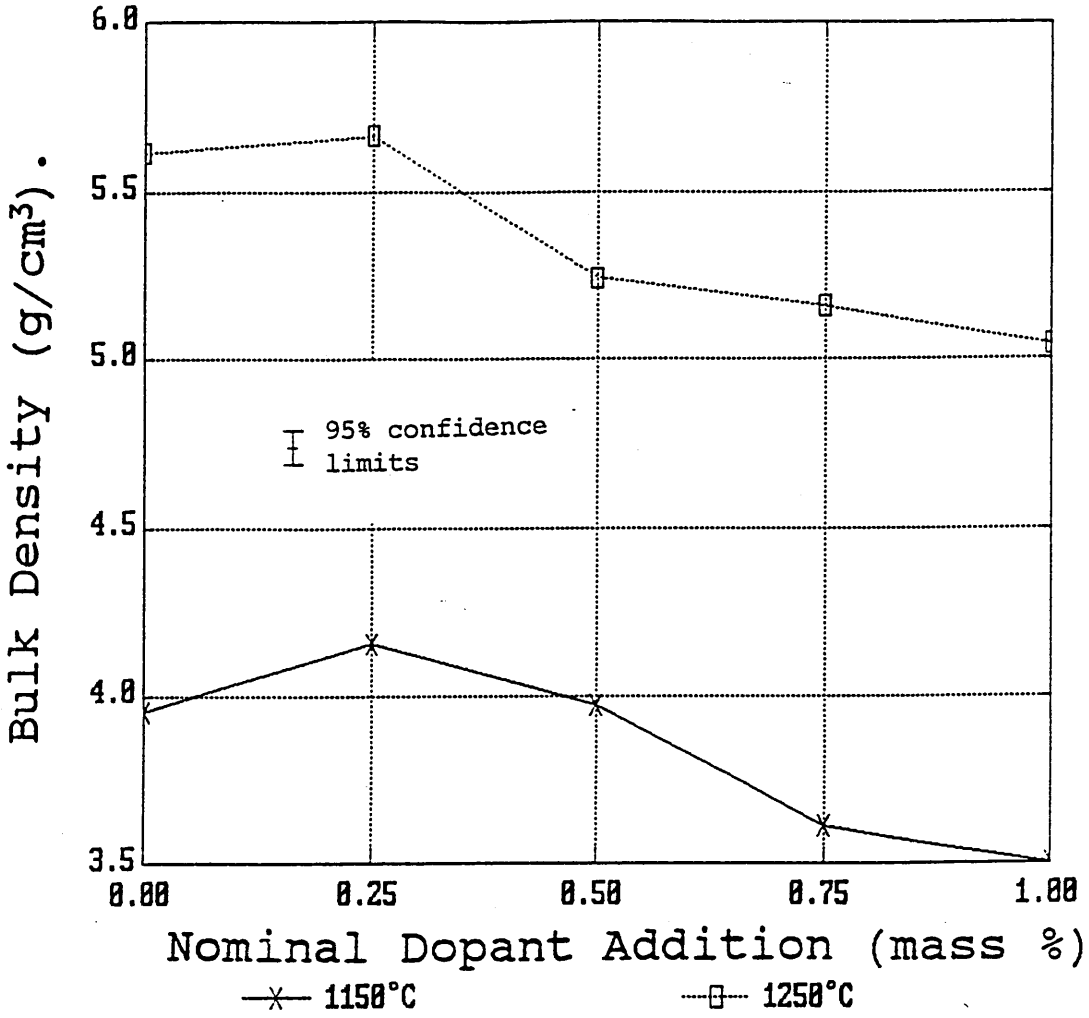

Figure 4.3.5 (c).

Effect of titania addition on densification behaviour of doped TZP for 1350-1750°C sintering temperature.

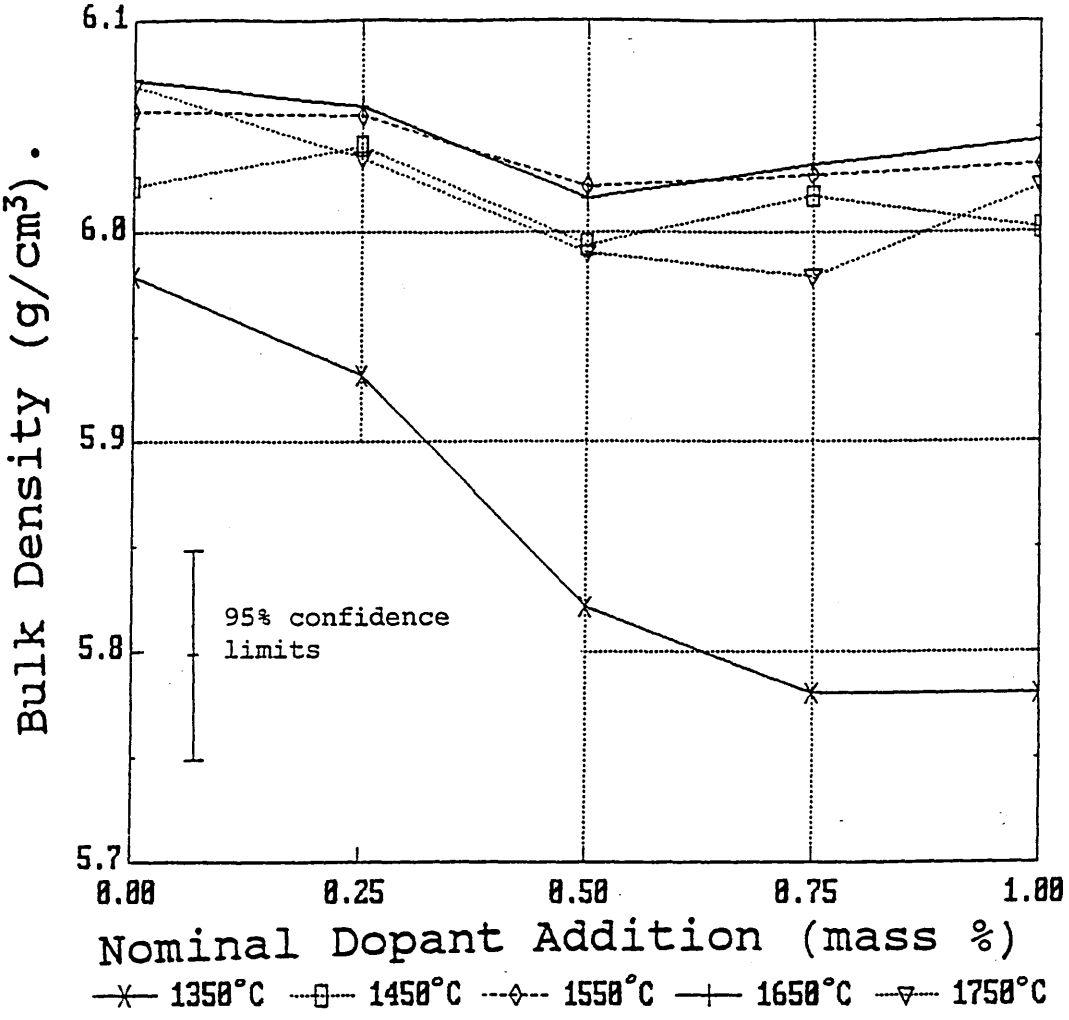

4.3.6 Multiple dopant additions.

The density results for the TZP with multiple oxide dopant additions (at the 1 mass % level) are shown in table 4.3.6 (appendix 1), with the effect of sintering temperature on the densification behaviour shown in figure 4.3.6.

The results show that the powders containing combinations of silica and alumina additions underwent the majority of their densification at lower temperatures (up to 1150°C) compared to the other doped powders.

The material containing 1 mass % additions of silica with titania had a substantially lower density at 1150°C, although the maximum density was reached at the same temperature (1250°C) as the alumina and silica doped specimens.

The material containing alumina and titania in combination underwent densification at higher temperatures than the other material, but sintered to a higher maximum density value at around 1450°C.

The other notable result from these experiments was that all of the multiple doped specimens containing alumina underwent a gradual reduction in density with increasing sintering temperature above approximately 1450°C, with a substantial decrease in density for sintering temperatures in excess of 1650°C. The onset of this phenomena occured at a higher temperature for the alumina plus titania doped specimens than other samples containing alumina.

Figure 4.3.6

Effect of sintering temperature on density of sintered samples with multiple dopant additions.

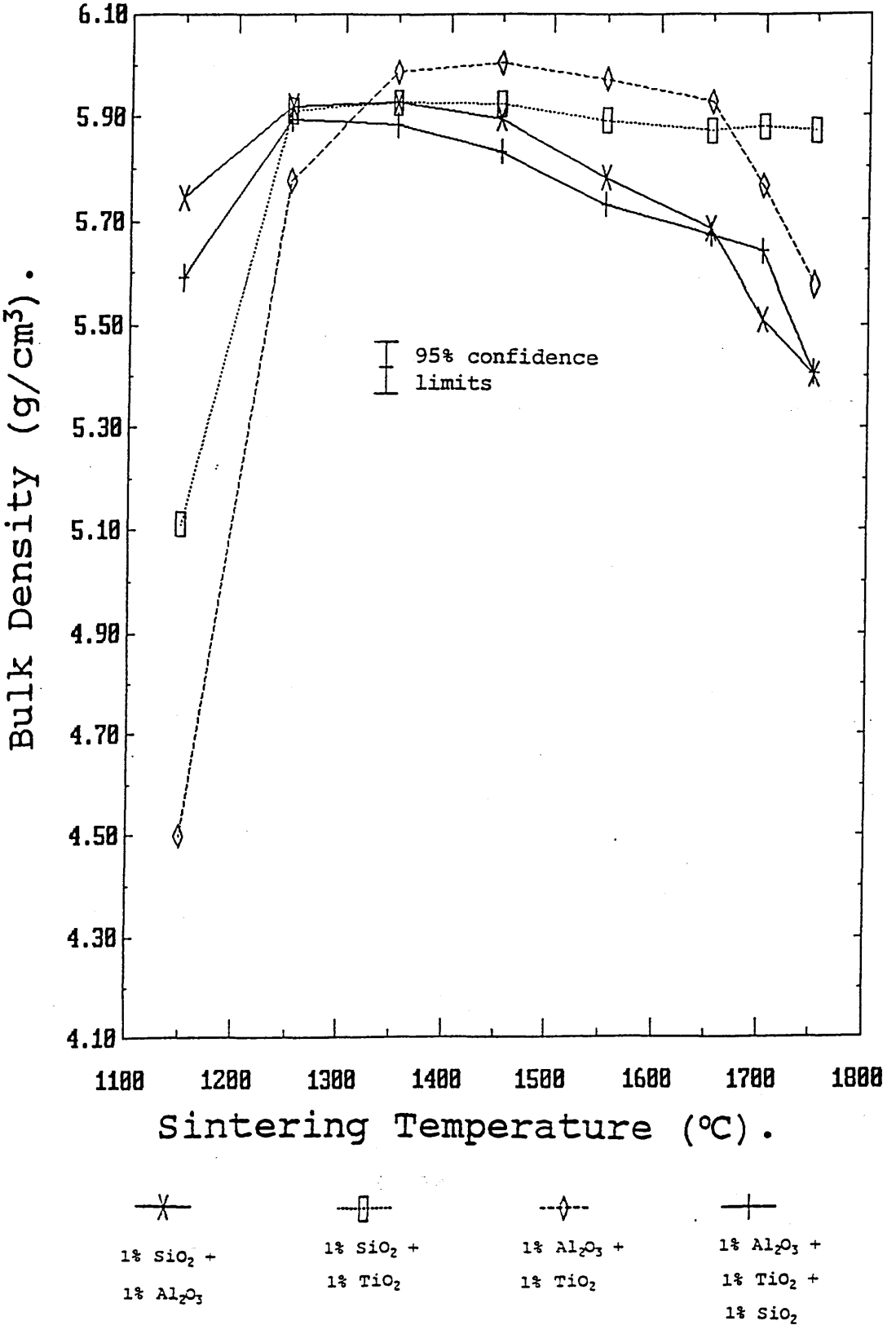

4.3.7 Mechanically mixed doped samples.

The results of the density and porosity determinations for the mechanically mixed doped samples are shown in table 4.3.7 (appendix 1).

The effects of sintering temperature on the density of the mechanically mixed doped samples and the unmodified TZ3Y material are compared in figure 4.3.7.

The results show that the mechanically mixed silica additions produced a significant increase in the density of samples sintered at low temperatures (<1350°C), with small increases in density also apparently resulting from mechanically mixed Al_2O_3 and TiO_2 additions at these sintering temperatures.

The maximum density in all the specimens appeared to occur for sintering temperatures between 1350 and 1550°C, with all the doped samples exhibiting similar behaviour over this range of sintering temperature, resulting in a decrease in density relative to the unmodified material.

The impaired densification at low temperatures observed in the TiO_2 doped materials prepared via the alkoxide doping route was not observed in these samples.

The samples sintered at 1750°C all exhibited a decrease density compared to the samples sintered at lower temperatures, with this being especially pronounced for the alumina doped samples which showed similar de-densification effects to those observed with the equivalent alkoxide doped material.

Figure 4.3.7
Effect of sintering temperature on the density of mechanically mixed, doped specimens.

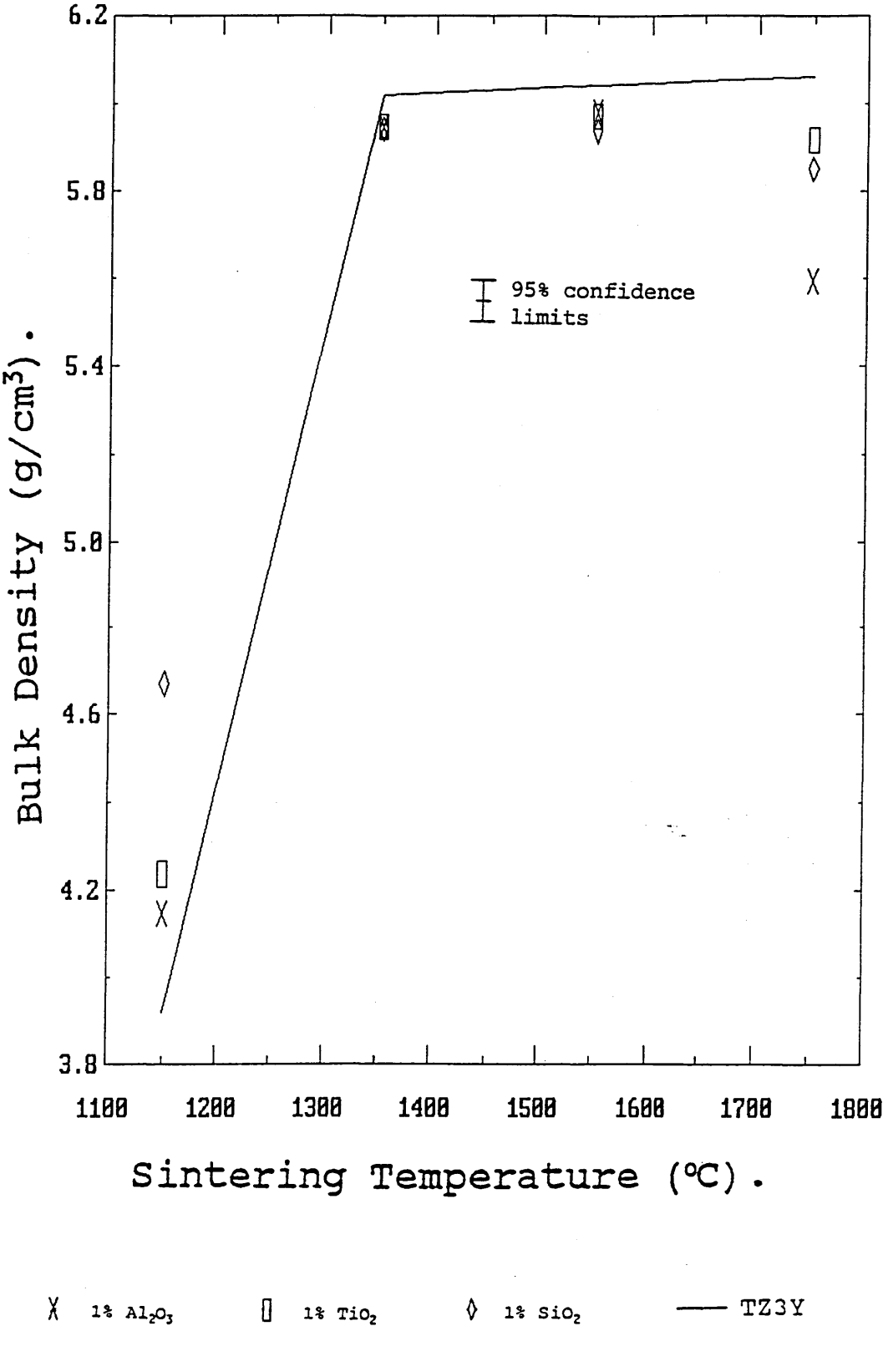

4.3.8 Factorial experiments.

The results of the factorial experiment(s) to investigate the effects of sintering temperature and impurity content, and their interactions on the density of the sintered samples are shown in these sections.

The results comprise 6 separate factorial experiments each over a 100°C temperature interval, to cover the full range of 1250° to 1750°c sintering temperatures investigated in these experiments.

The results are shown in the form of the calculated factorial effects from the data (Yate's method) in tables 4.3.8 (a)-(f), with the corresponding analyses of variance, and estimates of significance in tables 4.3.8 (g)-(l) (see appendix 1).

The analysis of variance (ANOVA) tables, and the significance tests include two sets of results based upon the use of an internal estimate of error based on high order (assumed to be negligible) interaction terms, and the external estimate of error derived in the one factor at a time experiments (method (c)). These error estimates (and the associated significance tests) differ substantially at high and low sintering temperatures due to the presence of significant three and four factor interactions. In general, the external estimate of error appears to be more reliable.

The significance of the (single factor) main effects in these results is difficult to ascertain from these experiments since the (significantly large) two, three and four factor interaction effects will obscure the main effects. The one factor at a time experiments thus give a better indication of these.

The calculated factorial interaction effects are illustrated schematically in figures 4.3.8 (a), (b) and (c) for the two and three factor impurity interactions 4.3.8 (a), and the impurity-temperature interactions 4.3.8 (b) and (c).

The results for the SiO_2-TiO_2 factorial interaction effect (BC), show a large and positive factorial effect (ie enhanced densification when both are present compared to their individual effects) at sintering temperatures below 1350°C, with the interaction effect becoming insignificant for sintering temperatures in excess of this.

The impurity interaction between Al_2O_3 and SiO_2 (AB) indicates a negative effect (ie the impurities interact to reduce the density) for all sintering temperatures, with the largest effects occurring at lower sintering temperatures..

The interaction between Al_2O_3 and TiO_2 (AC) appears to produce a negative effect for sintering temperatures up to 1250°C, whilst the three factor interaction between Al_2O_3, SiO_2, and TiO_2 (ABC) appears to produce a negative effect for sintering temperatures up to 1450°C. In both cases the interaction effects become less significant with increasing sintering temperature, and insignificant for sintering temperatures above 1450°C.

The calculated impurity-temperature factorial effects for alumina (AD), and silica (BD), show significant interactions in the 1150 to 1250°C and the 1250-1350°C temperature intervals, with alumina and temperature (AD) also showing significant interaction effects over the 1650-1750°C temperature interval suggesting that the effect of these impurities changes over these temperature intervals.

Large three factor interactions (two impurities and temperature) were observed for the Al_2O_3-TiO_2 system (ACD) over the 1150 to 1250°C temperature interval, for the SiO_2-TiO_2 system (BCD) over the 1150-1250° and 1250-1350° temperature intervals, and for the Al_2O_3-SiO_2 system (ABD) over the 1150-1250°C temperature interval implying that the interaction effect was changing between these temperatures.

A small impurity - temperature interaction effect was also observed for the Al_2O_3-SiO_2-TiO_2 impurity system in the 1150-1250, 1250-1350, 1350-1450°C and 1650-1750°C temperature intervals.

The magnitude of the impurity - temperature interaction effects generally increased with decreasing temperature

Figure 4.3.8 (a).
Factorial experiments (sintered density).
Schematic representation of factorial effects.
Impurity interaction effects.

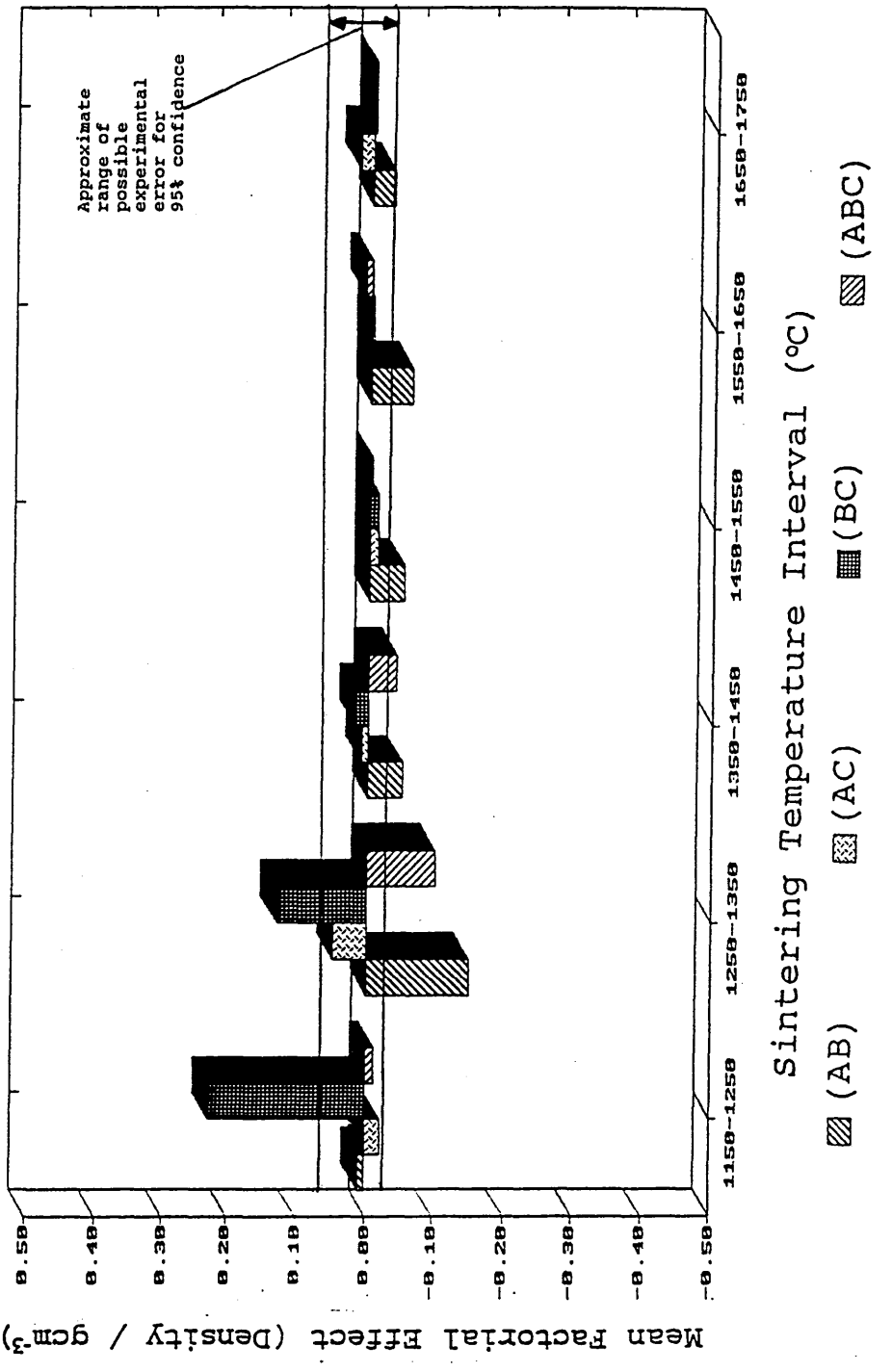

Key to Notation.
e.g.
A = 1 mass % Al_2O_3 addition.
B = 1 mass % SiO_2 addition.
C = 1 mass % TiO_2 addition.
D = Higher value of sintering temperature (in range) used.
ABCD = Interaction between factors A,B,C and D.

Figure 4.3.8 (b).

Factorial experiments (sintered density)

Schematic representation of factorial effects.

Impurity-temperature interaction effects (two factor).

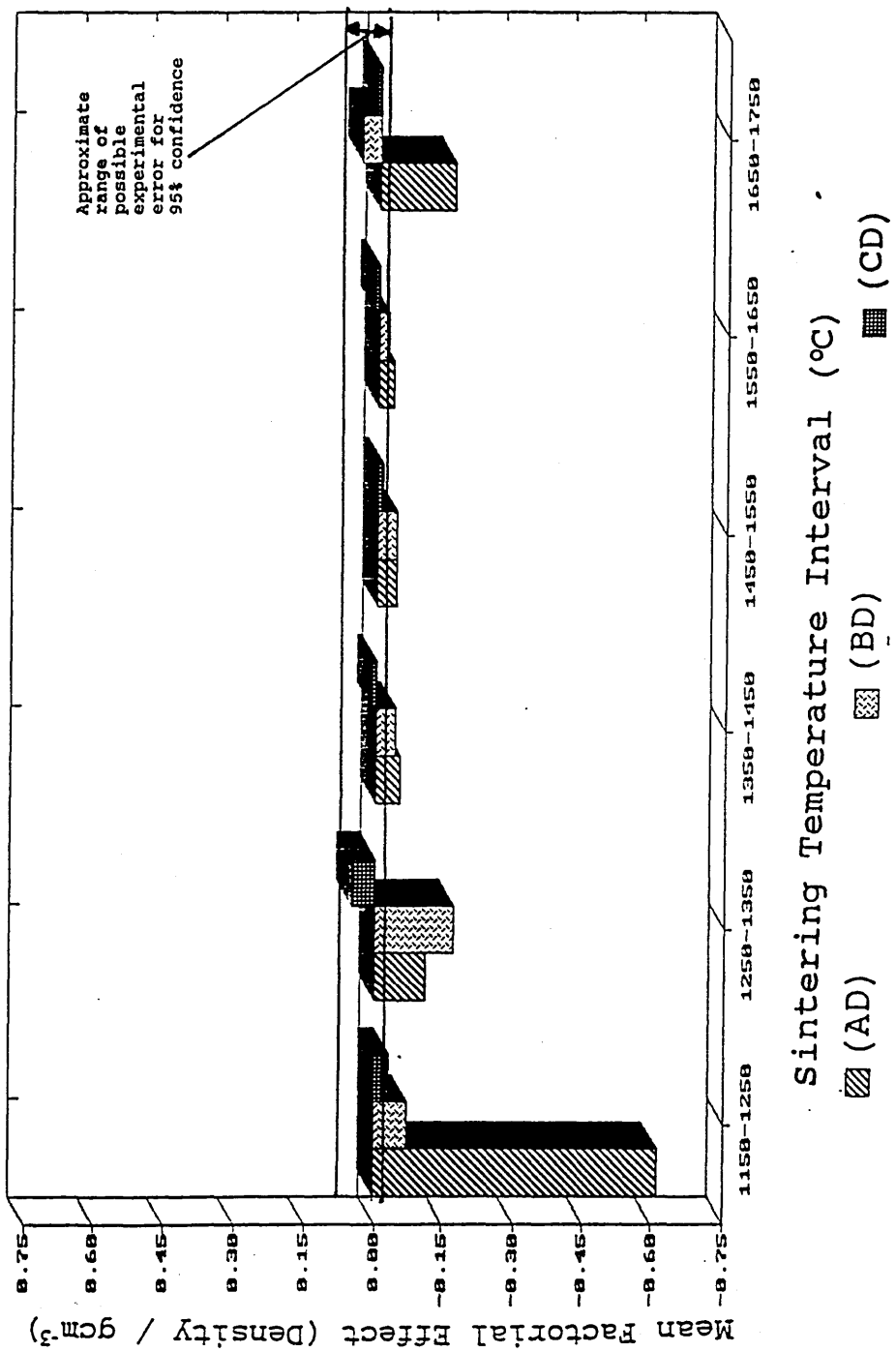

Key to Notation.
e.g.
A = 1 mass % Al_2O_3 addition.
B = 1 mass % SiO_2 addition.
C = 1 mass % TiO_2 addition.
D = Higher value of sintering temperature (in range) used.
ABCD = Interaction between factors A,B,C and D.

Figure 4.3.8 (c).

Factorial experiments (sintered density)

Schematic representation of factorial effects.

Impurity-temperature interaction effects (3 & 4 factor).

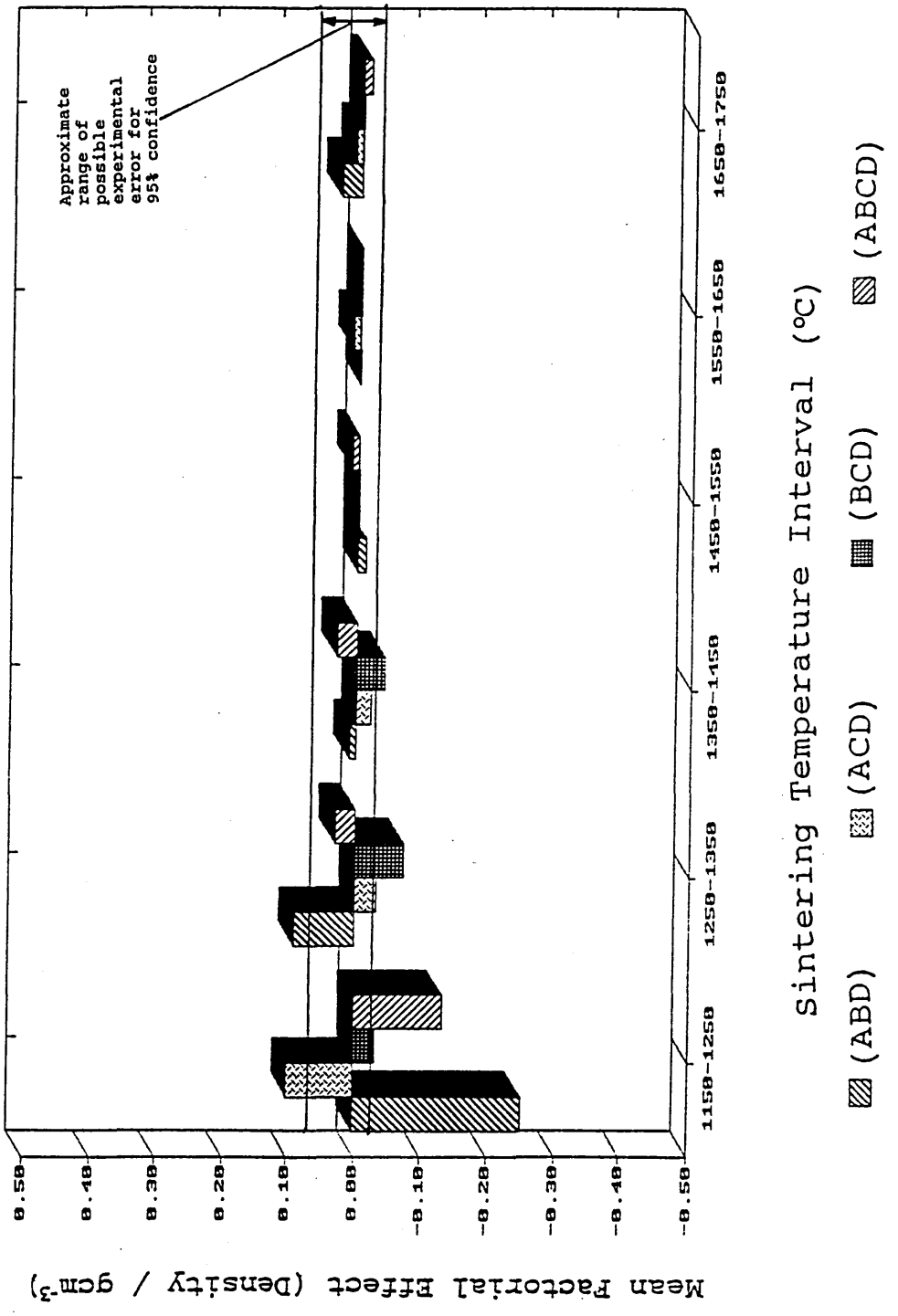

Key to Notation.
e.g.
A = 1 mass % Al_2O_3 addition.
B = 1 mass % SiO_2 addition.
C = 1 mass % TiO_2 addition.
D = Higher value of sintering temperature (in range) used.
ABCD = Interaction between factors A,B,C and D.

4.4 Determination of defect area and surface damage by optical microscopy and image analysis.

The results of the quantification of sintering and polishing induced defect area by optical microscopy and Seescan image analysis are reported in the following sections.

4.4.1 Sources and estimation of experimental error.

Two estimates of error in these experiments were made. These were: (a) an estimate of the error inherent in the measurement (of defect area) in the sintered specimens, and (b) an estimate of total experimental error.

(a) The estimate of error in the measurements was obtained from the output of the image analyser programme. This gave the mean defect area (from an average of ten fields of view), and the standard deviation of the data. This data was used to calculate the 95% confidence limits for the mean defect area.

A crude estimate of measuring error was taken as the average value of the 95% confidence limits for all samples of a given type.

The calculation and value of estimated error by this method is shown for the various dopant additions in table 4.4.1 (a) (appendix 1).

The sources of the error in the measurements were thought to be the inhomogenous distribution of defects within the samples, combined with the relatively small number of fields of view (10) analysed.

(b) An estimate of total experimental error was obtained from a comparison between the measured defect areas of sintered pellets produced from two separate batches of 0.25 and 0.75% alumina doped powders, similarly to the equivalent estimate of error in the shrinkage and density measurements.

Table 4.4.1 (b) (appendix 1) shows the results and calculation used to produce the estimate of experimental

error. The estimated value for the total experimental error was approximately plus or minus 0.35% defect area. This result is of the same order of magnitude as the estimate of measuring error by the previous method, and suggests that the errors arising from powder doping, pressing, sintering and specimen polishing operations are relatively small compared to the errors in the measurements.

The large measuring error in these experiments made it impossible to identify clear differences between the various dopant levels of each type. However there did appear to be trends associated with the various types of impurity addition.

To attempt to demonstrate these trends, the average effect of each dopant type over all of the addition levels used was calculated. The average effects of each addition type are shown in the following sections:

4.4.2 Undoped powders.

The results of the defect area determination from sintered specimens of the blank treated and as supplied undoped TZ3Y material are shown in table 4.4.2 (appendix 1), with the effects of sintering temperature on the defect area shown in figure 4.4.2.

These results show a consistently increased defect area in the blank treated specimens when compared to the as supplied (unmodified) material for all sintering temperatures.

The differences recorded between the two samples are greater than the estimated experimental confirming that the results are showing a real effect.

Figure 4.4.2.
Effect of sintering temperature on the measured defect area of sintered specimens of unmodified and blank treated TZ3Y.

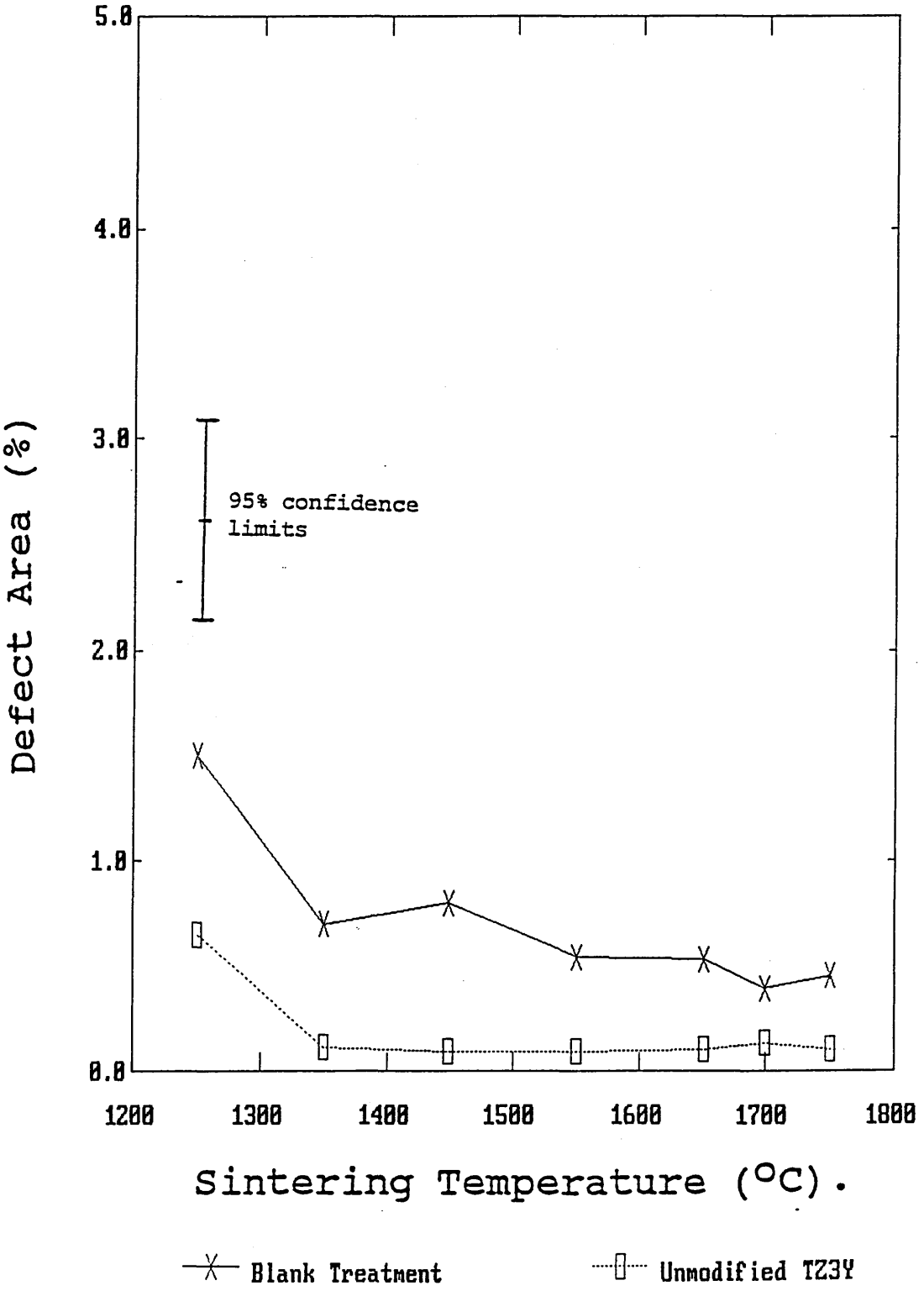

4.4.3 Alumina doped powders.

The Seescan defect area results for these samples are shown in table 4.4.3 (appendix 1), with the average effect of the alumina additions for the various sintering temperature illustrated in figure 4.4.3 (solid black line), and compared to the blank treated material (dashed line). The results for each of the individual addition levels are also shown as data points on the graph.

As can be seen from the graph, it is not possible to draw absolute conclusions from these results due to the large range of possible error. However there appears to be a general trend of a decrease in defect area where alumina additions are present for low sintering temperatures (compared to the blank treated material), with a gradual increase in defect area for sintering temperatures between 1450 and 1650°C, and a very large increase in measured defect area for sintering temperatures in excess of 1650°C.

Figure 4.4.3

Effect of sintering temperature on the measured defect area of sintered alumina doped specimens (average effect for all alumina additions shown).

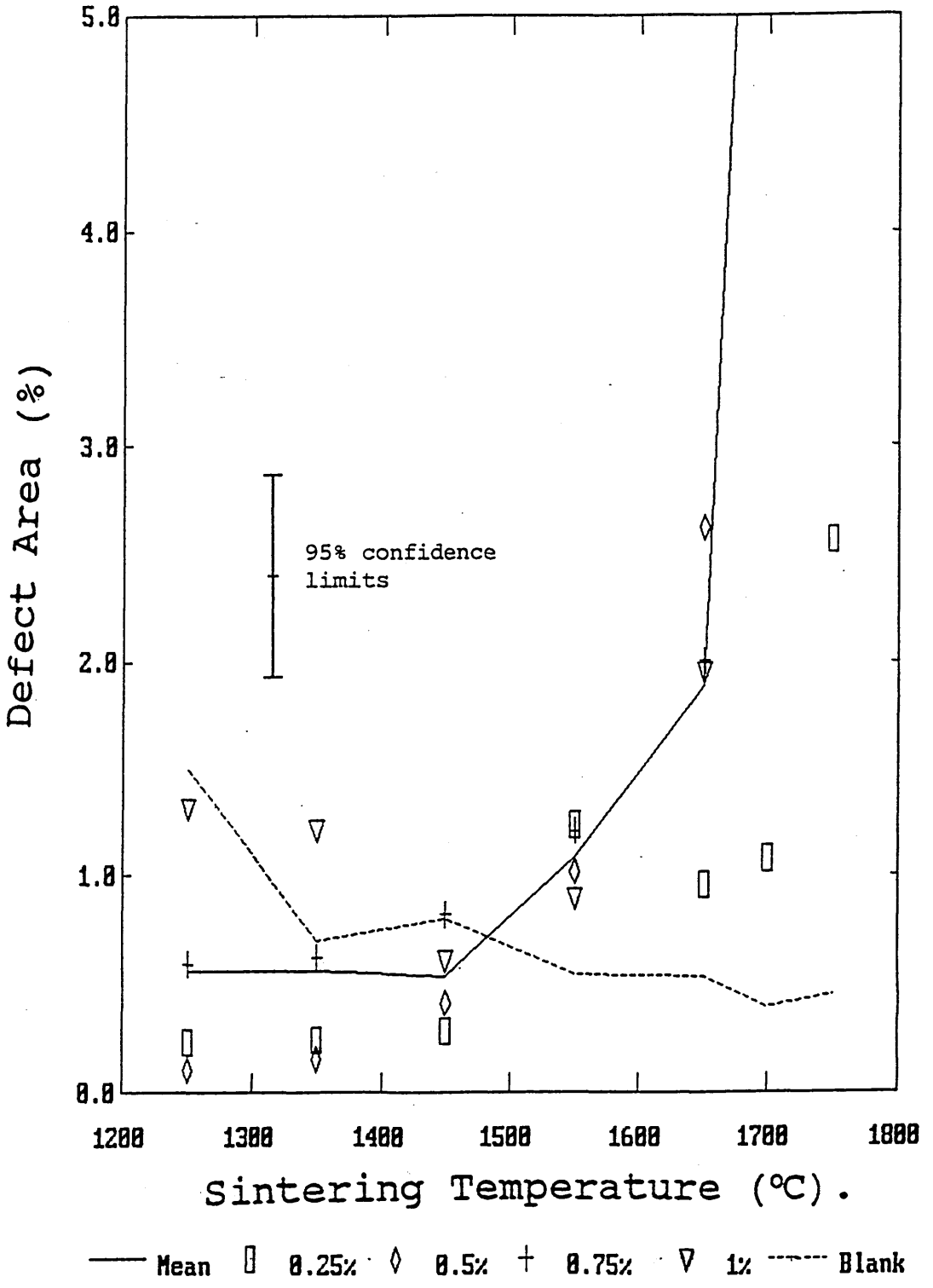

4.4.4 Silica doped powders.

The Seescan defect area results for the silica doped materials are shown in table 4.4.4 (appendix 1), with the average effect of the silica additions for the various sintering temperatures illustrated in figure 4.4.4. The results obtained for the 0.75% SiO_2 doped sample were considered anomalous (see figure 4.4.4 (b)) and were not used to calculate the average effect in figure 4.4.4(a))

The results (fig 4.4.4(a)) appear to suggest that silica additions result in a slight decrease in defect area for low sintering temperatures (compared to the undoped blank), whilst for sintering temperatures in excess of 1550°C, the measured defect area increases relative to both the undoped material, and the silica doped material at lower sintering temperatures.

Figure 4.4.4(a)
Effect of sintering temperature on the measured defect area of sintered silica doped specimens (average effect for 0.25,0.5 and 1% silica additions shown).

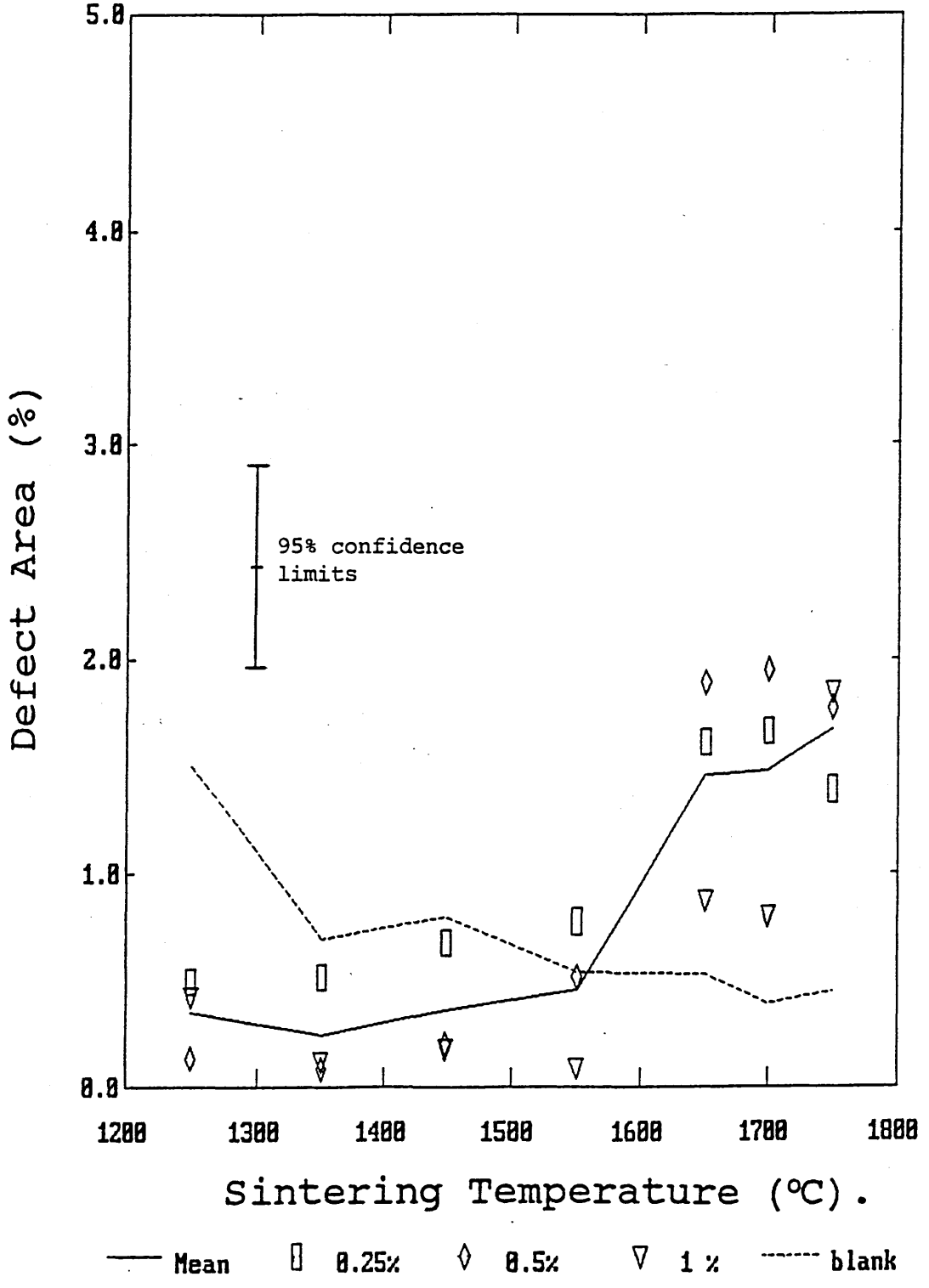

Figure 4.4.4(b)
Effect of sintering temperature on the measured defect area of anomalous 0.75% silica doped sintered specimens

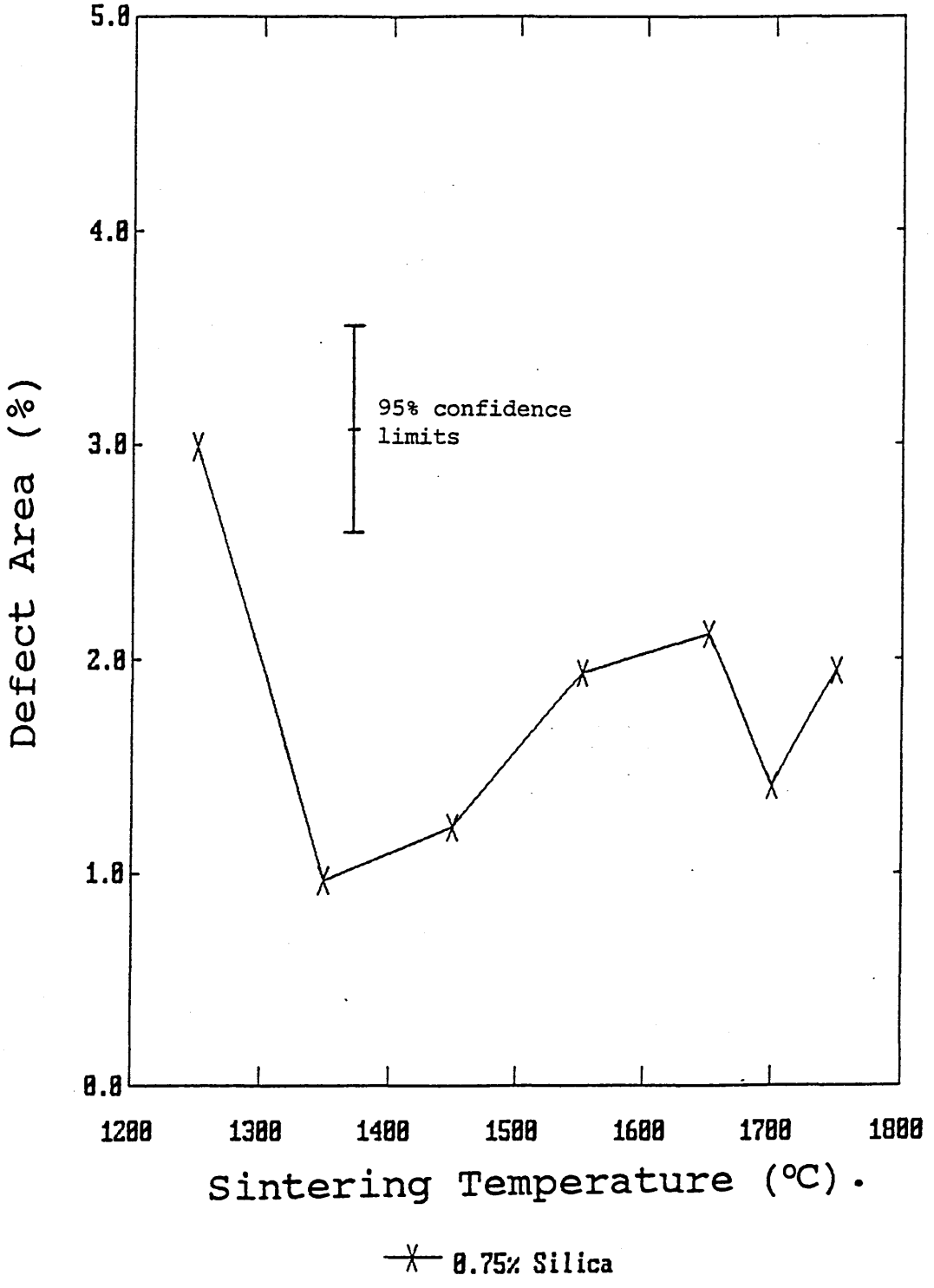

4.4.5 Titania doped samples.

The Seescan defect area results for the titania doped materials are shown in table 4.4.5 (appendix 1), with the average effect of these additions for the various sintering temperatures illustrated in figure 4.4.4.

The results (figure 4.4.5) appear to show that titania additions result in a significant increase in measured defect area, compared to the undoped sample, for sintering temperatures below 1450°C, whilst for sintering temperatures of 1450°C and above there appears to be little difference between the doped and undoped materials.

Figure 4.4.5(a)
Effect of sintering temperature on the measured defect area of sintered titania doped specimens (average effect for all TiO_2 additions shown).

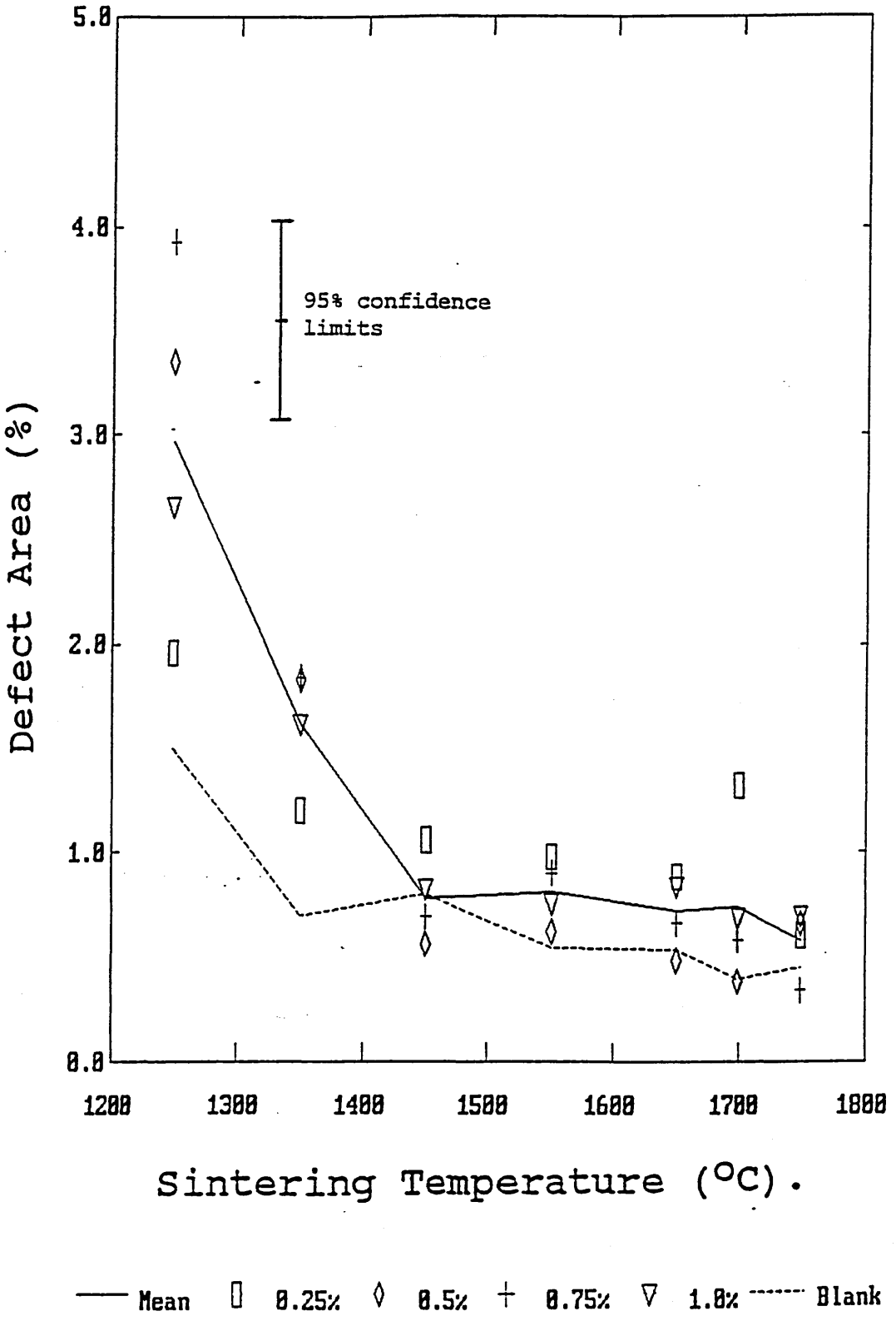

4.4.6 Multiple dopant additions.

The results of the defect area determination from sintered specimens with multiple oxide dopant additions are shown in table 4.4.6 (appendix 1), with the effects of sintering temperature on the defect area shown in figure 4.4.6.

These results show a consistent decrease in the measured defect area for all of the multiple doped samples compared to the undoped material at sintering temperatures below 1350^{o}C.

All of the samples show a trend of increasing defect area with sintering temperature, with this being particularly pronounced in the alumina containing specimens at temperatures in excess of 1450°C, or in excess of 1650°C for the alumina and titania doped material.

Figure 4.4.6
Effect of sintering temperature on measured defect area of sintered samples containing multiple oxide dopant additions.

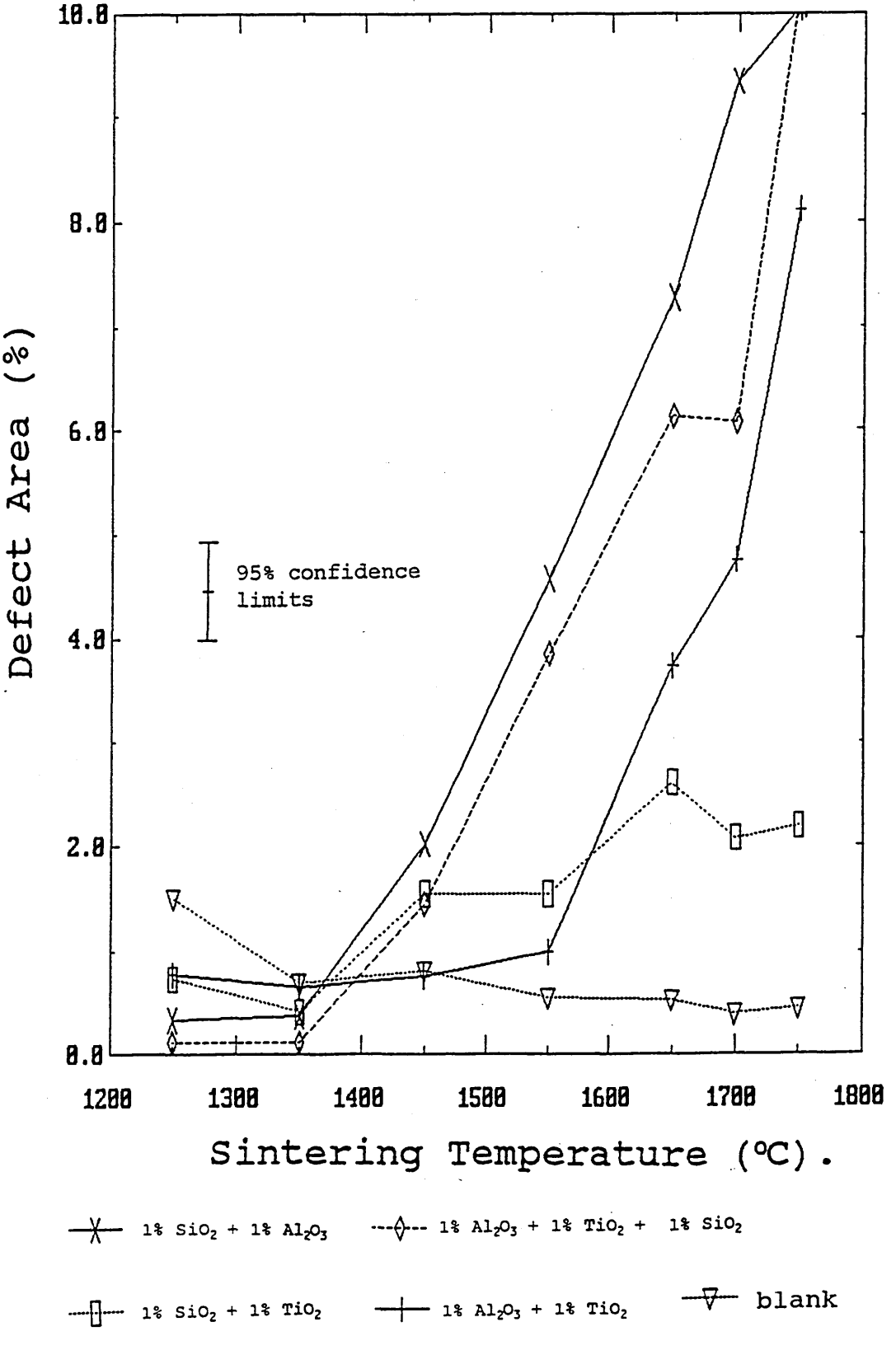

4.4.7 Mechanically mixed dopant additions.

The results of the defect area determination from sintered specimens with mechanically mixed (particulate) single oxide dopant additions are shown in table 4.4.7 (appendix 1), with the effects of sintering temperature on the defect area shown in figure 4.4.7.

These results show basically similar trends to the equivalent alkoxide doped compositions, with the alumina doped material showing an increase in defect area with sintering temperature, with a large increase for sintering temperatures in excess of 1550°C.

The silica doped specimens show a smaller but consistent increase in measured defect area with increasing sintering temperature.

The defect area of the mechanically mixed titania sample appears to be approximately independent of sintering temperature over the range of temperatures measured. This is apparently inconsistent with the results for the titanium alkoxide doped material which exhibited a much larger measured defect area at lower sintering temperatures (compared to sintering temperatures in excess of 1450°C).

Figure 4.4.7

Effect of sintering temperature on measured defect area of sintered samples containing mechanically mixed, particulate dopant additions.

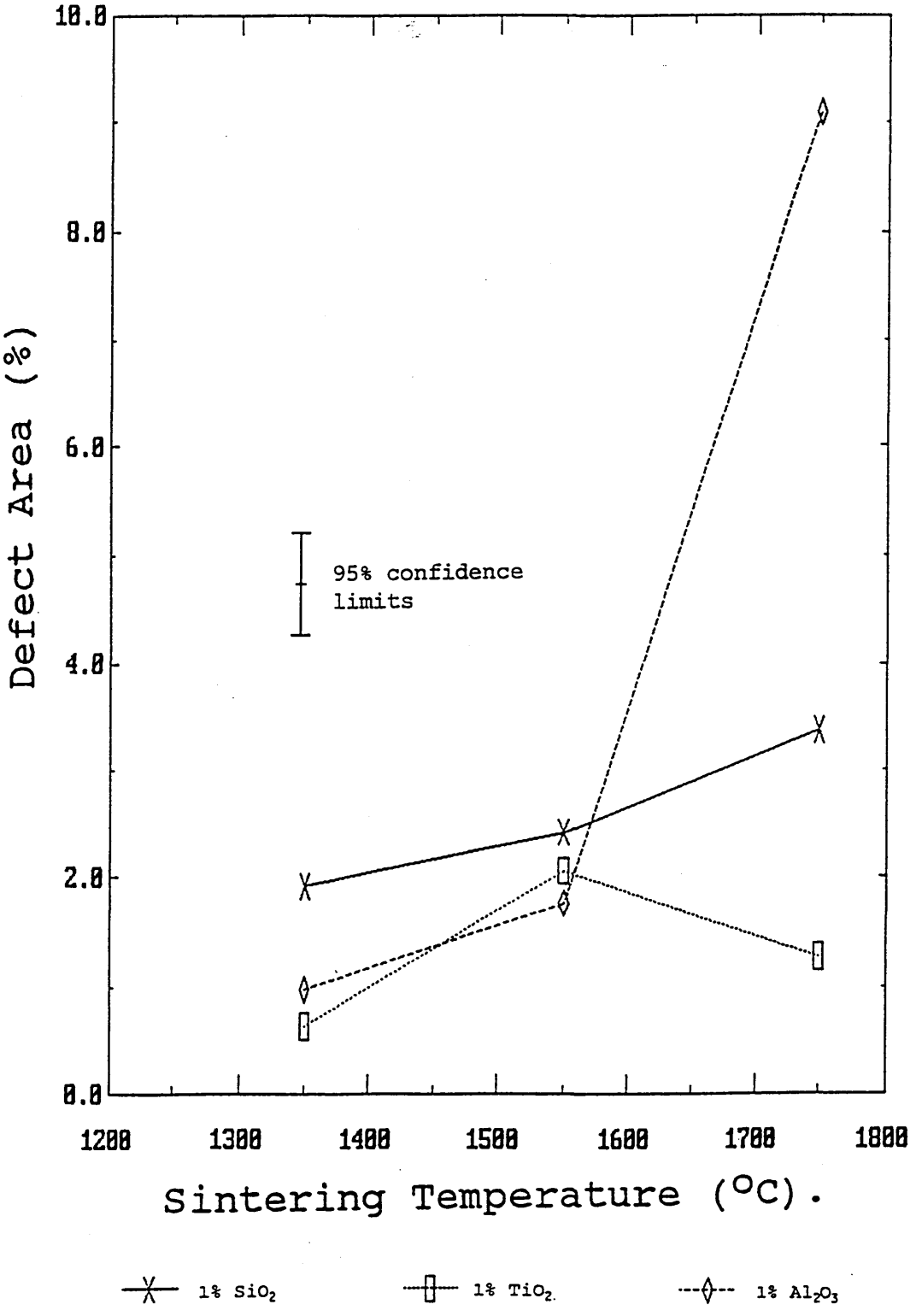

4.5 Microstructural analysis and grain size determination by SEM and EDX.

The results of the grain size determinations for the doped specimens are presented in the following section, together with the micrographs produced from the thermally etched specimens by S.E.M. and E.D.X. analysis for the nominally 1 mass percent doped specimens.

4.5.1 Determination of experimental error.

Two estimates of experimental error were carried out for the grain size determinations. These comprised (a) an estimate of the measuring error, and (b) an estimate of the total experimental error.

(a) The measuring error in the mean linear intercept determination of grain size was estimated by measuring the grain sizes on photomicrographs produced from three different areas on two of the specimens. These were the undoped (blank treated) material, and the 0.75% TiO_2 doped material.

The results and calculations used to generate this estimate of error are shown in table 4.5.1(a) (appendix 1).

(b) The total experimental error was estimated by comparing the results of grain size determinations from sintered pellets produced with duplicate batches of two of the doped powder compositions (the nominally 0.25 and 0.75 mass % alumina doped powders).

These values were used to generate 95% confidence limits for the measurements using the same method described for the seescan microstructural analysis.

The results and calculations used to generate this estimate of experimental error are shown in table 4.5.1(b) (appendix 1).

4.5.2 Undoped material.

The results of the grain size determinations on the sintered specimens of undoped and blank treated TZ3Y powder are shown in table 4.5.2 (appendix 1), with the effect of sintering temperature on the grain size illustrated in figure 4.5.2(a).

The microstructural development of the undoped powders sintering temperatures between 1350 and 1750°C is shown in figures 4.5.2 (b)-(d).

The results show an increase in grain size with increasing sintering temperature, with this becoming increasingly significant at sintering temperatures in the range 1550-1750°C.

No grain boundary phases, intra or intergranular inclusions can be identified in these specimens.

Figure 4.5.2 (a)
Effect of sintering temperature on the grain growth of undoped T.Z.P. (TZ3Y).

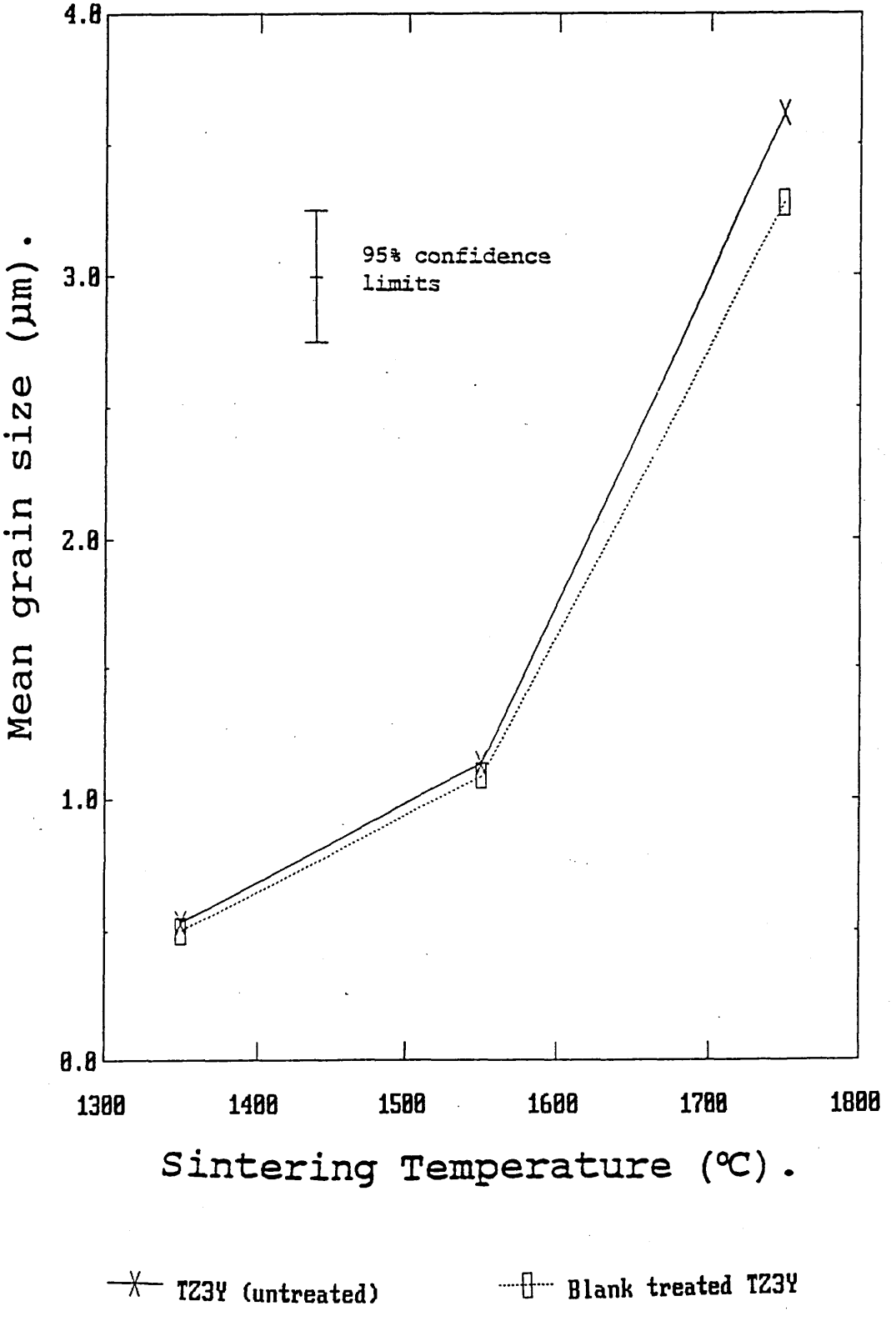

Figures 4.5.2 (b) - (c).
S.E.M. Micrographs, Thermally etched, sintered specimens.
Undoped TZP.

(b) 1350°C sintering temperature.

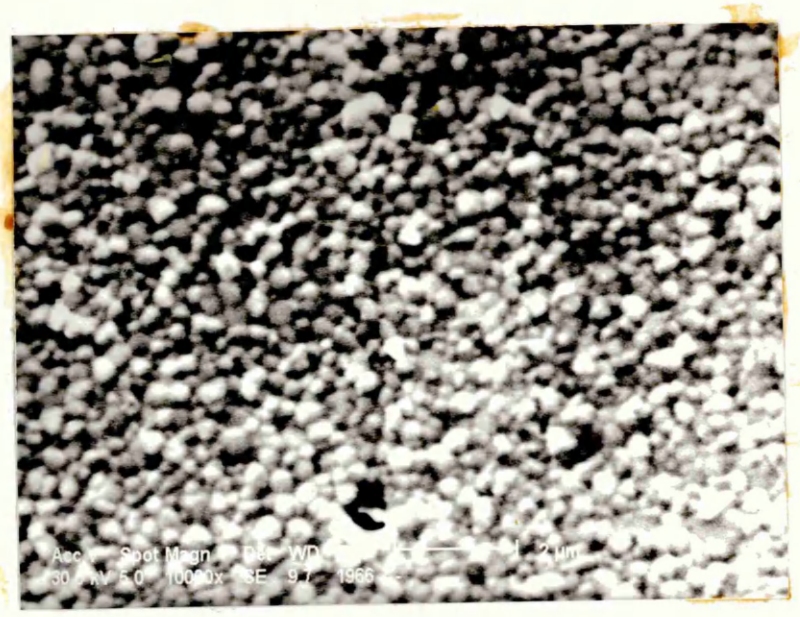

(c) 1550°C sintering temperature.

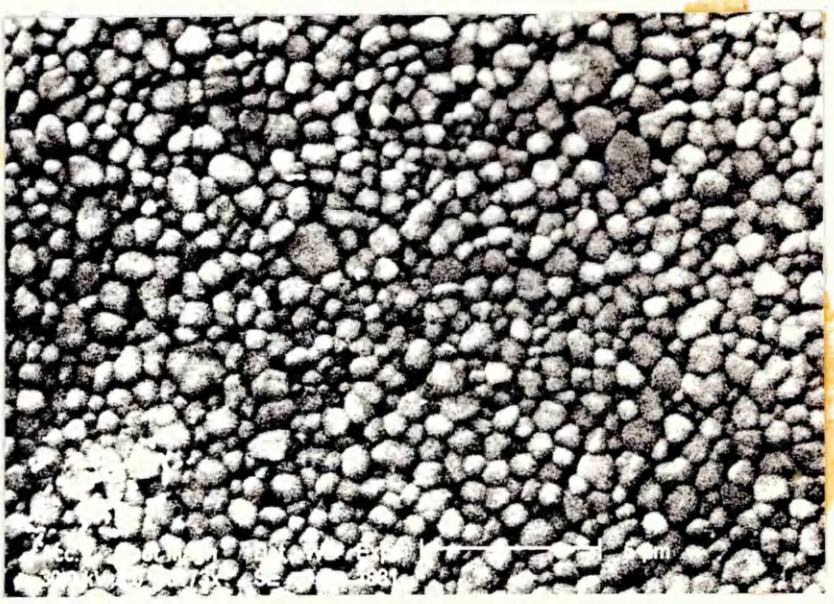

Figure 4.5.2
S.E.M. Micrograph, Thermally etched,
sintered specimens.
Undoped TZP.
(d) 1750°C sintering temperature.

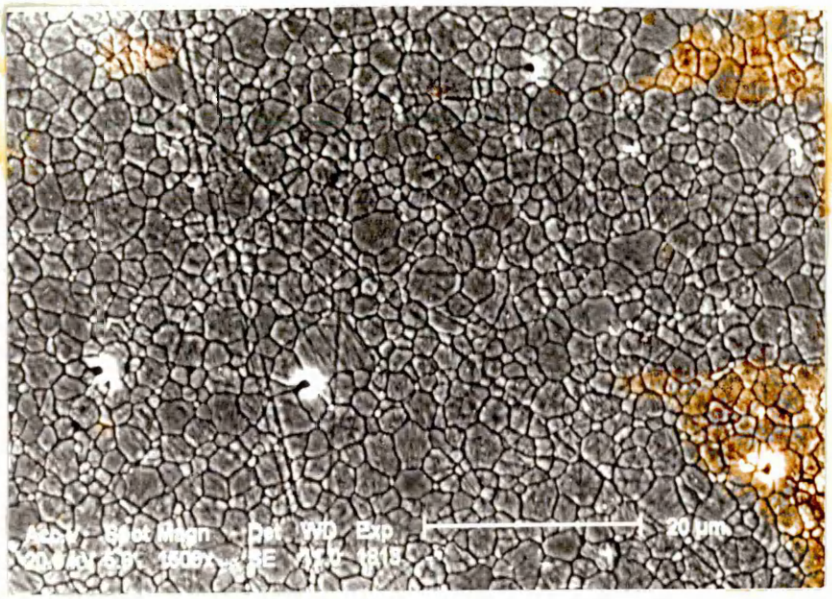

4.5.3 Alumina doped material.

The results of the grain size determinations on the sintered specimens of the alumina doped TZ3Y powder are shown in table 4.5.3 (appendix 1), with the effect of sintering temperature on the grain size illustrated in figure 4.5.3 (a).

The microstructural development of the nominally 1 mass percent alumina doped powders at sintering temperatures between 1350 and 1750°C is shown in figures 4.5.3 (b)-(d), with the results of the x-ray mapping experiments on these specimens shown in figures 4.5.3 (e)-(h). The results show an increase in grain size with increasing sintering temperature similar to the undoped material at sintering temperatures up to 1550°C, with a much greater rate of grain growth for sintering temperatures in the range 1550-1750°C.

The materials also contain a substantial number of alumina containing inclusions in the microstructure of the 1350 and 1550°C sintered specimens. The volume fraction of these inclusions present in the 1750°C sintered material was substantially reduced.

Variations in ytrria concentration between grains in the microstructure can also be identified, particularly where lower magnification values were used.

Figure 4.5.3 (a)
Effect of sintering temperature on the grain growth of alumina doped T.Z.P. (TZ3Y).

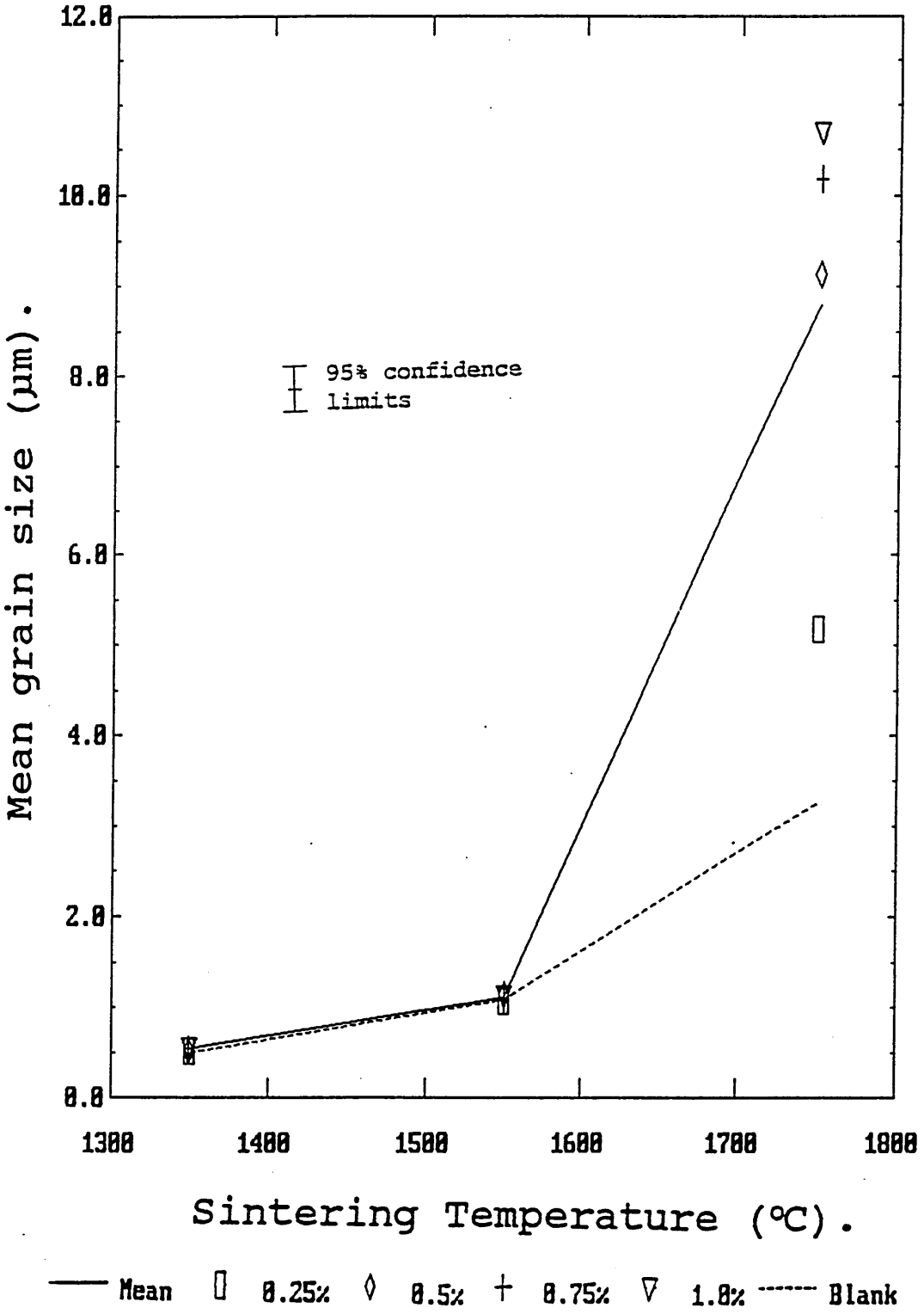

Figures 4.5.3 (b) - (c).
S.E.M. Micrographs, Thermally etched, sintered specimens.
Nominal 1 mass percent alumina doped TZP.

(b) 1350°C sintering temperature.

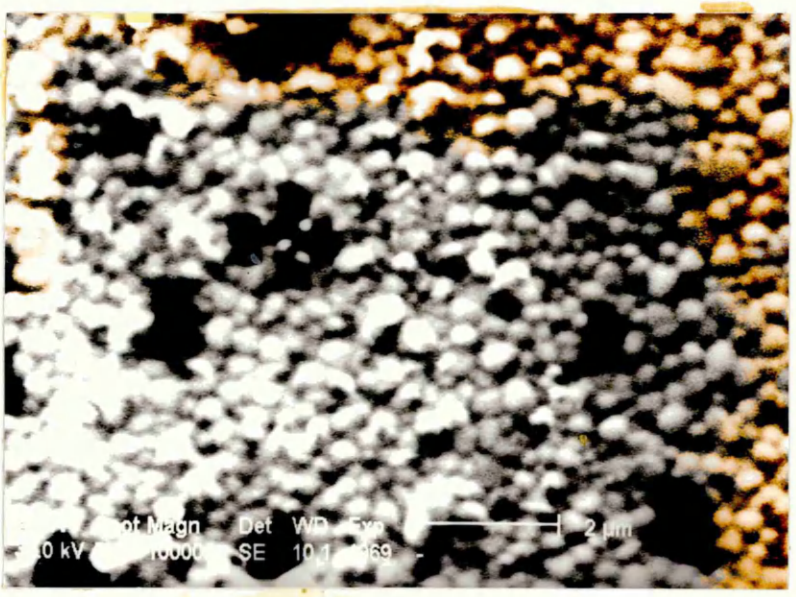

(c) 1550°C sintering temperature.

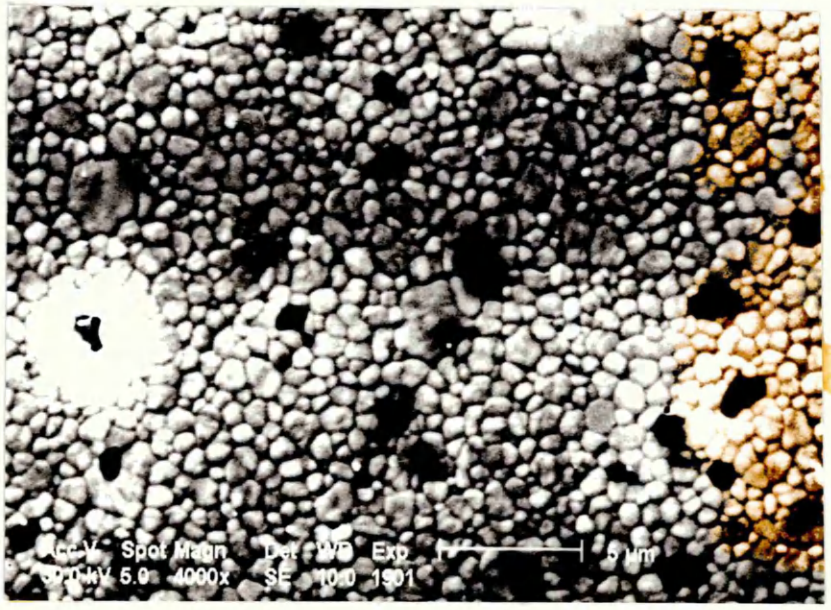

Figure 4.5.3 (d)
S.E.M. Micrograph, Thermally etched,
sintered specimens.
Nominal 1 mass percent alumina doped T.Z.P.
1750°C sintering temperature.

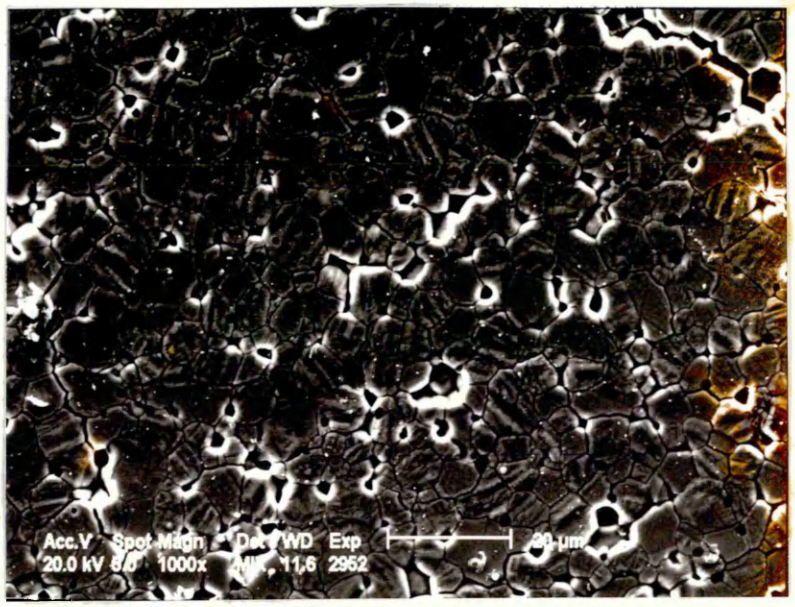

Figures 4.5.3 (e)-(f).
Compositional x -ray dot maps of thermal etched and sintered alumina doped specimens.
Nominal 1 mass % alumina addition.
1550°C sintering temperature.

(e) Secondary electron image of mapped area.

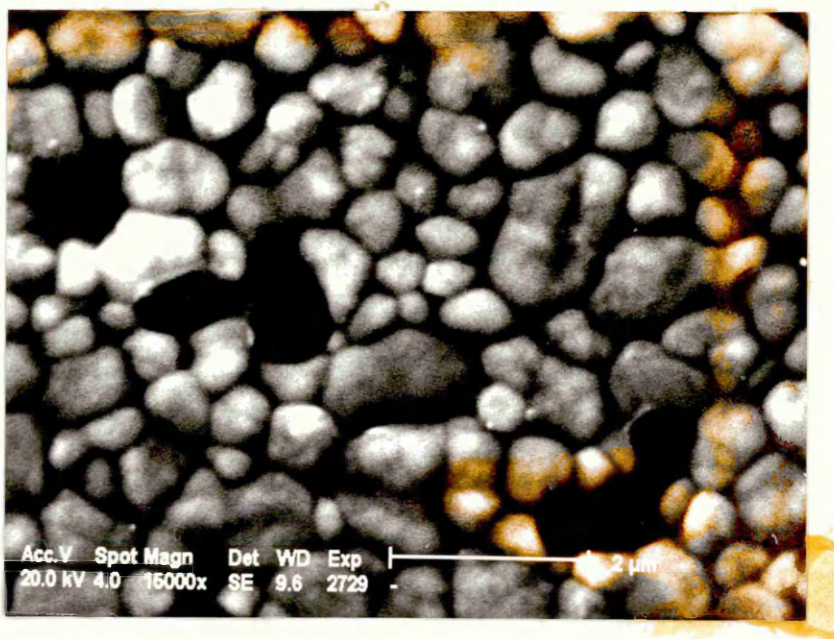

(f) E.D.X. Dot maps.

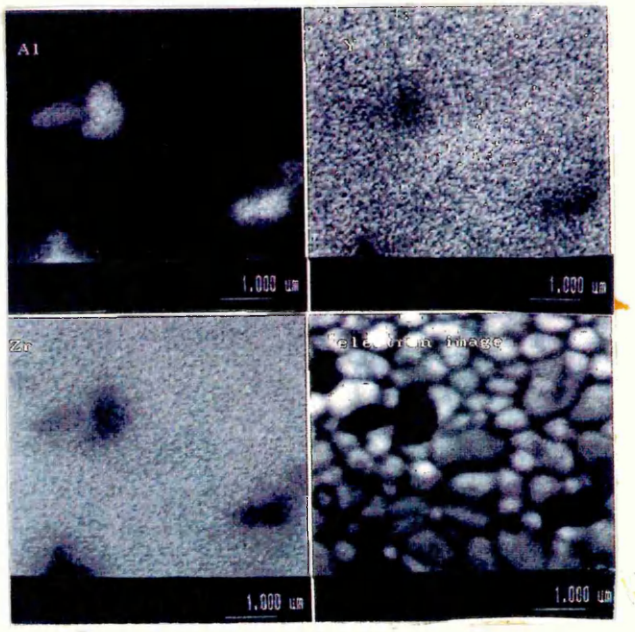

Figures 4.5.3 (g)-(h).
Compositional x-ray dot maps of thermal etched and sintered alumina doped specimens.
Nominal 1 mass % alumina addition.
1750°C sintering temperature.

(g) Secondary electron image of mapped area.

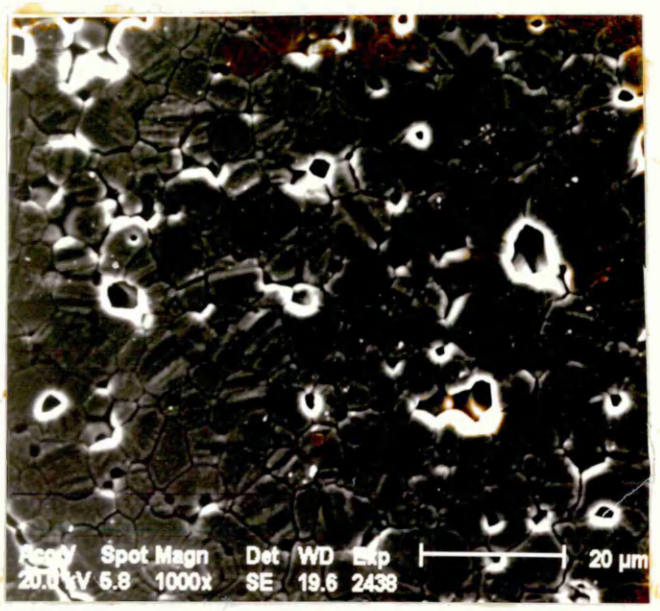

(h) E.D.X. Dot maps.

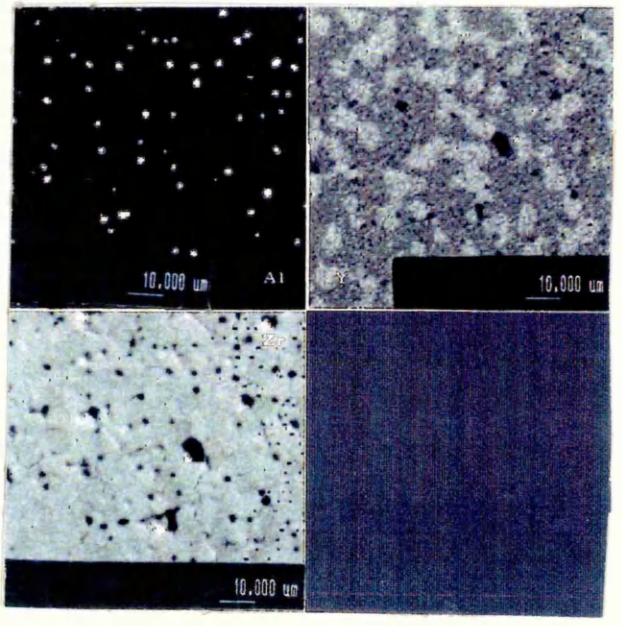

4.5.4 Silica doped specimens.

The results of the grain size determinations on the sintered specimens of silica doped Y-T.Z.P. powder are shown in table 4.5.4 (appendix 1), with the effect of sintering temperature on the grain size illustrated in figure 4.5.4(a).

The microstructural development of the undoped powders sintering temperatures between 1350 and 1750°C is shown in figures 4.5.4 (b)-(d), with the results of the X-ray mapping experiments on the blank treated powder shown in figures 4.5.4 (e)-(h).

The results show an increase in grain size with increasing sintering temperature, with this becoming increasingly significant at sintering temperatures in the range 1550-1750°C.

The micrographs, and E.D.X. dot maps show the presence of a grain boundary phase, particularly at triple points between the grains which becomes increasingly significant with increased sintering temperature.

Figure 4.5.4 (i) shows the microstructure of the anomalous 0.75 mass % (nominally) silica doped specimens, particularly the presence of sintering defects arising from agglomerate formation.

Figure 4.5.4 (a)
Effect of sintering temperature on the grain growth of silica doped T.Z.P. (TZ3Y).

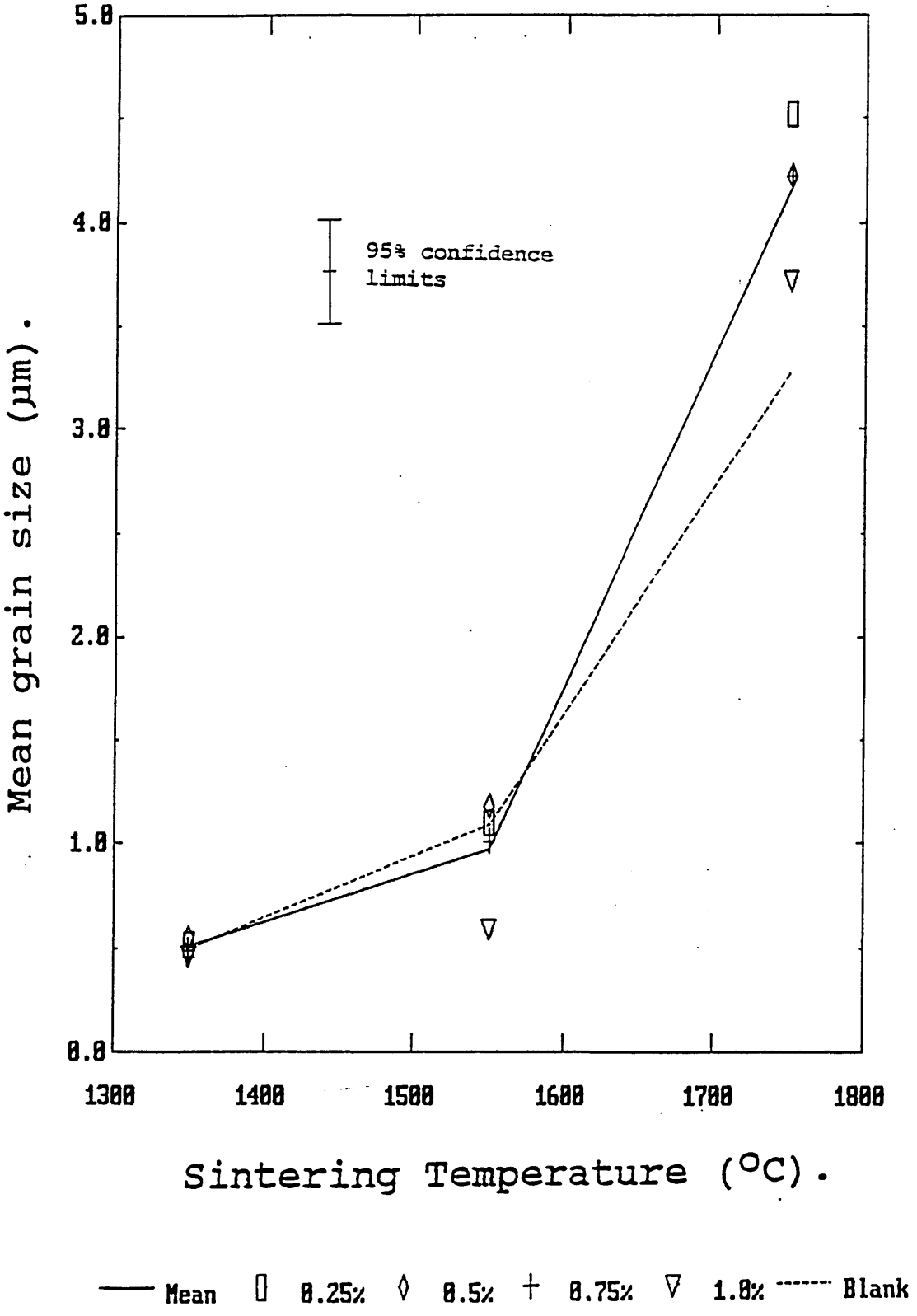

Figures 4.5.4 (b) - (c).
S.E.M. Micrographs. Thermally etched, sintered specimens.
Nominal 1 mass percent silica doped TZP.

(b) 1350°C sintering temperature.

(c) 1550°C sintering temperature.

Figure 4.5.4 (d)
S.E.M. Micrograph. Thermally etched, sintered specimen.
Nominal 1 mass percent silica doped TZP.
1750°C sintering temperature.

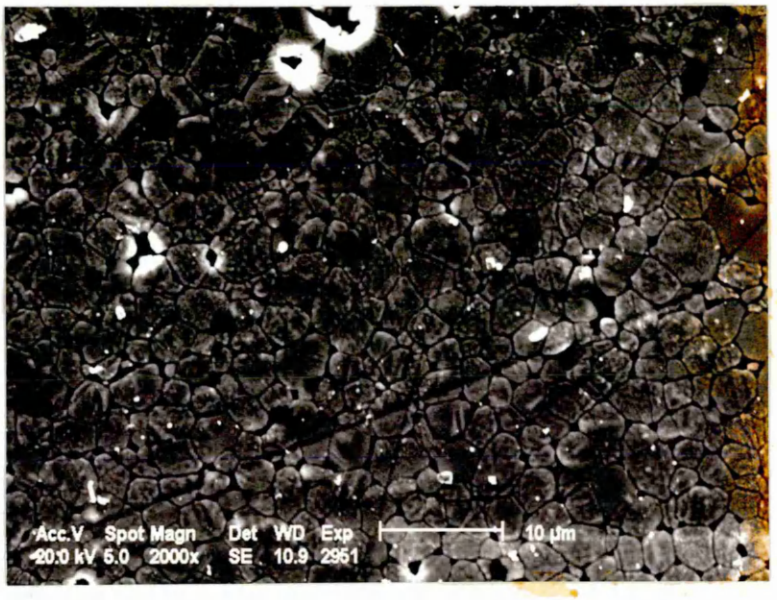

Figures 4.5.4 (e)-(f).
Compositional x -ray dot maps of thermal etched and sintered silica doped specimens.
Nominal 1 mass % silica addition.
1550°C sintering temperature.

(e) Secondary electron image of mapped area.

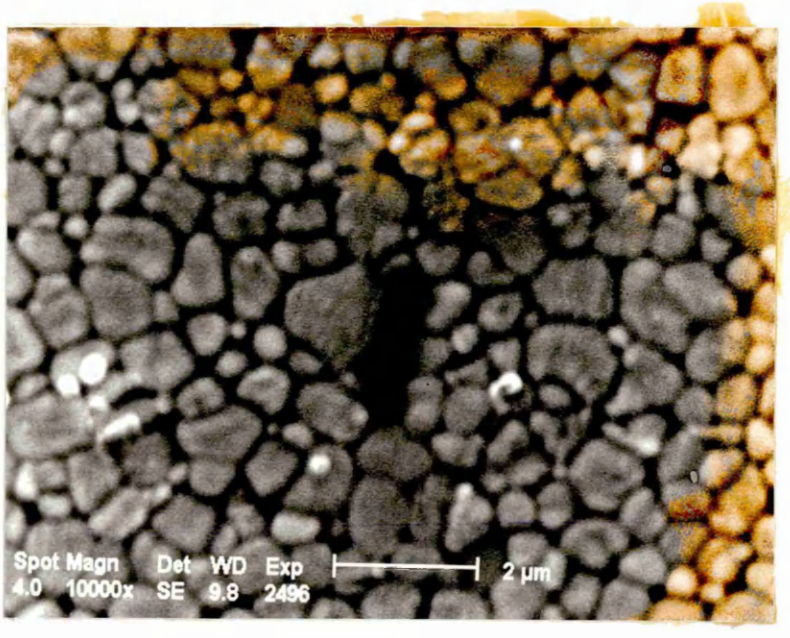

(f) E.D.X. Dot maps.

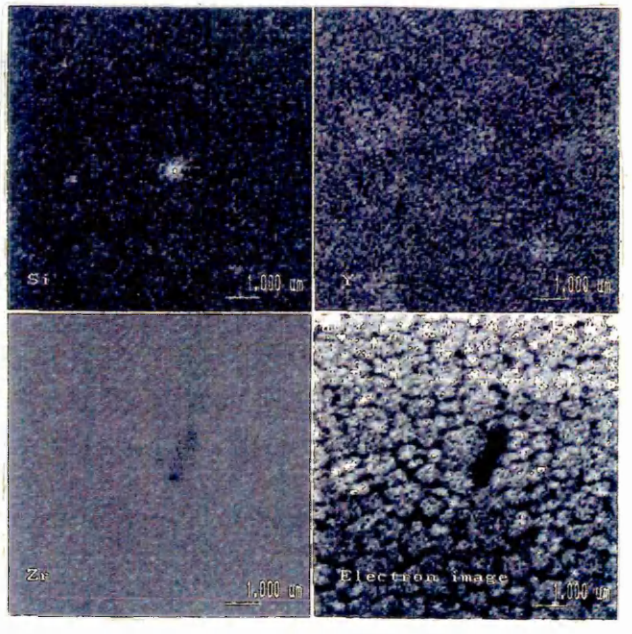

Figures 4.5.4 (g)-(h).
Compositional x-ray dot maps of thermal etched and sintered silica doped specimens.
Nominal 1 mass % silica addition.
1750°C sintering temperature.

(g) Secondary electron image of mapped area.

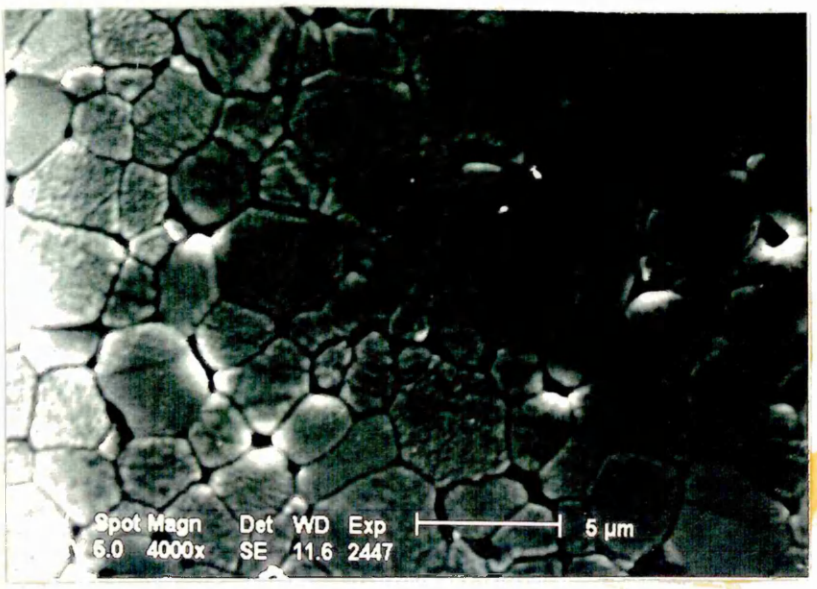

(h) E.D.X. Dot maps.

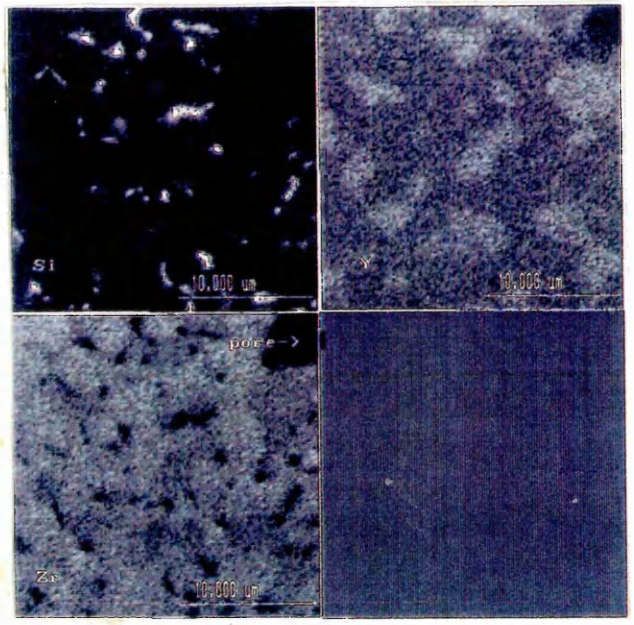

Figure 4.5.4 (i)
Sintering defects from agglomerate formation in the anomalous nominally 0.75 mass % silica doped specimens.

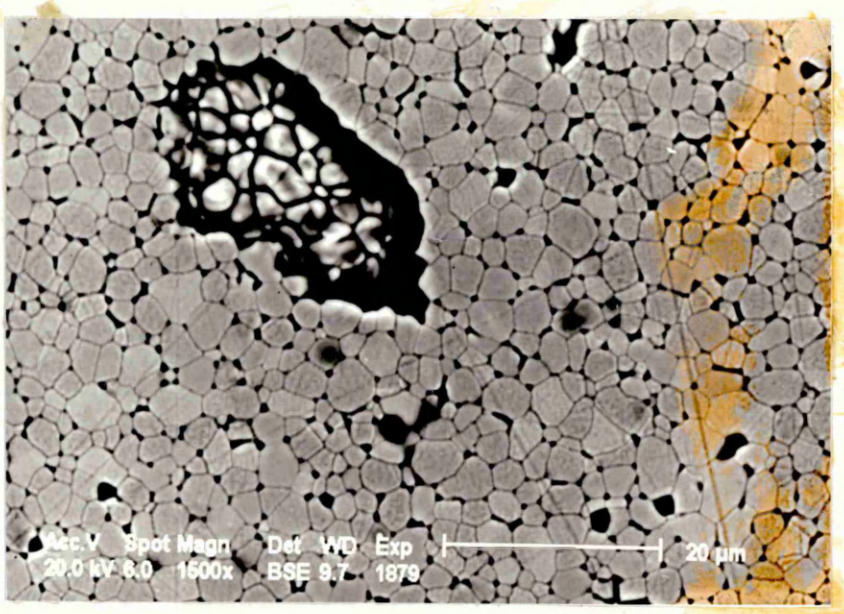

4.5.5 Titania doped specimens.

The results of the grain size determinations on the sintered specimens of titania doped TZ3Y powder are shown in table 4.5.5 (appendix 1), with the effect of sintering temperature on the grain size illustrated in figure 4.5.5(a).

The microstructural development of the nominally 1 mass percent titania doped material, for sintering temperatures between 1350 and 1750°C is shown in figures 4.5.5 (b)-(d), with the results of the X-ray mapping experiments on the blank treated powder shown in figures 4.5.5 (e)-(h).

The results show a similar increase in grain size with increasing sintering temperature to the undoped material, although the grain size appears to be consistently slightly larger for the titania doped material, particularly for higher sintering temperatures.

No grain boundary phases can be identified in these specimens.

Figure 4.5.5 (a)
Effect of sintering temperature on the grain growth of titania doped T.Z.P. (TZ3Y).

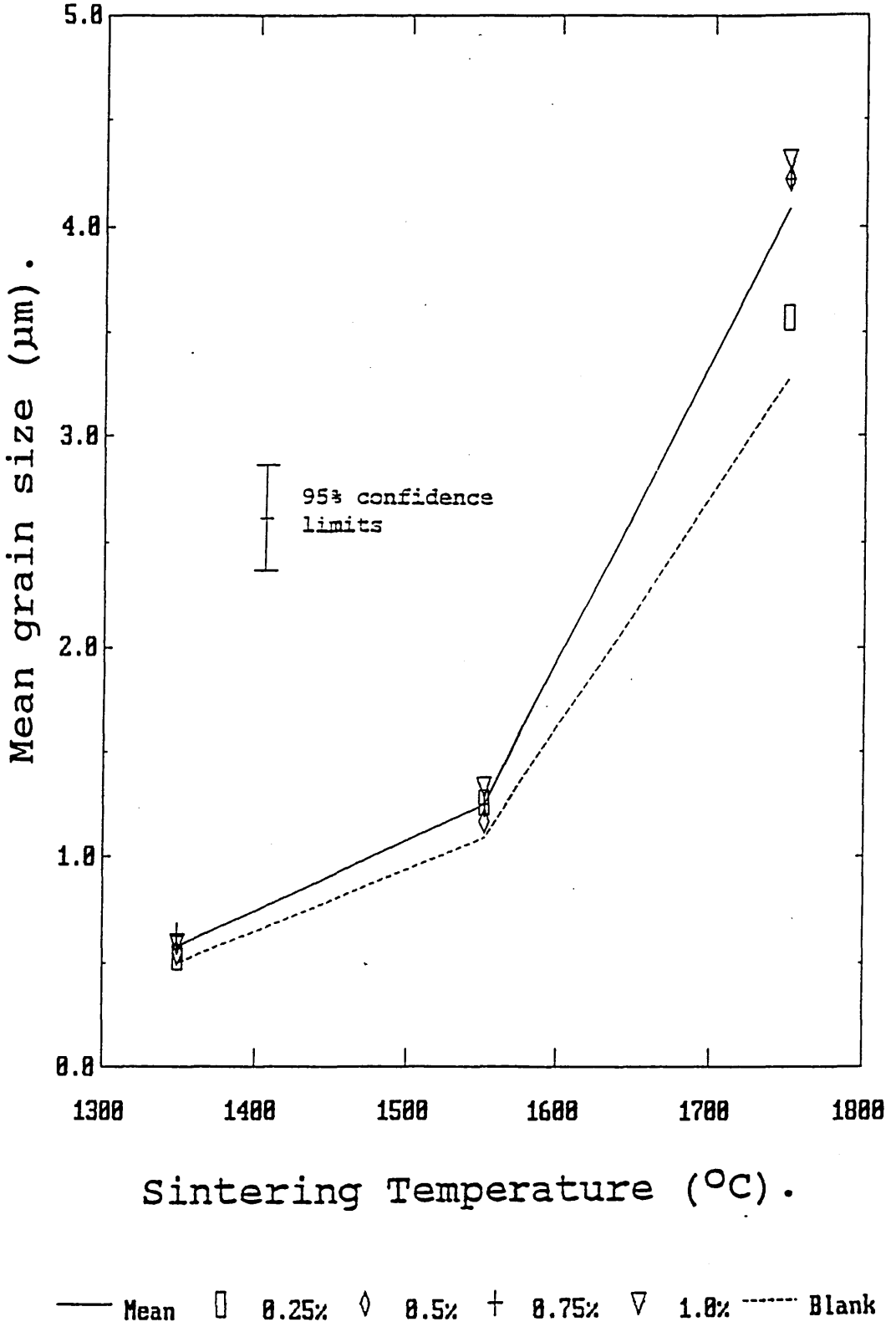

Figures 4.5.5 (b) - (c).

S.E.M. Micrographs. Thermally etched, sintered specimens. Nominal 1 mass percent titania doped TZP.

(b) 1350°C sintering temperature.

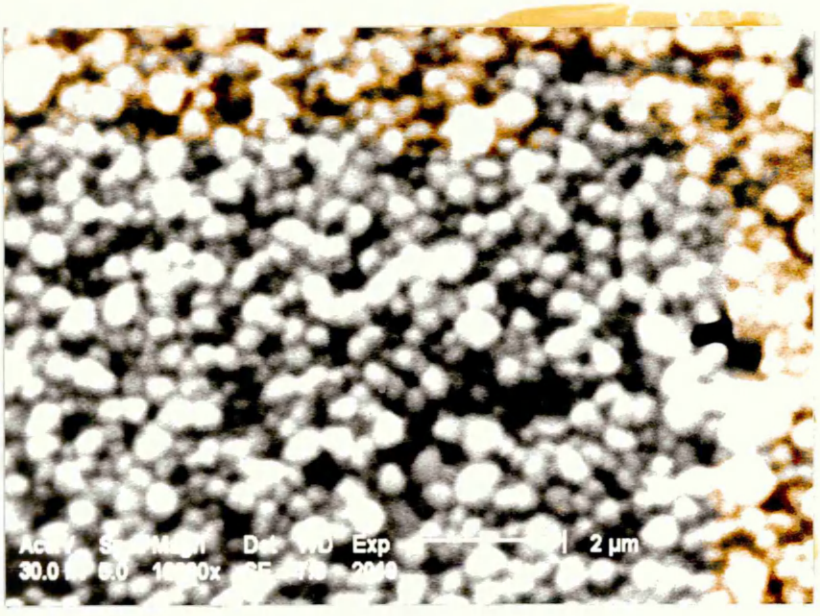

(c) 1550°C sintering temperature.

Figure 4.5.5 (d).
S.E.M. Micrograph. Thermally etched,
sintered specimen.
Nominal 1 mass percent titania doped TZP.
1750°C sintering temperature.

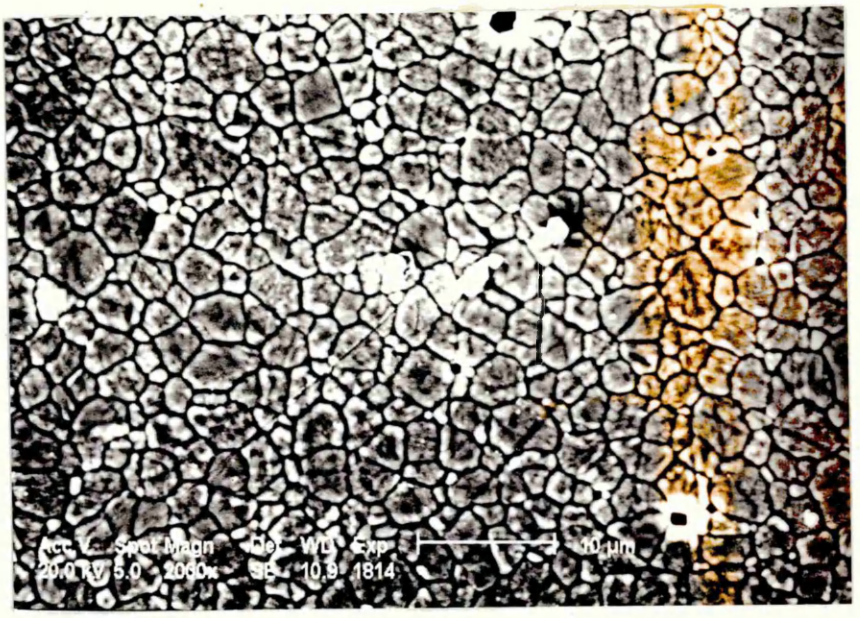

Figures 4.5.5 (e)-(f).

Compositional x -ray dot maps of thermal etched and sintered titania doped specimens.

Nominal 1 mass % titania addition.

1550°C sintering temperature.

(e) Secondary electron image of mapped area.

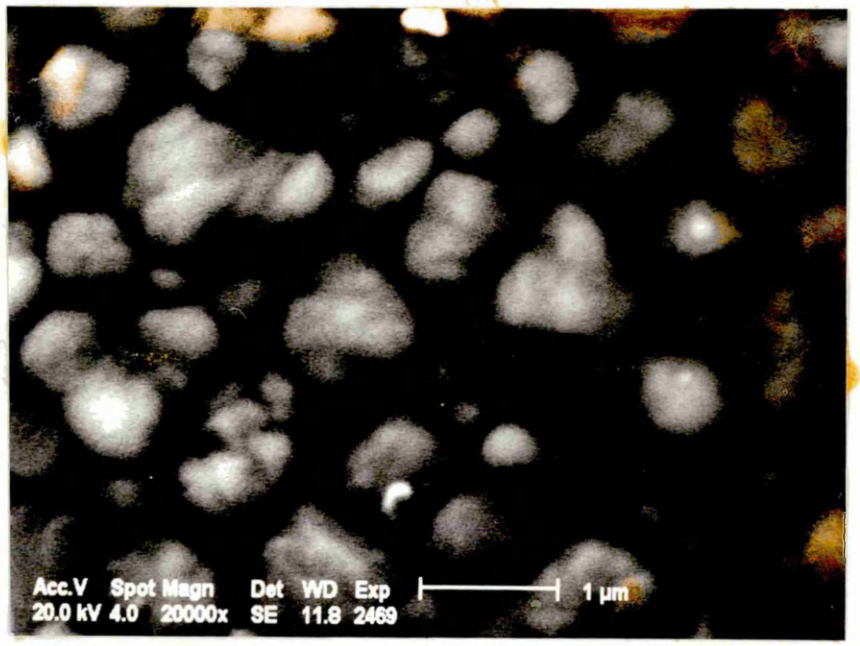

(f) E.D.X. Dot maps.

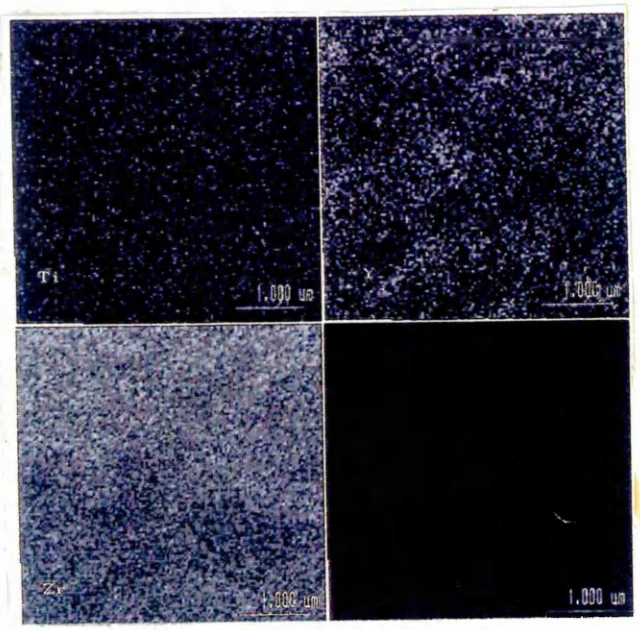

Figures 4.5.5 (g)-(h).
Compositional x-ray dot maps of thermal etched and sintered titania doped specimens.
Nominal 1 mass % titania addition.
1750°C sintering temperature.

(g) Secondary electron image of mapped area.

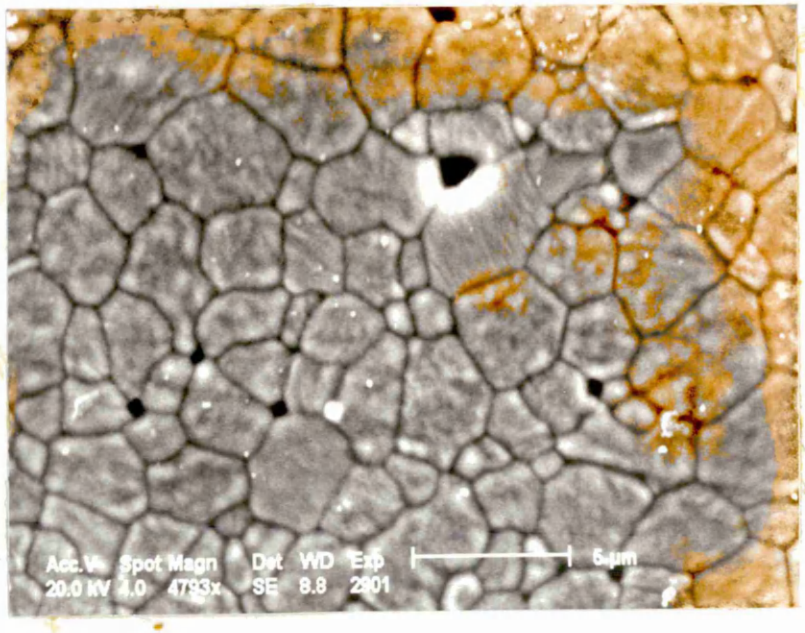

(h) E.D.X. Dot maps.

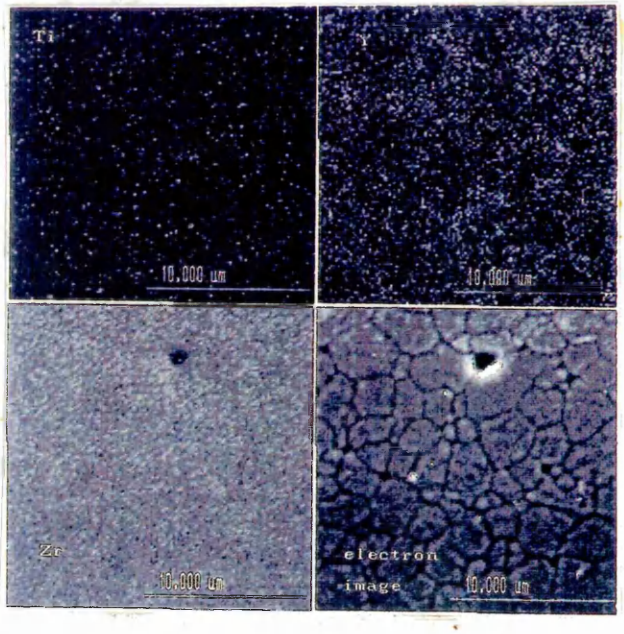

4.5.6 Multiple oxide doped samples.

The results of the grain size determinations on the sintered TZ3Y containing multiple dopant additions are shown in table 4.5.6 (appendix 1), with the effect of sintering temperature on the grain size illustrated in figure 4.5.6(a), and on microstructural development in figures 4.5.6 (b)-(i).

The results for the alumina plus titania, and the silica plus titanium doped materials show similar trends to the undoped materials, although with increased grain growth at high sintering temperatures, whilst the samples containing both alumina and silica (with or without TiO_2) show much larger grain growth at 1550 and 1650°C sintering temperature, with a bimodal grain size distribution present in the 1550°C sintered materials.

Figure 4.5.6 (a)

Effect of sintering temperature on the grain growth of multiple oxide doped T.Z.P.

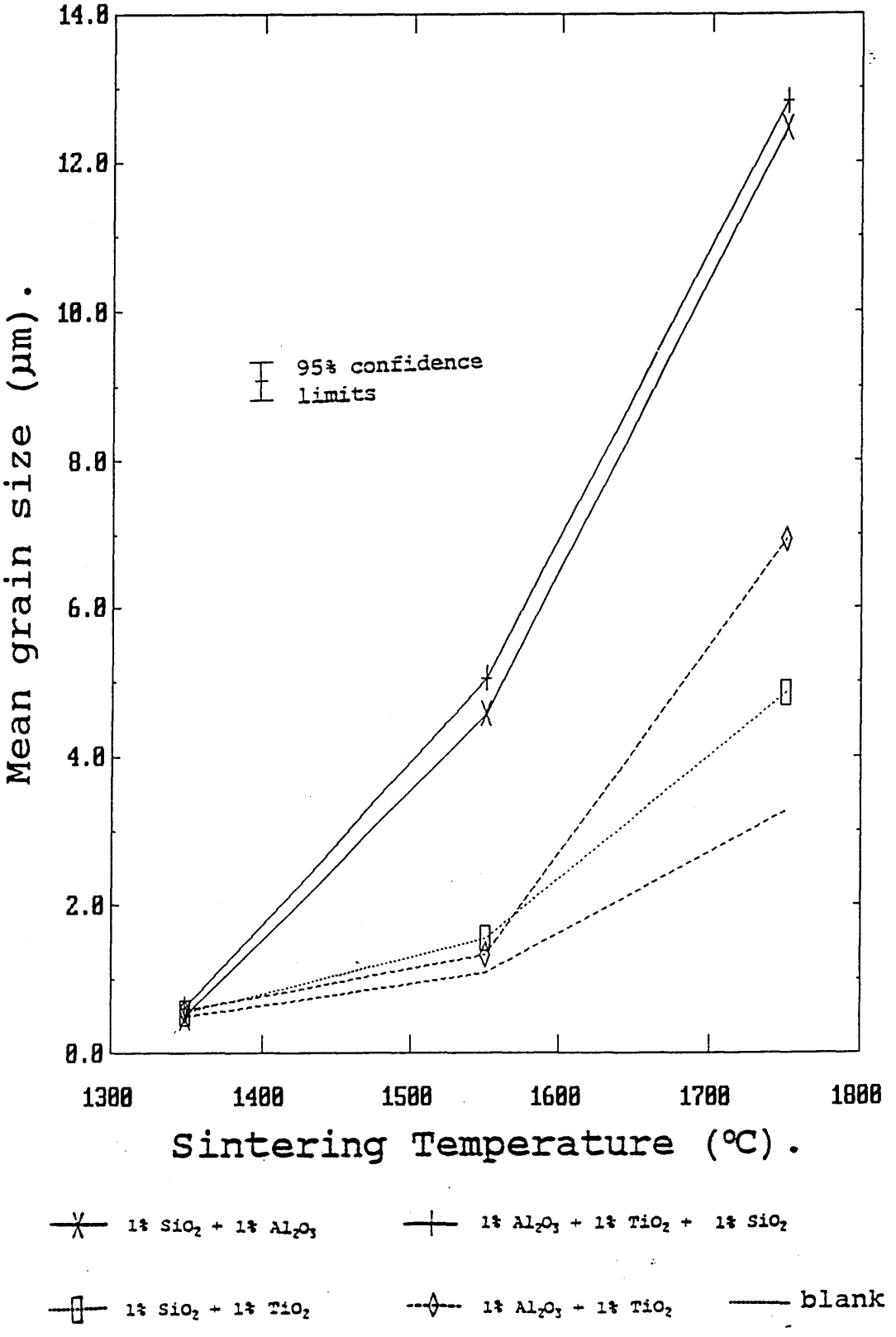

Figures 4.5.6 (b) - (c).
S.E.M. Micrographs. Thermally etched, sintered specimens.
Silica plus titania doped material.

(b) 1550°C sintering temperature.

(c) 1750°C sintering temperature.

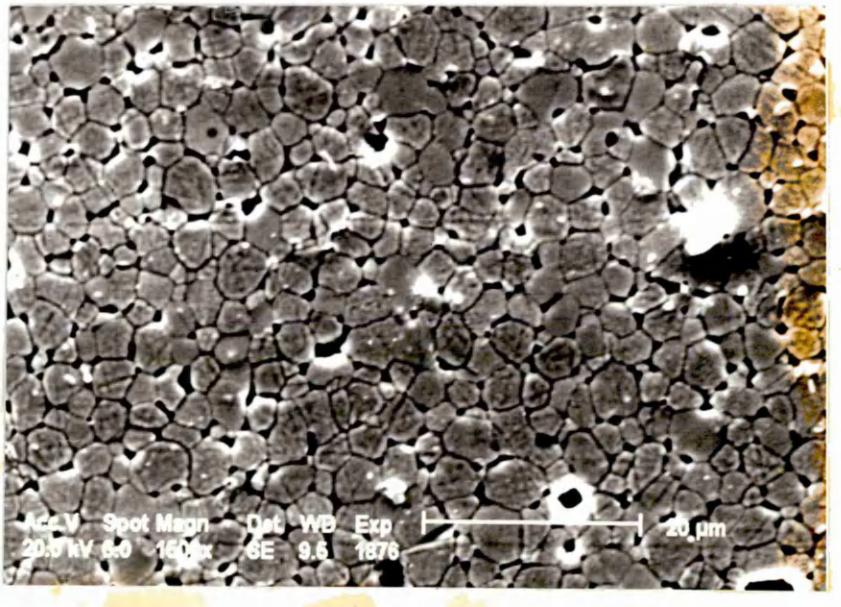

Figures 4.5.6 (d) - (e).
S.E.M. Micrographs. Thermally etched, sintered specimens.
Alumina plus titania doped TZP.

(d) 1550°C sintering temperature.

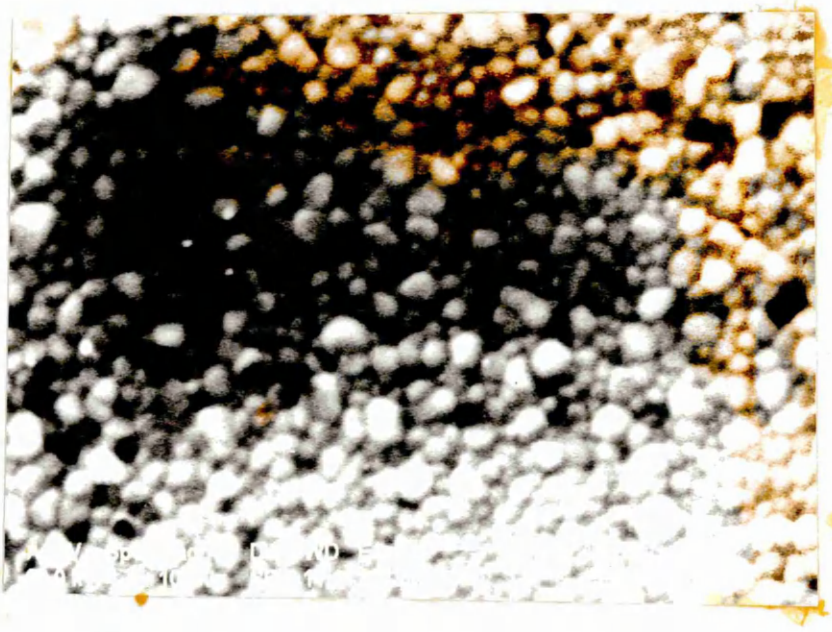

(e) 1750°C sintering temperature.

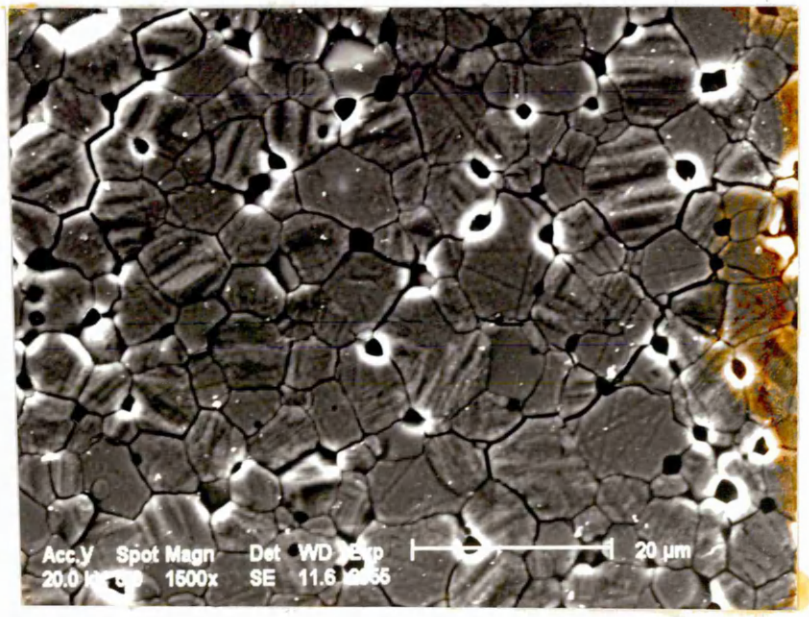

Figures 4.5.6 (f) - (g).
S.E.M. Micrographs. Thermally etched, sintered specimens.
Alumina plus silica doped TZP.

(f) 1550°C sintering temperature.

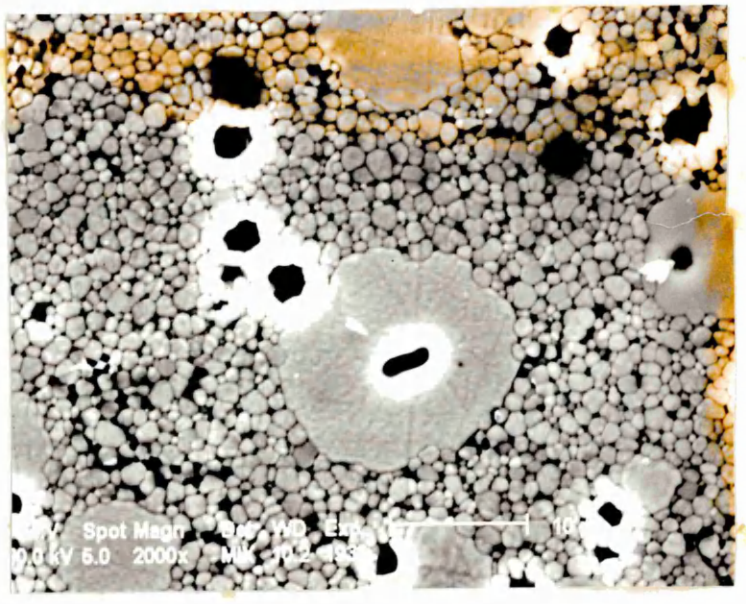

(g) 1750°C sintering temperature

Figures 4.5.6 (h) - (i).
S.E.M. Micrographs. Thermally etched, sintered specimens.
Alumina plus silica plus titania doped TZP.

(h) 1550°C sintering temperature.

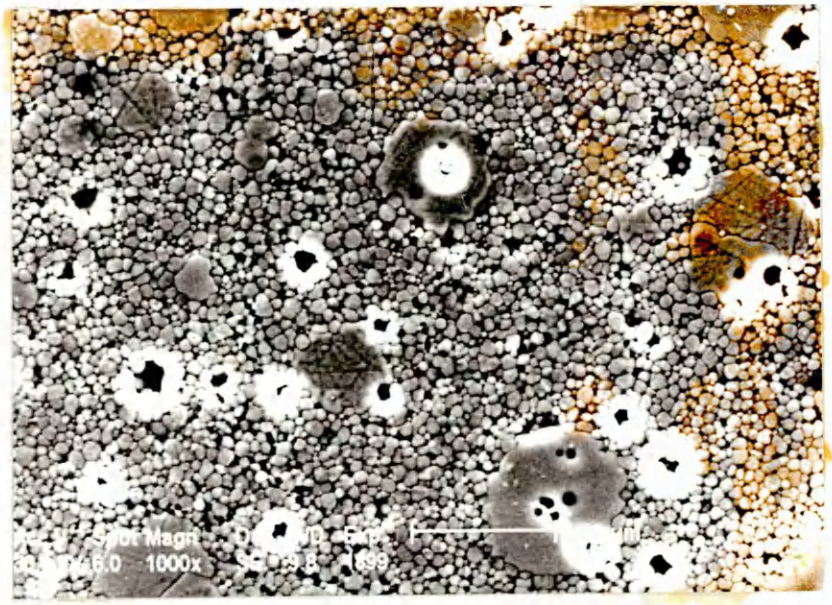

(i) 1750°C sintering temperature

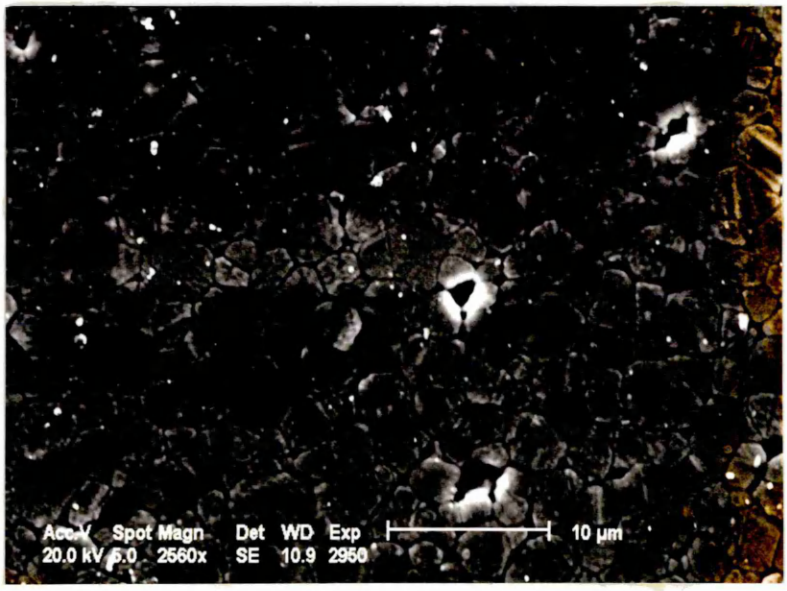

4.6 X-ray diffraction studies of phase composition.

The effects of sintering temperature, type of dopant and dopant addition level on the phase composition of the sintered samples are reported in this section.

4.6.1 Sources and estimation of experimental error.

The possible sources of experimental error in these experiments were (a) errors arising from the measurement technique used, including the curve fitting estimate (measuring error); and (b) errors arising from variability in the powder doping process, specimen fabrication and heat treatment in addition to the measuring error (total experimental error).

Two estimates of experimental error were therefore made to attempt to quantify these.

Due to time constraints, it was not possible to undertake multiple measurements for all of the X-ray diffraction studies, and the results reported are not mean values.

(a) An estimate of the measuring error, was undertaken by carrying out duplicate measurements on a subset of the total experiments, and comparing the results between the original and duplicate measurements using a similar technique to that described for the sintering shrinkage and density determinations.

The measuring error was estimated from the (upper) 95% confidence limit of the mean difference between the two sets of results, with the assumption being made that the measuring error in the subset of experiments chosen were representative of the measuring errors in the experiment as a whole.

The results and calculation used to estimate the measuring error are shown in table 4.6.1(a) (appendix 1).

(b) An estimate of total experimental error was also made using a similar technique to that described for the shrinkage and density determinations.

The entire experiment was repeated for 2 dopant addition levels, and the results compared as a measure of reproducibility.

The results and calculation used to generate this estimate of experimental error are shown in table 4.6.1 (b) (appendix 1).

The estimate of error by method (a) gave similar results to the estimate by method (b), indicating that the total experimental error was not significantly greater than the measuring error in the phase determination.

4.6.2 Undoped samples.

The development of the cubic, tetragonal and monoclinic phases in undoped TZP is illustrated in figures 4.6.2(a), (b) and (c) respectively, for a range of sintering temperatures between 1350 and 1750°C. The results are tabulated in full in table 4.6.2 (appendix 1).

The results indicate that there is generally little if any difference between the as received and the blank treated powder within the limits of measuring error.

The results appear to show a trend of increasing amounts of cubic and monoclinic phase with increasing sintering temperature up to 1650°C, with a corresponding decrease in tetragonal phase.

The results for the samples sintered at 1750°C appear to reverse this trend however, with the amount of tetragonal phase increasing and the proportions of cubic and possibly monoclinic phase decreasing.

Figure 4.6.2(a).

Effect of sintering temperature on phase composition of undoped T.Z.P.

Cubic Phase.

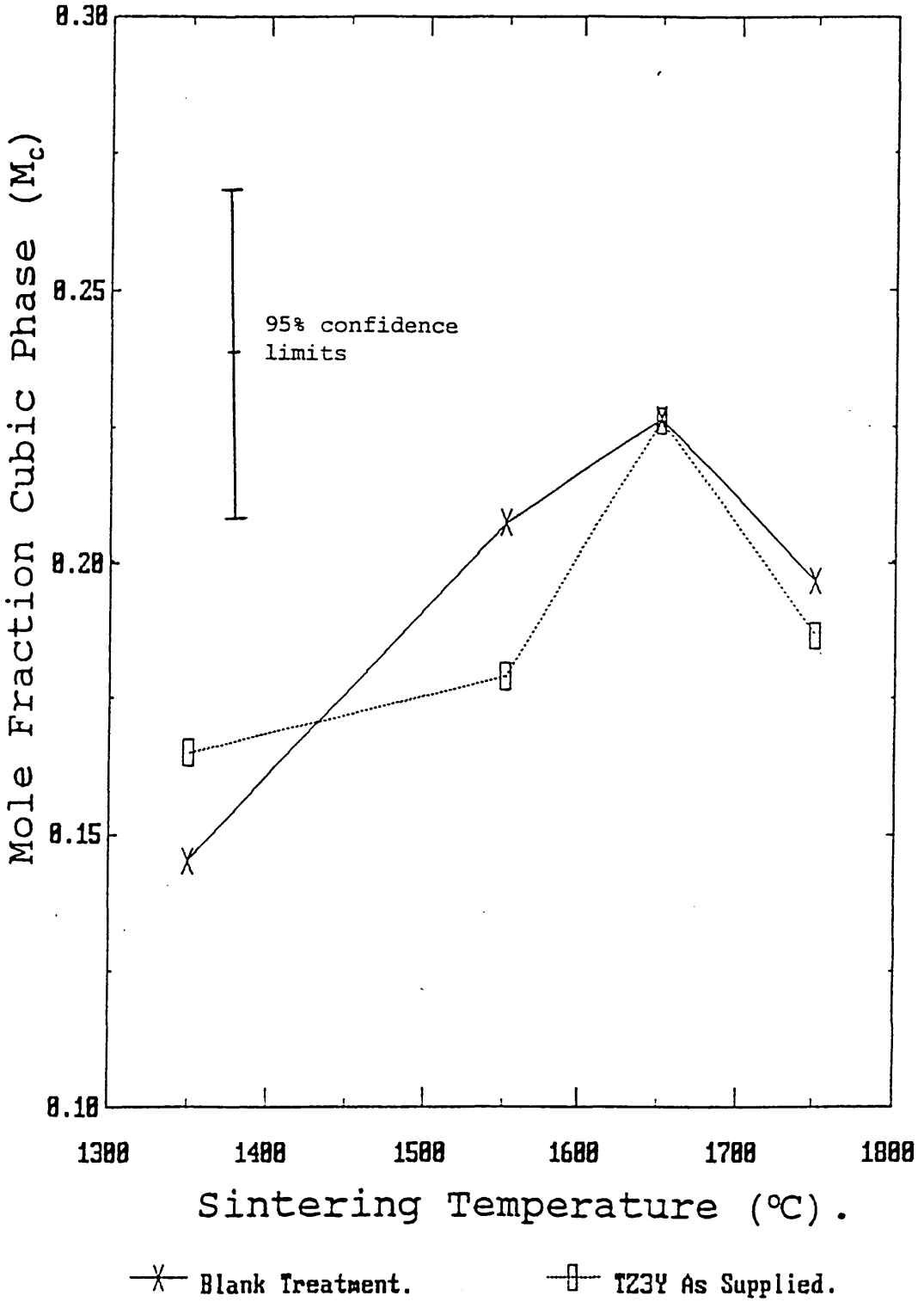

Figure 4.6.2(b).
Effect of sintering temperature on phase composition of undoped T.Z.P.
Tetragonal Phase.

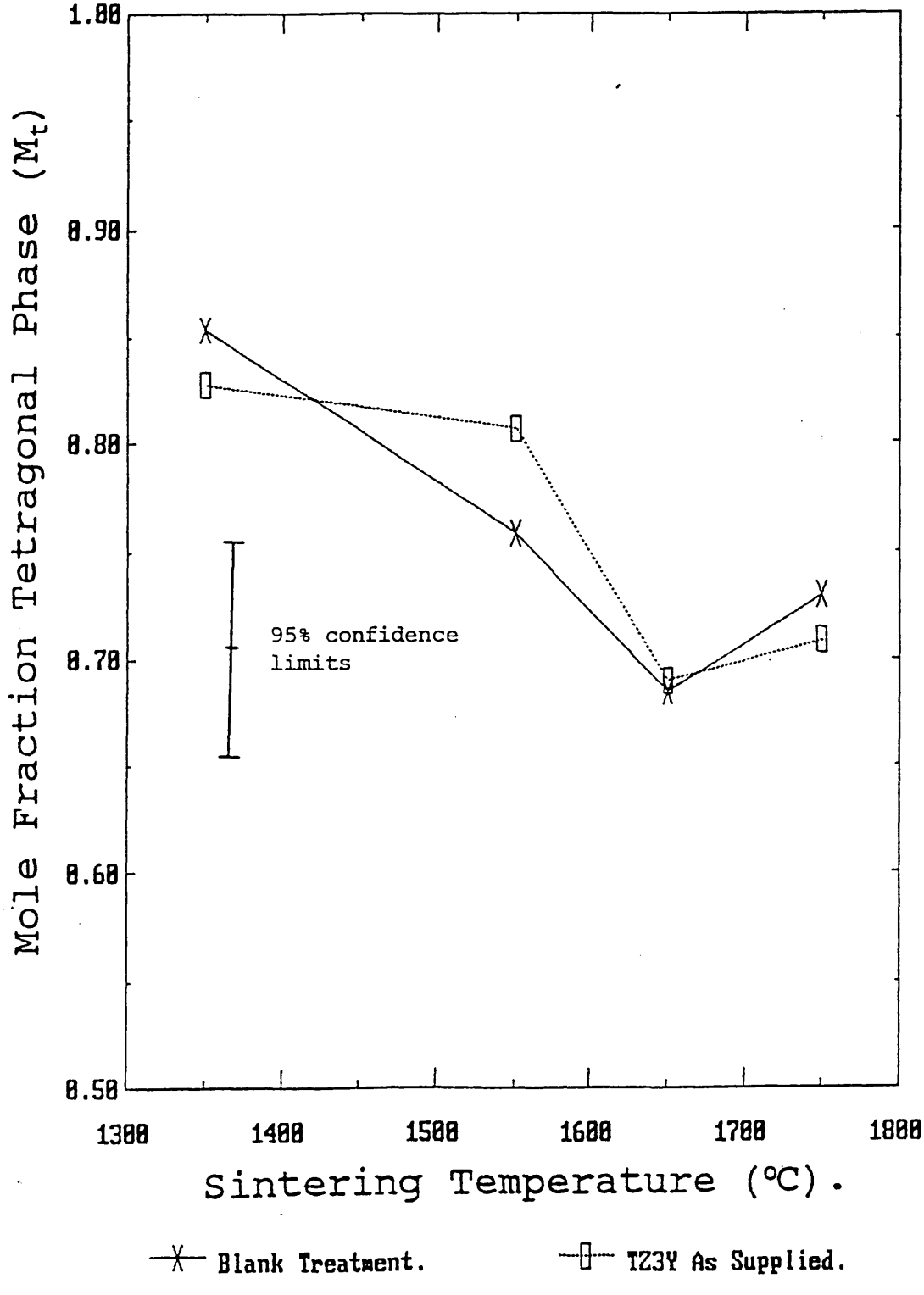

Figure 4.6.2(c).

Effect of sintering temperature on phase composition of undoped T.Z.P.

Monoclinic Phase.

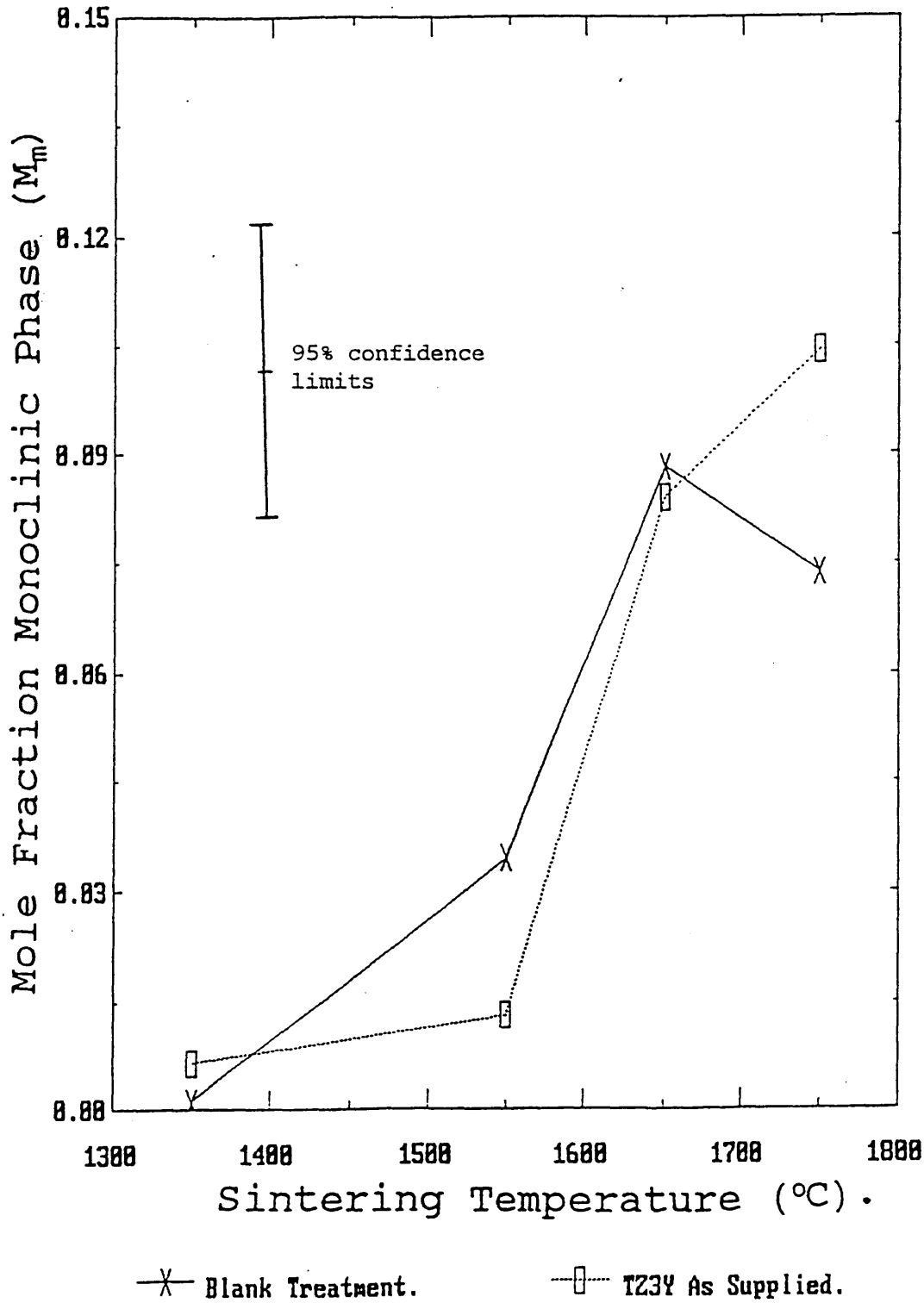

4.6.3 Alumina doped powders.

The results of the X-ray diffraction measurements for the phase determination of the sintered, alumina doped specimens are shown in table 4.6.3 (appendix 1).

Figures 4.6.3(a)-(c) show the effect of sintering temperature on the phase development of TZP with various levels of dopant addition.

The results appear to indicate a general trend of an increase in cubic phase with sintering temperature up to 1650°C, with a decrease in cubic phase for 1750°C sintering temperature similar to the undoped samples (figure 4.6.3(a)).

The 0.25% alumina addition at 1750°C sintering temperature is the only exception to this trend and may be anomalous.

The amount of tetragonal phase (figure 4.6.3 (b)) appears to follow a trend of decreasing with increasing sintering temperature, with a dramatic decrease occurring for sintering temperatures in excess of 1650°C, except for the 0.25% addition. The amount of monoclinic phase appears to vary inversely with the amount of tetragonal phase (figure 4.6.3(c)).

Figures 4.6.3 (d)-(i) show the effect of alumina addition on the phase development. These results appear to indicate that the amount of cubic phase present is independent of the alumina dopant content for all sintering temperatures (figures 4.6.3 (d) & (e)).

The effect of the alumina addition on the amount of tetragonal phase appears two distinct regions of behaviour. For sintering temperatures up to 1650°, the amount of retained tetragonal phase appears to be independent of or show a slight increase with increasing alumina content (figure 4.6.3(f)). However, the 1750° sintered sample shows a dramatic decrease in the amount of tetragonal phase as the alumina content is increased over approximately 0.25% (figure 4.6.3(g)).

The effects described for the tetragonal phase development can be more clearly identified when the monoclinic phase development is considered, where the opposite trends occur.

For sintering temperatures below 1650°C, the amount of monoclinic phase formed decreases with increased alumina addition and decreasing sintering temperature (figure 4.6.3(h)). Above this temperature, the amount of monoclinic phase appears to increase with increasing alumina content (figure 4.6.3(i)).

Figure 4.6.3(a).

Effect of sintering temperature on phase composition of alumina doped T.Z.P.

Cubic Phase.

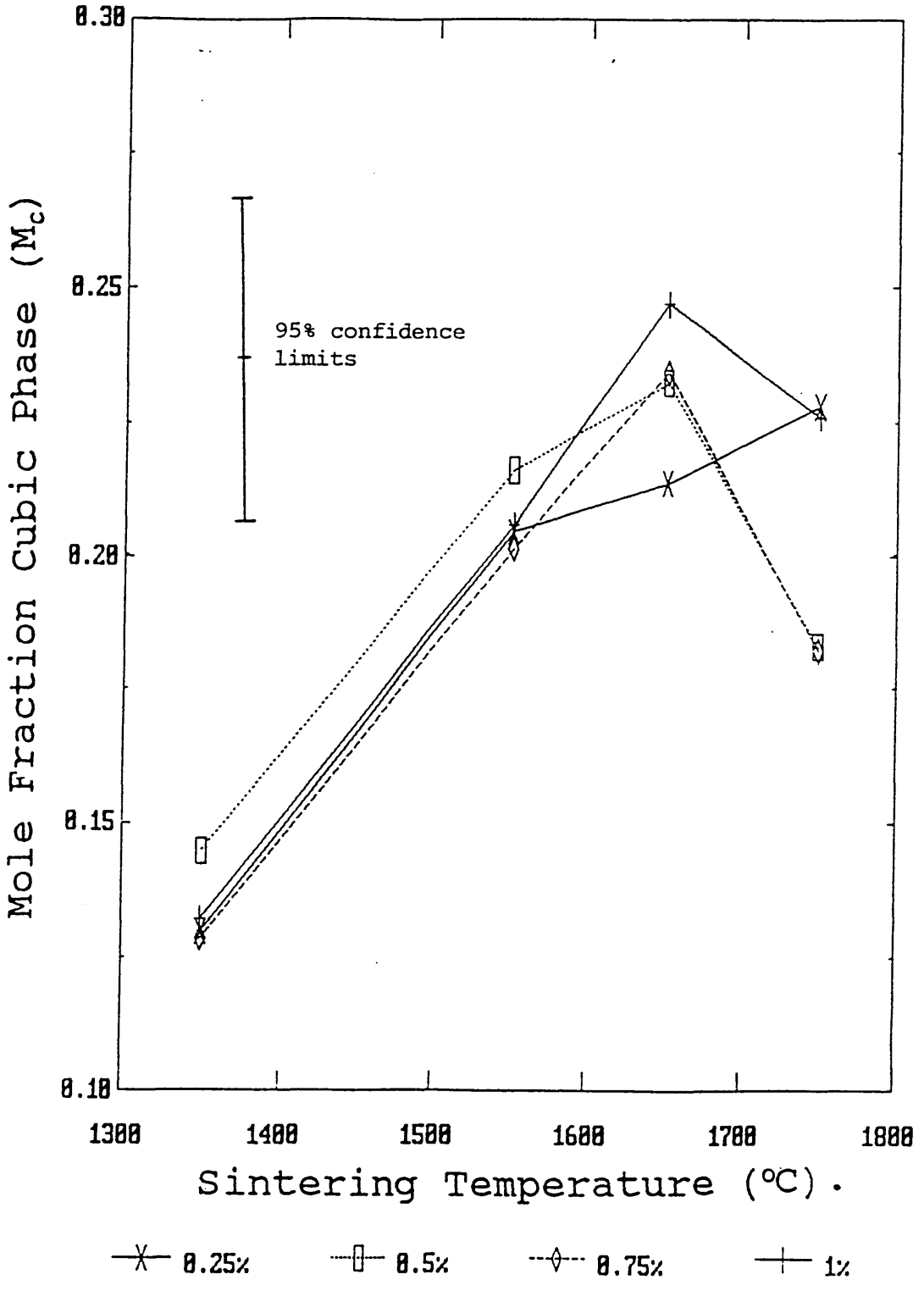

Figure 4.6.3(b).

Effect of sintering temperature on phase composition of alumina doped T.Z.P.

Tetragonal Phase.

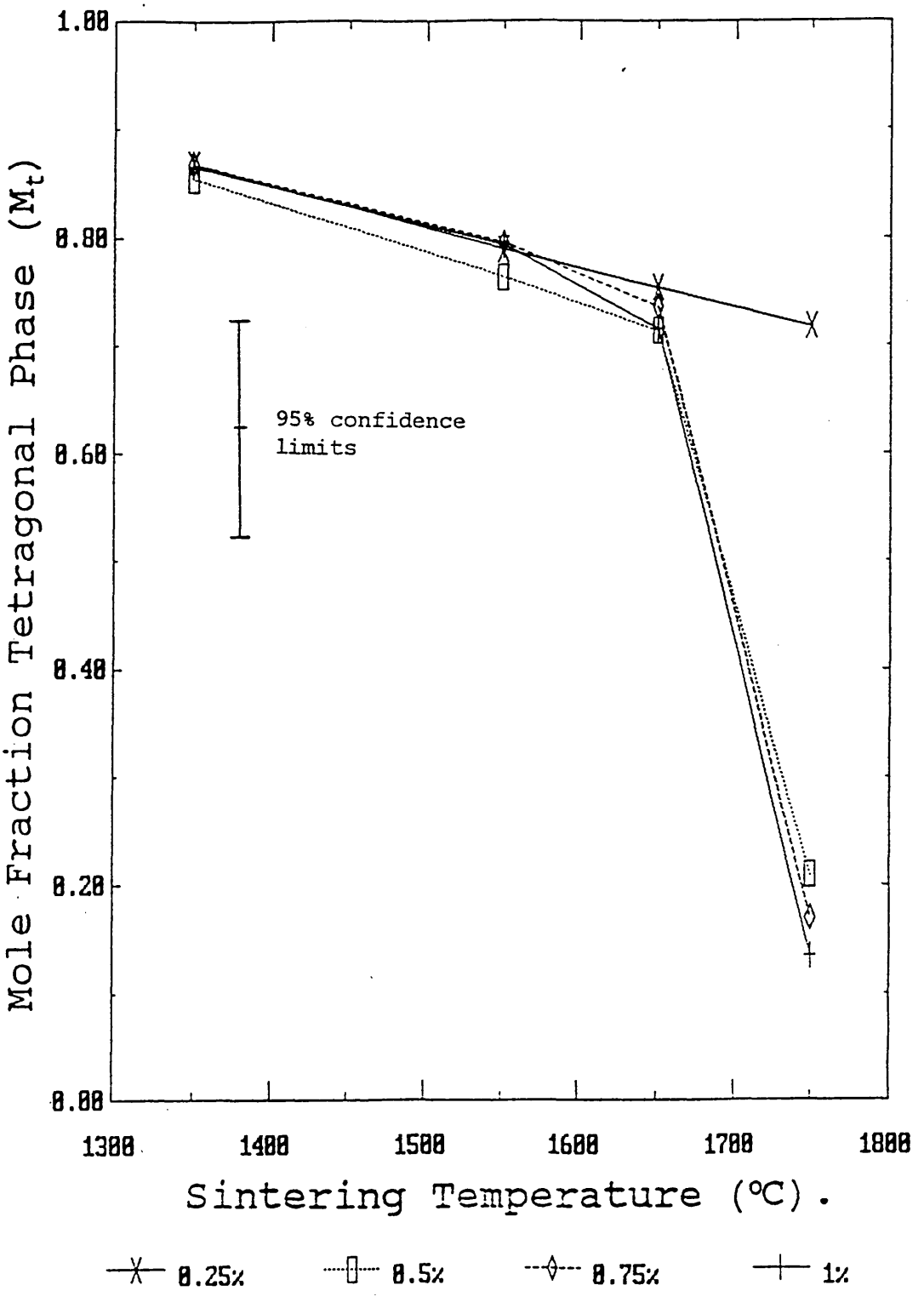

Figure 4.6.3(c).

Effect of sintering temperature on phase composition of alumina doped T.Z.P.

Monoclinic Phase.

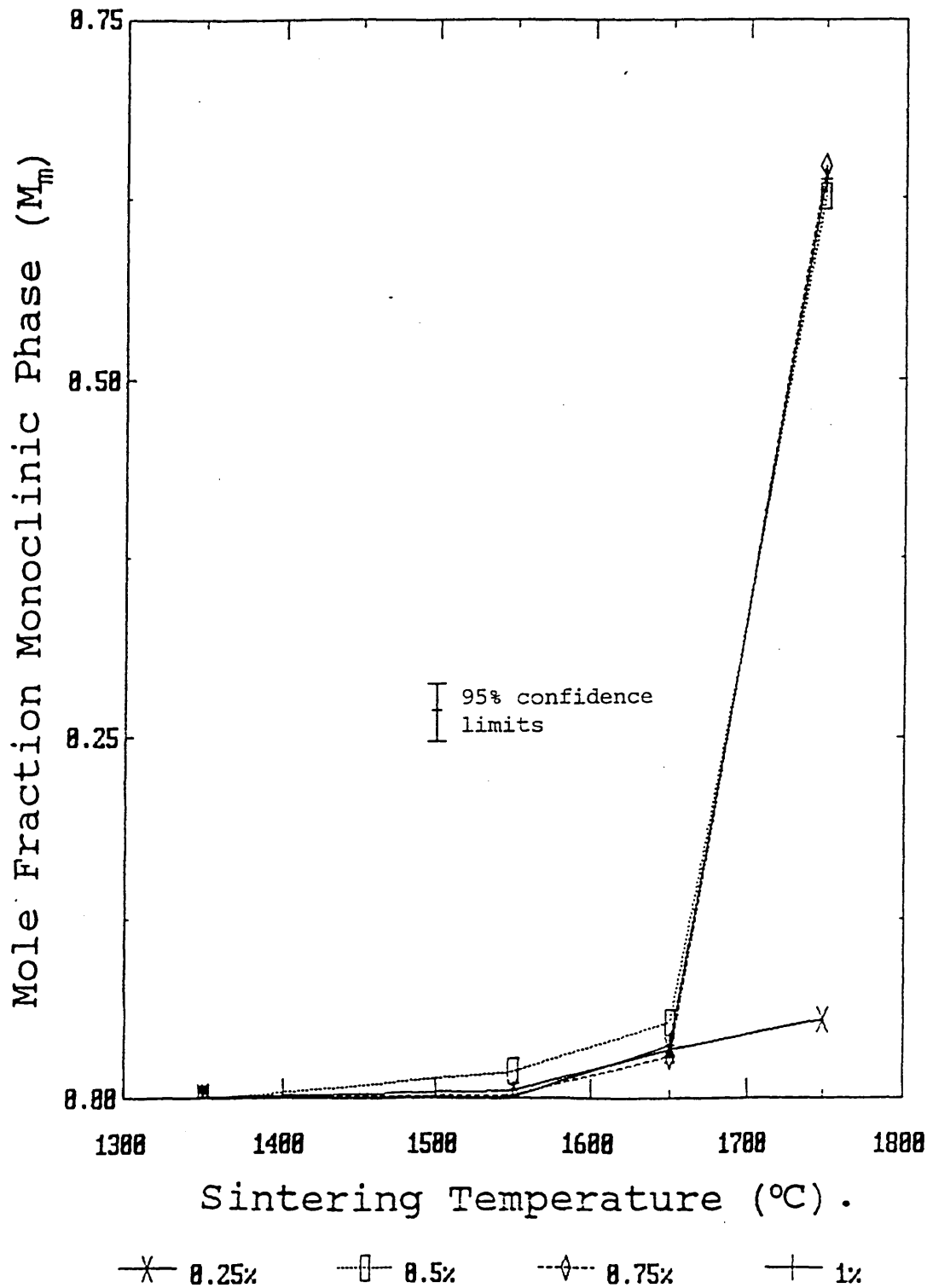

Figure 4.6.3(d) Effect of alumina addition on phase composition of sintered samples.

Cubic Phase
1350-1650°C sintering temperature.

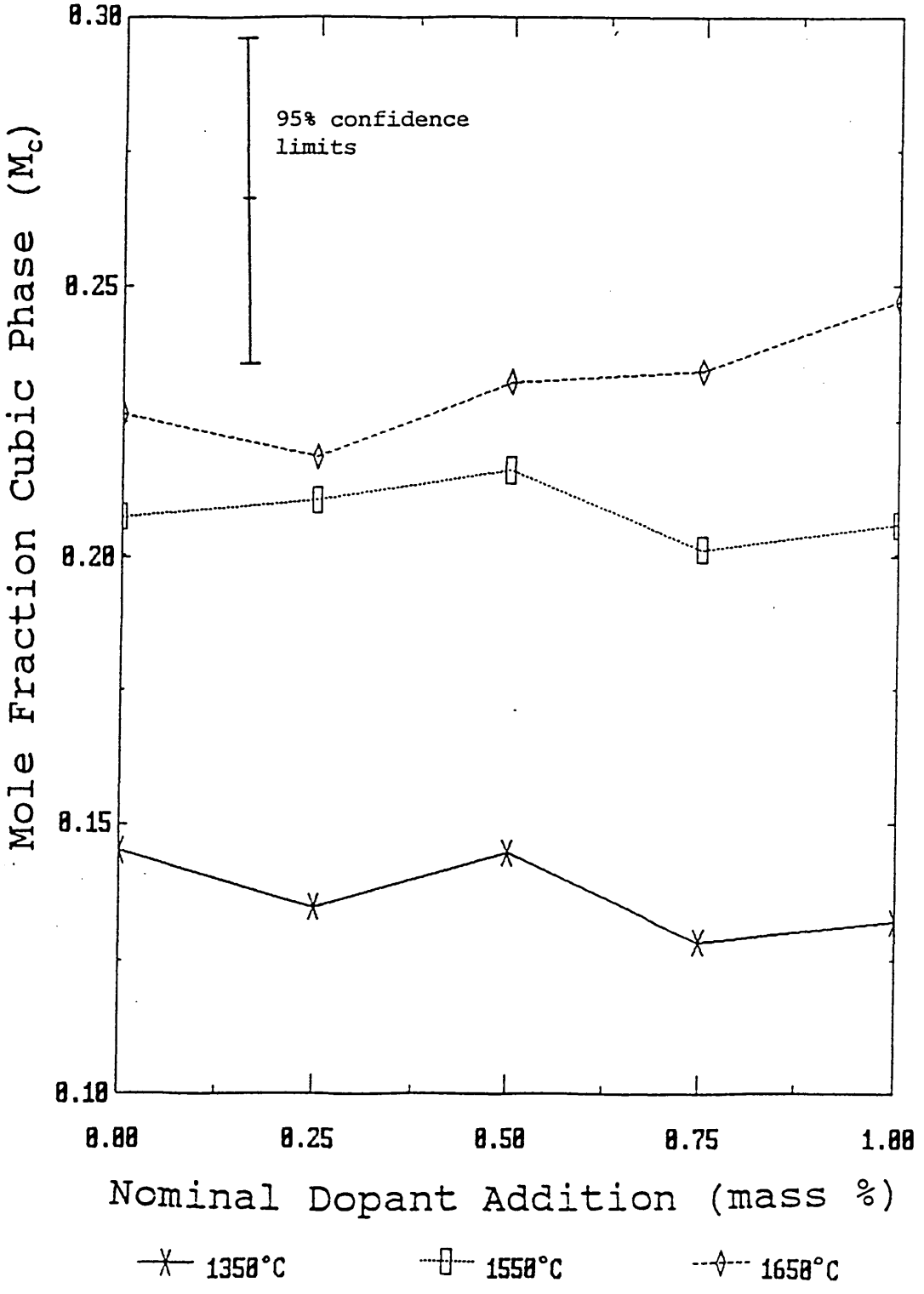

Figure 4.6.3(e) Effect of alumina addition on phase composition of sintered samples.

Cubic Phase

1750°C sintering temperature.

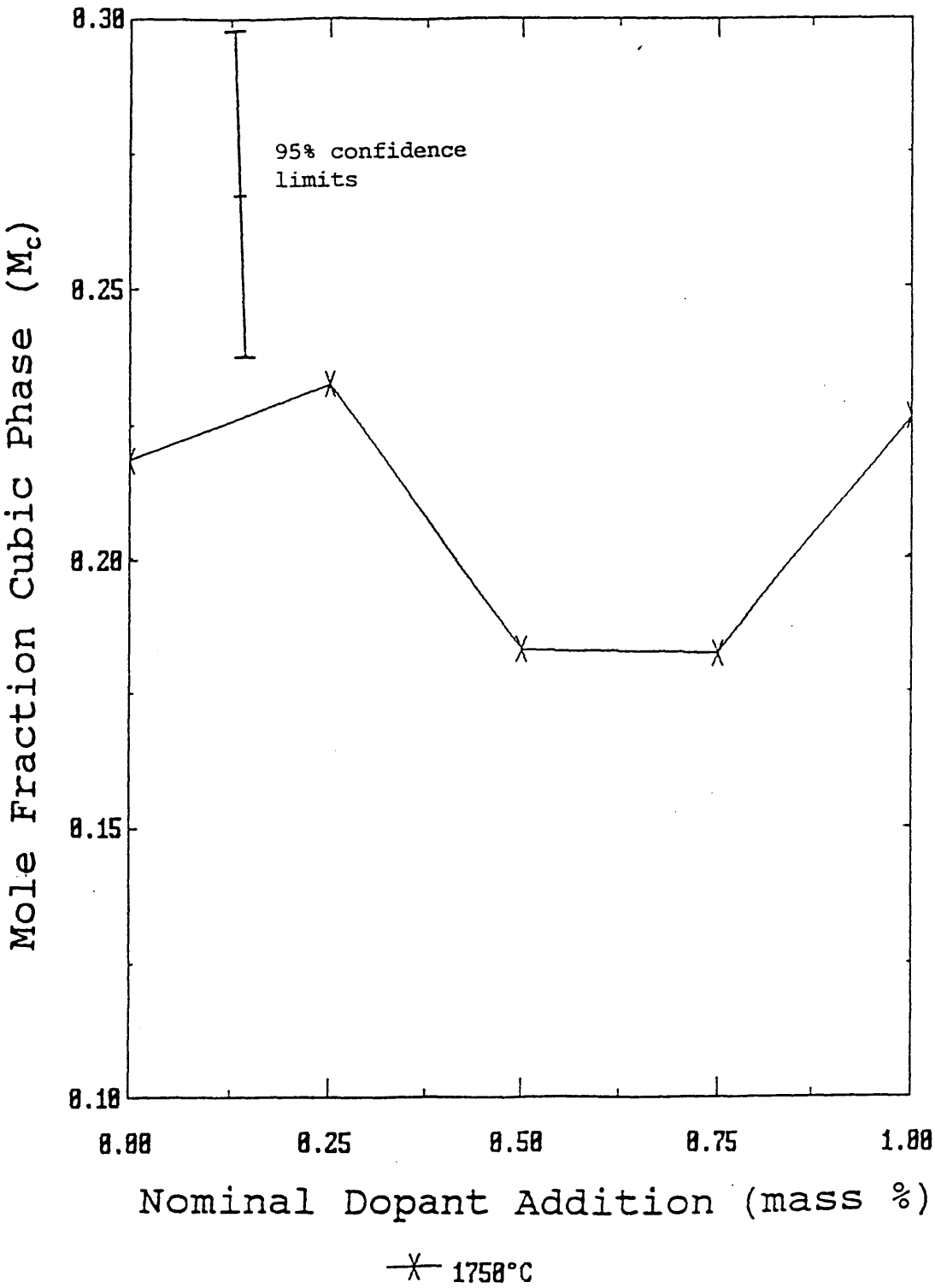

Figure 4.6.3(f) Effect of alumina addition on phase composition of sintered samples.

Tetragonal Phase
1350-1650°C sintering temperature.

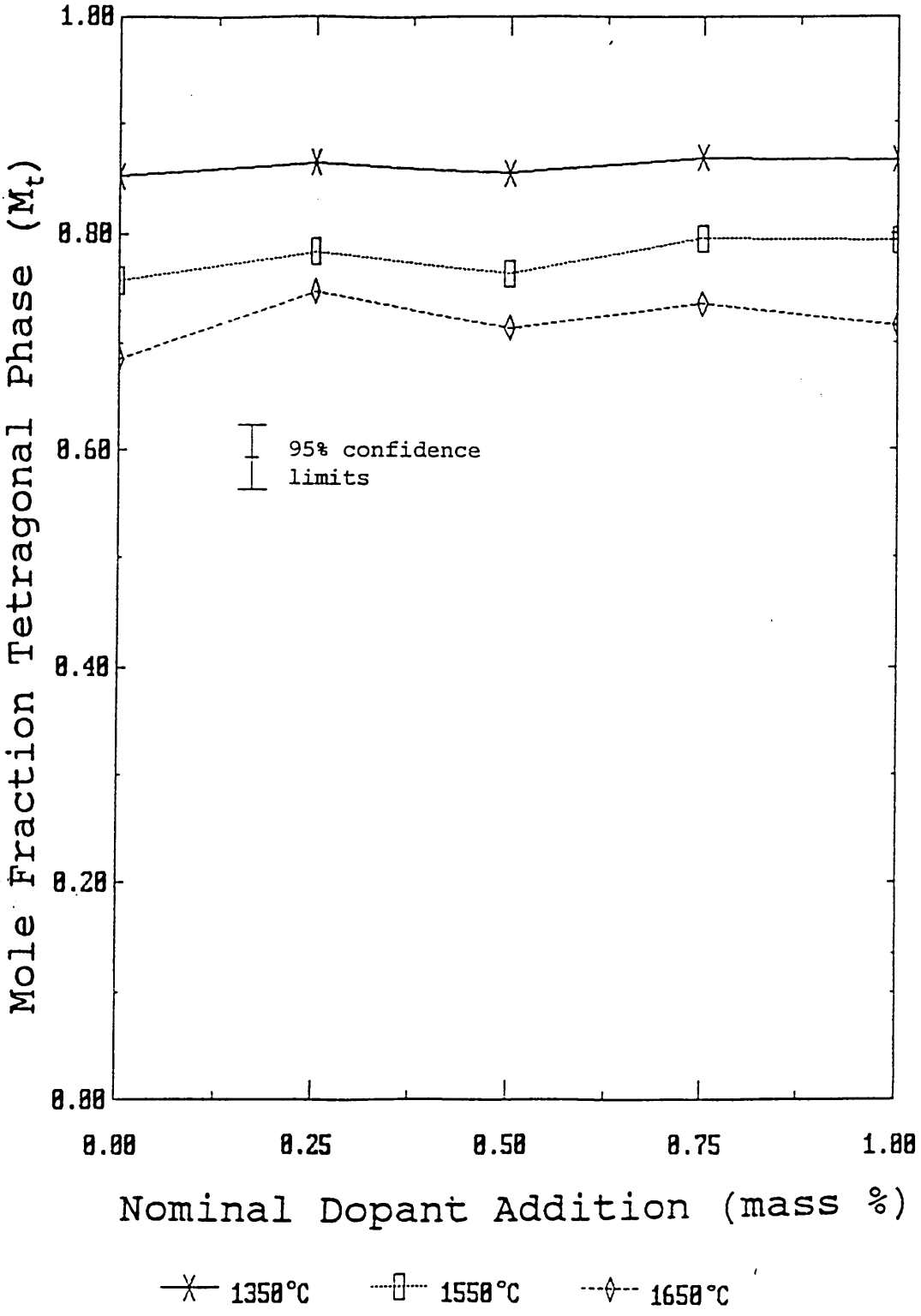

Figure 4.6.3(g) Effect of alumina addition on phase composition of sintered samples.

Tetragonal Phase
1750°C sintering temperature.

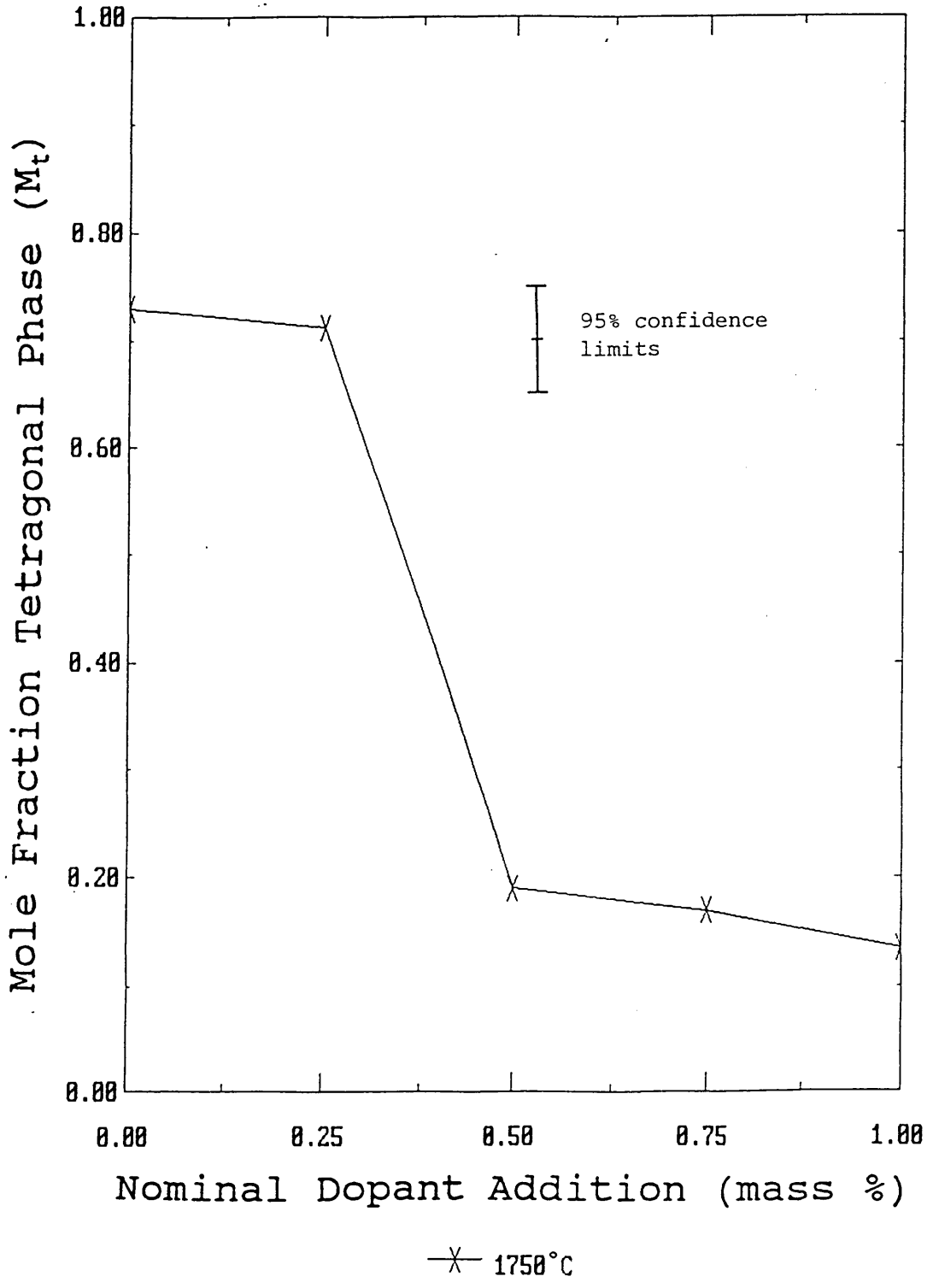

Figure 4.6.3(h) Effect of alumina addition on phase composition of sintered samples.

Monoclinic Phase
1350-1650°C sintering temperature.

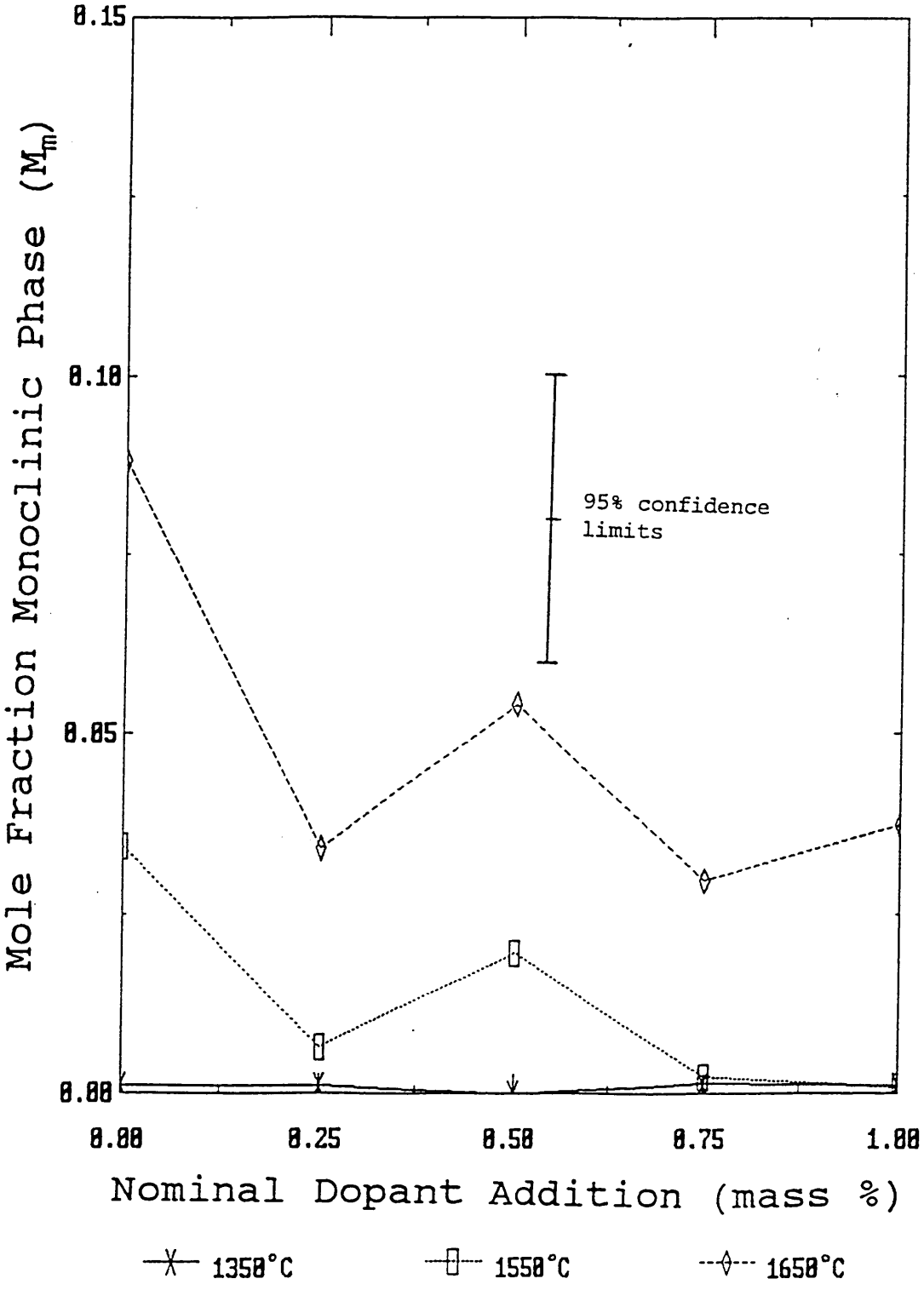

Figure 4.6.3(i) Effect of alumina addition on phase composition of sintered samples.

Monoclinic Phase
1750°C sintering temperature.

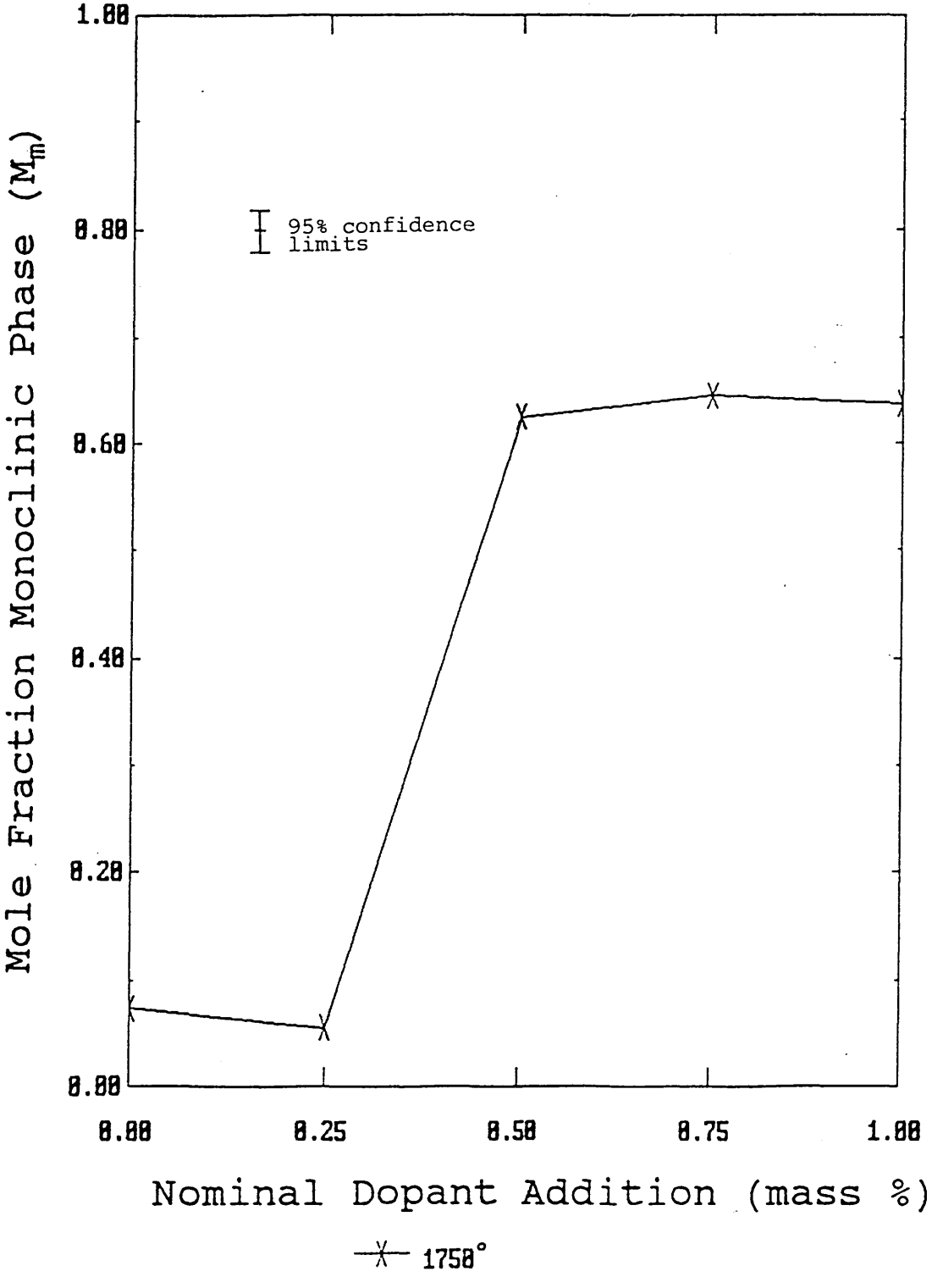

4.6.4 Silica Doped Samples.

The results of the x-ray diffraction measurements for the phase determination of the sintered, silica doped specimens are shown in table 4.6.4 (appendix 1), with the effect of sintering temperature on the phase composition in these samples shown in figures 4.6.4(a)-(c).

The effect of temperature on cubic phase development is very similar in these samples to the undoped and alumina doped samples, with a maxima in cubic phase development occurring at 1650°C (figure 4.6.4(a)).

The effect of sintering temperature on the tetragonal and monoclinic phases is also similar to the undoped samples. The amount of retained tetragonal phase shows a steady decrease with increased sintering temperature, whilst the monoclinic phase shows the reverse trend (figures 4.6.4(b) & (c)), with the exception of the 0.75% silica addition, which may be a rogue result.

The effects of the silica content on phase composition are less significant, and less clearly defined for the silica doped than for the alumina doped material. This may be partially due to a series of apparently anomalous results for the 0.75% addition level material, particularly regarding the monoclinic phase.
The results of these experiments suggest that the amount of tetragonal phase does not appear to vary significantly with silica content (figures 4.6.4 (e) and (f)), whilst there is some suggestion that the amount of monoclinic phase may decrease (figure 4.6.4 (g)) and cubic phase increase (figure 4.6.4 (d)) with silica addition. However it should be pointed out that both of these trends are poorly defined, and well within the limits of possible experimental error and may not be significant.

Figure 4.6.4(a).
Effect of sintering temperature on phase composition of silica doped T.Z.P.
Cubic Phase.

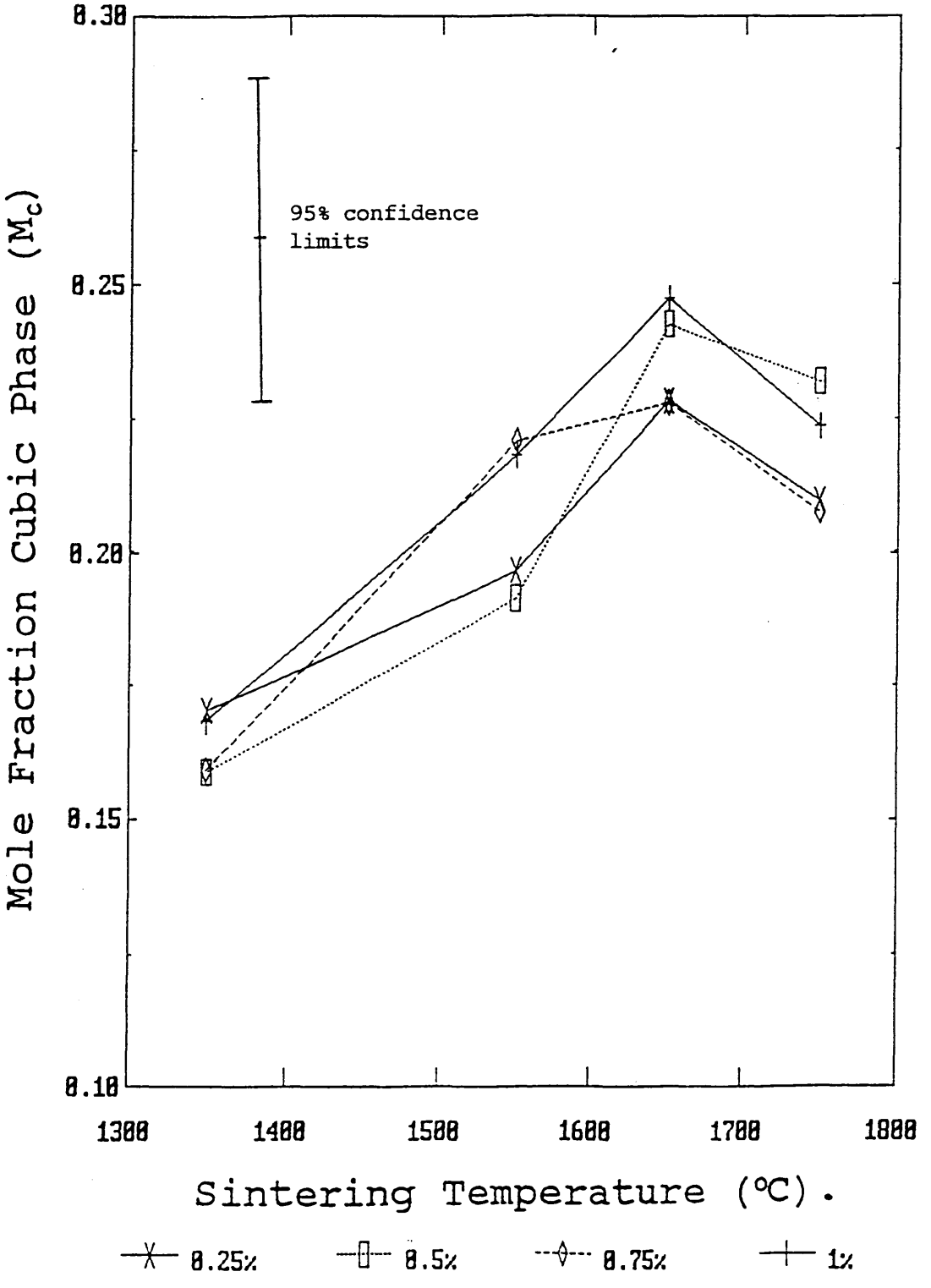

Figure 4.6.4(b).

Effect of sintering temperature on phase composition of silica doped T.Z.P.

Tetragonal Phase.

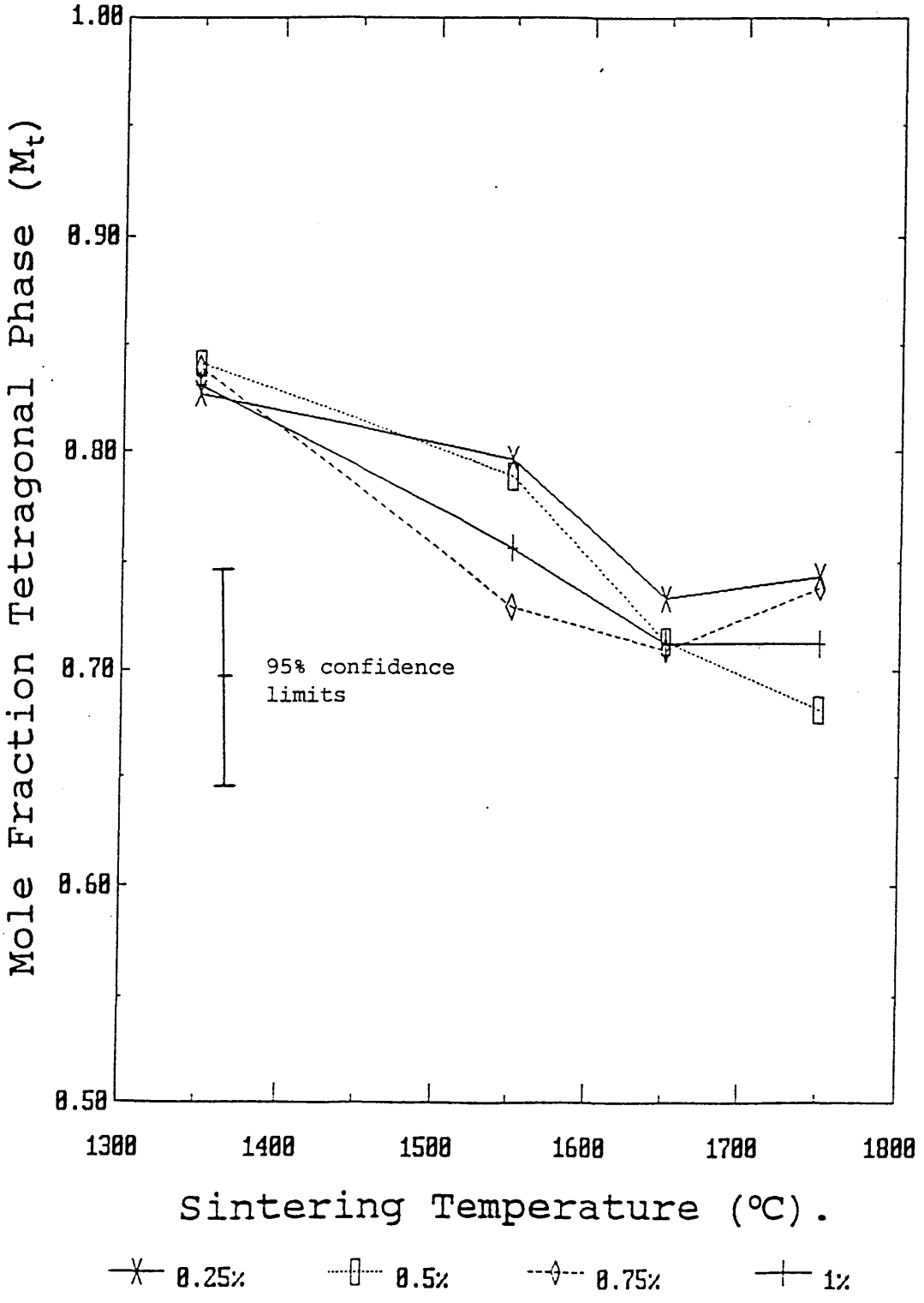

Figure 4.6.4(c).

Effect of sintering temperature on phase composition of silica doped T.Z.P.

Monoclinic Phase.

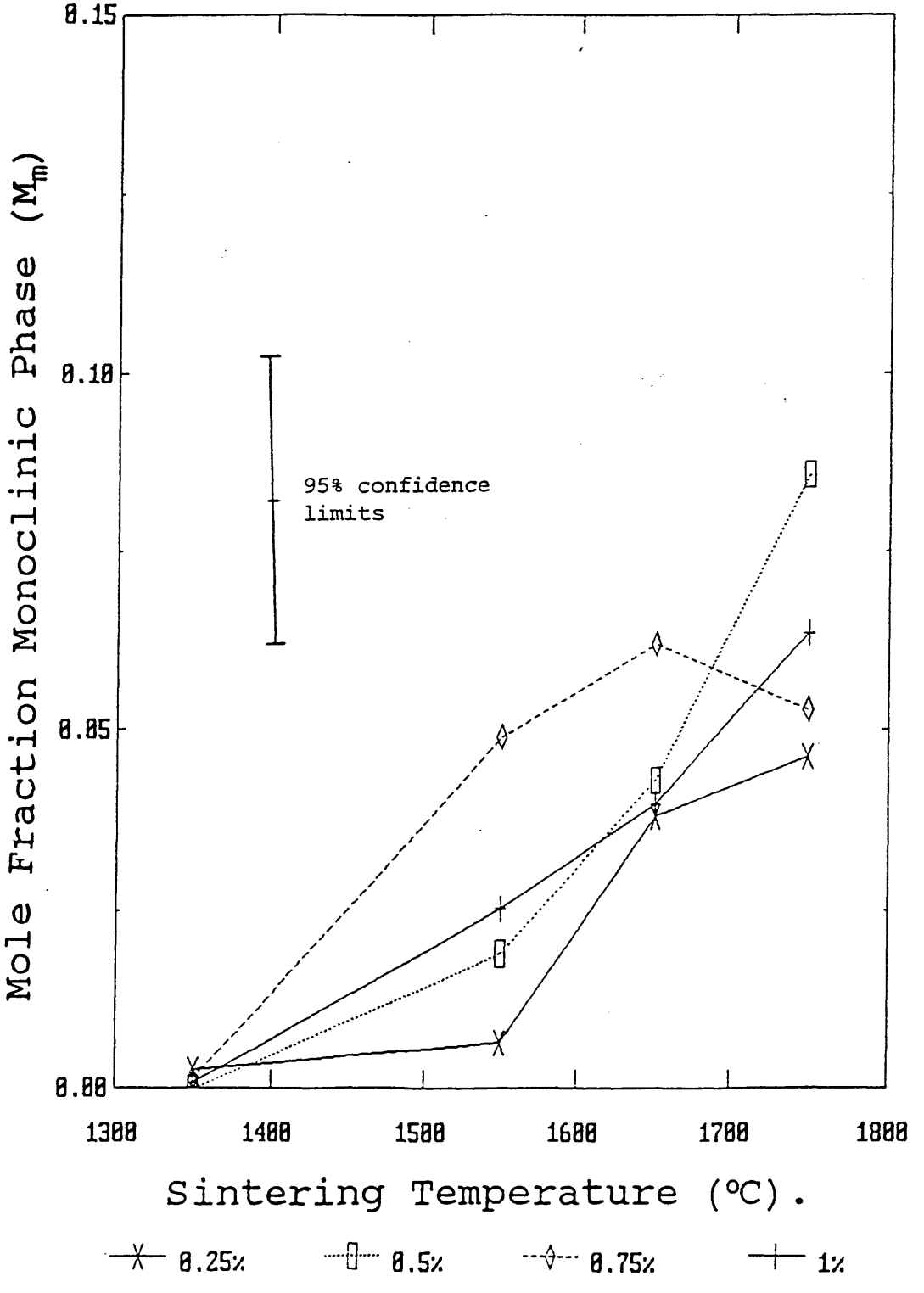

Figure 4.6.4(d) Effect of silica addition on phase composition of sintered samples.

Cubic Phase

1350-1750°C sintering temperature.

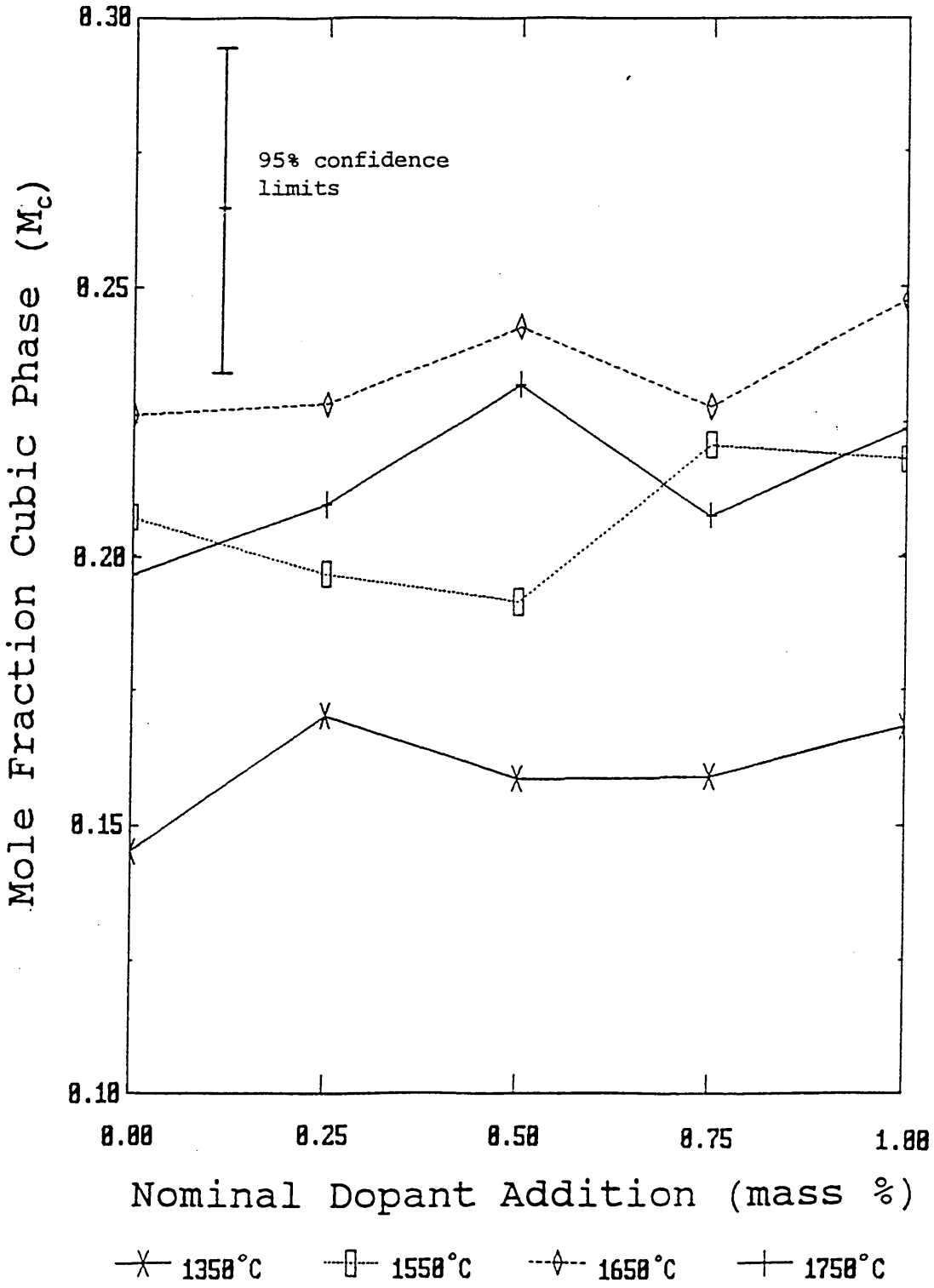

Figure 4.6.4(e) Effect of silica addition on phase composition of sintered samples.

Tetragonal Phase
1350-1650°C sintering temperature.

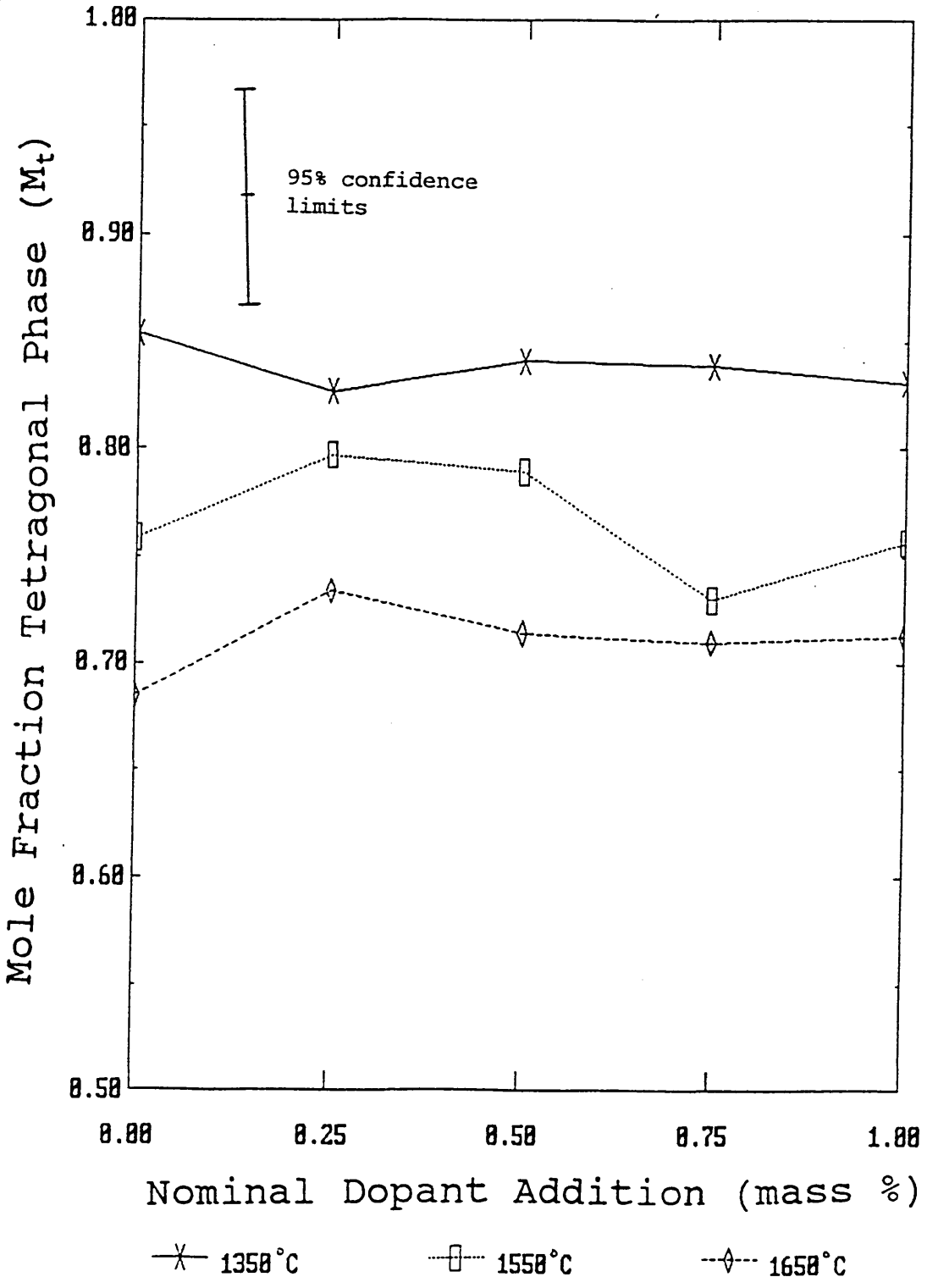

Figure 4.6.4(f) Effect of silica addition on phase composition of sintered samples.

Tetragonal Phase
1750°C sintering temperature.

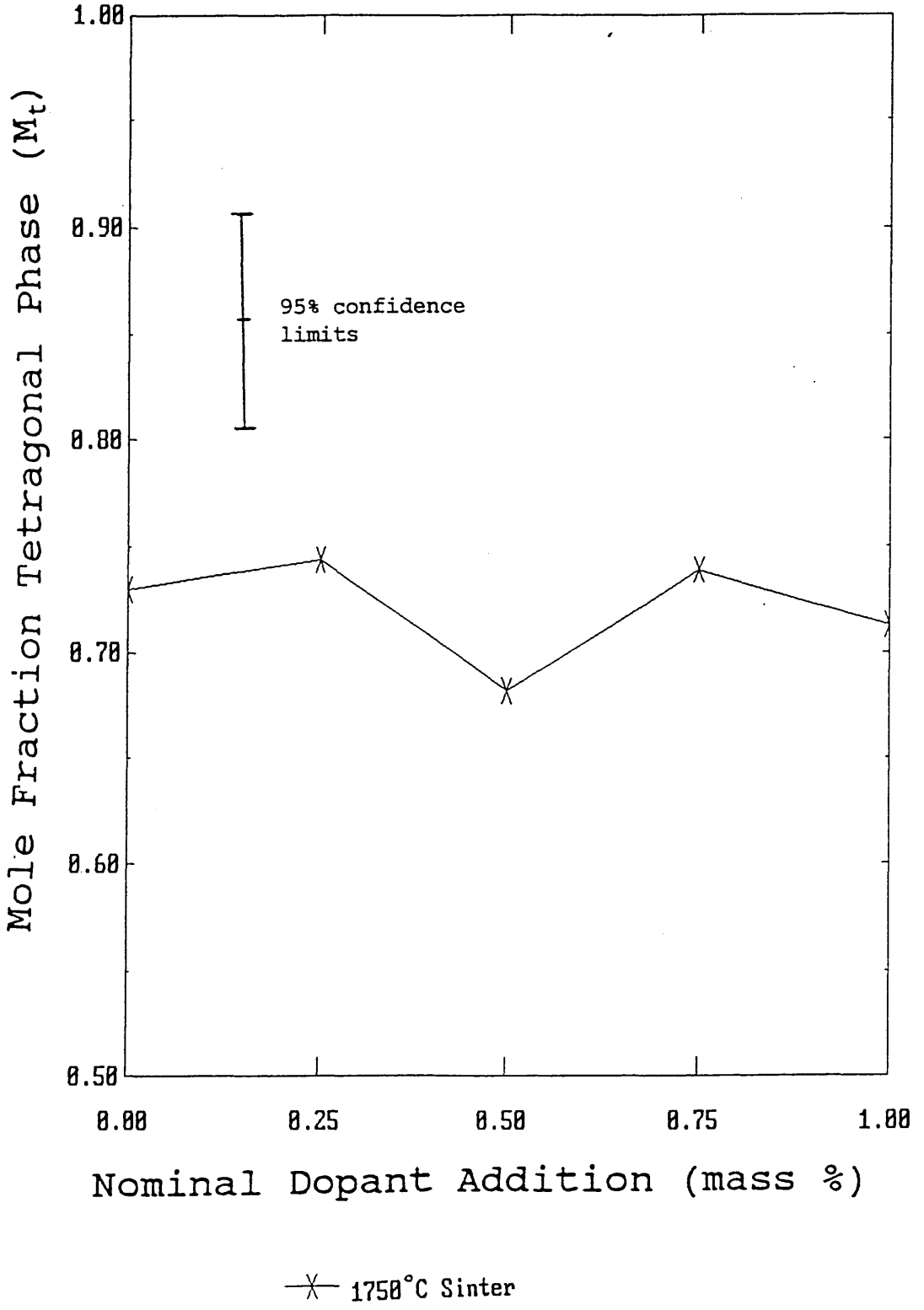

Figure 4.6.4 (g) Effect of alumina addition on phase composition of sintered samples.

Monoclinic Phase
1350-1650°C sintering temperature.

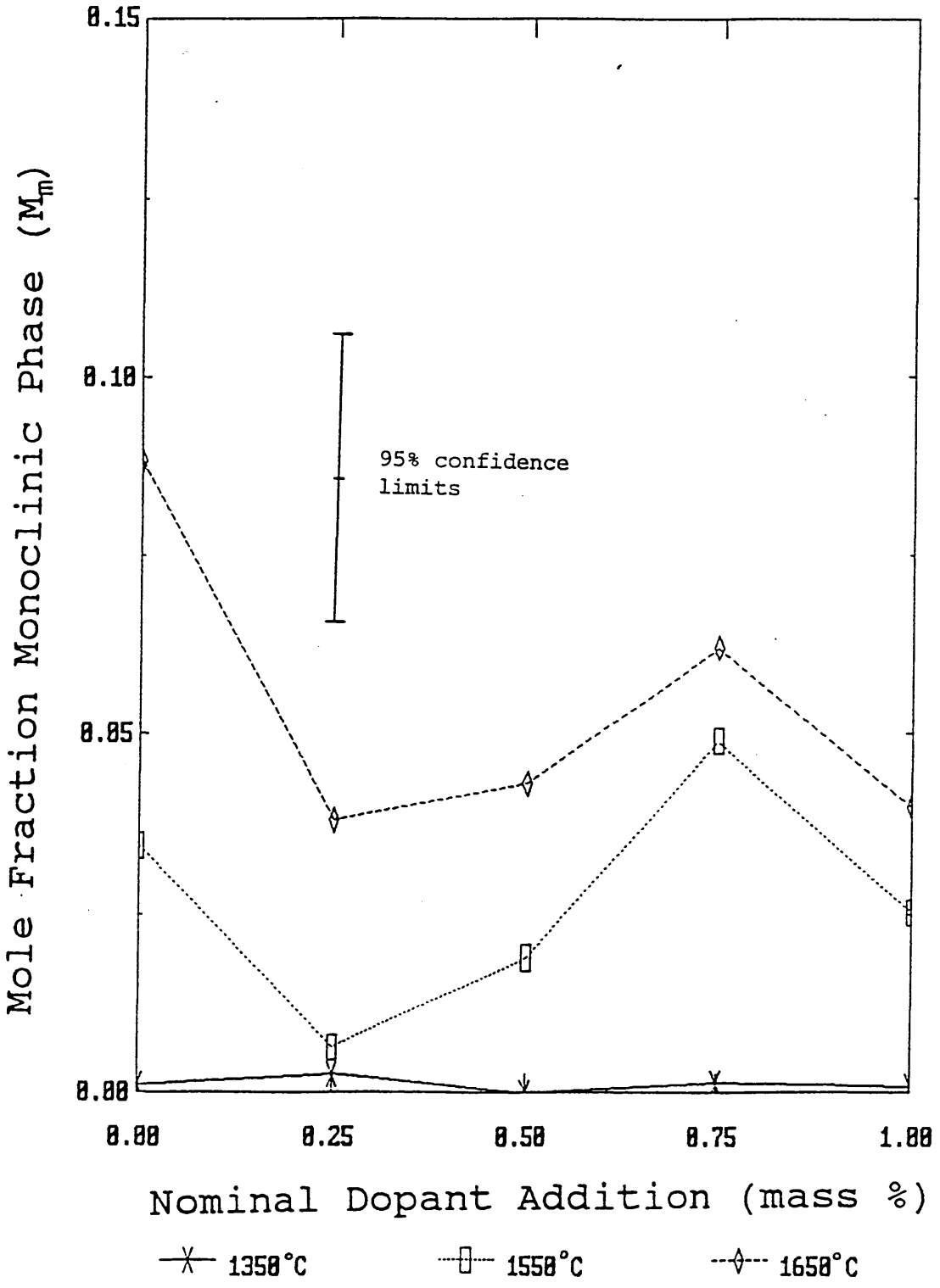

4.6.5 Titania doped samples.

The effect of sintering temperature on the cubic monoclinic and tetragonal phase composition of the titania doped samples is illustrated in figures 4.6.5(a)-(c).

The results show a trend for an increase in cubic phase formation with increasing sintering temperature. The reduction in cubic phase for sintering temperatures above 1650°C observed with the other undoped and doped samples is either not present or is much less significant in these samples.

The tetragonal phase shows a decrease in tetragonal phase with increased sintering temperature, although this effect appears to be reversed for higher dopant additions in the 1750°C sintered samples.

The formation of monoclinic phase appears to increase with increased sintering temperature, with the trend reversed for the higher dopant levels and sintering temperatures similarly to (although the inverse of) the tetragonal phase.

The effects of the dopant addition level are shown in figures 4.5.5 (d)-(f) for the various sintering temperatures.

The most significant effect is a decrease in the amount of cubic phase present with increasing titania addition. This effect becomes increasingly apparent as the sintering temperature is increased (figure 4.6.5(d)).

Figure 4.6.5(e) shows a corresponding trend for an increase in the amount of retained tetragonal phase with increased titania addition.

The variation in the amount of monoclinic phase present is insignificant compared to the experimental error, and no clear trends can be identified suggesting that this phase is independent of the titania content (figure 4.6.5(f)).

Figure 4.6.5(a).

Effect of sintering temperature on phase composition of titania doped T.Z.P.
Cubic Phase.

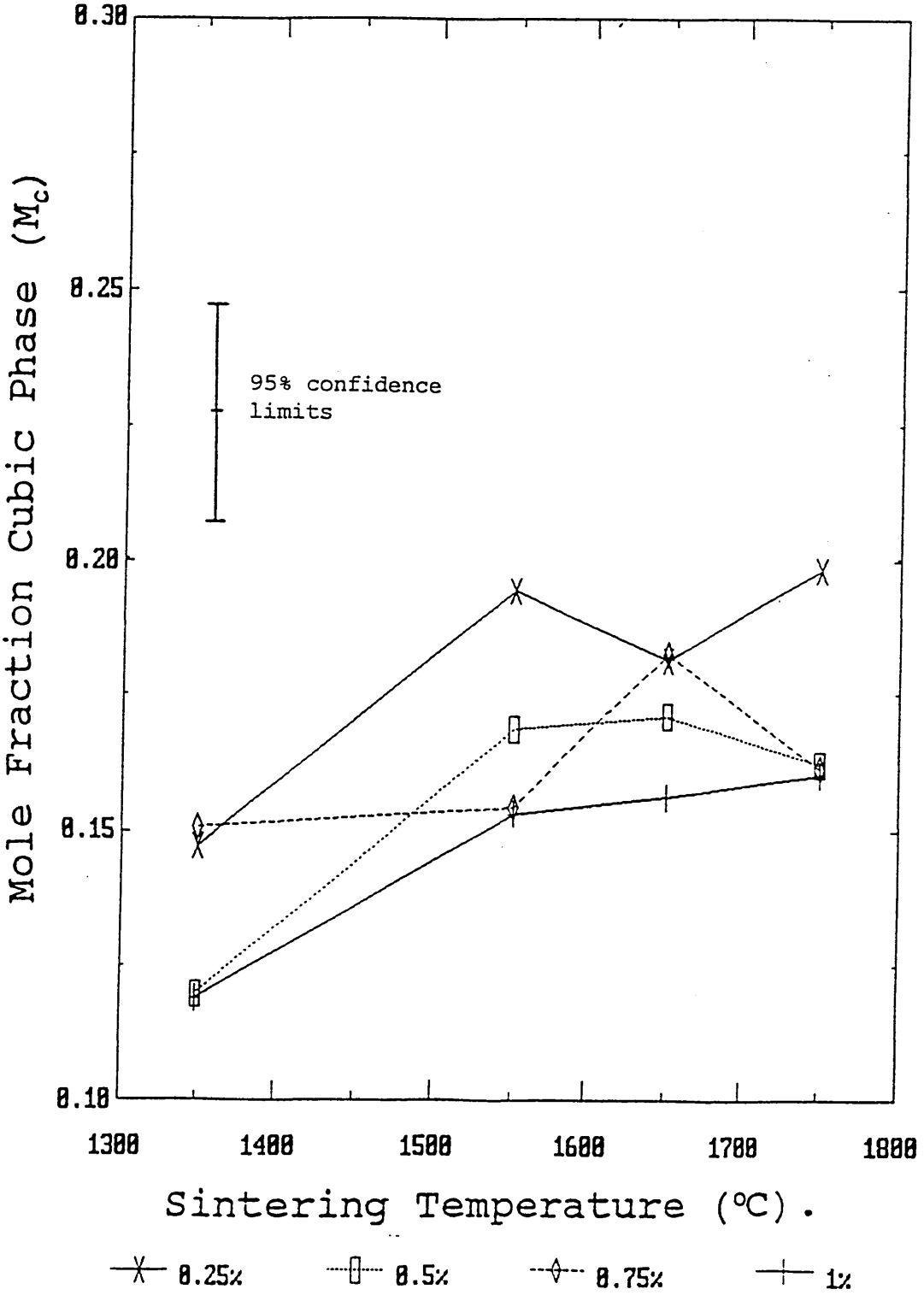

Figure 4.6.5(b).

Effect of sintering temperature on phase composition of titania doped T.Z.P.

Tetragonal Phase.

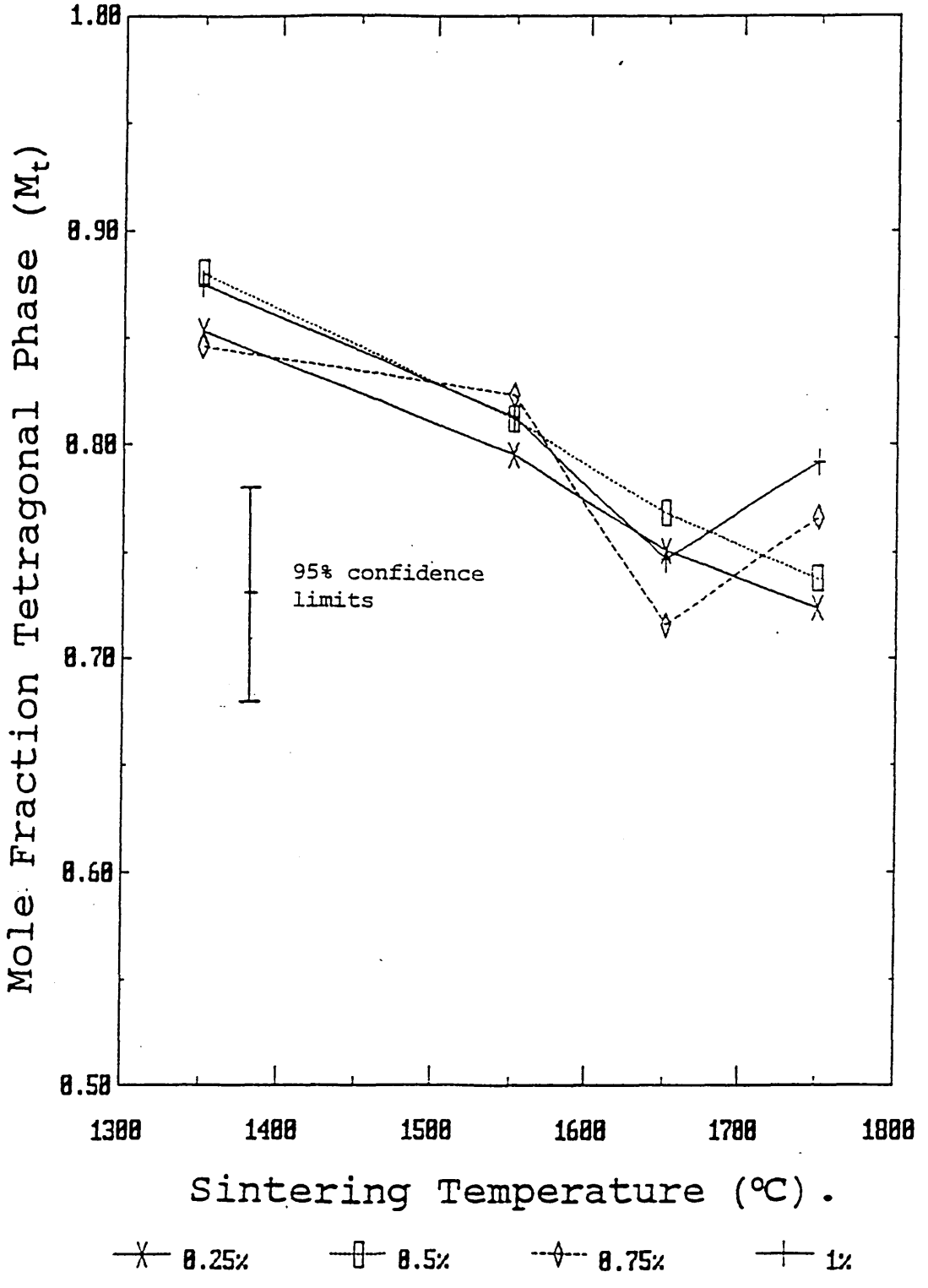

Figure 4.6.5(c).

Effect of sintering temperature on phase composition of titania doped T.Z.P.

Monoclinic Phase.

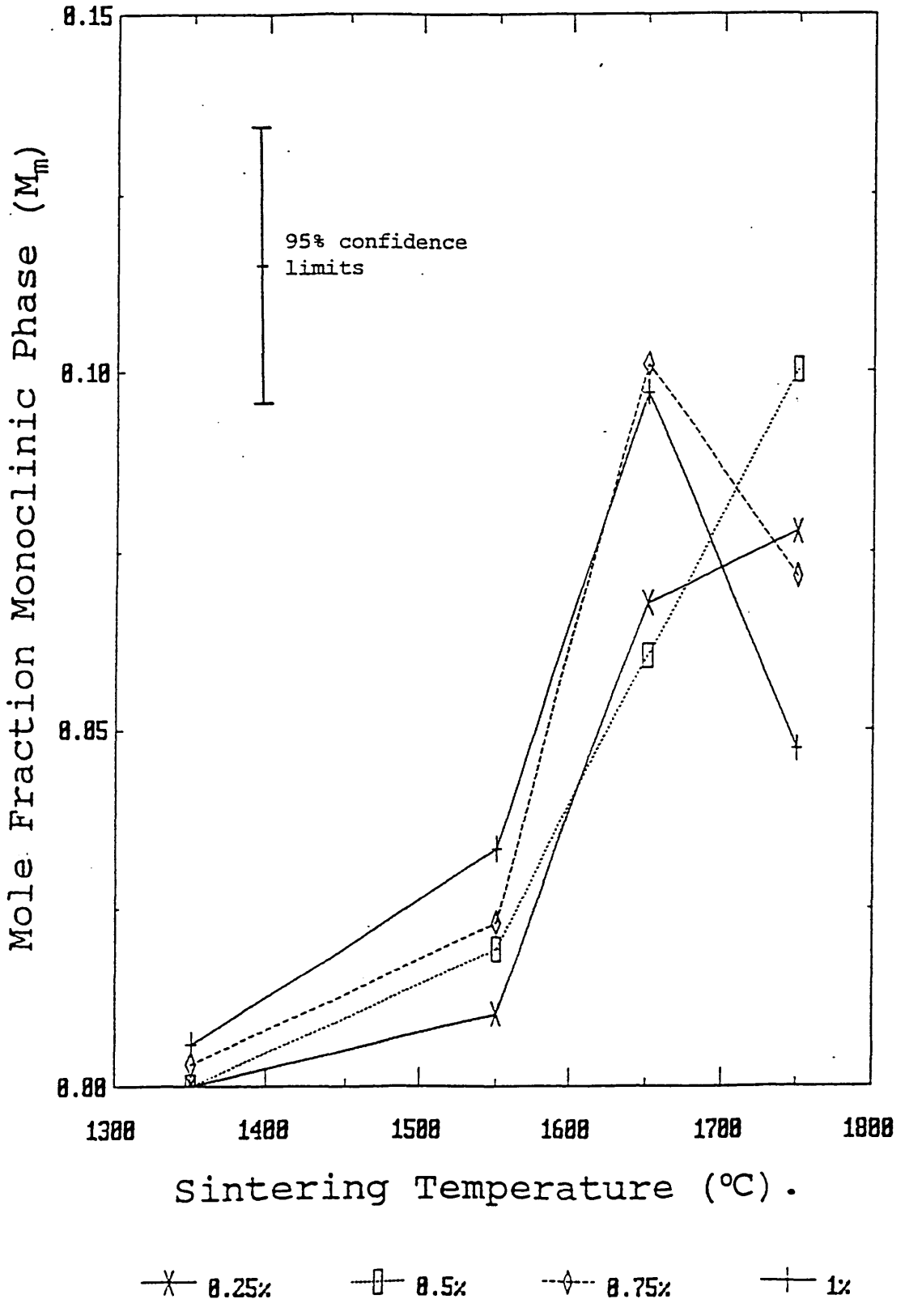

Figure 4.6.5(d) Effect of titania addition on phase composition of sintered samples.

Cubic Phase

1350-1650°C sintering temperature.

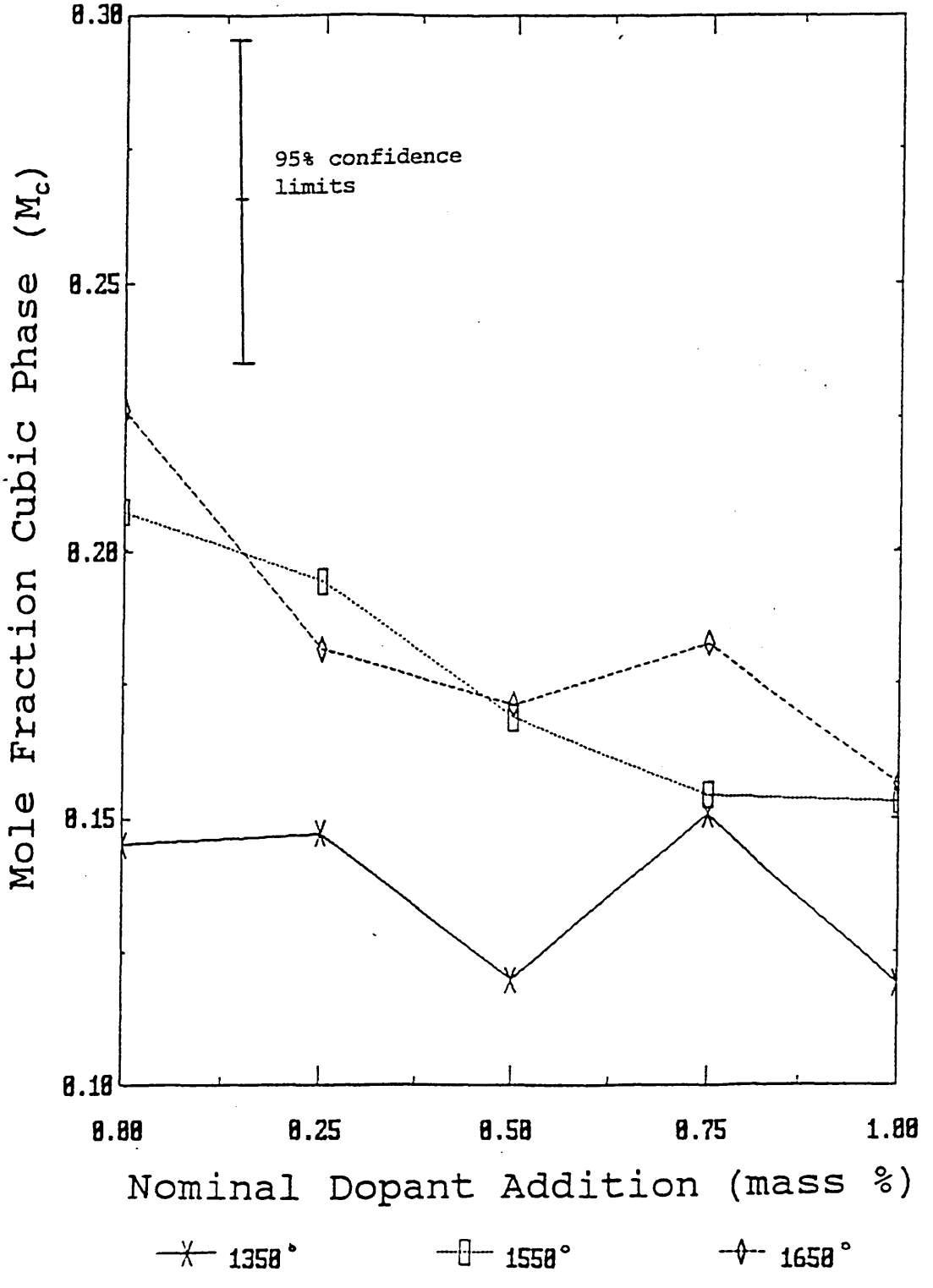

Figure 4.6.5(e) Effect of titania addition on phase composition of sintered samples.

Tetragonal Phase

1350-1750°C sintering temperature.

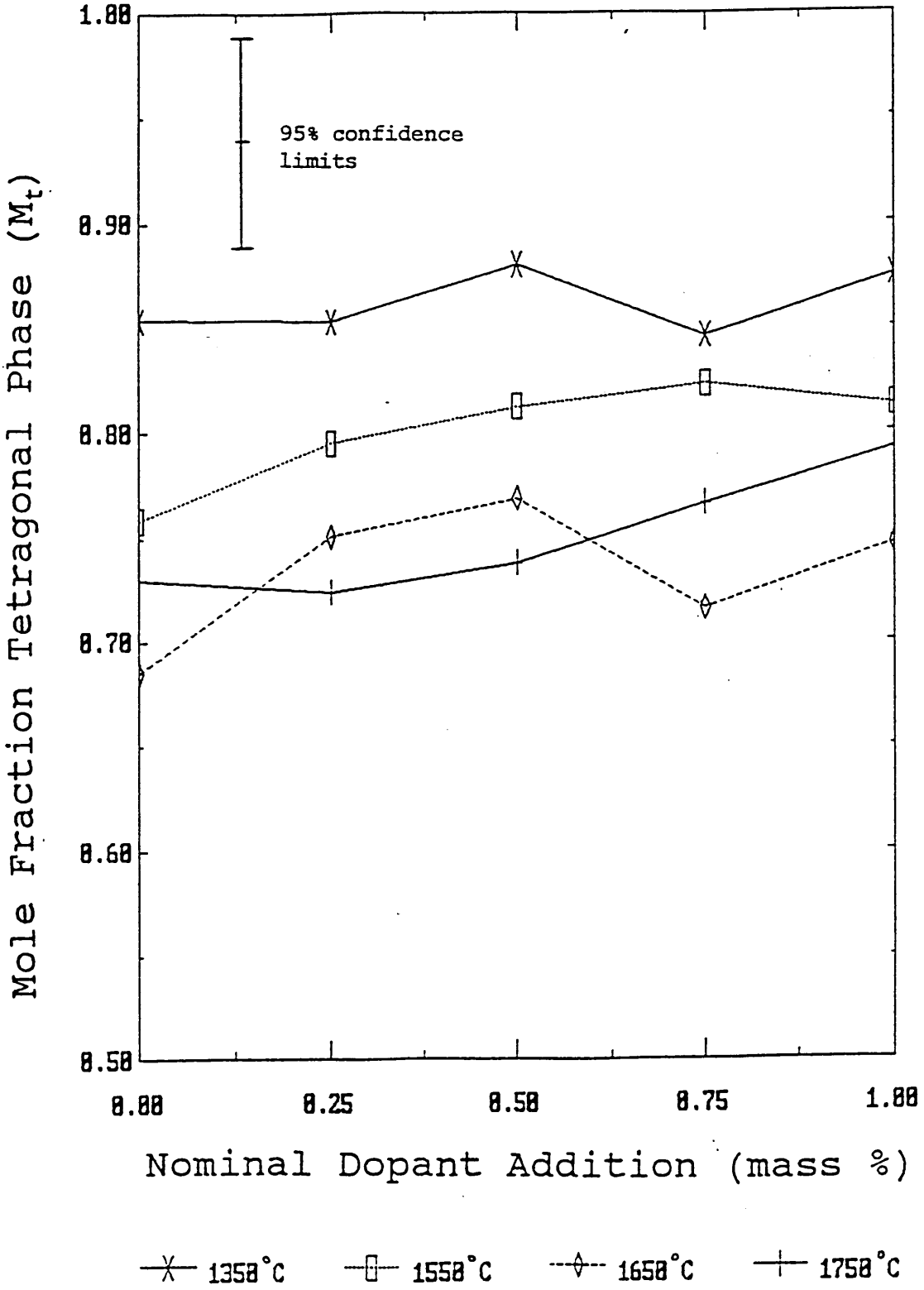

Figure 4.6.5(f) Effect of titanium oxide addition on phase composition of sintered samples.

Monoclinic Phase
1350-1750°C sintering temperature.

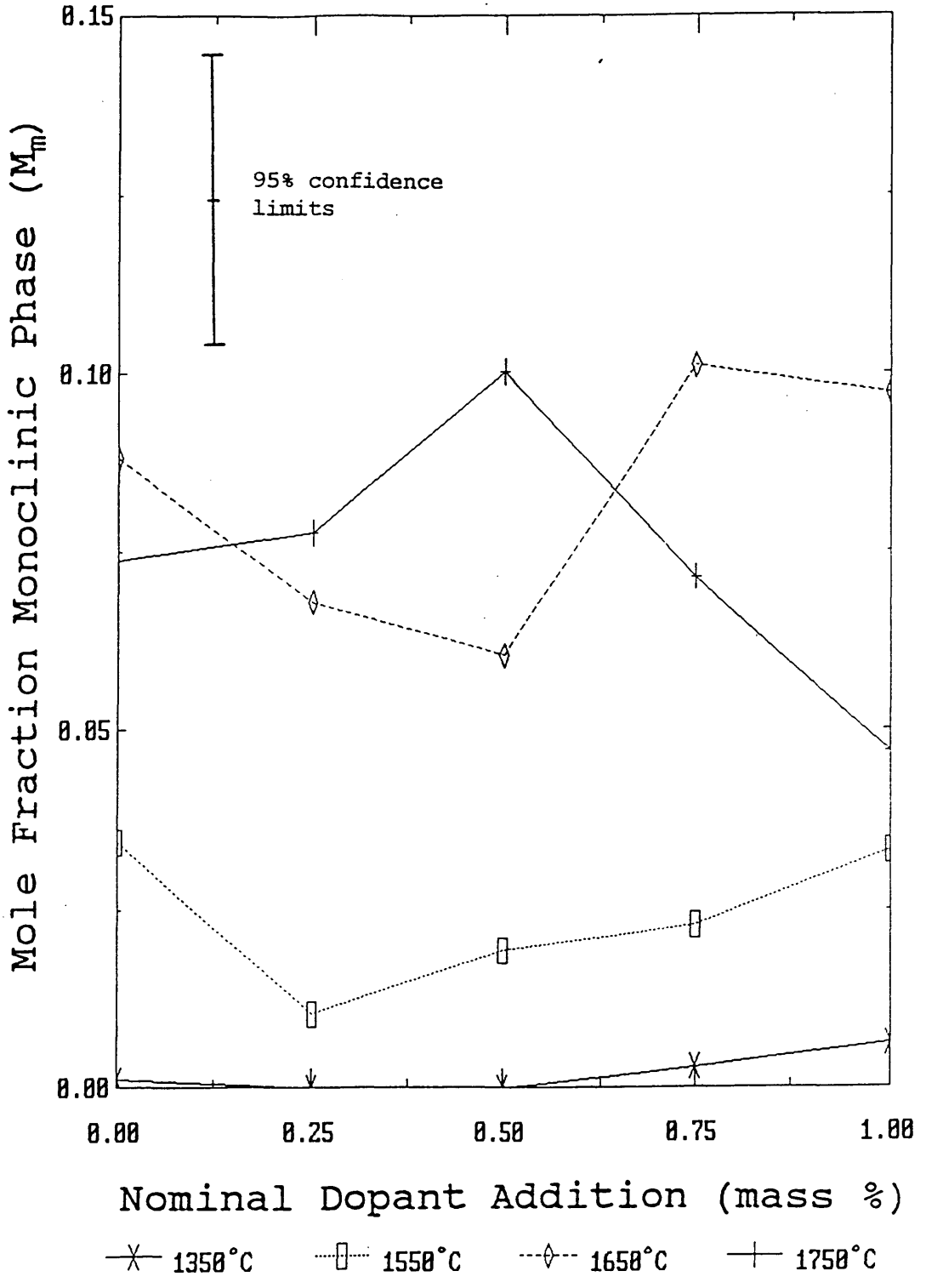

4.6.6 Multiple doped samples.

Figures 4.6.6(a)-(c) illustrate the effect of sintering temperature on the cubic, tetragonal and monoclinic phase compositions of the TZP with multiple dopant additions.

The results appear to show that all of the specimens containing alumina additions behave similarly, with a dramatic change in phase composition for the 1750° sintered samples.

The SiO_2-TiO_2 doped sample shows an increase in cubic phase with increasing sintering temperature over the range 1350-1750°C, whilst all of the remaining samples containing alumina show an increase in cubic phase with sintering temperature, with a large reduction in the cubic phase content for the 1750°C sintered samples.

The tetragonal phase of the SiO_2-TiO_2 sample appears to decrease for sintering temperatures above 1350°C, with a possible minima at 1550-1650°C. However for sintering temperatures between 1550 and 1750°C, the change in tetragonal phase content is very small, and within the limits of experimental error.

The alumina containing samples all show a decrease in tetragonal phase content with increasing sintering temperature, with a dramatic decrease for the 1750°C sintered samples.

The monoclinic phase content varies approximately inversely with the tetragonal phase for all samples.

Figure 4.6.6(a).

Effect of sintering temperature on phase composition of T.Z.P. with multiple oxide dopant additions.

Cubic Phase.

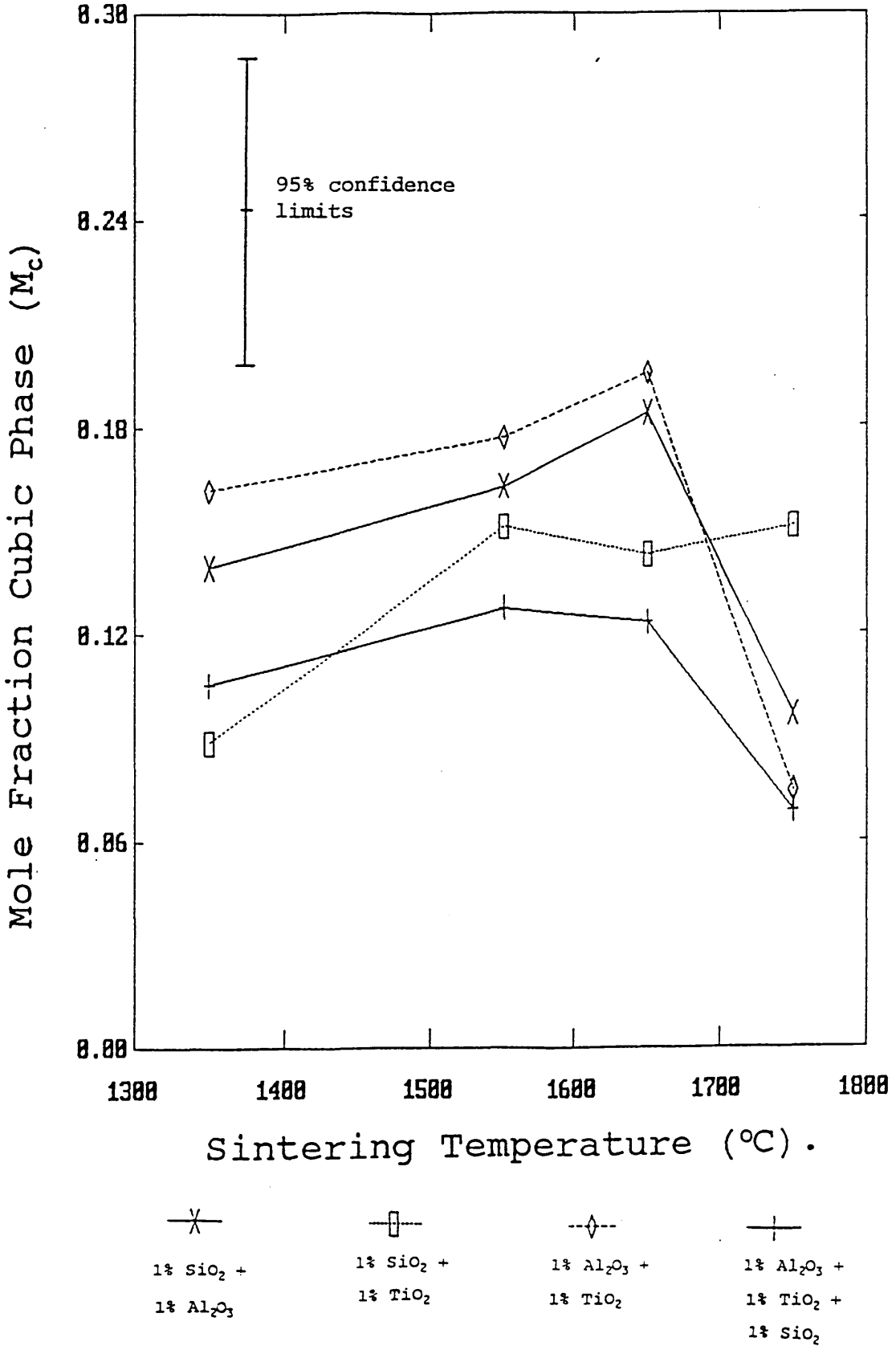

Figure 4.6.6(b).
Effect of sintering temperature on phase composition of T.Z.P. with multiple oxide dopant additions.
Tetragonal Phase.

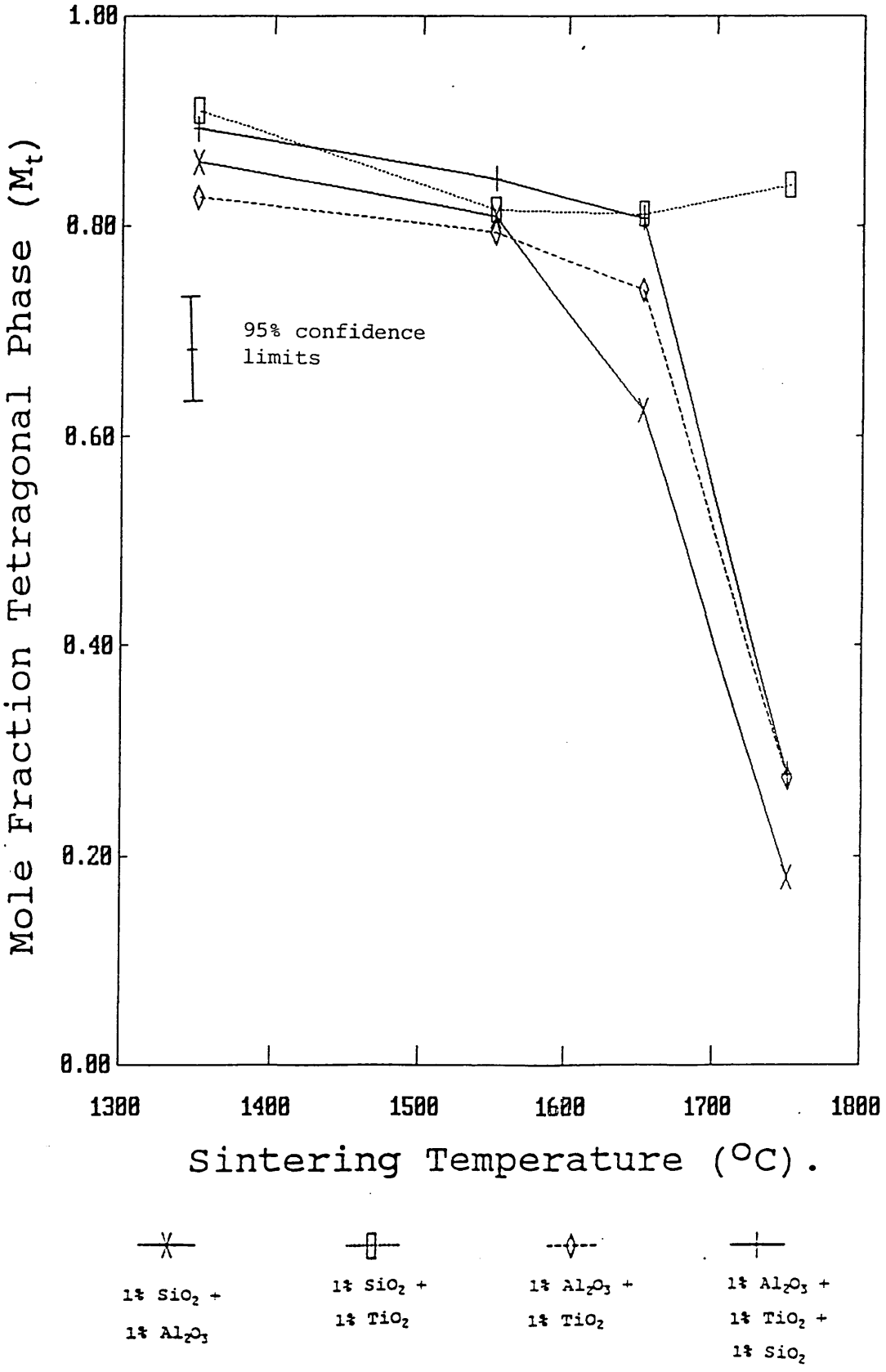

Figure 4.6.6(c).
Effect of sintering temperature on phase composition of T.Z.P. with multiple oxide dopant additions
Monoclinic Phase.

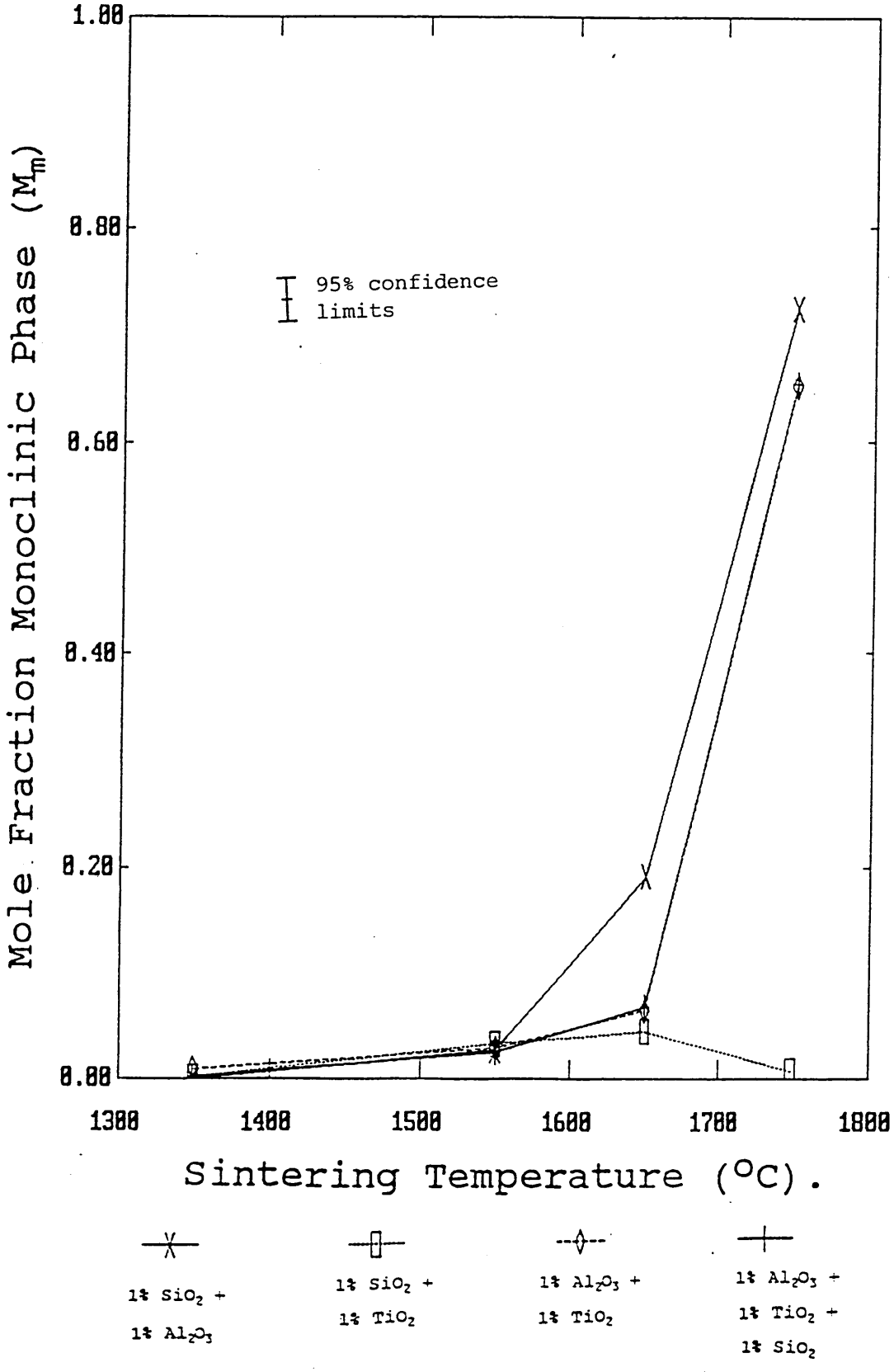

4.6.7 Factorial experiments for phase development.

The results of the factorial experiments to investigate the effects of sintering temperature and impurities (together with their interactions) on the phase development of the sintered specimens are shown in the following sections.

The results comprise three separate factorial experiments for both the cubic and tetragonal phases to cover the sintering temperature ranges 1350-1550°C, 1550°-1650°C, and 1650-1750°C.

It was not deemed necessary to carry out a separate investigation into the monoclinic phase content, since the one factor at a time experiments showed that this was inversely related to the amount of tetragonal phase.

The results are presented in the same form as the factorial experiments for density (section 4.3.8), with both internal and external estimates of error included in the variance analyses and significance tests as described previously.

4.6.7.1 Factorial experiments for cubic phase development

The experimental data and calculated factorial effects of impurity content and sintering temperature on the cubic phase development in the sintered specimens are shown in tables 4.6.7.1(a)-(c), with the corresponding analyses of variance and estimates of significance in tables 4.6.7.1((d)-(f) (see appendix 1).

Figures 4.6.7.1(a)-(d) are schematic representations of the main effects, impurity interactions and impurity-temperature interactions for two and three/four factors respectively.

Generally, the magnitude of the interaction effects is small in these experiments, with the most significant (at f(<5%) level) being a negative (AB) interaction effect between Al_2O_3 and SiO_2 over the 1550-1650° and 1650-1750°C temperature intervals (i.e. less cubic phase than

predicted).

A significant impurity-temperature interaction is present for alumina addition (AD) for the 1650-1750°C sintering temperature interval.

The single factor (main) effects identified in these experiments should be generally meaningful, due to the limited number and small magnitude of multi factor interactions. However, the calculated main effect for alumina addition (A) over the 1650-1750°C temperature interval may not be reliable due to the significant interactions present involving this factor.

The calculated main effects from the factorial experiment are in accordance with the results of the one factor at a time experiments for alumina addition over the 1350-1550°C and 1550-1650°C sintering temperature intervals showing no significant effect on the cubic phase development, with no effect also being confirmed for silica addition over all temperature intervals.

The calculated main (factorial) effect of titania addition (C) shows a significant negative effect (ie reduction in cubic phase) for all sintering temperature intervals, with the magnitude of the effect increasing with sintering temperature.

The calculated factorial effect of temperature (D) shows a significant positive effect on cubic phase formation over the 1350-1550° sintering temperature interval, and a significant negative effect for the 1650-1750°C temperature interval.

Figure 4.6.7.1(a)

Factorial Experiment (cubic phase development).

Schematic representation of factorial effects.

Main (single factor) effects.

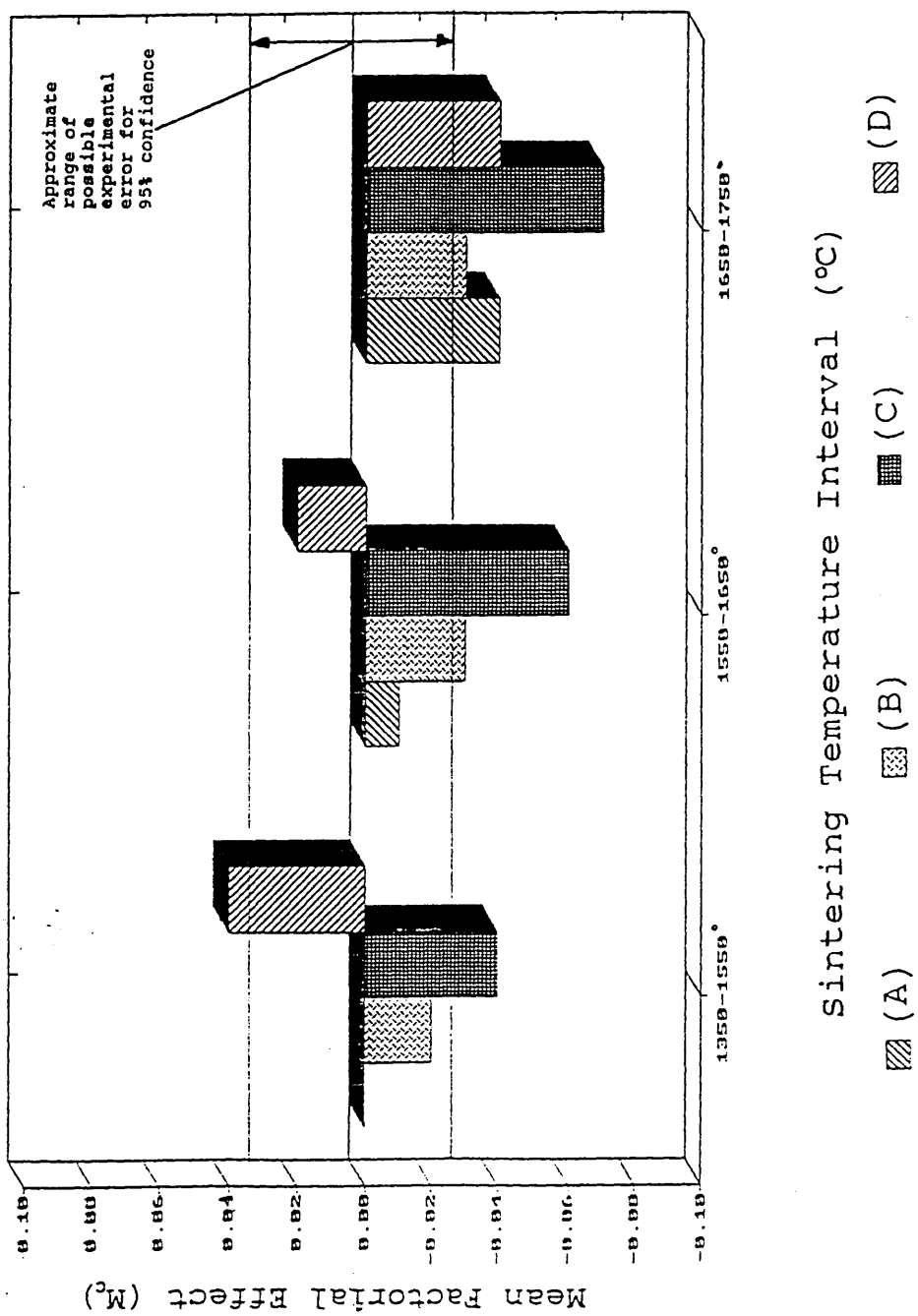

Key to Notation.
e.g.
A = 1 mass % Al_2O_3 addition.
B = 1 mass % SiO_2 addition.
C = 1 mass % TiO_2 addition.
D = Higher value of sintering temperature (in range) used.
ABCD = Interaction between factors A,B,C and D.

Figure 4.6.7.1(b)

Factorial Experiment (cubic phase development).
Schematic representation of factorial effects.
Impurity interaction effects.

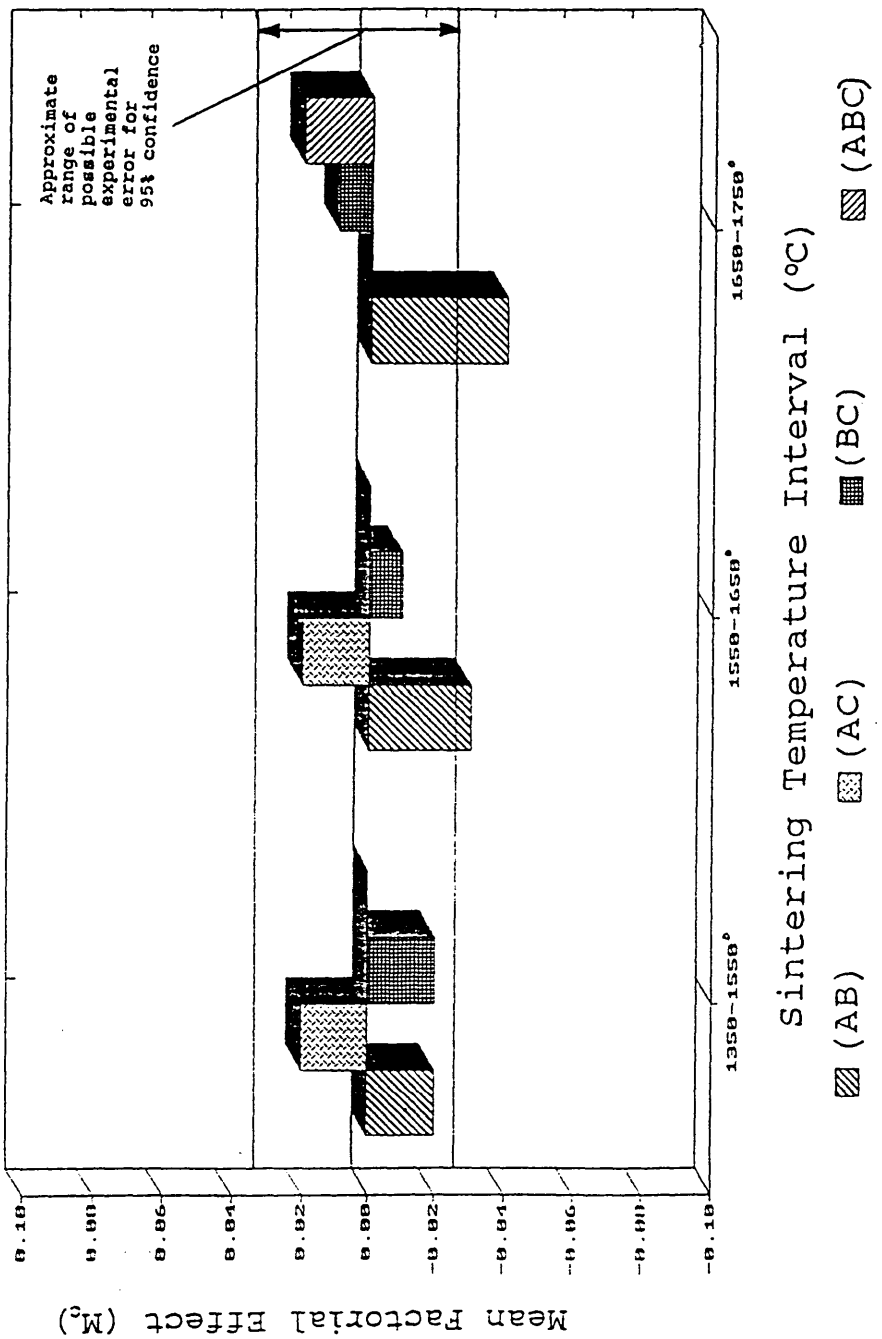

Key to Notation.
e.g.
A = 1 mass % Al_2O_3 addition.
B = 1 mass % SiO_2 addition.
C = 1 mass % TiO_2 addition.
D = Higher value of sintering temperature (in range) used.
ABCD = Interaction between factors A,B,C and D.

Figure 4.6.7.1(c)

Factorial Experiment (cubic phase development).

Schematic representation of factorial effects.

Impurity-temperature interaction effects (two factor).

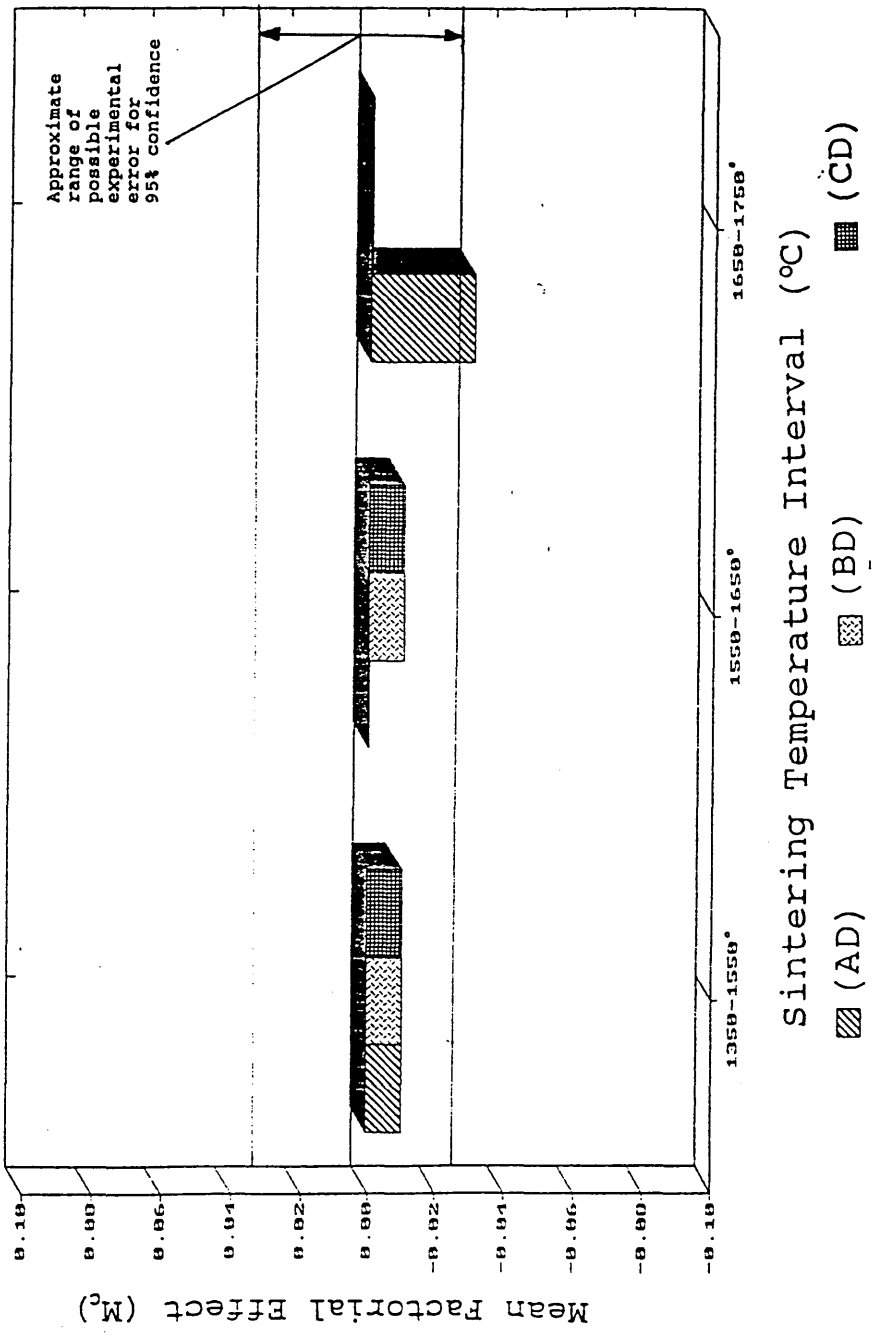

Key to Notation.
e.g.
A = 1 mass % Al_2O_3 addition.
B = 1 mass % SiO_2 addition.
C = 1 mass % TiO_2 addition.
D = Higher value of sintering temperature (in range) used.
ABCD = Interaction between factors A,B,C and D.

Figure 4.6.7.1(d)

Factorial Experiment (cubic phase development).

Schematic representation of factorial effects.

Impurity-temperature interaction effects (3 & 4 factor).

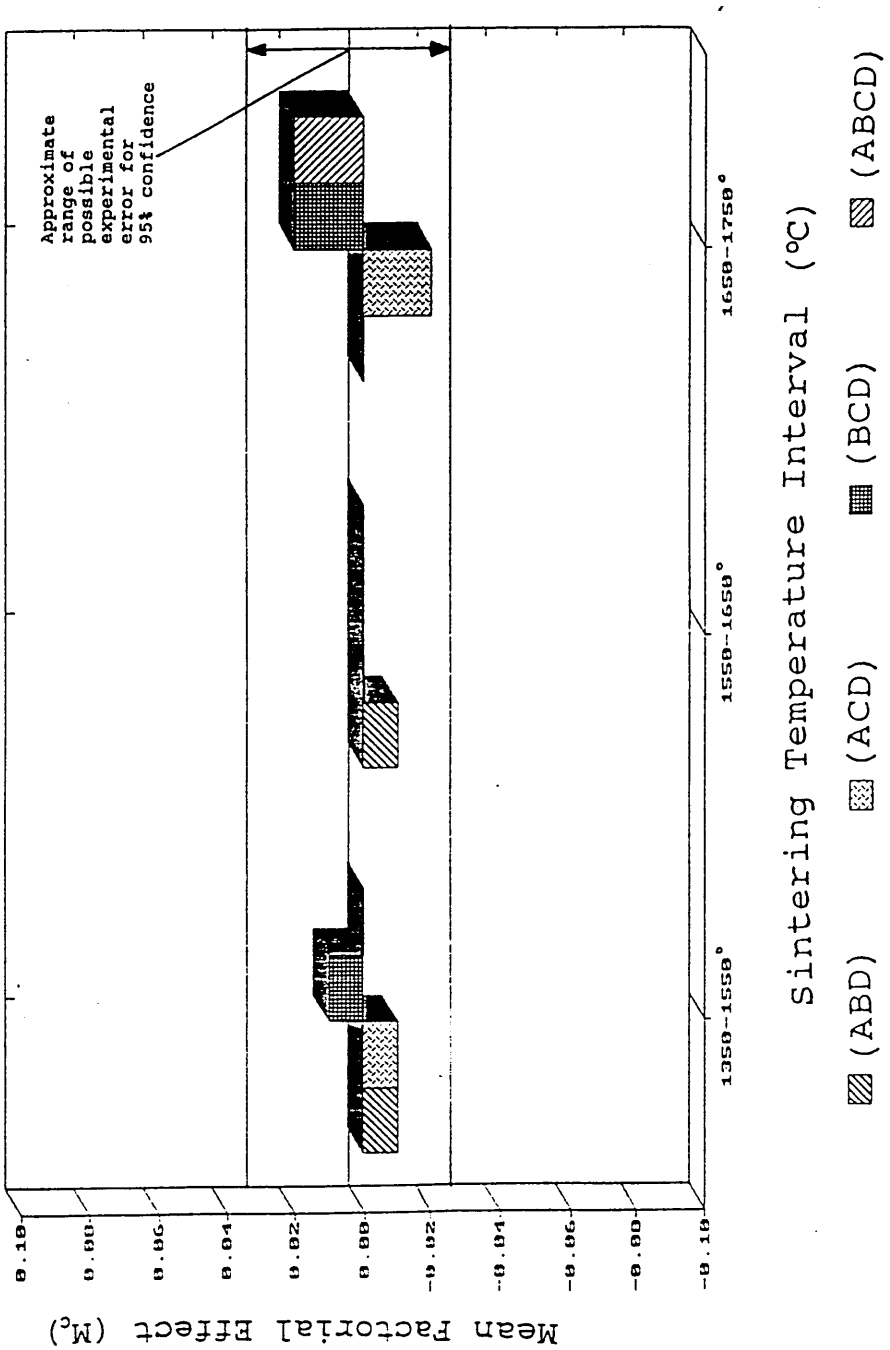

Key to Notation.
e.g.
A = 1 mass % Al_2O_3 addition.
B = 1 mass % SiO_2 addition.
C = 1 mass % TiO_2 addition.
D = Higher value of sintering temperature (in range) used.
ABCD = Interaction between factors A,B,C and D.

4.6.7.2 Factorial experiments for tetragonal phase development.

The experimental data and calculated factorial effects of impurity content and sintering temperature on the development and stability of the tetragonal phase in the sintered specimens are shown in tables 4.6.7.2 (a)-(c), with the corresponding analyses of variance and estimates of significance in tables 4.6.7.2 (d)-(f) (see appendix 1).

Figures 4.6.7.2 (a)-(d) are schematic representations of the main effects, impurity interactions and impurity-temperature interactions for two and three/four factors respectively.

The calculated impurity interaction effects show that none of the impurities produce large (significant at the f(<1%) level) interaction effects for sintering temperatures in the 1350-1550°c and 1550-1650°C temperature intervals. However there may be an interaction between Al_2O_3 and SiO_2 (AB) and Al_2O_3 and TiO_2 (AC) over the 1650-1750°C temperature interval (significant at the f(5%) level), whilst there also appears to be a significant (at f(1%) level) three factor interaction between Al_2O_3 and SiO_2 and TiO_2 (ABC) for this sintering temperature interval.

Similarly no significant impurity temperature interaction effects are present for the 1350-1550 and 1550-1650°C temperature intervals. However there appear to be large and highly significant impurity-temperature interaction effects on the amount of tetragonal phase for all the single and multiple dopant additions over the 1650-1750°C sintering temperature interval. Of these, the largest effects are the Al_2O_3 impurity-temperature interaction effect (AD), the Al_2O_3-SiO_2-TiO_2 (ABCD) impurity -temperature interaction effect, and SiO_2-TiO_2 (BCD) impurity-temperature interaction effect all of which are negative suggesting that the interactions increase the tendency for the tetragonal-monoclinic phase

transformation.

The values for the calculated main effects for the 1650-1750°C temperature interval should be interpreted with some scepticism since the numerous and highly significant interaction effects may render the main effect values meaningless. However the calculated values for the main effects should be reliable for the other temperature intervals where no significant interactions are present.

The calculated values of these main effects suggest that titania addition (C) produces a small but significant increase in the amount of tetragonal phase in the sintered specimens. The negative values for the calculated effects of sintering temperature (D), suggest that an increase in sintering temperature results in a decrease in the amount of tetragonal phase over the 1350-1550 and 1550-1650°C sintering temperature ranges. These results confirm the findings of the one factor at a time experiments.

No significant (main) effects are present for alumina and silica addition over the 1350-1550 and 1550-1650°C temperature intervals which is also in accordance with the one factor at a time experiments.

Figure 4.6.7.2(a)

Factorial Experiment (tetragonal phase development).
Schematic representation of factorial effects.
Main (single factor) effects.

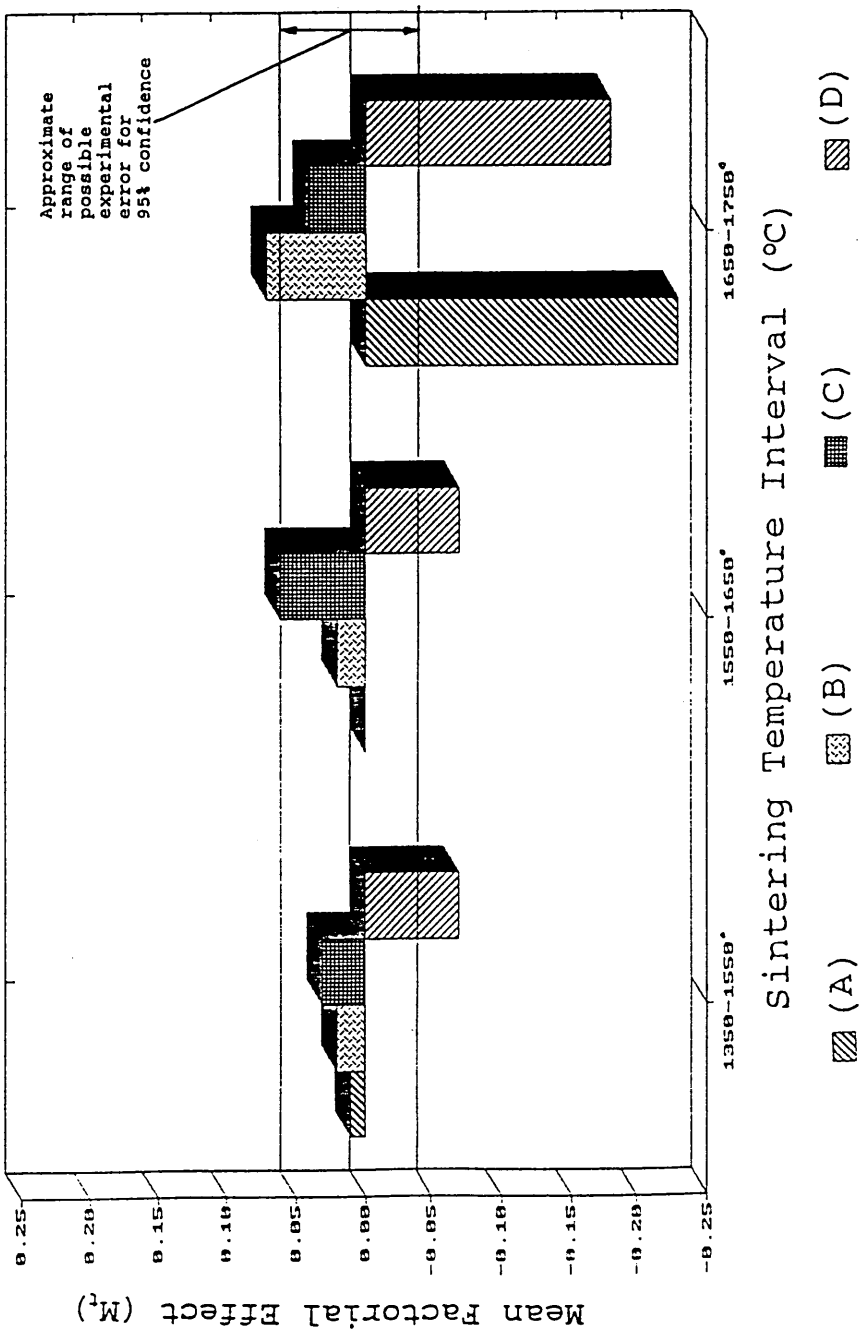

Key to Notation.
e.g.
A = 1 mass % Al_2O_3 addition.
B = 1 mass % SiO_2 addition.
C = 1 mass % TiO_2 addition.
D = Higher value of sintering temperature (in range) used.
ABCD = Interaction between factors A,B,C and D.

Figure 4.6.7.2(b)

Factorial Experiment (tetragonal phase development).

Schematic representation of factorial effects.

Impurity interaction effects.

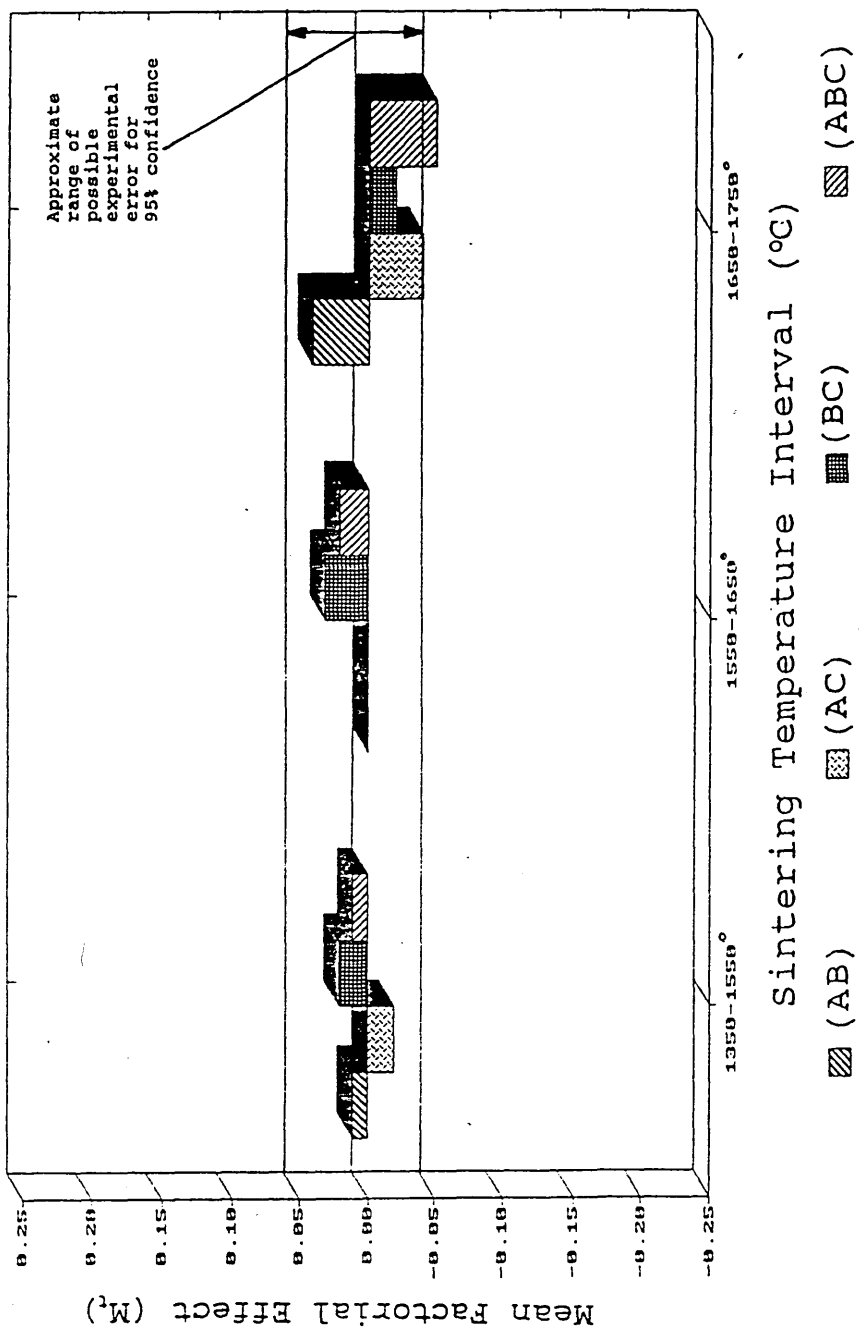

Key to Notation.
e.g.
A = 1 mass % Al_2O_3 addition.
B = 1 mass % SiO_2 addition.
C = 1 mass % TiO_2 addition.
D = Higher value of sintering temperature (in range) used.
ABCD = Interaction between factors A,B,C and D.

Figure 4.6.7.2(c)

Factorial Experiment (tetragonal phase development).

Schematic representation of factorial effects.

Impurity-temperature interaction effects (two factor).

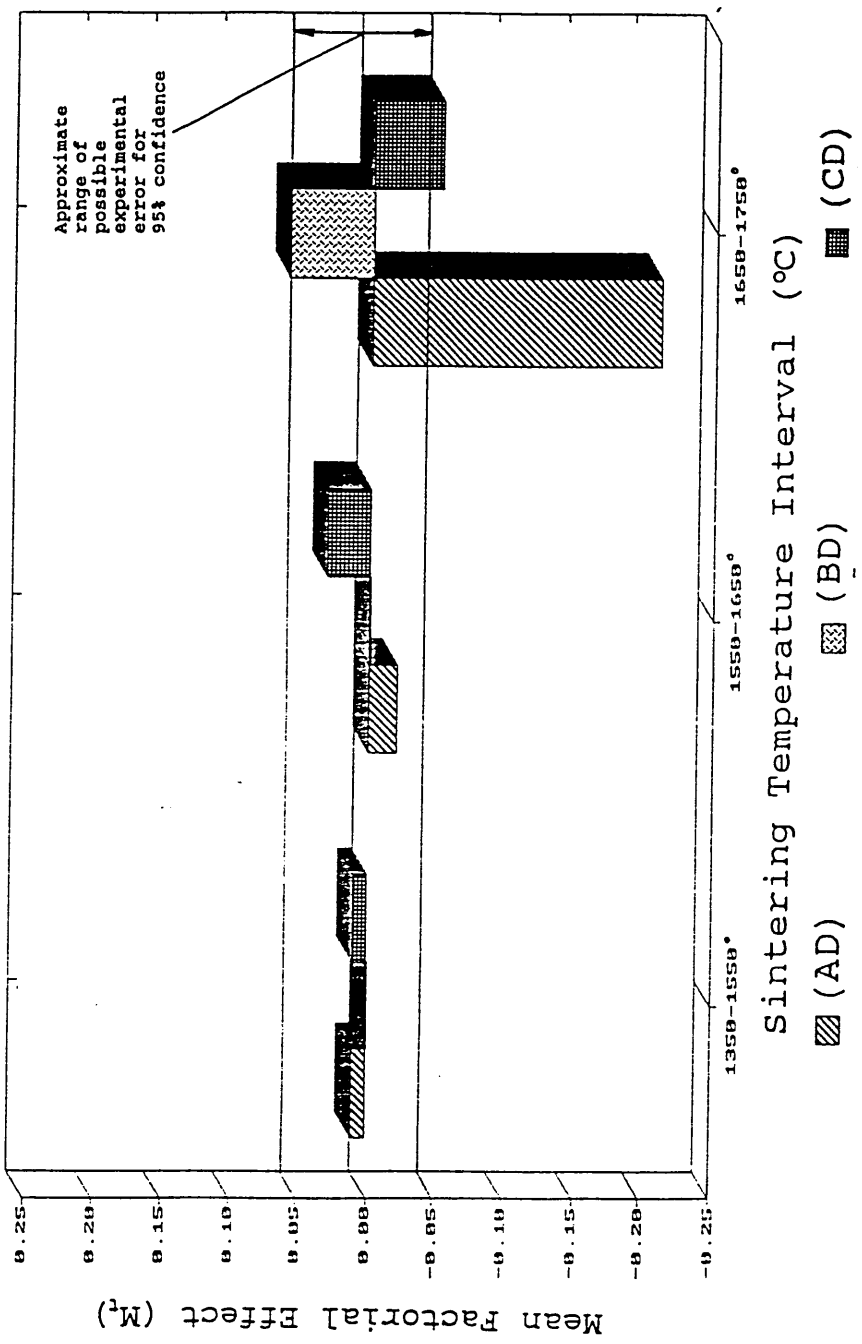

Key to Notation.
e.g.
A = 1 mass % Al_2O_3 addition.
B = 1 mass % SiO_2 addition.
C = 1 mass % TiO_2 addition.
D = Higher value of sintering temperature (in range) used.
ABCD = Interaction between factors A,B,C and D.

Figure 4.6.7.2(d)

Factorial Experiment (tetragonal phase development).

Schematic representation of factorial effects.

Impurity-temperature interaction effects (3 & 4 factor).

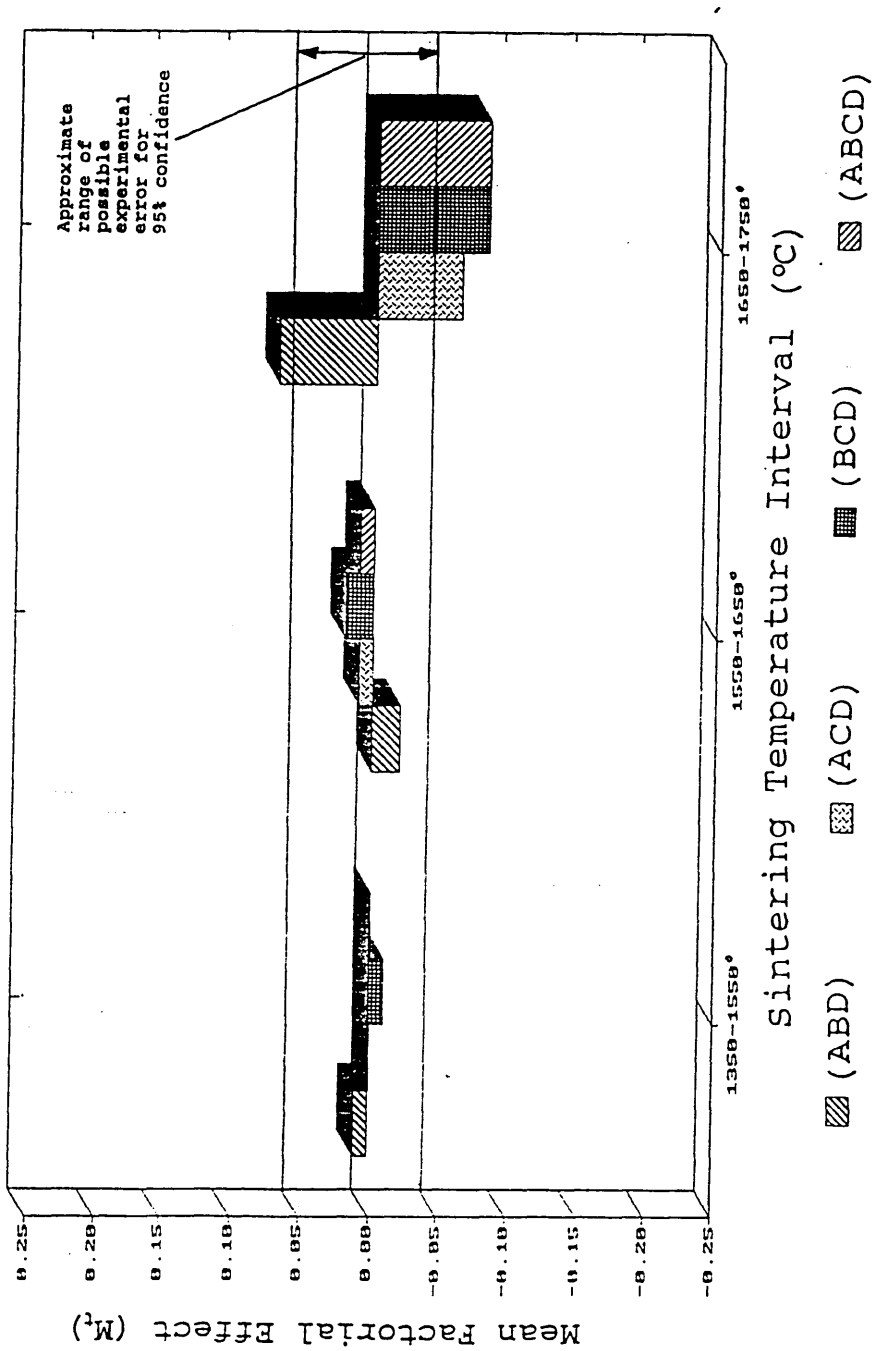

Key to Notation.
e.g.
A = 1 mass % Al_2O_3 addition.
B = 1 mass % SiO_2 addition.
C = 1 mass % TiO_2 addition.
D = Higher value of sintering temperature (in range) used.
ABCD = Interaction between factors A,B,C and D.

4.7 Hardness and fracture toughness determinations.

The results of the determination of the effect of the impurities on the mechanical properties of T.Z.P. are reported in this section. The results comprise the calculated hardness values from the Vicker's indentations, and the calculated toughness values from the indentation crack length measurements.

4.7.1 Sources and estimation of experimental error.

As for the other experiments, there are a number of possible sources of experimental error in these results. These include:

- Errors arising from the hardness and fracture toughness measurements.
  e.g. Errors in measuring the indentation diameters, errors from frictional forces in the Vickers indenting equipment.
  Difficulties in accurately determining the crack length.
- Errors from the doping and fabrication process.
  e.g. As described in the previous sections.

To account for and distinguish between these, two estimates of experimental error were made for these results comprising an estimate of measuring error (a), and total experimental error (b).
The methods used to estimate the error were similar to those used in the other results.

(a) An estimate of measuring error was made from the standard error in the mean of the indentation diameter measurements and crack length measurements for the hardness and fracture toughness results respectively on each specimen.

The 95% confidence limits around the mean value were used as the estimate of the measuring error in each case.

The measuring error was estimated separately for each composition as an average over all sintering

temperatures, with the results being combined to give an overall estimate of experimental error.

The results and calculations used to generate this estimate are shown in table 4.7.1(a) (appendix 1).

(b) An estimate of total experimental error was made by comparing the hardness and fracture toughness results obtained from sintered pellets produced from two different batches of doped powder of nominally identical composition.
The difference between the calculated values for each batch was calculated for each sintering temperature and the average value of the difference (over all sintering temperatures) was calculated together with the standard deviation in this mean value.

The overall experimental error was estimated to be less than the (upper) 95% confidence limit in the average value of the difference recorded between the two sets of results.
eg.

$$\text{Experimental error} < [\text{mean difference} + 1.96 \times (\text{standard error in mean difference})]$$

The results and calculations used to produce this estimate are shown in table 4.7.1(b) (appendix 1).

4.7.2 Undoped powders.

The hardness and fracture toughness results for the undoped T.Z.P. material are shown in table 4.7.2 (appendix 1). The results are compared for the as received TZ3Y material and the blank treated material.

Figures 4.7.2 (a) and (b) illustrate the effect of sintering temperature on the hardness and fracture toughness respectively of these specimens.

The results show very similar behaviour in both cases with a large increase in hardness occurring between 1250 and 1350°C sintering temperature, and a plateau value of approximately 13 GN/m^2 for sintering temperatures between 1350° and 1650°C. The results also suggest the possibility of a decrease in hardness for sintering temperatures in excess of 1650° although this is within the range of possible experimental error.

There appears to be a small reduction in hardness for the blank treated material compared to the as received TZ3Y for a similar sintering temperature. The magnitude of this difference is within the range of possible experimental error for 95% confidence, although the consistency of the trend does suggest that it may be real.

The toughness results also show very similar behaviour in both materials, and no clear differences can be identified in the toughness of the two materials when sintered under similar conditions.

There is a consistent trend in both specimens showing a minimum in toughness for sintering temperatures in the range 1350° to 1450°C, after which the toughness increases significantly with increasing sintering temperature.

Figure 4.7.2(a) Effect of sintering temperature on hardness of undoped T.Z.P.

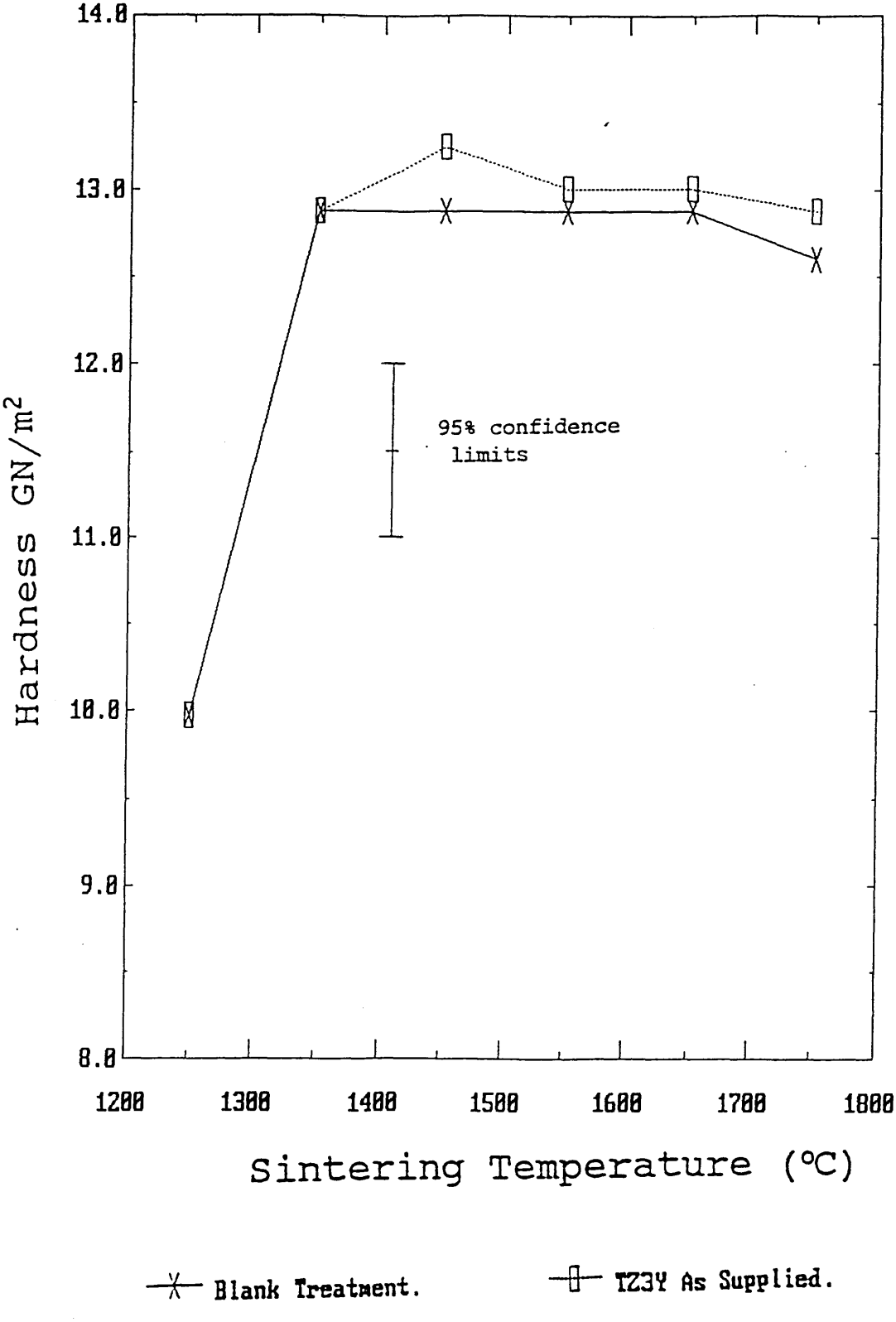

Figure 4.7.2(b) Effect of sintering temperature on fracture toughness of undoped T.Z.P.

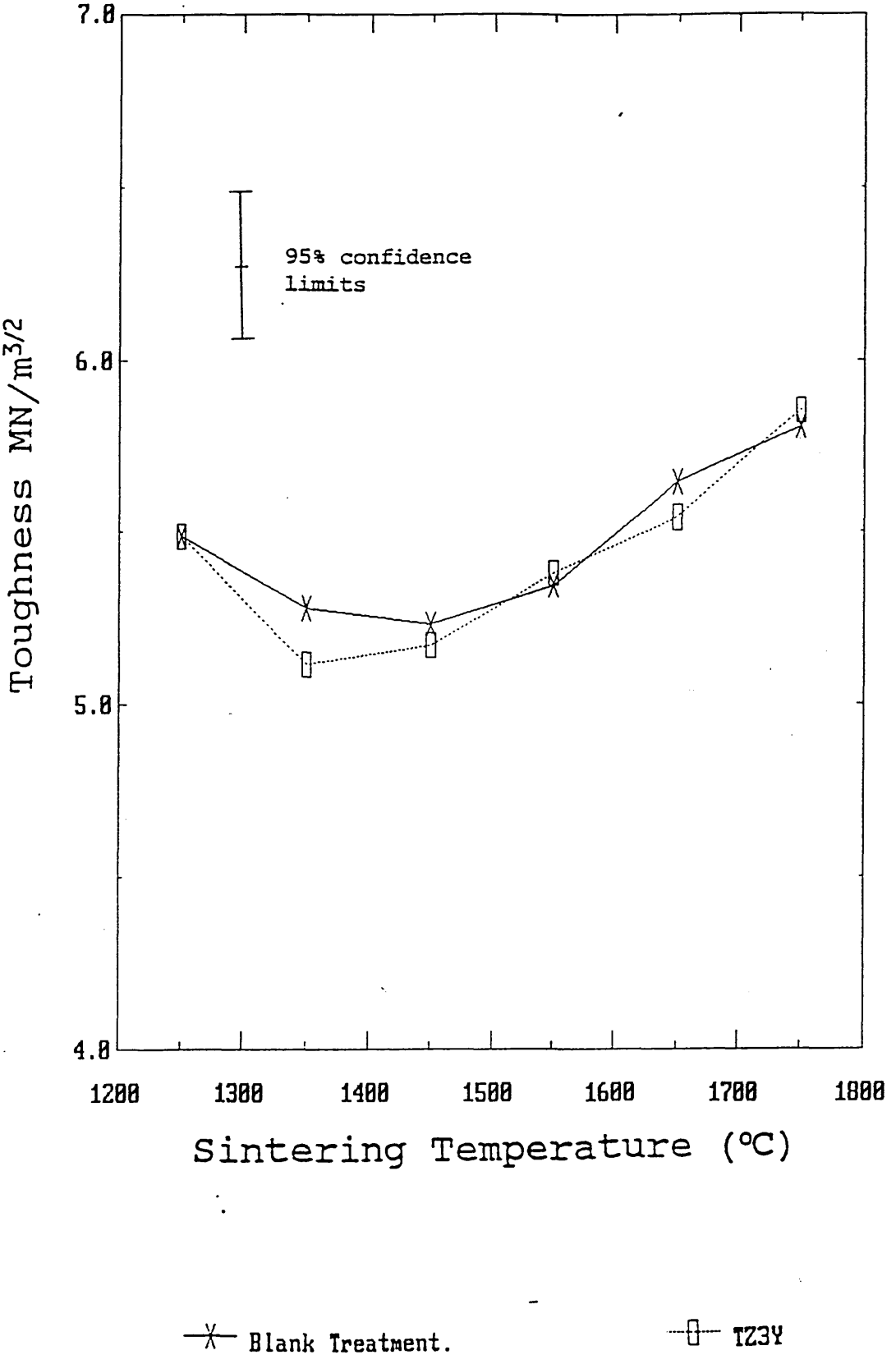

4.7.3 Alumina doped material.

The hardness and fracture toughness results for the sintered alumina doped material are shown in table 4.7.3 (appendix 1).

The effect of sintering temperature on the hardness and fracture toughness of the alumina doped material is also shown in figures 4.7.3 (a) and (b) respectively.

Figures 4.7.3 (c)-(e) show the effect of the alumina content on the hardness for a range of sintering temperatures. These results appear to show that for lower sintering temperatures ie 1250°C -1450°C, small additions of alumina (up to 0.25 mass % result in significant increases in hardness, whilst further dopant additions produce no further improvement, with a possible reduction in hardness for additions in the range 0.75 to 1 mass %.

However the magnitude of this effect in the 1350°C and 1450°C sintered specimens is similar (although slightly greater than) the estimated range of possible experimental error, and it is difficult to draw clear conclusions from these results.

For sintering temperatures of 1650°C and above, the hardness appears to decrease with increased alumina addition. However, the hardness of samples containing more than 0.25% alumina additions could not be determined for 1750°C sintering temperature due to the porosity and cracking present in the specimens.

The effect of the various levels of alumina dopant addition on the toughness of the material could not be ascertained, since the magnitude of the differences between the variously doped samples lay well within the range of possible experimental error. However, by taking an average of the toughness results for all the addition levels at each sintering temperature, it was possible to calculate an average effect (of the presence of alumina) on the toughness.

These results do appear to show clear trends when

compared to the undoped material.

The average effect of alumina addition appears to show that alumina additions of up to 1 mass % produce a significant increase in the toughness when compared to the blank treated material for sintering temperatures in excess of 1350°C

Figure 4.7.3(a)
Effect of sintering temperature on the hardness of alumina doped specimens.

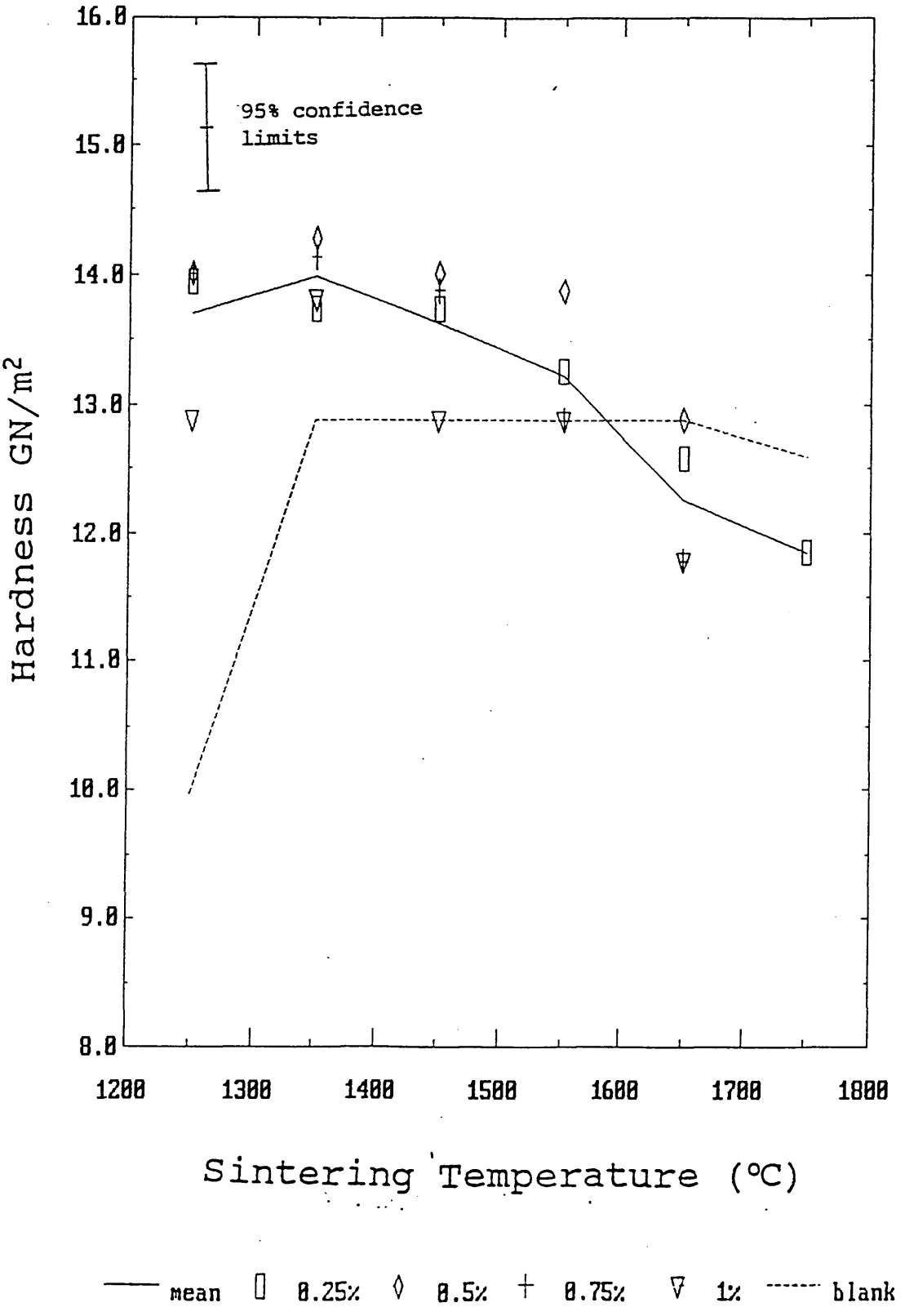

Figure 4.7.3(b)
Effect of sintering temperature on the toughness of alumina doped specimens.

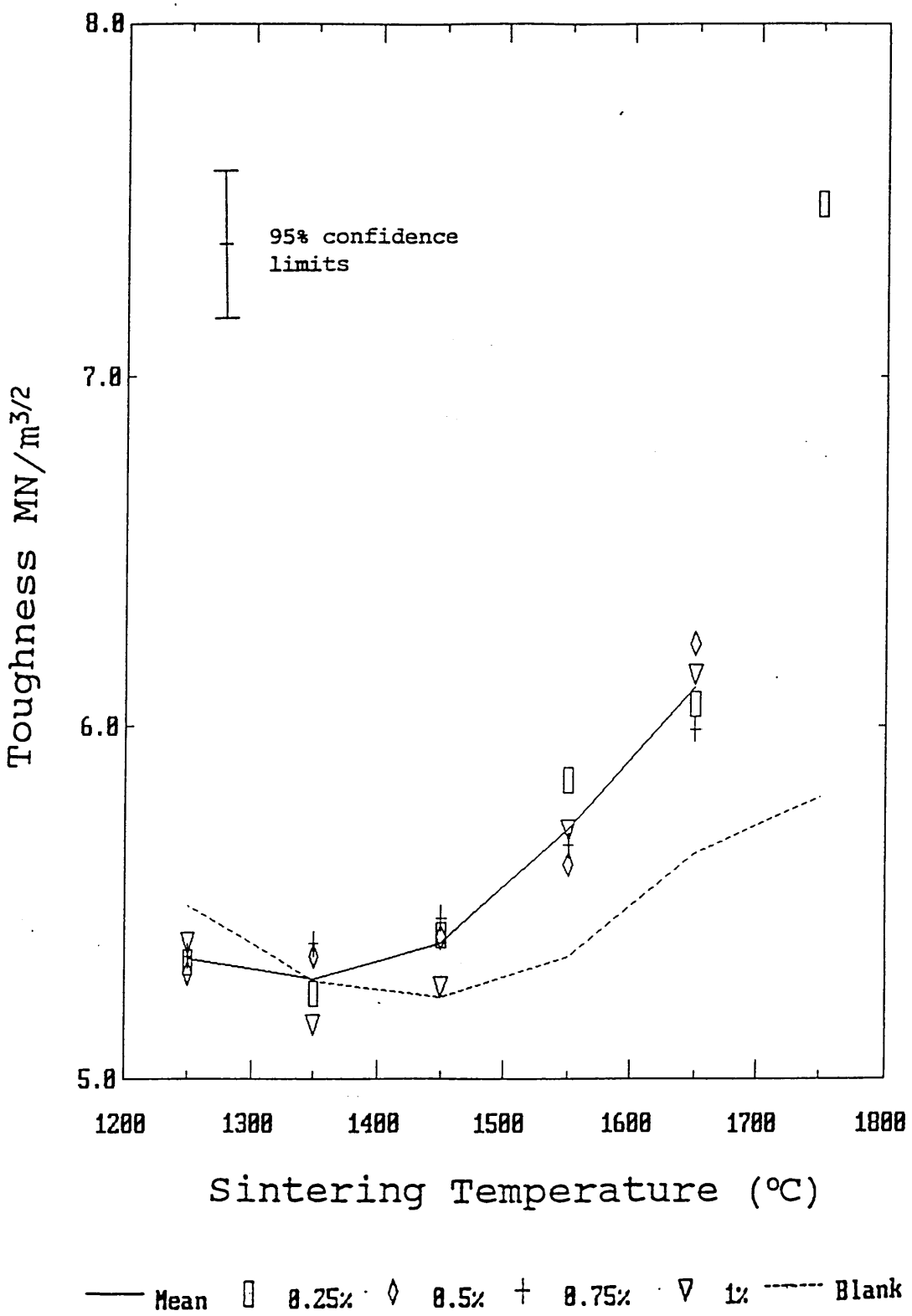

Figure 4.7.3 (c)
Effect of alumina dopant addition on the hardness of sintered specimens
1250°-1450°C sintering temperature.

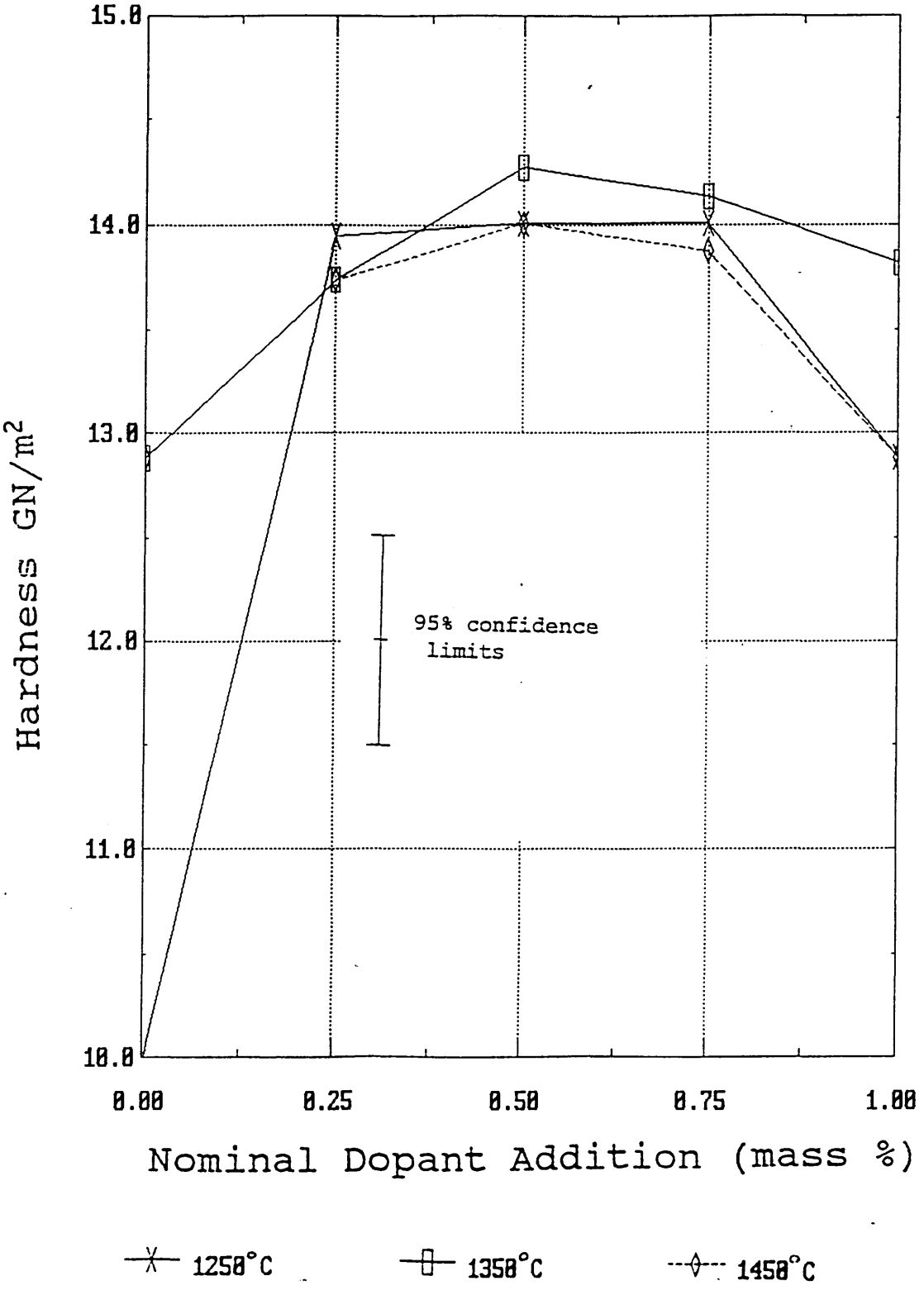

Figure 4.7.3 (d)
Effect of alumina dopant addition on the hardness of sintered specimens
1550°C sintering temperature.

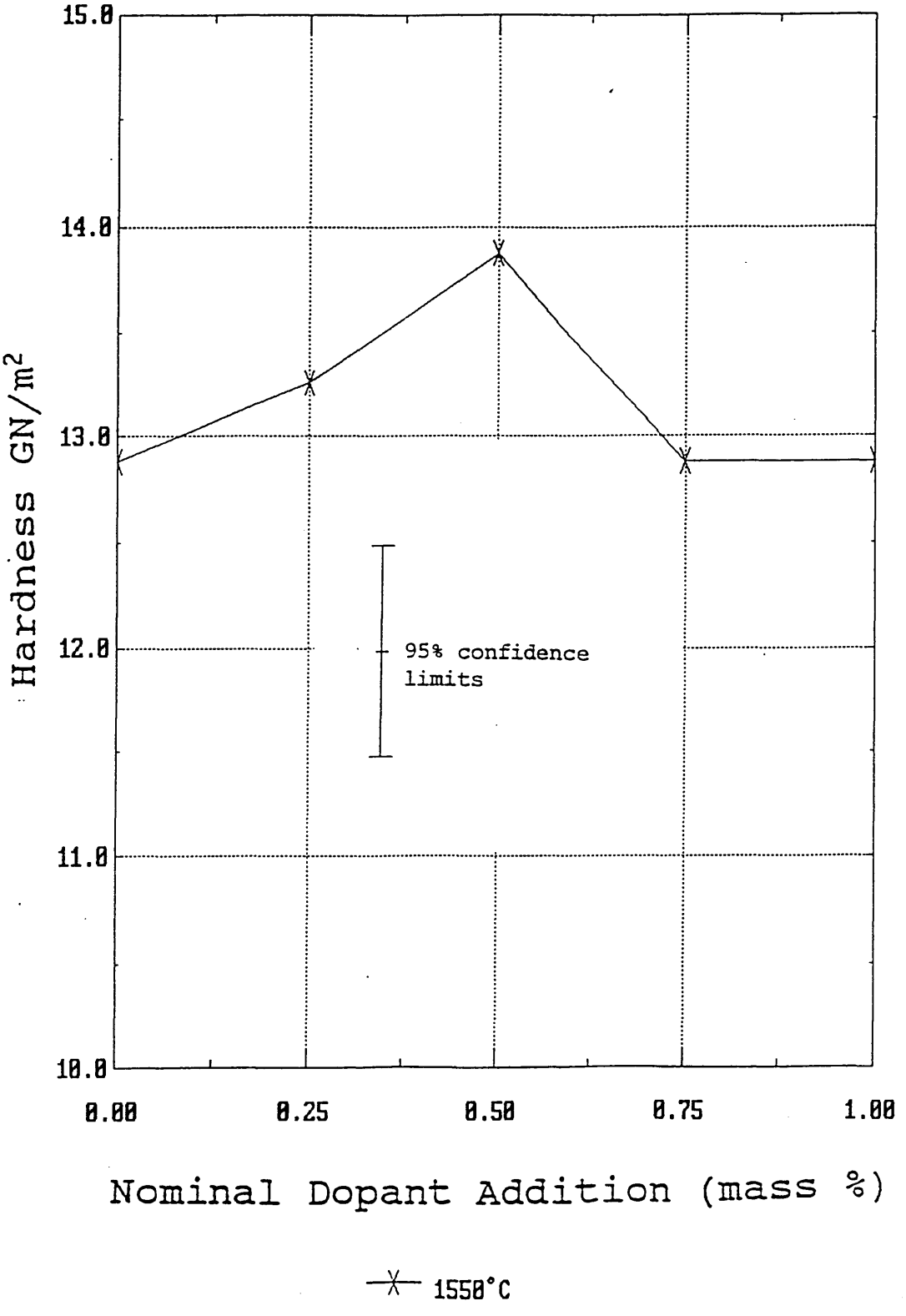

Figure 4.7.3 (e)
Effect of alumina dopant addition on the hardness of sintered specimens
1650 - 1750°C sintering temperature.

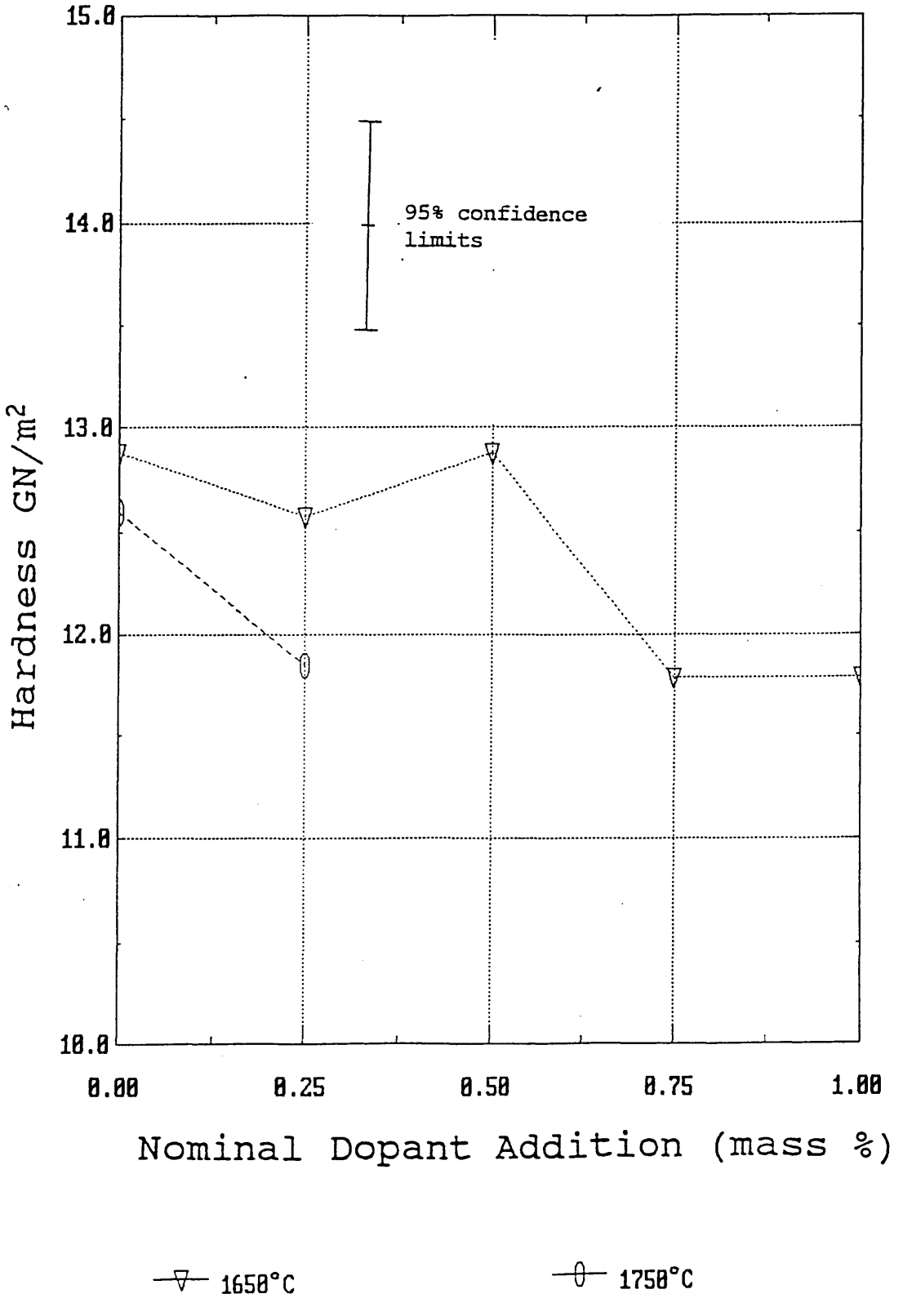

4.7.4 Silica doped specimens.

The hardness and fracture toughness results for the sintered silica doped specimens are shown in table 4.7.4 (appendix 1), with the effect of sintering temperature on the hardness and fracture toughness shown in figures 4.7.4 (a) to (c).

As with the previous results, the hardness and fracture toughness results for the 0.75% silica dopant addition appear to be anomalous.

The differences observed between the other silica doped specimens lie within the range of possible experimental error for both the hardness and fracture toughness determinations, and it is not possible to identify any trends over the range of addition levels investigated. However there do appear to be significant differences between the silica doped and undoped materials for equivalent sintering temperatures.

To attempt to show these trends, and to attempt to reduce the effect of experimental error on the results, the average effect of the silica additions on the hardness and fracture toughness were calculated as described in section 4.7.3. The calculated mean effect of silica over the 0.25 to 1 mass % addition level are shown in figures 4.7.4(a) and (c) as a solid black line (the apparently anomalous 0.75% SiO_2 results are omitted from the calculated mean values).

The hardness results for the silica doped samples show a large increase for sintering temperatures between 1250 and 1350°C, and a higher maximum hardness value than the undoped material.

For sintering temperatures in excess of 1350°C, the hardness of the silica doped materials appears to decrease significantly, and for sintering temperatures in excess of 1550°C produces lower hardness values than the undoped material in which the hardness is relatively invariant with temperature above 1350°C sintering

temperature.

The hardness of the 0.75% SiO_2 doped material also appears to show the same trends with increasing sintering temperature. However the results all appear to be shifted to lower than expected values.

The effect of silica addition on toughness is less clear than observed on the hardness results. However there does appear to be a **small** but consistent reduction in toughness compared to the undoped (blank treated) material for sintering temperatures below 1550°C and a consistent **slight** increase in toughness relative to the undoped material for sintering temperatures above 1650°C. It is difficult to draw clear conclusions from these results since the magnitude of the effects observed lies within the estimated range of experimental error for 95% confidence (for individual results), however the consistency of the results would appear to suggest that the effect is probably significant.

Figure 4.7.4 (a)
The effect of sintering temperature on the hardness of silica doped specimens.
(0.25, 0.5 and 1 mass % addition levels)

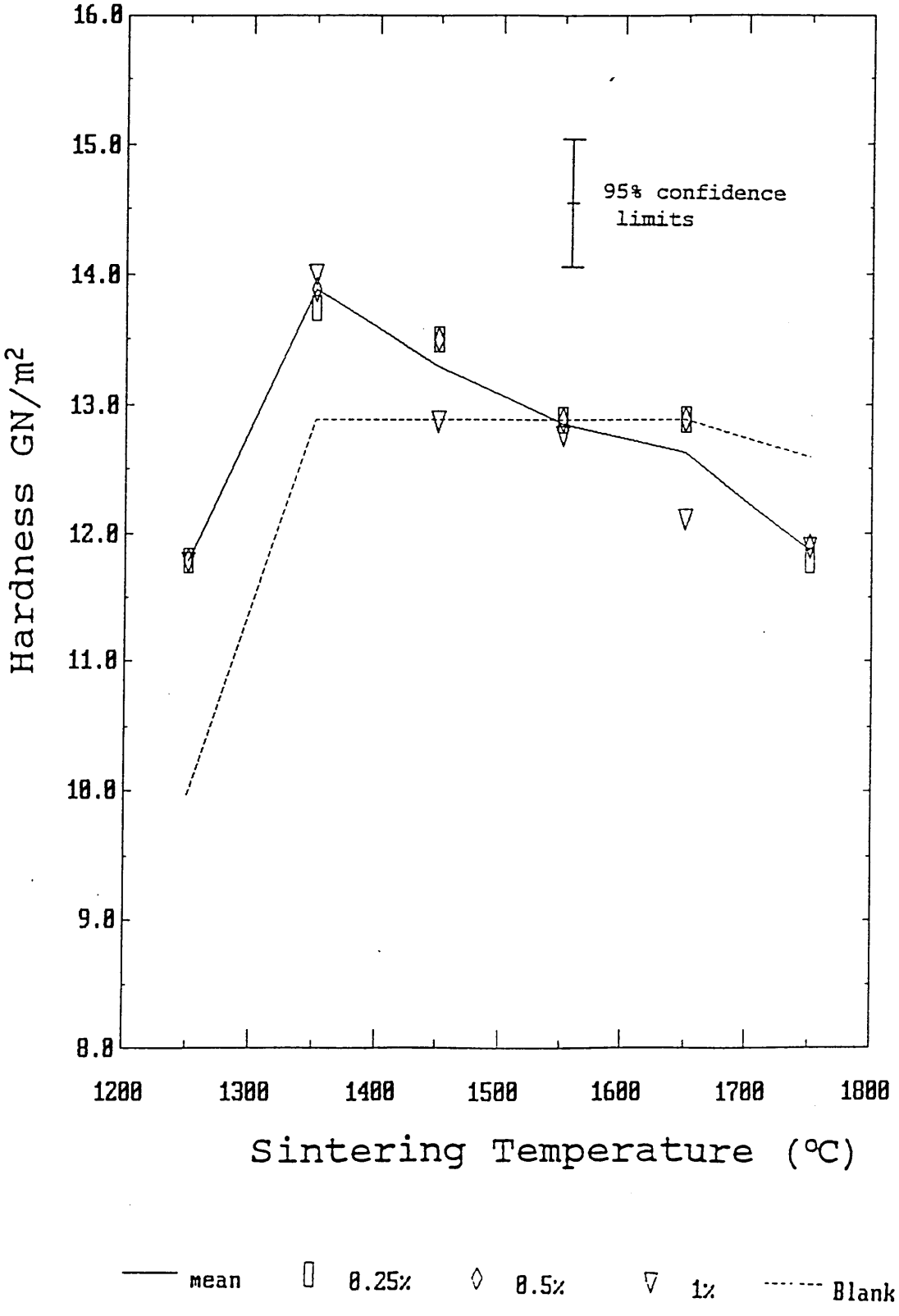

Figure 4.7.4 (b)

The effect of sintering temperature on the hardness of the anomalous 0.75 mass % silica doped specimens.

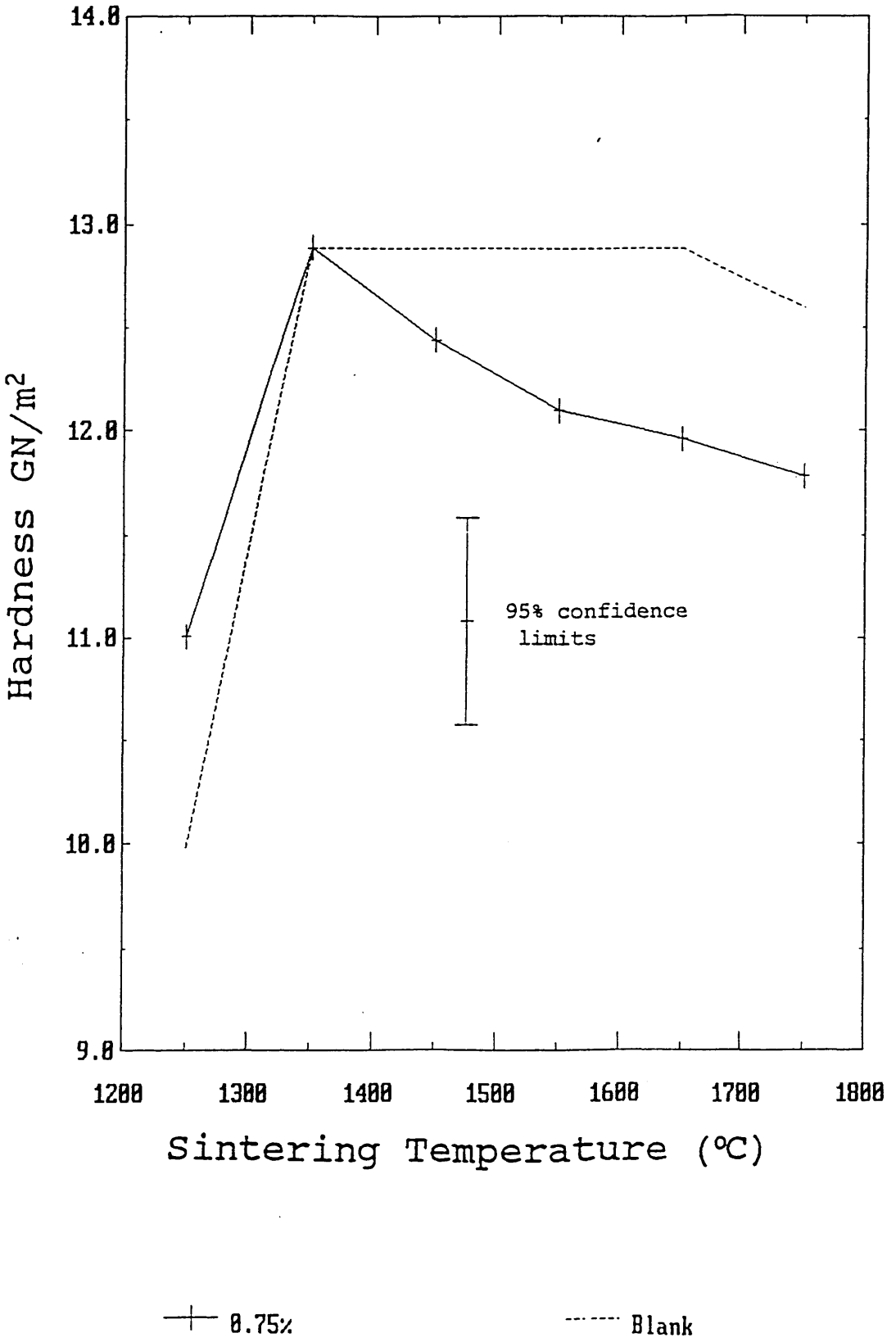

Figure 4.7.4 (c).
The effect of sintering temperature on the fracture toughness of silica doped specimens.

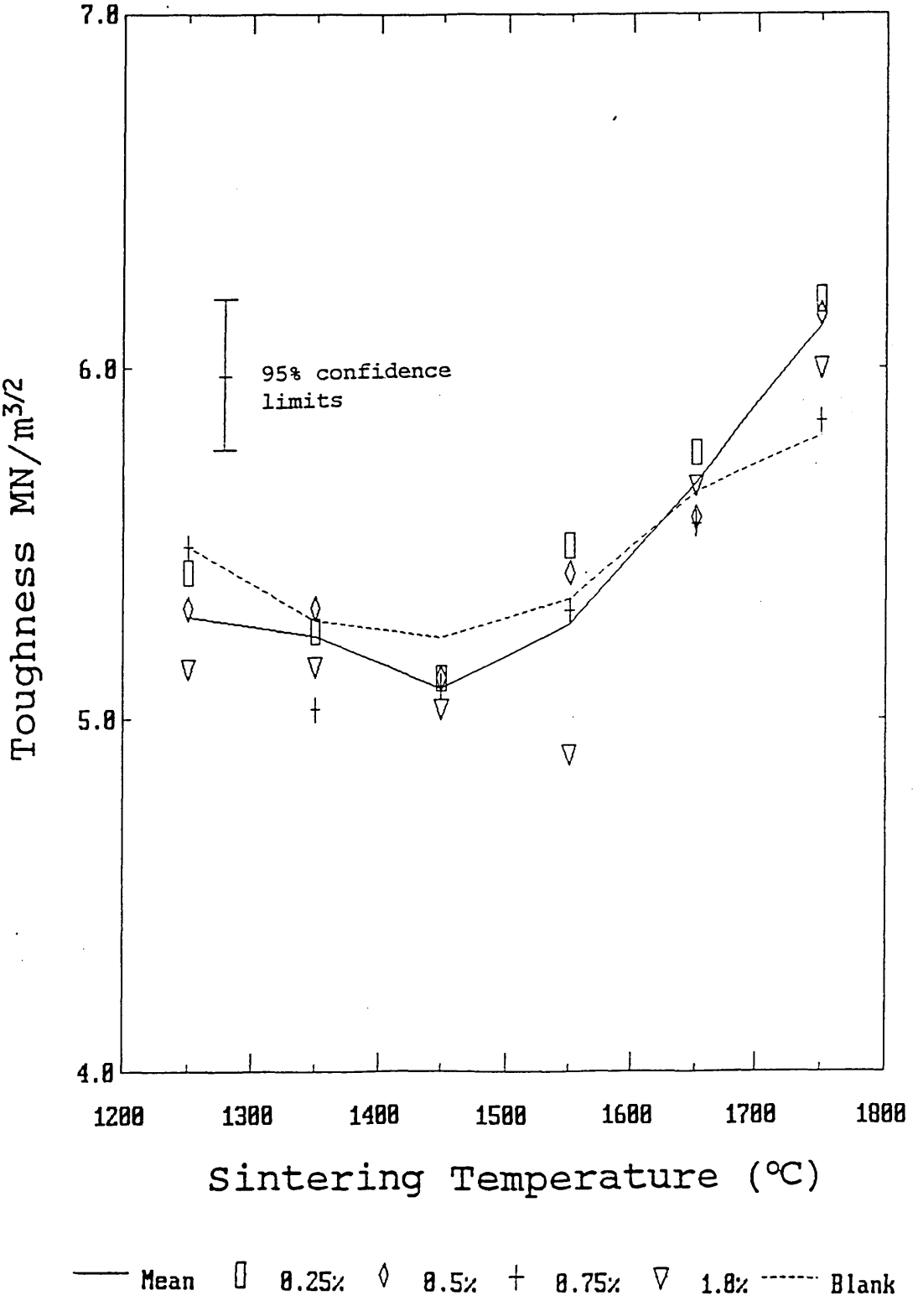

4.7.5 Titania doped samples.

The hardness and fracture toughness results for the sintered titania doped samples are shown in table 4.7.5 (appendix 1), with the effect of sintering temperature on the hardness and fracture toughness of these specimens shown and compared to the undoped (blank treated) material in figures 4.7.5 (a) and 4.7.5 (b) respectively.

The results show a substantial increase in hardness with increasing sintering temperature over the range 1250-1450°C in the titanium doped samples, with a plateau value of hardness, similar to that in the undoped material (around 13 GN/m^2), occurring over the temperature range 1450 - 1650°C. For sintering temperatures in excess of 1650°C, the hardness appears to decrease.

The effect of titania addition on the hardness of samples sintered at various sintering temperatures is shown in figures 4.7.5 (c)-(d).

These results show that additions of TiO_2 above 0.25 mass % appear to produce a significant reduction in hardness for sintering temperatures up to 1350°C (see figure 4.7.5(c)), whilst for sintering temperatures between 1450 and 1650°C the dopant additions produce no obvious effect (figure 4.7.5(d)). For sintering temperatures in excess of 1650°, the hardness appears to decrease with dopant additions of more than 0.25 mass % TiO_2.

The effect of TiO_2 addition on the toughness is less clearly defined, and the differences in toughness observed between the different levels of TiO_2 addition generally lie within the range of possible experimental error. The results of the additions were therefore combined to produce a figure representing the average effect of TiO_2 additions (in the 0.25 to 1 mass % range) on the toughness of the sintered specimens. This is shown in figure 4.7.5(b) as a solid black line.

The toughness of the TiO_2 doped material generally shows the same trends as the undoped (blank treated) reference material over the range of sintering temperatures investigated. However there appears to be a small but consistent increase in toughness for the TiO_2 doped material over the range of sintering temperatures. The magnitude of the difference between the toughness of the TiO_2 doped and blank treated material lies within the estimated range of possible experimental error for 95% confidence. However the consistency of the trend would again appear to suggest that this does represent a real effect.

Figure 4.7.5(a)
Effect of sintering temperature on the hardness of titania doped samples.

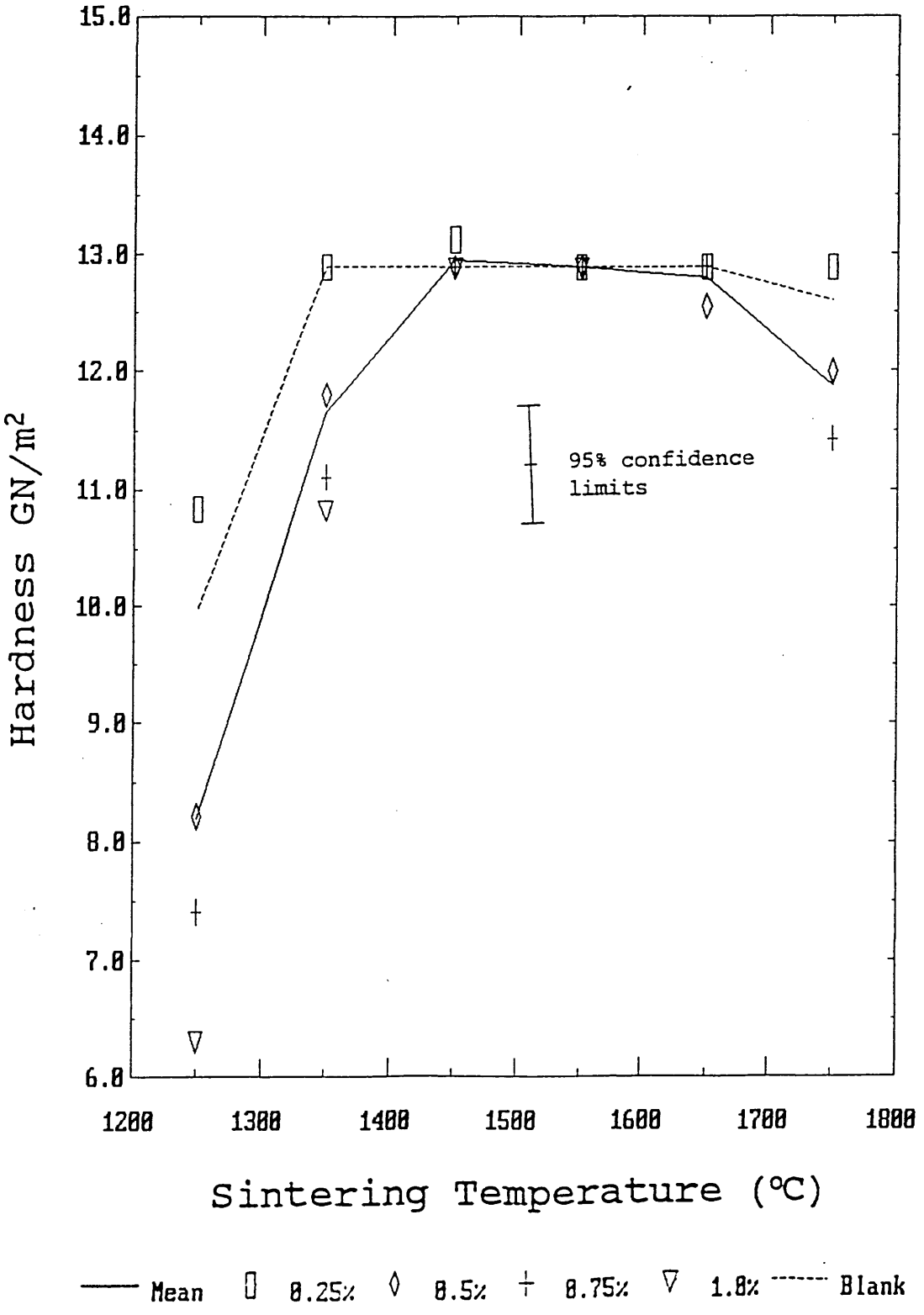

Figure 4.7.5 (b)
Effect of sintering temperature on the toughness of titania doped samples.

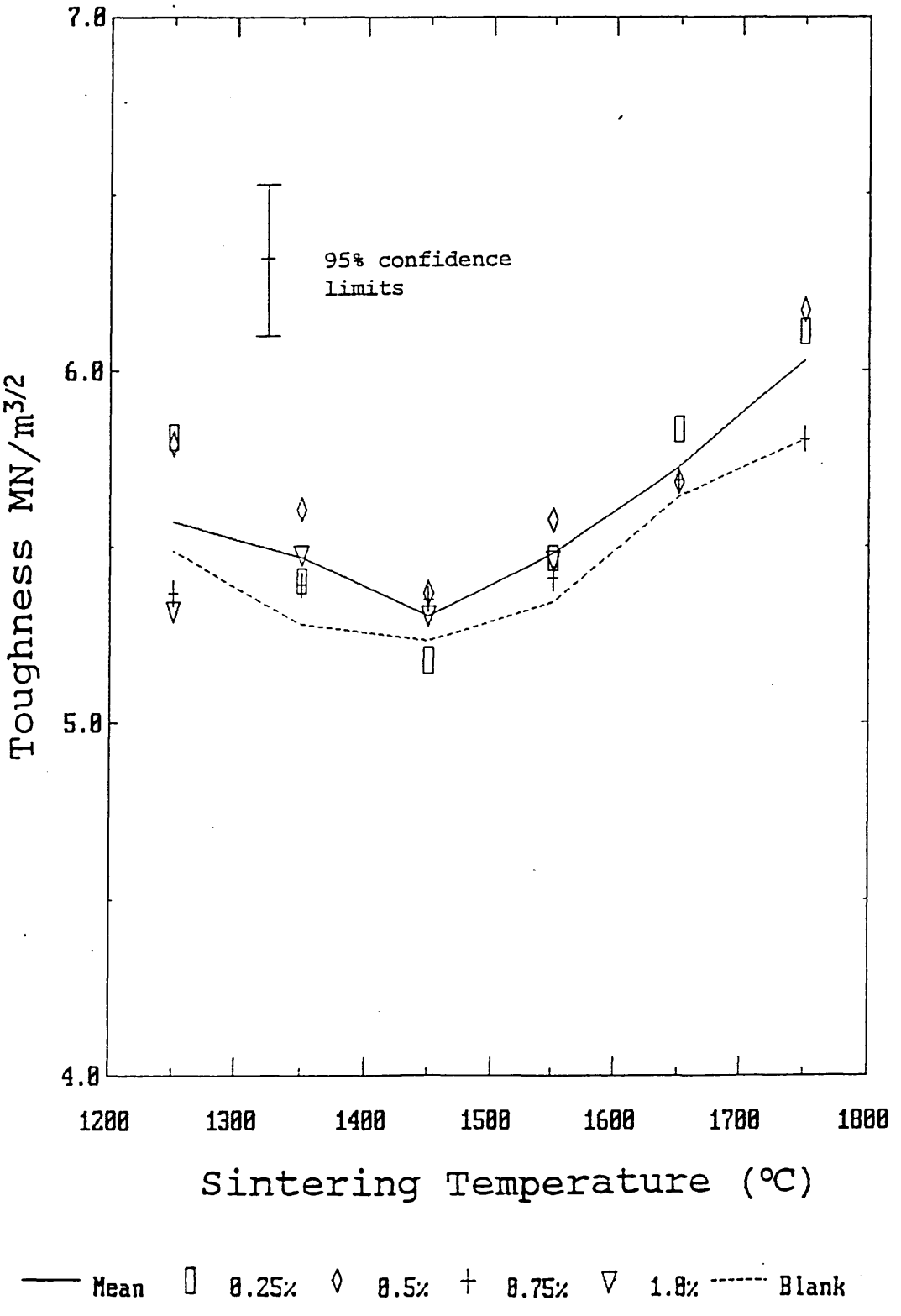

Figure 4.7.5 (c)
Effect of titania dopant addition on the hardness of sintered specimens.
1250-1350°C sintering temperature.

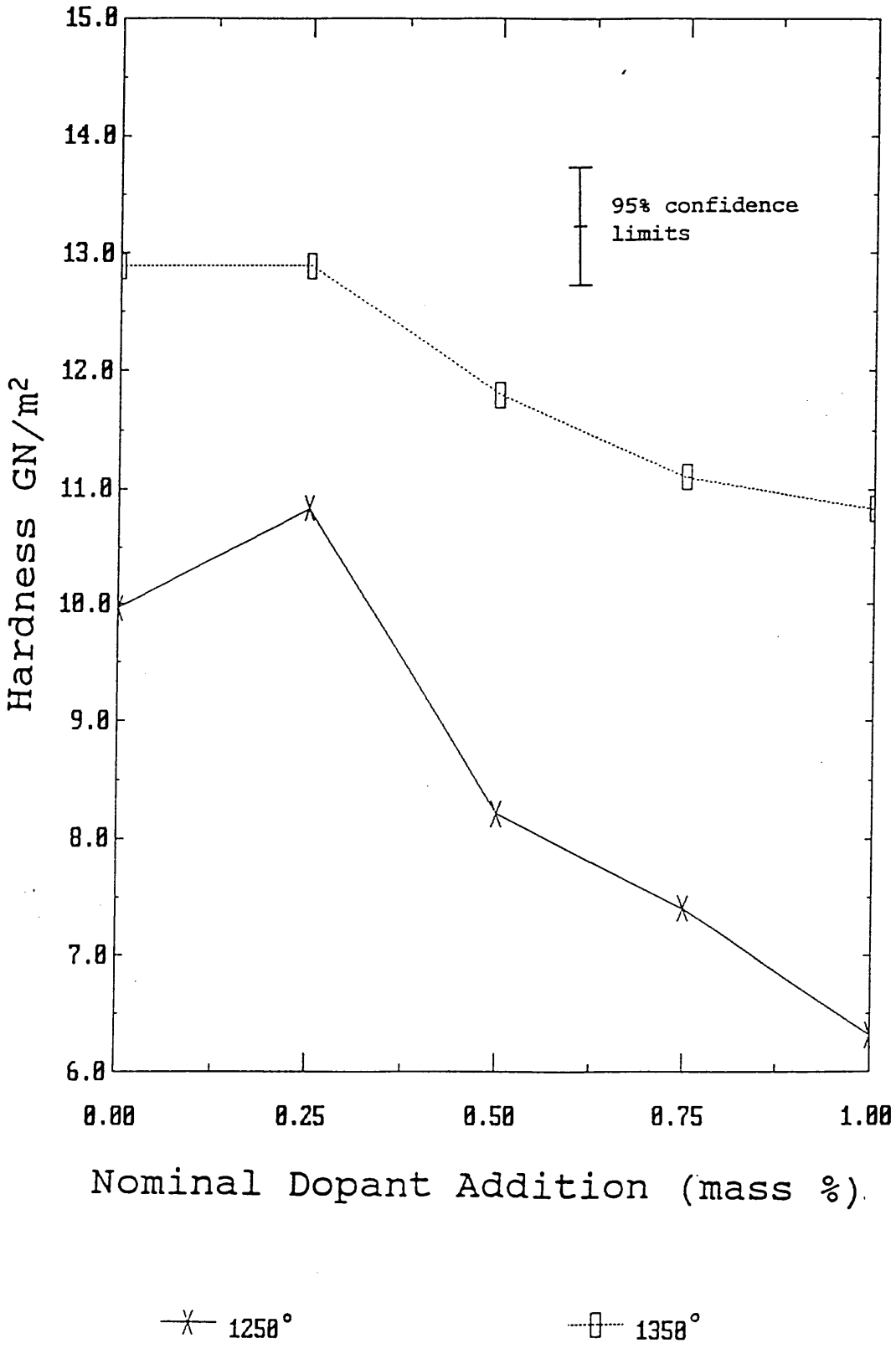

Figure 4.7.5 (d)

Effect of titania addition on the hardness of sintered specimens.

1450-1650°C sintering temperature.

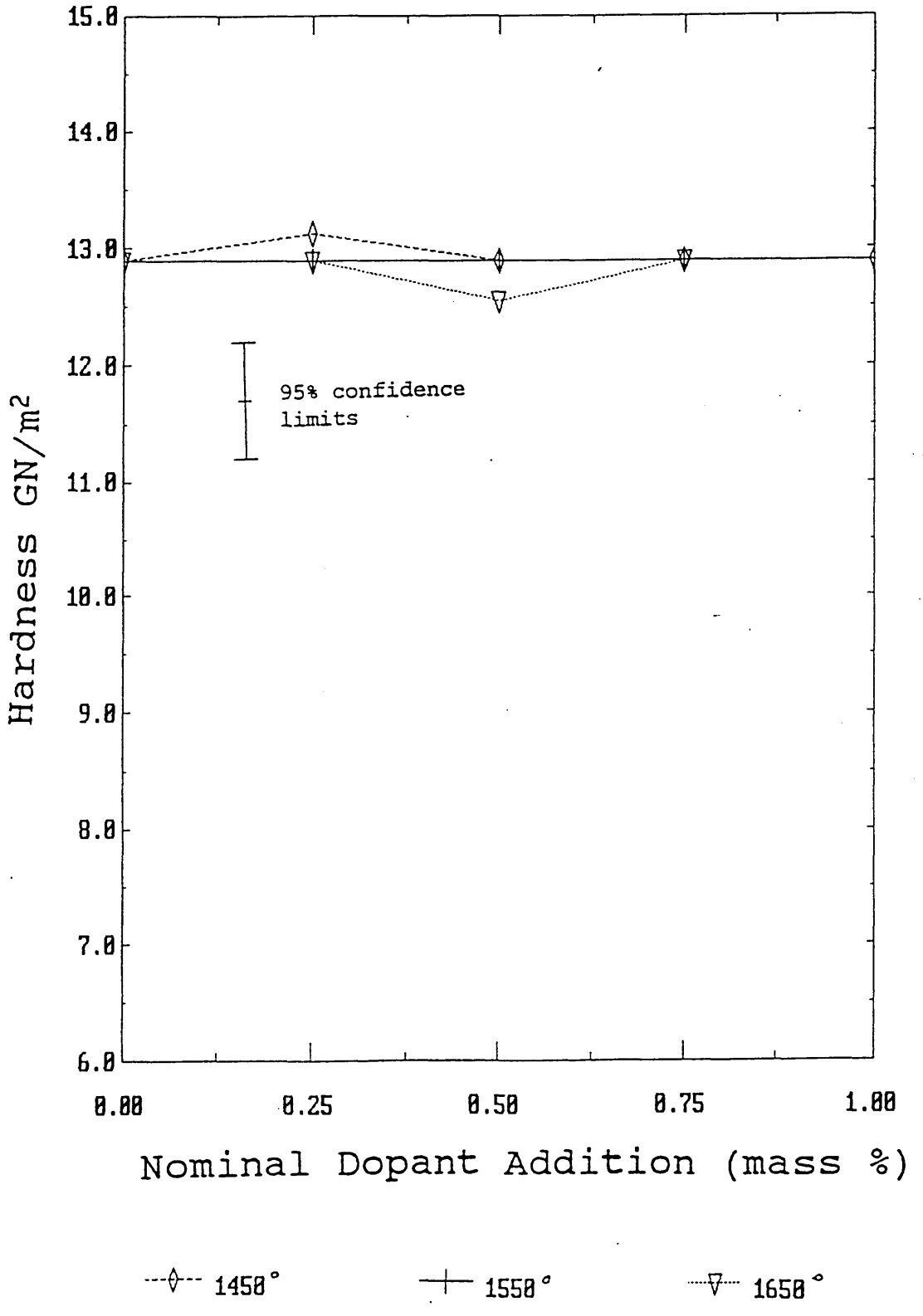

Figure 4.7.5 (e)
Effect of titania dopant addition on the hardness of sintered specimens
1750°C sintering temperature.

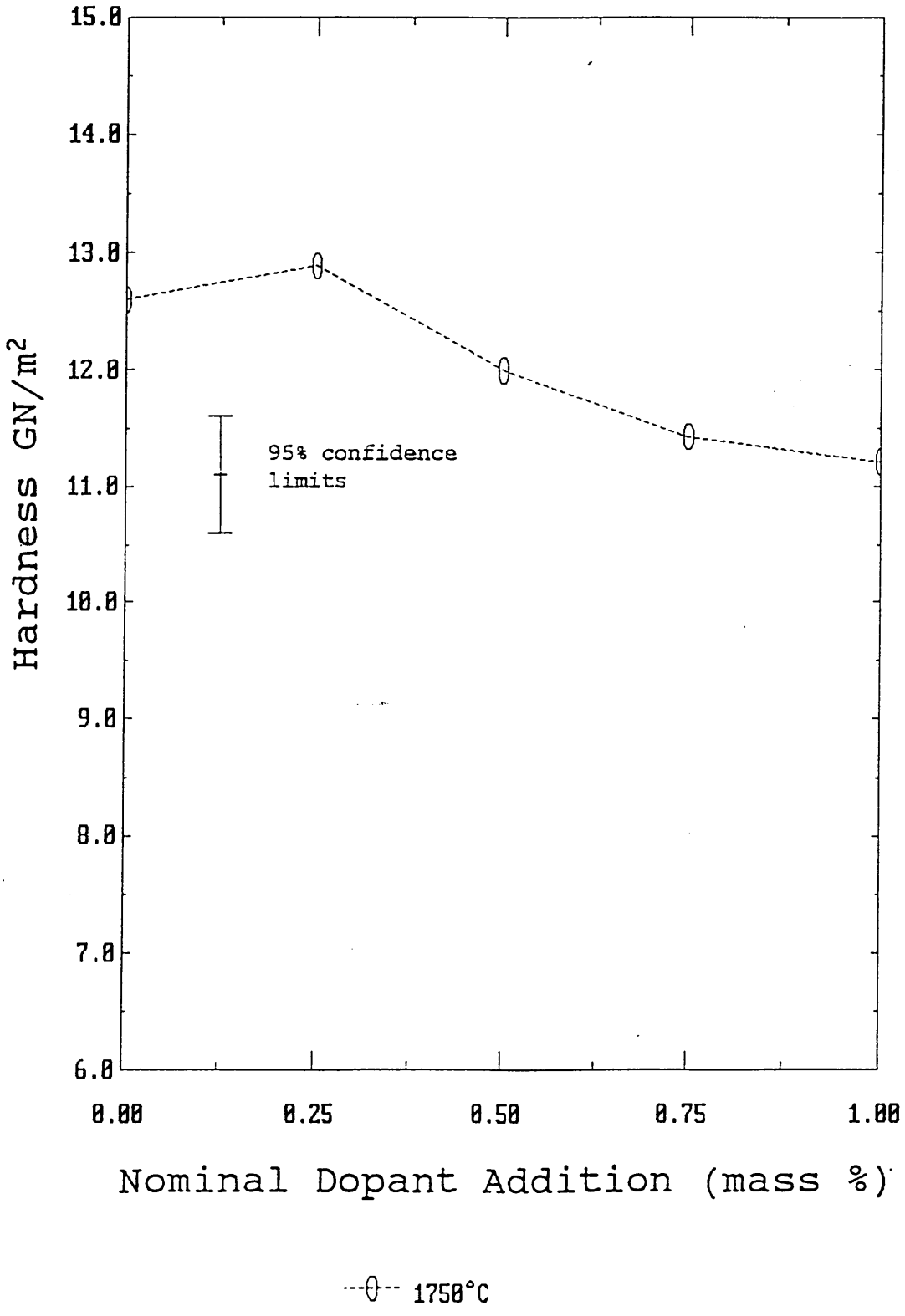

4.7.6 Multiple dopant additions.

The hardness and fracture toughness results for the sintered specimens with multiple dopant additions are shown in table 4.7.6 (appendix 1).

The effect of sintering temperature on the hardness and fracture toughness of these specimens is shown, and compared to the blank treated reference material in figures 4.7.6(a) and 4.7.6(b) respectively.

The hardness of the multiple doped specimens, and the effects of sintering temperature on these materials differs significantly in these materials.

In particular, the hardness at temperatures below 1350°C is significantly higher for all of the multiple doped specimens compared to the undoped blank.

The hardness of the multiple doped specimens generally appears to decrease dramatically with increasing sintering temperature above 1350°C, although the effect is much less marked for the 1% SiO_2 with 1% TiO_2 doped material.

The effect of sintering temperature on the toughness of the multiple doped specimens also differs significantly from the behaviour of the undoped and singly doped materials, with the exception of the 1% SiO_2 with 1% TiO_2 doped compositions which appears to exhibit similar behaviour to the blank treated reference material for sintering temperatures of 1450°C or above.

The most significant effect appears to be a large apparent increase in toughness with increasing sintering temperature up to 1650°C, with a rapid reduction in fracture toughness for sintering temperatures in excess of this.

All of the multiple doped specimens appeared to exhibit a small reduction in toughness compared to to blank treated reference for sintering temperatures below 1350°C

Figure 4.7.6(a)
Effect of sintering temperature on the hardness of multiple doped specimens.

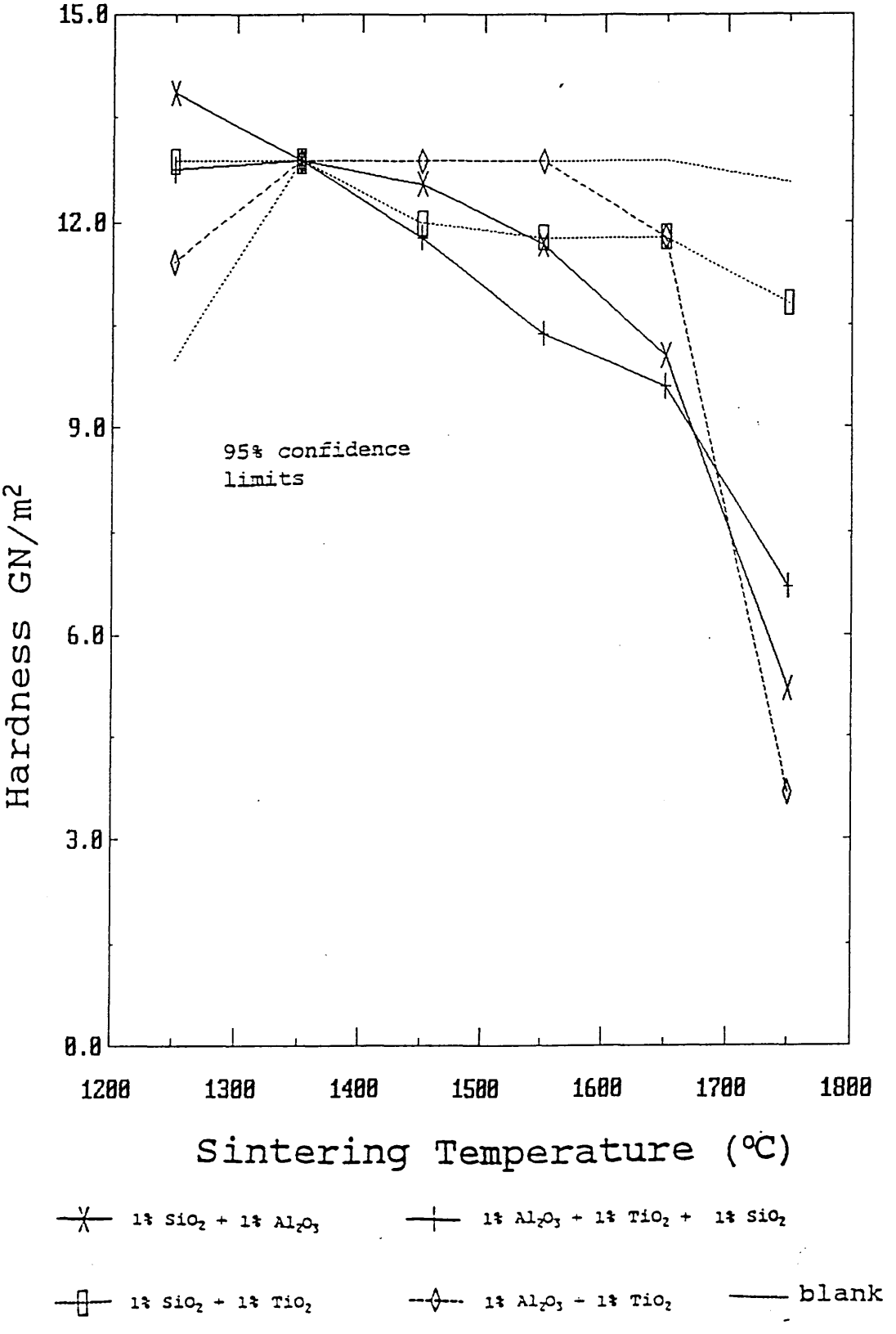

Figure 4.7.6(b)

Effect of sintering temperature on the toughness of multiple doped specimens.

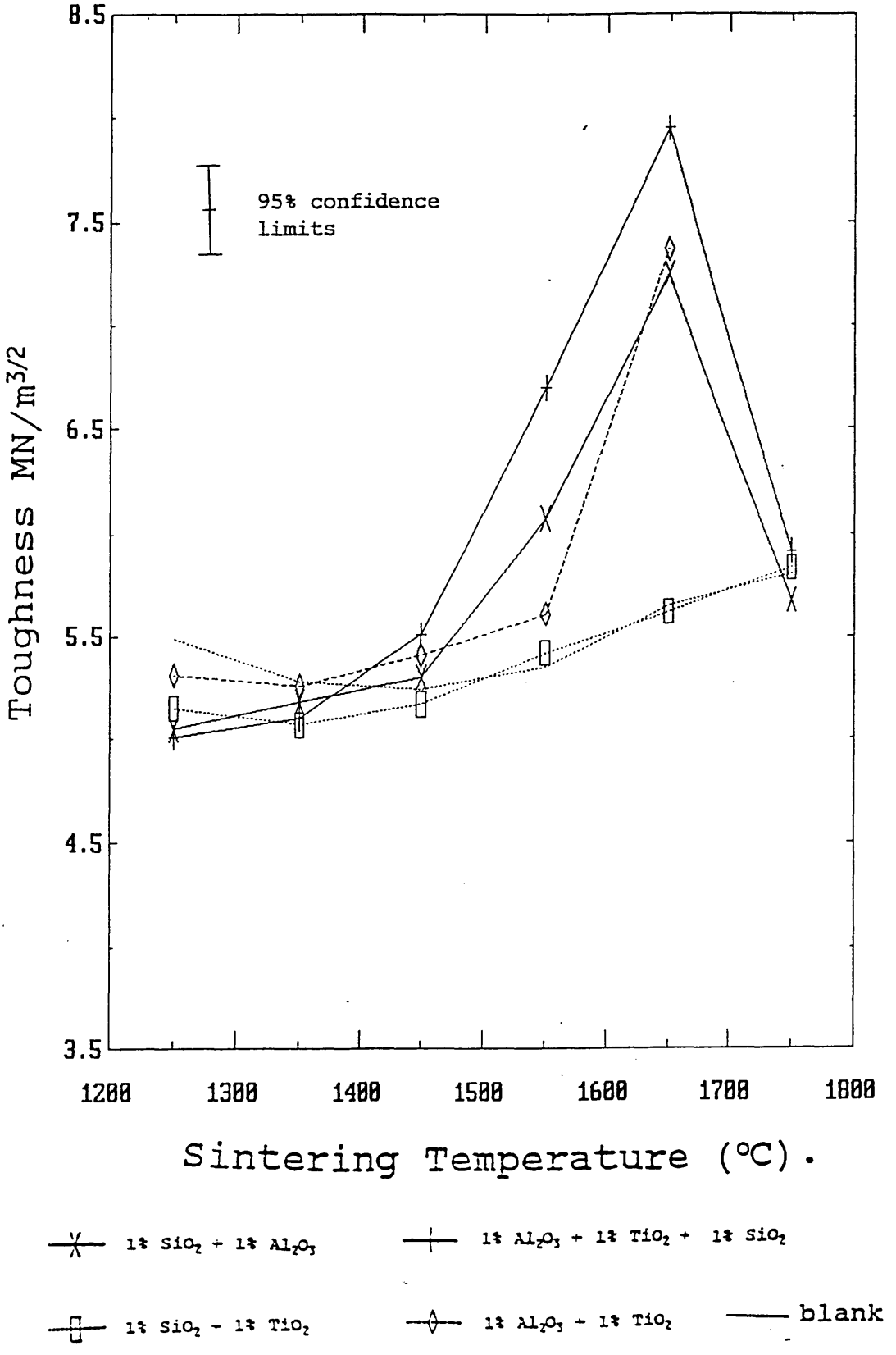

4.7.7 Factorial experiment.

The results of the factorial experiment(s) to investigate the effect of sintering temperature and impurity content (together with their interactions) on the mechanical properties of the sintered specimens are shown in the following sections.

As for the one factor at a time experiments, both hardness and fracture toughness results are reported.

The results for each study comprise three separate factorial experiments to cover the sintering temperature ranges 1250°C - 1450°C, 1450°C - 1550°C, and 1550°C - 1650°C. Due to difficulties in obtaining meaningful results in some of the 1750°C sintered samples, the factorial experiment could not be extended to include samples produced at this sintering temperature.

The results are presented in the same form as the factorial experiments for density and phase developments, with the calculated factorial effects from the data (by Yates' method) and the corresponding analyses of variance shown.

Both internal and external estimates of error are included in the variance analysis and significance tests as described for the density factorial experiments.

4.7.7.1 Factorial experiments for hardness.

The analysis of data for the calculated factorial effects of sintering temperature and impurity content on the hardness of the sintered specimens is shown in tables 4.7.7.1(a)-(c), with the corresponding analyses of variance and estimates of significance in tables 4.7.7.1(d)-(f) (see appendix 1).

The factorial effects are also shown schematically in figures 4.7.7.1(a) for the main effects, 4.7.7.1(b) for the impurity interactions, and figures 4.7.7.1(c) and (d) for the impurity-temperature interactions.

The calculated factorial effects for the main effects should be interpreted with caution due to the presence of significant two and three factor interactions which may obscure the true single factor effects. However the results do appear to correspond with the one factor at a time experiments.

There appears to be a significant positive effect (ie increase in hardness) associated with alumina addition and silica addition over the 1250° - 1450° C temperature interval, and a significant positive effect associated with an increase in sintering temperature over this range, whilst TiO_2 addition appears to produce a negative effect over this temperature interval.

The main effects of alumina (A) and temperature (D) over the 1450°C -1550°C temperature interval are less significant {f(5%) level}, but may show a small decrease in hardness, whilst their appears to be a more significant negative effect {f(1%) level} associated with SiO_2 and TiO_2 addition over this temperature interval.

The main effects of SiO_2 and Al_2O_3, addition and increase in sintering temperature all appear to be significantly large and negative over the 1550°-1650°C temperature interval.

The calculated impurity-temperature interaction factorial effects appear to show significant interaction in the hardness results when Al_2O_3 and SiO_2 (AB) are present over the full range of sintering temperatures, and When SiO_2 and TiO_2 (BC) are present over the 1450-1550 and 1550-1650°C temperature intervals.

The calculated impurity-temperature factorial effects for alumina (AD) and silica (BD) show large and highly significant interactions over the 1250-1450°C temperature interval, with large three factor interactions occurring for the multiple doped Al_2O_3 and SiO_2 (ABD) system over this temperature interval.

Figure 4.7.7.1(a)

Factorial experiments (Hardness)

Schematic representation of factorial effects

Main (single factor) effects.

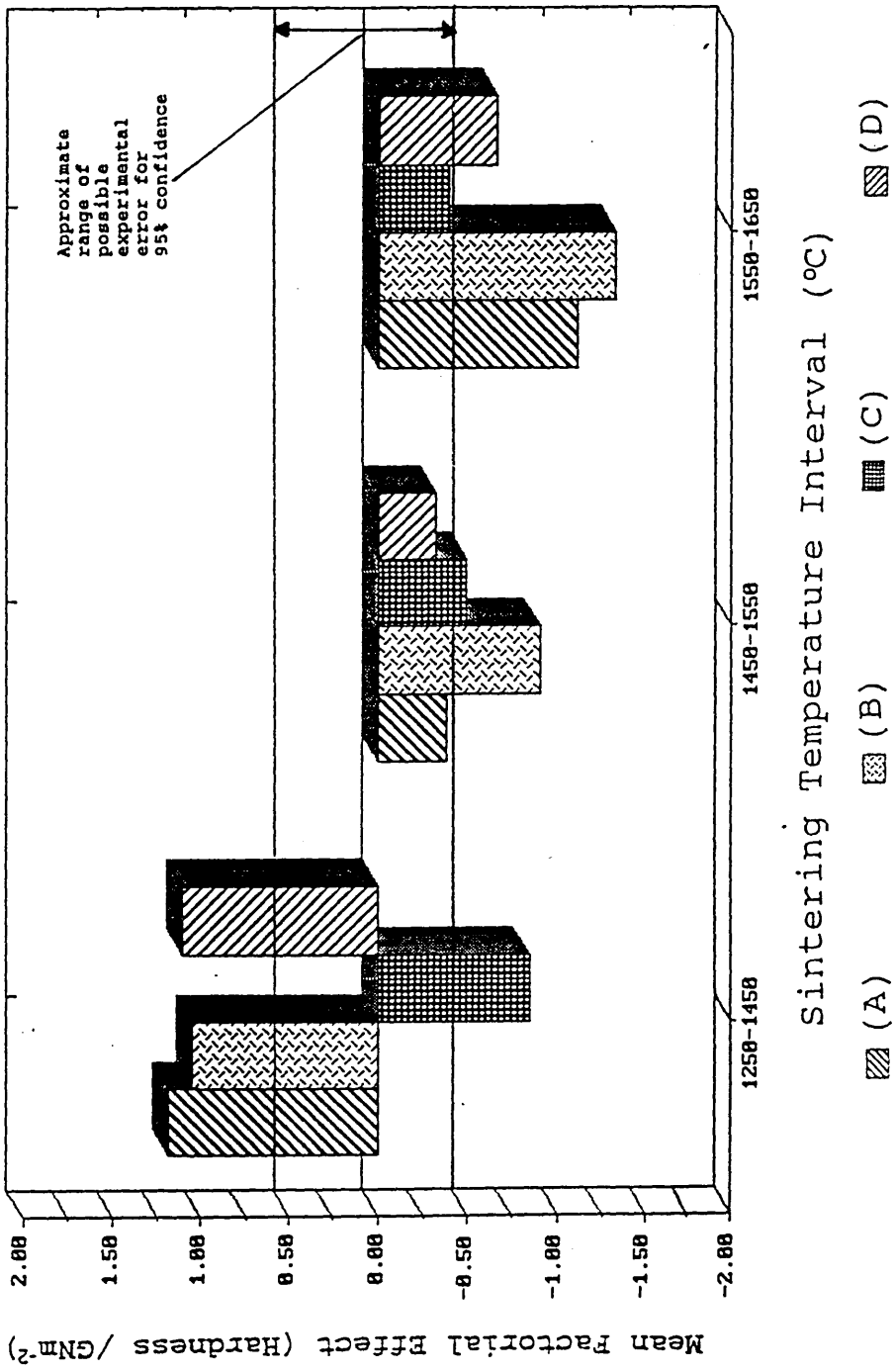

Key to Notation.
e.g.
A = 1 mass % Al_2O_3 addition.
B = 1 mass % SiO_2 addition.
C = 1 mass % TiO_2 addition.
D = Higher value of sintering temperature (in range) used.
ABCD = Interaction between factors A,B,C and D.

Figure 4.7.7.1(b)
Factorial experiments (Hardness)
Schematic representation of factorial effects
Impurity interaction effects.

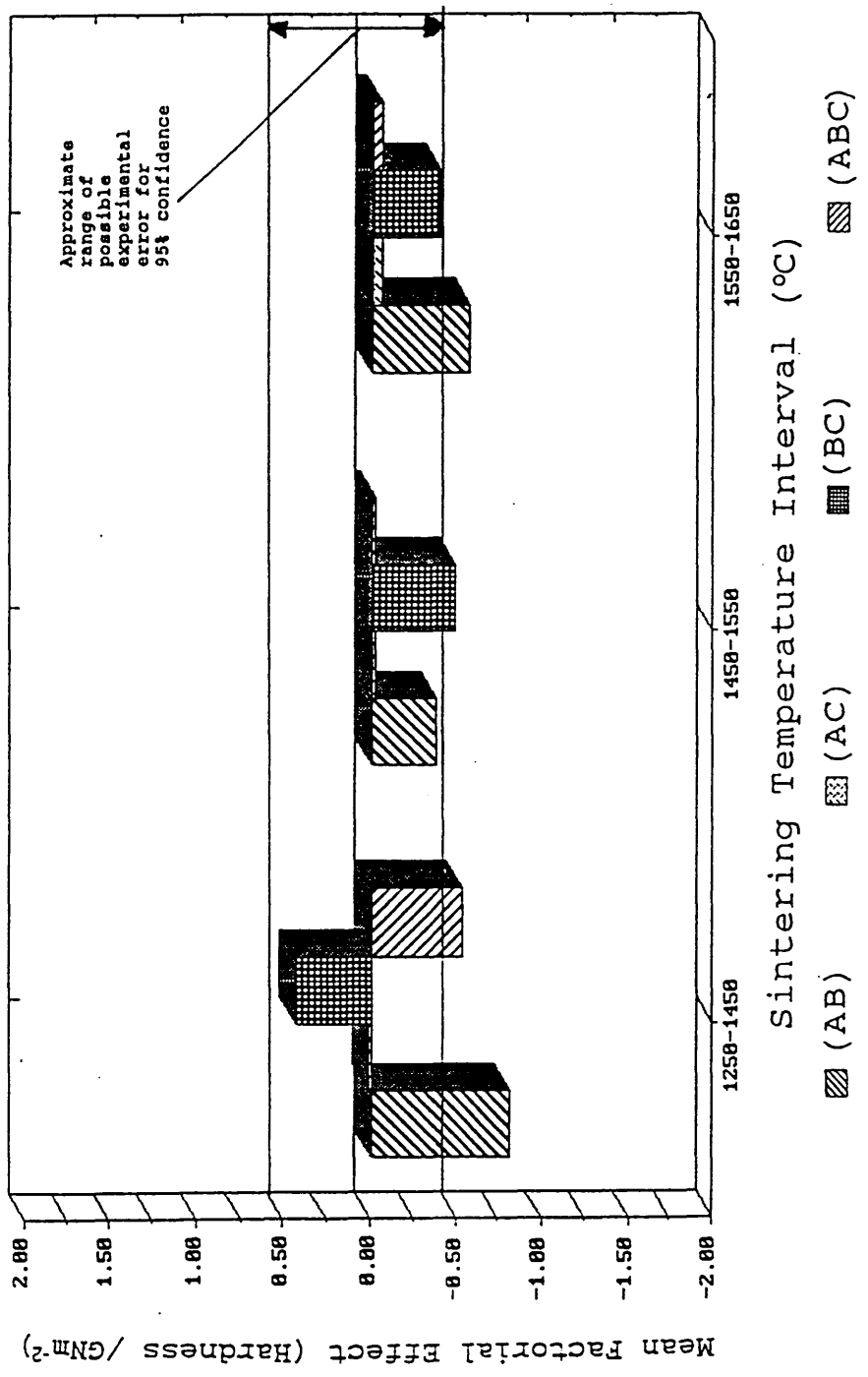

Key to Notation.
e.g.
A = 1 mass % Al_2O_3 addition.
B = 1 mass % SiO_2 addition.
C = 1 mass % TiO_2 addition.
D = Higher value of sintering temperature (in range) used.
ABCD = Interaction between factors A,B,C and D.

Figure 4.7.7.1(c)

Factorial experiments (Hardness)

Schematic representation of factorial effects

Impurity - temperature interaction effects (two factor).

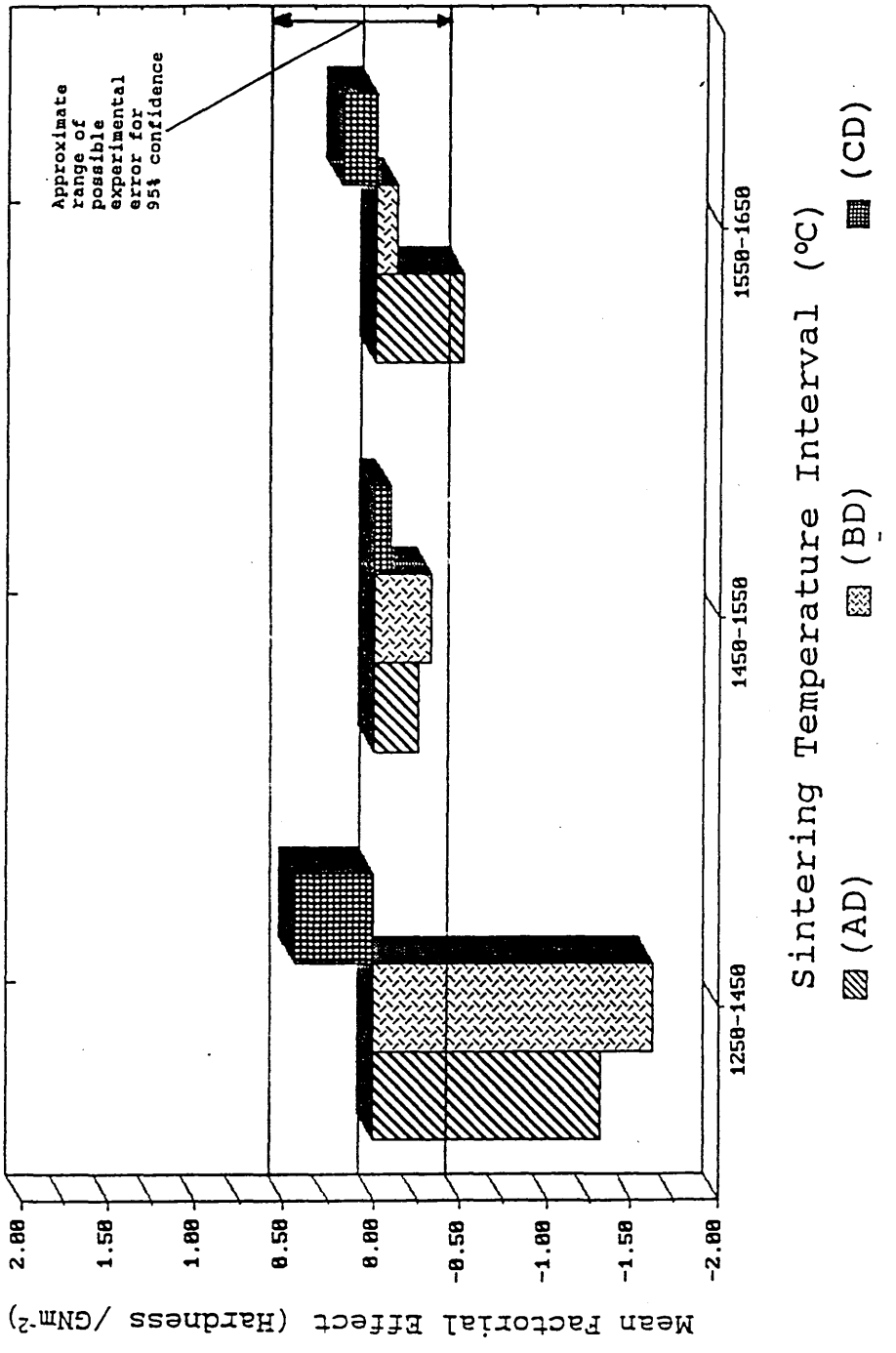

Key to Notation.
e.g.
A = 1 mass % Al_2O_3 addition.
B = 1 mass % SiO_2 addition.
C = 1 mass % TiO_2 addition.
D = Higher value of sintering temperature (in range) used.
ABCD = Interaction between factors A,B,C and D.

Figure 4.7.7.1(d)

Factorial experiments (Hardness)

Schematic representation of factorial effects

Impurity - temperature interaction effects (3 & 4 factor).

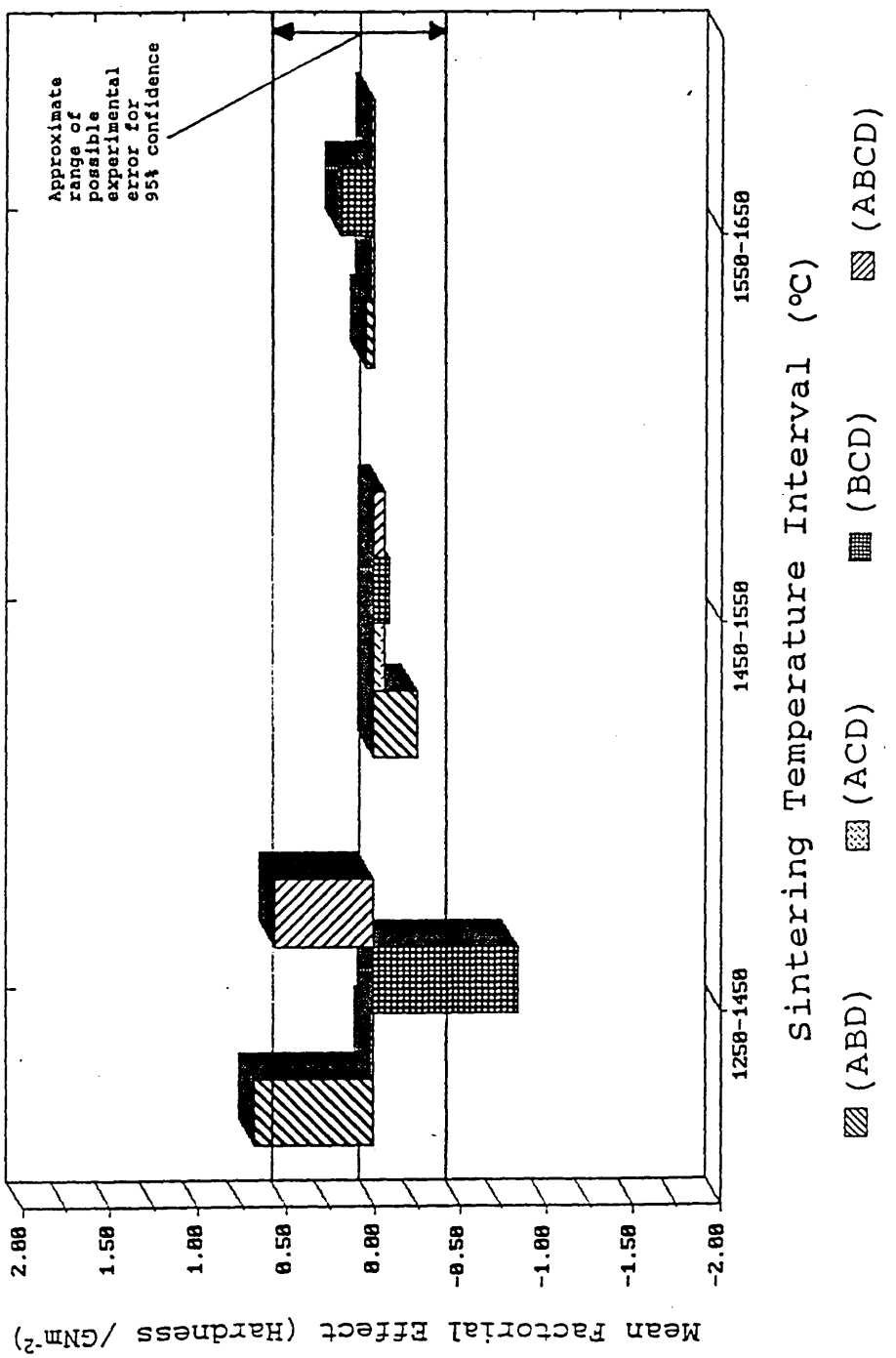

Key to Notation.
e.g.
A = 1 mass % Al_2O_3 addition.
B = 1 mass % SiO_2 addition.
C = 1 mass % TiO_2 addition.
D = Higher value of sintering temperature (in range) used.
ABCD = Interaction between factors A,B,C and D.

4.7.7.2 Factorial experiments for toughness.

The calculated factorial effects of sintering temperature and impurity content on the fracture toughness of the sintered specimens are shown in tables 4.7.7.2(a)-(c), with the corresponding analyses of variance, and estimates of significance in tables 4.7.7.2 (d)-(f) (see appendix 1).

The calculated factorial effects for the single factors (main effects),, the impurity interactions and the two, and three factor impurity-temperature interactions are shown schematically in figures 4.7.7.2 (a)-(f) respectively.

As for the hardness results, the interpretation of the single factor calculated factorial effects requires considerable caution due to the presence of significant multi factor interactions in these experiments. However, the effects do generally correspond with the one factor at a time experiments.

The results appear to show that there is a significant positive factorial effect (toughness increase) associated with the Al_2O_3 addition and TiO_2 addition for the 1450-1550 and 1550-1650°C temperature intervals.

There also appears to be a smaller negative effect (significant at f(5%) level) associated with SiO_2 addition in the 1250-1450°C temperature interval, and a larger positive effect associated with SiO_2 addition over the 1550-1650°C temperature interval.

There appear to be significant positive effects associated with an increase in sintering temperature over the 1450-1550°C and 1550°-1650°C temperature intervals.

The calculated values for the AB (Al_2O_3 + SiO_2) interaction term suggests that there is a significant positive interaction effect on the toughness over the 1450-1550°C and 1550-1650° temperature intervals, with significant positive interactions also observed for the Al_2O_3 with TiO_2 system over the 1550-1650°C temperature

interval. The results also appear to show a possible slight (positive) interaction effect between SiO_2 and TiO_2 (BC) over the 1450-1550°C temperature interval (significant at f(5%) level).

The calculated temperature-impurity interaction terms for alumina addition (AD) show a significant and increasingly positive interaction effect over the 1450-1550° and 1550-1650°C temperature intervals. A similar positive interaction with temperature also appears to occur for alumina and silica addition (ABD) over the 1450-1550°C sintering temperature interval.

The SiO_2-TiO_2 (BCD) impurity-temperature interaction term shows a significant negative interaction effect over the 1550-1650°C sintering temperature interval.

The other interaction effects are less clearly defined, their magnitudes being very similar to the experimental error in the analysis, with no clear trends identifiable.

Figure 4.7.7.2 (a)

Factorial experiments (toughness)

Schematic representation of factorial effects

Main (single factor) effects.

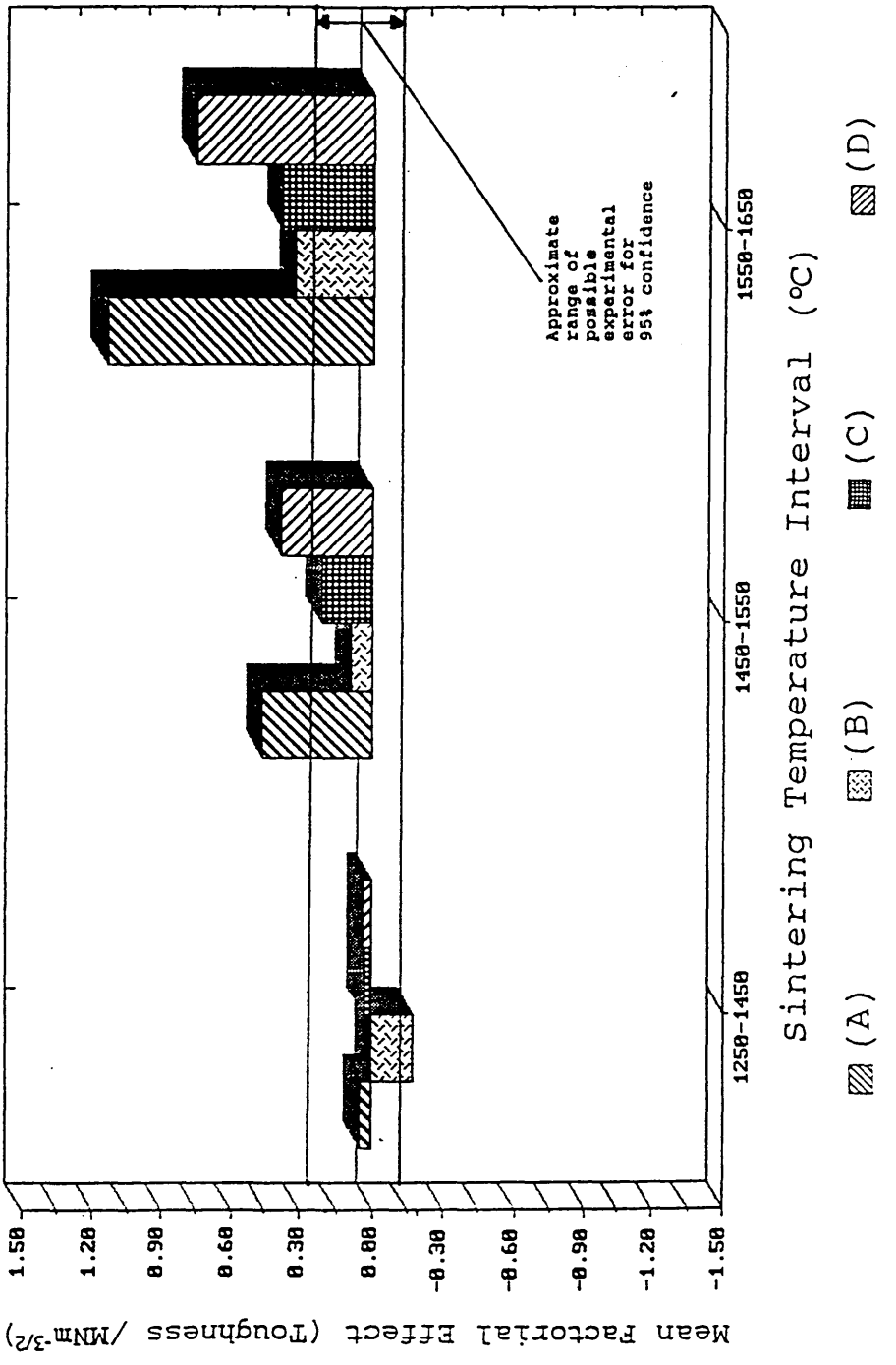

Key to Notation.
e.g.
A = 1 mass % Al_2O_3 addition.
B = 1 mass % SiO_2 addition.
C = 1 mass % TiO_2 addition.
D = Higher value of sintering temperature (in range) used.
ABCD = Interaction between factors A,B,C and D.

Figure 4.7.7.2 (b)

Factorial experiments (toughness)

Schematic representation of factorial effects

Impurity interaction effects.

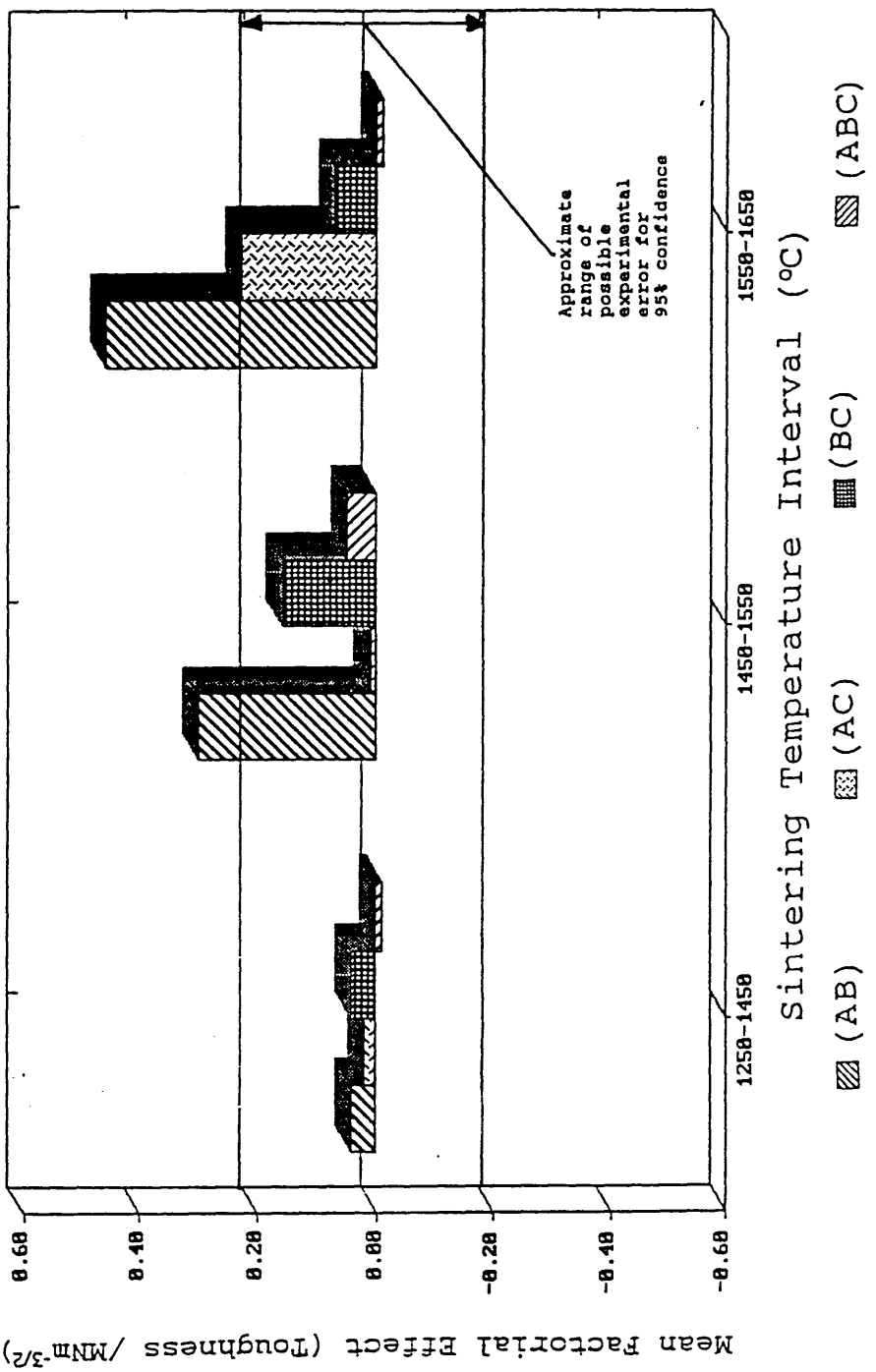

Key to Notation.
e.g.
A = 1 mass % Al_2O_3 addition.
B = 1 mass % SiO_2 addition.
C = 1 mass % TiO_2 addition.
D = Higher value of sintering temperature (in range) used.
ABCD = Interaction between factors A,B,C and D.

Figure 4.7.7.2 (c)

Factorial experiments (toughness)

Schematic representation of factorial effects

Impurity - temperature interaction effects (two factor).

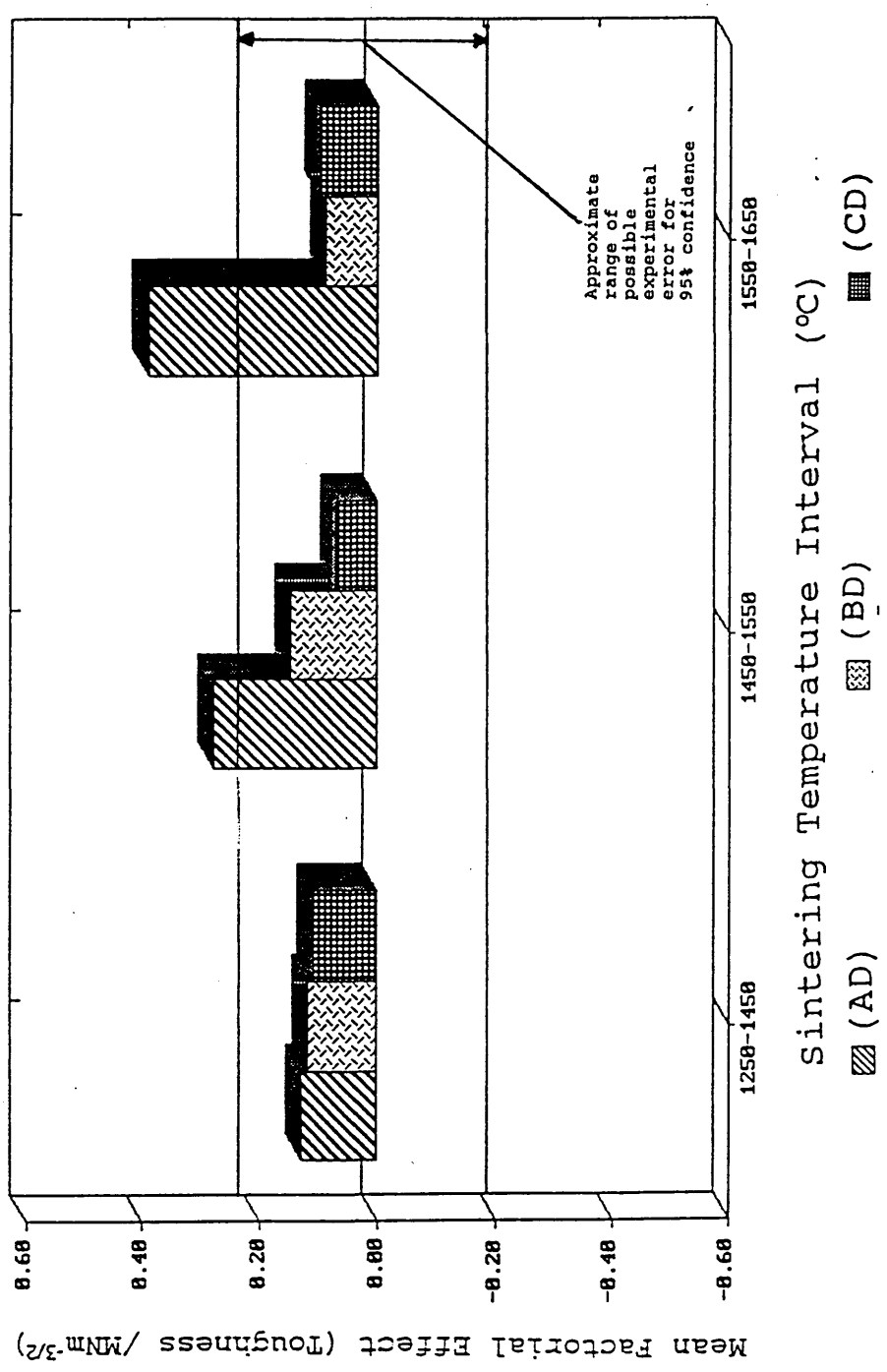

Key to Notation.
e.g.
A = 1 mass % Al_2O_3 addition.
B = 1 mass % SiO_2 addition.
C = 1 mass % TiO_2 addition.
D = Higher value of sintering temperature (in range) used.
ABCD = Interaction between factors A,B,C and D.

Figure 4.7.7.2(d)

Factorial experiments (toughness)

Schematic representation of factorial effects

Impurity - temperature interaction effects (3 & 4 factor).

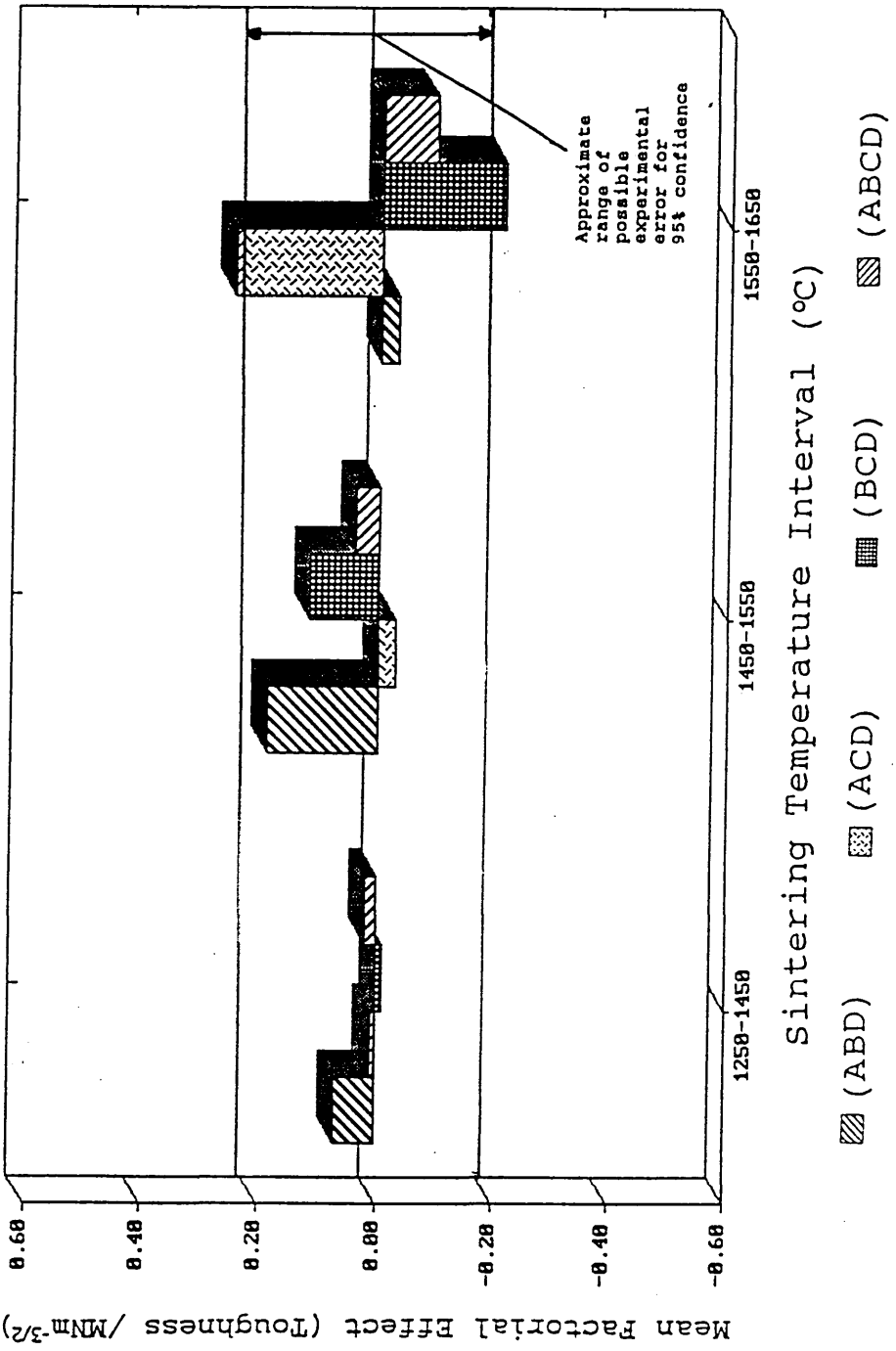

Key to Notation.
e.g.
A = 1 mass % Al_2O_3 addition.
B = 1 mass % SiO_2 addition.
C = 1 mass % TiO_2 addition.
D = Higher value of sintering temperature (in range) used.
ABCD = Interaction between factors A,B,C and D.

5. Discussion.

In this section of the report, an attempt will be made to explain the underlying principles of the processes developed, and phenomena observed during the work.

Separate attention is given to the following:

(i) The development and effectiveness of the alkoxide doping process (section 5.1 and subsections)

(ii) The effects of the impurities on the properties and behaviour of doped Y-T.Z.P. (sections 5.2-5.4 & subsections).

(iii) The efficacy of the experimental design and the factorial experimental method (section 5.5).

5.1 The alkoxide doping process.

The alkoxide doping process developed for introducing the oxide impurities into the powder was a novel technique, based upon the technology of sol-gel coating, with the objective being to produce a thin, even coating of dopant oxide on the surface of the primary zirconia particles which would undergo further homogenisation during sintering heat treatment.

This section of the report will consider the effectiveness of the technique, and will attempt to explain the main phenomena observed during its development.

5.1.1 Effect of alkoxide doping process on the powder characteristics.

Key findings:
Alkoxide doping process produced:

(i) Change in size and morphology of powder agglomerates, and powder flow properties.

(ii) Increase in agglomerate strength.

The physical characteristics of the powders after undergoing the doping process were generally similar for

all the dopant types and additions (including the blank treatment process). The resultant powders were generally less free flowing than the as supplied TZ3Y, which would be consistent with the observed change in particle morphology from spherical to irregular.

The change in particle size distribution and morphology suggested by the change in physical characteristics of the doped powders was confirmed by the results of the Sedigraph particle size distributions.

The increase in agglomerate strength of the doped powders compared to the blank treated samples, which had undergone the same process, was presumably due to the layer of dopant oxide on the particle surfaces bonding the particles in the former case. This may have been significant, since the difference between the behaviour of the blank treated and as supplied powders may in fact have underestimated the true difference between the doped and as supplied materials. However it was not possible to distinguish between those effects arising from changes in physical characteristics of the doped powders, and those arising from chemical effects due to the effect of the dopant oxide.

5.1.2 The yield of the doping process and the effect of process conditions.

Key findings:

(i) Yield of doping process low for SiO_2 additions unless water addition levels, evaporation rate, and catalyst addition controlled.

(ii) Small discrepancy between calculated dopant addition and chemical analysis results for alumina doped powders.

The primary objectives of the development of the doping process were to produce powders with even, controlled and reproducible levels of dopant additive, whilst minimising other changes to the sintering characteristics of the material.

The conditions used during the doping reaction were

found to have a very significant bearing upon the control of the doping process. In particular, it was found that the yield of reaction, and the nature of the doped powders, were strongly dependent upon the catalyst system used, water content and evaporation conditions, particularly for the tetraethyl silicate (SiO_2 precursor) alkoxide addition.

The yield of reaction was found to be low where basic catalysis was used, and/or excess water was present in the system, and/or evaporation of the ethanol was carried out too quickly.

These observations suggest that a large proportion of the alkoxide species could be lost by evaporation, presumably as an azeotropic mixture, together with the ethanol, leading to low and non reproducible yields of reaction.

Evidence for this was offered by the fact that the yield could be increased by reducing the overall evaporation rate, either by covering the reaction vessel, or by carrying out the initial stages of the reaction in a reaction vessel equipped with a condenser apparatus.

Relating the results obtained with theory (see sections 2.8.2,2.8.3), it appears that for the silicon alkoxide system, the optimum values of yield were obtained under conditions which should favour the formation of a network polymer structure. It would appear that alkoxide molecules which were either unhydrolysed, or reacted species of low molecular weight (i.e. in the early stages of the polycondensation reaction) were more susceptible to loss by volatalisation than more highly reacted species of greater molecular weight. This was also thought to explain the improved yield of reaction obtained by partially pre-reacting the alkoxide (in a suitable condenser equipped reaction vessel) prior to evaporation of the ethanol.

Similarly, it is probable that the long chain polymers

produced under conditions of acid catalysis or low water contents were less susceptible to volatalisation than the smaller molecular species produced under other conditions.

Although such a phenomena has not previously been reported in the literature, it is thought that it may have arisen due to the low concentration of alkoxide used, which may have affected the kinetics of the polycondensation reaction, particularly in its early stages.

The flow properties and agglomeration behaviour of the doped powders were both found to be impaired under conditions which favoured high yields of reaction. This can be explained in terms of the reaction characteristics under these conditions. It would appear that the long chain polymers (which give high yields of reaction) tend to bond the particles together, producing agglomeration and aggregation in the doped powders produced under these conditions.

The optimisation of the yield of the reaction was found to be important, since those systems which gave very low yields of reaction were also found to give very poor reproducibility, presumably due to variations in the evaporation rate from changes in atmospheric conditions.

The results of the X.R.F. chemical analysis carried out on the doped powders shows that there was a linear relationship between the nominal dopant addition level, calculated from the amount of alkoxide added, and the composition of the doped powders. In the case of the silica and titania doped powders, the calculated and measured addition levels gave virtually identical values. In the case of the alumina doped specimens there was a small but consistent discrepancy between the two values where the measured alumina content of the doped powders was 0.86 times the nominal dopant addition level.

This discrepancy can be explained either as arising from an error in calculating the yield of reaction from the

preliminary experiments, or from a calibration error in the X.R.F. analysis programme. The former seems the most probable, and would have resulted in too little alkoxide precursor being added during the doping process to give the required alumina content.

5.2 Sintering and microstructural development of doped and undoped T.Z.P.

The key aspects of interest to the commercial collaborators for this research regarding the sintering behaviour of the material were: Did the impurities adversely or beneficially affect the densification and fired density of the material?, if so to what degree?, what effect did changes in sintering conditions produce on the behaviour of Y-T.Z.P. with different amounts and combinations of these impurities?, and how did all of these factors affect the microstructure (and thus properties) of the sintered products?

The experiments carried out were therefore designed to produce this information through shrinkage and density determinations on sintered specimens of various composition produced at various sintering temperatures.

However, the nature of the experiments performed does not allow the mechanisms responsible for the various effects to be unequivocally determined, and the interpretation of the sintering behaviour is therefore somewhat speculative. Further experiments, involving shrinkage determinations obtained in the early stages of sintering under isothermal conditions[91], would be required to fully determine the sintering mechanisms.

Determinations of microstructure and grain size were also carried out. This information was also useful in the interpretation of the X-ray diffraction and mechanical property results.

5.2.1 Sintering and microstructural development of undoped T.Z.P.

Key Results:

(i) As received and blank treated specimens showed indistinguishable density and shrinkage behaviour.

(ii) Seescan microstructural analysis showed increased numbers of defects in "blank treated" specimens.

The similar behaviour observed for the shrinkage and density measurements for the as received, and blank treated material suggests that the doping process resulted in little change to the bulk sintering behaviour of the powder. However there appears to be some discrepancy between these results, and the "Seescan" microstructural analysis results which showed clear differences between these two materials, with the blank treated powder containing consistently increased numbers and measured area of sintering defects (eg voids, pores etc.)

It is suggested that the discrepancy arises from the increased sensitivity of the microstructural analysis to the presence of relatively small numbers of sintering defects when compared to the bulk measurements.

The most probable source of the increased numbers of defects in the blank treated powder is the presence of small agglomerates, arising from the (blank) doping and powder preparation processes, which may disrupt the packing in the green state and produce inhomogenous sintering behaviour (see section 2.5.5[116][117][118]).

Presumably, a small proportion of small, but strongly bonded agglomerates passed through the final mesh during the grinding and sieving operation.

The close correlation between the bulk behaviour of the undoped (blank treated) and as supplied material shown in the shrinkage, density, phase composition and mechanical property (hardness and toughness) determinations suggests

that the number of these agglomerates was relatively small. It is probable however that they would have resulted in a significant reduction in strength by acting as Griffith flaws or sites for crack propagation.

5.2.2 Densification and microstructural development of alumina doped T.Z.P.

Key Results:

(i) Al_2O_3 additions increased sintering activity at low sintering temperatures (1050°C to 1350°C).

(ii) Al_2O_3 additions produced a reduction in density in samples sintered at high sintering temperatures (above 1550°C), and an increase in the number of microstructural defects.

(iii) Al_2O_3 additions produced substantial increase in grain size at high sintering temperatures (above 1550°C).

The shrinkage and density determinations and microstructural examination by optical microscopy of the polished specimens showed similar results for the alumina doped samples. This is of some significance, since it offers confirmatory evidence for trends which are in some cases quite small in magnitude relative to the possible experimental error in the system.

(i) low sintering temperature effects.

Alumina additions by the alkoxide doping process produced a substantial increase in density in the early stages of sintering, particularly for specimens sintered at temperatures in the range 1050-1250°C, with the largest effects occurring for a sintering temperature of 1150°C. The final sintered density for this sintering temperature was of the order of 85-90% of the theoretical density. The sintering activity also appeared to increase with increasing alumina content over this range of temperature.

The sintering behaviour of the mechanically mixed,

alumina doped specimens did not appear to exhibit any significant increase in densification at these sintering temperatures, presumably due to the poor homogeneity in these specimens.

The grain size determinations carried out on the sintered, alumina doped specimens did not identify any significant difference between the grain growth behaviour of the alumina doped and blank treated specimens for sintering temperatures up to and including 1550°C suggesting that reduced grain growth rates were not responsible for the enhanced sintering behaviour.

The results for the alkoxide doped specimens were generally in agreement with the findings of Lu and Chen[159] for the densification behaviour of TZ3Y with alumina additions, however the alumina distribution in this study was expected to be significantly better than that achieved in their work. Experiments were also carried out over a wider range of sintering temperatures in this study, in particular much lower sintering temperatures were investigated, which lead to some questions over the interpretation given by Lu and Chen[159] to explain their findings.

The enhanced densification observed by these workers in alumina doped specimens at sintering temperatures in excess of 1250°C was interpreted as being due to the occurrence of a liquid phase sintering mechanism. This was confirmed in their work by a difference in the calculated activation energy for the sintering process in undoped and alumina doped Y-T.Z.P. at 1350°C.

The results obtained in this study, for sintering temperatures in excess of 1250°C, appear to be consistent with the findings and proposed mechanisms described above. However, there remains some doubt regarding the large increases in density observed with alumina addition in this work at sintering temperatures between 1050°C and 1250°C, in particular the problem of addressing how a liquid phase could be formed at such low temperatures.

The lowest melting composition identified for alumina and other relevant species is the eutectic point in the Al_2O_3-SiO_2-Y_2O_3 system (figure 2.6.2(vii)) between 1300°C and 1400°C. Although no phase diagrams have been published for the quaternary system ZrO_2-Al_2O_3-SiO_2-Y_2O_3, the most likely explanation for liquid phase formation at temperatures below 1350°C, would appear to involve the interaction of these constituents. However, given the mutual, extremely limited solubilty of alumina and zirconia at low temperatures this would require a highly significant effect to produce a liquid phase at temperatures as low as the 1050°C temperature at which the enhancing effect of alumina on the sintering behaviour becomes apparent.

An alternative, and perhaps more probable explanation of the observed increase in sintering activity at low sintering temperatures (in the range 1050-1350°C) would appear to be a solid state mechanism involving an increase in diffusivity of the (rate controlling) zirconia ions in the system.

It has been proposed[159] [237] that the limited solid solubility of alumina in zirconia (0.1% at 1300°C) would be expected to result in the formation of charge compensating vacancies in the oxygen sublattice to account for the different valencies of the Al^{3+} and Zr^{4+} ions. This would be expected in turn to produce an increase in diffusion and sintering rates, through an increase in the number of (rate controlling) cation interstitials by an identical mechanism to that proposed by Wu and Brook[125] for the effects of Y_2O_3 described in section 2.5.6, and could explain the effect observed in this. However, further experiments would be required to substantiate this, and determine which of the possible sintering mechanisms described above was in fact operating.

The significant negative impurity temperature interaction effects identified in the density factorial experiments

for the alumina doped specimens (AD) over the 1150-1250°C and 1250-1350°C sintering temperature intervals imply a change in the effect of alumina on the sintering behaviour over these temperature ranges, with the alumina becoming decreasingly effective at promoting densification with increasing temperature. This may simply be a consequence of a smaller relative difference between the undoped and alumina doped samples as the undoped specimens begin to approach maximum density.

(ii) and (iii) De-densification and grain growth at higher sintering temperatures.

For sintering temperatures of around 1550°C and above, alumina additions appear to produce the reverse effect on the densification behaviour to that identified for lower sintering temperatures. The density, and shrinkage values appear to decrease with increasing sintering temperature and dopant addition, with the measured defect area from the Seescan microstructural analysis increasing. All of the measured parameters indicate a substantially increased effect for sintering temperatures in excess of 1650°C. This suggests a change in the mechanism by which alumina addition affects the densification behaviour at intermediate and higher sintering temperatures, and appears to indicate the presence of a de-densification mechanism for alumina additions at higher sintering temperatures.

These results are generally in agreement with the findings of Lu and Chen[159], who attributed the de-densification effect to destabilisation of the tetragonal phase and the effects of the resultant phase transformation on the density of the sintered material, and appear consistent with many of the findings of Lange et al[160], who identified a similar de-densification effect in milled zirconia specimens but attributed this to a bloating mechanism arising from the release of high pressure oxygen during heat treatment.

The microstructural changes apparent in the alumina doped

specimens sintered at 1750°C, particularly the reduction in the volume fraction of the alumina inclusions compared to the 1350° and 1550°C sintered specimens, is thought to be due to the increased solid solubility of alumina in zirconia at this temperature, allowing a proportion of the alumina inclusion phases, presumably together with any alumina present as grain boundary phases to go into solid solution in the primary zirconia grains.

This effect was coincident with the onset of rapid grain growth, with the average grain size of these specimens being typically three times larger than in the undoped material, and being found to increase with increased dopant addition, suggesting that alumina in solid solution in the zirconia grains is responsible for the accelerated grain growth phenomena.

This would also be consistent with the proposed solid state mechanism described to account for the improved sintering of alumina doped T.Z.P. specimens at low temperatures, due to an increase in atomic mobility associated with the presence of Al^{3+} ions in solid solution.

The microstructures of thermally etched specimens produced at these sintering temperatures revealed extensive grain boundary cracking, with frequent interlinking of these cracks to form much larger cracks within the structure. The large grains within these specimens also showed evidence of twinning, characteristic of the monoclinic polymorph and suggests that the intergranular cracking arises from the volume expansion associated with the tetragonal to monoclinic phase transformation.

This is consistent with the findings of the grain size determinations, which showed the average grain size in these materials to be of the order of 5 to 10 times larger than the critical, maximum grain size for Y-T.Z.P. of this stabiliser content[127].

The microstructures revealed by S.E.M. examination also appeared to suggest that the cause of the increased defect areas identified by the optical microscopy and Seescan microstructural analysis, was loss or removal of a number of the surface grains. Given the extensive nature of the grain boundary cracking, this would almost certainly have occurred during the polishing of the samples prior to microstructural examination.

The increase in apparent (or open) porosity in the 1700°C and 1750°C sintered samples, identified in the density measurements was thought to be associated with the network of intergranular cracking which was present in these specimens.

5.2.3 Densification and microstructural development in silica doped T.Z.P.

Key Findings:

(i) Anomalous results for 0.75% SiO_2 addition.

(ii) SiO_2 produced little or no significant density increase for sintering temperatures below 1250°C.

(iii) SiO_2 produced a significant increase in density for 1250-1350°C sintering temperature.

(iv) Maximum density achieved decreased with increasing SiO_2 content and sintering temperature above 1350°C, with increasing amounts of microstructural defects and grain boundary phases observed.

(v) Slight increase in grain growth rate with SiO_2 at high sintering temperatures.

The results of the shrinkage and density determinations and the Seescan microstructural analysis for the silica doped T.Z.P. generally show similar trends, offering some confirmatory evidence for the microstructural development and sintering behaviour in this material.

Taken together the results show that the effect of silica on the densification and microstructure of Y-T.Z.P. appears to fall into three regimes of behaviour for low (950-

1200°C), intermediate (1200-1400°C) and high (1450°C and above) sintering temperatures.

(i) Anomalous results for 0.75% SiO_2

The results for the nominal 0.75% SiO_2 doped specimens appear to show apparently contradictory results for the density measurements when compared with the results of the shrinkage determinations and optical microscopy. These results are also inconsistent with the results of the other levels of SiO_2 addition.

The origin of this apparent anomaly is thought to lie in the powder grinding and sieving operations carried out on the doped powders. The (nominally) 0.75% doped powder was found to contain a substantial proportion of strongly bonded aggregates or agglomerates which were not broken down during the powder pressing operations and produced large voids and defects in the microstructure of the sintered specimens and reduced shrinkage.

Examination of laboratory notebooks for the period in question showed that the sieving operation carried out on the subsequently produced doped powder batch were repeated due to the discovery of a damaged area in one of the sieves used. It is thought that this damage must have occurred but gone unnoticed during the sieving of the previous powder batch (the nominal 0.75% SiO_2 doped material), allowing large agglomerates to pass into the final doped powder.

The discrepancies between the density and other measurements was thought to arise in the "wet" density determination method used.

This method relied on the retention of water by capillary action in the pore spaces of the specimens after immersion, to produce a measure of the apparent or open porosity in the specimens. It is thought that the size of pore produced from these agglomerates was sufficiently large as to allow the water to be lost from the pore spaces between immersion and the subsequent weighing,

thus producing erroneously high density values which effectively ignored the presence of the (open) pore spaces from the bulk volume.

(ii) Low temperature sintering behaviour.

Although the densification behaviour of some of the silica doped specimens appeared to show a slight increase for sintering temperatures as low as 1050 to 1150°C, the magnitude of this effect was very small, and was not consistent for all the dopant additions. It is therefore probable that this did not represent a "real" effect.

(iii) Intermediate temperature sintering behaviour.

The considerably enhanced densification evidenced by the density, shrinkage and Seescan analysis results for the SiO_2 doped material sintered at temperatures in the range 1250-1350°C suggests that this represents a real and significant effect. The most probable explanation for this effect, particularly for the 1250°C sintered specimens is that the improved sintering of these specimens was due to the appearance of a liquid phase sintering mechanism at sintering temperatures between 1150 and 1250°C.

The magnitude of this effect became decreasingly significant with increasing sintering temperature as the density of the undoped specimens approached the theoretical maximum value, and the difference between the densities achieved by the silica doped and undoped material was therefore reduced. The results for the 1450°C sintered specimens, did not show any significant density improvement.

These findings were confirmed by the results of the factorial experiment for density which showed significant negative impurity-temperature interaction terms (BD) for the 1150-1250°C and 1250-1350°C sintering temperature intervals suggesting that the enhancing effect of silica addition on the sintered density undergoes a gradual diminution over these ranges of sintering temperature and

relative density.

The microstructures of the thermally etched samples, and the results of the grain size determinations for the 1350°C sintered specimens did not reveal any significant change in grain morphology, and the expected curved sided grains were not observed in these specimens. This would appear to contradict the theory that that liquid phase sintering did occur at these temperatures. However, the combination of small grain size and low thermal etching temperature made resolution of the microstructure very difficult, and it is probable that the amounts of grain boundary phase and changes in morphology were too small to identify under these conditions.

(iv) and (v) Higher sintering temperature effects.

The increasing amounts of grain boundary phase identified in the silica doped T.Z.P. specimens with increasing sintering temperature appear to confirm the formation of a liquid phase during sintering at these temperatures, with the amount of liquid phase increasing with increasing temperature. It appears that the maximum density achieved by the samples decreased proportionally with the amount of grain boundary phase formed. This may be a simple mixture effect due to the difference in relative densities between the zirconia (density approximately 6.1 gcm^{-3}) and the silicate grain boundary phases (density typically < 2.5 gcm^{-3})

The microstructure of the silica doped materials exhibited silica rich grain boundary phases (dark areas in the S.E.M. micrographs) located both in the triple points between grains, and along the grain boundaries.

The apparent increase in grain growth rate for silica containing specimens at the 1750°C sintering temperature compared to the undoped material may be due to a change in the grain growth mechanism as increasing amounts of liquid phase are formed in the microstructure.

In the case of the undoped material containing trace

levels of impurities and very small amounts (if any) of grain boundary phase, the grain growth mechanism would be expected to be essentially a solid state process, whilst in the silica doped materials, containing up to 1 mass percent oxide impurity, with extensive liquid phase, the grain growth may well occur by a (more rapid) Ostwald ripening process through the liquid phase.

The increase in measured defect area identified for the silica doped materials at sintering temperatures in excess of 1550°C appears to be due to increased amounts of surface damage induced during polishing of the specimens. The microstructures of the thermally etched specimens showed significant numbers of defects in the structure which appeared to be grains which had been lost from the surface.

5.2.4 Densification and microstructural development in titania doped T.Z.P.

Key Findings:

(i) TiO_2 additions reduced sintering activity for sintering temperatures below 1450°C.

(ii) Possible increase in grain growth rate for all sintering temperatures.

(i) Low sintering temperature effects.

The impaired sintering characteristics associated with titania addition for sintering temperatures below 1450°C was the reverse of the behaviour associated with alumina and silica additions at low and intermediate sintering temperatures.

The reduction in density achieved at these temperatures suggests that liquid phase formation and liquid assisted sintering processes (which normally enhance densification) do not play a significant role in the mechanisms by which titania impurities affect the densification behaviour.

Although, liquid phase sintering behaviour has been

reported in yttria stabilised F.S.Z. containing 12 mole % Y_2O_3 and 2-5 mole % TiO_2[152], this was produced at sintering temperatures of 1480°C. The density of both undoped and titania doped specimens in this work were close to the theoretical density at this sintering temperature, and thus the formation of a liquid phase would not be expected to significantly affect the densification.

Liquid phase formation would not be expected in this system from the simple zirconia-titania binary system at temperatures below approximately 1700°C (figure 2.6.2(iii)), and any liquid phase sintering phenomena at temperatures below this would be expected to involve interactions between the TiO_2, the stabiliser, zirconia, and probably other impurities in the system to form lower melting compounds.

The microstructures of the titania doped systems did not indicate any significant change in grain morphology (compared to the undoped material) suggesting that the amount of liquid phase formed in these specimens (if any) was very small. This is consistent with the findings of Radford and Bratton[152][161] for titania doped Y-F.S.Z. in which titanium ions were found to be distributed in solid solution throughout the grains of the sintered material, with limited segregation at the grain boundaries.

The reduction in sintering activity associated with TiO_2 addition at low sintering temperatures is therefore most probably due to a solid state mechanism. It is suggested that this could occur by a reduction in the concentration of free oxygen vacancies, and related anion vacancies by the opposite effect to that described in section 5.2.2 for alumina.

This could occur by a defect clustering mechanism, similar to that described by Wu and Brook[125] to explain the reduction in sintering activity (and ionic conductivity) in yttria stabilised zirconia at high levels of yttria addition (see section 2.5.4).

Some confirmatory evidence for such a mechanism would appear to be offered by the synchotron radiation study of Zschech et al[163] (see section 2.6.3.3). This identified (i) that Ti^{4+} ions do not substitute randomly for Zr^{4+} ions in the lattice, but form clusters due to ion interactions, and (ii) that these Ti^{4+} ions occupy off centre positions in the lattice which leave some oxygen ions less strongly bonded (presumably resulting in a preferential site for an oxygen vacancy).

Taken together these two effects could result in a reduction in a number of mobile defects able to participate in the sintering process (with TiO_2 addition), as increasing numbers of oxygen vacancies become "tied" to clustered Ti^{4+} ions in the lattice.

It should be stressed that as with the similar (but reverse) mechanism proposed for the effect of alumina addition, <u>further experiments would be required to substantiate this.</u>

(ii) Effect of TiO_2 on Grain size.

The small, but consistent and apparently significant increase in grain size of the TiO_2 doped specimens relative to the undoped material was not considered to be sufficient to account for the significant differences in sintering and densification behaviour. However, this could be consistent with a decrease in the atomic mobility, from the reduction in free vacancy concentration postulated above.

5.2.5 Densification and microstructural development in multiple doped samples, and results of factorial experiment.

The shrinkage, density results and Seescan analysis show similar trends, and combination of the results from these experiments appears to show consistent behaviour.

Generally, the effects the of impurities in combination were consistent with their individual effects. However the

results of the factorial experiments did show significant interaction effects between the impurities.

5.2.5.1 Silica plus titania doped material.

Key findings:

- **Positive interaction effect on density for 1150-1250°C and 1250-1350°C sintering temperatures.**

The net effect of combined silica and titania additions on the sintering activity was found to be strongly dependent upon sintering temperature, particularly during the early stages of sintering and/or at low sintering temperatures. However, this can be explained in terms of interactions between these oxides.

At very low sintering temperatures (1150°C), this combination of dopants appeared to result in a slight decrease in sintering activity relative to the undoped and silica doped specimens (evidenced by the shrinkage and density results). However the presence of SiO_2 appeared to ameliorate the reducing effect of TiO_2 on the sintering activity.

At slightly higher sintering temperatures (1250°C) the sintering activity of the T.Z.P. with these additions was increased relative to the undoped material, and the individually silica and titania doped materials, suggesting the possibility of a liquid assisted sintering mechanism at these temperatures.

Both effects suggest that the TiO_2 was removed from solid solution in zirconia, where it appears to impair densification, and was presumably partitioned into the silica rich grain boundary phases, possibly forming a lower melting liquid phase, particularly at sintering temperatures of 1250°C and above.

These effects were confirmed by the calculated (BC) interaction effect in the factorial experiments for the 1150-1250°C and 1250-1350°C sintering temperature intervals.

For sintering temperatures in excess of 1450°C, the density of the TiO_2 plus SiO_2 doped specimens was lower than that of the undoped or singly TiO_2 or SiO_2 doped materials. This may be due to the effect of the grain boundary phases on the bulk density of the material, similarly to the effect proposed to account for the reduction in density in the silica doped materials. However, no significant BC interaction effect was identified in the factorial experiments for the 1450-1550°C, 1550-1650°C, and 1650-1750°C sintering temperature intervals.

5.2.5.2 Alumina plus titania doped material.

Key Findings:

(i) Slight increase in density relative to undoped material at low sintering temperatures.

(ii) No evidence of interactions.

(iii) Grain size at high sintering temperatures smaller than with alumina additions alone.

This combination of dopant additives appeared to produce a slight increase in sintering activity relative to the undoped material for sintering temperatures of 1350°C or less, with the density and shrinkage values lying between those obtained with single additions of TiO_2 or Al_2O_3 at this level. There is a slight discrepancy between the shrinkage and density results for the 1350°C sintering temperature, which may be due to the experimental error in the measurements.

Since alumina additions produced an increase in sintering activity, and TiO_2 additions produced a generally smaller decrease in sintering activity over this range of temperatures, a NET slight increase in density relative to undoped material would be consistent with the dopants operating independently (i.e. not interacting).

The calculated interaction effect (AC) between these impurities would appear to confirm this for the 1150-1250°C sintering temperature interval, with no significant interaction effects identified. However,

there does appear to be a small positive interaction over the 1250-1350°C sintering temperature interval. This could be explained by partitioning of some of the titania impurity to the alumina inclusions formed in the microstructure.

For sintering temperatures of 1450°C and above, the sintering and microstructural development of the alumina and titania containing material was generally similar to that of the alumina containing material, and it would appear that at higher sintering temperatures, the effect of alumina dominates the behaviour, with these samples exhibiting similar grain growth and de-densification effects to the material containing alumina alone.

This would appear to be confirmed by the results of the density factorial experiments which did not identify any significant interaction effects between alumina and titania (AC) at higher sintering temperatures.

The grain size of the alumina and titania containing material was smaller than that obtained when alumina alone was present at higher sintering temperature. This would be expected if the titania resulted in a decrease in ionic mobility to counteract the increase in vacancy concentration and ionic mobility associated with alumina addition, suggested as a possible mechanism to account for the effects of the single factors on the densification.

5.2.5.3 Alumina plus silica doped material.

Key findings:

(i) Small increase in density for alumina plus silica dopant additions relative to alumina doped specimens at low sintering temperatures.

(ii) Negative Al_2O_3-SiO_2 interaction, (i.e. decrease in density) at higher sintering temperatures, and increase in microstructural defects.

(iii) Large increase in grain size for sintering

temperatures above 1450°C, with discontinuous grain growth for sintering temperatures between 1450 and 1650°C.

(i) Low sintering temperature effects.

The material doped with both alumina and silica exhibited slightly enhanced sintering activity at the 1150°C sintering temperature compared to the singly alumina doped materials. However, the results of the factorial experiments did not indicate the presence of a significant alumina-silica interaction (AB) for the 1150 to 1250°C sintering temperature range.

This discrepancy may be due to the way in which the factorial effects were calculated over the 1150-1250°C temperature range, as the magnitude of the effect was greatly diminished for the 1250°C sintered material, or may be due to an anomolously high density value being obtained for the alumina plus silica doped sample for 1150°C sintering temperature.

Enhanced sintering activity when both alumina and silica were present may be evidence for the presence of a mechanism involving (Al_2O_3 and SiO_2 containing) liquid phase assisted sintering. However the same problems arise as previously discussed for the single dopant additives, in explaining the formation of liquid phases at temperatures as low as 1150°C.

Alternatively, the presence of silica may have increased the wetting behaviour of the (alumina containing) grain boundary phase, facilitating the dissolution of increasing amounts of alumina in the primary grains and thereby increasing its effect according to the solid state mechanism postulated in section 5.2.2(i).

(ii) and (iii) Densification and grain growth at higher sintering temperatures.

The negative alumina plus silica interaction effects identified in the factorial experiments for the 1250-

1350°C and 1350-1450°C sintering temperature ranges indicate that the enhancing effects of alumina or silica on the densification have been reduced over this range of sintering temperature. This result would be consistent with the findings of Butler and Drennan[153], who found that alumina inclusions could act as a scavenger for SiO_2 impurities, thus reducing the effect of SiO_2 rich liquid phase on the sintering behaviour.

The decrease in density and shrinkage, for intermediate sintering temperatures between 1450 and 1650°C, identified in the specimens containing both alumina and silica additions was coincident with the occurrence of a bimodal grain size distribution and discontinuous grain growth in the etched microstructures, and may also have arisen as a result of this.

The microstructures of these specimens showed intergranular porosity, with some intragranular porosity also present in the large grains of the thermally etched specimens, with the Seescan analysis of the microstructures offering confirmatory evidence for the formation of increasing numbers of defects in the structure for increasing sintering temperature

The formation of the large grains in the microstructure can be explained in terms of the alumina distribution within the material. The microstructures of all of the alumina containing materials contained a characteristic distribution of alumina rich grains or inclusions. However, in the case of the samples exhibiting discontinuous grain growth, these inclusions were either no longer apparent or present on a much smaller scale, with the large grains having a similar distribution in the microstructure to these previously existing inclusions.

This would appear to suggest that the alumina rich rich regions have acted as sites for the onset of discontinuous grain growth, with the alumina inclusions being redistributed, presumably into the silica

containing grain boundary phase. Since discontinuous grain growth was not observed in the specimens unless both silica and alumina were present together, it would appear that the silica containing grain boundary phase is essential to facilitate the redistribution and grain growth processes.

The very large grain sizes identified in the alumina and silica doped materials at the 1750°C sintering temperatures was presumably due to the continued growth of the large grain population (from the bimodal size distribution formed at lower temperatures), with the smaller grains being consumed within these.

5.2.5.4 Alumina plus silica plus titania doped material.

Key findings:

(i) Negative Al_2O_3-SiO_2-TiO_2 interaction at low to intermediate sintering temperatures.

(ii) Grain growth and microstructural development otherwise very similar to the alumina plus silica doped specimens.

The sintering behaviour of the material containing the three additives in combination was extremely similar to that of the alumina and silica containing material discussed in section 5.2.5.3, and It would appear that the behaviour of these multiple doped materials was generally dominated by the effects of the silica and alumina, and that the titania produced little effect.

However the results of the density factorial experiments appear to indicate the presence of a (negative) three factor interaction effect over the 1250-1350°C and 1350-1450°C sintering temperature intervals. A negative three factor interaction implies that the presence of the third factor either reduces the magnitude of any positive two factor interaction, or alternatively, that any negative two factor interaction is increased in magnitude by the

presence of the third factor.

There are a large number of possible explanations for this apparent effect. However, since the effect was observed over both the 1250-1350 and 1350-1450°C sintering temperature intervals, and since there is only one consistent two factor interaction over these two sintering temperature intervals (i.e. the negative alumina plus silica interaction), the most plausible of these is that this interaction is increased in magnitude (i.e. made more negative) by the presence of TiO_2. This could occur if the presence of TiO_2 in the alumina rich inclusions increased their propensity for scavenging SiO_2 as discussed by Butler and Drennan[153].

The microstructural development and grain growth of the alumina plus silica plus titania doped material was very similar to the alumina and silica doped material, showing bimodal grain size distributions at intermediate sintering temperatures, and extensive grain growth at the 1750°C sintering temperatures. Presumably the mechanisms responsible for this behaviour were the same as those discussed for the silica plus alumina doped material.

5.3 Phase development and stability in doped and undoped T.Z.P.

The results of the X-ray diffraction studies of the phase composition of the doped and undoped materials sintered at various temperatures indicated that monoclinic, cubic, and tetragonal phases were present, as demonstrated in a range of other studies into the microstructure of T.Z.P. (see section 2.5.5[19][122]).

No additional phases were identified in any of the doped or undoped materials by X-ray diffraction, suggesting that the assumption of a three phase system made for the quantitative phase determination calculations was reasonable. However, this appeared to contradict the findings of the microstructural determinations, particularly for the SiO_2 and Al_2O_3 doped samples which

demonstrated the presence of (small volume fractions of) additional phases. It is thought that the amounts of these phases present were below the limits of detection for the technique and conditions used in this work.

5.3.1 Effect of sintering conditions on phase development and stability in undoped Y-T.Z.P.

Key Findings:

(i) Cubic phase content increases with increasing sintering temperature to 1650°C

(ii) Tetragonal phase content decreases with increasing sintering temperature to 1650°C

(iii) Effects (i) and (ii) reversed for sintering temperatures above 1650°C.

(i) Cubic phase development for sintering temperatures up to 1650°C.

The formation of cubic phase on sintering can be explained from the phase diagram for the ZrO_2-Y_2O_3 system (figure 2.3.3 (ii)), which shows the equilibrium phase field for the composition and sintering temperature range to be the two phase cubic and tetragonal region.

The phase composition of the unsintered T.Z.P. showed little or no cubic phase to be present. Thus sintering of the material in the two phase region should result in the development of cubic phase, the amount of which should increase (from the lever rule) with increased sintering temperature.

Although the room temperature equilibrium phase for T.Z.P. of this composition should be completely tetragonal, the specimens were found to contain the commonly observed non equilibrium cubic phase on cooling, which is though to arise from inhomogenous distributions of yttria in the material (see section 2.5.5[122][130]). The amount of retained cubic phase appeared to increase with increased sintering temperature.

This is consistent with the theory that the amount of yttria rich, non equilibrium, cubic phase retained on cooling is related to the amount of cubic phase formed during sintering, and that the retention of this phase is due to the slow transformation kinetics of the cubic to tetragonal phase transformation.

The slow furnace cooling used in the sintering schedules for these specimens was expected to produce a microstructure containing mainly tetragonal phase (with some non equilibrium yttria rich cubic regions) as opposed to the non transformable cubic related tetragonal (t') microstructure. This would seem to be confirmed by the results of this work, although some uncertainty does arise from the broad nature of the cubic (400) peak obtained in the X-ray diffraction experiments.

(ii) Tetragonal phase content for sintering temperatures up to 1650°C.

The observed decrease in the amount of tetragonal phase and increase in monoclinic phase content with increasing sintering temperature can be explained in terms of the grain growth behaviour of the sintered specimens, with increasing numbers of grains growing to a grain size in excess of the critical grain size[127] and transforming to the monoclinic polymorph.

(iii) Change in phase composition for sintering temperatures in excess of 1650°C.

The apparent reversal of the cubic and tetragonal phase composition-sintering temperature relationships for sintering temperatures in excess of 1650°C can be explained by an increase in the homogeneity of the yttria stabiliser in the microstructure for these sintering temperatures.

In particular the diffusion of yttria from the yttria rich cubic grains to the (lower yttria content), tetragonal grains would be expected to produce an

increase in the stability and amount of the retained tetragonal phase at room temperature.

The mechanism responsible for the homogenisation of the yttria within the microstructure is not clear. However, the rapid increase in grain growth rate, which was also observed in samples at sintering temperatures in excess of 1650°C does suggest that the migration and dissolution of grain boundary phases may be associated with the phenomena.

5.3.2 Phase development and stability in alumina doped T.Z.P.

Key Findings:

(i) No significant change in phase composition associated with alumina addition for sintering temperatures up to 1650°C

(ii) Large decrease in tetragonal phase content and increase in monoclinic phase content for sintering temperatures in excess of 1650°C.

(i) Low and intermediate sintering temperature effects.

The similarity in the behaviour of the phase development of the undoped and alumina doped materials, and the absence of a clear trend for the effect of increasing alumina content over the 0 to 1 mass % level suggests that alumina produced little or no effect on the phase development for sintering temperatures up to 1650°C. This would be consistent with the very limited solubilty of the alumina dopant in the primary grains for sintering temperatures in this range (figure 2.6.2(i)).

The results of the single factor experiments for alumina addition would appear to be confirmed by the factorial experiment results for the main effects of alumina (A) on the phase development, which were not significantly large.

Taken together, the two sets of results would appear to

suggest that any effects which did occur were small, and may be explained by experimental error.

Similar studies produced by other workers have produced contradictory results, with Tsubakino et al[154] obtaining similar results to this work, whilst Lu and Chen[159] report that the presence of alumina produced very large changes in the phase composition of Y-T.Z.P.

The latter study[159] identified an increase in the monoclinic phase content for alumina additions at sintering temperatures as low as 1400°C , which was attributed to removal (or partitioning) of the yttria stabilising additive into alumina rich liquid phase thought to be formed on sintering at these temperatures.

It is possible that experimental errors in the X-ray diffraction measurements obscured the occurrence of a similar phenomena in this work. However this cannot explain the very large discrepancies between the measured monoclinic phase contents in this work, and those observed by Lu et al[159], who claimed the presence of up to 45% monoclinic phase in their alumina doped specimens as opposed to less than 10 % monoclinic phase in this work for equivalent sintering temperatures and compositions.

However, Lu et al[159] state that the phase analysis in their study was carried out according to the method of Garvie and Nicholson[226] (incorrectly referenced in their work), which is based upon a two component cubic and monoclinic system. This would be inappropriate for a three component system consisting of predominantly tetragonal phase and may explain the large discrepancies between the two sets of results.

The presence of yttria in the liquid phase is prerequisite to produce melting compositions at these temperatures, and this would therefore be expected to produce some destabilisation of the tetragonal grains, although the magnitude of this destabilising effect is not clear, and depends upon the degree of yttria

partitioning. Therefore, the stability of the tetragonal phase identified in the X-ray diffraction studies of the alumina doped materials would appear to be inconsistent with the formation of a liquid phase.

Two possible explanations are proposed to account for this apparent inconsistency, as follows:

(a) The amount of partitioning and associated destabilisation produced under these conditions (impurity and stabiliser content, sintering temperature and time) may be within the limits of experimental error for the X-ray diffraction technique used for the phase determination, and therefore undetectable.

(b) An alternative explanation for the stability of the tetragonal phase in alumina containing T.Z.P. can be found in the work of Tsubakino et al[154]. This work involved a study into the phase distribution and grain boundary composition of alumina doped Y-T.Z.P. specimens, and showed that destabilisation of samples containing between 1 and 12 mass % alumina did not appear to take place despite evidence of yttria partitioning to alumina grain boundary phases evidenced by E.D.X. studies, and that the presence of alumina appeared to suppress the tetragonal to monoclinic phase transformation. Tsubakino et al[154] proposed a mechanism whereby the formation of an yttria and alumina containing grain boundary phase promotes stronger cohesion between grains, preventing the nucleation of the tetragonal to monoclinic phase transformation at grain boundary microcracks.

The apparent lack of a destabilising effect in this work, for sintering temperatures up to 1650°C can be explained in terms of an equilibrium between these two conflicting mechanisms. Thus the destabilising effect of the removal of yttria to the alumina containing grain boundary phase must be balanced by the increase in stability arising from the enhanced grain boundary cohesion in the presence of this phase.

(ii) Effect of alumina addition at high sintering temperatures.

The change in the tetragonal phase content-sintering temperature relationship for sintering temperatures in excess of 1650°C suggests the appearance of a new mechanism for the effect of alumina on the material, with increasing amounts of alumina addition promoting rapid destabilisation of the tetragonal phase, and transformation to the monoclinic form.

The onset of this mechanism appears to be coincident with the onset of rapid grain growth at high sintering temperatures, suggesting a possible link between these two phenomena. The average grain size of these materials is of the order of 10 times larger than the critical (maximum) grain size for this stabiliser content[127], and transformation to the monoclinic form would therefore be predicted.

The X-ray diffraction studies are confirmed by the appearance of the characteristic twinned monoclinic grains in the microstructure of these specimens.

There is some evidence, particularly from the factorial experiments carried out on these samples that the presence of alumina produces a reduction in the cubic phase content, particularly at high sintering temperatures, exaggerating a trend which was also apparent in the undoped specimens.

A significant (negative) main effect was identified for alumina addition (A) over the 1650-1750°C sintering temperature interval in the factorial experiment for cubic phase development.

This can be explained in terms of a similar mechanism to that proposed for the similar effect in the undoped specimens involving an increase in yttria homogenisation, but suggests that the presence of alumina, perhaps as a component of grain boundary phases, plays a significant part in the process.

The factorial experiment also identified a significant interaction effect (AD) over this temperature interval confirming that the mechanism by which alumina affects the cubic phase development changes over this sintering temperature range.

5.3.3 Phase development and stability of silica doped samples.

Key findings:

(i) SiO_2 addition produced no significant effect on phase composition for sintering temperatures up to 1550°C.

(ii) Small decrease in cubic phase content, and increase in tetragonal phase content for higher sintering temperatures.

The similarity between the behaviour of the undoped and silica doped materials would appear to suggest that silica addition produced little effect on the phase development and retention of T.Z.P. at these addition levels. Certainly, the magnitude of any effect was considerably smaller than the effect of changing the sintering conditions.

The experimental error (arising predominantly in the X.R.D. measurements) in these experiments was highly significant in comparison with the magnitude of any effects arising from the impurity addition, and caused significant problems in the analysis of the experiments.

(i) Low sintering temperature effects.

No significant effects on the phase composition of the silica doped samples were observed in either the factorial experiments or the single factor experiments for sintering temperatures up to 1350°C.

Such a result was not expected, since given the effect of silica addition on the formation of grain boundary phases (which were far more extensive than observed with alumina

addition), and the apparent formation of liquid phases at low sintering temperatures (thought to involve yttria to form a low melting quaternary eutectic), it would appear to be a reasonable assumption that considerable partitioning of the silica to the grain boundaries had taken place in these specimens. Such a phenomena would be also be consistent with the findings of other workers as discussed in section 2.6.3.

However, the phase development and stability of these specimens was extremely similar to that of the alumina doped specimens, and it is probable that similar explanations of the phenomena would apply in both cases i.e. either some destabilisation did occur, but this was below the limits of detection for the X-ray diffraction technique used, or alternatively that grain boundary effects produced a corresponding increase in stability (see section 5.3.2(i)).

(ii) High sintering temperature effects.

The interpretation of these effects is complicated by an apparent contradiction between the results of (a) the one factor experiments and (b) the calculated factorial effects of silica addition from the factorial experiment for the 1550-1650° and 1650-1750°C sintering temperature intervals. The two experimental techniques suggest respectively (a) no significant effect on the cubic phase content with silica addition, and (b) a slight reduction in cubic phase content with silica addition. The latter technique is expected to be the most reliable.

The calculated main factorial effects of silica addition (B) in the factorial experiments for cubic and tetragonal phase development suggest that silica addition resulted in a small but significant reduction in the amount of cubic phase present at higher sintering temperatures (1550-1650° and 1650-1750°C), with a similar increase in the amount of retained tetragonal phase for the 1650-1750°C temperature interval. This phenomena is very similar to that observed in the alumina doped materials

over the 1650-1750°C range of sintering temperature.

It should be noted that the magnitude of these effects was small, and of the same order of magnitude of the experimental error in these experiments. However the results of the f test for significance do indicate that these results are (just) significant at the f(1%) level.

The phenomena could be explained by an identical mechanism to that proposed in section 5.3.3(ii) to explain the same effect in the alumina doped samples, involving partitioning of yttria from the yttria rich cubic grains into the impurity phases.

5.3.4 Phase development and stability in titania doped T.Z.P.

Key effects:

(i) TiO_2 additions resulted in decrease in cubic phase and increase in tetragonal phase content.

(ii) The significance of this effect increased with increasing sintering temperature.

The effect of titania on the phase development of the doped samples produced significant effects for all sintering temperatures in excess of 1350°C. In particular, titania produced a decrease in the amount of cubic phase, and an equivalent increase in the amount of retained tetragonal phase present. This can be explained from the effect of the titania in solid solution in the zirconia on the phase equilibria of the system.

As explained in section 5.3.1, the development of the cubic phase is due to the sintering temperatures used, which lie in the two phase cubic and tetragonal region of the zirconia-yttria phase diagram. The reduction in the amount of cubic phase developed during sintering thus suggests that the titania has resulted in a change in the position of the phase boundary between the tetragonal, and the cubic and tetragonal phase fields with this boundary being moved to the right (i.e. towards the high

yttria end of the diagram - see figure 5.3.4(i))

The results for the cubic phase contents of the sintered samples also appear to show that the magnitude of this effect was increased for increasing sintering temperature, suggesting that the slope of the phase boundary between the tetragonal and the tetragonal plus cubic phase fields may have been changed by the addition of TiO_2, closer to the vertical over these sintering temperatures (see figure 5.3.4(ii)). However, this trend was less identifiable for the tetragonal phase content.

It is not possible to calculate the new position of the phase boundary from these experiments due to the relatively short heat treatments used (thus the samples may not have reached equilibrium during heat treatment), and the slow furnace cooling schedules used (which would have resulted in changes in the chemical equilibrium during cooling).

The increase in the amount of retained tetragonal phase would be expected if less cubic phase were produced during sintering. Since the cubic phase evolves from the starting material which was virtually 100% tetragonal, a reduction in the amount of cubic phase produced during heat treatment implies a corresponding increase in the amount of retained parent tetragonal phase.

The formation of cubic phase involves the depletion of yttria from the tetragonal grains, and a reduction in the amount of cubic phase formed would therefore be expected to result in a slight increase in stability of the tetragonal phase, and consequent reduction in the amount of monoclinic phase present in the specimens relative to the undoped material. However, whilst an increase in tetragonal phase content of the TiO_2 containing specimens was observed, no clear indication of a reduction in the monoclinic phase content was observed in the X-ray diffraction results for this phase. This was presumably due to the (increased stability) effect being too small

Figure 5.2.4.2

Schematic representation of the effect of Titania on the cubic and tetragonal phase equilibrium in Y-TZP.

Modification to phase diagram of Scott[34].

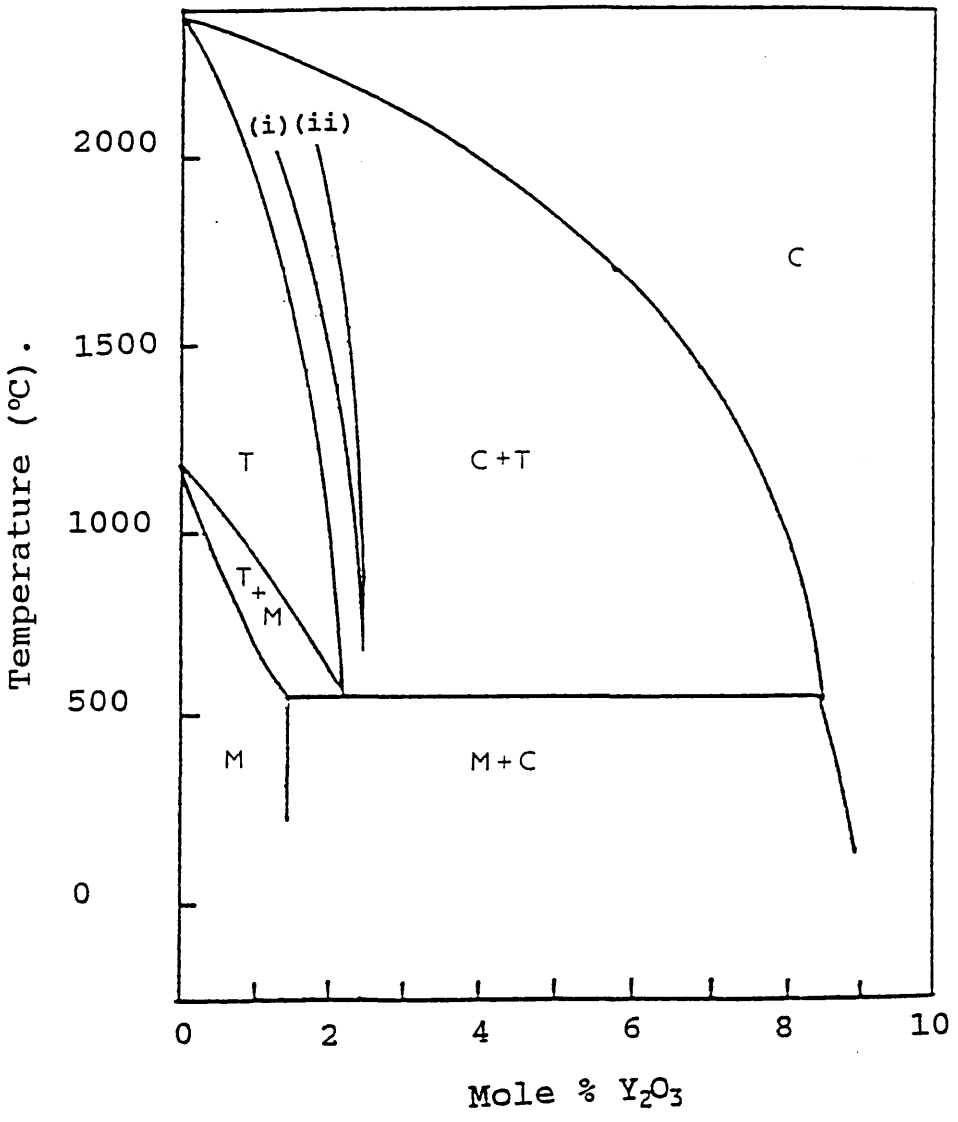

(i) T:C+T Phase boundary shifted to right by titania addition.
(results in decreased cubic phase formation)

(ii) Phase boundary shifted to right with slope of boundary increased closer to the vertical.
(results in decreased cubic phase formation relative to Y-TZP, becoming increasingly significant as temperature increased)

to detect in comparison with the experimental error in the measurements.

The results of the factorial experiments confirmed the findings of the one factor at a time experiments for phase development of the titania doped samples with significant, and increasingly negative main effects of titania addition (C) being identified for cubic phase development in the 1350-1550°C, 1550-1650°C, and 1650-1750°C sintering temperature interval, with corresponding but smaller positive effects being identified for the tetragonal phase development (significant at between f(10%) and f(1%) level depending upon sintering temperature interval).

5.3.5 Phase development and stability of samples containing multiple dopant additions, and results of factorial experiments.

Key findings:

(i) Few significant interactions identified.

(ii) Significant alumina plus silica (AB) interactions for samples sintered at high temperatures comprising:

- **Negative interaction for cubic phase (i.e. cubic phase content reduced).**
- **Positive interaction for tetragonal phase (i.e. tetragonal phase content increased).**

(iii) Apparently significant alumina plus silica plus titania (ABC) interaction for samples sintered at high temperatures comprising:

- **Negative interaction for tetragonal phase.**

(i) General observations.

Generally, the phase development of the multiple doped samples was consistent with the individual effects of the dopants, suggesting that the effects of any interactions were small.

This would appear to be confirmed by the factorial

experiments for the cubic and tetragonal phase development, in which the majority of the calculated interaction effects were insignificant. However, interaction effects were identified for alumina plus silica, and alumina plus silica plus titania.

Interpretation of these results is complicated by the magnitude of experimental error present in these measurements, relative to the magnitude of the effects of the dopant additives. It is quite plausible that the errors present masked the presence of other smaller (but real) interactions.

(ii) Alumina plus silica interaction effects.

The significant interaction effects identified for alumina and silica on the cubic phase development for 1550-1650ºC and 1650-1750ºC sintering temperatures, and the corresponding positive interaction on the tetragonal phase for the 1650-1750ºC sintering temperature range, would appear to represent a real effect whereby the presence of these two elements in combination results in a significant decrease in the stability of the cubic phase regions, and increases the stability of the tetragonal phase.

The similarity of this phenomena to the smaller effect observed for the alumina (alone) containing material when sintered at high temperatures, suggests that a similar mechanism, presumably involving homogenisation of the yttria content within the microstructure (see sections 5.3.2(ii), and 5.3.1(iii)), is responsible for the phenomena in this case.

The greater magnitude of the effect (i.e. the interaction) in the multiple doped material may be due to the presence of increased amounts of grain boundary phase, and the increased wetting behaviour of this phase relative to that in the singly doped alumina containing specimens.

(iii) Alumina plus silica plus titania interaction effects.

The interpretation of the apparently significant negative three factor interaction for the tetragonal phase content for the 1650°C to 1750°C sintering temperature range is complicated by the lack of the expected corresponding positive effect for the cubic phase content. This leads to the possible interpretation that this did not in fact represent a real effect.

However, it is possible that the presence of a corresponding effect for the cubic phase content was obscured by the relatively large experimental error, and that it was in fact present. This would then suggest that the negative three factor (ABC) interaction effect for the tetragonal phase development may be due to the loss of TiO_2 into the alumina and silica rich liquid phases formed during sintering at high temperatures. The amount of tetragonal phase would therefore be lower than expected due to the loss of TiO_2 from the zirconia grains, with concomitant loss of the change in phase equilibria (i.e. increase in tetragonal phase content) associated with TiO_2 addition described in section 5.3.4.

5.4 Mechanical Properties of doped and undoped T.Z.P.

The hardness and fracture toughness of sintered T.Z.P. might be affected by microstructural changes and/or changes in the phase composition and/or transformation toughening behaviour in the specimens.

In particular, a reduction in grain size and transformability, or tetragonal phase content, or the presence of significant amounts of low fracture toughness grain boundary phases might be expected to produce a reduction in fracture toughness, whilst the presence of second phases, microcracking and increases in grain size might be expected to produce an increase in fracture toughness. These are discussed in more detail in the following sections.

The hardness of the material might also be affected by the presence of microcracking, grain boundary phases and changes in transformability and/or tetragonal phase content. However, the nature of these effects is not obvious, and for example it can be argued that the tetragonal to monoclinic phase transformation in these materials might produce an increase in apparent hardness by producing a constraining effect on an indentation, or a decrease in hardness due to the pseudoplastic deformation associated with the transformation. The latter argument appears to explain the effects observed in this work.

5.4.1 Mechanical properties of undoped T.Z.P.

Key findings:

(i) Hardness of undoped specimens increased with increasing sintering temperature for sintering temperatures up to 1350°C

(ii) Little variation in hardness with increasing sintering temperature above 1350°C

(iii) Toughness of undoped specimens decreased with increasing sintering temperature over the range 1250-1350°C

(iv) Toughness of undoped samples increased with increasing sintering temperature over the range 1350-1750°C.

(i) and (ii) Effect of sintering temperature on hardness of sintered specimens.

For samples sintered at temperatures up to 1350°C, the large increase in hardness with increased sintering temperature can be related to the increase in density over this range of sintering temperature. For sintering temperatures above this, the hardness appears to be independent of the sintering temperature suggesting that the changes in grain size and phase composition identified over this temperature range have little effect on the hardness.

(iii) and (iv) Effect of sintering temperature on fracture toughness of sintered specimens.

The effect of sintering temperature on the fracture toughness of the material, also showed two discrete regions of behaviour suggesting that two mechanisms were operating. The apparent **increase** in fracture toughness with **decreasing** sintering temperature below 1350°C can be explained in terms of the effect of (increasing amounts of) retained porosity in the microstructure, which could act as a crack stopping mechanism. The increase in fracture toughness with increasing sintering temperatures in excess of 1350°C (for which the density values were close to the theoretical value) would be expected due to the increased transformability of the tetragonal grains associated with the increase in the grain size for increasing sintering temperature.

The mechanism proposed (in section 5.3.1(ii)) involving yttria homogenisation to explain the decrease in cubic phase and increase in tetragonal phase content for sintering temperatures in excess of 1650°C would be expected to increase the stability (i.e. decrease the transformability) of the tetragonal grains, and might therefore be expected to result in a slight decrease in the fracture toughness of the material. However no such effect could be detected in the fracture toughness determinations. It is possible that this did occur, but was disguised by the relatively large range of possible experimental error in the results.

5.4.2 Mechanical properties of alumina doped T.Z.P.

Key findings:

(i) The hardness of samples sintered at temperatures up to 1350°C was increased by alumina addition.

(ii) The hardness was approximately independent of sintering temperature used in the range 1350-1550°C, and was increased relative to the undoped material.

(iii) The hardness decreased with increasing sintering temperature above approximately 1550°C.

(iv) The toughness of samples sintered at temperatures up to 1350°C was decreased by alumina addition.

(v) Alumina additions produced a slight increase in toughness of samples sintered at temperatures between 1350 and 1650°C.

(vi) Samples sintered at temperatures above 1650°C showed large apparent fracture toughness increase with alumina addition.

The effect of sintering temperature on the hardness and fracture toughness of the alumina doped specimens appears to show two distinct types of behaviour corresponding to low and high sintering temperatures. There is also evidence of a transitional stage, corresponding to sintering temperatures between these extremes.

(i) Effect of alumina on hardness for sintering temperatures up to 1350°C.

The hardness results for the alumina doped sintered specimens appear to show that the development of hardness was a function of the alumina addition level and increased with it. This was confirmed by the calculated main effects for alumina (A) in the hardness factorial experiments which were found to be large and positive for the 1250-1450°C sintering temperature interval.

The increase in hardness associated with alumina additions at sintering temperatures between 1250° and 1350°C corresponds approximately with the enhancing effect of alumina addition on the densification behaviour at these temperatures, suggesting that the hardness increase was due to the higher density in these specimens. The density of the undoped T.Z.P. sintered at 1250°C was approximately 90% of the theoretical density compared with around 98% for the alumina doped specimens at the same sintering temperature.

(ii) Effect of alumina on hardness for 1350-1550°C sintering temperature.

The apparent increase in hardness associated with alumina addition at higher sintering temperatures, at which the density of both the undoped and blank treated materials approaches the theoretical value cannot be adequately explained by a mechanism based solely upon an increase in density.

A possible explanation for this phenomena might be a decrease in transformability (and hence pseudoplastic deformation) of the primary tetragonal grains in the material. This would be consistent with the mechanism proposed to explain the lack of an apparent destabilising effect in these materials in section 5.3.2 (i).

However, the calculated factorial effects for alumina in the factorial experiment over the 1450-1550°C sintering temperature interval did not identify the presence of any significant effect associated with alumina addition for these sintering temperatures, and it is therefore not clear whether a real effect does in fact exist, particularly at the higher end of this sintering temperature range.

(iii) Effect of alumina on hardness for higher sintering temperatures.

The decreases in hardness observed in both the single factor and factorial experiments for sintering temperatures in excess of 1550°C are thought to be associated with the onset of grain growth, destabilisation and grain boundary microcracking in the material.

The hardness determinations would appear to be a more sensitive indicator of the onset of this phenomena than the X-ray diffraction measurements, which did not identify a significant change in the tetragonal phase content for the 1650°C sintering temperature.

(iv) Effect of alumina on fracture toughness of specimens sintered at low sintering temperatures.

The similarity of the fracture toughness of the undoped and alumina doped specimens sintered at low temperatures would appear to suggest that the same mechanisms, thought to involve the interaction of retained porosity on the growing crack, were responsible for the change in properties over this range of sintering conditions (see section 5.4.1(iii)).

The enhanced density of the alumina doped specimens would be expected to produce a reduction in fracture toughness relative to the undoped T.Z.P. due to the presence of less residual porosity at these sintering temperatures.

(v) Effect of alumina addition on fracture toughness for sintering temperatures between 1350 and 1650°C.

The fracture toughness of the alumina doped specimens appeared to show a consistent increase relative to the undoped specimens over this sintering temperature range.

The curves representing the effect of sintering temperature on the fracture toughness of the undoped and alumina doped materials appear to be approximately parallel, suggesting that the toughening enhancement in the alumina doped specimens is a consistent effect superimposed upon the transformation toughening mechanism.

Two possible mechanisms are suggested to explain this apparent effect.

(a) The microstructures of the alumina containing materials sintered at temperatures up to 1650°C all contained second phase grains or inclusions of alumina. These second phase particles may have interfered with crack propagation, perhaps by the formation of microcracks at the zirconia/alumina particle interface.

(b) The fracture toughness of the alumina containing materials may have been increased by an increase in the

transformability of the tetragonal grains caused by yttria partitioning to the grain boundaries. However, as explained in section 5.3.2(i), the amount of destabilisation expected by this phenomena would be relatively small, and it would appear unlikely that such a significant change in mechanical properties would result from it.

(vi) Effect of alumina additions on fracture toughness for sintering temperatures in excess of 1650°C.

The apparent increase in fracture toughness associated with alumina addition would appear to be inconsistent with the decrease in the amount of retained tetragonal phase for alumina doped Y-TZP at sintering temperatures above 1650°C, and the similar phase composition between the alumina and undoped material for sintering temperature up to this value.

However, these findings are in agreement with other studies, particularly the work of Kihara et al[237], and would therefore appear to represent a real effect.

The most probable explanation of this apparent anomaly is that the increase in fracture toughness in these alumina doped specimens arose from an alternative toughening mechanism (or mechanisms) to conventional transformation toughening behaviour.

The increase in the measured fracture toughness for specimens sintered at 1650°C and above is thought to arise from a further toughening mechanism, involving the interaction of the propagating cracks with the residual stress fields and grain boundary microcracks in these extensively transformed materials.

It is possible that this effect arose in part due to the micro-indentation method used. The presence of large amounts of intergranular cracking and surface damage, arising from the tetragonal to monoclinic phase transformation and the polishing technique, made accurate determination of the crack length very difficult. This

may have resulted in an over-estimation of the true fracture toughness.

5.4.3 Mechanical properties of silica doped T.Z.P.

Key Findings:

(i) Silica additions result in large increase in hardness for sintering temperatures up to 1450°C

(ii) Hardness of silica doped specimens sintered at temperatures above 1350°C, decreases with increasing sintering temperature.

(iii) Silica additions produce a decrease in fracture toughness for all sintering temperatures up to 1550°C.

(iv) Silica additions produce apparent increase in fracture toughness for sintering temperatures above 1650°C.

(i) Low sintering temperature effects.

At low sintering temperatures, the increase in hardness relative to the undoped material can be explained as arising from the enhanced densification in these materials as described for the effect of alumina. However, at higher sintering temperatures in the range 1350-1450°C, which produce virtually theoretical density in both doped and undoped specimens, this cannot account for the difference between the hardness of the two materials.

The increase in hardness in the silica doped material relative to undoped T.Z.P., suggests that the resistance to the martensitic transformation (and the associated pseudoplastic deformation) was increased by the addition of silica, particularly at low sintering temperatures.

This could be explained in terms of the mechanism, proposed to account for the similar effect in the alumina doped specimens (section 5.4.2(i)), involving the effect of grain boundary phases on the grain boundary integrity.

Alternatively, the presence of significant amounts of grain boundary phase in these specimens (this was far more extensive than in the alumina doped

specimens) could increase the hardness by interfering with the nucleation of the tetragonal to monoclinic phase transformation at the grain boundaries. It is possible that the grain boundary phase acts as a "buffer" between the tetragonal grains, and impedes the transgranular nucleation and propagation of the martensitic phase transformation, and the associated pseudoplastic deformation.

Such a mechanism would also be expected to produce a decrease in the fracture toughness by reduction in the size of the transformation zone around a propagating crack (see section 2.4.1).

(ii) Effect of silica addition on the hardness of specimens sintered at temperatures above 1350°C.

The decrease in hardness with increasing sintering temperature above 1350°C would not appear to be consistent with the mechanisms proposed to explain the increased in hardness relative to the undoped material at lower sintering temperatures, and it would appear that a secondary mechanism was operative in these specimens.

The decrease in hardness coincided with the formation of increasing amounts of grain boundary phase, in the microstructure as the sintering temperature was increased, suggesting a possible link between these phenomena.

It is possible that the hardness of this phase may be lower than that of the primary zirconia, and that this accounted directly for the hardness decrease. However, the relatively small proportions of glassy phase in the microstructure (<1%) would not be expected to produce such a significant change in the hardness (approximately 15% decrease in hardness) by a simple mixture effect.

The appearance of significant amount of grain boundary phase in the microstructures of the silica doped specimens (for sintering temperatures of 1550°C or more also coincided with an increase in susceptibility to surface

(polishing) damage by grain pull out, evidenced in the Seescan results. This suggests that any enhancing effect of the grain boundary phase on the grain boundary integrity or effect on the phase transformation diminishes at higher sintering temperatures. One possibility is that an increase in the amount of grain boundary phase above a critical value enables it to act as a low toughness fracture path in the materials with associated grain boundary microcracking under load (i.e. on polishing, or hardness testing), resulting in lower values of apparent hardness.

(iii) Effect of silica addition on fracture toughness for sintering temperatures up to 1550°C.

Generally, silica additions appeared to produce a reduction in the fracture toughness for sintering temperatures up to 1550°C.

The microstructures of the silica doped specimens exhibited significant amounts of silica containing phase distributed primarily at triple points and along grain boundaries, the amounts of which were found to increase with increasing sintering temperature. This is thought to produce the observed change in mechanical properties with sintering temperature.

Two possible mechanisms are suggested to explain how the grain boundary silica phase might affect the fracture toughness:

(i) The fracture toughness of the silica doped specimens may be reduced relative to the undoped material by the grain boundary phase acting as a low toughness pathway for intergranular crack propagation.

(ii) Alternatively, the grain boundary phase might interfere with the nucleation of the tetragonal to monoclinic phase transformation across grain boundaries, thus reducing the size of the transformation zone around a propagating crack thereby reducing the transformation toughening

effect and fracture toughness.
This would be consistent with the mechanism proposed to explain the increase in hardness in these specimens.

(iii) Effect of silica addition on fracture toughness for sintering temperatures in excess of 1650°C.

At higher sintering temperatures, the apparent increase in fracture toughness appears to be inconsistent with the mechanism proposed to account for the decrease in fracture toughness at lower sintering temperatures, particularly since the amounts of grain boundary phase present increased with increasing sintering temperature. This suggests the onset of a new mechanism affecting the fracture toughness of these specimens.

The increase in fracture toughness relative to the undoped material for the 1650 and 1750°C sintering temperature was similar (although smaller in magnitude) to the effect observed for the alumina doped specimens for similar sintering temperatures.

In the alumina doped materials, this was attributed to the formation of grain boundary microcracking from the martensitic phase transformation, and the interaction between the propagating macrocrack with the grain boundary microcracking resulting.

The increase in polishing damage (grain pullout) identified in the Seescan analysis, and the decrease in hardness for the silica doped specimens sintered at 1650°C and 1750°C offers some evidence for the existence of grain boundary microcracking in these materials, and would be consistent with the existence of a similar toughening mechanism in this case.

5.4.4 Mechanical properties of titania doped T.Z.P.

Key Findings:

(i) TiO_2 additions resulted in decrease in hardness for samples sintered at temperatures up to 1450°C.

(ii) TiO_2 additions produced small, but consistent

increases in fracture toughness for all sintering temperatures.

Generally, the effects of sintering temperature on the hardness and fracture toughness of the titania doped material were similar to the undoped material, suggesting that similar mechanisms were responsible for determining the mechanical properties in both cases.

(i) Effects of TiO_2 on hardness.

The significant reductions in hardness for titania doped materials at low sintering temperatures (1250-1450°C) can be attributed to the lower density of these materials due to the impaired sintering. The hardness results also appear to show an apparent decrease in hardness for the TiO_2 doped specimens sintered at 1750°C.

The findings of the single factor experiments for the 1250 to 1450°C sintering temperature range are confirmed by the results of the factorial experiments for hardness, in which the calculated main effects of titania addition (C) were found to be significantly large and negative.

However the factorial experiment also appears to show smaller negative factorial effects (i.e. hardness reductions) associated with titania additions for the 1450 to 1550°C and 1550 to 1650°C sintering temperature ranges. These can be explained in terms of an increase in pseudoplastic deformation associated with the increased amounts of the tetragonal phase present in these specimens.

(ii) Effect of TiO_2 on fracture toughness of sintered T.Z.P.

The increased fracture toughness of the titania doped material relative to the undoped material can be explained in terms of the crack stopping effect of the increased porosity at lower sintering temperatures, by the mechanism described in section 5.4.1(iii), whilst for sintering temperatures of 1450° and above, the increased

amounts of tetragonal phase available to produce the transformation toughening effect, from the change in phase composition associated with titania addition, would explain the toughness increase.

The calculated main effects (C) for the factorial experiment would appear to confirm these findings, with significant and increasingly large positive effects (i.e. fracture toughness increases) being identified in the 1450-1550 and 1550-1650°C temperature intervals.

5.4.5 Mechanical properties of Y-T.Z.P. with multiple dopant additions and interpretation of factorial experiment.

As with the phase development results, the interpretation of the mechanical properties data for these specimens is complicated by the magnitude of the errors present in the measurements relative to the limited magnitude of the effects produced by the dopant additives.

However, the results did appear to show the presence of a number of significant interactions, particularly between alumina and silica (hardness and fracture toughness), silica plus titania (hardness), alumina and titania (fracture toughness) and alumina plus silica plus titania (hardness).

5.4.5.1 Alumina plus silica.

Key Findings:

Significant alumina plus silica (AB) interactions comprising:

(i) Negative interaction for hardness (for 1250-1450°C, 1450-1550°C, and 1550-1650°C sintering temperature ranges)

(ii) Positive interaction for toughness phase for 1450 -1550°C, and 1550-1650°C sintering temperature ranges (i.e. tetragonal phase content increased).

(i) Hardness effects.

The physical meaning of the negative (AB) interaction effect identified between alumina and silica on the hardness of the sintered material over all sintering temperatures was that the effect of alumina (A) was reduced (i.e. less positive) or more negative in the presence of silica.

Thus for sintering temperatures up to 1550°C, the positive effects associated with alumina addition were decreased in magnitude, whilst for sintering temperatures in excess of this, the negative effects associated with alumina addition were decreased in magnitude.

The negative interaction on the hardness of the alumina plus silica doped material, can be explained in terms of an increase in the amount of grain boundary phase formed when both silica and alumina are present relative to samples containing single additions of these oxides. This might be expected to decrease the hardness in the same way as was proposed to explain the similar effect in the silica doped specimens (see section 5.4.3.2 (iii)), although to a greater degree.

(ii) Toughness effects.

The significant positive interactions identified for these impurities on toughness for specimens sintered at temperatures between 1450-1550° and 1550-1650°C could also be due the presence of increasing amounts of grain boundary phase in this material, due to increased partitioning of yttria stabiliser into this phase, and associated partial destabilisation and increased transformability of the tetragonal phase.

However, the microstructures of these specimens also differed significantly from the undoped and singly doped specimens, due to the occurrence of discontinuous grain growth. It would appear probable that the change in fracture toughness was related to this highly significant microstructural effect, perhaps due to a change in the

crack propagation path. Unfortunately, fractography was not carried out on the cracks in the thermally etched specimens to confirm this.

5.4.5.2 Silica plus titania.

Key findings:

- **Negative interaction effect for hardness (hardness reduced) for sintering temperatures in excess of 1450°C.**

The inconsistent nature of the BC interaction for hardness which showed a positive effect (at f(5%)) level for the 1250-1450°C sintering temperature range, and negative for the 1450-1550°C and 1550-1650°C sintering temperature ranges (significant at the f(1%), and f(5%) levels respectively) poses some difficulty in interpreting the behaviour, and does offer some doubt as to whether (and which of) these represent a real effect.

Assuming that the two largest and negative effects in the higher sintering temperature ranges do represent "real" effects, these can be interpreted as follows:

The physical meaning of the negative two factor interaction between silica and titania could be either that the mean effect of silica was reduced (i.e. was less positive or more negative) when titania was present, or the mean effect of titania was reduced when silica was present. These two possible interpretations are indistinguishable in the calculated factorial effects.

Since single additions of silica or titania both produced a reduction in hardness at higher sintering temperatures, the interaction effect suggests that the combination of the two dopants produces an even greater reduction than their combined individual effects.

The most probable mechanism for this interaction would be the formation of grain boundary phases containing silica and titania, producing a reduction in hardness by the same mechanism described to explain the similar effect in the alumina plus silica doped material (section 5.4.5.1). This must have entailed the partitioning of

some of the titania from the tetragonal grains to the grain boundaries.

5.4.5.3 Alumina plus silica plus titania doped specimens.

Key findings:

- **Negative interaction effect on hardness for 1250-1450°C range of sintering temperature.**

The negative three factor interaction effect (i.e. reduction in hardness) in these specimens can be explained in terms of an identical mechanism to that proposed to explain the similar negative interaction effects for alumina plus silica and silica plus titania, but involving a silica, alumina and titania containing grain boundary phase.

5.4.5.4 Alumina plus titania doped T.Z.P.

Key results:

- **Apparent positive interaction effect on toughness for 1650-1750°C range of sintering temperature.**

The positive interaction identified in the toughness results of the alumina plus titania doped materials sintered at temperatures in the range 1550-1650°C, is a surprising effect. Both of these impurities produced apparent toughness increases when present singly, by what seem to be quite different mechanisms, (i.e. crack stopping by second phase particles and/or microcracking for alumina (5.4.2 (v)), and increased tetragonal phase content for titania (5.4.4 (ii)). It is not clear what mechanism(s) could be produce an increase in toughness from an interaction between these oxides.

The most probable explanation is that the occurrence of these two impurities in combination increased the propensity for the material to form microcracks or second phase particles, thereby increasing the fracture toughness according to the mechanisms proposed to explain the similar (but smaller) effects associated with alumina addition.

The presence of a positive interaction effect may be of significance as a potential mechanism for improving the performance of Y-T.Z.P.

5.5 The experimental design and the factorial experiments.

The use of a factorially designed experiment to identify the presence of interactions between the impurity dopants has been shown to be successful. The results have yielded useful information regarding the nature of the multi factor interactions on the sintering, phase development and mechanical properties of Y-T.Z.P., notably the occurrence of discontinuous grain growth in the presence of alumina and silica, and possible improvements in mechanical properties (hardness and fracture toughness) associated with alumina plus silica interactions, and perhaps alumina plus silica, although in the latter case, it is expected that discontinuous grain growth would have resulted in a reduction in strength.

The work has also demonstrated the need for a "belt and braces" approach utilising both factorial experimental design and conventional one factor at a time experiments to enable reliable conclusions to be drawn, particularly regarding single factor effects in systems in which significant multi factor interactions occur. A good example of this can be seen in the density results

For example the calculated factorial effects for titania (C) over the 1250-1350°C sintering temperature range (-0.10 gcm^{-3} or about -2%) considerably underestimate the real effect of this addition on the density due to the presence of significant positive alumina plus silica and silica plus titania interactions, which bias the calculated mean main effect. The calculated factorial effect can be compared to the results of the single factor experiments for titania which show a reduction in density of 0.6 gcm^{-3} (or about -10%) for the 1250°C sintering temperature.

The validity and suitability of the 2^4 type factorial experimental design used in this work, warrants some discussion. In particular, the effect of the adoption of this experimental design on the reliability and amount of information obtained.

The choice of a 2^4 factorial experimental design investigating the effects of both the impurities and sintering temperature had some drawbacks associated with it. The calculated factorial effects for the impurities and interactions were calculated as average effects over a range of sintering temperatures (i.e. over each of the sintering temperature intervals), reducing the amount of information available regarding the impurity and impurity interactions at each sintering temperature, and thus the resolution available from the experiments.

However, this design also had some advantages notably regarding the increased amount of information available on the effects of sintering temperature and impurity-sintering temperature interactions. The method also reduced the susceptibility of the experiments to occasional spurious results, and this was considered to be a powerful argument in favour of the adoption of the 2^4 design in these unreplicated experiments.

In retrospect, more reliable results might have been obtained by carrying out a number of replicates of the experiment, using fewer temperature intervals, and perhaps a 2^3 type design investigating only the impurities and their interactions. However, this would have resulted in a significant reduction in the amount of information available from the experiment and it is debatable whether this would have been justified.

On balance, the loss of resolution associated with the 2^4 design was considered to be an acceptable trade-off for the greater information offered regarding impurity-temperature interaction effects and the "smoothing" effect attained by calculating each of the factorial effects from a greater number of experimental results.

As with all experimental determinations, the study involved a compromise between obtaining the maximum amount of information from the experiment by investigating the effect of the maximum number of variables, and increasing the reliability of the experiment by investigating the effects of fewer variables, but duplicating these experiments a number of times to reduce the effects of the unavoidable occasional spurious result.

Whilst the factorial experiment was successful in identifying the presence of interactions, the technique cannot (in isolation) identify the mechanisms responsible for those effects. This is perhaps the most significant limitation of factorial experimental designs, which tend to provide insufficient information to explain the effects observed. In the case of this work, tentative interpretation of the mechanisms responsible for the apparent effects was made possible by inter-relating the results of both factorial experiments and (multi-level) single factor experiments for the effects of sintering temperature and impurity additions on the density, microstructure, phase development and mechanical properties of the material.

5.6 In summary.....

The results of the investigations carried out in this work suggest that alumina, silica and titania impurities in T.Z.P. do produce significant effects on the properties and behaviour of the material, particularly for very low and high sintering temperatures.

However, by no means all of these effects are detrimental to the properties of the material, and the majority of those which are, can be limited in their effect by control of the sintering conditions.

Titania additions at the 0.25 to 1 mass percent level have been shown to result in an improvement of the tetragonal phase content and fracture toughness of the sintered material, but do appear to impair the (initial) sintering behaviour, particularly at the higher end of this range of addition.

Alumina additions have been shown to enhance the densification, and produce an increase in fracture toughness, particularly for sintering temperatures in the 1350° to 1550°C temperature range. However, the presence of alumina has been shown to result in detrimental effects for sintering temperatures in excess of 1650°C.

Silica additions appear to enhance the densification particularly for sintering temperatures in the 1250-1350°C range. However, the presence of silica appears to be generally detrimental to the attainment of maximum density, and to the fracture toughness of the sintered materials, and also results in undesirable discontinuous grain growth when present in combination with alumina.

A combination of alumina and silica additions has been shown to ameliorate the reduction in sintering activity associated with TiO_2 additions, and may also produce an increase in fracture toughness, perhaps combining the positive aspects associated with single additions of these oxides. Further investigation of this system may

produce significant performance advantages. It is suggested that he excellent properties of the Tosoh Y-T.Z.P. investigated in this work appear to be primarily due, not to the high degrees of chemical purity as originally thought, but to other physical parameters, notably the fine particle size and low agglomerate strength.

6. Conclusions.

1. The alkoxide doping technique developed in this work produced doped powders of high homogeneity with minimal disruption to the other physical properties.

2. The distribution of the impurity phases in the microstructure was found to be dependent upon type of impurity and the sintering temperatures used:

(a) At low to intermediate sintering temperatures, alumina impurity formed inclusions within the microstructure.

(b) At sintering temperatures of 1650°C and above, the alumina inclusions reduced in both size and volume fraction, and the alumina appeared to go into solid solution in the zirconia grains. This would be a non equilibrium effect on cooling.

(c) The silica impurity tended to form a grain boundary phase, particularly at triple points in the microstructure. The amount of grain boundary phase appeared to increase with increasing sintering temperature.

(d) Titania impurity was distributed throughout the microstructure, in solid solution in the zirconia grains for all sintering temperatures.

3. Alumina impurity additions produced increased sintering activity at low temperatures, possibly due to a solid state mechanism involving an increase in vacancy concentration associated with substitution of Al^{3+} ions on Zr^{4+} lattice sites.

4. Alumina impurity additions produced rapid grain growth and associated destabilisation of the tetragonal phase, and de-densification of the sintered specimens.

5. Silica additions facilitated enhanced sintering at intermediate sintering temperatures (1250-1350°C, probably due to a liquid assisted sintering mechanism.

6. Silica additions produced a substantial increase in hardness at lower sintering temperatures, thought to be associated with the effects of the grain boundary phase on the nucleation of the martensitic phase transformation. This effect decreased with increasing sintering temperature and amount of grain boundary phase.

7. Titania additions produced a decrease in the sintering activity at low sintering temperatures, possibly due to a solid state mechanism involving a reduction in ionic mobility associated with a reduction in the concentration of mobile anion vacancies.

8. Titania additions produced a reduction in the amount of cubic phase formed during sintering, with a corresponding increase in the amount of retained tetragonal phase. This can be explained in terms of a shift in the position of the phase boundary between the tetragonal and the cubic plus tetragonal phase fields.

9. Titania additions produced an increase in fracture toughness and decrease in hardness in the sintered specimens. This was thought to be due to the increase in tetragonal phase content in the material.

10. The factorial experiments identified the presence of significant interactions between the impurities on the sintering behaviour, phase development and mechanical properties. The majority of these were associated with the formation of increased amounts of liquid phase during sintering of multiple doped materials, partitioning of the various oxides into these phases, and the effects of these phases on crack propagation and the nucleation of the tetragonal to monoclinic phase transformation.

11. Some of the impurity interactions, notably alumina plus titania suggest that improvements in the performance of Y-T.Z.P. may be attainable with appropriate additions of these oxides.

12. High chemical purity does not appear to be essential in the production of Y-T.Z.P. materials with good properties.

5.5 Suggestions for future work

There are a number of areas in which the work carried out in this study could be usefully extended by further work. The most significant of these are as follows:

(i) Although the doping process developed in this work was successful in producing homogenously doped powders, it did entail a great deal of effort and time in grinding and sieving the doped powders, which formed a solid "cake" on drying. This could also be a possible source of impurity contamination. It would be beneficial to further develop the process to avoid the formation of the solid cake of doped particles, and eliminate the grinding stage of the process. Possible ways in which this could be achieved include spray drying of the suspensions, or perhaps fluidised bed drying of the powders.

(ii) The microstructural determinations carried out in these studies were hampered by the limited resolution (particularly for the E.D.X. analysis techniques) of the scanning electron microscope compared to the grain size and thickness of grain boundary phases formed. It would be useful to carry out further studies using transmission electron microscopy to confirm the composition and distribution of the grain boundary and impurity inclusion phases.

(iii) Elucidation of the sintering mechanisms involved in the sintering of these materials requires further experiments involving determination of shrinkage during isothermal sintering.

(iv) The mechanical properties results carried out in this work did not include a determination of the effect of the variables measured on the strength of the sintered ceramic. This would be a useful area for further investigation, which would allow a more complete interpretation of the effects of the impurities.

(iv) The range of impurities investigated could be extended to cover other common T.Z.P. impurity oxides such as CaO, Fe_2O_3, Na_2O, and perhaps HfO_2.

References.

[1] Proceedings of International Seminar on Advanced Ceramics.
Hannover Messe Industrie '88, 26/4/1988.
Pub. Tosoh Corporation, Tokyo, Japan, (1988).

[2] Private Communication.
S. Jones, C. Norman, Alcan Chemicals ltd.
Gerrards Cross, M. Clubley, Magnesium Elektron,
Swinton, Manchester.

[3] Toyo-Soda Manufacturing Co. Ltd.
Fine Ceramics Dept. Tokyo, Japan.
(Now TOSOH Corporation).
Manufacturer's Technical Bulletins,
Numbers Z-003, Z-001, Z-010, (1989).

[4] A.H. Heuer and M. Ruhle.
"Phase Transformations in ZrO_2 Containing Ceramics-I. The Instability of c-ZrO_2 and the Resulting Diffusion Controlled Reactions."
Advances in Ceramics. Vol. 12, pp 1-13, (1984).

[5] A.H. Heuer.
"Transformation Toughening in ZrO_2 Containing Ceramics".
J. Am. Ceram. Soc. 70,[10], pp 689-698 (1987)

[6] O. Ruff, F. Ebert and E. Stephen.
"Contributions to the Ceramics of Highly Refractory - Materials II: The System Zirconia-Lime."
Z. Anorg. Allg. Chem. 180, [1], pp 215-224 (1929)

[7] C.E. Curtiss.
"Development of Zirconia Resistant to Thermal Shock".
J. Am. Ceram. Soc. 30, [6], pp 180-196 (1947)

[8] A.G. Karaulov, A.A. Grebenyuk and I.N. Rudyak.
"Effect of Phase Composition of Zirconium Dioxide on Spalling Resistance".
Izv. Akad. Nauk. SSSR, Neorg. Mater. 3, [6], pp 1101-1103 (1967).

[9] L.S. Alekseenko, I.S. Kainarskii and E.G. Degtyareva.
"Methods of Improving Spalling Resistance of Hot-Pressed Zirconia."
Ogneupory. 31, [12], pp 40-45 (1966).

[10] A.G. King and P.J. Yavorsky.
"Stress Relief Mechanisms in Magnesia and Yttria-Partially Stabilised Zirconia."
J. Am. Ceram. Soc. 51, [1], pp 38-42 (1968).

[11] R.C. Garvie.
"Theory of Enhanced Thermal Shock Resistance in Partially Stabilised Zirconia Ceramics."
Am. Ceram. Bull. 48, [8], pp 825. (1969)

[12] R.C. Garvie and P.S. Nicholson.
"Structure and Thermomechanical Properties of Partially Stabilised Zirconia in the $CaO-ZrO_2$ System".
J. Am. Ceram. Soc. 55, [3], pp 152-157. (1972)

[13] R.C. Garvie, R.H. Hannink and R.T. Pascoe.
"Ceramic Steel?"
Nature, 258, pp 703-704 (1975).

[14] D.L. Porter and A .H. Heuer.
"Mechanism of Toughening Partially Stabilised Zirconia".
J. Am. Ceram. Soc. 60, [3-4], pp 280-281 (1977).

[15] A.H. Heuer, F.F. Lang, M.V. Swain and A.G. Evans.
"Transformation Toughening: An Overview."
J. Am. Ceram. Soc. 69,[3], pp i-iv (1986).

[16] P. Rieth and J. Reed.
"Fabrication and Flexural Strength of Ultrafine-Grained Yttria Stabilised Zirconia".
Ceramic Bulletin, 55, [8], pp 717-727, (1976).

[17] E.C. Subbarao
"Zirconia, An Overview."
Advances in Ceramics, vol 3, pp 1-24, (1981)

[18] R. Stevens.
"An Introduction to Zirconia"
Magnesium Elektron Publication no. 113.
2nd ed.
Pub. Magnesium Elektron Ltd. (1986)

[19] I. Nettleship and R. Stevens.
"Tetragonal Zirconia Polycrystal (TZP), A Review".
Int. J. High Tech Ceramics, 3, pp 1-32, (1987).

[20] High Temperature Technology.
Pub. John Wiley and Sons, New-York. (1956)
Ed. I.E. Campbell.

[21] B.C. Weber.
"Inconsistencies in Zirconia Literature."
J. Am. Ceram. Soc. 45, [12], pp 614-615. (1962)

[22] D.K. Smith and C.F. Cline
"Verification of the Existence of Cubic Zirconia at High Temperatures"
J. Amer. Ceram. Soc. 45, [5], pp 249-250. (1962)

[23] V.S. Stubican, G.S. Corman, J.R. Hellmann and G. Senft.
"Phase Relationships in Some ZrO_2 Systems".
Advances in Ceramics, Vol. 12, pp 96-105 (1984)

[24] R.C. Garvie.
High Temperature Oxides, Part II.
Pub. Academic Press, New York. (1970)

[25] J.D. Mc Cullough and K.N. Trueblood.
"The Crystal Structure of Baddelyite (Monoclinic ZrO_2)."
Acta Cryst. 12, pp 507-511. (1959)

[26] V.M. Goldschmidt, T. Barth, D. Holmsen, G. Lunde, W. Zachariasen.
"Geochemical Distribution Law of the Elements VI, Crystal Structures of the Rutile Type, With Remarks on the Geochemistry of the Bivalent and Quadrivalent elements".
Skrifter Norske Videnskaps Akad. Oslo, Mat-Nat Kl. 1, pp 5-21, (1926).

[27] O. Ruff and F. Ebert.
"Contributions to the Ceramics of Highly Refractory Materials I:- The Forms of Zirconium Dioxide."
Z. Anorg U. Allg. Chem. 180, [1], pp 19-41, (1929).

[28] D.K. Smith and H.W. Newkirk.
"The Crystal Structure of Baddelyite (Monoclinic ZrO_2) and its Relation to the Polymorphism of ZrO_2".
Acta Cryst. 18, pp 983-991, (1965).

[29] G. Teuffer.
"The Crystal Structure of Tetragonal ZrO_2".
Acta Cryst. 15, pp 1187-1188, (1962).

[30] C.A. Andersson, J. Greggi and T.K. Gupta.
"Diffusionless Transformations in Zirconia Alloys".
Advances in Ceramics, Vol 12, pp 78-85, (1984).

[31] G.M. Wolten.
"Diffusionless Phase Transformations in Zirconia and Hafnia."
J. Am. Ceram. Soc. 46, [9], pp 418-422. (1963)

[32] E.C. Subbarao, H.S. Maiti and K.K. Srivastava.
"Martensistic Transformation in Zirconia".
Phys. Stat. Sol. A, 21, [9], pp 7-40, (1974).

[33] M. Ruhle and A.H. Heuer.
"Phase Transformations in ZrO_2 Ceramics II; The Martensitic Reaction in t-ZrO_2."
Advances in Ceramics , Vol. 12, pp 14-32, (1984).

[34] H.G. Scott.
"Phase Relationships in the Zirconia-Yttria System".
J. Mat. Sci 10, pp 1527-1535, (1975)

[35] A. Paterson and R. Stevens.
"Phase Analysis of Sintered Zirconia Ceramics by X Ray Diffraction."
J. Mat. Res. 1, [2], pp 295-298, (1986).

[36] R.A. Miller, J.L. Smialek and R.G. Garlick.
"Phase Stability in Plasme Sprayed, Partially Stabilised Zirconia".
Advances in Ceramics, Vol. 3, pp 241-253, (1981).

[37] T.S. Sheu and T.Y. Tien.
"Cubic to Tetragonal (t') Transformation in Zirconia Containing Systems."
J. Amer. Ceram. Soc, 75, [5], pp 1108-1116, (1992).

[38] H.S. Maiti, K.V. Gokhale and E.C. Subbarao.
"Kinetics and Burst Phenomenon in ZrO_2 Transformation".
J. Amer. Ceram. Soc. 55, [6], pp 317-322, (1972).

[39] G. S. Machlin and M. Cohen.
Trans. A.I.M.E. 191, p 746, (1951).

[40] L. Ma and M. Ruhle.
Unpublished work, cited in reference [43].

[41] M. Ruhle, A. Strecker, D. Waidelich and B. Kraus.
"In-Situ Observations of Stress Induced Phase Transformations in ZrO_2 Containing Ceramics.
Advances in Ceramics, Vol. 12, pp 256-274 (1984).

[42] M. Ruhle and A.H. Heuer
Proceedings of the 7th international Conference on High Voltage Electron Microscopy.
Ed. R.M. Fisher, R. Gronsky, K.H. Westmacott.
Pub. U.S. Dept. Commerce, (1983) p 359.

[43] T.H. Etsell and S.N. Flengas.
"The Electrical Properties of Solid Oxide Electrolytes".
Chem. Rev. 70, [3], pp 339-376, (1970).

[44] C.R. Catlow, A.V. CHadwick and G.N. Greaves
"EXAFS Study of Yttria Stabilised Zirconia"
J. Am. Ceram. Soc. [69], pp 272-277 (1986)

[45] M. Yashima, N. Ishizawa and M. Yoshimura.
"Application of an Ion Packing Model Based Upon Defect Clusters to Zirconia Solid Solutions: I, Modelling and Local Strcucture of Solid Solutions".
J. Am. Ceram. Soc. 75, [6], pp 1541-1549 (1992)

[46] R.C. Garvie.
"The Occurrence of Metastable Tetragonal Zirconia as a Crystalite Size Effect".
J. Phys. Chem. 69, pp 1238-1243, (1965).

[47] R.C. Garvie and M.F. Goss.
"Intrinsic Size Dependence of the Phase Transformation Temperature in Zirconia Microcrystals."
J. Mat. Sci, 21, pp 1253-1257, (1986).

[48] J.R. Hellmann and V.S. Stubican.
"Stable and Metastable Phase Relations in the System ZrO_2-CaO."
J. Am. Ceram. Soc. 66, [4] pp 260-264 (1983).

[49] C.F. Grain.
"Phase Relations in the ZrO_2-MgO System."
J. Am. Ceram. Soc, 50, [6], pp 288-290, (1967).

[50] L.S. Pauling.
"The Nature of the Chemical Bond". 3rd ed.
Pub. Cornell University Press, New York.

[51] I.J. McColm.
"Ceramic Science for Materials Technologists".
Pub. Leonard Hill, Glasgow. ISBN 0-249-44163-2

[52] H.Y. Lu and S.Y. Chen.
"Sintering and Compensation Effect of Donor and Acceptor Codoped 3 mol% Y_2O_3-ZrO_2".
J. Mat. Sci. 27, pp 4791-4796, (1992).

[53] R. Ruh and H.J. Garrett.
"Nonstoichiometry of ZrO_2 and its Relation to Tetragonal-Cubic Inversion in ZrO_2".
J. Am. Ceram. Soc 50, [5], pp 257-261, (1967).

[54] A.N. Cormack and S.C.Parker
"Some Observatons on the Role of Dopants in Phase Transitions in Zirconia from Atomistic Simulations."
J. Am. Ceram. Soc, 73, [11], pp 3220-3224, (1990)

[55] P. Duwez, F.H. Brown and F. Odell.
"Ziconia-Yttria System."
J. Electrochem. Soc, 98, p356, (1951).

[56] K.S. Masdiyasni, C.T. Lynch and J.S. Smith,
"Cubic Phase Stabilisation of Transluscent Yttria Zirconia at Very Low Temperatures".
J. Am. Ceram. Soc, 50, pp 532-537, (1967).

[57] K.K. Srivistana, R.N. Patil, C.B. Choudhart, K.V. Gokhale and E.C. Subbarao.
Trans. J. Brit. Ceram. Soc, 73, p85, (1974)

[58] V.S. Stubican, R.C. Hink and S.P. Ray.
"Phase Equilibria and Ordering in the System ZrO_2-Y_2O_3".
J. Am. Ceram. Soc, 61, [1] pp 17-21, (1971).

[59] C. Pascual and P. Duran.
"Subsolidus Phase Equilibria and Ordering in the System ZrO_2-Y_2O_3".
J. Am. Ceram. Soc, 66, [1] pp 23-27, (1983).

[60] V. Lanteri, A.H. Heuer and T.E. Mitchell.
"Tetragonal Phase in the System ZrO_2-Y_2O_3".
Advances in Ceramics, Vol 12, pp 118-130 (1984).

[61] W. H. Rhodes and R.E. Carter.
"Cationic Self Diffussion in Stabilised Zirconia".
J. Am Ceram Soc. 49, [5] pp 244-249, (1966).

[62] L. Rose and M.V. Swain,
"Two R Curves for Stabilised Zirconia".
J. Am Ceram Soc 69, [3], pp 203-207, (1986)

[63] M.V. Swain.
"Inelastic Deformation of Mg-PSZ and its Significance for Strength Toughness Relationships of Zirconia Toughened Ceramics".
Acta Metall. 33 pp 2083-2988 (1985).

[64] I. Wei Chen
"Implications of Transformation Plasticity in ZrO_2 Containing Ceramics II, Elastic-Plastic Indentation"
J. Am. Ceram. Soc, 69 [3] pp 189-194 (1986)

[65] I. Wei-Chen and P. Reyes Morel.
"Implications of Transformation Plasticity in ZrO_2 Containing Ceramics I, Shear and Dilatation Effects"
J. Am. Ceram. Soc. 69, [3], pp 181-189 (1986)

[66] R.W. Leslie.
"The Physical Metallurgy of Steels"
2nd ed. (1982)
Pub. Mc Graw Hill, London.

[67] S. Burns and M.V. Swain.
"Fracture Toughness of Mgo Partially Stabilised ZrO_2 Specimens with K_R curve Behaviour from Transformation Toughening."
J. Amer. Ceram. Soc. 69, [3] pp 226-230 (1986).

[68] W. Pompe and W. Kreher.
"Theoretical Approach to Energy Dissipative Mechanisms in Zirconia and Other Ceramics"
Advances in Ceramics, Vol 12, pp 283-292 (1984).

[69] A.G.Evans, D.B. Marshall and N.H. Burlingame.
"The Origin of Transformation Toughening in Ceramics"
Advances in Ceramics, Vol 3, pp 202-216, (1981).

[70] R. Mc Meeking and A. Evans.
"Mechanisms of Transformation Toughening in Brittle Materials".
J. Am. Ceram Soc. 65 [5], p 242 (1982).

[71] M.V. Swain and L.R.F. Rose.
"Strength Limitations of Transformation Toughened Zirconia Alloys"
J. Am. Ceram. Soc. 69,[7] pp 511-518. (1986).

[72] M.V. Swain and R.H.J. Hannink.
"R-Curve Behaviour in Zirconia Ceramics."
Advances in Ceramics, Vol.12, pp 225-239. (1984)

[73] H. Ewalds, R. Wanhill,
"Fracture Mechanics"
Pub. Edward Arnold, London (1984)

[74] D.B. Marshall.
"Strength Characteristics of Transformation Toughened Zirconia"
J. Am. Ceram. Soc. 69, [3], pp173-180, (1986).

[75] D.J. Green, F.F. Lange and M.R. James.
"Residual Surface Stresses in Al_2O_3 Composites".
Advances in Ceramics vol 12 pp 240-250 (1986).

[76] N. Claussen and M. Ruhle.
"Design of Transformation Toughened Ceramics".
Advances in Ceramics, Vol 3, pp 137-163 (1981).

[77] W.D. Kingery, H.K. Bowen and D.R. Uhlman.
"Introduction to Ceramics."
Pub. John Wiley and Sons, New York,
Second Ed. (1976).

[78] O.S. Narayanaswamy and R. Gardon.
"Calculation of Residual Stresses in Glass"
J. Amer. Ceram. Soc, 52, (1969) pp 554-558.

[79] D.J. Green and B.R. Maloney.
"Influence of Surface Stress on Indentation Cracking".
J. Amer. Ceram. Soc. 69, [3],pp 223-225, (1986).

[80] M. Watanabe, S. Iio and I. Fukuura.
"Ageing Behaviour of T.Z.P."
Advances in Ceramics, vol 12, pp 391-398 (1986)

[81] K. Nakajima, K. Kobayashi and Y. Murata.
"Phase Stability of Y-P.S.Z. in Aqueous Solutions."
Advances in Ceramics, vol 12, pp 399-407 (1986).

[82] J.J. Swab,
"Low Temperature Degradation of Y-T.Z.P Materials"
J. Mat. Sci, 26, pp 6706-6714 (1991)

[83] M. Hirano,
"Inhibition of Low Temperature Degradation of Tetragonal Zirconia Ceramics"
Br. Ceram. Trans. J., 91, pp 139-147, (1992)

[84] T. Masaki.
"Mechanical Properties of Y-PSZ After Ageing at Low Temperature."
Int. J. High Tech. Ceramics 2, p 85, (1986)

[85] T. Sato, S. Ohtaki and M. Shimada.
"Transformation of Yttrai Partially Stabilised Zirconia by Low Temperature Annnealing in Air".
J. Mat Sci, 20, p 1466 (1985).

[86] T. Sato and M. Shimada.
"Transformation of Yttria Doped Tetragonal Zirconia Polycrystals by Annealing in Water"
J. Am. Ceram. Soc. 68, p 356, (1985).

[87] F.F. Lange, G.L. Dunlop and B.I. Davis.
"Degradation During Ageing of Transformation Toughened ZrO_2-Y_2O_3 Materials at 250°C"
J. Am. Ceram Soc, 69, p 237, (1986).

[88] H. Schubert, N. Claussen and M. Ruhle.
"Surface Stabilisation of Y-TZP".
Proc. Brit. Ceram. Soc. 34, p157, (1984)

[89] K. Tsukama and M. Shimada.
"Thermal Stability of Y_2O_{32} Partially Stabilised Zirconia (Y-PSZ) and Y-PSZ/Al_2O_3 Composites".
J. Mat. Sci. Letters, 4, p 857, (1985)

[90] H. Hofmann, B. Michel and L.J. Gauckler.
"Zirconia Powder for TZP Ceramics, Ti-Y-TZP"
Zirconia 88, Advances in Zirconia Science and Technology. pp 119-129
ed. S. Meriani, C. Palmonari.
Pub. Elsevier, London.(1989).

[91] I.J. McColm and N.J. Clark.
"Forming, Shaping and Working of High Performance Ceramics".
Pub. Blackie and Son, London. First ed. (1988).

[92] F.F. Lange.
"Powder Processing Science and Technology for Increased Reliability."
J. Am. Ceram. Soc. 72, [1], pp 3-15, (1989).

[93] J.Y. Kim, M. Miyashita, N. Uchica and K. Uematsu.
"Change of Internal/Pore Structure in alumina
green body during initial sintering.
J. Mat Sci 27, pp 6609-6614 (1992)

[94] M.F. Ashby.
"Sintering Diagrams",
Acta Metall., [22] p 275, (1974).

[95] F.B. Swinkells and M.F. Ashby.
"A Second Report on Sintering Diagrams".
Acta Metall, [29], pp 259-281 (1980).

[96] R.L. Coble and J.E. Burke,
"Progress in Ceramic Science", Vol 3.
Ed. J. E. Burke,
Pub Pergamon Press (1963).

[97] R.J. Brook.
"Fabrication Principles for Ceramics with
Superior Mechanical Properties".
Proc. Brit. Ceram. Soc. [32], pp 7-24, (1987).

[98] W.D. Kingery and B Francois.
"The Sintering of Crystalline Oxides I."
in Sintering and Related Phenomena,
Ed G.C. Kuczynski et al.
Pub Gordon and Breach, New York (1967).

[99] R.J. Brook.
Treatise on Mat. Sci and Tech [9], p 331 (1976).

[100] H.J. Frost.
"Overview 17 - Cavities in Dense Random Packing"
Acta Metall, 30, [5] pp 899-904 (1982).

[101] B.J. Kellet and F.F. Lange.
"Thermodynamics of Densification: I, Sintering of
Simple Particle Arrays, Equilibrium Configurations,
Pore Stability, and Shrinkage"
J Am. Ceram Soc., 72, [5], pp725-734, (1989).

[102] F.F. Lange and M.J. Claussen.
"Some Processing Requirements for Transformation
Toughened Ceramics."
in "Ultrastructure Processing of Ceramics, Glasses,
and Composites".
Ed. R.C. Bradt et al.
Pub. J. Wiley, New York, (1984). p 493.

[103] J.H. Jean and T.K. Gupta.
"Liquid Phase Sintering in the Glass-Cordierite
System".
J.Mat. Sci 27, (1992) pp 1575-1584.

[104] T.J. Whale and M. Humenik.
"Sintering in the Presence of a Liquid Phase".
in "Sintering and Related Phenomena",
Ed. G.C. Kuczynski et al.
Pub. Gordon and Breach, New York (1967), (p715)

[105] W.J. Huppman and H. Riegger.
"Modelling of Rearrangement Processes in Liquid Phase Sintering"
Acta Metall, 23, pp 965-971, (1975).

[106] W.D. Kingery.
"Densification during Sintering in the Presence of a Liquid Phase I. - Theory".
J. Appl. Phys. 30, pp 301-306, (1959).

[107] J. W. Cahn and R.B. Heady.
"Analysis of Cappillry Forces in Liquid Phase Sintering of Jagged Particles".
J. Am. Ceram. Soc. 53, p 406, (1970).

[108] S.J.L. Kang, K.H. Kim and D.N. Yoon
"Densification and Shrinkage During Liquid Phase Sintering".
J. Am. Ceram. Soc. 74, [2], pp 425-427, (1991)

[109] B. Jackson, W Ford and J. White.
"The Influence of Cr_2O_3 and Fe_2O_3 on the Wetting of Periclase Grains by Liquid Silicate".
Trans. Brit. Ceram. Soc. 62 pp 577-601, (1963)

[110] J.H. Jean and C.H. Lin.
"Coarsening of Tungsten Particles in W-Ni-Fe Alloys".
J. Mater Sci, 24, p 500, (1989).

[111] S-X. Wu.
"Sintering Additives for Zirconia Ceramics."
PhD Thesis, University of Leeds (1982)

[112] J.W. Cahn.
"The Impurity Drag Effect in Grain Boundary Motion".
Acta Met. 10, pp. 789-798, (1962).

[113] P.J. Jorgensen and J.H. Westbrook.
"Role of Solute Segregation at Grain Boundaries During Final Stage Sintering of Alumina".
J. Am. Ceram. Soc. 47, pp 332-338, (1964)

[114] F.A. Kroger and V.J. Vink.
"Solid State Physics", Vol. 3. p307-435 (1966).
Eds. F. Seitz, D. Turnbull.
Pub. Academic Press.

[115] P. Pena, P. Miranzo, J.S. Moya and S. De Aza.
"Multicomponent toughened ceramic materials obtained by reaction sintering - Part 1 ZrO_2-Al_2O_3-SiO_2-CaO System".
J. Mat Sci. 20 (1985) pp 2011-2022.

[116] K. Kendall.
"Influence of Powder Structure on Processing and Properties of Advanced Ceramics"
Powder Technology, 58, pp 151-161, (1989).

[117] N. Mc Alford, J.D. Birchall and K. Kendall.
"High Strength Ceramics Through Colloidal Control to Remove Defects".
Nature, 330, pp 51-53, (1987).

[118] J. Sung and P.S. Nicholson.
"Strength improvement if Yttria Partially Stabilised Zirconia by Flaw Elimination."
J. Am. Ceram. Soc. 71, [9], pp 788-795, (1988)

[119] W.F.M. Groot Zevart, A.J. Winnubst, GS. Theunissen, and A.J. Burgraaf.
"Powder Preparation and Compaction Behaviour of Fine Grained Y-TZP."
J. Mat Sci 25 (1990) pp 3449-3455.

[120] J.Y. Kim. M. Miyashita, M. Inoue, N. Uchida, K. Saito, and K. Uematsu.
"Characterisation of Internal Structure of Y-TZP Powder Compacts."
J. Mat Sci. 27, pp 587-591, (1992).

[121] J.L. Shi, J.H. Gao, Z.X. Lin, and D.S. Yan.
"Effect of Agglomerates in ZrO_2 Powder Compacts on Microstructural Development"
J. Mat. Sci. 28, p 342-348 (1993).

[122] M. Ruhle, N. Claussen, and A.H. Heuer.
"Microstructural studies of Y_2O_3 containing Tetragonal Zirconia Polycrystals (Y-TZP)."
Advances in Ceramics, Vol.12, pp 352-371. (1984)

[123] G.S. Theunissen, A.J. Winnubst, W.F. Groot Zevert, and A.J. Burgraaf.
"Microstructure Development During Sintering of Ultra Fine Grained Y-T.Z.P."
In "Zirconia '88, Advances in Zirconia Science and Technology". (pp 325-336)
Pub. Elsevier, New York (1989)

[124] W.S. Young and I.B. Cutler.
"Initial Sintering with Constant Rates of Heating".
J. Am. Ceram. Soc. 53, pp 659-663, (1970).

[125] S.X. Wu and R.J. Brook.
"Kinetics of Densification in Stabilised Zirconia"
Solid State Ionics, 14, pp 123-130, (1984).

[126] E.B. Slamovich and F.F. Lange.
"Densification of Large Pores: I, Experiments"
J. Am. Ceram. Soc. 75, [9], pp 2498-2508. (1992).

[127] F.F. Lange.
"Transformation toughening - part 3: Experimental Observations in the ZrO_2-Y_2O_3 system".
J. Mat. Sci. 17, p240, (1982).

[128] A.J. Winnubst and A.J. Burgraaf.
Advances in Ceramics, Vol 24, p 39, (1989)
Ed. S. Sorniya et al.
Pub. Amer. Ceram. Soc.

[129] T.K. Gupta.
"Sintering of Tetragonal Zirconia and its Characteristics".
Sci. of Sint. 10, p 205, (1978).

[130] K. Tsukama, Y. Kubota and T. Tsukidate.
"Thermal and Mechanical Properties of Y_2O_3 Stabilised Tertagonal Zirconia Polycrystals".
Advances in Ceramics, Vol.12, pp 382-390. (1984)

[131] Magnesium Elektron ltd.
Manchester, England.
Manufacturer's Data Sheet No. 307.

[132] Zirconia Sales (U.K.) Ltd.
Lightwater, Surrey, U.K.
Manufacturer's Data.

[133] T.E. Garnar.
"Zircon". (annual minerals review).
Ceramic Bulletin, 68, [5], pp 1029-1074, (1989).

[134] T.K. Gupta, J.H. Bechtold, R.C. Kuzicnici, L.H. Cadoff and B.R. Rossing.
"Stabilisation of Tetragonal Phase in Polycrystalline Zirconia"
J. Mat Sci., 12, pp 2421-2426, (1977).

[135] Phase Diagrams for Ceramists.
1975 Supplement.
Eds. E.M. Levin, H.F. McMurdie and M.K. Reser.
Pub. Amer. Ceram. Soc, Columbus, Ohio (1975).
Figure 4378- "System Al_2O_3-ZrO_2 in Air".

[136] Phase Diagrams for Ceramists.
Volume VI.
Eds. R.S. Roth, J.R. Dennis and H.F. McMurdie.
Pub. Amer. Ceram. Soc, Columbus, Ohio.
Figure 6514 - "System ZrO_2-SiO_2 (calculated)".

[137] Phase Diagrams for Ceramists.
Volume VI.
Eds. R.S. Roth, J.R. Dennis and H.F. McMurdie.
Pub. Amer. Ceram. Soc, Columbus, Ohio.
Figure 6521 - "System TiO_2-ZrO_2".

[138] Phase Diagrams for Ceramists.
Volume VI.
Eds. R.S. Roth, J.R. Dennis and H.F. McMurdie.
Pub. Amer. Ceram. Soc, Columbus, Ohio.
Figure 6825- "System Al_2O_3-Y_2O_3-ZrO_2 at 1450^oC".

[139] E.M. Levin, C.R. Robbins and H.F. Mc Hurdie.
"Phase Diagrams for Ceramists".
Ed. M.K. Reser.
Pub. Am. Ceram. Soc, Columbus, Ohio, (1964)
Figure 311.

[140] P. Pena and S. De Aza.
"The Zircon Thermal Behaviour; - Effect of
Impurities, Part 1."
J. Mat Sci, 19, pp 135-142, (1984).

[141] P. Pena, F. Guitian and S. De Aza.
"The Zircon Thermal Behaviour;- Effect of
Impurities, Part 2".
J. Mat. Sci, 19, pp 143-149, (1984).

[142] M.F. Melo, J.S. Moya, P. Pena and S. De Aza.
"Multicomponent toughened Ceramic Materials
Obtained Through Reaction Sintering - Part 3:
System ZrO_2-Al_2O_3-SiO_2-TiO_2."
J. Mat Sci, 20, pp2711-2718, (1985).

[143] M.J. Hyatt and D.E. Day.
"Glass Properties in the Yttria-Alumina-Silica
System".
Com. Am. Ceram. Soc., 70, [10], pp 283-287, (1987).

[144] F.F. Lange and M.M. Hirlinger,
"Hindrance of Grain Growth in Al_2O_3 by ZrO_2
Inclusions"
J. Am. Ceram. Soc. 67,[3], pp 164-168, (1984)

[145] N. Claussen.
"Microstructural design of Zirconia Toughened
Ceramics."
Advances in Ceramics, Vol.12, pp 325-351. (1984)

[146] M. Ruhle, M. Bischoff and O. David.
"Structure of Grain Boundaries in Ceramics."
Ultramicroscopy, 14, pp.37-46, (1984).

[147] M. Verkeerk, J. Middelhuis and A. Burgraaf.
"Effect of Grain Boundaries on the Conductivity of
High Purity ZrO_2-Y_2O_3 Ceramics."
Solid State Ionics, [6], pp. 159-170, (1982).

[148] J.F. Shackelford, P.S. Nicholson and W.F. Smeltzer.
"Influence of SiO_2 on Sintering of Partially Stabilised Zirconia".
Bull Am. Ceram Soc. 53, [12], (1974).

[149] D.V. Mallinckrodt, P. Reynen and C. Zografou.
"The Effect of Impurities on Sintering and Stabilisation of ZrO_2 (CaO)."
Interceram, 2, pp 126-129, (1982)

[150] M.L. Mecartney.
"Influence of Amorphous Second Phase on the Properties of Yttria Stabilised Tetragonal Zirconia Poycrystals (Y-TZP)"
J. Am. Ceram Soc, 70, [1], pp 54-58, (1987).

[151] Y.J. Lin, P. Angelini and M. Mecartney.
"Microstructural and Chemical Influences of Silicate Grain Boundary Phases in Yttria Stabilised Zirconia".
J. Am. Ceram Soc, 73, [9], pp 2728-2735, (1990)

[152] K.C. Radford and R.J. Bratton.
"Zirconia Electrolyte Cells - Part 1: Sintering Studies".
J. Mat. Sci. 14, pp59-65, (1979).

[153] E.P. Butler and J. Drennan.
"Microstructural Analysis of Sintered High Conductivity Zirconia with Al_2O_3 Addittions".
J. Am. Ceram. Soc. 65, [10], pp 474-478, (1982).

[154] H. Tsubakino, R. Nozato and R. Hamamoto.
"Effect of Alumina Addittion on The Tetragonal-Monoclinic Phase Transformation in ZrO_2 -3 mol% Y_2O_3".
J. Am. Ceram. Soc. 74, [2], pp 440-443, (1991).

[155] T. Stoto, M. Nauer and C. Carry.
"Influence of Residual Impurities on Phase Partitioning and Grain Growth Processes of Y-TZP Materials".
J. Am. Ceram. Soc. 74, [10], pp 2615-2621, (1991).

[156] H. Bernard.
"Sintered Stabilised Zirconia Microstructure and Conductivity"
Report CEA-R-5090.
Pub. Commissariat a l'Energia Atomique,
CEN- Saclay, France, (1981).

[157] G. Rossi and C.E. Knapp.
"Microstructure and Mechanical Properties of Y_2O_3-ZrO_2 Toughened Ceramics".
High Temperatures - High Pressures, 20,[3], pp 315-323, (1988).

[158] R.V. Wilhelm and D.S. Howarth.
"Iron Oxide Doped Yttria Stabilised Zirconia Ceramic :- Iron Solubility and Electrical Conductivity"
J. Am. Ceram. Soc. 58, [2], pp. 228-232, (1979).

[159] H.Y. Lu and S.Y. Chen.
"Sintering and Compensation Effect of Donor and Acceptor Codoped 3 mol% Y_2O_3-ZrO_2".
J. Mat. Sci. 27, pp 4791-4796, (1992).

[160] F.F. Lange, H. Shubert, N. Claussen and M. Ruhle.
"Effects of Attrittion Milling and Post Sintering Heat Treatment on Fabrication, Microstructure, and Properties of Transformation Toughened ZrO_2".
J. Mat. Sci., 21, pp 768-774, (1986).

[161] K.C. Radford and R.J. Bratton.
"Zirconia Electrolyte Cells, Part 2:- Electrical Properties".
J. Mat. Sci 14, pp. 66-69, (1979).

[162] G.S. Theunissen, A.J. Winubst and A.J. Burgraaf.
"Surface and Grain Boundary Analysis of Doped Zirconia Ceramics Studied by AES and XPS"
J. Mat. Sci, 27, pp 5057-5066, (1992).

[163] E. Zschech, P. Kountouros and G. Petzow.
"Synchotron Radiation Ti-k XANES Study of TiO_2-Y_2O_3 Stabilised Tetragonal Zirconia Polycrystals".
J. Am. Ceram. Soc. 76, [11], pp 197-201, (1993).

[164] T. Sato, S. Ohtaki, T. Endo and M. Shimada.
"Improvement of Thermal Stability of Y Doped Tetragonal Zirconia Polycrystals of Alloying with Various Oxides".
Int. J. High. Tech. Ceramics, 2, (1986), p167.

[165] J. Wang, M. Rainforth and R. Stevens.
"The Grain Size Dependence of the Mechanical Properties in T.Z.P. Ceramics"
Br. Ceram. Trans. J., 88, pp1-6, (1989).

[166] H. Tsubakino, R. Nozato and R. Hamamoto.
"Effect of Alumina Addittion on The Tetragonal-Monoclinic Phase Transformation in ZrO_2 -3 mol% Y_2O_3".
J. Am. Ceram. Soc. 74, [2], pp 440-443, (1991).

[167] T. Sato and M. Shimada.
"Control of the Tetragonal to Monoclinic Phase Transformation of Y_2O_3 PSZ in Hot Water".
J. Mat. Sci. 20, p 3988, (1985).

[168] G.F. Tu, Z.T. Sui, Q. Huang and C.Z. Wang.
"Sol-Gel Processed Y-P.S.Z. Ceramics with 5 wt% Al_2O_3."
J. Am. Ceram Soc. 75, [4] p 1032-1034, (1992)

[169] J. Williams.
"Mixing and Segregation in Powders."
in "Principles of Powder Technology"
ed. M. Rhodes.
Pub. John Wiley and Sons, Chichester, England.
ISBN 0-471-92422

[170] P.M.C. Lacey.
"Mixing of Solid particles I: Application of Theory to Practice"
Chem. Age, 53, pp 119-124, (1945).

[171] D. Buslik.
"Mixing and Sampling with Special Reference to Multi Sized Granular Material".
A.S.T.M. Bull., [165], pp 66-73 (1950)

[172] P.F. Messer,
Department of Ceramics, Glasses and Polymers,
University of Sheffield.
"Uniformity in Processing".
Unpublished Work.

[173] Y. Lin and P.F. Messer.
"Mixing Prior to Calcination"
Br. Ceram. Trans. J., 86, pp 85-90 (1987)

[174] R. Hogg.
"Grinding and Mixing of Non-Metallic Powders."
Ceramic Bulletin, 60, [2], pp 206-211, (1981)

[175] P.M.C. Lacey.
"Developments in the Theory of Particles Mixing"
J. Apl. Chem., 4, pp 257-268, (1954).

[176] K.R. Poole, R.F. Taylor and G.P. Wall.
"Mixing Powders to Fine Scale Homogeneity, Studies of Batch Mixing."
Trans. Inst. Chem. Eng., 42 [8] T305-315 (1964)

[177] S. Weidenbaum.
"Mixing of Solids"
in Advances in Chemical Engineering, Vol. II,
pp 211-321, (1958)
ed. T. Drew, J. Hoopes.
Pub. Academic Press, New York.

[178] K. Hyun and L. Marc de Chazal.
"A Statistical Definition of Perfect Mixtures of Solids of Different Sizes."
Ind. Eng. Chem. Process Des.Dev.,
5, [2], pp 105-110, (1966).

[179] K. Stange.
"Mixing Quality in a Random Mixture of Three or More Components".
Chem. Ing. Tech., 35, [8], pp 580-582, (1963).

[180] L. Levene and I. Thomas. (Owens-Illinois inc.)
U.S. Patent no. 3,640,093. 8th February 1972

[181] H. Dislich.
"New Routes to multicomponent Oxide Glasses."
Angewandte Chemie, Int. ed. 10, pp 363-370,
(1971).

[182] H. Schroeder and G. Gliemroth.
(J.Glaswerk Schott and Gen.)
U.S. Patent no. 3,597,252. 3rd August 1971.

[183] D.M. Roy and R. Roy.
"Synthesis and Stability of Minerals in the System $MgO-Al_2O_3-SiO_2-H_2O$".
American Mineralogist, 40, pp 147-178, (1955).

[184] H. Schroeder.
"Oxide Layer Deposited From Organic Solutions"
in "Physics of Thin Films", Vol. 3,
pp. 87-141 (1969).
Ed. G. Hass, R. Thun.

[185] H. Dislich and P. Hinz.
"History and Principles of the Sol-Gel Process and
Some New Multi-Component Oxide Coatings."
J. Non Cryst. Solids, 48, pp 11-16, (1982).

[186] I.M. Thomas.
"Multi-Component Glasses from the Sol-Gel Process."
In "Sol-Gel Technology". pp 1-15
Ed. L.C. Klein.
Pub. Noyes Publications, New Jersey, U.S.A.

[187] B.E. Yoldas.
"Preparation of Glasses and Ceramics from Metal-
Organic Compounds."
J. Mater. Sci. 12, pp 1203-1208, (1977)

[188] K.S. Mazdyansi, C.T. Lynch and J.S. Smith.
"Cubic Phase Stabilisation of Yttria-Zirconia at
Very Low Temperatures".
Proc. 78th Ann. Meet. of American Ceramic Soc.
Ceramic Bulletin, 45, [4], p 367. (1966).

[189] K. Uchimimyama, T. Ogihara, T. Ikemoto, N.
Mizutani and M. Kato
"Preparation of Monodispersed Y Doped T.Z.P.
Powders".
J. Mater. Sci. 22, pp 4343-4347, (1987).

[190] M. Yamane, S. Inoue and K. Nakazawa.
"Preparation of Gels to Obtain Glasses of High
Homogeneity by Low Temperature Synthesis".
J. Non. Cryst. Solids, 48, pp 153-159, (1982)

[191] H. Dislich.
"Glassy and Crystalline Systems from Gels, Chemical Basis, and Technical Application."
J. Non Cryst. Solids, 57, pp 371-388, (1983).

[192] S.P. Mukherjee, J. Zarzycki, J. Traverse.
"A Comparative Study of "Gels" and Oxide Mixtures as Starting Materials for the Nucleation and Crystallisation of Silicate Glasses".
J. Mater. Sci. 11, pp 341-355, (1976).

[193] C.J. Brinker, G.W. Scherer, E.P. Roth.
"Sol->Gel->Glass II, Physical and Structural Evolution During Constant Heating Rate Experiments."
J. Non Cryst Solids, 72, pp 345-368, (1985).

[194] G.W. Scherer, C.J. Brinker, E.P. Roth.
"Sol->Gel->Glass III, Viscous Sintering"
J. Non Cryst. Solids, 72, pp 369-389, (1985).

[195] L.C. Klein.
"Sol-Gel Processing of Silicates"
Ann Rev. Mater. Sci. 15, pp 227-248, (1985).

[196] R.W. Jones.
"Fundamental Principles of Sol-Gel Technology."
Pub. The Institute of Metals, London, (1990).

[197] R. C. Mehrotra
"Polymetallic Alkoxides, Precursors for Ceramics."
Mat. Res. Soc. Symp. Proc. 121, pp 81-92, (1988).

[198] D.C. Bradley, R.C. Mehrotra and D. Gaur.
"Metal Alkoxides".
Pub. Academic Press, New York (1978).

[199] D.P. Partlow and B.E. Yoldas.
"Colloidal Versus Polymer Gels, and Monolithic Transformation in Glass Forming Systems".
J. Non Cryst. Solids, 46, pp 153-161, (1981).

[200] B.E. Yoldas
"Alumina Sol Preparation From Alkoxides"
Bull. Am. Ceram. Soc. 54, [3], pp 289-290, (1975).

[201] B.E. Yoldas.
"Zirconium Oxides Formed by Hydrolytic Polycondensation and Factors that Affect their Morphology".
J. Mat. Sci. 21, pp 1080-1086, (1986).

[202] B.E. Yoldas.
"Hydrolysis of Titanium Alkoxide, and effects of Hydrolytic Polycondensation Parameters".
J. Mater. Sci. 21, pp 1087-1092, (1986).

[203] C.J. Brinker and G.W. Scherer.
"Sol-Gel-Glass I: Gelation and Gel Structure".
J. Non Cryst. Solids. 87, pp 301-322, (1985).

[204] E. Pope and J. Mackenzie.
"Sol-Gel Processing of Silica II - The Role of the Catalyst".
J. Non Cryst. Solids. 87, pp 185-198, (1986)

[205] C. Brinker, K, Keefer, D. Schaefer and C. Ashley.
"Sol-Gel Transition in Simple Silicates".
J. Non Cryst. Solids. 48, pp 47-64, (1982).

[206] L.C. Klein and G. Garvey.
"Kinetics of the Sol/Gel Transition"
J. Non Cryst. Solids, 38/39, pp 45-50, (1980).

[207] A. Ayral, J. Phalippou and J. Droguet.
"Alumina Powders from Aluminium Alkoxide."
Mat. Res. Soc. Symp. Proc 121, pp 239-244, (1988).

[208] J. Livage.
"Synthesis, Structure, and Applications of TiO_2 Gels".
Mat. Res. Soc. Symp. Proc. 73, pp 717-724, (1986).

[209] G.E.P. Box, W.G. Hunter and J.S. Hunter.
"Statistics for Experimenters".
Pub. John Wiley & Sons, New York (1978).

[210] D.C. Montgomery.
"Design and Analysis of Experiments".
Pub. John Wiley & Sons, 2nd ed. (1984).

[211] J.A. John and M.H. Quenouille.
"Experiments, Design and Analysis."
Pub. Griffin, London, (1977).

[212] O.L. Davies (ed).
"The Design and Analysis of Industrial Experiments".
Pub. Oliver and Boyd, London. 2nd ed. (1956)

[213] C. Daniel.
"Applications of Statistics to Industrial Experimentation."
Pub. John Wiley and Sons, New York, (1976).

[214] R.A. Fisher.
"The Arrangement of Field Experiments"
J. Ministry of Agriculture, Vol XXXIII, pp 503-513, (1926).

[215] R.A. Fisher and J. Wishart.
"The Arrangement of Field Experiments, and the Statistical Reduction of the Results".
Imperial Bureau of Soil Science,
Tech. Comm. No. 10, (1930).

[216] F. Yates.
"The Design and Analysis of Factorial Experiments."
Imperial Bureau of Soil Science,
Tech. Comm. No. 35, (1937).

[217] G.E.P. Box and N.R. Draper.
"Evolutionary Operation".
Pub. John Wiley, New York, (1969).

[218] M.W. Weiser and K.B. Fong.
"Experimental Design for Improved Ceramic Processing - Emphasising the Taguchi Method".
Bull. Am. Ceram. Soc. 72, [12], pp 87-92, (1993)

[219] M.S. Marschner.
"Additives for Processing Alumina Ceramics"
PhD thesis, Rutgers University, (1992).

[220] O. Grossmann and A.N. Turanov.
"Spectrophotometric Multi-Component Determination of yttrium, Barium, and Copper in microsamples of $YBa_2Cu_3O_x$ Ceramics"
Anal. Chim. Acta, 257, [2], pp 195-202, (1992).

[221] G. Pouskouleli and T.A. Wheat.
"Statistical Design in Ceramics I - Role of Statistics in Materials Development and Production".
Canad. Ceram. Quart., 59, [4], pp 41-46, (1990).

[222] J.G. Malinka, D.J. Varacalle and W.L. Riggs.
"Thermal Sprayed Tiatnia Coatings Using Liquid Stabilised Plasma Technology".
In Conference Proceedings
International Advances in Coating Technology,
Orlando, Florida, May-June 1992.
Pub ASM International, Ohio, pp 87-92, (1992).

[223] R.L. Allor, T.J. Whalen, J.R. Baer and K.V. Kumar.
"Machining of Silicon Nitride, Experimental Determination of Process/Property Relationships".
in Conference Proceedings
Machining of Advanced Materials, Maryland, USA.
July 1993.
NIST Special Publication 847, pp 223-234, (1993).

[224] F. Singer and S.S. Singer.
"Industrial Ceramics"
Pub. Chapman and Hall, London, (1963).

[225] L.A Lay.
"Metallographic Procedures for Advanced Ceramics.
Metals and Materials, 7, [9], pp 543-547, (1991).

[226] R.C. Garvie and P.S. Nicholson.
"Phase Analysis in Zirconia Systems".
J. Am. Ceram. Soc. 55, [6], pp 303-305, (1972).

[227] H.P. Klug and L.E. Alexander.
"X-Ray Diffraction Procedures".
Pub. John Wiley and Sons, New York, (1954)

[228] D.L. Porter and A.H. Heuer.
"Microstructural Development in Mgo Partially
Stabilised Zirconia (Mg-PSZ)".
J. Am. Ceram. Soc. 62, [5-5], pp 298-305, (1979).

[229] P.A. Evans, R. Stevens and J.G. Binner.
"Quantitative X-Ray Diffraction Analysis of
Polymorphic Mixes of Pure Zirconia".
Br. Ceram. Trans. J. 83, pp 39-43, (1984)

[230] A. Paterson and R. Stevens.
"Phase Diffraction of Sintered Yttria Zirconia
Ceramics by X-Ray Diffraction."
J. Mat. Res. 1, [2], pp 295-299, (1986).

[231] A.G. Evans and E.A. Charles.
"Fracture Toughness Determinations by
Indentation".
J. Am. Ceram. Soc. 59, [7-8], pp 371-372, (1976).

[232] B. Lawn and R. Wilshaw.
"Review, Indentation Fracture: Principles and
Applications".
J. Mat. Sci. 10, pp 1049-1081, (1975).

[233] D.J. Green and B.R. Maloney.
"Influence of Surface Stress on Indentation
Cracking".
J. Am. Ceram. Soc. 69, [3], pp 223-225, (1986).

[234] K. Niihara, R. Morena and D.P. Hasselman.
"Evaluation of K_{1c} of Brittle Solids by the
Indentation Method with Low Crack to Indent
Ratios".
J. Mat. Sci. Letts. 1, pp 13-16, (1982).

[235] H.G. Gemmell
"The Characterisation of Hot Pressed Zirconia
-Yttria Compacts".
Final Year BEng Project, Sheffield City
Polytechnic, (1988)

[236] M.I. Mendelson.
"Average Grain Size in Polycrystalline Ceramics"
J. Am. Ceram. Soc, 52, [8], pp 443-446, (1969).

[237] M. Kihara, T. Ogata, K. Nakamura and K. Kobayashi.
"Effect of Al_2O_3 Addition on Mechanical Properties
and Microstructures of Y-T.Z.P."
J. Jpn. Ceram. Soc., 96, pp 643-653, (1988).

Contents.

Appendix 1. - Tables of Experimental Data.

Table 4.2.1 (a)

Estimation of measuring error in shrinkage measurements for doped and undoped specimens.

Undoped specimens.
average for all sinter temperatures.

	Mean value of Std. Deviation in Shrinkage (%)	Mean value of 95% confidence limits (plus or minus)
Powder 15 (TZ3Y powder, as supplied)	0.10 %	0.06 %
Powder 11 (blank treatment)	0.07 %	0.04 %
Average, all undoped samples.	0.09 %	0.06 %

Al_2O_3 doped specimens.
average for all sinter temperatures.

	Mean value of Std. Deviation in Shrinkage (%)	Mean value of 95% confidence limits (plus or minus)
Powder 1 (0.25% Al_2O_3)	0.10 %	0.06 %
Powder 18 (0.5% Al_2O_3)	0.05 %	0.03 %
Powder 2 (0.75% Al_2O_3)	0.09 %	0.06 %
Powder 13 (1% Al_2O_3)	0.07 %	0.04 %
Average, all Al_2O_3 doped samples.	0.08 %	0.05 %

SiO_2 doped specimens.
average for all sinter temperatures.

	Mean value of Std. Deviation in Shrinkage (%)	Mean value of 95% confidence limits (plus or minus)
Powder 5 (0.25% SiO_2)	0.09 %	0.06 %
Powder 17 (0.5% SiO_2)	0.06 %	0.04 %
Powder 7 (0.75% SiO_2)	0.07 %	0.04 %
Powder 3 (1% SiO_2)	0.14 %	0.09 %
Average, all SiO_2 doped samples.	0.09 %	0.06 %

Table 4.2.1 (a)

Estimation of measuring error in shrinkage measurements for doped and undoped specimens (continued...).

TiO_2 doped specimens.
average for all sinter temperatures.

	Mean value of Std. Deviation in Shrinkage (%)	Mean value of 95% confidence limits (plus or minus)
Powder 4 (0.25% TiO_2)	0.13 %	0.08 %
Powder 19 (0.5% TiO_2)	0.06 %	0.04 %
Powder 8 (0.75% TiO_2)	0.09 %	0.06 %
Powder 12 (1% TiO_2)	0.07 %	0.04 %
Average, all TiO_2 doped samples.	0.09 %	0.06 %

Multiple doped specimens.
average for all sinter temperatures.

	Mean value of Std. Deviation in Shrinkage (%)	Mean value of 95% confidence limits (plus or minus)
Powder 6	0.11 %	0.07 %
Powder 9	0.08 %	0.05 %
Powder 14	0.06 %	0.04 %
Powder 10	0.06 %	0.04 %
Average, multiple doped samples.	0.08 %	0.05 %

Average values for all dopant additions.

(All sinter temperatures).

Mean value of Standard Deviation (shrinkage) = 0.09%

Mean value of 95% confidence limits = (+ or -) 0.06%

Table 4.2.1 (b).

Estimate of experimental error using duplicate samples from same doped powder batch (method (b)).

Sintering Temperature (°C)	950	1050	1150	1250	1350	1450	1550	1650	1700	1750
	Linear shrinkage (%).									
0.75% SiO_2 Powder 7.	1.32	5.04	13.75	20.87	21.93	21.66	21.53	21.48	21.46	21.59
Powder 7 (duplicate).	0.63	4.47	13.75	20.39	21.45	21.58	21.28	21.23	21.32	21.26
| difference |	0.69	0.57	0.00	0.48	0.48	0.08	0.25	0.25	0.14	0.33

Sintering Temperature (°C)	950	1050	1150	1250	1350	1450	1550	1650	1700	1750
	Linear shrinkage (%).									
0.75% TiO_2 Powder 8.	0.78	2.09	8.66	19.04	22.19	23.13	23.37	22.98	22.67	22.79
Powder 8 (duplicate).	0.52	1.66	9.79	18.87	21.90	23.03	23.02	22.98	22.96	22.79
| difference |	0.26	0.43	1.13	0.17	0.29	0.10	0.35	0.00	0.29	0.00

Estimated error (average for all sintering temperatures).

0.75% SiO_2 doped samples

Mean difference (between samples)	0.33
Std. Dev. in Difference.	0.21
Std. Error in Difference.	0.07
95% Confidence limit error <	+/- 0.06

Estimated error (average for all sintering temperatures).

0.75% TiO_2 doped samples

Mean difference (between samples)	0.30
Std. Dev. in Difference.	0.31
Std. Error in Difference.	0.10
95% Confidence limit error <	+/- 0.49

Estimated error (average for all sintering temperatures).

Combined results for 0.75% SiO_2 and TiO_2 doped samples.

Mean difference (between samples)	0.31
Std. Dev. in Difference.	0.26
Std. Error in Difference.	0.06
95% Confidence limit error <	+/- 0.43

Table 4.2.1(c) Estimate of total experimental error from repeat powder batches (method (c)).

Sintering Temperature (°C)	950	1050	1150	1250	1350	1450	1550	1650	1700	1750
	Linear shrinkage (%).									
0.25% Al_2O_3 Powder 1.	1.12	8.41	19.69	22.89	23.08	23.09	23.31	23.15	22.68	22.79
Powder 20.	0.92	8.07	18.10	22.09	22.70	22.51	22.88	22.61	22.81	22.61
| difference |	0.19	0.35	1.58	0.79	0.38	0.58	0.43	0.55	0.13	0.18

Sintering Temperature (°C)	950	1050	1150	1250	1350	1450	1550	1650	1700	1750
	Linear shrinkage (%).									
0.75% Al_2O_3 Powder 1.	1.41	9.78	20.96	22.63	22.62	23.14	23.14	22.74	21.71	21.13
Powder 16	1.02	9.93	20.64	23.11	23.29	23.28	23.51	22.75	22.26	21.50
| difference |	0.39	0.15	0.32	0.48	0.67	0.14	0.37	0.02	0.55	0.37

Estimated experimental error (average for all sintering temperatures).

Mean difference (between samples)	0.43
Std. Dev. in Difference.	0.33
Std. Error in Difference.	0.07
95% Confidence limit error <	+/- 0.57

Table 4.2.2 (a)

Shrinkage results. Undoped TZ3Y Powder, as received from manufacturer.

Powder 15: (TZ3Y Unmodified Powder).

Sintering temperature	950°C	1050°C	1150°C	1250°C	1350°C	1450°C	1550°C	1650°C	1700°C	1750°C
Pellet diameter (mm).	15.99	15.45	14.35	12.86	12.54	12.51	12.48	12.53	12.49	12.52
	15.98	15.41	14.34	12.81	12.53	12.54	12.52	12.53	12.50	12.54
	16.00	15.47	14.35	12.81	12.53	12.51	12.50	12.50	12.50	12.54
	15.99	15.45	14.35	12.83	12.54	12.49	12.49	12.51	12.51	12.51
	15.99	15.45	14.34	12.86	12.56	12.54	12.51	12.53	12.49	12.50
	15.98	15.46	14.34	12.82	12.56	12.53	12.54	12.51	12.50	12.57
	15.98	15.48	14.35	12.81	12.56	12.55	12.48	12.56	12.51	12.51
	15.99	15.45	14.33	12.83	12.52	12.52	12.54	12.54	12.49	12.53
	15.98	15.44	14.33	12.81	12.54	12.52	12.55	12.52	12.50	12.54
	16.00	15.47	14.33	12.82	12.53	12.52	12.46	12.57	12.53	12.53

Initial pellet diameter = 16.23 mm.

Mean diameter (mm).	15.99	15.45	14.34	12.83	12.54	12.52	12.51	12.53	12.50	12.53
Std. deviation (mm).	0.01	0.02	0.01	0.02	0.01	0.02	0.03	0.02	0.01	0.02
Mean shrinkage (%).	1.49	4.79	11.64	20.97	22.73	22.84	22.94	22.80	22.97	22.80
Std. deviation (%)	0.05	0.11	0.05	0.11	0.08	0.10	0.18	0.13	0.07	0.12

Powder 15: (TZ3Y unmodified powder, duplicate pellets).

Sintering temperature	950°C	1050°C	1150°C	1250°C	1350°C	1450°C	1550°C	1650°C	1700°C	1750°C
Pellet diameter (mm).	16.19	15.40	14.35	13.03	12.54	12.51	12.52	12.53	12.54	12.54
	16.17	15.40	14.34	13.03	12.53	12.54	12.52	12.56	12.53	12.54
	16.15	15.40	14.35	13.04	12.53	12.52	12.51	12.55	12.53	12.55
	16.15	15.38	14.35	13.03	12.54	12.51	12.52	12.53	12.54	12.55
	16.15	15.42	14.34	13.02	12.56	12.52	12.52	12.54	12.54	12.54
	16.17	15.40	14.34	13.02	12.56	12.51	12.52	12.57	12.53	12.53
	16.15	15.41	14.35	13.03	12.56	12.54	12.53	12.55	12.54	12.54
	16.16	15.41	14.33	13.03	12.52	12.53	12.52	12.56	12.55	12.54
	16.15	15.41	14.33	13.03	12.54	12.51	12.51	12.57	12.53	12.56
	16.15	15.43	14.33	13.02	12.53	12.51	12.52	12.54	12.54	12.53

Initial pellet diameter = 16.23 mm.

Mean diameter (mm)	16.16	15.41	14.34	13.03	12.54	12.52	12.52	12.55	12.54	12.54
Std. deviation (mm).	0.01	0.01	0.01	0.01	0.01	0.01	0.01	0.01	0.01	0.01
Mean shrinkage (%).	0.44	5.08	11.64	19.73	22.73	22.86	22.87	22.67	22.75	22.72
Std. deviation (mm).	0.08	0.08	0.05	0.04	0.08	0.07	0.03	0.09	0.04	0.05

Table 4.2.2(b)

Shrinkage results. Undoped TZ3Y powder, subjected to blank doping treatment.

Powder 11: Blank Treatment TZ3Y (undoped, alkoxide doping method).

Sintering temperature	950°C	1050°C	1150°C	1250°C	1350°C	1450°C	1550°C	1650°C	1700°C	1750°C
Pellet diameter (mm).	16.03	15.53	14.44	12.82	12.48	12.46	12.49	12.48	12.50	12.47
	16.03	15.50	14.43	12.81	12.49	12.46	12.49	12.46	12.49	12.46
	16.03	15.52	14.43	12.78	12.50	12.48	12.51	12.46	12.49	12.45
	16.03	15.50	14.43	12.77	12.49	12.42	12.51	12.46	12.48	12.46
	16.04	15.55	14.43	12.81	12.49	12.46	12.53	12.45	12.50	12.49
	16.03	15.53	14.44	12.80	12.49	12.44	12.50	12.45	12.49	12.46
	16.02	15.51	14.43	12.77	12.49	12.46	12.49	12.46	12.49	12.44
	16.03	15.52	14.43	12.78	12.50	12.46	12.49	12.47	12.49	12.46
	16.02	15.54	14.43	12.77	12.49	12.43	12.52	12.46	12.49	12.45
	16.03	15.55	14.44	12.78	12.50	12.44	12.49	12.46	12.49	12.44

Initial pellet diameter = 16.23 mm.

Mean diameter (mm)	16.03	15.52	14.43	12.79	12.49	12.45	12.50	12.46	12.49	12.46
Std. Deviation (mm)	0.01	0.02	0.00	0.02	0.01	0.02	0.01	0.01	0.01	0.01
Mean shrinkage (%).	1.24	4.34	11.07	21.20	23.03	23.28	22.97	23.22	23.04	23.24
Std. Deviation (%).	0.03	0.11	0.03	0.11	0.04	0.10	0.09	0.05	0.03	0.09

Table 4.2.3

Sintering Shrinkage Results, Alumina doped samples.

Powder 1: (0.25% Al_2O_3 addition)

Initial pellet diameter = 16.23 mm.

Sintering temperature.	950°C	1050°C	1150°C	1250°C	1350°C	1450°C	1550°C	1650°C	1700°C	1750°C
Mean diameter (mm).	16.05	14.87	13.03	12.51	12.48	12.48	12.45	12.47	12.55	12.53
Std. Deviation (mm).	0.01	0.01	0.00	0.03	0.02	0.02	0.01	0.02	0.02	0.02
Mean shrinkage (%).	1.12	8.41	19.69	22.89	23.08	23.09	23.31	23.15	22.68	22.79
Std. Deviation (%).	0.05	0.04	0.03	0.19	0.12	0.14	0.09	0.12	0.10	0.10

Powder 20: (0.25% Al_2O_3 addition, repeat).

Initial pellet diameter = 16.23 mm.

Sintering temperature.	950°C	1050°C	1150°C	1250°C	1350°C	1450°C	1550°C	1650°C	1700°C	1750°C
Mean diameter (mm).	16.08	14.92	13.29	12.64	12.55	12.58	12.52	12.56	12.53	12.56
Std. Deviation (mm).	0.01	0.01	0.01	0.00	0.01	0.02	0.00	0.01	0.02	0.01
Mean shrinkage (%).	0.92	8.07	18.10	22.09	22.70	22.51	22.88	22.61	22.81	22.61
Std. Deviation (%).	0.05	0.04	0.04	0.03	0.03	0.10	0.03	0.05	0.13	0.06

Powder 18: (0.5% Al_2O_3 addition).

Initial pellet diameter = 16.23 mm.

Sintering temperature.	950°C	1050°C	1150°C	1250°C	1350°C	1450°C	1550°C	1650°C	1700°C	1750°C
Mean diameter (mm).	16.06	14.76	12.89	12.47	12.47	12.47	12.46	12.52	12.76	12.80
Std. Deviation (mm).	0.01	0.01	0.00	0.01	0.01	0.01	0.01	0.01	0.01	0.01
Mean shrinkage (%).	1.04	9.07	20.58	23.17	23.19	23.19	23.20	22.88	21.36	21.15
Std. Deviation (%).	0.04	0.04	0.03	0.03	0.06	0.04	0.06	0.04	0.08	0.07

Powder 2: (0.75% Al_2O_3 addition)

Initial pellet diameter = 16.23 mm.

Sintering temperature.	950°C	1050°C	1150°C	1250°C	1350°C	1450°C	1550°C	1650°C	1700°C	1750°C
Mean diameter (mm)	16.00	14.64	12.83	12.56	12.56	12.47	12.47	12.54	12.71	12.80
Std. Deviation (mm).	0.01	0.01	0.01	0.01	0.01	0.02	0.02	0.03	0.01	0.03
Mean shrinkage (%).	1.41	9.78	20.96	22.63	22.62	23.14	23.14	22.74	21.71	21.13
Std. Deviation (%).	0.06	0.06	0.04	0.09	0.06	0.11	0.10	0.17	0.06	0.19

Table 4.2.3

Sintering Shrinkage results

- alumina doped samples (continued...).

Powder 16: (0.75% Al_2O_3 addition, repeat).

Initial pellet diameter = 16.23 mm.

Sintering temperature.	950°C	1050°C	1150°C	1250°C	1350°C	1450°C	1550°C	1650°C	1700°C	1750°C
Mean diameter (mm).	16.07	14.62	12.88	12.48	12.45	12.45	12.42	12.54	12.62	12.74
Std. Deviation (mm).	0.01	0.01	0.01	0.01	0.01	0.00	0.01	0.01	0.01	0.01
Mean shrinkage (%).	1.02	9.93	20.64	23.11	23.29	23.28	23.51	22.75	22.26	21.50
Std. Deviation (%).	0.07	0.09	0.05	0.05	0.05	0.02	0.06	0.06	0.08	0.06

Powder 13 (1% Al_2O_3 addition).

Initial pellet diameter = 16.23 mm.

Sintering temperature.	950°C	1050°C	1150°C	1250°C	1350°C	1450°C	1550°C	1650°C	1700°C	1750°C
Mean diameter (mm).	15.99	14.57	12.86	12.51	12.52	12.41	12.43	12.45	12.63	12.78
Std. Deviation (mm).	0.01	0.01	0.01	0.01	0.02	0.01	0.01	0.01	0.01	0.01
Mean shrinkage (%).	1.48	10.26	20.74	22.95	22.85	23.55	23.41	23.28	22.18	21.24
Std. Deviation (%).	0.08	0.09	0.05	0.09	0.10	0.04	0.04	0.04	0.07	0.09

Table 4.2.4

Sintering Shrinkage Results, Silica doped samples.

Powder 5: (0.25% SiO_2 addition).

Initial pellet diameter = 16.23 mm.

Sintering temperature.	950°C	1050°C	1150°C	1250°C	1350°C	1450°C	1550°C	1650°C	1700°C	1750°C
Mean diameter (mm).	16.03	15.13	13.89	12.63	12.44	12.49	12.50	12.48	12.54	12.54
Std. Deviation (mm).	0.01	0.02	0.01	0.02	0.15	0.01	0.02	0.01	0.01	0.02
Mean shrinkage (%).	1.24	6.81	14.40	22.16	23.37	23.04	22.96	23.11	22.72	22.75
Std. Deviation (%).	0.06	0.14	0.06	0.13	0.09	0.07	0.14	0.07	0.04	0.11

Powder 17: (0.5% SiO_2 addition)

Initial pellet diameter = 16.23 mm.

Sintering temperature.	950°C	1050°C	1150°C	1250°C	1350°C	1450°C	1550°C	1650°C	1700°C	1750°C
Mean diameter (mm)	16.07	15.24	14.14	12.72	12.50	12.53	12.53	12.54	12.57	12.58
Std. Deviation (mm).	0.01	0.01	0.01	0.01	0.01	0.01	0.01	0.02	0.01	0.02
Mean shrinkage (%).	1.01	6.11	12.85	21.62	22.98	22.80	22.81	22.73	22.54	22.51
Std. Deviation (%).	0.06	0.05	0.04	0.06	0.03	0.09	0.05	0.10	0.04	0.12

Powder 7: (0.75% SiO_2 addition).

Initial pellet diameter = 16.23 mm.

Sintering temperature.	950°C	1050°C	1150°C	1250°C	1350°C	1450°C	1550°C	1650°C	1700°C	1750°C
Mean diameter (mm)	16.02	15.41	14.00	12.84	12.67	12.71	12.73	12.74	12.75	12.73
Std. Deviation (mm).	0.00	0.02	0.01	0.01	0.01	0.01	0.02	0.01	0.01	0.01
Mean shrinkage (%).	1.32	5.04	13.75	20.87	21.93	21.66	21.53	21.48	21.46	21.59
Std. Deviation (%).	0.03	0.14	0.04	0.09	0.07	0.06	0.09	0.07	0.06	0.05

Table 4.2.4

Sintering shrinkage results,

- silica doped samples (continued....)..

Powder 7: (0.75% SiO_2 addition, duplicate pellets).

Initial pellet diameter = 16.23 mm.

Sintering temperature.	950°C	1050°C	1150°C	1250°C	1350°C	1450°C	1550°C	1650°C	1700°C	1750°C
Mean diameter (mm).	16.13	15.50	14.00	12.92	12.75	12.73	12.78	12.78	12.77	12.78
Std. Deviation (mm).	0.02	0.02	0.01	0.01	0.01	0.00	0.01	0.02	0.01	0.01
Mean shrinkage (%).	0.63	4.47	13.75	20.39	21.45	21.58	21.28	21.23	21.32	21.26
Std. Deviation (%).	0.09	0.12	0.04	0.05	0.05	0.02	0.06	0.10	0.04	0.04

Powder 3: (1% SiO_2 addition).

Initial pellet diameter = 16.23 mm.

Sintering temperature.	950°C	1050°C	1150°C	1250°C	1350°C	1450°C	1550°C	1650°C	1700°C	1750°C
Mean diameter (mm).	16.04	15.42	14.35	12.62	12.50	12.53	12.52	12.56	12.57	12.59
Std. Deviation (mm).	0.00	0.02	0.01	0.02	0.03	0.04	0.03	0.03	0.01	0.04
Mean shrinkage (%).	1.15	5.00	11.60	22.22	22.99	22.82	22.88	22.62	22.54	22.45
Std. Deviation (%).	0.03	0.11	0.05	0.12	0.16	0.22	0.18	0.17	0.08	0.23

Table 4.2.5 Shrinkage results - Titania doped specimens.

Powder 4: (0.25% TiO_2 addition)

Initial pellet diameter = 16.23 mm.

Sintering temperature.	950°C	1050°C	1150°C	1250°C	1350°C	1450°C	1550°C	1650°C	1700°C	1750°C
Mean diameter (mm).	16.05	15.51	14.26	12.89	12.61	12.54	12.53	12.51	12.62	12.52
Std. Deviation (mm).	0.01	0.02	0.00	0.04	0.01	0.02	0.02	0.03	0.04	0.01
Mean shrinkage (%).	1.10	4.41	12.16	20.59	22.33	22.77	22.79	22.91	22.23	22.86
Std. Deviation (%).	0.04	0.11	0.03	0.27	0.09	0.14	0.10	0.15	0.25	0.09

Powder 19: (0.5% TiO_2 addition)

Initial pellet diameter = 16.23 mm.

Sintering temperature.	950°C	1050°C	1150°C	1250°C	1350°C	1450°C	1550°C	1650°C	1700°C	1750°C
Mean diameter (mm).	16.09	15.51	14.64	13.15	12.62	12.52	12.55	12.50	12.64	12.51
Std. Deviation (mm).	0.01	0.01	0.01	0.00	0.02	0.01	0.01	0.01	0.02	0.01
Mean shrinkage (%).	0.86	4.47	9.80	18.96	22.27	22.88	22.70	22.96	22.11	22.90
Std. Deviation (%).	0.05	0.06	0.05	0.03	0.10	0.07	0.03	0.06	0.13	0.05

Powder 8: (0.75% TiO_2 addition).

Initial pellet diameter = 16.23 mm.

Sintering temperature.	950°C	1050°C	1150°C	1250°C	1350°C	1450°C	1550°C	1650°C	1700°C	1750°C
Mean diameter (mm).	16.10	15.89	14.82	13.14	12.63	12.48	12.44	12.50	12.55	12.53
Std. Deviation (mm).	0.01	0.01	0.00	0.03	0.01	0.01	0.01	0.02	0.01	0.02
Mean shrinkage (%).	0.78	2.09	8.66	19.04	22.19	23.13	23.37	22.98	22.67	22.79
Std. Deviation (%).	0.05	0.06	0.03	0.19	0.05	0.07	0.09	0.15	0.06	0.12

Powder 8 (Rpt.): (0.75% TiO_2 addition, duplicate pellets).

Initial pellet diameter = 16.23 mm.

Sintering temperature.	950°C	1050°C	1150°C	1250°C	1350°C	1450°C	1550°C	1650°C	1700°C	1750°C
Mean diameter (mm).	16.15	15.96	14.64	13.17	12.68	12.49	12.49	12.50	12.50	12.53
Std. Deviation (mm).	0.03	0.01	0.01	0.01	0.01	0.01	0.01	0.02	0.01	0.01
Mean shrinkage (%).	0.52	1.66	9.79	18.87	21.90	23.03	23.02	22.98	22.96	22.79
Std. Deviation (%).	0.16	0.08	0.08	0.07	0.08	0.08	0.06	0.15	0.04	0.06

Table 4.2.5 Shrinkage results

- Titania doped specimens (continued....).

Powder 12: (1 % TiO_2 addition)

Initial pellet diameter = 16.23 mm.

Sintering temperature.	950°C	1050°C	1150°C	1250°C	1350°C	1450°C	1550°C	1650°C	1700°C	1750°C
Mean diameter (mm).	16.16	15.89	15.02	13.24	12.63	12.49	12.49	12.49	12.49	12.49
Std. Deviation (mm).	0.01	0.02	0.01	0.01	0.01	0.01	0.01	0.01	0.01	0.02
Mean shrinkage (%).	0.46	2.08	7.48	18.40	22.16	23.07	23.06	23.05	23.02	23.04
Std. Deviation (%).	0.05	0.11	0.04	0.08	0.06	0.06	0.09	0.08	0.04	0.12

Table 4.2.6 Shrinkage Results, Multiple doped specimens.

Powder 6: (1% SiO_2 + 1% Al_2O_3 additions).

Initial pellet diameter = 16.23 mm.

Sintering temperature.	950°C	1150°C	1250°C	1350°C	1450°C	1550°C	1650°C	1700°C	1750°C
Mean diameter (mm)	15.99	12.56	12.37	12.39	12.47	12.47	12.51	12.75	13.26
Std. Deviation (mm).	0.01	0.00	0.03	0.02	0.03	0.01	0.01	0.02	0.02
Mean shrinkage (%).	1.51	22.64	23.80	23.66	23.17	23.19	22.90	21.41	18.31
Std. Deviation (%).	0.04	0.03	0.18	0.14	0.16	0.09	0.08	0.11	0.14

Powder 9: (1% SiO_2 + 1% TiO_2 additions).

Initial pellet diameter = 16.23 mm.

Sintering temperature.	950°C	1150°C	1250°C	1350°C	1450°C	1550°C	1650°C	1700°C	1750°C
Mean diameter (mm).	15.98	14.72	12.56	12.47	12.50	12.51	12.51	12.59	12.65
Std. Deviation (mm).	0.00	0.01	0.03	0.01	0.01	0.01	0.01	0.01	0.02
Mean shrinkage (%).	1.53	17.76	22.60	23.19	23.01	22.95	22.90	22.40	22.06
Std. Deviation (%).	0.02	0.06	0.18	0.06	0.08	0.04	0.09	0.07	0.14

Powder 14: (1% Al_2O_3 + 1% TiO_2 additions)

Initial pellet diameter = 16.23 mm.

Sintering temperature.	950°C	1150°C	1250°C	1350°C	1450°C	1550°C	1650°C	1700°C	1750°C
Mean diameter (mm).	16.06	13.57	12.54	12.33	12.34	12.37	12.38	12.56	12.67
Std. Deviation (mm).	0.01	0.01	0.01	0.01	0.02	0.01	0.01	0.02	0.01
Mean shrinkage (%).	1.05	16.38	23.35	24.00	23.99	23.78	23.74	22.61	21.93
Std. Deviation (%).	0.04	0.04	0.04	0.05	0.10	0.04	0.04	0.12	0.04

Powder 10: (1% SiO_2 + 1% Al_2O_3 + 1% TiO_2 additions).

Initial pellet diameter = 16.23 mm.

Sintering temperature.	950°C	1150°C	1250°C	1350°C	1450°C	1550°C	1650°C	1700°C	1750°C
Mean diameter (mm)	16.02	12.55	12.34	12.34	12.37	12.45	12.50	12.57	12.69
Std. Deviation (mm).	0.01	0.01	0.01	0.01	0.01	0.01	0.01	0.02	0.01
Mean shrinkage (%).	1.31	22.66	23.98	23.96	23.81	23.27	23.00	22.57	21.82
Std. Deviaton (%).	0.04	0.06	0.05	0.08	0.04	0.07	0.06	0.10	0.03

Table 4.2.7 Shrinkage results.
Mechanically mixed doped specimens
(1 mass % additions).

Powder MA (Mechanically mixed: 1% Al_2O_3 addition).

Initial pellet diameter = 16.23 mm.

Sintering temperature.	1050°C	1150°C	1350°C	1550°C	1750°C
Mean diameter (mm).	15.42	14.21	12.60	12.57	12.83
Std. Deviation (mm).	15.42	14.21	0.01	0.01	0.01
Mean shrinkage (%).	5.02	12.45	22.40	22.56	20.96
Std. Deviation (%).	0.07	0.03	0.04	0.03	0.05

Powder MT (Mechanically mixed: 1% TiO_2 addition).

Initial pellet diameter = 16.23 mm.

Sintering temperature.	1050°C	1150°C	1350°C	1550°C	1750°C
Mean diameter (mm)	15.43	14.14	12.62	12.57	12.63
Std. Deviation (mm).	0.01	0.00	0.01	0.01	0.02
Mean shrinkage (%).	4.95	12.85	22.26	22.54	22.15
Std. Deviation (%).	0.04	0.03	0.04	0.04	0.11

Powder MS (Mechanically mixed 1% SiO_2)

Initial pellet diameter = 16.23 mm.

Sintering temperature.	1050°C	1150°C	1350°C	1550°C	1750°C
Mean diameter (mm).	15.32	13.72	12.56	12.57	12.61
Std. Deviation (mm).	0.01	0.30	0.01	0.02	0.01
Mean shrinkage (%).	5.59	15.47	22.61	22.56	22.30
Std. Deviation (%).	0.05	1.85	0.07	0.12	0.04

Table 4.3.1 (a)

Estimation of measuring error in bulk density measurements for doped and undoped specimens.

Undoped specimens.
average for all sinter temperatures.

	Mean value of S.D (bulk density)	Mean value of 95% confidence (plus or minus)
TZ3Y (as supplied)	0.002	0.002
Blank treatment.	0.003	0.003
Average, all undoped samples.	0.003	0.003

Al_2O_3 doped specimens.
average for all sinter temperatures.

	Mean value of S.D (bulk density)	Mean value of 95% confidence (plus or minus)
Powder 1 (0.25% Al_2O_3)	0.003	0.003
Powder 18 (0.5% Al_2O_3)	0.002	0.002
Powder 2 (0.75% Al_2O_3)	0.002	0.002
Powder 13 (1% Al_2O_3)	0.002	0.002
Average, all Al_2O_3 doped samples.	0.002	0.002

SiO_2 doped specimens.
average for all sinter temperatures.

	Mean value of S.D (bulk density)	Mean value of 95% confidence (plus or minus)
Powder 5 (0.25% SiO_2)	0.001	0.001
Powder 17 (0.5% SiO_2)	0.002	0.002
Powder 7 (0.75% SiO_2)	0.003	0.003
Powder 3 (1% SiO_2)	0.003	0.003
Average, all SiO_2 doped samples.	0.002	0.002

TiO_2 doped specimens.
average for all sinter temperatures.

	Mean value of S.D (bulk density)	Mean value of 95% confidence (plus or minus)
Powder 4 (0.25% TiO_2)	0.002	0.002
Powder 19 (0.5% TiO_2)	0.002	0.002
Powder 8 (0.75% TiO_2)	0.002	0.002
Powder 12 (1% TiO_2)	0.003	0.003
Average, all TiO_2 doped samples.	0.002	0.002

Table 4.3.1 (a)

Estimation of measuring error in bulk density measurements for doped and undoped specimens (continued....).

Multiple doped specimens.
average for all sinter temperatures.

	Mean value of std. deviation in density (g/cm^3)	Mean value of 95% confidence limits (plus or minus(g/cm^3))
Powder 6	0.002	0.002
Powder 9	0.002	0.002
Powder 14	0.002	0.002
Powder 10	0.002	0.002
Average, multiple doped samples.	0.002	0.002

Average values for all dopant additions.

(All sinter temperatures).

Mean value of standard deviation= 0.002 g/cm^3

Mean value of 95% confidence limits = (+ or -) 0.002 g/cm^3

Table 4.3.1 (b) Estimate of experimental error in density measurements, from duplicate samples made from same powder batch (post doping experimental error).

Sintering Temperature (°C)	1150	1250	1350	1450	1550	1650	1700	1750
	Measured bulk density values (g/cm^3).							
Powder 7, 0.75% SiO_2	4.05	5.80	5.91	5.92	5.93	5.91	5.92	5.90
Powder 7, 0.75% SiO_2 (duplicate)	4.05	5.70	5.97	5.93	5.96	5.95	5.93	5.87
| difference |	0.00	0.10	0.06	0.01	0.03	0.04	0.01	0.03

Sintering Temperature (°C)	1150	1250	1350	1450	1550	1650	1700	1750
	Measured bulk density values (g/cm^3).							
Powder 8, 0.75% TiO_2	3.61	5.16	5.78	6.02	6.03	6.03	5.96	5.98
Powder 8, 0.75% TiO_2 (duplicate)	3.68	5.22	5.82	6.00	6.02	6.00	5.99	5.97
| difference |	0.07	0.06	0.04	0.02	0.01	0.03	0.03	0.01

Average values for all dopant additions.

(All sinter temperatures).

Mean value of standard deviation= 0.003 g/cm^3

Mean value of 95% confidence limits = (+ or -) 0.003 g/cm^3

Table 4.3.1 (c) Estimate of experimental error in density measurements, from samples of duplicate composition produced from different powder batches. (Total experimental error).

Sintering Temperature (°C)	1150	1250	1350	1450	1550	1650	1700	1750
	Measured bulk density values (g/cm^3).							
Powder 1, 0.25% Al_2O_3	5.34	6.00	6.04	6.05	6.04	5.99	5.96	5.98
Powder 20, 0.25% Al_2O_3 Rpt.	5.19	6.02	6.05	6.04	6.03	6.00	5.98	5.96
| difference |	0.15	0.01	0.01	0.01	0.01	0.02	0.02	0.02

Sintering Temperature (°C)	1150	1250	1350	1450	1550	1650	1700	1750
	Measured bulk density values (g/cm^3).							
Powder 2, 0.75% Al_2O_3	5.49	5.96	6.03	6.02	6.02	5.96	5.65	5.59
Powder 16, 0.75% Al_2O_3 Rpt.	5.45	5.97	6.04	6.03	6.02	5.98	5.70	5.53
| difference |	0.04	0.01	0.01	0.02	0.00	0.02	0.05	0.06

Estimated error (average for all sintering temperatures).

Mean difference (between samples)	0.03	(g/cm^3)
Std. Dev. in Difference.	0.04	(g/cm^3)
Std. Error in Difference.	0.01	(g/cm^3)
95% Confidence limits, error < +/-	0.05	(g/cm^3)

Table 4.3.2 Sintering density and porosity results. Undoped samples.

Powder 11 (Undoped, Blank Treatment).

Sintering temperature (°C)	1150	1250	1350	1450	1550	1650	1700	1750
Bulk density (g/cm^3).	3.95	5.61	5.98	6.02	6.06	6.07	6.06	6.07
Standard deviation (g/cm^3).	0.000	0.002	0.004	0.004	0.002	0.002	0.004	0.004
Apparent solid density (g/cm^3).	5.93	5.85	5.98	6.02	6.06	6.08	6.06	6.07
Standard deviation (g/cm^3).	0.001	0.003	0.004	0.004	0.002	0.002	0.004	0.004
Apparent porosity (%)	33.33	4.07	0.00	0.00	0.08	0.08	0.00	0.00
True porosity (%)	35.19	7.96	2.00	1.29	0.70	0.47	0.62	0.51
Standard deviation (g/cm^3).	0.01	0.04	0.06	0.06	0.03	0.03	0.06	0.06
% of theoretical density.	64.81	92.04	98.00	98.71	99.30	99.53	99.38	99.49
Standard deviation (%).	0.01	0.04	0.06	0.06	0.03	0.03	0.06	0.06
Bulk density change (g/cm^3). (compared with undoped blank)	0.00	0.00	0.00	0.00	0.00	0.00	0.00	0.00
Bulk density change (%).	0.00	0.00	0.00	0.00	0.00	0.00	0.00	0.00

Powder 15 (Unmodified TZ3Y, as supplied).

Sintering temperature (°C)	1150	1250	1350	1450	1550	1650	1700	1750
Bulk density (g/cm^3).	3.92	5.62	6.02	6.03	6.04	6.08	6.07	6.06
Standard deviation (g/cm^3).	0.001	0.002	0.002	0.002	0.003	0.001	0.002	0.002
Apparent solid density (g/cm^3).	5.99	5.69	6.03	6.03	6.04	6.08	6.08	6.07
Standard deviation (g/cm^3).	0.002	0.002	0.002	0.002	0.003	0.001	0.002	0.002
Apparent porosity (%)	34.52	1.24	0.22	0.00	0.00	0.00	0.08	0.04
True porosity (%)	35.73	7.85	1.30	1.14	0.91	0.29	0.44	0.60
Standard deviation (g/cm^3).	0.01	0.04	0.04	0.03	0.05	0.02	0.03	0.03
% of theoretical density.	64.27	92.15	98.70	98.86	99.09	99.71	99.56	99.40
Standard deviation (%).	0.01	0.04	0.04	0.03	0.05	0.02	0.03	0.03
Bulk density change (g/cm^3). (compared with undoped blank)	-0.03	0.01	0.04	0.01	-0.01	0.01	0.01	-0.01
Bulk density change (%).	-0.83	0.11	0.71	0.16	-0.22	0.17	0.19	-0.09

Table 4.3.3

Sintering density and porosity results

- Alumina doped samples.

Powder 1 (0.25% Al_2O_3)

Sintering temperature (°C)	1150	1250	1350	1450	1550	1650	1700	1750
Bulk density (g/cm^3).	5.34	6.00	6.04	6.05	6.04	5.99	5.96	5.98
Standard deviation (g/cm^3).	0.001	0.005	0.003	0.004	0.002	0.003	0.003	0.004
Apparent solid density (g/cm^3).	5.89	6.00	6.04	6.05	6.04	5.99	5.96	5.98
Standard deviation (g/cm^3).	0.001	0.005	0.003	0.004	0.002	0.003	0.001	0.004
Apparent porosity (%)	9.39	0.00	0.00	0.00	0.00	0.00	0.00	0.04
True porosity (%)	12.50	1.57	0.92	0.80	0.97	1.85	2.33	1.97
Standard deviation (g/cm^3).	0.01	0.08	0.05	0.06	0.03	0.04	0.04	0.06
% of theoretical density.	87.50	98.43	99.08	99.20	99.03	98.15	97.67	98.03
Standard deviation (%).	0.01	0.08	0.05	0.06	0.03	0.04	0.04	0.06
Bulk density change (g/cm^3). (compared with undoped blank)	1.39	0.39	0.06	0.03	-0.02	-0.08	-0.11	-0.09
Bulk density change (%).	35.12	7.03	1.07	0.52	-0.31	-1.37	-1.85	-1.48

Powder 20 (0.25% Al_2O_3 Rpt.)

Sintering temperature (°C)	1150	1250	1350	1450	1550	1650	1700	1750
Bulk density (g/cm^3).	5.19	6.02	6.05	6.04	6.03	6.00	5.98	5.96
Standard deviation (g/cm^3).	0.001	0.003	0.002	0.001	0.001	0.002	0.002	0.001
Apparent solid density (g/cm^3).	5.90	6.02	6.05	6.05	6.03	6.00	5.99	5.97
Standard deviation (g/cm^3).	0.002	0.003	0.002	0.001	0.001	0.002	0.002	0.001
Apparent porosity (%)	12.12	0.00	0.00	0.08	0.09	0.00	0.12	0.04
True porosity (%)	14.98	1.39	0.80	0.97	1.19	1.60	1.99	2.22
Standard deviation (g/cm^3).	0.02	0.05	0.03	0.02	0.02	0.03	0.03	0.02
% of theoretical density.	85.02	98.61	99.20	99.03	98.81	98.40	98.01	97.78
Standard deviation (%).	0.02	0.05	0.03	0.02	0.02	0.03	0.03	0.02
Bulk density change (g/cm^3). (compared with undoped blank)	1.24	0.41	0.07	0.02	-0.03	-0.07	-0.09	-0.11
Bulk density change (%).	31.30	7.22	1.19	0.34	-0.54	-1.11	-1.51	-1.74

Table 4.3.3

Sintering density and porosity results

- Alumina doped samples (continued....)

Powder 18 (0.5% Al_2O_3).

Sintering temperature (°C)	1150	1250	1350	1450	1550	1650	1700	1750
Bulk density (g/cm^3).	5.42	6.02	6.06	6.05	6.03	5.99	5.69	5.56
Standard deviation (g/cm^3).	0.001	0.001	0.003	0.001	0.002	0.002	0.002	0.001
Apparent solid density (g/cm^3).	5.81	6.02	6.06	6.05	6.03	5.99	5.77	5.63
Standard deviation (g/cm^3).	0.001	0.001	0.003	0.001	0.002	0.002	0.002	0.001
Apparent porosity (%)	6.72	0.00	0.00	0.00	0.00	0.04	1.38	1.09
True porosity (%)	11.16	1.23	0.72	0.80	1.21	1.87	6.73	8.78
Standard deviation (g/cm^3).	0.01	0.02	0.04	0.02	0.03	0.03	0.03	0.02
% of theoretical density.	88.84	98.77	99.28	99.20	98.79	98.13	93.27	91.22
Standard deviation (%).	0.01	0.02	0.04	0.02	0.03	0.03	0.03	0.02
Bulk density change (g/cm^3). (compared with undoped blank)	1.47	0.41	0.08	0.03	-0.03	-0.08	-0.38	-0.51
Bulk density change (%).	37.20	7.40	1.28	0.52	-0.56	-1.39	-6.27	-8.32

Powder 2 (0.75% Al_2O_3).

Sintering temperature (°C)	1150	1250	1350	1450	1550	1650	1700	1750
Bulk density (g/cm^3).	5.49	5.96	6.03	6.02	6.02	5.96	5.65	5.59
Standard deviation (g/cm^3).	0.001	0.003	0.002	0.002	0.001	0.004	0.001	0.004
Apparent solid density (g/cm^3).	5.85	5.96	6.03	6.02	6.02	5.96	5.78	5.76
Standard deviation (g/cm^3).	0.001	0.003	0.002	0.002	0.001	0.004	0.002	0.004
Apparent porosity (%)	6.15	0.00	0.00	0.00	0.00	0.00	2.38	2.98
True porosity (%)	9.96	2.33	1.16	1.36	1.34	2.33	7.44	8.36
Standard deviation (g/cm^3).	0.02	0.04	0.03	0.03	0.02	0.07	0.02	0.06
% of theoretical density.	90.04	97.67	98.84	98.64	98.66	97.67	92.56	91.64
Standard deviation (%).	0.02	0.04	0.03	0.03	0.02	0.07	0.02	0.06
Bulk density change (g/cm^3). (compared with undoped blank)	1.54	0.35	0.05	-0.00	-0.04	-0.11	-0.42	-0.48
Bulk density change (%).	39.06	6.20	0.82	-0.05	-0.69	-1.85	-6.98	-7.91

Table 4.3.3

Sintering density and porosity results

- Alumina doped samples (continued....)

Powder 16 (0.75% Al_2O_3 Rpt.).

Sintering temperature (°C)	1150	1250	1350	1450	1550	1650	1700	1750
Bulk density (g/cm^3).	5.45	5.97	6.04	6.03	6.02	5.98	5.70	5.53
Standard deviation (g/cm^3).	0.002	0.002	0.004	0.003	0.001	0.001	0.001	0.001
Apparent solid density (g/cm^3).	5.76	5.98	6.04	6.04	6.02	5.98	5.82	5.70
Standard deviation (g/cm^3).	0.002	0.002	0.004	0.003	0.001	0.001	0.001	0.001
Apparent porosity (%)	5.33	0.20	0.00	0.04	0.00	0.00	2.21	2.95
True porosity (%)	10.61	2.16	0.94	1.10	1.29	2.00	6.63	9.35
Standard deviation (g/cm^3).	0.03	0.03	0.07	0.05	0.02	0.02	0.02	0.02
% of theoretical density.	89.39	97.84	99.06	98.90	98.71	98.00	93.37	90.65
Standard deviation (%).	0.03	0.03	0.07	0.05	0.02	0.02	0.02	0.02
Bulk density change (g/cm^3). (compared with undoped blank)	1.50	0.36	0.06	0.01	-0.04	-0.09	-0.37	-0.54
Bulk density change (%).	38.05	6.39	1.05	0.22	-0.63	-1.52	-6.16	-8.90

Powder 13 (1% Al_2O_3).

Sintering temperature (°C)	1150	1250	1350	1450	1550	1650	1700	1750
Bulk density (g/cm^3).	5.42	5.92	6.01	6.03	6.03	5.98	5.66	5.54
Standard deviation (g/cm^3).	0.001	0.001	0.002	0.003	0.001	0.001	0.001	0.003
Apparent solid density (g/cm^3).	5.81	5.92	6.01	6.03	6.03	5.98	5.79	5.70
Standard deviation (g/cm^3).	0.002	0.001	0.002	0.003	0.001	0.001	0.001	0.003
Apparent porosity (%)	6.68	0.04	0.04	0.00	0.00	0.00	2.24	2.75
True porosity (%)	11.19	2.94	1.45	1.21	1.10	1.97	7.15	9.17
Standard deviation (g/cm^3).	0.02	0.02	0.03	0.05	0.02	0.02	0.02	0.05
% of theoretical density.	88.81	97.06	98.55	98.79	98.90	98.03	92.85	90.83
Standard deviation (%).	0.02	0.02	0.03	0.05	0.02	0.02	0.02	0.05
Bulk density change (g/cm^3). (compared with undoped blank)	1.47	0.31	0.03	0.01	-0.03	-0.09	-0.41	-0.53
Bulk density change (%).	37.15	5.53	0.53	0.10	-0.45	-1.48	-6.69	-8.72

Table 4.3.4

Sintering density and porosity results - silica doped samples.

Powder 5 (0.25% SiO_2)

Sintering temperature (°C)	1150	1250	1350	1450	1550	1650	1700	1750
Bulk density (g/cm^3).	4.16	5.83	6.04	6.03	6.03	6.01	5.99	6.00
Standard deviation (g/cm^3).	0.001	0.001	0.001	0.002	0.002	0.002	0.001	0.001
Apparent solid density (g/cm^3).	5.93	5.86	6.04	6.03	6.03	6.01	5.99	6.00
Standard deviation (g/cm^3).	0.001	0.001	0.001	0.002	0.002	0.002	0.001	0.001
Apparent porosity (%)	29.93	0.36	0.00	0.00	0.00	0.00	0.00	0.00
True porosity (%)	31.85	4.35	1.06	1.12	1.15	1.40	1.88	1.61
Standard deviation (g/cm^3).	0.01	0.02	0.02	0.03	0.04	0.03	0.02	0.02
% of theoretical density.	68.15	95.65	98.94	98.88	98.85	98.60	98.12	98.39
Standard deviation (%).	0.01	0.02	0.02	0.03	0.04	0.03	0.02	0.02
Bulk density change (g/cm^3). (compared with undoped blank)	0.20	0.22	0.06	0.01	-0.03	-0.06	-0.08	-0.07
Bulk density change (%).	5.16	3.92	0.96	0.17	-0.45	-0.94	-1.36	-1.11

Powder 17 (0.5% SiO_2)

Sintering temperature (°C)	1150	1250	1350	1450	1550	1650	1700	1750
Bulk density (g/cm^3).								
Standard deviation (g/cm^3).	4.16	5.81	6.03	6.02	6.01	6.00	5.98	5.95
	0.001	0.003	0.001	0.000	0.003	0.002	0.004	0.002
Apparent solid density (g/cm^3).								
Standard deviation (g/cm^3).	5.95	5.88	6.03	6.02	6.01	6.00	5.99	5.96
	0.001	0.003	0.001	0.000	0.003	0.002	0.004	0.002
Apparent porosity (%)	30.16	1.19	0.00	0.04	0.12	0.12	0.08	0.04
True porosity (%)								
Standard deviation (g/cm^3).	31.86	4.69	1.15	1.29	1.52	1.69	1.92	2.40
	0.01	0.04	0.02	0.00	0.05	0.03	0.07	0.03
% of theoretical density.								
Standard deviation (%).	68.14	95.31	98.85	98.71	98.48	98.31	98.08	97.60
	0.01	0.04	0.02	0.00	0.05	0.03	0.07	0.03
Bulk density change (g/cm^3).								
(compared with undoped blank)	0.20	0.20	0.05	-0.00	-0.05	-0.07	-0.08	-0.12
Bulk density change (%).	5.14	3.55	0.87	-0.00	-0.82	-1.24	-1.40	-1.90

Table 4.3.4

Sintering density and porosity results - silica doped samples (continued...).

Powder 7 (0.75% SiO_2)

Sintering temperature (°C)	1150	1250	1350	1450	1550	1650	1700	1750
Bulk density (g/cm^3).	4.05	5.80	5.91	5.92	5.93	5.91	5.92	5.90
Standard deviation (g/cm^3).	0.001	0.004	0.002	0.003	0.003	0.003	0.002	0.003
Apparent solid density (g/cm^3).	5.92	5.92	5.98	5.98	5.97	5.95	5.96	5.94
Standard deviation (g/cm^3).	0.002	0.004	0.002	0.003	0.003	0.003	0.002	0.003
Apparent porosity (%)	31.61	2.17	1.11	0.88	0.70	0.71	0.60	0.76
True porosity (%)	33.67	4.99	3.12	2.89	2.81	3.10	2.96	3.29
Standard deviation (g/cm^3).	0.02	0.07	0.03	0.04	0.04	0.05	0.03	0.04
% of theoretical density.	66.33	95.01	96.88	97.11	97.19	96.90	97.04	96.71
Standard deviation (%).	0.02	0.07	0.03	0.04	0.04	0.05	0.03	0.04
Bulk density change (g/cm^3). (compared with undoped blank)	0.09	0.18	-0.07	-0.10	-0.13	-0.16	-0.15	-0.17
Bulk density change (%).	2.35	3.23	-1.14	-1.62	-2.13	-2.65	-2.44	-2.80

Powder 7, Repeat. (0.75% SiO_2 duplicate sintered pellets)

Sintering temperature (°C)	1150	1250	1350	1450	1550	1650	1700	1750
Bulk density (g/cm^3).	4.05	5.70	5.97	5.93	5.96	5.95	5.93	5.87
Standard deviation (g/cm^3).	0.001	0.001	0.003	0.003	0.003	0.003	0.002	0.003
Apparent solid density (g/cm^3).	5.92	5.93	5.98	5.98	5.98	5.97	5.96	5.92
Standard deviation (g/cm^3).	0.002	0.001	0.003	0.003	0.003	0.003	0.002	0.003
Apparent porosity (%)	31.61	3.85	0.16	0.76	0.36	0.28	0.48	0.87
True porosity (%)	33.67	6.48	2.19	2.75	2.33	2.45	2.84	3.79
Standard deviation (g/cm^3).	0.02	0.02	0.04	0.05	0.04	0.05	0.03	0.04
% of theoretical density.	66.33	93.52	97.81	97.25	97.67	97.55	97.16	96.21
Standard deviation (%).	0.02	0.02	0.04	0.05	0.04	0.05	0.03	0.04
Bulk density change (g/cm^3). (compared with undoped blank)	0.09	0.09	-0.01	-0.09	-0.10	-0.12	-0.14	-0.20
Bulk density change (%).	2.35	1.60	-0.19	-1.48	-1.64	-1.99	-2.32	-3.29

Table 4.3.4

Sintering density and porosity results - silica doped samples (continued...).

Powder 3 (1% SiO_2)

Sintering temperature (°C)	1150	1250	1350	1450	1550	1650	1700	1750
Bulk density (g/cm^3).	3.99	5.81	5.88	5.96	5.95	5.93	5.92	5.92
Standard deviation (g/cm^3).	0.002	0.002	0.004	0.002	0.003	0.004	0.003	0.004
Apparent solid density (g/cm^3).	5.91	5.84	5.91	5.97	5.95	5.93	5.92	5.92
Standard deviation (g/cm^3).	0.004	0.002	0.004	0.002	0.003	0.004	0.003	0.004
Apparent porosity (%)	32.54	0.63	0.60	0.16	0.00	0.00	0.00	0.00
True porosity (%)	34.65	4.83	3.62	2.26	2.48	2.74	2.89	2.98
Standard deviation (g/cm^3).	0.03	0.03	0.06	0.03	0.05	0.07	0.05	0.06
% of theoretical density.	65.35	95.17	96.38	97.74	97.52	97.26	97.11	97.02
Standard deviation (%).	0.03	0.03	0.06	0.03	0.05	0.07	0.05	0.06
Bulk density change (g/cm^3). (compared with undoped blank)	0.03	0.19	-0.10	-0.06	-0.11	-0.14	-0.14	-0.15
Bulk density change (%).	0.84	3.39	-1.66	-0.98	-1.79	-2.28	-2.37	-2.47

Table 4.3.5

Sintering density results - titania doped samples.

Powder 4 (0.25% TiO_2)

Sintering temperature (°C)	1150	1250	1350	1450	1550	1650	1700	1750
Bulk density (g/cm^3).	4.16	5.66	5.93	6.04	6.05	6.06	6.05	6.03
Standard deviation (g/cm^3).	0.001	0.002	0.003	0.002	0.001	0.004	0.001	0.004
Apparent solid density (g/cm^3).	5.93	5.80	5.93	6.04	6.05	6.06	6.05	6.03
Standard deviation (g/cm^3).	0.001	0.002	0.003	0.002	0.001	0.004	0.001	0.004
Apparent porosity (%)	29.93	2.40	0.04	0.00	0.00	0.00	0.00	0.00
True porosity (%)	31.85	7.14	2.76	0.97	0.74	0.67	0.90	1.07
Standard deviation (g/cm^3).	0.01	0.03	0.05	0.03	0.02	0.06	0.02	0.07
% of theoretical density.	68.15	92.86	97.24	99.03	99.26	99.33	99.10	98.93
Standard deviation (%).	0.01	0.03	0.05	0.03	0.02	0.06	0.02	0.07
Bulk density change (g/cm^3). (compared with undoped blank)	0.20	0.05	-0.05	0.02	-0.00	-0.01	-0.02	-0.03
Bulk density change (%).	5.16	0.88	-0.78	0.32	-0.04	-0.20	-0.28	-0.56

Powder 19 (0.5% TiO_2)

Sintering temperature (°C)	1150	1250	1350	1450	1550	1650	1700	1750
Bulk density (g/cm^3).	3.97	5.24	5.82	5.99	6.02	6.02	5.97	5.99
Standard deviation (g/cm^3).	0.001	0.001	0.003	0.002	0.002	0.001	0.001043	0.001
Apparent solid density (g/cm^3).	5.98	5.70	5.88	6.00	6.02	6.02	6.00	5.99
Standard deviation (g/cm^3).	0.001	0.001	0.003	0.002	0.002	0.001	0.001054	0.001
Apparent porosity (%)	33.62	8.06	1.02	0.04	0.00	0.00	0.53	0.00
True porosity (%)	34.92	14.09	4.57	1.75	1.29	1.38	2.19	1.81
Standard deviation (g/cm^3).	0.01	0.01	0.04	0.03	0.03	0.02	0.02	0.02
% of theoretical density.	65.08	85.91	95.43	98.25	98.71	98.62	97.81	98.19
Standard deviation (%).	0.01	0.01	0.04	0.03	0.03	0.02	0.02	0.02
Bulk density change (g/cm^3). (compared with undoped blank)	0.02	-0.37	-0.16	-0.03	-0.04	-0.06	-0.10	-0.08
Bulk density change (%).	0.42	-6.66	-2.62	-0.46	-0.59	-0.92	-1.57	-1.30

Table 4.3.5

Sintering density results

- titania doped samples (continued...).

Powder 8 (0.75% TiO_2)

Sintering temperature (°C)	1150	1250	1350	1450	1550	1650	1700	1750
Bulk density (g/cm^3).	3.61	5.16	5.78	6.02	6.03	6.03	5.96	5.98
Standard deviation (g/cm^3).	0.000	0.002	0.004	0.001	0.003	0.001	0.001046	0.001
Apparent solid density (g/cm^3).	5.76	5.64	5.78	6.02	6.03	6.03	5.96	5.98
Standard deviation (g/cm^3).	0.001	0.002	0.004	0.001	0.003	0.001	0.001046	0.001
Apparent porosity (%)	37.32	8.48	0.00	0.00	0.00	0.00	0.00	0.00
True porosity (%)	40.83	15.45	5.24	1.37	1.20	1.12	2.32	1.99
Standard deviation (g/cm^3).	0.01	0.03	0.06	0.02	0.04	0.02	0.02	0.02
% of theoretical density.	59.17	84.55	94.76	98.63	98.80	98.88	97.68	98.01
Standard deviation (%).	0.01	0.03	0.06	0.02	0.04	0.02	0.02	0.02
Bulk density change (g/cm^3). (compared with undoped blank)	-0.34	-0.46	-0.20	-0.00	-0.03	-0.04	-0.10	-0.09
Bulk density change (%).	-8.69	-8.14	-3.31	-0.08	-0.50	-0.66	-1.71	-1.48

Powder 8 (0.75% TiO_2 duplicate pellets.)

Sintering temperature (°C)	1150	1250	1350	1450	1550	1650	1700	1750
Bulk density (g/cm^3).	3.68	5.22	5.82	6.00	6.02	6.00	5.99	5.97
Standard deviation (g/cm^3).	0.001	0.003	0.002	0.002	0.002	0.003	0.002	0.001
Apparent solid density (g/cm^3).	5.68	5.58	5.82	6.00	6.02	6.00	5.99	5.97
Standard deviation (g/cm^3).	0.001	0.003	0.002	0.002	0.002	0.003	0.002	0.001
Apparent porosity (%)	35.2	6.40	0.00	0.00	0.00	0.00	0.00	0.00
True porosity (%)	39.67	14.43	4.59	1.64	1.31	1.64	1.80	2.13
Standard deviation (g/cm^3).	0.01	0.04	0.03	0.03	0.03	0.04	0.03	0.01
% of theoretical density.	59.17	84.55	94.76	98.63	98.80	98.88	97.68	98.01
Standard deviation (%).	0.01	0.04	0.03	0.03	0.03	0.04	0.03	0.01
Bulk density change (g/cm^3). (compared with undoped blank)	-0.27	-0.39	-0.16	-0.02	-0.04	-0.07	-0.07	-0.10
Bulk density change (%).	-4.55	-6.95	-2.68	-0.33	-0.66	-1.15	-1.16	-1.65

Table 4.3.5

Sintering density results

- titania doped samples (continued...).

Powder 12 (1% TiO_2)

Sintering temperature (°C)	1150	1250	1350	1450	1550	1650	1700	1750
Bulk density (g/cm^3).	3.50	5.04	5.78	6.00	6.03	6.04	6.03	6.02
Standard deviation (g/cm^3).	0.001	0.003	0.002	0.004	0.002	0.004	0.002	0.003
Apparent solid density (g/cm^3).	5.87	5.74	5.80	6.00	6.03	6.04	6.03	6.03
Standard deviation (g/cm^3).	0.002	0.004	0.002	0.004	0.002	0.004	0.002	0.003
Apparent porosity (%)	40.41	12.18	0.39	0.00	0.00	0.00	0.00	0.16
True porosity (%)	42.64	17.37	5.24	1.62	1.11	0.93	1.11	1.29
Standard deviation (g/cm^3).	0.01	0.05	0.04	0.06	0.03	0.06	0.04	0.04
% of theoretical density.	57.36	82.63	94.76	98.38	98.89	99.07	98.89	98.71
Standard deviation (%).	0.01	0.05	0.04	0.06	0.03	0.06	0.04	0.04
Bulk density change (g/cm^3). (compared with undoped blank)	-0.45	-0.57	-0.20	-0.02	-0.03	-0.03	-0.03	-0.05
Bulk density change (%).	-11.49	-10.22	-3.30	-0.33	-0.42	-0.47	-0.49	-0.78

Table 4.3.6

Sintering density and porosity results

- Multiple dopant additions.

Powder 6 (1.00% SiO_2, 1.00% Al_2O_3)

Sintering temperature (°C)	1150	1250	1350	1450	1550	1650	1750
Bulk density (g/cm^3).	5.75	5.92	5.93	5.90	5.78	5.68	5.41
Standard deviation (g/cm^3).	0.002	0.004	0.004	0.003	0.001	0.001	0.002
Apparent solid density (g/cm^3).	5.75	5.92	5.93	5.90	5.78	5.69	5.52
Standard deviation (g/cm^3).	0.002	0.004	0.004	0.003	0.001	0.001	0.002
Apparent porosity (%)	0.00	0.00	0.00	0.00	0.00	0.19	1.98
True porosity (%)	5.80	2.92	2.82	3.35	5.22	6.86	11.38
Standard deviation (g/cm^3).	0.03	0.06	0.06	0.06	0.02	0.02	0.03
% of theoretical density.	94.20	97.08	97.18	96.65	94.78	93.14	88.62
Standard deviation (%).	0.03	0.06	0.06	0.06	0.02	0.02	0.03
Bulk density change (g/cm^3). (compared with undoped blank)	1.79	0.31	-0.05	-0.13	-0.28	-0.39	-0.66
Bulk density change (%).	45.35	5.48	-0.84	-2.08	-4.55	-6.43	-10.92

Powder 9 (1.00% SiO_2, 1.00% TiO_2)

Sintering temperature (°C)	1150	1250	1350	1450	1550	1650	1750
Bulk density (g/cm^3).	3.82	5.91	5.93	5.92	5.89	5.87	5.87
Standard deviation (g/cm^3).	0.001	0.002	0.003	0.003	0.002	0.001	0.002
Apparent solid density (g/cm^3).	5.85	5.91	5.93	5.92	5.89	5.87	5.87
Standard deviation (g/cm^3).	0.001	0.002	0.003	0.003	0.002	0.001	0.002
Apparent porosity (%)	34.80	0.00	0.00	0.00	0.00	0.00	0.00
True porosity (%)	37.43	3.08	2.83	2.88	3.40	3.70	3.70
Standard deviation (g/cm^3).	0.02	0.03	0.04	0.04	0.03	0.02	0.03
% of theoretical density.	62.57	96.92	97.17	97.12	96.60	96.30	96.30
Standard deviation (%).	0.02	0.03	0.04	0.04	0.03	0.02	0.03
Bulk density change (g/cm^3). (compared with undoped blank)	-0.07	0.30	-0.05	-0.10	-0.16	-0.20	-0.19
Bulk density change (%).	-1.82	5.30	-0.85	-1.61	-2.71	-3.25	-3.20

Table 4.3.6

Sintering density and porosity results

- Multiple dopant additions (continued....).

Powder 14 (1% Al_2O_3, 1% TiO_2)

Sintering temperature (°C)	1150	1250	1350	1450	1550	1650	1750
Bulk density (g/cm^3).	4.50	5.78	5.99	6.00	5.97	5.93	5.57
Standard deviation (g/cm^3).	0.002	0.001	0.002	0.004	0.002	0.002	0.002
Apparent solid density (g/cm^3).	5.87	5.79	5.99	6.00	5.97	5.93	5.77
Standard deviation (g/cm^3).	0.003	0.001	0.002	0.004	0.002	0.002	0.003
Apparent porosity (%)	23.26	0.23	0.04	0.00	0.00	0.00	3.33
True porosity (%)	26.18	5.27	1.80	1.56	2.09	2.79	8.61
Standard deviation (g/cm^3).	0.03	0.02	0.03	0.06	0.03	0.03	0.04
% of theoretical density.	73.82	94.73	98.20	98.44	97.91	97.21	91.39
Standard deviation (%).	0.03	0.02	0.03	0.06	0.03	0.03	0.04
Bulk density change (g/cm^3). (compared with undoped blank)	0.55	0.16	0.01	-0.02	-0.08	-0.14	-0.49
Bulk density change (%).	13.91	2.92	0.21	-0.27	-1.40	-2.33	-8.14

Powder 10 (1% SiO_2, 1% Al_2O_3, 1% TiO_2)

Sintering temperature (°C)	1150	1250	1350	1450	1550	1650	1750
Bulk density (g/cm^3).	5.59	5.90	5.89	5.84	5.73	5.67	5.41
Standard deviation (g/cm^3).	0.001	0.002	0.001	0.003	0.002	0.001	0.002
Apparent solid density (g/cm^3).	5.63	5.91	5.89	5.84	5.73	5.67	5.44
Standard deviation (g/cm^3).	0.002	0.002	0.001	0.003	0.002	0.001	0.002
Apparent porosity (%)	0.72	0.24	0.12	0.12	0.04	0.00	0.58
True porosity (%)	8.35	3.34	3.49	4.34	6.09	7.07	11.31
Standard deviation (g/cm^3).	0.02	0.03	0.02	0.05	0.03	0.02	0.04
% of theoretical density.	91.65	96.66	96.51	95.66	93.91	92.93	88.69
Standard deviation (%).	0.02	0.03	0.02	0.05	0.03	0.02	0.04
Bulk density change (g/cm^3). (compared with undoped blank)	1.64	0.28	-0.09	-0.19	-0.33	-0.40	-0.66
Bulk density change (%).	41.42	5.02	-1.52	-3.09	-5.43	-6.63	-10.85

Table 4.3.7

Sintering density and porosity results

- Mechanically mixed dopant additions.

Powder MA: 1% Al_2O_3 addition, mechanically mixed.

Sintering temperature (°C)	1150	1350	1550	1750
Bulk density (g/cm^3).	4.15	5.95	5.98	5.59
Standard deviation (g/cm^3).	0.001	0.001	0.002	0.001
Apparent solid density (g/cm^3).	5.95	5.96	5.99	5.69
Standard deviation (g/cm^3).	0.001	0.001	0.002	0.002
Apparent porosity (%)	30.24	0.20	0.16	1.72
True porosity (%)	31.98	2.51	1.93	8.33
Standard deviation (g/cm^3).	0.01	0.02	0.03	0.02
% of theoretical density.	68.02	97.49	98.07	91.67
Standard deviation (%).	0.01	0.02	0.03	0.02
Bulk density change (g/cm^3). (compared with undoped blank)	0.23	-0.07	-0.06	-0.47
Bulk density change (%).	5.84	-1.23	-1.02	-7.78

Powder MT : 1% TiO_2 addition mechanically mixed.

Sintering temperature (°C)	1150	1350	1550	1750
Bulk density (g/cm^3).	4.24	5.95	5.97	5.92
Standard deviation (g/cm^3).	0.001	0.001	0.002	0.000
Apparent solid density (g/cm^3).	5.92	5.96	5.97	5.92
Standard deviation (g/cm^3).	0.002	0.001	0.002	0.000
Apparent porosity (%)	28.37	0.20	0.00	0.08
True porosity (%)	30.47	2.51	2.15	2.99
Standard deviation (g/cm^3).	0.02	0.02	0.03	0.00
% of theoretical density.	69.53	97.49	97.85	97.01
Standard deviation (%).	0.02	0.02	0.03	0.00
Bulk density change (g/cm^3). (compared with undoped blank)	0.32	-0.07	-0.08	-0.15
Bulk density change (%).	8.18	-1.23	-1.25	-2.40

Table 4.3.7

Sintering density and porosity results

- Mechanically mixed dopant additions (continued...).

Powder MS: 1% SiO_2 addition, mechanically mixed.

Sintering temperature (°C)	1150	1350	1550	1750
Bulk density (g/cm^3).	4.67	5.94	5.94	5.85
Standard deviation (g/cm^3).	0.001	0.001	0.001	0.002
Apparent solid density (g/cm^3).	5.92	5.94	5.94	5.85
Standard deviation (g/cm^3).	0.002	0.001	0.001	0.002
Apparent porosity (%)	21.10	0.00	0.04	0.00
True porosity (%)	23.41	2.62	2.67	4.09
Standard deviation (g/cm^3).	0.02	0.02	0.02	0.03
% of theoretical density.	76.59	97.38	97.33	95.91
Standard deviation (%).	0.02	0.02	0.02	0.03
Bulk density change (g/cm^3). (compared with undoped blank)	0.75	-0.08	-0.11	-0.21
Bulk density change (%).	19.17	-1.33	-1.78	-3.51

Table 4.3.8 (a)
Analysis of data for factorial experiment
1150-1250°C temperature interval.
(Yates' method).

a = 1% Al_2O_3, b = 1% SiO_2, c = 1% TiO_2,
d = higher sintering temperature

Treatment	Mean density	(1)	(2)	(3)	(4)	EFFECT.	degrees of freedom	Sum of squares
1	3.95	9.37	19.11	36.52	82.41 = T			
a	5.42	9.74	17.41	45.89	7.15 = [A]	0.89	1	3.195
b	3.99	8.00	23.26	6.00	2.97 = [B]	0.37	1	0.551
ab	5.75	9.11	22.63	1.15	0.11 = [AB]	0.01	1	0.001
c	3.50	11.53	3.23	1.78	-2.23 = [C]	-0.29	1	0.339
ac	4.50	11.73	2.77	1.19	-0.15 = [AC]	-0.02	1	0.001
bc	3.82	10.82	0.42	1.06	1.83 = [BC]	0.23	1	0.209
abc	5.59	11.81	0.73	-0.95	-0.07 = [ABC]	-0.01	1	0.000
d	5.61	1.47	0.37	-1.70	9.37 = [D]	1.17	1	5.487
ad	5.92	1.76	1.41	-0.63	-4.85 = [AD]	-0.61	1	1.470
bd	5.81	1.00	0.20	-0.46	0.59 = [BD]	-0.07	1	0.022
abd	5.92	1.77	0.99	0.31	2.01 = [ABD]	-0.25	1	0.253
cd	5.04	0.31	0.29	2.33	-0.22 = [CD]	-0.03	1	0.003
acd	5.78	0.11	0.77	0.79	0.77 = [ACD]	0.10	1	0.037
bcd	5.91	0.74	-0.20	0.48	-0.25 = [BCD]	-0.03	1	0.004
abcd	5.90	-0.01	-0.75	-0.55	-1.03 = [ABCD]	-0.13	1	0.066
Total (T) =	82.41							

Table 4.3.8 (b)
Analysis of data for factorial experiment
1250-1350°C temperature interval.
(Yates' method).

a = 1% Al_2O_3, b = 1% SiO_2, c = 1% TiO_2,
d = higher sintering temperature

Treatment	Mean density	(1)	(2)	(3)	(4)	EFFECT.	degrees of freedom	Sum of squares
1	5.61	11.53	23.26	45.89	93.28 = T			
a	5.92	11.73	22.63	47.39	1.40 = [A]	0.17	1	0.122
b	5.81	10.82	23.80	1.15	1.06 = [B]	0.13	1	0.070
ab	5.92	11.81	23.59	0.25	-1.18 = [AB]	-0.15	1	0.087
c	5.04	11.99	0.42	1.19	-0.84 = [C]	-0.10	1	0.044
ac	5.78	11.81	0.73	-0.13	0.40 = [AC]	0.05	1	0.010
bc	5.91	11.77	0.08	-0.95	1.02 = [BC]	0.13	1	0.065
abc	5.90	11.82	0.17	-0.23	-0.82 = [ABC]	-0.10	1	0.042
d	5.98	0.31	0.20	-0.63	1.50 = [D]	0.19	1	0.141
ad	6.01	0.11	0.99	-0.21	-0.90 = [AD]	-0.11	1	0.051
bd	5.88	0.74	-0.18	0.31	-1.32 = [BD]	-0.17	1	0.109
abd	5.93	-0.01	0.05	0.09	0.72 = [ABD]	0.09	1	0.032
cd	5.78	0.03	-0.20	0.79	0.42 = [CD]	0.05	1	0.011
acd	5.99	0.05	-0.75	0.23	-0.22 = [ACD]	-0.03	1	0.003
bcd	5.93	0.21	0.02	-0.55	-0.56 = [BCD]	-0.07	1	0.020
abcd	5.89	-0.04	-0.25	-0.27	0.28 = [ABCD]	0.03	1	0.005
Total (T) =	93.28							

Table 4.3.8 (c)
Analysis of data for factorial experiment
1350-1450°C temperature interval.
(Yates' method).

a = 1% Al_2O_3, b = 1% SiO_2, c = 1% TiO_2,
d = higher sintering temperature

Treatment	Mean density	(1)	(2)	(3)	(4)	EFFECT.	degrees of freedom	Sum of squares
1	5.98	11.99	23.80	47.39	95.06 = T			
a	6.01	11.81	23.59	47.67	0.12 = [A]	0.02	1	0.001
b	5.88	11.77	23.91	0.25	-0.56 = [B]	-0.07	1	0.020
ab	5.93	11.82	23.76	-0.13	-0.38 = [AB]	-0.05	1	0.009
c	5.78	12.05	0.08	-0.13	-0.36 = [C]	-0.04	1	0.008
ac	5.99	11.86	0.17	-0.43	0.06 = [AC]	0.01	1	0.000
bc	5.93	12.00	-0.05	-0.23	0.18 = [BC]	0.02	1	0.002
abc	5.89	11.76	-0.08	-0.15	-0.28 = [ABC]	-0.04	1	0.005
d	6.02	0.03	-0.18	-0.21	0.28 = [D]	0.03	1	0.005
ad	6.03	0.05	0.05	-0.15	-0.38 = [AD]	-0.05	1	0.009
bd	5.96	0.21	-0.19	0.09	-0.30 = [BD]	-0.04	1	0.006
abd	5.90	-0.04	-0.24	-0.03	0.08 = [ABD]	0.01	1	0.000
cd	6.00	0.01	0.02	0.23	0.06 = [CD]	0.01	1	0.000
acd	6.00	-0.06	-0.25	-0.05	-0.12 = [ACD]	-0.02	1	0.001
bcd	5.92	0.00	-0.07	-0.27	-0.28 = [BCD]	-0.04	1	0.005
abcd	5.84	-0.08	-0.08	-0.01	0.26 = [ABCD]	0.03	1	0.004
Total (T) =	95.06							

Table 4.3.8 (d)
Analysis of data for factorial experiment
1450-1550°C temperature interval.
(Yates' method).

a = 1% Al_2O_3, b = 1% SiO_2, c = 1% TiO_2,
d = higher sintering temperature

Treatment	Mean density	(1)	(2)	(3)	(4)	EFFECT.	degrees of freedom	Sum of squares
1	6.02	12.05	23.91	47.67	95.11 = T			
a	6.03	11.86	23.76	47.44	-0.55 = [A]	-0.07	1	0.019
b	5.96	12.00	23.82	-0.13	-1.17 = [B]	-0.15	1	0.086
ab	5.90	11.76	23.62	-0.42	-0.39 = [AB]	-0.05	1	0.010
c	6.00	12.09	-0.05	-0.43	-0.35 = [C]	-0.04	1	0.008
ac	6.00	11.73	-0.08	-0.74	-0.05 = [AC]	-0.01	1	0.000
bc	5.92	12.00	-0.20	-0.15	-0.07 = [BC]	-0.01	1	0.000
abc	5.84	11.62	-0.22	-0.24	0.03 = [ABC]	0.00	1	0.000
d	6.06	0.01	-0.19	-0.15	-0.23 = [D]	-0.03	1	0.003
ad	6.03	-0.06	-0.24	-0.20	-0.29 = [AD]	-0.04	1	0.005
bd	5.95	0.00	-0.36	-0.03	-0.31 = [BD]	-0.04	1	0.006
abd	5.78	-0.08	-0.38	-0.02	-0.09 = [ABD]	-0.01	1	0.001
cd	6.03	-0.03	-0.07	-0.05	-0.05 = [CD]	-0.01	1	0.000
acd	5.97	-0.17	-0.08	-0.02	0.01 = [ACD]	0.00	1	0.000
bcd	5.89	-0.06	-0.14	-0.01	0.03 = [BCD]	0.00	1	0.000
abcd	5.73	-0.16	-0.10	0.04	0.05 = [ABCD]	0.01	1	0.000
Total (T) =	95.11							

Table 4.3.8 (e)
Analysis of data for factorial experiment
1550-1650°C temperature interval.
(Yates' method).

a = 1% Al_2O_3, b = 1% SiO_2, c = 1% TiO_2,
d = higher sintering temperature

Treatment	Mean density	(1)	(2)	(3)	(4)	EFFECT.	degrees of freedom	Sum of squares
1	6.06	12.09	23.82	47.44	94.61 = T			
a	6.03	11.73	23.62	47.17	-1.07 = [A]	-0.13	1	0.072
b	5.95	12.00	23.66	-0.42	-1.61 = [B]	-0.20	1	0.162
ab	5.78	11.62	23.51	-0.65	-0.49 = [AB]	-0.06	1	0.015
c	6.03	12.05	-0.20	-0.74	-0.35 = [C]	-0.04	1	0.008
ac	5.97	11.61	-0.22	-0.87	0.01 = [AC]	0.00	1	0.000
bc	5.89	11.97	-0.34	-0.24	-0.01 = [BC]	-0.00	1	0.000
abc	5.73	11.54	-0.31	-0.25	0.11 = [ABC]	0.01	1	0.001
d	6.07	-0.03	-0.36	-0.20	-0.27 = [D]	-0.03	1	0.005
ad	5.98	-0.17	-0.38	-0.15	-0.23 = [AD]	-0.03	1	0.003
bd	5.93	-0.06	-0.44	-0.02	-0.13 = [BD]	-0.02	1	0.001
abd	5.68	-0.16	-0.43	0.03	-0.01 = [ABD]	-0.00	1	0.000
cd	6.04	-0.09	-0.14	-0.02	0.05 = [CD]	0.01	1	0.000
acd	5.93	-0.25	-0.10	0.01	0.05 = [ACD]	0.01	1	0.000
bcd	5.87	-0.11	-0.16	0.04	0.03 = [BCD]	0.00	1	0.000
abcd	5.67	-0.20	-0.09	0.07	0.03 = [ABCD]	0.00	1	0.000
Total (T) =	94.61							

Table 4.3.8 (f)
Analysis of data for factorial experiment
1650-1750°C temperature interval.
(Yates' method).

a = 1% Al_2O_3, b = 1% SiO_2, c = 1% TiO_2,
d = higher sintering temperature

Treatment	Mean density	(1)	(2)	(3)	(4)	EFFECT.	degrees of freedom	Sum of squares
1	6.07	12.05	23.66	47.17	92.98 = T			
a	5.98	11.61	23.51	45.81	-2.60 = [A]	-0.32	1	0.422
b	5.93	11.97	22.94	-0.65	-1.46 = [B]	-0.18	1	0.133
ab	5.68	11.54	22.87	-1.95	-0.24 = [AB]	-0.03	1	0.004
c	6.04	11.61	-0.34	-0.87	-0.22 = [C]	-0.03	1	0.003
ac	5.93	11.33	-0.31	-0.59	0.16 = [AC]	0.02	1	0.002
bc	5.87	11.59	-1.04	-0.25	-0.02 = [BC]	-0.00	1	0.000
abc	5.67	11.28	-0.91	0.01	0.04 = [ABC]	0.00	1	0.000
d	6.07	-0.09	-0.44	-0.15	-1.36 = [D]	-0.17	1	0.116
ad	5.54	-0.25	-0.43	-0.07	-1.30 = [AD]	-0.16	1	0.106
bd	5.92	-0.11	-0.28	0.03	0.28 = [BD]	0.04	1	0.005
abd	5.41	-0.20	-0.31	0.13	0.26 = [ABD]	0.03	1	0.004
cd	6.02	-0.53	-0.16	0.01	0.08 = [CD]	0.01	1	0.000
acd	5.57	-0.51	-0.09	-0.03	0.10 = [ACD]	0.01	1	0.001
bcd	5.87	-0.45	0.02	0.07	-0.04 = [BCD]	-0.00	1	0.000
abcd	5.41	-0.46	-0.01	-0.03	-0.10 = [ABCD]	-0.01	1	0.001
Total (T) =	92.98							

Table 4.3.8 (g)

Analysis of Variance (ANOVA Table),

Factorial Experiment 1150-1250°C temperature interval.

Source of variation	degrees of freedom	sum of squares	mean square	(Pooled error estimate) mean square/ error mean square	F test signif-icance.	(External error estimate) mean square/ error mean square	F test signif-icance.
Al_2O_3 addition (A)	1	3.1952	3.1952	44.37	***	3350.17	***
SiO_2 Addition (B)	1	0.5513	0.5513	7.66	**	612.56	***
TiO_2 addition (C)	1	0.3393	0.3393	4.71	*	377.01	***
Sintering temperature (D)	1	5.4873	5.4873	76.20	***	6097.01	***
Interactions: (2nd order)							
AB	1	0.0008	0.0008	0.01	N/S	0.84	N/S
AC	1	0.0014	0.0014	0.02	N/S	1.56	N/S
AD	1	1.4702	1.4702	20.41	***	1633.51	***
BC	1	0.2093	0.2093	2.91	*	232.56	***
BD	1	0.0218	0.0218	0.30	N/S	24.17	***
CD	1	0.0716	0.0716	0.99	N/S	79.51	***
(3rd order)							
ABC	1	0.0003	0.0003	0.00	---	0.34	N/S
ABD	1	0.2525	0.2525	3.51	---	280.56	***
ACD	1	0.0371	0.0371	0.51	---	41.17	***
BCD	1	0.0039	0.0039	0.05	---	4.34	*
(4th order)							
ABCD	1	0.0663	0.0663	0.92	---	73.67	***
Error terms: Internal (pooled 3rd and 4th order terms)	5	0.3601	0.0702	----			
External estimate of error (method c difference values)	16	0.0144	0.0009	----			

f test values for significance		(5 & 1 degrees of freedom)
f (1 %) (highly significant)	16.3	Indicated as *** in results.
f (5 %)	6.61	Indicated as ** in results.
f (10 %) (less significant)	4.06	Indicated as * in results.
		(16 & 1 degrees of freedom)
f (1 %) (highly significant)	8.53	Indicated as *** in results.
f (5 %)	4.49	Indicated as ** in results.
f (10 %) (less significant)	3.05	Indicated as * in results.

Calculation of external error estimate.

Mean difference (method c) = 0.030
Difference squared = 0.0009
Sum of squares of differences = 0.0144
Mean square difference = sum squares /degrees freedom = 0.0009

Table 4.3.8 (h)

Analysis of Variance (ANOVA Table),

Factorial Experiment 1250-1350°C temperature interval.

Source of variation	degrees of freedom	sum of squares	mean square	(Pooled error estimate) mean square/ error mean square	F test signif-icance.	(External error estimate) mean square/ error mean square	F test signif-icance.
Al2O3 addition (A)	1	0.1225	0.1225	6.01	*	136.11	***
SiO2 Addition (B)	1	0.0702	0.0702	3.44	N/S	78.03	***
TiO2 addition (C)	1	0.0441	0.0441	2.16	N/S	49.03	***
sintering temperature (D)	1	0.1406	0.1406	6.90	**	156.25	***
Interactions:							
(2nd order)							
AB	1	0.0878	0.0878	4.27	*	96.69	***
AC	1	0.0100	0.0100	0.49	N/S	11.11	***
AD	1	0.0506	0.0506	2.48	N/S	56.25	***
BC	1	0.0650	0.0650	3.19	N/S	72.25	***
BD	1	0.1089	0.1089	5.34	*	121.00	***
CD	1	0.0110	0.0110	0.54	N/S	12.25	***
(3rd order)							
ABC	1	0.0420	0.0420	2.06	---	46.69	***
ABD	1	0.0324	0.0324	1.59	---	36.00	***
ACD	1	0.0030	0.0030	0.15	---	3.36	*
BCD	1	0.0196	0.0196	0.96	---	21.78	***
(4th order)							
ABCD	1	0.0049	0.0049	0.24	---	0.24	N/S
Error terms:							
Internal							
(pooled 3rd and 4th order terms)	5	0.1020	0.0204	----			
External estimate of error							
(method c difference values)	16	0.0144	0.0009	----			

f test values for significance		(5 & 1 degrees of freedom)
f (1 %) (highly significant)	16.3	Indicated as *** in results.
f (5 %)	6.61	Indicated as ** in results.
f (10 %) (less significant)	4.06	Indicated as * in results.
		(16 & 1 degrees of freedom)
f (1 %) (highly significant)	8.53	Indicated as *** in results.
f (5 %)	4.49	Indicated as ** in results.
f (10 %) (less significant)	3.05	Indicated as * in results.

Calculation of external error estimate.

Mean difference (method c) = 0.030
Difference squared = 0.0009
Sum of squares of differences = 0.0144
Mean square difference = sum squares /degrees freedom = 0.0009

Table 4.3.8 (i)

Analysis of Variance (ANOVA Table),

Factorial Experiment 1350-1450°C temperature interval.

Source of variation	degrees of freedom	sum of squares	mean square	(Pooled error estimate) mean square/ error mean square	F test signif-icance.	(External error estimate) mean square/ error mean square	F test signif-icance.
Al_2O_3 addition (A)	1	0.0009	0.0009	0.29	N/S	1.00	N/S
SiO_2 Addition (B)	1	0.0196	0.0196	6.39	*	21.78	***
TiO_2 addition (C)	1	0.0081	0.0081	2.64	N/S	9.00	***
Sintering temperature (D)	1	0.0049	0.0049	1.60	N/S	5.44	**
Interactions:							
(2nd order)							
AB	1	0.0090	0.0090	2.94	N/S	10.03	***
AC	1	0.0002	0.0002	0.07	N/S	0.25	N/S
AD	1	0.0090	0.0090	2.94	N/S	10.03	***
BC	1	0.0020	0.0020	0.66	N/S	2.25	N/S
BD	1	0.0056	0.0056	1.84	N/S	6.25	**
CD	1	0.0002	0.0002	0.07	N/S	0.25	N/S
(3rd order)							
ABC	1	0.0049	0.0049	1.60	---	5.44	**
ABD	1	0.0004	0.0004	0.13	---	0.44	N/S
ACD	1	0.0009	0.0009	0.29	---	1.00	N/S
BCD	1	0.0049	0.0049	1.60	---	5.44	**
(4th order)							
ABCD	1	0.0042	0.0042	1.38	---	1.38	N/S
Error terms:							
Internal							
(pooled 3rd and 4th order terms)	5	0.0153	0.0031	----			
External estimate of error							
(method c difference values)	16	0.0144	0.0009	----			

f test values for significance		(5 & 1 degrees of freedom)
f (1 %) (highly significant)	16.3	Indicated as *** in results.
f (5 %)	6.61	Indicated as ** in results.
f (10 %) (less significant)	4.06	Indicated as * in results.
		(16 & 1 degrees of freedom)
f (1 %) (highly significant)	8.53	Indicated as *** in results.
f (5 %)	4.49	Indicated as ** in results.
f (10 %) (less significant)	3.05	Indicated as * in results.

Calculation of external error estimate.

Mean difference (method c) = 0.030
Difference squared = 0.0009
Sum of squares of differences = 0.0144
Mean square difference = sum squares /degrees freedom = 0.0009

Table 4.3.8 (j)

Analysis of Variance (ANOVA Table),

Factorial Experiment 1450-1550°C temperature interval.

Source of variation	degrees of freedom	sum of squares	mean square	(Pooled error estimate) mean square/ error mean square	F test signif-icance.	(External error estimate) mean square/ error mean square	F test signif-icance.
Al_2O_3 addition (A)	1	0.0189	0.0189	121.00	***	21.01	***
SiO_2 Addition (B)	1	0.0856	0.0856	547.56	***	95.06	***
TiO_2 addition (C)	1	0.0077	0.0077	49.00	***	8.57??	**
Sintering temperature (D)	1	0.0033	0.0033	21.16	***	3.67	N/S
Interactions:							
(2nd order)							
AB	1	0.0095	0.0095	60.84	***	10.56	***
AC	1	0.0002	0.0002	1.00	N/S	0.00	N/S
AD	1	0.0053	0.0053	33.64	***	5.84	**
BC	1	0.0003	0.0003	1.96	N/S	0.34	N/S
BD	1	0.0060	0.0060	38.44	***	6.67	**
CD	1	0.0002	0.0002	1.00	N/S	0.17	N/S
(3rd order)							
ABC	1	0.0001	0.0001	0.36	---	0.06	N/S
ABD	1	0.0005	0.0005	3.24	---	0.56	N/S
ACD	1	0.0000	0.0000	0.00	---	0.00	N/S
BCD	1	0.0001	0.0001	0.36	---	0.06	N/S
(4th order)							
ABCD	1	0.0002	0.0002	1.00	---	1.00	N/S
Error terms:							
Internal							
(pooled 3rd and 4th order terms)	5	0.0008	0.0002	----			
External estimate of error							
(method c difference values)	16	0.0144	0.0009	----			

f test values for significance		(5 & 1 degrees of freedom)
f (1 %) (highly significant)	16.3	Indicated as *** in results.
f (5 %)	6.61	Indicated as ** in results.
f (10 %) (less significant)	4.06	Indicated as * in results.
		(16 & 1 degrees of freedom)
f (1 %) (highly significant)	8.53	Indicated as *** in results.
f (5 %)	4.49	Indicated as ** in results.
f (10 %) (less significant)	3.05	Indicated as * in results.

Calculation of external error estimate.

Mean difference (method c) = 0.030
Difference squared = 0.0009
Sum of squares of differences = 0.0144
Mean square difference = sum squares /degrees freedom = 0.0009

Table 4.3.8 (k)

Analysis of Variance (ANOVA Table),

Factorial Experiment 1550-1650°C temperature interval.

Source of variation	degrees of freedom	sum of squares	mean square	(Pooled error estimate) mean square/ error mean square	F test signif-icance.	(External error estimate) mean square/ error mean square	F test signif-icance.
Al_2O_3 addition (A)	1	0.0716	0.0716	346.94	***	79.51	***
SiO_2 Addition (B)	1	0.1620	0.1620	785.48	***	180.01	***
TiO_2 addition (C)	1	0.0077	0.0077	37.12	***	8.51	**
Sintering temperature (D)	1	0.0046	0.0046	22.09	***	5.06	**
Interactions:							
(2nd order)							
AB	1	0.0150	0.0150	72.76	***	16.67	***
AC	1	0.0000	0.0000	0.00	N/S	0.00	N/S
AD	1	0.0033	0.0033	16.03	**	3.67	**
BC	1	0.0000	0.0000	0.00	N/S	0.00	N/S
BD	1	0.0011	0.0011	5.12	*	1.17	N/S
CD	1	0.0002	0.0002	0.76	N/S	0.17	N/S
(3rd order)							
ABC	1	0.0008	0.0008	3.67	---	0.84	N/S
ABD	1	0.0000	0.0000	0.00	---	0.00	N/S
ACD	1	0.0002	0.0002	0.76	---	0.17	N/S
BCD	1	0.0001	0.0001	0.27	---	0.06	N/S
(4th order)							
ABCD	1	0.0001	0.0001	0.27	---	0.27	N/S
Error terms:							
Internal							
(pooled 3rd and 4th order terms)	5	0.0010	0.0002	----			
External estimate of error							
(method c difference values)	16	0.0144	0.0009	----			

f test values for significance		(5 & 1 degrees of freedom)
f (1 %) {highly significant}	16.3	Indicated as *** in results.
f (5 %)	6.61	Indicated as ** in results.
f (10 %) {less significant}	4.06	Indicated as * in results.
		(16 & 1 degrees of freedom)
f (1 %) {highly significant}	8.53	Indicated as *** in results.
f (5 %)	4.49	Indicated as ** in results.
f (10 %) {less significant}	3.05	Indicated as * in results.

Calculation of external error estimate.

Mean difference (method c) = 0.030
Difference squared = 0.0009
Sum of squares of differences = 0.014
Mean square difference = sum squares /degrees freedom = 0.0009

Table 4.3.8 (1)

Analysis of Variance (ANOVA Table),

Factorial Experiment 1650-1750°C temperature interval.

Source of variation	degrees of freedom	sum of squares	mean square	(Pooled error estimate) mean square/ error mean square	F test signif-icance.	(External error estimate) mean square/ error mean square	F test signif-icance.
Al_2O_3 addition (A)	1	0.4225	0.4225	372.25	***	469.44	***
SiO_2 Addition (B)	1	0.1332	0.1332	117.38	***	148.03	***
TiO_2 addition (C)	1	0.0030	0.0030	2.67	N/S	3.36	*
Sintering temperature (D)	1	0.1156	0.1156	101.85	***	128.44	**
Interactions:							
(2nd order)							
AB	1	0.0036	0.0036	3.17	N/S	4.00	*
AC	1	0.0016	0.0016	1.41	N/S	1.78	N/S
AD	1	0.1056	0.1056	93.06	***	117.36	***
BC	1	0.0000	0.0000	0.00	N/S	0.00	N/S
BD	1	0.0049	0.0049	4.32	*	5.44	**
CD	1	0.0004	0.0004	0.35	N/S	0.44	N/S
(3rd order)							
ABC	1	0.0001	0.0001	0.09	---	0.11	N/S
ABD	1	0.0042	0.0042	3.72	---	4.69	**
ACD	1	0.0006	0.0006	0.55	---	0.69	N/S
BCD	1	0.0001	0.0001	0.09	---	0.11	N/S
(4th order)							
ABCD	1	0.0006	0.0006	0.55	---	0.69	N/S
Error terms:							
Internal							
(pooled 3rd and 4th order terms)	5	0.0057	0.0057	----			
External estimate of error							
(method c difference values)	16	0.0144	0.0009	----			

f test values for significance		(5 & 1 degrees of freedom)
f (1 %) (highly significant)	16.3	Indicated as *** in results.
f (5 %)	6.61	Indicated as ** in results.
f (10 %) (less significant)	4.06	Indicated as * in results.
		(16 & 1 degrees of freedom)
f (1 %) (highly significant)	8.53	Indicated as *** in results.
f (5 %)	4.49	Indicated as ** in results.
f (10 %) (less significant)	3.05	Indicated as * in results.

Calculation of external error estimate.

Mean difference (method c) = 0.030
Difference squared = 0.0009
Sum of squares of differences = 0.0144
Mean square difference = sum squares /degrees freedom = 0.0009

Table 4.4.1 (a)

Estimation of measuring error in Seescan results for doped and undoped specimens.

Undoped specimens	
Mean 95% confidence limits:	
all sinter temps.	0.13
1250-1650°C sinter.	0.13
1700-1750°C sinter.	0.10
Alumina doped specimens.	
Mean 95% confidence limits:	
all sinter temps.	0.51
1250-1650°C sinter.	0.22
1700-1750°C sinter.	1.32
Silica doped specimens	
Mean 95% confidence limits:	
all sinter temps.	0.22
1250-1650°C sinter.	0.19
1700-1750°C sinter.	0.28
Titania doped specimens	
Mean 95% confidence limits:	
All sinter temps.	0.30
1250-1650°C sinter.	0.32
1700-1750°C sinter.	0.27
Multiple dopant addns.	
All sinter temps.	0.55
1250-1650 C sinter.	0.37
1700-1750 C sinter.	1.01
Average for all specimens	
Mean 95% confidence limits:	
all sinter temps.	0.34
1250-1650°C sinter.	0.25
1700-1750°C sinter.	0.60

Table 4.4.1 (b).

Estimate of total experimental error in Seescan results from repeat powder batches (method (b)).

Sintering Temperature (°C)	1250	1350	1450	1550	1650	1700
	Seescan measured defect area values (%).					
Powder 1, 0.25% Al_2O_3	0.24	0.25	0.29	1.24	0.96	1.09
Powder 20, 0.25% Al_2O_3 Rpt.	0.71	0.52	0.63	1.52	1.50	1.34
| difference |	0.47	0.27	0.34	0.28	0.53	0.25

Sintering Temperature (°C)	1250	1350	1450	1550	1650	1700
	Seescan measured defect area values (%).					
Powder 2, 0.75% Al_2O_3	0.59	0.62	0.83	1.21	2.01	10.55
Powder 16, 0.75% Al_2O_3 Rpt.	0.58	0.52	0.69	1.43	2.13	11.65
| difference |	0.01	0.11	0.14	0.22	0.12	1.10

Estimated error

(average for 1250-1700°C sintering temperatures).

Mean difference (between samples) = 0.32%
Std. Deviation in difference values = 0.28%
Std. Error in difference values = 0.08%
95% confidence limit, error < + or - 0.48%

Table 4.4.2

Seescan analysis results - undoped samples.

Powder no.11

(Blank Treatment on TZ3Y)

Sintering Temp (°C).	No. of Defects counted	Total Defect area (mm^2)	Mean Defect area (%)	S.D. area (%)	Std. Error (%)
1250	529	0.00588	1.50	0.45	0.14
1350	214	0.00276	0.70	0.25	0.08
1450	303	0.00316	0.81	0.38	0.12
1550	232	0.00214	0.55	0.32	0.10
1650	253	0.00212	0.54	0.32	0.10
1700	140	0.00157	0.40	0.24	0.08
1750	223	0.00180	0.46	0.28	0.09

Powder no.15

(Unmodified TZ3Y, as supplied).

Sintering Temp (°C).	No. of Defects counted	Total Defect area (mm^2)	Mean Defect area (%)	S.D. area (%)	Std. Error (%)
1250	301	0.00255	0.65	0.13	0.04
1350	74	0.00046	0.12	0.03	0.01
1450	59	0.00040	0.10	0.08	0.03
1550	38	0.00039	0.10	0.06	0.02
1650	37	0.00045	0.11	0.09	0.03
1700	69	0.00055	0.14	0.09	0.03
1750	59	0.00043	0.11	0.04	0.01

(note S.D. = standard deviation)

Table 4.4.3

Seescan analysis results - Alumina doped samples.

Powder no. 1

(0.25% Al_2O_3 addition)

Sintering Temp (°C).	No. of Defects counted	Total Defect area (mm^2)	Mean Defect area (%)	S.D. area (%)	Std. Error (%)
1250	75	0.00093	0.24	0.24	0.08
1350	95	0.00097	0.25	0.18	0.06
1450	128	0.00112	0.29	0.24	0.08
1550	489	0.00485	1.24	0.43	0.14
1650	506	0.00377	0.96	0.38	0.12
1700	488	0.00425	1.09	0.45	0.14
1750	1522	0.01003	2.57	0.67	0.21

Powder no.20

(0.25% Al_2O_3 addition repeat.)

Sintering Temp (°C).	No. of Defects counted	Total Defect area (mm^2)	Mean Defect area (%)	S.D. area (%)	Std. Error (%)
1250	101	0.00278	0.71	0.65	0.21
1350	195	0.00204	0.52	0.20	0.06
1450	146	0.00246	0.63	0.50	0.16
1550	699	0.00594	1.52	0.73	0.23
1650	389	0.00585	1.50	1.05	0.33
1700	412	0.00524	1.34	0.49	0.16
1750	688	0.00575	1.47	0.89	0.28

Powder no.18

(0.5% Al_2O_3 addition)

Sintering Temp (°C).	No. of Defects counted	Total Defect area (mm^2)	Mean Defect area (%)	S.D. area (%)	Std. Error (%)
1250	56	0.00044	0.11	0.05	0.02
1350	96	0.00064	0.16	0.05	0.02
1450	197	0.00165	0.42	0.09	0.03
1550	506	0.00401	1.02	0.31	0.10
1650	1516	0.01028	2.63	0.86	0.27
1700	2144	0.03534	9.04	0.71	0.22
1750	2282	0.08906	22.78	6.18	1.96

(note S.D. = standard deviation)

Table 4.4.3

Seescan analysis results

- Alumina doped samples (continued....).

Powder no. 2

(0.75% Al_2O_3)

Sintering Temp (°C).	No. of Defects counted	Total Defect area (mm^2)	Mean Defect area (%)	S.D. area (%)	Std. Error (%)
1250	189	0.00232	0.59	0.33	0.104
1350	202	0.00243	0.62	0.31	0.098
1450	249	0.00324	0.83	0.27	0.085
1550	815	0.00475	1.21	0.32	0.101
1650	1075	0.00785	2.01	0.45	0.142
1700	3396	0.04124	10.55	1.05	0.332
1750	2208	0.07472	19.11	3.47	1.098

Powder no.16

(0.75% Al_2O_3 addition repeat)

Sintering Temp (°C).	No. of Defects counted	Total Defect area (mm^2)	Mean Defect area (%)	S.D. area (%)	Std. Error (%)
1250	101	0.00227	0.58	0.43	0.14
1350	159	0.00202	0.52	0.24	0.08
1450	237	0.00271	0.69	0.30	0.09
1550	723	0.00561	1.43	0.14	0.04
1650	1119	0.00833	2.13	0.39	0.12
1700	1751	0.04557	11.65	1.07	0.34
1750	2200	0.10456	26.74	5.91	1.87

Powder no.13

(1% Al_2O_3 addition)

Sintering Temp (°C).	No. of Defects counted	Total Defect area (mm^2)	Mean Defect area (%)	S.D. area (%)	Std. Error (%)
1250	473	0.00518	1.32	0.30	0.09
1350	467	0.00480	1.23	0.28	0.09
1450	287	0.00240	0.61	0.17	0.05
1550	459	0.00354	0.91	0.23	0.07
1650	1060	0.00766	1.96	0.31	0.10
1700	3928	0.04726	12.09	2.51	0.79
1750					

(note S.D. = standard deviation)

Table 4.4.4

Seescan analysis results - Silica doped samples.

Powder no. 5
(0.25% SiO_2 addition)

Sintering Temp (°C).	No. of Defects counted	Total Defect area (mm^2)	Mean Defect area (%)	S.D. area (%)	Std. Error (%)
1250	242	0.00198	0.51	0.19	0.06
1350	107	0.00206	0.53	0.15	0.05
1450	258	0.00270	0.69	0.29	0.09
1550	425	0.00307	0.79	0.35	0.11
1650	752	0.00630	1.61	0.55	0.17
1700	936	0.00651	1.66	0.28	0.09

Powder no.17
(0.5% SiO_2 addition)

Sintering Temp (°C).	No. of Defects counted	Total Defect area (mm^2)	Mean Defect area (%)	S.D. area (%)	Std. Error (%)
1250	48	0.00054	0.14	0.09	0.03
1350	39	0.00037	0.09	0.05	0.02
1450	89	0.00083	0.21	0.09	0.03
1550	312	0.00206	0.53	0.12	0.04
1650	986	0.00738	1.89	0.71	0.22
1700	1054	0.00762	1.95	0.54	0.17
1750	1000	0.00693	1.77	0.23	0.07

Powder no. 7
(0.75% SiO_2 addition)

Sintering Temp (°C).	No. of Defects counted	Total Defect area (mm^2)	Mean Defect area (%)	S.D. area (%)	Std. Error (%)
1250	735	0.01172	3.00	0.98	0.31
1350	231	0.00378	0.97	0.40	0.13
1450	307	0.00472	1.21	0.38	0.12
1550	817	0.00757	1.94	0.48	0.15
1650	575	0.00829	2.12	0.73	0.23
1700	623	0.00549	1.40	0.59	0.19
1750	438	0.00762	1.95	0.61	0.19
1550 rpt.	441	0.00495	1.27	0.30	0.09
1650 rpt	592	0.00453	1.16	0.73	0.23

(note S.D. = standard deviation)

Table 4.4.4

Seescan analysis results

- silica doped samples (continued...).

Powder no. 3
(1% SiO_2 addition)

Sintering Temp (^oC).	No. of Defects counted	Total Defect area (mm^2)	Mean Defect area (%)	S.D. area (%)	Std. Error (%)
....	...	.....	....	....	....
1250	192	0.00170	0.44	0.13	0.04
1350	23	0.00049	0.13	0.05	0.02
1450	90	0.00075	0.19	0.07	0.02
1550	33	0.00039	0.10	0.10	0.03
1650	364	0.00347	0.89	0.36	0.11
1700	481	0.00321	0.82	0.36	0.11
1750	565	0.00722	1.85	0.55	0.17

(note S.D. = standard deviation)

Table 4.4.5

Seescan analysis results - Titania doped samples.

Powder no. 4

(0.25% TiO_2 addition)

Sintering Temp (°C).	No. of Defects counted	Total Defect area (mm^2)	Mean Defect area (%)	S.D. area (%)	Std. Error (%)
1250	469	0.00765	1.96	0.45	0.14
1350	359	0.00471	1.21	0.43	0.14
1450	406	0.00416	1.06	0.31	0.10
1550	349	0.00384	0.98	0.39	0.12
1650	357	0.00346	0.88	0.35	0.11
1700	399	0.00515	1.32	1.21	0.38
1750	252	0.00236	0.60	0.28	0.09

Powder no.19

(0.5% TiO_2)

Sintering Temp (°C).	No. of Defects counted	Total Defect area (mm^2)	Mean Defect area (%)	S.D. area (%)	Std. Error (%)
1250	1272	0.01310	3.35	1.14	0.36
1350	462	0.00716	1.83	0.54	0.17
1450	362	0.00223	0.57	0.79	0.25
1550	356	0.00246	0.63	0.83	0.26
1650	357	0.00192	0.49	0.65	0.21
1700	352	0.00152	0.39	0.34	0.11
1750	182	0.00262	0.67	0.35	0.11

Powder no. 8

(0.75% TiO_2)

Sintering Temp (°C).	No. of Defects counted	Total Defect area (mm^2)	Mean Defect area (%)	S.D. area (%)	Std. Error (%)
1250	1067	0.01536	3.93	1.18	0.37
1350	467	0.00718	1.84	0.55	0.17
1450	329	0.00271	0.69	0.30	0.09
1550	319	0.00353	0.90	0.39	0.12
1650	269	0.00262	0.67	0.30	0.09
1700	304	0.00229	0.59	0.31	0.10
1750	183	0.00137	0.35	0.11	0.03

(note S.D. = standard deviation)

Table 4.4.5

Seescan analysis results

- Titania doped samples (continued...).

Powder no.12

(1% TiO_2 addition)

Sintering Temp (°C).	No. of Defects counted	Total Defect area (mm^2)	Mean Defect area (%)	S.D. area (%)	Std. Error (%)
1250	772	0.01040	2.66	0.41	0.13
1350	549	0.00634	1.62	0.47	0.15
1450	390	0.00325	0.83	0.26	0.08
1550	430	0.00299	0.76	0.13	0.04
1650	356	0.00330	0.84	0.39	0.12
1700	313	0.00274	0.70	0.30	0.09
1750	267	0.00277	0.71	0.19	0.06

(note S.D. = standard deviation)

Table 4.4.6

Seescan analysis results - Multiple doped samples.

Powder no. 6
(1% SiO_2 + 1% Al_2O_3 additions)

Sintering Temp (°C).	No. of Defects counted	Total Defect area (mm^2)	Mean Defect area (%)	S.D. area (%)	Std. Error (%)
1250	83	0.00130	0.33	0.12	0.04
1350	106	0.00147	0.38	0.16	0.05
1450	910	0.00790	2.02	0.80	0.25
1550	1455	0.01787	4.57	1.65	0.52
1650	1098	0.02842	7.27	2.57	0.81
1700	1629	0.03655	9.35	2.39	0.76
1750	1278	0.03942	10.08	3.92	1.24

Powder no. 9

(1% SiO_2 + 1% TiO_2 additions)

Sintering Temp (°C).	No. of Defects counted	Total Defect area (mm^2)	Mean Defect area (%)	S.D. area (%)	Std. Error (%)
1250	200	0.00287	0.73	0.52	0.16
1350	124	0.00161	0.41	0.33	0.10
1450	439	0.00607	1.55	0.50	0.16
1550	535	0.00603	1.54	0.41	0.13
1650	810	0.01026	2.62	0.27	0.09
1700	979	0.00820	2.10	0.27	0.09
1750	875	0.00866	2.21	0.43	0.14

Powder no.14

(1% TiO_2 + 1% Al_2O_3 additions)

Sintering Temp (°C).	No. of Defects counted	Total Defect area (mm^2)	Mean Defect area (%)	S.D. area (%)	Std. Error (%)
1250	246	0.00306	0.78	0.30	0.09
1350	285	0.00257	0.66	0.23	0.07
1450	372	0.00292	0.75	0.22	0.07
1550	513	0.00388	0.99	0.25	0.08
1650	1944	0.01460	3.73	1.36	0.43
1700	1564	0.01860	4.76	1.20	0.38
1750	1344	0.03175	8.12	1.86	0.59

(note S.D. = standard deviation)

Table 4.4.6

Seescan analysis results

- Multiple doped samples (continued...).

Powder no.10

(1% SiO_2 + 1% TiO_2 + 1% Al_2O_3 additions).

Sintering Temp (^oC).	No. of Defects counted	Total Defect area (mm^2)	Mean Defect area (%)	S.D. area (%)	Std. Error (%)
....	...	.....	....	....	....
1250	34	0.00050	0.13	0.09	0.03
1350	81	0.00050	0.13	0.33	0.10
1450	684	0.00566	1.45	0.54	0.17
1550	1089	0.01508	3.86	0.56	0.18
1650	924	0.02404	6.15	0.74	0.23
1700	956	0.02378	6.08	1.37	0.43
1750	1254	0.04018	10.28	1.65	0.52

(note S.D. = standard deviation)

Table 4.4.7

Seescan results - mechanically mixed doped samples.

Powder identification MS

(Mechanically Mixed 1% SiO_2 addition)

Sintering Temp (°C).	No. of Defects counted	Total Defect area (mm^2)	Mean Defect area (%)	S.D. area (%)	Std. Error (%)
1350	350	0.00751	1.92	0.95	0.30
1550	486	0.00950	2.43	0.64	0.20
1750	402	0.01318	3.37	0.57	0.18

Powder identification MT

(Mechanically mixed 1% TiO_2 addition).

Sintering Temp (°C).	No. of Defects counted	Total Defect area (mm^2)	Mean Defect area (%)	S.D. area (%)	Std. Error (%)
1350	96	0.00249	0.64	0.67	0.21
1550	271	0.00807	2.06	1.68	0.53
1750	744	0.00501	1.28	0.67	0.21

Powder identification MA

(Mechanically Mixed 1% Al_2O_3)

Sintering Temp (°C).	No. of Defects counted	Total Defect area (mm^2)	Mean Defect area (%)	S.D. area (%)	Std. Error (%)
1350	143	0.00381	0.97	1.12	0.35
1550	73	0.00692	1.77	3.79	1.20
1750	2732	0.00346	9.10	0.67	0.21

(note S.D. = standard deviation)

Table 4.5.1(a) Estimate of measuring error in grain size determinations.

Method (a)

Undoped specimens

Powder no.	Dopant. (nominal mass %)	Grain size at (sintering temp. (°C)) 1350	1550	1750
11	Blank treatment (measurement #1)	0.48um	1.06um	3.20um
11	Blank treatment (measurement #2)	0.48um	1.14um	3.48um
11	Blank treatment (measurement #3)	0.53um	1.08um	3.17um
---	Average of 3 measurements.	0.50um	1.09um	3.28um
---	Standard deviation	0.02um	0.03um	0.14um
---	95 % confidence limits [+ or -]	0.02um	0.04um	0.16um

Titania doped specimens.

Powder no.	Dopant. (nominal mass %)	Grain size at (sintering temp. (°C)) 1350	1550	1750
8	0.75% TiO_2 (measurement #1)	0.59um	1.26um	4.29um
8.	0.75% TiO_2 (measurement #2)	0.66um	1.23um	4.21um
8.	0.75% TiO_2 (measurement #3)	0.61um	1.25um	4.20um
---	Average of 3 measurements.	0.62um	1.25um	4.23um
---	Standard deviation (um).	0.03um	0.01um	0.04um
	95 % confidence limits [+ or -]	0.03um	0.01um	0.05um

Combined error estimate

(average value of 95% confidence limits for repeat measurements).

95% confidence limits for measuring error = [+ or -] 0.05

Table 4.5.1(b) Estimate of total experimental error in grain size determinations.
Method (b).

Powder No.	Sample identification.	Grain size at sintering temperature (°C) 1350	1550	1750
1	0.25% Al_2O_3	0.53um	1.08um	5.19um
20	0.25% Al_2O_3 (repeat batch)	0.56um	1.17um	4.65um
	| difference |	0.03um	0.09um	0.55um
2	0.75% Al_2O_3	0.55um	1.11um	10.19um
16	0.75% Al_2O_3 (repeat batch)	0.59um	1.26um	9.94um
	| difference |	0.05um	0.16um	0.25um

Mean difference	= 0.19 um
Standard deviation in difference	= 0.18 um
Standard error in difference	= 0.07 um
95% confidence limit, error < (+ or -)	0.25 um

Table 4.5.2 (a)

Grain size results, undoped materials.

Powder no.	Dopant. (nominal mass %)	Grain size in um at (sintering temp. (°C)) 1350	1550	1750
11	Blank treatment.	0.48um	1.06um	3.20um
11 rpt. #1	Blank treatment (repeat)	0.48um	1.14um	3.47um
11 rpt. #2	Blank treatment (repeat)	0.53um	1.08um	3.17um
11 rpt. #3	Blank treatment (repeat)	0.50um	1.04um	3.28um
	Blank treatment (average)	0.50um	1.09um	3.28um
15	TZ3Y (as supplied)	0.53um	1.14um	3.62um

Table 4.5.3

Grain size results, alumina doped materials.

Powder no.	Dopant. (nominal mass %)	Grain size at (sintering temp. (°C)) 1350	1550	1750
	nil	0.50um	1.09um	3.28um
1	0.25% Al_2O_3	0.53um	1.08um	5.19um
18	0.5% Al_2O_3	0.53um	1.15um	9.13um
2	0.75% Al_2O_3	0.55um	1.11um	10.19um
13	1% Al_2O_3	0.56um	1.14um	10.70um
	Average for alumina additions	0.54um	1.12um	8.80um
20	0.25% Al_2O_3 (repeat batch)	0.56um	1.17um	4.65um
16	0.75% Al_2O_3 (repeat batch)	0.59um	1.26um	9.94um

Table 4.5.4

Grain size results, Silica doped materials.

Powder no.	Dopant. (nominal mass %)	Grain size at (sintering temp. (°C)) 1350	1550	1750
	nil	0.50um	1.09um	3.28um
5	0.25% SiO_2	0.51um	1.11um	4.52um
17	0.5% SiO_2	0.55um	1.19um	4.23um
7	0.75% SiO_2	0.48um	1.01um	4.23um
3	1% SiO_2	0.47um	0.59um	3.73um
Ave.	Average for all SiO_2 additions.	0.50um	0.98um	4.18um
7 Rpt.	0.75% SiO_2 (duplicate pellets).	0.51um	1.06um	4.26um

Table 4.5.5

Grain size results, titania doped materials.

Powder no.	Dopant. (nominal mass %)	Grain size at (sintering temp. (°C)) 1350	1550	1750
	nil	0.50um	1.09um	3.28um
4	0.25% TiO_2	0.53um	1.26um	3.57um
19	0.5% TiO_2	0.55um	1.17um	4.23um
12	1% TiO_2	0.59um	1.34um	4.32um
	Average for TiO_2 additions	0.57um	1.26um	4.09um

Table 4.5.6

Grain size results, multiple oxide doped materials.

Powder no.	Dopant. (nominal mass %)	Grain size at sintering temp. (°C) 1350	1550	1750
6	1% SiO_2 + 1% Al_2O_3	0.50um	4.59um (bimodal) (1.33 + 17.6 um)	12.46um
9	1% SiO_2 + 1% TiO_2	0.55um	1.56um	4.88um
10	1% SiO_2 + 1% Al_2O_3 + 1% TiO_2	0.62um	5.05um (bimodal) (2.23 + 16.4 um)	12.84um
12	1% Al_2O_3 + 1% TiO_2	0.59um	1.34um	6.94um

Table 4.6.1(a)

Estimation of measuring error in x ray diffraction results from duplicate analysis.

Powder No.	15			15					
Dopant addn.	Undoped TZ3Y			Undoped TZ3Y repeat analysis					
	Phase Composition.			Phase composition.			| Difference |		
	M_t	M_c	M_m	M_t	M_c	M_m	M_t	M_c	M_m
Sinter temp.									
1350°C	0.83	0.17	0.01	0.79	0.21	0.01	0.04	0.04	0.00
1550°C	0.81	0.18	0.01	0.75	0.24	0.01	0.06	0.06	0.00
1650°C	0.69	0.23	0.08	0.68	0.23	0.09	0.01	0.00	0.01
1750°C	0.71	0.19	0.10	0.73	0.17	0.10	0.02	0.02	0.00

Powder No.	12			12					
Dopant addn.	1% TiO_2			1% TiO_2 repeat analysis.					
	Phase Composition.			Phase composition.			| Difference |		
	M_t	M_c	M_m	M_t	M_c	M_m	M_t	M_c	M_m
Sinter temp.									
1350°C	0.87	0.12	0.01	0.83	0.15	0.02	0.04	0.03	0.01
1550°C	0.81	0.15	0.03	0.82	0.17	0.01	0.01	0.02	0.02
1650°C	0.75	0.16	0.10	0.73	0.21	0.06	0.02	0.05	0.04
1750°C	0.79	0.16	0.07	0.76	0.19	0.05	0.03	0.03	0.02

Estimated error in tetragonal phase measurements.

	Mean difference	S.D.	95% confidence limit error <
All sinter temps.	0.03	0.02	0.05
1350-1650°C Sinter temps.	0.02	0.01	0.03
1750°C sinter temp.	0.06	0.03	0.10

Estimated error in cubic phase measurements.

	Mean difference	S.D.	95% confidence limit error <
All sinter temps.	0.02	0.02	0.03
1350-1650°C Sinter temps.	0.01	0.01	0.02
1750°C sinter temp.	0.04	0.02	0.06

Estimated error in monoclinic phase measurements.

	Mean difference	S.D.	95% confidence limit error <
All sinter temps.	0.01	0.02	0.02
1350-1650°C Sinter temps.	0.01	0.01	0.02
1750°C sinter temp.	0.02	0.02	0.04

Table 4.5.1(b) Estimation of total experimental error in x ray diffraction results using measurements obtained from duplicate compositions.

Powder No.	1			20					
Dopant addn.	0.25% Al_2O_3			0.25% Al_2O_3 repeat batch.					
	Phase Composition.			Phase composition.			| Difference |		
	M_t	M_c	M_m	M_t	M_c	M_m	M_t	M_c	M_m
Sinter temp.									
1350°C	0.86	0.13	0.00	0.86	0.14	0.00	0.00	0.01	0.00
1550°C	0.78	0.21	0.01	0.75	0.23	0.02	0.03	0.02	0.01
1650°C	0.75	0.22	0.03	0.71	0.22	0.08	0.04	0.00	0.05
1750°C	0.71	0.23	0.06	0.62	0.29	0.09	0.09	0.06	0.03

Powder No.	2			16					
Dopant addn.	0.75% Al_2O_3			0.75% Al_2O_3 repeat batch.					
	Phase Composition.			Phase composition.			| Difference |		
	M_t	M_c	M_m	M_t	M_c	M_m	M_t	M_c	M_m
Sinter temp.									
1350°C	0.86	0.14	0.00	0.87	0.13	0.00	0.01	0.01	0.00
1550°C	0.77	0.22	0.00	0.80	0.20	0.00	0.03	0.02	0.00
1650°C	0.75	0.23	0.02	0.74	0.23	0.03	0.01	0.01	0.01
1750°C	0.19	0.16	0.65	0.17	0.18	0.65	0.02	0.02	0.00

Estimated error in tetragonal phase measurements.

	Mean difference	S.D.	95% confidence limit error <
All sinter temps.	0.03 **	0.02	0.05
1350-1650°C Sinter temps.	0.02	0.01	0.03
1750°C sinter temp.	0.06	0.03	0.10

** indicates error value used for factorial experiment analysis of variance.

Estimated error in cubic phase measurements.

	Mean difference	S.D.	95% confidence limit error <
All sinter temps.	0.02 **	0.02	0.03
1350-1650°C Sinter temps.	0.01	0.01	0.02
1750°C sinter temp.	0.04	0.02	0.06

Estimated error in monoclinic phase measurements.

	Mean difference	S.D.	95% confidence limit error <
All sinter temps.	0.01	0.02	0.02
1350-1650°C Sinter temps.	0.01	0.01	0.02
1750°C sinter temp.	0.02	0.02	0.04

Table 4.6.2 X Ray Diffraction Results, for phase composition of sintered samples of undoped Y-T.Z.P.

Powder No. 11.

Blank Treatment, No Dopant Addition.

Sintering Temperature (°C)	Integrated Peak Intensity [counts]. 111_t	$\bar{1}11_m$	111_m	004_t	400_c	400_t	M_m/M_{ct}	M_c/M_t	mol.fract. Tetragonal	mol.fract. Cubic	mol.fract. Monoclinic
1350	1977.75	2.92	0	41.92	27.57	100.54	0.001	0.170	0.85	0.15	0.00
1550	2353.79	87.58	15.64	37.22	38.77	87.53	0.036	0.273	0.76	0.21	0.03
1650	1761.92	174.63	33.35	35.31	41.97	76.4	0.097	0.331	0.69	0.23	0.09
1750	2023.38	159.38	37.86	36.43	35.46	79.28	0.080	0.270	0.73	0.20	0.07

Powder No. 15

TZ3Y As Supplied.

Sintering Temperature (°C)	Integrated Peak Intensity [counts]. 111_t	$\bar{1}11_m$	111_m	004_t	400_c	400_t	M_m/M_{ct}	M_c/M_t	mol.fract. Tetragonal	mol.fract. Cubic	mol.fract. Monoclinic
1350	1876.04	15.2	0	35.07	37.67	131.1	0.007	0.199	0.83	0.17	0.01
1550	1904.14	31.16	0	43.57	33.69	89.97	0.013	0.222	0.81	0.18	0.01
1650	1635.16	151.22	31.97	36.99	43.23	78.98	0.092	0.328	0.69	0.23	0.08
1750	2537.08	307.32	53.44	40.31	38.75	89.01	0.117	0.264	0.71	0.19	0.10

Table 4.6.3 X Ray Diffraction Results, for phase composition of sintered samples of alumina doped Y-T.Z.P.

Powder No. 1
0.25% Alumina.

Sintering Temperature (°C)	Integrated Peak Intensity [counts]. 111_t	$\bar{1}11_m$	111_m	004_t	400_c	400_t	M_m/M_{ct}	M_c/M_t	mol.fract. Tetragonal	mol.fract. Cubic	mol.fract. Monoclinic
1350	1639.38	2.66	0	41.9	24.31	95.18	0.001	0.156	0.86	0.13	0.00
1550	1949.23	15.82	0	36.55	37.04	84.55	0.007	0.269	0.78	0.21	0.01
1650	2149.4	67.17	25.96	36.62	39.15	81.13	0.036	0.293	0.75	0.22	0.03
1750	1825.84	89.22	41.67	30.51	38.81	74.25	0.059	0.326	0.71	0.23	0.06

Powder No. 20
0.25 % Alumina addition, repeat batch.

Sintering Temperature (°C)	Integrated Peak Intensity [counts]. 111_t	$\bar{1}11_m$	111_m	004_t	400_c	400_t	M_m/M_{ct}	M_c/M_t	mol.fract. Tetragonal	mol.fract. Cubic	mol.fract. Monoclinic
1350	2028.78	3.59	0	35.44	22.76	85.35	0.001	0.166	0.86	0.14	0.00
1550	2135.53	44.32	12.52	38.4	43.21	88.02	0.022	0.301	0.75	0.23	0.02
1650	1624.22	129.72	34.57	37.43	43.51	86.49	0.083	0.309	0.71	0.22	0.08
1750	545.62	727.02	358.67	0	23.91	13.61	1.632	1.546	0.15	0.23	0.62

Powder No. 18
0.5% alumina addition.

Sintering Temperature (°C)	Integrated Peak Intensity [counts]. 111_t	$\bar{1}11_m$	111_m	004_t	400_c	400_t	M_m/M_{ct}	M_c/M_t	mol.fract. Tetragonal	mol.fract. Cubic	mol.fract. Monoclinic
1350	2164.03	0	0	42.42	28.27	104.13	0.000	0.170	0.85	0.15	0.00
1550	2522.54	48.81	12.6	39.48	43.08	94.67	0.020	0.283	0.76	0.22	0.02
1650	1909.94	106.74	26.83	36.62	45.66	86.58	0.057	0.326	0.71	0.23	0.05
1750	631.94	893.64	393.58	3.06	25.95	20.77	1.670	0.958	0.19	0.18	0.63

Powder No. 2.
0.75% alumina addition.

Sintering Temperature (°C)	Integrated Peak Intensity [counts]. 111_t	$\bar{1}11_m$	111_m	004_t	400_c	400_t	M_m/M_{ct}	M_c/M_t	mol.fract. Tetragonal	mol.fract. Cubic	mol.fract. Monoclinic
1350	1819.53	0	0	43.75	25.02	92.92	0.000	0.161	0.86	0.14	0.00
1550	2188.52	12.42	0	32.38	36.21	77.81	0.005	0.289	0.77	0.22	0.00
1650	2285.88	41.32	23.33	36.7	43.01	88	0.023	0.304	0.75	0.23	0.02
1750	512.37	847.64	289.08	0	21.42	22.8	1.819	0.827	0.19	0.16	0.65

Table 4.6.3 X Ray Diffraction Results, for phase composition of sintered samples of alumina doped Y-T.Z.P. Continued....

Powder No. 16
0.75% Alumina addition, repeat batch.

Sintering Temperature (°C)	Integrated Peak Intensity [counts]. 111_t	$\bar{1}11_m$	111_m	004_t	400_c	400_t	M_m/M_{ct}	M_c/M_t	mol.fract. Tetragonal	mol.fract. Cubic	mol.fract. Monoclinic
1350	2036.14	0	3.78	39.5	22.79	95.95	0.002	0.148	0.87	0.13	0.00
1550	2279.3	7.03	0	37.68	35.91	87.11	0.003	0.253	0.80	0.20	0.00
1650	1886.35	56.1	14.77	36.91	43.85	84.18	0.031	0.319	0.74	0.23	0.03
1750	356.25	593.15	201.5		10.08	8.34	1.829	1.064	0.17	0.18	0.65

Powder No. 13
1% alumina addition.

Sintering Temperature (°C)	Integrated Peak Intensity [counts]. 111_t	$\bar{1}11_m$	111_m	004_t	400_c	400_t	M_m/M_{ct}	M_c/M_t	mol.fract. Tetragonal	mol.fract. Cubic	mol.fract. Monoclinic
1350	1277.79	1.83	0	30.04	17.94	73.5	0.001	0.152	0.87	0.13	0.00
1550	2463.88	2.62	0	37.64	37.7	90.28	0.001	0.259	0.79	0.21	0.00
1650	1824.36	66.46	20.68	35.85	45.5	80.1	0.039	0.345	0.72	0.25	0.04
1750	681.8	1127.16	337.93		28.74	15.24	1.762	1.660	0.14	0.23	0.64

Table 4.6.4 X Ray Diffraction Results, for phase composition of sintered samples of silica doped Y-T.Z.P.

Powder No. 5
0.25% silica addition.

Sintering Temperature (°C)	Integrated Peak Intensity [counts]. 111_t	$\bar{1}11_m$	111_m	004_t	400_c	400_t	M_m/M_{ct}	M_c/M_t	mol.fract. Tetragonal	mol.fract. Cubic	mol.fract. Monoclinic
1350	1930.65	6.16	0	40.11	31.68	95.34	0.003	0.206	0.83	0.17	0.00
1550	2341.3	18.9	0	37.48	35.23	88.29	0.007	0.247	0.80	0.20	0.01
1650	2133.08	83.87	19.66	35.14	41.28	81.52	0.040	0.311	0.73	0.23	0.04
1750	2175.93	100.46	29.11	33.08	34.65	74.95	0.049	0.282	0.74	0.21	0.05

Powder No. 17
0.5% silica addition.

Sintering Temperature (°C)	Integrated Peak Intensity [counts]. 111_t	$\bar{1}11_m$	111_m	004_t	400_c	400_t	M_m/M_{ct}	M_c/M_t	mol.fract. Tetragonal	mol.fract. Cubic	mol.fract. Monoclinic
1350	2203.9	0	0	45.89	32.45	105.33	0.000	0.189	0.84	0.16	0.00
1550	2464.48	47.61	10.73	40.23	37.68	96.68	0.019	0.242	0.79	0.19	0.02
1650	1612.06	72.31	16.58	36.41	45.61	81.52	0.045	0.340	0.71	0.24	0.04
1750	1901.17	188.16	29.28	28.09	38.59	71.69	0.094	0.340	0.68	0.23	0.09

Powder No. 7.
0.75% silica addition.

Sintering Temperature (°C)	Integrated Peak Intensity [counts]. 111_t	$\bar{1}11_m$	111_m	004_t	400_c	400_t	M_m/M_{ct}	M_c/M_t	mol.fract. Tetragonal	mol.fract. Cubic	mol.fract. Monoclinic
1350	1802.4	3.33	0	42.18	30.5	99.47	0.002	0.189	0.84	0.16	0.00
1550	2247.43	114.61	26.89	34.8	41.6	86.25	0.052	0.302	0.73	0.22	0.05
1650	1475.76	94.43	24.94	34	41.11	78.7	0.066	0.321	0.71	0.23	0.06
1750	1797.15	97.99	25.21	37.38	41.18	91.47	0.056	0.281	0.74	0.21	0.05

Powder No. 3.
1% silica addition.

Sintering Temperature (°C)	Integrated Peak Intensity [counts]. 111_t	$\bar{1}11_m$	111_m	004_t	400_c	400_t	M_m/M_{ct}	M_c/M_t	mol.fract. Tetragonal	mol.fract. Cubic	mol.fract. Monoclinic
1350	1876.16	1.87	0	41.48	32.19	98.33	0.001	0.203	0.83	0.17	0.00
1550	2386.4	45.6	30.2	38.99	44.93	98.06	0.026	0.288	0.76	0.22	0.03
1650	2353.8	92.79	26.85	36.07	46.05	80.5	0.042	0.348	0.71	0.25	0.04
1750	2186.7	149.86	31.94	38.25	42.29	80.31	0.068	0.314	0.71	0.22	0.06

Table 4.6.5 X Ray Diffraction Results, for phase composition of sintered samples of titania doped Y-T.Z.P.

Powder No. 4
0.25% TiO_2 addition.

Sintering Temperature (°C)	Integrated Peak Intensity [counts]. 111_t	$\bar{1}11_m$	111_m	004_t	400_c	400_t	M_m/M_{ct}	M_c/M_t	mol.fract. Tetragonal	mol.fract. Cubic	mol.fract. Monoclinic
1350	1628.1	0	0	38.35	25.63	92.32	0.000	0.173	0.85	0.15	0.00
1550	2405.8	30.5	0	39.08	35.46	88.76	0.010	0.244	0.80	0.19	0.01
1650	1858.12	128.35	36.88	37.41	33.53	84.73	0.073	0.242	0.75	0.18	0.07
1750	1997.69	162.67	43.08	34.24	35.58	80.25	0.084	0.273	0.72	0.20	0.08

Powder No. 19
0.5% TiO_2 addition.

Sintering Temperature (°C)	Integrated Peak Intensity [counts]. 111_t	$\bar{1}11_m$	111_m	004_t	400_c	400_t	M_m/M_{ct}	M_c/M_t	mol.fract. Tetragonal	mol.fract. Cubic	mol.fract. Monoclinic
1350	2021.33	0	0	44.87	23.6	107.42	0.000	0.136	0.88	0.12	0.00
1550	2446.03	45.74	12.96	44.73	33.61	97.38	0.020	0.208	0.81	0.17	0.02
1650	1836.94	108.35	35.86	42.32	34.65	94.53	0.064	0.223	0.77	0.17	0.06
1750	1791.15	217.09	26.27	33.46	28.05	78.61	0.111	0.220	0.74	0.16	0.10

Powder No. 8
0.75% TiO_2 addition.

Sintering Temperature (°C)	Integrated Peak Intensity [counts]. 111_t	$\bar{1}11_m$	111_m	004_t	400_c	400_t	M_m/M_{ct}	M_c/M_t	mol.fract. Tetragonal	mol.fract. Cubic	mol.fract. Monoclinic
1350	1556.52	5.93	0	40.32	26.56	90.76	0.003	0.178	0.85	0.15	0.00
1550	2242.22	48.24	16.1	37.63	26.15	84.98	0.024	0.188	0.82	0.15	0.02
1650	1565.31	176.8	38.11	34.03	32.82	79.03	0.113	0.255	0.72	0.18	0.10
1750	1971.23	150.91	34.64	34.42	28.21	83.37	0.077	0.211	0.77	0.16	0.07

Powder No. 12.
1% TiO_2 addition.

Sintering Temperature (°C)	Integrated Peak Intensity [counts]. 111_t	$\bar{1}11_m$	111_m	004_t	400_c	400_t	M_m/M_{ct}	M_c/M_t	mol.fract. Tetragonal	mol.fract. Cubic	mol.fract. Monoclinic
1350	1693.5	9.82	2.91	35.94	18.85	85.99	0.006	0.136	0.87	0.12	0.01
1550	2164.65	65.49	25.53	38.52	27.21	88.51	0.034	0.188	0.81	0.15	0.03
1650	1662.87	187.98	30.69	37.98	28.68	82.47	0.108	0.210	0.75	0.16	0.10
1750	2000.77	96.91	24.05	36.6	28.73	88.09	0.050	0.203	0.79	0.16	0.05

Table 4.6.6 X Ray Diffraction Results, for phase composition of sintered samples of Y-T.Z.P. with multiple oxide dopant additions.

Powder No. 6
1% SiO_2 + 1% Al_2O_3 additions.

Sintering Temperature (°C)	Integrated Peak Intensity [counts]. 111_t	$\bar{1}11_m$	111_m	004_t	400_c	400_t	M_m/M_{ct}	M_c/M_t	mol.fract. Tetragonal	mol.fract. Cubic	mol.fract. Monoclinic
1350	1819.67	0.27	0	41.29	25.26	95.98	0.000	0.162	0.86	0.14	0.00
1550	2257.95	55.85	20.08	41.14	31.48	96.59	0.028	0.201	0.81	0.16	0.03
1650	1398.58	330.41	73.7	33.11	36.83	77.09	0.237	0.294	0.62	0.18	0.19
1750	495.81	1055.27	529.98	0	12.78	20.81	2.622	0.540	0.18	0.10	0.72

Powder No. 9.
1% SiO_2 + 1% TiO_2 additions.

Sintering Temperature (°C)	Integrated Peak Intensity [counts]. 111_t	$\bar{1}11_m$	111_m	004_t	400_c	400_t	M_m/M_{ct}	M_c/M_t	mol.fract. Tetragonal	mol.fract. Cubic	mol.fract. Monoclinic
1350	1791.93	2.4	0	39.49	14.9	95.89	0.001	0.097	0.91	0.09	0.00
1550	908.39	29.08	7.82	37.83	27.69	94.05	0.033	0.185	0.82	0.15	0.03
1650	1634.09	71.82	21.45	37.22	25.85	92.17	0.047	0.176	0.81	0.14	0.04
1750	1493.27	12.1	3.61	34.52	25.02	87.63	0.009	0.180	0.84	0.15	0.01

Powder No. 14
1% Al_2O_3 + 1% TiO_2 additions.

Sintering Temperature (°C)	Integrated Peak Intensity [counts]. 111_t	$\bar{1}11_m$	111_m	004_t	400_c	400_t	M_m/M_{ct}	M_c/M_t	mol.fract. Tetragonal	mol.fract. Cubic	mol.fract. Monoclinic
1350	1455.46	12.65	5.09	36.47	26.34	82.11	0.010	0.195	0.83	0.16	0.01
1550	2204.06	59	21.81	37.85	31.22	85.55	0.030	0.223	0.79	0.18	0.03
1650	1739	115.86	30.42	36.34	36.8	86.03	0.069	0.265	0.74	0.20	0.06
1750	554.67	917.52	346.65	34.27	35.43	80.28	1.869	0.272	0.27	0.07	0.65

Powder No. 10.
1% SiO_2 + 1% Al_2O_3 + 1% TiO_2 additions.

Sintering Temperature (°C)	Integrated Peak Intensity [counts]. 111_t	$\bar{1}11_m$	111_m	004_t	400_c	400_t	M_m/M_{ct}	M_c/M_t	mol.fract. Tetragonal	mol.fract. Cubic	mol.fract. Monoclinic
1350	1640.44	3.96	0	37.9	17.77	94.26	0.002	0.118	0.89	0.11	0.00
1550	2367.01	59.68	18.28	43.78	25.93	107.44	0.027	0.151	0.85	0.13	0.03
1650	1694.29	121.3	29.57	46.32	27.1	109.78	0.073	0.153	0.81	0.12	0.07
1750	667.78	1019.17	525.54	19.52	17.52	42.54	1.897	0.248	0.28	0.07	0.65

Table 4.6.7.1 (a)
Analysis of data for factorial experiment.
Cubic phase development.
1350-1550°C temperature interval.

a = 1% Al_2O_3, b = 1% SiO_2, c = 1% TiO_2,
d = higher sintering temperature

Treatment	Mol. fract. cubic phase	(1)	(2)	(3)	FACTORIAL EFFECT..... (4) [total]	(mean)	degrees of freedom	Sum of squares
1	0.15	0.28	0.59	1.07	2.48 = T			
a	0.13	0.31	0.48	1.41	-0.04 = [A]	-0.00	1	0.00010
b	0.17	0.28	0.80	0.01	-0.14 = [B]	-0.02	1	0.00123
ab	0.14	0.20	0.61	-0.05	-0.14 = [AB]	-0.02	1	0.00123
c	0.12	0.42	-0.05	-0.05	-0.30 = [C]	-0.04	1	0.00563
ac	0.16	0.38	0.06	-0.09	0.18 = [AC]	0.02	1	0.00203
bc	0.09	0.33	-0.06	-0.03	-0.12 = [BC]	-0.02	1	0.00090
abc	0.11	0.28	0.01	-0.11	-0.00 = [ABC]	-0.00	1	0.00000
d	0.21	-0.02	0.03	-0.11	0.34 = [D]	0.04	1	0.00723
ad	0.21	-0.03	-0.08	-0.19	-0.06 = [AD]	-0.01	1	0.00023
bd	0.22	0.04	-0.04	0.11	-0.04 = [BD]	-0.01	1	0.00010
abd	0.16	0.02	-0.05	0.07	-0.08 = [ABD]	-0.01	1	0.00040
cd	0.15	0.00	-0.01	-0.11	-0.08 = [CD]	-0.01	1	0.00040
acd	0.18	-0.06	-0.02	-0.01	-0.04 = [ACD]	-0.01	1	0.00010
bcd	0.15	0.03	-0.06	-0.01	0.10 = [BCD]	0.01	1	0.00063
abcd	0.13	-0.02	-0.05	0.01	0.02 = [ABCD]	0.00	1	0.00003
Total (T) =	2.48							

no. of treatments (t) =	16
no of replicates (r) =	1

Table 4.6.7.1 (b)

Analysis of data for factorial experiment.

Cubic phase development.

1550-1650°C temperature interval.

a = 1% Al_2O_3, b = 1% SiO_2, c = 1% TiO_2,

d = higher sintering temperature

Treatment	Mol. fract. cubic phase	(1)	(2)	(3)	FACTORIAL EFFECT..... (4) [total]	(mean)	degrees of freedom	Sum of squares
1	0.21	0.42	0.80	1.41	2.94 = T			
a	0.21	0.38	0.61	1.53	-0.08 = [A]	-0.01	1	0.00040
b	0.22	0.33	0.91	-0.05	-0.24 = [B]	-0.03	1	0.00360
ab	0.16	0.28	0.62	-0.03	-0.26 = [AB]	-0.03	1	0.00423
c	0.15	0.48	-0.06	-0.09	-0.48 = [C]	-0.06	1	0.01440
ac	0.18	0.43	0.01	-0.15	0.14 = [AC]	0.02	1	0.00122
bc	0.15	0.36	-0.05	-0.11	-0.06 = [BC]	-0.01	1	0.00023
abc	0.13	0.26	0.02	-0.15	0.04 = [ABC]	0.00	1	0.00010
d	0.23	0.00	-0.04	-0.19	0.12 = [D]	0.02	1	0.00090
ad	0.25	-0.06	-0.05	-0.29	0.02 = [AD]	0.00	1	0.00002
bd	0.25	0.03	-0.05	0.07	-0.06 = [BD]	-0.01	1	0.00022
abd	0.18	-0.02	-0.10	0.07	-0.04 = [ABD]	-0.01	1	0.00010
cd	0.16	0.02	-0.06	-0.01	-0.10 = [CD]	-0.01	1	0.00063
acd	0.20	-0.07	-0.05	-0.05	-0.00 = [ACD]	-0.00	1	0.00000
bcd	0.14	0.04	-0.09	0.01	-0.04 = [BCD]	-0.00	1	0.00010
abcd	0.12	-0.02	-0.06	0.03	0.02 = [ABCD]	0.00	1	0.00002
Total (T) =	2.94							

no. of treatments (t) =	16
no of replicates (r) =	1

Table 4.6.7.1 (c)

Analysis of data for factorial experiment.

Cubic phase development.

1650-1750°C temperature interval.

a = 1% Al_2O_3, b = 1% SiO_2, c = 1% TiO_2,

d = higher sintering temperature

Treatment	Mol. fract. cubic phase	(1)	(2)	(3)	FACTORIAL EFFECT..... (4) [total]	(mean)	degrees of freedom	Sum of squares
1	0.23	0.48	0.91	1.53	2.73 = T			
a	0.25	0.43	0.62	1.20	-0.29 = [A]	-0.04	1	0.00526
b	0.25	0.36	0.75	-0.03	-0.27 = [B]	-0.03	1	0.00456
ab	0.18	0.26	0.45	-0.26	-0.29 = [AB]	-0.04	1	0.00526
c	0.16	0.43	-0.05	-0.15	-0.59 = [C]	-0.07	1	0.02176
ac	0.20	0.32	0.02	-0.12	-0.01 = [AC]	-0.00	1	0.00001
bc	0.14	0.23	-0.09	-0.15	0.05 = [BC]	0.01	1	0.00016
abc	0.12	0.22	-0.17	-0.14	0.19 = [ABC]	0.02	1	0.00226
d	0.20	0.02	-0.05	-0.29	-0.33 = [D]	-0.04	1	0.00681
ad	0.23	-0.07	-0.10	-0.30	-0.23 = [AD]	-0.03	1	0.00331
bd	0.22	0.04	-0.11	0.07	0.03 = [BD]	0.00	1	0.00006
abd	0.10	-0.02	-0.01	-0.08	0.01 = [ABD]	0.00	1	0.00001
cd	0.16	0.03	-0.09	-0.05	-0.01 = [CD]	-0.00	1	0.00001
acd	0.07	-0.12	-0.06	0.10	-0.15 = [ACD]	-0.02	1	0.00141
bcd	0.15	-0.09	-0.15	0.03	0.15 = [BCD]	0.02	1	0.00141
abcd	0.07	-0.08	0.01	0.16	0.13 = [ABCD]	0.02	1	0.00106
Total (T) =	2.73							

no. of treatments (t) =	16
no of replicates (r) =	1

Table 4.6.7.1 (d)

Analysis of Variance (ANOVA) table

Factorial Experiment:- Cubic phase Development

1350 - 1550°C temperature interval.

Source of variation	degrees of freedom	sum of squares	mean square	(Pooled error estimate) mean square/ error mean square	F test signif-icance.	(External error estimate) mean square/ error mean square	F test signif-icance.
Al_2O_3 addition (A)	1	0.00010	0.00010	0.43	N/S	0.25	N/S
SiO_2 Addition (B)	1	0.00123	0.00123	5.33	*	3.06	N/S
TiO_2 addition (C)	1	0.00563	0.00563	24.46	***	14.06	***
Sintering temperature (D)	1	0.00723	0.00723	31.41	***	18.06	***
Interactions:							
(2nd order)							
AB	1	0.00123	0.00123	5.33	*	3.06	N/S
AC	1	0.00203	0.00203	8.80	**	5.06	*
AD	1	0.00023	0.00023	0.98	N/S	0.56	N/S
BC	1	0.00090	0.00090	3.91	N/S	2.25	N/S
BD	1	0.00010	0.00010	0.43	N/S	0.25	N/S
CD	1	0.00040	0.00040	1.74	N/S	1.00	N/S
(3rd order)							
ABC	1	0.00000	0.00000	0.00	---	0.00	N/S
ABD	1	0.00040	0.00040	1.74	---	1.00	N/S
ACD	1	0.00010	0.00010	0.43	---	0.25	N/S
BCD	1	0.00063	0.00063	2.72	---	1.56	N/S
(4th order)							
ABCD	1	0.00003	0.00003	0.11	---	0.06	N/S
Error term:							
(pooled 3rd and 4th order terms)	5	0.00115	0.00023	----			
External estimate of error							
(method b difference values)	8	0.00320	0.00040	----			

f test values for significance (5 & 1 degrees of freedom)

f (1 %) (highly significant) = 16.3 Indicated as *** in results.
f (5 %) = 6.61 Indicated as ** in results.
f (10 %) (less significant) = 4.06 Indicated as * in results.
f (>10%) considered to be not significant. Indicated as N/S in results.

(8 & 1 degrees of freedom)

f (1 %) (highly significant) = 11.3 Indicated as *** in results.
f (5 %) = 5.32 Indicated as ** in results.
f (10 %) (less significant) = 3.46 Indicated as * in results.
f (>10%) considered to be not significant. Indicated as N/S in results.

Calculation of external error estimate.

Mean difference (method b) = 0.020
Difference squared = 0.0004
Sum of squares of differences = 0.0032
No. of data values (degrees of freedom) = 8
mean square difference = sum squares /degrees freedom = 0.0004

Table 4.6.7.1 (e)

Analysis of Variance (ANOVA) table

Factorial Experiment:- Cubic phase Development

1550 - 1650°C temperature interval.

Source of variation	degrees of freedom	sum of squares	mean square	(Pooled error estimate) mean square/ error mean square	F test signif-icance.	(External error estimate) mean square/ error mean square	F test signif-icance.
Al_2O_3 addition (A)	1	0.00040	0.00040	6.15	*	1.00	N/S
SiO_2 Addition (B)	1	0.00360	0.00360	55.38	***	9.00	**
TiO_2 addition (C)	1	0.01440	0.01440	221.54	***	36.00	***
Sintering temperature (D)	1	0.00090	0.00090	13.85	***	2.25	N/S
Interactions:							
(2nd order)							
AB	1	0.00423	0.00423	65.00	***	10.56	**
AC	1	0.00122	0.00122	18.85	***	3.06	N/S
AD	1	0.00002	0.00002	0.38	N/S	0.06	N/S
BC	1	0.00023	0.00023	3.46	N/S	0.56	N/S
BD	1	0.00022	0.00022	3.46	N/S	0.56	N/S
CD	1	0.00063	0.00063	9.62	**	1.56	N/S
(3rd order)							
ABC	1	0.00010	0.00010	1.54	---	0.25	N/S
ABD	1	0.00010	0.00010	1.54	---	0.25	N/S
ACD	1	0.00000	0.00000	0.00	---	0.00	N/S
BCD	1	0.00010	0.00010	1.54	---	0.25	N/S
(4th order)							
ABCD	1	0.00002	0.00002	0.38	---	0.06	N/S
Error term:							
(pooled 3rd and 4th order terms)	5	0.00032	0.00007	----			
External estimate of error							
(method b difference values)	8	0.00320	0.00040	----			

f test values for significance (5 & 1 degrees of freedom)

f (1 %) (highly significant) = 16.3	Indicated as *** in results.
f (5 %) = 6.61	Indicated as ** in results.
f (10 %) (less significant) = 4.06	Indicated as * in results.
f (>10%) considered to be not significant.	Indicated as N/S in results.

(8 & 1 degrees of freedom)

f (1 %) (highly significant) = 11.3	Indicated as *** in results.
f (5 %) = 5.32	Indicated as ** in results.
f (10 %) (less significant) = 3.46	Indicated as * in results.
f (>10%) considered to be not significant.	Indicated as N/S in results.

Calculation of external error estimate.

Mean difference (method b) = 0.020
Difference squared = 0.0004
Sum of squares of differences = 0.0032
No. of data values (degrees of freedom) = 8
mean square difference = sum squares /degrees freedom = 0.0004

Table 4.6.7.1 (f)

Analysis of variance (ANOVA) table

Factorial experiment:- Cubic phase development

1650 - 1750°C temperature interval.

Source of variation	degrees of freedom	sum of squares	mean square	(Pooled error estimate) mean square/ error mean square	F test signif-icance.	(External error estimate) mean square/ error mean square	F test signif-icance.
Al_2O_3 addition (A)	1	0.00526	0.00526	4.29	*	13.14	***
SiO_2 Addition (B)	1	0.00456	0.00456	3.72	N/S	11.39	***
TiO_2 addition (C)	1	0.02176	0.02176	17.74	***	54.39	***
Sintering temperature (D)	1	0.00681	0.00681	5.55	*	17.02	***
Interactions: (2nd order)							
AB	1	0.00526	0.00526	4.29	*	13.86	***
AC	1	0.00001	0.00001	0.01	N/S	0.02	N/S
AD	1	0.00331	0.00331	2.70	N/S	8.27	**
BC	1	0.00016	0.00016	0.13	N/S	0.39	N/S
BD	1	0.00006	0.00006	0.05	N/S	0.14	N/S
CD	1	0.00001	0.00001	0.01	N/S	0.02	N/S
(3rd order)							
ABC	1	0.00226	0.00226	1.84	---	5.64	**
ABD	1	0.00001	0.00001	0.01	---	0.02	N/S
ACD	1	0.00141	0.00141	1.15	---	3.52	*
BCD	1	0.00141	0.00141	1.15	---	3.52	*
(4th order)							
ABCD	1	0.00106	0.00106	0.86	---	0.58	N/S
Error term: (pooled 3rd and 4th order terms)	5	0.00613	0.00123	----			
External estimate of error (method b difference values)	8	0.00320	0.00040	----			

f test values for significance (5 & 1 degrees of freedom)

f (1 %) (highly significant) = 16.3 Indicated as *** in results.
f (5 %) = 6.61 Indicated as ** in results.
f (10 %) (less significant) = 4.06 Indicated as * in results.
f (>10%) considered to be not significant. Indicated as N/S in results.

(8 & 1 degrees of freedom)

f (1 %) (highly significant) = 11.3 Indicated as *** in results.
f (5 %) = 5.32 Indicated as ** in results.
f (10 %) (less significant) = 3.46 Indicated as * in results.
f (>10%) considered to be not significant. Indicated as N/S in results.

Calculation of external error estimate.

Mean difference (method b) = 0.020
Difference squared = 0.0004
Sum of squares of differences = 0.0032
No. of data values (degrees of freedom) = 8
mean square difference = sum squares /degrees freedom = 0.0004

Table 4.6.7.2 (a)
Analysis of data for factorial experiment.
Tetragonal phase development.
1350-1550°C temperature interval.

a = 1% Al_2O_3, b = 1% SiO_2, c = 1% TiO_2,
d = higher sintering temperature

Treatment	Mol. fract. cubic phase	(1)	(2)	(3)	FACTORIAL EFFECT..... (4) [total]	(mean)	degrees of freedom	Sum of squares
1	0.85	1.72	3.41	6.91	13.30 = T			
a	0.87	1.69	3.50	6.39	0.08 = [A]	0.01	1	0.00040
b	0.83	1.70	3.12	-0.01	0.16 = [B]	0.02	1	0.00160
ab	0.86	1.80	3.27	0.09	0.10 = [AB]	0.01	1	0.00063
c	0.87	1.55	0.05	0.07	0.24 = [C]	0.03	1	0.00360
ac	0.83	1.57	-0.06	0.09	-0.18 = [AC]	-0.02	1	0.00202
bc	0.91	1.60	0.08	0.03	0.18 = [BC]	0.02	1	0.00203
abc	0.89	1.67	0.01	0.07	0.04 = [ABC]	0.01	1	0.00010
d	0.76	0.02	-0.03	0.09	-0.52 = [D]	-0.07	1	0.01690
ad	0.79	0.03	0.10	0.15	0.10 = [AD]	0.01	1	0.00063
bd	0.76	-0.04	0.02	-0.11	0.02 = [BD]	0.00	1	0.00003
abd	0.81	-0.02	0.07	-0.07	0.04 = [ABD]	0.01	1	0.00010
cd	0.81	0.03	0.01	0.13	0.06 = [CD]	0.01	1	0.00022
acd	0.79	0.05	0.02	0.05	0.04 = [ACD]	0.00	1	0.00010
bcd	0.82	-0.02	0.02	0.01	-0.08 = [BCD]	-0.01	1	0.00040
abcd	0.85	0.03	0.05	0.03	0.02 = [ABCD]	0.00	1	0.00003
Total (T) =	13.3							

no. of treatments (t) =	16
no of replicates (r) =	1

Table 4.6.7.2 (b)

Analysis of data for factorial experiment.

Tetragonal Phase Development.

1550-1650°C temperature interval.

a = 1% Al_2O_3, b = 1% SiO_2, c = 1% TiO_2,

d = higher sintering temperature

Treatment	Mol. fract. cubic phase	(1)	(2)	(3)	FACTORIAL EFFECT..... (4) [total]	(mean)	degrees of freedom	Sum of squares
1	0.76	1.55	3.12	6.39	12.24 = T			
a	0.79	1.57	3.27	5.85	0.02 = [A]	0.00	1	0.00003
b	0.76	1.60	2.74	0.09	0.14 = [B]	0.02	1	0.00123
ab	0.81	1.67	3.11	-0.07	-0.04 = [AB]	-0.00	1	0.00010
c	0.81	1.41	0.08	0.09	0.52 = [C]	0.06	1	0.01690
ac	0.79	1.33	0.01	0.05	-0.02 = [AC]	-0.00	1	0.00003
bc	0.82	1.49	-0.06	0.07	0.26 = [BC]	0.03	1	0.00423
abc	0.85	1.62	-0.01	-0.11	0.16 = [ABC]	0.02	1	0.00160
d	0.69	0.03	0.02	0.15	-0.54 = [D]	-0.07	1	0.01823
ad	0.72	0.05	0.07	0.37	-0.16 = [AD]	-0.02	1	0.00160
bd	0.71	-0.02	-0.08	-0.07	-0.04 = [BD]	-0.00	1	0.00010
abd	0.62	0.03	0.13	0.05	-0.18 = [ABD]	-0.02	1	0.00203
cd	0.75	0.03	0.02	0.05	0.22 = [CD]	0.03	1	0.00303
acd	0.74	-0.09	0.05	0.21	0.12 = [ACD]	0.01	1	0.00090
bcd	0.81	-0.01	-0.12	0.03	0.16 = [BCD]	0.02	1	0.00160
abcd	0.81	0.00	0.01	0.13	0.10 = [ABCD]	0.01	1	0.00063
Total (T) =	12.24							

no. of treatments (t) =	16
no of replicates (r) =	1

Table 4.6.7.2 (c)
Analysis of data for factorial experiment.
Tetragonal Phase Development.
1650-1750°C temperature interval.

a = 1% Al_2O_3, b = 1% SiO_2, c = 1% TiO_2,
d = higher sintering temperature

Treatment	Mol. fract. cubic phase	(1)	(2)	(3)	FACTORIAL EFFECT..... (4) [total]	(mean)	degrees of freedom	Sum of squares
1	0.69	1.41	2.74	5.85	10.23 = T			
a	0.72	1.33	3.11	4.38	-1.83 = [A]	-0.23	1	0.20931
b	0.71	1.49	2.20	-0.07	0.57 = [B]	0.07	1	0.02031
ab	0.62	1.62	2.18	-1.76	0.35 = [AB]	0.04	1	0.00766
c	0.75	0.87	-0.06	0.05	0.35 = [C]	0.04	1	0.00766
ac	0.74	1.33	-0.01	0.52	-0.35 = [AC]	-0.04	1	0.00766
bc	0.81	1.06	-0.68	-0.11	-0.19 = [BC]	-0.02	1	0.00226
abc	0.81	1.12	-1.08	0.46	-0.41 = [ABC]	-0.05	1	0.01051
d	0.73	0.03	-0.08	0.37	-1.47 = [D]	-0.18	1	0.13506
ad	0.14	-0.09	0.13	-0.02	-1.69 = [AD]	-0.21	1	0.17851
bd	0.71	-0.01	0.46	0.05	0.47 = [BD]	0.06	1	0.01381
abd	0.62	0.00	0.06	-0.40	0.57 = [ABD]	0.07	1	0.02031
cd	0.79	-0.59	-0.12	0.21	-0.39 = [CD]	-0.05	1	0.00951
acd	0.27	-0.09	0.01	-0.40	-0.45 = [ACD]	-0.06	1	0.01266
bcd	0.84	-0.52	0.50	0.13	-0.61 = [BCD]	-0.08	1	0.02326
abcd	0.28	-0.56	-0.04	-0.54	-0.67 = [ABCD]	-0.08	1	0.02806
Total (T) =	10.23							

no. of treatments (t) =	16
no of replicates (r) =	1

Table 4.6.7.2 (d)

Analysis of variance (ANOVA) table

Factorial experiment:- Tetragonal phase development

1350 - 1550°C temperature interval.

Source of variation	degrees of freedom	sum of squares	mean square	(Pooled error estimate) mean square/ error mean square	F test signif-icance.	(External error estimate) mean square/ error mean square	F test signif-icance.
Al_2O_3 addition (A)	1	0.00040	0.00040	2.76	N/S	0.44	N/S
SiO_2 Addition (B)	1	0.00160	0.00160	11.03	**	1.78	N/S
TiO_2 addition (C)	1	0.00360	0.00360	24.83	***	4.00	*
Sintering temperature (D)	1	0.01690	0.01690	116.55	***	18.78	***
Interactions:							
(2nd order)							
AB	1	0.00063	0.00063	4.31	*	0.69	N/S
AC	1	0.00202	0.00202	13.97	**	2.25	N/S
AD	1	0.00063	0.00063	4.31	*	0.69	N/S
BC	1	0.00203	0.00203	13.97	**	2.25	N/S
BD	1	0.00003	0.00003	0.17	N/S	0.03	N/S
CD	1	0.00022	0.00022	1.55	N/S	0.25	N/S
(3rd order)							
ABC	1	0.00010	0.00010	0.69	---	0.11	N/S
ABD	1	0.00010	0.00010	0.69	---	0.11	N/S
ACD	1	0.00010	0.00010	0.69	---	0.11	N/S
BCD	1	0.00040	0.00040	2.76	---	0.44	N/S
(4th order)							
ABCD	1	0.00003	0.00003	0.17	---	0.03	N/S
Error term:							
(pooled 3rd and 4th order terms)	5	0.00073	0.00015	----			
External estimate of error							
(method b difference values)	8	0.00720	0.00090	----			

f test values for significance (5 & 1 degrees of freedom)

f (1 %) (highly significant) = 16.3	Indicated as *** in results.
f (5 %) = 6.61	Indicated as ** in results.
f (10 %) (less significant) = 4.06	Indicated as * in results.
f (>10%) considered to be not significant.	Indicated as N/S in results.

(8 & 1 degrees of freedom)

f (1 %) (highly significant) = 11.3	Indicated as *** in results.
f (5 %) = 5.32	Indicated as ** in results.
f (10 %) (less significant) = 3.46	Indicated as * in results.
f (>10%) considered to be not significant.	Indicated as N/S in results.

Calculation of external error estimate.

Mean difference (method b) = 0.030
Difference squared = 0.0009
Sum of squares of differences = 0.007
No. of data values (degrees of freedom) = 8
mean square difference = sum squares /degrees freedom = 0.0009

Table 4.6.7.2 (e)

Analysis of variance (ANOVA) table

Factorial experiment:- Tetragonal phase development

1550 - 1650°C temperature interval.

Source of variation	degrees of freedom	sum of squares	mean square	(Pooled error estimate) mean square/ error mean square	(Pooled error estimate) F test signif-icance.	(External error estimate) mean square/ error mean square	(External error estimate) F test signif-icance.
Al_2O_3 addition (A)	1	0.00003	0.00003	0.02	N/S	0.03	N/S
SiO_2 Addition (B)	1	0.00123	0.00123	0.91	N/S	1.36	N/S
TiO_2 addition (C)	1	0.01690	0.01690	12.52	**	18.78	***
Sintering temperature (D)	1	0.01823	0.01823	13.50	**	20.25	***
Interactions: (2nd order)							
AB	1	0.00010	0.00010	0.07	N/S	0.11	N/S
AC	1	0.00003	0.00003	0.02	N/S	0.03	N/S
AD	1	0.00160	0.00160	1.19	N/S	1.78	N/S
BC	1	0.00423	0.00423	3.13	N/S	4.69	*
BD	1	0.00010	0.00010	0.07	N/S	0.11	N/S
CD	1	0.00303	0.00303	2.24	N/S	3.36	N/S
(3rd order)							
ABC	1	0.00160	0.00160	1.19	---	1.78	N/S
ABD	1	0.00203	0.00203	1.50	---	2.25	N/S
ACD	1	0.00090	0.00090	0.67	---	1.00	N/S
BCD	1	0.00160	0.00160	1.19	---	1.78	N/S
(4th order)							
ABCD	1	0.00063	0.00063	0.46	---	0.69	N/S
Error term: (pooled 3rd and 4th order terms)	5	0.00675	0.00135	----			
External estimate of error (method b difference values)	8	0.00720	0.00090	----			

f test values for significance (5 & 1 degrees of freedom)

f (1 %) (highly significant) = 16.3 Indicated as *** in results.
f (5 %) = 6.61 Indicated as ** in results.
f (10 %) (less significant) = 4.06 Indicated as * in results.
f (>10%) considered to be not significant. Indicated as N/S in results.

(8 & 1 degrees of freedom)

f (1 %) (highly significant) = 11.3 Indicated as *** in results.
f (5 %) = 5.32 Indicated as ** in results.
f (10 %) (less significant) = 3.46 Indicated as * in results.
f (>10%) considered to be not significant. Indicated as N/S in results.

Calculation of external error estimate.

Mean difference (method b) = 0.030
Difference squared = 0.0009
Sum of squares of differences = 0.0072
No. of data values (degrees of freedom) = 8
mean square difference = sum squares /degrees freedom = 0.0009

Table 4.6.7.2 (f)

Analysis of variance (ANOVA) table

Factorial experiment:- Tetragonal phase development

1650 - 1750°C temperature interval.

Source of variation	degrees of freedom	sum of squares	mean square	(Pooled error estimate) mean square/ error mean square	F test signif-icance.	(External error estimate) mean square/ error mean square	F test signif-icance.
Al_2O_3 addition (A)	1	0.20931	0.20931	11.04	**	232.56	***
SiO_2 Addition (B)	1	0.02031	0.02031	1.07	N/S	22.56	***
TiO_2 addition (C)	1	0.00766	0.00766	0.40	N/S	8.51	**
Sintering temperature (D)	1	0.13506	0.13506	7.12	**	150.06	***
Interactions: (2nd order)							
AB	1	0.00766	0.00766	0.40	N/S	8.51	**
AC	1	0.00766	0.00766	0.40	N/S	8.51	**
AD	1	0.17851	0.17851	9.42	**	198.34	***
BC	1	0.00226	0.00226	0.12	N/S	2.51	N/S
BD	1	0.01381	0.01381	0.73	N/S	15.34	***
CD	1	0.00951	0.00951	0.50	N/S	10.56	***
(3rd order)							
ABC	1	0.01051	0.01051	0.55	---	11.67	***
ABD	1	0.02031	0.02031	1.07	---	22.56	***
ACD	1	0.01266	0.01266	0.67	---	14.06	***
BCD	1	0.02326	0.02326	1.23	---	25.84	***
(4th order)							
ABCD	1	0.02806	0.02806	1.48	---	31.17	***
Error term: (pooled 3rd and 4th order terms)	5	0.09478	0.01896	----			
External estimate of error (method b difference values)	8	0.00320	0.00040	----			

f test values for significance (5 & 1 degrees of freedom)

f (1 %) (highly significant)	= 16.3	Indicated as *** in results.
f (5 %)	= 6.61	Indicated as ** in results.
f (10 %) (less significant)	= 4.06	Indicated as * in results.
f (>10%) considered to be not significant.		Indicated as N/S in results.

(8 & 1 degrees of freedom)

f (1 %) (highly significant)	= 11.3	Indicated as *** in results.
f (5 %)	= 5.32	Indicated as ** in results.
f (10 %) (less significant)	= 3.46	Indicated as * in results.
f (>10%) considered to be not significant.		Indicated as N/S in results.

Calculation of external error estimate.

Mean difference (method b) = 0.03
Difference squared = 0.0009
Sum of squares of differences = 0.0072
No. of data values (degrees of freedom) = 8
mean square difference = sum squares /degrees freedom = 0.0009

Table 4.7.1(a) Estimate of measuring error in Hardness and Fracture toughness results.

Alumina doped Specimens:	
Mean value of 95% confidence limits	
Hardness (plus or minus)	0.10
Toughness (plus or minus)	0.09

Silica doped Specimens:	
Mean value of 95% confidence limits	
Hardness (plus or minus)	0.08
Toughness (plus or minus)	0.07

Titania doped Specimens:	
Mean value of 95% confidence limits	
Hardness (plus or minus)	0.06
Toughness (plus or minus)	0.08

Multiple oxide doped Specimens:	
Mean value of 95% confidence limits	
Hardness (plus or minus)	0.06
Toughness (plus or minus)	0.14

Average for all doped Specimens:	
Mean value of 95% confidence limits	
Hardness (plus or minus)	0.08
Toughness (plus or minus)	0.10

Figure 4.7.1(b)

Estimate of total experimental error.

(i) Hardness results.

Sintering Temperature (°C)	1250	1350	1450	1550	1650	1750
Powder 1	13.94	13.74	13.74	13.26	12.57	11.85
Powder 20	14.44	14.42	14.01	12.60	12.88	11.15
| difference |	0.49	0.68	0.27	0.66	0.31	0.70
Powder 2	14.01	14.14	13.88	12.88	11.79	
Powder 16	13.88	14.01	14.14	13.00	12.11	
| difference |	0.13	0.13	0.26	0.12	0.33	

Mean Difference	= 0.37
Standard deviation in mean	= 0.27
Standard error in mean	= 0.06
95% Confidence limit error	< 0.50

(ii) Toughness Results

Sintering Temperature (°C)	1250	1350	1450	1550	1650	1750
Powder 1	5.34	5.25	5.41	5.85	6.07	7.49
Powder 20	5.24	5.32	5.49	6.07	5.55	7.38
| difference |	0.09	0.07	0.08	0.22	0.52	0.11
Powder 2	5.35	5.39	5.46	5.67	5.99	
Powder 16	5.36	5.26	5.50	5.82	5.99	
| difference |	0.01	0.13	0.04	0.15	0.01	

Mean Difference	= 0.13
Standard deviation in mean	= 0.14
Standard error in mean	= 0.04
95% Confidence limit error	< 0.21

Table 4.7.2

Hardness and fracture toughness results for undoped T.Z.P.

Blank Treatment

Sintering temperature (°C).	1250	1350	1450	1550	1650	1750
Mean Hardness GN/m^2	9.98	12.88	12.88	12.88	12.88	12.60
Std. Dev. Hardness GN/m^2	0.00	0.00	0.00	0.00	0.00	0.25
Std. Error (Hardness) GN/m^2	0.00	0.00	0.00	0.00	0.00	0.06
95% confidence limit (hardness) GN/m^2	0.00	0.00	0.00	0.00	0.00	0.11
Mean Toughness $MN/m^{3/2}$	5.49	5.28	5.23	5.35	5.64	5.81
Std. Dev. (Toughness) $MN/m^{3/2}$	0.16	0.11	0.08	0.06	0.13	0.24
Std. Error (Toughness) $MN/m^{3/2}$	0.03	0.03	0.02	0.01	0.03	0.05
95% confidence limit (toughness) $Mn/m^{3/2}$	0.07	0.05	0.04	0.03	0.06	0.10

Mean 95% Confidence limit (hardness) GN/m^2 = 0.02
Mean 95% confidence limit (toughness) $MN/m^{3/2}$ = 0.06

Unmodified TZ3Y.

Sintering temperature (°C).	1250	1350	1450	1550	1650	1750
Mean Hardness GN/m^2	9.98	12.88	13.25	13.00	13.00	12.88
Std. Dev. Hardness GN/m^2	0.00	0.00	0.30	0.24	0.24	0.00
Std. Error (Hardness) GN/m^2	0.00	0.00	0.07	0.05	0.05	0.00
95% confidence limit (hardness) GN/m^2	0.00	0.00	0.13	0.11	0.11	0.00
Mean Toughness $MN/m^{3/2}$	5.49	5.12	5.18	5.39	5.55	5.85
Std. Dev. (Toughness) $MN/m^{3/2}$	0.16	0.10	0.09	0.12	0.08	0.14
Std. Error (Toughness) $MN/m^{3/2}$	0.03	0.02	0.02	0.03	0.02	0.03
95% confidence limit (toughness) $Mn/m^{3/2}$	0.07	0.05	0.04	0.05	0.04	0.06

Mean 95% Confidence limit (hardness) GN/m^2 = 0.06
Mean 95% confidence limit (toughness) $MN/m^{3/2}$ = 0.05

Table 4.7.3

Hardness and fracture toughness results: Alumina doped specimens.

0.25% Al_2O_3

Sintering Temperature (°C).	1250	1350	1450	1550	1650	1750
Mean Hardness GN/m^2	13.94	13.74	13.74	13.26	12.57	11.85
Std. Dev. Hardness GN/m^2	0.54	0.00	0.00	0.30	0.00	0.41
Std. Error (Hardness) GN/m^2	0.12	0.00	0.00	0.07	0.00	0.09
95% Confidence limit (hardness)	0.24	0.00	0.00	0.13	0.00	0.18
Mean Toughness MN/m^2	5.34	5.25	5.41	5.85	6.07	7.49
Std. Dev. (Toughness) GN/m^2	0.37	0.18	0.23	0.10	0.18	1.26
Std. Error (Toughness) MN/m^2	0.08	0.04	0.05	0.02	0.04	0.28
95% Confidence limit (Toughness)	0.16	0.08	0.10	0.04	0.08	0.55

Mean 95% Confidence limit (hardness) GN/m^2 = 0.09
Mean 95% confidence limit (toughness) $MN/m^{3/2}$ = 0.17

0.25% Al_2O_3 Repeat (powder 20)

Sintering Temperature (°C).	1250	1350	1450	1550	1650	1750
Mean Hardness GN/m^2	14.44	14.42	14.01	12.60	12.88	11.15
Std. Dev. Hardness GN/m^2	0.59	0.30	0.26	0.28	0.00	1.46
Std. Error (Hardness) GN/m^2	0.13	0.07	0.06	0.06	0.00	0.52
95% Confidence limit (hardness)	0.26	0.13	0.11	0.12	0.00	1.01
Mean Toughness MN/m^2	5.24	5.32	5.49	6.07	5.55	7.38
Std. Dev. (Toughness) GN/m^2	0.21	0.27	0.17	0.16	0.24	0.55
Std. Error (Toughness) MN/m^2	0.05	0.06	0.04	0.04	0.05	0.11
95% Confidence limit (Toughness)	0.09	0.12	0.08	0.07	0.10	0.22

Mean 95% Confidence limit (hardness) GN/m^2 = 0.27
Mean 95% confidence limit (toughness) $MN/m^{3/2}$ = 0.11

0.50% Al_2O_3

Sintering Temperature (°C).	1250	1350	1450	1550	1650	1750
Mean Hardness GN/m^2	14.01	14.28	14.01	13.88	12.88	N/A
Std. Dev. Hardness GN/m^2	0.26	0.28	0.26	0.32	0.00	N/A
Std. Error (Hardness) GN/m^2	0.06	0.06	0.06	0.07	0.00	N/A
95% Confidence limit (hardness)	0.11	0.12	0.11	0.14	0.00	N/A
Mean Toughness MN/m^2	5.31	5.35	5.40	5.62	6.24	N/A
Std. Dev. (Toughness) GN/m^2	0.12	0.09	0.11	0.14	0.16	N/A
Std. Error (Toughness) MN/m^2	0.03	0.02	0.02	0.03	0.03	N/A
95% Confidence limit (Toughness)	0.05	0.04	0.05	0.06	0.07	N/A

Mean 95% Confidence limit (hardness) GN/m^2 = 0.10
Mean 95% confidence limit (toughness) $MN/m^{3/2}$ = 0.05

Table 4.6.3

Hardness and fracture toughness results: Alumina doped specimens (continued...).

0.75% Al_2O_3

Sintering Temperature (°C).	1250	1350	1450	1550	1650	1750
Mean Hardness GN/m^2	14.01	14.14	13.88	12.88	11.79	N/A
Std. Dev. Hardness GN/m^2	0.26	0.00	0.32	0.00	0.00	N/A
Std. Error (Hardness) GN/m^2	0.06	0.00	0.07	0.00	0.00	N/A
95% Confidence limit (hardness)	0.11	0.00	0.14	0.00	0.00	N/A
Mean Toughness MN/m^2	5.35	5.39	5.46	5.67	5.99	N/A
Std. Dev. (Toughness) GN/m^2	0.19	0.07	0.14	0.12	0.12	N/A
Std. Error (Toughness) MN/m^2	0.04	0.02	0.03	0.03	0.03	N/A
95% Confidence limit (Toughness)	0.08	0.03	0.06	0.05	0.07	N/A

Mean 95% Confidence limit (hardness) GN/m^2 = 0.05
Mean 95% confidence limit (toughness) $MN/m^{3/2}$ = 0.06

0.75% Al_2O_3 Duplicate, (powder 16)

Sintering Temperature (°C).	1250	1350	1450	1550	1650	1750
Mean Hardness GN/m^2	13.88	14.01	14.14	13.00	12.11	N/A
Std. Dev. Hardness GN/m^2	0.32	0.26	0.00	0.24	0.44	N/A
Std. Error (Hardness) GN/m^2	0.07	0.06	0.00	0.05	0.10	N/A
95% Confidence limit (hardness)	0.14	0.11	0.00	0.11	0.19	N/A
Mean Toughness MN/m^2	5.36	5.26	5.50	5.82	5.99	N/A
Std. Dev. (Toughness) GN/m^2	0.14	0.12	0.17	0.14	0.20	N/A
Std. Error (Toughness) MN/m^2	0.03	0.03	0.04	0.03	0.04	N/A
95% Confidence limit (Toughness)	0.06	0.05	0.07	0.06	0.09	N/A

Mean 95% Confidence limit (hardness) GN/m^2 = 0.11
Mean 95% confidence limit (toughness) $MN/m^{3/2}$ = 0.07

1.00% Al_2O_3

Sintering Temperature (°C).	1250	1350	1450	1550	1650	1750
Mean Hardness GN/m^2	12.88	13.82	12.88	12.88	11.79	N/A
Std. Dev. Hardness GN/m^2	0.00	0.00	0.00	0.00	0.00	N/A
Std. Error (Hardness) GN/m^2	0.00	0.00	0.00	0.00	0.00	N/A
95% Confidence limit (hardness)	0.00	0.00	0.00	0.00	0.00	N/A
Mean Toughness MN/m^2	5.40	5.16	5.27	5.72	6.16	N/A
Std. Dev. (Toughness) GN/m^2	0.15	0.19	0.13	0.14	0.17	N/A
Std. Error (Toughness) MN/m^2	0.03	0.04	0.03	0.03	0.04	N/A
95% Confidence limit (Toughness)	0.06	0.08	0.06	0.06	0.07	N/A

Mean 95% Confidence limit (hardness) GN/m^2 = 0.00
Mean 95% confidence limit (toughness) $MN/m^{3/2}$ = 0.07

Table 4.6.4

Hardness and toughness results:

- Silica doped specimens.

0.25% SiO_2

Sintering Temperature (°C).	1250	1350	1450	1550	1650	1750
Mean Hardness GN/m^2	11.79	13.75	13.50	12.88	12.88	11.79
Std. Dev. Hardness GN/m^2	0.00	0.32	0.40	0.00	0.00	0.00
Std. Error (Hardness) GN/m^2	0.00	0.07	0.09	0.00	0.00	0.00
95% Confidence limit (hardness)	0.00	0.14	0.17	0.00	0.00	0.00
Mean Toughness MN/m^2	5.42	5.25	5.12	5.50	5.76	6.20
Std. Dev. (Toughness) GN/m^2	0.16	0.09	0.29	0.10	0.17	0.33
Std. Error (Toughness) MN/m^2	0.04	0.02	0.06	0.02	0.04	0.07
95% Confidence limit (toughness).	0.07	0.04	0.13	0.04	0.07	0.15

Mean 95% Confidence limit (hardness) GN/m^2 = 0.05
Mean 95% confidence limit (toughness) $MN/m^{3/2}$ = 0.08

0.50% SiO_2

Sintering Temperature (°C).	1250	1350	1450	1550	1650	1750
Mean Hardness GN/m^2	11.79	13.88	13.50	12.88	12.88	11.89
Std. Dev. Hardness GN/m^2	0.00	0.32	0.40	0.00	0.00	0.21
Std. Error (Hardness) GN/m^2	0.00	0.07	0.09	0.00	0.00	0.05
95% Confidence limit (hardness)	0.00	0.14	0.17	0.00	0.00	0.09
Mean Toughness MN/m^2	5.32	5.32	5.12	5.42	5.57	6.15
Std. Dev. (Toughness) GN/m^2	0.11	0.13	0.29	0.09	0.09	0.20
Std. Error (Toughness) MN/m^2	0.02	0.03	0.06	0.02	0.02	0.04
95% Confidence limit (toughness).	0.05	0.06	0.13	0.04	0.04	0.09

Mean 95% Confidence limit (hardness) GN/m^2 = 0.07
Mean 95% confidence limit (toughness) $MN/m^{3/2}$ = 0.07

0.75% SiO_2.

Sintering Temperature (°C).	1250	1350	1450	1550	1650	1750
Mean Hardness GN/m^2	11.01	12.88	12.44	12.10	11.96	11.79
Std. Dev. Hardness GN/m^2	0.23	0.00	0.41	0.26	0.56	0.00
Std. Error (Hardness) GN/m^2	0.05	0.00	0.09	0.06	0.13	0.00
95% Confidence limit (hardness)	0.10	0.00	0.18	0.11	0.25	0.00
Mean Toughness MN/m^2	5.49	5.03	5.09	5.31	5.56	5.85
Std. Dev. (Toughness) GN/m^2	0.18	0.15	0.20	0.11	0.12	0.19
Std. Error (Toughness) MN/m^2	0.04	0.03	0.04	0.02	0.03	0.04
95% Confidence limit (toughness).	0.08	0.07	0.09	0.05	0.05	0.08

Mean 95% Confidence limit (hardness) GN/m^2 = 0.11
Mean 95% confidence limit (toughness) $MN/m^{3/2}$ = 0.07

Table 4.7.4

Hardness and toughness results:

- Silica doped specimens (continued....).

1.00% SiO_2

Sintering Temperature (°C).	1250	1350	1450	1550	1650	1750
Mean Hardness GN/m^2	11.79	14.01	12.88	12.77	12.11	11.89
Std. Dev. Hardness GN/m^2	0.00	0.26	0.00	0.23	0.44	0.21
Std. Error (Hardness) GN/m^2	0.00	0.06	0.00	0.05	0.10	0.05
95% Confidence limit (hardness)	0.00	0.11	0.00	0.10	0.19	0.09
Mean Toughness MN/m^2	5.15	5.16	5.04	4.91	5.67	6.00
Std. Dev. (Toughness) GN/m^2	0.08	0.08	0.07	0.10	0.12	0.20
Std. Error (Toughness) MN/m^2	0.02	0.02	0.01	0.02	0.03	0.04
95% Confidence limit (toughness).	0.03	0.03	0.03	0.04	0.05	0.09

Mean 95% Confidence limit (hardness) GN/m^2 = 0.08

Mean 95% confidence limit (toughness) $MN/m^{3/2}$ = 0.04

Table 4.7.5

Hardness and fracture toughness results: Titania doped material.

0.25% TiO_2

Sintering Temperature (°C).	1250	1350	1450	1550	1650	1750
Mean Hardness GN/m^2	10.83	12.88	13.13	12.88	12.88	12.88
Std. Dev. Hardness GN/m^2	0.00	0.00	0.30	0.00	0.00	0.00
Std. Error (Hardness) GN/m^2	0.00	0.00	0.07	0.00	0.00	0.00
95% Confidence limit (hardness)	0.00	0.00	0.13	0.00	0.00	0.00
Mean Toughness MN/m^2	5.81	5.41	5.18	5.47	5.84	6.11
Std. Dev. (Toughness) GN/m^2	0.43	0.20	0.16	0.14	0.31	0.22
Std. Error (Toughness) MN/m^2	0.10	0.04	0.04	0.03	0.07	0.05
95% Confidence limit (toughness).	0.19	0.09	0.07	0.06	0.14	0.09

Mean 95% Confidence limit (hardness) GN/m^2 = 0.02
Mean 95% confidence limit (toughness) $MN/m^{3/2}$ = 0.11

0.50% TiO_2

Sintering Temperature (°C).	1250	1350	1450	1550	1650	1750
Mean Hardness GN/m^2	8.23	11.79	12.88	12.88	12.55	12.00
Std. Dev. Hardness GN/m^2	0.71	0.32	0.00	0.00	0.44	0.26
Std. Error (Hardness) GN/m^2	0.16	0.07	0.00	0.00	0.10	0.06
95% Confidence limit (hardness)	0.31	0.14	0.00	0.00	0.19	0.11
Mean Toughness MN/m^2	5.79	5.61	5.37	5.58	5.69	6.17
Std. Dev. (Toughness) GN/m^2	0.62	0.22	0.08	0.11	0.14	0.31
Std. Error (Toughness) MN/m^2	0.14	0.05	0.02	0.02	0.03	0.07
95% Confidence limit (toughness).	0.27	0.09	0.03	0.05	0.06	0.14

Mean 95% Confidence limit (hardness) GN/m^2 = 0.13
Mean 95% confidence limit (toughness) $MN/m^{3/2}$ = 0.11

0.75% TiO_2.

Sintering Temperature (°C).	1250	1350	1450	1550	1650	1750
Mean Hardness GN/m^2	7.41	11.10	12.88	12.88	12.88	11.42
Std. Dev. Hardness GN/m^2	0.00	0.23	0.00	0.00	0.00	0.72
Std. Error (Hardness) GN/m^2	0.00	0.05	0.00	0.00	0.00	0.16
95% Confidence limit (hardness)	0.00	0.10	0.10	0.00	0.00	0.32
Mean Toughness MN/m^2	5.37	5.39	5.35	5.41	5.69	5.81
Std. Dev. (Toughness) GN/m^2	0.16	0.16	0.19	0.11	0.11	0.14
Std. Error (Toughness) MN/m^2	0.04	0.04	0.04	0.02	0.02	0.03
95% Confidence limit (toughness).	0.07	0.07	0.08	0.05	0.05	0.06

Mean 95% Confidence limit (hardness) GN/m^2 = 0.07
Mean 95% confidence limit (toughness) $MN/m^{3/2}$ = 0.06

Table 4.7.5

Hardness and fracture toughness results: Titania doped material (continued...).

1.00% TiO_2

Sintering Temperature (^{o}C).	1250	1350	1450	1550	1650	1750
Mean Hardness GN/m^2	6.33	10.83	12.88	12.88	12.88	11.20
Std. Dev. Hardness GN/m^2	0.92	0.00	0.00	0.00	0.00	0.00
Std. Error (Hardness) GN/m^2	0.21	0.00	0.00	0.00	0.00	0.00
95% Confidence limit (hardness)	0.42	0.00	0.00	0.00	0.00	0.00
Mean Toughness MN/m^2	5.32	5.49	5.31	5.46	5.69	6.02
Std. Dev. (Toughness) GN/m^2	0.10	0.13	0.10	0.12	0.12	0.18
Std. Error (Toughness) MN/m^2	0.02	0.03	0.02	0.03	0.03	0.03
95% Confidence limit (toughness).	0.04	0.06	0.04	0.05	0.05	0.05

Mean 95% Confidence limit (hardness) GN/m^{2} = 0.03
Mean 95% confidence limit (toughness) $MN/m^{3/2}$ = 0.05

Table 4.7.6.

Hardness and fracture toughness results.

Multiple doped specimens.

1% Al_2O_3, 1% SiO_2

Sintering Temperature (°C).	1250	1350	1450	1550	1650	1750
Mean Hardness GN/m^2	13.88	12.88	12.55	11.70	10.06	5.23
Std. Dev. Hardness GN/m^2	0.32	0.00	0.44	0.48	0.16	0.13
Std. Error (Hardness) GN/m^2	0.07	0.00	0.10	0.11	0.04	0.07
95% Confidence limit (hardness)	0.14	0.00	0.20	0.22	0.08	0.14
Mean Toughness MN/m^2	5.05	5.18	5.29	6.08	7.25	5.68
Std. Dev. (Toughness) GN/m^2	0.10	0.18	0.14	0.27	0.90	0.94
Std. Error (Toughness) MN/m^2	0.02	0.04	0.03	0.06	0.20	0.21
95% Confidence limit (toughness).	0.04	0.08	0.06	0.12	0.40	0.42

Mean 95% Confidence limit (hardness) GN/m^2 = 0.13
Mean 95% confidence limit (toughness) $MN/m^{3/2}$ = 0.18

1% SiO_2, 1% TiO_2

Sintering Temperature (°C).	1250	1350	1450	1550	1650	1750
Mean Hardness GN/m^2	12.88	12.88	12.00	11.79	11.79	10.83
Std. Dev. Hardness GN/m^2	0.00	0.00	0.26	0.00	0.00	0.00
Std. Error (Hardness) GN/m^2	0.00	0.00	0.06	0.00	0.00	0.00
95% Confidence limit (hardness)	0.00	0.00	0.12	0.00	0.00	0.00
Mean Toughness MN/m^2	5.15	5.07	5.17	5.41	5.62	5.83
Std. Dev. (Toughness) GN/m^2	0.16	0.10	0.07	0.10	0.15	0.17
Std. Error (Toughness) MN/m^2	0.04	0.02	0.02	0.02	0.03	0.04
95% Confidence limit (toughness).	0.08	0.04	0.04	0.04	0.06	0.08

Mean 95% Confidence limit (hardness) GN/m^2 = 0.02
Mean 95% confidence limit (toughness) $MN/m^{3/2}$ = 0.05

1% Al_2O_3, 1% TiO_2

Sintering Temperature (°C).	1250	1350	1450	1550	1650	1750
Mean Hardness GN/m^2	11.42	12.88	12.88	12.88	11.79	3.71
Std. Dev. Hardness GN/m^2	0.22	0.00	0.00	0.00	0.00	0.19
Std. Error (Hardness) GN/m^2	0.05	0.00	0.00	0.00	0.00	0.04
95% Confidence limit (hardness)	0.10	0.00	0.00	0.00	0.00	0.08
Mean Toughness MN/m^2	5.31	5.26	5.41	5.61	7.36	0.00
Std. Dev. (Toughness) GN/m^2	0.13	0.10	0.10	0.08	1.05	0.00
Std. Error (Toughness) MN/m^2	0.03	0.02	0.02	0.02	0.23	0.00
95% Confidence limit (toughness).	0.06	0.04	0.04	0.04	0.46	0.00

Mean 95% Confidence limit (hardness) GN/m^2 = 0.03
Mean 95% confidence limit (toughness) $MN/m^{3/2}$ = 0.11

Table 4.7.6.

Hardness and fracture toughness results.

Multiple doped specimens (continued...).

1.00% Al_2O_3, SiO_2, TiO_2

Sintering Temperature (°C).	1250	1350	1450	1550	1650	1750
Mean Hardness GN/m^2	12.77	12.88	11.79	10.39	9.59	6.72
Std. Dev. Hardness GN/m^2	0.23	0.00	0.00	0.00	0.00	0.36
Std. Error (Hardness) GN/m^2	0.05	0.00	0.00	0.00	0.00	0.08
95% Confidence limit (hardness)	0.10	0.00	0.00	0.00	0.00	0.16
Mean Toughness MN/m^2	5.01	5.10	5.51	6.70	7.96	5.91
Std. Dev. (Toughness) GN/m^2	0.08	0.08	0.11	0.49	1.63	0.76
Std. Error (Toughness) MN/m^2	0.02	0.02	0.02	0.11	0.36	0.17
95% Confidence limit (toughness).	0.05	0.04	0.05	0.21	0.71	0.33

Mean 95% Confidence limit (hardness) GN/m^2 = 0.04

Mean 95% confidence limit (toughness) $MN/m^{3/2}$ = 0.23

Table 4.7.7.1 (a)

Analysis of data for factorial experiment (Yates' method)

Hardness results.

1250 - 1450°C temperature interval.

a = 1% Al_2O_3, b = 1% SiO_2, c = 1% TiO_2,

d = higher sintering temperature

Treatment	Mean hardness. (GN/m^2)	(1)	(2)	(3)	FACTORIAL EFFECT..... (4) [total]	(mean)	degrees of freedom	Sum of squares
1	9.98	22.86	48.53	91.93	192.67 = T			
a	12.88	25.67	43.40	100.74	9.43 = [A]	1.18	1	5.56
b	11.79	17.75	51.19	9.97	8.41 = [B]	1.05	1	4.42
ab	13.88	25.65	49.55	-0.54	-6.55 = [AB]	-0.82	1	2.68
c	6.33	25.76	4.99	10.71	-6.77 = [C]	-0.85	1	2.86
ac	11.42	25.43	4.98	-2.30	0.11 = [AC]	0.01	1	0.00
bc	12.88	25.76	-0.33	-6.01	3.45 = [BC]	0.43	1	0.74
abc	12.77	23.79	-0.21	-0.54	-4.27 = [ABC]	-0.53	1	1.14
d	12.88	2.90	2.81	-5.13	8.81 = [D]	1.10	1	4.85
ad	12.88	2.09	7.90	-1.64	-10.51 = [AD]	-1.31	1	6.90
bd	12.88	5.09	-0.33	-0.01	-13.01 = [BD]	-1.63	1	10.58
abd	12.55	-0.11	-1.97	0.12	5.47 = [ABD]	0.68	1	1.87
cd	12.88	0.00	-0.81	5.09	3.49 = [CD]	0.44	1	0.76
acd	12.88	-0.33	-5.20	-1.64	0.13 = [ACD]	0.02	1	0.00
bcd	12.00	0.00	-0.33	-4.39	-6.73 = [BCD]	-0.84	1	2.83
abcd	11.79	-0.21	-0.21	0.12	4.51 = [ABCD]	0.56	1	1.27

Total (T) = 192.67

no. of treatments (t) = 16

no of replicates (r) = 1

Table 4.7.7.1 (b)

Analysis of data for factorial experiment (Yates' method)

Hardness results.

1450 - 1550°C temperature interval.

a = 1% Al_2O_3, b = 1% SiO_2, c = 1% TiO_2,

d = higher sintering temperature

Treatment	Mean hardness. (GN/m^2)	(1)	(2)	(3)	FACTORIAL EFFECT..... (4) [total]	(mean)	degrees of freedom	Sum of squares
1	12.88	25.76	51.19	100.74	198.91 = T			
a	12.88	25.43	49.55	98.17	-3.01 = [A]	-0.38	1	0.57
b	12.88	25.76	50.23	-0.54	-7.17 = [B]	-0.90	1	3.21
ab	12.55	23.79	47.94	-2.47	-3.01 = [AB]	-0.38	1	0.57
c	12.88	25.76	-0.33	-2.30	-3.93 = [C]	-0.49	1	0.97
ac	12.88	24.47	-0.21	-4.87	-0.21 = [AC]	-0.03	1	0.00
bc	12.00	25.76	-1.07	-0.54	-3.93 = [BC]	-0.49	1	0.97
abc	11.79	22.18	-1.40	-2.47	-0.21 = [ABC]	-0.03	1	0.00
d	12.88	0.00	-0.33	-1.64	-2.57 = [D]	-0.32	1	0.41
ad	12.88	-0.33	-1.97	-2.29	-1.93 = [AD]	-0.24	1	0.23
bd	12.77	0.00	-1.29	0.12	-2.57 = [BD]	-0.32	1	0.41
abd	11.70	-0.21	-3.58	-0.33	-1.93 = [ABD]	-0.24	1	0.23
cd	12.88	0.00	-0.33	-1.64	-0.65 = [CD]	-0.08	1	0.03
acd	12.88	-1.07	-0.21	-2.29	-0.45 = [ACD]	-0.06	1	0.01
bcd	11.79	0.00	-1.07	0.12	-0.65 = [BCD]	-0.08	1	0.03
abcd	10.39	-1.40	-1.40	-0.33	-0.45 = [ABCD]	-0.06	1	0.01
Total (T) =	198.91							

no. of treatments (t) =	16
no of replicates (r) =	1

Table 4.7.7.1 (c)

Analysis of data for factorial experiment (Yates' method)

Hardness results.

1550 - 1650°C temperature interval.

a = 1% Al_2O_3, b = 1% SiO_2, c = 1% TiO_2,

d = higher sintering temperature

Treatment	Mean Hardness. (GN/m^2)	(1)	(2)	(3)	FACTORIAL EFFECT..... (4) [total]	(mean)	degrees of freedom	Sum of squares
1	12.88	25.76	50.23	98.17	191.06 = T			
a	12.88	24.47	47.94	92.89	-8.90 = [A]	-1.11	1	4.95
b	12.77	25.76	46.84	-2.47	-10.66 = [B]	-1.33	1	7.10
ab	11.70	22.18	46.05	-6.43	-4.54 = [AB]	-0.57	1	1.29
c	12.88	24.67	-1.07	-4.87	-3.08 = [C]	-0.39	1	0.59
ac	12.88	22.17	-1.40	-5.79	-0.48 = [AC]	-0.06	1	0.01
bc	11.79	24.67	-3.14	-2.47	-3.08 = [BC]	-0.39	1	0.59
abc	10.39	21.38	-3.29	-2.07	-0.48 = [ABC]	-0.06	1	0.01
d	12.88	0.00	-1.29	-2.29	-5.28 = [D]	-0.66	1	1.74
ad	11.79	-1.07	-3.58	-0.79	-3.96 = [AD]	-0.50	1	0.98
bd	12.11	0.00	-2.50	-0.33	-0.92 = [BD]	-0.11	1	0.05
abd	10.06	-1.40	-3.29	-0.15	0.40 = [ABD]	0.05	1	0.01
cd	12.88	-1.09	-1.07	-2.29	1.50 = [CD]	0.19	1	0.14
acd	11.79	-2.05	-1.40	-0.79	0.18 = [ACD]	0.02	1	0.00
bcd	11.79	-1.09	-0.96	-0.33	1.50 = [BCD]	0.19	1	0.14
abcd	9.59	-2.20	-1.11	-0.15	0.18 = [ABCD]	0.02	1	0.00
Total (T) =	191.06							

no. of treatments (t) =	16
no of replicates (r) =	1

Table 4.7.7.1(d)

Analysis of variance (ANOVA) table.

Factorial experiment (hardness)

1250 - 1450°C temperature interval.

Source of variation	degrees of freedom	sum of squares	mean square	(Pooled error estimate) mean square/ error mean square	F test signif-icance.	(External error estimate) mean square/ error mean square	F test signif-icance.
Al_2O_3 addition (A)	1	5.56	5.56	3.91	N/S	40.60	***
SiO_2 Addition (B)	1	4.42	4.42	3.11	N/S	32.29	***
TiO_2 addition (C)	1	2.86	2.86	2.01	N/S	20.92	***
Sintering temperature	1	4.85	4.85	3.41	N/S	35.43	***
Interactions:							
(2nd order)							
AB	1	2.68	2.68	1.88	N/S	19.59	***
AC	1	0.00	0.00	0.00	N/S	0.01	N/S
AD	1	6.90	6.90	4.85	**	50.43	***
BC	1	0.74	0.74	0.52	N/S	5.43	**
BD	1	10.58	10.58	7.44	**	77.27	***
CD	1	0.76	0.76	0.54	N/S	5.56	**
(3rd order)							
ABC	1	1.14	1.14	0.80		8.32	**
ABD	1	1.87	1.87	1.31		13.66	***
ACD	1	0.00	0.00	0.00		0.01	N/S
BCD	1	2.83	2.83	1.99		20.68	***
(4th order)							
ABCD	1	1.27	1.27	0.89		0.89	N/S
Error term:							
(pooled 3rd and 4th order term)	5	7.11	1.42	-----			
External estimate of error							
(method b difference values)	11	1.506	0.137	-----			

f test values for significance (5 & 1 degrees of freedom)

f (1 %) (highly significant) = 16.3	Indicated as *** in results.
f (5 %) = 6.61	Indicated as ** in results.
f (10 %) (less significant) = 4.06	Indicated as * in results.
f (>10%) considered to be not significant.	Indicated as N/S in results.

(11 & 1 degrees of freedom)

f (1 %) (highly significant) = 9.65	Indicated as *** in results.
f (5 %) = 4.84	Indicated as ** in results.
f (10 %) (less significant) = 3.23	Indicated as * in results.
f (>10%) considered to be not significant.	Indicated as N/S in results.

Calculation of external error estimate.

Mean difference (method b) = 0.37
Difference squared = 0.137
Sum of squares of differences = 1.506
No. of data values (degrees of freedom) = 11
mean square difference = sum squares /degrees freedom = 0.137

Table 4.7.7.1(e)

Analysis of variance (ANOVA) table.

Factorial experiment (hardness)

1450 - 1550°C temperature interval.

Source of variation	degrees of freedom	sum of squares	mean square	(Pooled error estimate) mean square/ error mean square	F test signif-icance.	(External error estimate) mean square/ error mean square	F test signif-icance.
Al_2O_3 addition (A)	1	0.57	0.57	9.86	**	4.14	**
SiO_2 Addition (B)	1	3.21	3.21	55.92	***	23.47	***
TiO_2 addition (C)	1	0.97	0.97	16.80	***	7.05	***
Sintering temperature (D)	1	0.41	0.41	7.18	**	3.02	**
Interactions:							
(2nd order)							
AB	1	0.57	0.57	9.86	**	4.14	**
AC	1	0.00	0.00	0.05	N/S	0.02	N/S
AD	1	0.23	0.23	4.05	N/S	1.70	N/S
BC	1	0.97	0.97	16.80	***	7.05	***
BD	1	0.41	0.41	7.18	**	3.02	**
CD	1	0.03	0.03	0.46	N/S	0.19	N/S
(3rd order)							
ABC	1	0.00	0.00	0.05		0.02	N/S
ABD	1	0.23	0.23	4.05		1.70	N/S
ACD	1	0.01	0.01	0.22		0.02	N/S
BCD	1	0.03	0.03	0.46		0.04	N/S
(4th order)							
ABCD	1	0.01	0.01	0.22		0.22	N/S
Error term: (pooled 3rd and 4th order terms)	5	0.29	0.06	----			
External estimate of error (method b difference values)	11	6.522	0.593	-----			

f test values for significance (5 & 1 degrees of freedom)

f (1 %) (highly significant)	= 16.3	Indicated as *** in results.
f (5 %)	= 6.61	Indicated as ** in results.
f (10 %) (less significant)	= 4.06	Indicated as * in results.
f (>10%) considered to be not significant.		Indicated as N/S in results.

(11 & 1 degrees of freedom)

f (1 %) (highly significant)	= 9.65	Indicated as *** in results.
f (5 %)	= 4.84	Indicated as ** in results.
f (10 %) (less significant)	= 3.23	Indicated as * in results.
f (>10%) considered to be not significant.		Indicated as N/S in results.

Calculation of external error estimate.

Mean difference (method b) = 0.37
Difference squared = 0.137
Sum of squares of differences = 1.506
No. of data values (degrees of freedom) = 11
mean square difference = sum squares /degrees freedom = 0.137

Table 4.7.7.1(f)

Analysis of variance (ANOVA) table.

Factorial experiment (hardness)

1550 - 1650°C temperature interval.

Source of variation	degrees of freedom	sum of squares	mean square	(Pooled error estimate) mean square/ error mean square	F test signif-icance.	(External error estimate) mean square/ error mean square	F test signif-icance.
Al_2O_3 addition (A)	1	4.95	4.95	146.40	***	36.16	***
SiO_2 Addition (B)	1	7.10	7.10	210.03	***	51.88	***
TiO_2 addition (C)	1	0.59	0.59	17.53	***	4.33	*
Sintering temperature (D)	1	1.74	1.74	51.53	***	12.73	***
Interactions:							
(2nd order)							
AB	1	1.29	1.29	38.10	***	9.41	**
AC	1	0.01	0.01	0.43	N/S	0.11	N/S
AD	1	0.98	0.98	28.98	***	7.16	**
BC	1	0.59	0.59	17.53	***	4.33	**
BD	1	0.05	0.05	1.56	N/S	0.39	N/S
CD	1	0.14	0.14	4.16	*	1.03	N/S
(3rd order)							
ABC	1	0.01	0.01	0.43		0.11	N/S
ABD	1	0.01	0.01	0.30		0.07	N/S
ACD	1	0.00	0.00	0.06		0.01	N/S
BCD	1	0.14	0.14	4.16		1.03	N/S
(4th order)							
ABCD	1	0.00	0.00	0.06		0.01	N/S
Error term:							
(pooled 3rd and 4th order terms)	5	0.17	0.03	-----			
External estimate of error							
(method b difference values)	11	1.506	0.137	-----			

f test values for significance (5 & 1 degrees of freedom)

f (1 %) (highly significant) = 16.3	Indicated as *** in results.
f (5 %) = 6.61	Indicated as ** in results.
f (10 %) (less significant) = 4.06	Indicated as * in results.
f (>10%) considered to be not significant.	Indicated as N/S in results.

(11 & 1 degrees of freedom)

f (1 %) (highly significant) = 9.65	Indicated as *** in results.
f (5 %) = 4.84	Indicated as ** in results.
f (10 %) (less significant) = 3.23	Indicated as * in results.
f (>10%) considered to be not significant.	Indicated as N/S in results.

Calculation of external error estimate.

Mean difference (method b) = 0.37
Difference squared = 0.137
Sum of squares of differences = 1.506
No. of data values (degrees of freedom) = 11
mean square difference = sum squares /degrees freedom = 0.137

Table 4.7.7.2 (a)

Analysis of data for factorial experiment (Yates' method)

Toughness results.

1250 - 1450°C temperature interval.

a = 1% Al_2O_3, b = 1% SiO_2, c = 1% TiO_2,

d = higher sintering temperature

Treatment	Mean toughness ($GNm^{3/2}$)	(1)	(2)	(3)	FACTORIAL EFFECT..... (4) [total]	(mean)	degrees of freedom	Sum of squares
1	5.49	10.89	21.09	41.88	84.11 = T			
a	5.40	10.20	20.79	42.23	0.39 = [A]	0.05	1	0.010
b	5.15	10.63	20.83	-0.34	-1.37 = [B]	-0.17	1	0.117
ab	5.05	10.16	21.40	0.73	0.31 = [AB]	0.04	1	0.006
c	5.32	10.50	-0.19	-1.16	0.27 = [C]	0.03	1	0.005
ac	5.31	10.33	-0.15	-0.21	0.19 = [AC]	0.02	1	0.002
bc	5.15	10.72	0.29	-0.14	0.35 = [BC]	0.04	1	0.008
abc	5.01	10.68	0.44	0.45	-0.09 = [ABC]	-0.01	1	0.001
d	5.23	-0.09	-0.69	-0.30	0.35 = [D]	0.04	1	0.008
ad	5.27	-0.10	-0.47	0.57	1.07 = [AD]	0.13	1	0.072
bd	5.04	-0.01	-0.17	0.04	0.95 = [BD]	0.12	1	0.056
abd	5.29	-0.14	-0.04	0.15	0.59 = [ABD]	0.07	1	0.022
cd	5.31	0.04	-0.01	0.22	0.87 = [CD]	0.11	1	0.047
acd	5.41	0.25	-0.13	0.13	0.11 = [ACD]	0.01	1	0.001
bcd	5.17	0.10	0.21	-0.12	-0.09 = [BCD]	-0.01	1	0.001
abcd	5.51	0.34	0.24	0.03	0.15 = [ABCD]	0.02	1	0.001
Total (T) =	84.11							

no. of treatments (t) =	16
no of replicates (r) =	1

Table 4.7.7.2 (b)

Analysis of data for factorial experiment (Yates' method)

Toughness results.

1450 - 1550°C temperature interval.

a = 1% Al_2O_3, b = 1% SiO_2, c = 1% TiO_2,

d = higher sintering temperature

Treatment	Mean toughness ($GNm^{3/2}$)	(1)	(2)	(3)	FACTORIAL EFFECT..... (4) [total]	(mean)	degrees of freedom	Sum of squares	
1	5.23	10.50	20.83	42.23	87.47 = T				
a	5.27	10.33	21.40	45.24	3.71 = [A]	0.46	1	0.860	0.860
b	5.04	10.72	22.06	0.73	0.75 = [B]	0.09	1	0.035	0.035
ab	5.29	10.68	23.18	2.98	2.39 = [AB]	0.30	1	0.357	0.357
c	5.31	11.07	0.29	-0.21	1.69 = [C]	0.21	1	0.179	0.179
ac	5.41	10.99	0.44	0.96	0.05 = [AC]	0.01	1	0.000	0.000
bc	5.17	11.07	1.54	0.45	1.25 = [BC]	0.16	1	0.098	0.098
abc	5.51	12.11	1.44	1.94	0.37 = [ABC]	0.05	1	0.009	0.009
d	5.35	0.04	-0.17	0.57	3.01 = [D]	0.38	1	0.566	0.566
ad	5.72	0.25	-0.04	1.12	2.25 = [AD]	0.28	1	0.316	0.316
bd	4.91	0.10	-0.08	0.15	1.17 = [BD]	0.15	1	0.086	0.086
abd	6.08	0.34	1.04	-0.10	1.49 = [ABD]	0.19	1	0.139	0.139
cd	5.46	0.37	0.21	0.13	0.55 = [CD]	0.07	1	0.019	0.019
acd	5.61	1.17	0.24	1.12	-0.25 = [ACD]	-0.03	1	0.004	0.004
bcd	5.41	0.15	0.80	0.03	0.99 = [BCD]	0.12	1	0.061	0.061
abcd	6.7	1.29	1.14	0.34	0.31 = [ABCD]	0.04	1	0.006	0.006
Total (T) =	87.47								

no. of treatments (t) =	16
no of replicates (r) =	1

Table 4.7.7.2 (c)

Analysis of data for factorial experiment (Yates' method)

Toughness results.

1550 - 1650°C temperature interval.

a = 1% Al_2O_3, b = 1% SiO_2, c = 1% TiO_2,

d = higher sintering temperature

Treatment	Mean toughness ($GNm^{3/2}$)	(1)	(2)	(3)	FACTORIAL EFFECT..... (4) [total]	(mean)	degrees of freedom	Sum of squares
1	5.35	11.07	22.06	45.24	96.59 = T			
a	5.72	10.99	23.18	51.35	9.09 = [A]	1.14	1	5.164
b	4.91	11.07	24.72	2.98	2.61 = [B]	0.33	1	0.426
ab	6.08	12.11	26.63	6.11	3.67 = [AB]	0.46	1	0.842
c	5.46	11.80	1.54	0.96	3.03 = [C]	0.38	1	0.574
ac	5.61	12.92	1.44	1.65	1.81 = [AC]	0.23	1	0.205
bc	5.41	13.05	2.10	1.94	0.53 = [BC]	0.07	1	0.018
abc	6.70	13.58	4.01	1.73	-0.05 = [ABC]	-0.01	1	0.000
d	5.64	0.37	-0.08	1.12	6.11 = [D]	0.76	1	2.333
ad	6.16	1.17	1.04	1.91	3.13 = [AD]	0.39	1	0.612
bd	5.67	0.15	1.12	-0.10	0.69 = [BD]	0.09	1	0.030
abd	7.25	1.29	0.53	1.91	-0.21 = [ABD]	-0.03	1	0.003
cd	5.69	0.52	0.80	1.12	0.79 = [CD]	0.10	1	0.039
acd	7.36	1.58	1.14	-0.59	2.01 = [ACD]	0.25	1	0.253
bcd	5.62	1.67	1.06	0.34	-1.71 = [BCD]	-0.21	1	0.183
abcd	7.96	2.34	0.67	-0.39	-0.73 = [ABCD]	-0.09	1	0.033
Total (T) =	96.59							

no. of treatments (t) =	16
no of replicates (r) =	1

Table 4.7.7.2(d)

Analysis of variance (ANOVA) table.

Factorial experiment (toughness)

1250 - 1450°C temperature interval.

Source of variation	degrees of freedom	sum of squares	mean square	(Pooled error estimate) mean square/ error mean square	F test signif-icance.	(External error estimate) mean square/ error mean square	F test signif-icance.
Al_2O_3 addition (A)	1	0.010	0.010	1.91	N/S	0.56	N/S
SiO_2 Addition (B)	1	0.117	0.117	23.53	***	6.94	**
TiO_2 addition (C)	1	0.005	0.005	0.91	N/S	0.27	N/S
Sintering temperature (D)	1	0.008	0.008	1.54	N/S?	0.45	N/S
Interactions:							
(2nd order)							
AB	1	0.006	0.006	1.20	N/S	0.36	N/S
AC	1	0.002	0.002	0.45	N/S	0.13	N/S
AD	1	0.072	0.072	14.35	**	4.23	*
BC	1	0.008	0.008	1.54	N/S	0.45	N/S
BD	1	0.056	0.056	11.31	**	3.34	*
CD	1	0.047	0.047	9.49	**	2.80	N/S
(3rd order)							
ABC	1	0.001	0.001	0.10	---	0.03	N/S
ABD	1	0.022	0.022	4.36	---	1.29	N/S
ACD	1	0.001	0.001	0.15	---	0.04	N/S
BCD	1	0.001	0.001	0.10	---	0.03	N/S

(4th order)							
ABCD	1	0.001	0.001	0.28	---	0.08	N/S
Error term:							
(pooled 3rd and 4th order terms)	5	0.025	0.005	-----	---	-----	---
External estimate of error							
(method b difference values)	11	0.186	0.017	-----	---	-----	---

f test values for significance (5 & 1 degrees of freedom)

f (1 %) (highly significant) = 16.3 Indicated as *** in results.
f (5 %) = 6.61 Indicated as ** in results.
f (10 %) (less significant) = 4.06 Indicated as * in results.
f (>10%) considered to be not significant. Indicated as N/S in results.

(11 & 1 degrees of freedom)

f (1 %) (highly significant) = 9.65 Indicated as *** in results.
f (5 %) = 4.84 Indicated as ** in results.
f (10 %) (less significant) = 3.23 Indicated as * in results.
f (>10%) considered to be not significant. Indicated as N/S in results.

Calculation of external error estimate.

Mean difference (method b) = 0.13
Difference squared = 0.017
Sum of squares of differences = 0.186
No. of data values (degrees of freedom) = 11
mean square difference = sum squares /degrees freedom = 0.017

Table 4.7.7.2(e)

Analysis of variance (ANOVA) table.

Factorial experiment (toughness)

1450 - 1550°C temperature interval.

Source of variation	degrees of freedom	sum of squares	mean square	(Pooled error estimate) mean square/ error mean square	F test signif-icance.	(External error estimate) mean square/ error mean square	F test signif-icance.
Al_2O_3 addition (A)	1	0.860	0.860	19.69	***	50.90	***
SiO_2 Addition (B)	1	0.035	0.035	0.80	N/S	2.08	N/S
TiO_2 addition (C)	1	0.179	0.179	4.09	*	10.56	***
Sintering temperature (D)	1	0.566	0.566	12.96	**	33.51	***
Interactions:							
(2nd order)							
AB	1	0.357	0.357	8.17	**	21.12	***
AC	1	0.000	0.000	0.00	N/S	0.01	N/S
AD	1	0.316	0.316	7.24	**	18.72	***
BC	1	0.098	0.098	2.23	N/S	5.78	**
BD	1	0.086	0.086	1.96	N/S	5.06	**
CD	1	0.019	0.019	0.43	N/S	1.12	N/S
(3rd order)							
ABC	1	0.009	0.009	0.20	---	0.51	N/S
ABD	1	0.139	0.139	3.18	---	8.21	**
ACD	1	0.004	0.004	0.09	---	0.23	N/S
BCD	1	0.061	0.061	1.40	---	3.62	*
(4th order)							
ABCD	1	0.006	0.006	0.14	---	0.36	N/S
Error term: (pooled 3rd and 4th order terms)	5	0.22	0.04	-----	---	-----	---
External estimate of error (method b difference values)	11	0.186	0.017	-----	---	-----	---

f test values for significance (5 & 1 degrees of freedom)

f (1 %) (highly significant) = 16.3	Indicated as *** in results.
f (5 %) = 6.61	Indicated as ** in results.
f (10 %) (less significant) = 4.06	Indicated as * in results.
f (>10%) considered to be not significant.	Indicated as N/S in results.

(11 & 1 degrees of freedom)

f (1 %) (highly significant) = 9.65	Indicated as *** in results.
f (5 %) = 4.84	Indicated as ** in results.
f (10 %) (less significant) = 3.23	Indicated as * in results.
f (>10%) considered to be not significant.	Indicated as N/S in results.

Calculation of external error estimate.

Mean difference (method b) = 0.13
Difference squared = 0.017
Sum of squares of differences = 0.186
No. of data values (degrees of freedom) = 11
mean square difference = sum squares /degrees freedom = 0.017

Table 4.7.7.2(f)

Analysis of variance (ANOVA) table.

Factorial experiment (toughness)

1550 - 1650°C temperature interval.

Source of variation	degrees of freedom	sum of squares	mean square	(Pooled error estimate) mean square/ error mean square	F test signif-icance.	(External error estimate) mean square/ error mean square	F test signif-icance.
Al_2O_3 addition (A)	1	5.164	5.164	54.77	***	305.58	***
SiO_2 Addition (B)	1	0.426	0.426	4.52	*	25.19	***
TiO_2 addition (C)	1	0.574	0.574	6.09	*	33.95	***
Sintering temperature (D)	1	2.333	2.333	24.74	***	138.06	***
Interactions:							
(2nd order)							
AB	1	0.842	0.842	8.93	**	49.81	***
AC	1	0.205	0.205	2.17	N/S	12.12	***
AD	1	0.612	0.612	6.49	*	36.23	***
BC	1	0.018	0.018	0.19	N/S	1.04	N/S
BD	1	0.030	0.030	0.32	N/S	1.76	N/S
CD	1	0.039	0.039	0.41	N/S	2.31	N/S
(3rd order)							
ABC	1	0.000	0.000	0.00	---	0.01	N/S
ABD	1	0.003	0.003	0.03	---	0.16	N/S
ACD	1	0.253	0.253	2.68	---	14.94	***
BCD	1	0.183	0.183	1.94	---	10.81	***
(4th order)							
ABCD	1	0.033	0.033	0.35	---	1.97	N/S
Error term:							
(pooled 3rd and 4th order terms)	5	0.471	0.094	-----	---	-----	---
External estimate of error							
(method b difference values)	11	0.186	0.017	-----	---	-----	---

f test values for significance (5 & 1 degrees of freedom)

f (1 %) (highly significant) = 16.3	Indicated as *** in results.
f (5 %) = 6.61	Indicated as ** in results.
f (10 %) (less significant) = 4.06	Indicated as * in results.
f (>10%) considered to be not significant.	Indicated as N/S in results.

(11 & 1 degrees of freedom)

f (1 %) (highly significant) = 9.65	Indicated as *** in results.
f (5 %) = 4.84	Indicated as ** in results.
f (10 %) (less significant) = 3.23	Indicated as * in results.
f (>10%) considered to be not significant.	Indicated as N/S in results.

Calculation of external error estimate.

Mean difference (method b) = 0.13
Difference squared = 0.017
Sum of squares of differences = 0.186
No. of data values (degrees of freedom) = 11
mean square difference = sum squares /degrees freedom = 0.017